Small-molecule inhibitors of eIF2α phosphatase

Matthew W. Halloran, Department of Chemistry
McGill University, Montreal

December 2017

A thesis submitted to McGill University in partial fulfillment of the requirements of the degree of Master of Science

Abstract

The investigation of protein-ligand interactions is essential in the development and discovery of biologically active small molecules. However, due to the complex nature of the native cellular environment, the elucidation of these fundamental biochemical processes remains challenging. Our lack of understanding of protein-ligand interactions in their native biological setting has hindered the discovery of new drug targets, and has influenced the progression of the pharmaceutical industry. Owing to the advancements made in the fields of organic synthesis, chemical biology, and proteomics, the ability to identify cellular targets of small molecules has come to fruition through the development of photoaffinity labelling (PAL), which involves the design and synthesis of a chemical probe capable of covalently modifying the target of interest through exposure to UV-light. Although PAL has proven to be effective, this technique harbors its own set of limitations which originate from the challenges associated with the development of a suitable chemical probe. In summarizing the requirements involved in a PAL experiment, current synthetic methods for the preparation of photoactive diazirines will be outlined, as well as their use for target identification studies in the recent literature.

Herein, we describe our efforts to apply PAL to a class of small molecules capable of regulating muscle stem cell differentiation to be used as therapeutic treatment for Duchenne's Muscular Dystrophy. The large-scale synthesis of this class of biologically active small molecules will be discussed, along with the design and synthesis of a PAL probe in order to identify their cellular target(s), and shed light on their mechanism of action.

Lastly, our work toward and atom-economical synthesis of 1,4-benzothiazines using our developed methodology for the selective installation of aryl carbon-sulfur bonds will be outlined.

Résumé

L'étude des interactions entre protéines et coordinats est essentielle au développement et à la découverte de molécule biologiquement active. Cependant, la nature complexe de l'environnement cellulaire naturel rend difficile l'analyse des processus biochimiques fondamentaux. Notre compréhension limitée des interactions protéine/coordinat dans leur milieu naturel a jusqu'ici empêché la découverte de nouveaux composés ciblés ce qui ralenti les progrès de l'industrie pharmaceutique. Toutefois les développements récents dans les champs des recherches en synthèse organique, en chimie biologique et en protéomique permettent d'identifier les cibles cellulaires de petite molécule grâce au développement d'une technique d'étiquetage par photo affinité (PhotoAffinity Labelling ou PAL), il s'agit de concevoir et de synthétiser une sonde chimique capable de modifier par covalence la cible recherchée après exposition a une lumière ultra violette. Bien que PAL se soit révélé efficace, la méthode rencontre ses propres limitations dues à des problèmes provenant des difficultés liées au développement de sondes chimiques convenables. Les méthodes de synthèses actuelles dans la préparation de diazines photoactives seront soulignées, ainsi que leurs utilités à identifier des cibles déjà décrites dans des publications récentes.

Ici, nous allons décrire nos travaux dans l'application de PAL a une catégorie de petites molécules capables de réguler la différentiation de cellules souches musculaires utilisées pour le traitement thérapeutique de la dystrophie musculaire de Duchenne. La synthèse à grande échelle de cette classe de petites molécules biologiquement actives sera abordé, ainsi que la conception et la synthèse d'une sonde PAL afin d'identifier leurs cibles cellulaires et d'illuminer leur mécanisme d'action.

Pour finir, nos travaux sur la synthèse atome-economique des 1,4-benzothiazines en utilisant notre méthodologie développée pour l'installation sélective de liaisons aryl carbone-soufre sera soulignée.

Acknowledgements

I am indebted to all who have made contributions to the research in this thesis. Foremost, I would like to express my deepest gratitude to my thesis supervisor and advisor, Dr. Jean-Philip Lumb. His constant guidance, enthusiasm, and relentless pursuit of excellence have been an unforgettable source of motivation during my graduate career

I would like to thank the laboratory of Dr. Colin Crist for performing the biological assays described in this thesis, as this project would not be possible without their contributions. I would also like to thank my committee members Dr. Jim Gleason and Dr. Bruce Arndsten, for their insightful comments and thought-provoking questions. I extend my gratitude to all of the faculty members and staff at McGill for allowing me the use of chemicals, equipment, and facilities in the department. I gratefully acknowledge the Stem Cell Network and McGill University for funding support throughout my degree.

During my time in the lab I was lucky enough to have worked alongside my friend and mentor, Dr. Kenneth Esguerra. From the day that I arrived, he was there to provide unlimited support without hesitation, and this work would not have been possible without him. I would also like to thank my good friend and roommate Dr. Naresh Vemula for keeping me motivated during the final stretch. I will always remember the good times and the laughs that we shared along the way. Finally, I would like to thank Océane Marescal for her contributions to this work and for enduring my sense of humour.

To my labmates past and present, Anna, Martin, Liz, Wenbo, Zheng, Ohhyeon, Haiyan, and Yalun, thank you so much for the constant support during the tough times, and for being the best company that made many sleepless nights pass all the quicker. To all my friends in the department, I feel honoured to have worked among such amazing people- thank you for all the great memories.

Lastly, I would like to thank my parents and my sister for keeping me grounded and supporting me during my degree.

Table of Contents

List of Abbreviations

°C- Degrees Celcius
μM- micromolar
1°- primary
2°-secondary
3°-tertiary
^{1}H- proton
Ac_2O- acetic anhydride
ADHD- attention-deficit/hyperactivity disorder
Ar- aryl
AR- adenosine receptor
AcOH- acetic acid
BARAC- biarylazacylcooctynone
Bn- benzyl
Boc- *tert*-Butyloxycarbonyl
CuAAC- copper catalyzed alkyne-azide cycloaddition
d- doublet
Da- Dalton
DIPEA- N,N-Diisopropylethylamine
DCE- 1,2-dichloroethane
DCM- dichloromethane
DMAP- 4-dimethylaminopyridine
DMF- dimethylformamide
DMSO- dimethyl sulfoxide
DNA- deoxyribonucleic acid
EC- endocannabinoid
ECS- endocannabinoid system
Et- ethyl
EtOAc- ethyl acetate
EtOH- ethanol
EtSH- ethanethiol
EWG- electron withdrawing group
h- hour(s)
GPCR- G protein-coupled receptor
HDAC- histone deacetylase
HIF- hypoxia inducible factor
HRMS- high resolution mass spectroscopy
Hz- Hertz
i-PrOH- isopropanol
i-PrSH- 2-propanethiol
J- coupling constant
Kcal/mol- kilocalorie per mol
KOH- potassium hydroxide
KO*t*Bu- potassium *tert*-butoxide
L- ligand
LC-MS/MS- liquid chromatography-mass spectrometry/mass spectrometry

m-multiplet
M- mol/L
$M^{-1}sec^{-1}$- /mol /sec
MDH2- malate dehydrogenase 2
Me- methyl
MeCN- acetonitrile
MeOH- methanol
$MgBr_2 \cdot Et_2O$- magnesium bromide di-ethyl etherate
Min- minute(s)
mM- millimolar
mol- mole (s)
Ms- mesyl
MsCl- methansulfonyl chloride
NAD- Nicotinamide adenine dinucleotide
NaOH- sodium hydroxide
NaOtBu- sodium *tert*-butoxide
NBD- nitrobenzoxadiazole
NMR- nuclear magnetic resonance
OAc- acetate
OH- Hydroxyl Group
PAL- photoaffinity labelling
PEG-400- low-molecular-weight grade of polyethylene glycol
Ph- Phenyl
PhSH- thiophenol
pH- decimal logarithm of the reciprocal of the hydrogen ion activity in a solution
pKa-acid dissociation constant
*p*TsOH- *para*-toluene sulfonic acid
q- quartet
QSAR- quantitative structure activity relationship
s- singlet
RNA- ribonucleic acid
SAR- Structure Activity Relationship
sec- second (s)
S_NAr- nucleophilic aromatic substitution
SIRT1- sirtuin 1
SIRT2- sirtuin 2
SIRT7- sirtuin 7
t- triplet
TPD- trifluoromethyl-phenyldiazirine
*t*Bu- *tert*-butyl
*t*BuOK- potassium *tert*-butoxide
TEMPO- (2,2,6,6-Tetramethylpiperidin-1-yl)oxyl
TFA- trifluoroacetic acid
THF- tetrahydrofuran
Ts- tosyl
UV- Ultraviolet Visible

List of Figures

List of Schemes

List of Tables

1 - Diazirines in Photoaffinity Labelling

1.1 - Introduction

Unraveling the intricate interactions of proteins and their ligands is crucial for the development of active pharmaceutical agents, and also aids in the understanding of enzyme structure.[1] A significant challenge in these studies is the elucidation of enzyme-substrate complexes at an atomic-level resolution. Our lack of understanding of these protein-ligand interactions in their native biological setting has hindered the discovery of new drug targets, as currently less than 1.5% genes in the human genome are used as pharmaceutical targets.[2] Despite the recent technological advancements in the screening capabilities for the identification of biologically active small-molecules, in some cases their biological targets and mechanisms of action remain unclear.[3-4] Having the ability to identify cellular targets of biologically active small-molecules provides the opportunity to discover new molecular pathways and therapeutic targets for currently untreatable diseases. In 1962, Frank Westheimer and coworkers introduced the concept of photoaffinity labelling (PAL) through the modification of the active site of chymotrypsin using a photo-induced acylation reaction involving the generation of a reactive carbene within the enzyme's active site.[5] This was the first reported example of a light-triggered covalent modification of an enzyme, thus introducing the concept of photoaffinity labelling (PAL). During the past 40 years, this technique has been successfully applied in the fields of structural biology, chemical biology, and medicinal chemistry for the identification of cellular targets of biologically active small-molecules, characterization of ligand-binding sites, and the identification of unknown receptors or enzymes.[6-8] Since its initial discovery, PAL has emerged as an important tool for studying protein-ligand interactions.

In this thesis, we will describe our efforts to apply PAL to the development of pharmacological agents capable of regulating muscle stem-cell differentiation. As a point of departure, we will review the synthesis and recent uses of photoactive diazirines in PAL studies from 2012-2017. In Chapter 2, we will describe our efforts to apply PAL towards a specific class of phosphatases with the long-term goal of developing of stem cell-based therapeutic strategies targeting skeletal muscle disorders.

1.2 - Overview of Chapter 1

In Section 1.3 the general mechanism of PAL will be discussed along with the requirements of developing and designing a suitable probe, including the commonly used groups for photo-crosslinking and reporter tagging. General methodologies for the synthesis of diazirines, including several recently developed methodologies, will then be discussed in Section 1.4. Finally, Section 1.5 will discuss the use of diazirines in PAL studies published within the past 5 years.

1.3 – Concept of PAL

1.3.1 – Mechanism of a PAL Experiment

In a PAL experiment, a bifunctional probe that has been functionalized with a reporter group and a photoactivatable group, is introduced into cell culture and binds to its biological target (Figure 1.3.1.1).[9] Upon irradiation with a specific wavelength of UV light, the photolabile group is activated, generating a highly reactive intermediate that forms a covalent bond with its cellular target; thereby permanently binding the small molecule to its biological target. Following cellular lysis, a tagging unit is introduced that reacts with the reporter group on the probe molecule to provide the tagged complex. Depending on the type of tagging unit that is applied, a range of purification techniques can be used to isolate the ligand-enzyme complex, which can then be analyzed using tandem pull-down experiments/mass spectrometry, or gel electrophoresis to identify the cellular target of the small molecule. Using this approach for target identification is advantageous because it does not require pre-purification of the macromolecule and is therefore amenable for use in the study of complex biological systems.

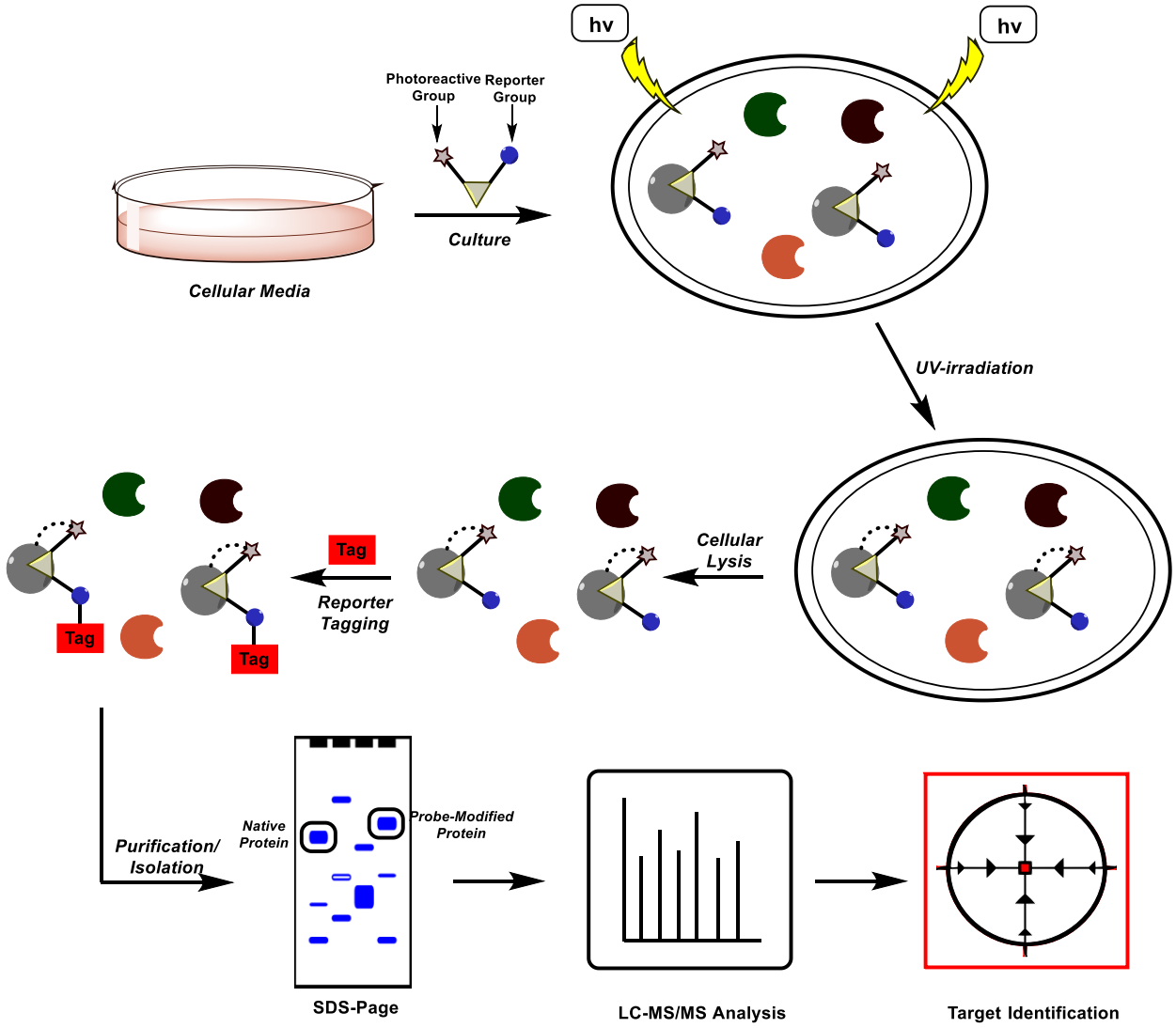

Figure 1.3.1.1 – General Workflow of a PAL Experiment

Although PAL has many advantages over previous methods used to probe small molecule interactions with their cellular targets, this technique comes with its own set of challenges. Firstly, a suitable photoaffinity probe needs to be designed that does not perturb the native biological activity of the small molecule. In essence, the introduction of the photoactive and reporter groups creates a new derivative, which must maintain the pharmacokinetic profile of the parent compound in order for the PAL study to be successful. This, in itself, poses many challenges during the design and development stages of the probe molecule. Therefore, these groups need to be small and installed in the optimal positions on the probe to prevent them from interfering with the overall biological activity of the parent molecule. They must also be photo-activated with fast kinetics, and preferably with low-wavelength light (< 300 nm) to avoid damage to the biological system.

The rate of photolysis is extremely important and must occur in a very short period of time to avoid the potential of non-specific labelling. Additionally, the reporter group must be accessible to the tagging group to allow subsequent cross-linking. For these reasons, a considerable amount of research has been devoted to the design and development of various photoactive and reporter groups, which has led to a diverse array of PAL constructs.[10]

1.3.2 – Photo-Crosslinking Groups

As previously mentioned, the photoactive group needs to be relatively small in size as well as readily activated under mild conditions to prevent any irradiation damage to the cellular material. This has led to the design and development of several different photoreactive groups, including benzophenones (**1.3.2.1**),[11] pyrimidones (**1.3.2.2**),[12] arylazides (**1.3.2.3**),[13] diazirines (**1.3.2.4**),[14] and tetrazoles (**1.3.2.5**) (Figure 1.3.2.1).[15] Of these, the most commonly employed groups in PAL experiments are benzophenones, arylazides, and diazirines.

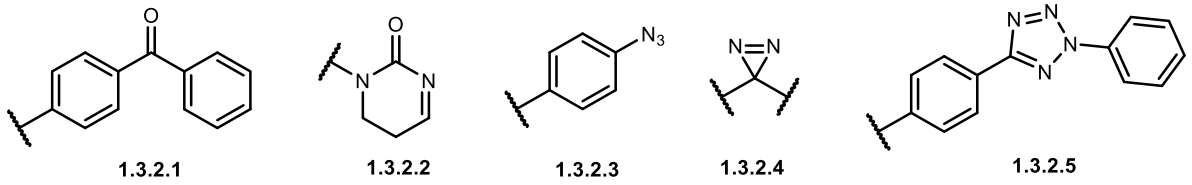

Figure 1.3.2.1 – Photoactive Groups

The drawbacks to using benzophenones are their relatively large size, and that they often require a prolonged irradiation time, which can cause damage to the biological system or lead to non-specific labelling.[16] The use of an arylazide also comes with significant drawbacks as they require short wavelengths (<300 nm) to be activated, which has the potential to damage cellular components. Additionally, upon irradiation, arylazides are known to undergo rearrangement reactions to a ketamine intermediate that can significantly decrease the yield of the photo-crosslinking reaction and can lead to non-specific labelling.[17] Therefore, amongst these three photo-crosslinking groups, the diazirine has proven to be the most popular choice owing to its relatively small size, overall chemical stability, and facile manner in which it undergoes photolysis to provide a highly reactive carbene intermediate.

The excitation wavelength for diazirines is in the 350-380 nm range, significantly lowering the possibility of causing UV-irradiation damage to the cell. Upon photolysis, diazirines expel N_2

to form the singlet carbene species **1.3.2.6**, along with a small amount (~30%) of its diazo-isomer **1.3.2.7** (Figure 1.3.2.2).[18] Upon further irradiation the diazo-isomer can be converted to the singlet carbene; however, this process is relatively slow and can lead to non-specific labelling or hydrolysis. To solve this issue, Brunner *et al.* developed the trifluoromethyl-phenyldiazirine group (TPD) **1.3.2.8**.[19] They reasoned that the strong electron-withdrawing effects of the trifluoromethyl substituent would stabilize the diazo-isomer, and prevent it from undergoing further undesired side reactions. Additionally, the presence of the trifluoromethyl and phenyl groups α to the diazirine are thought to provide stability during the extrusion of N_2, thereby supressing the formation of the diazo-isomer. Since this report in 1980, the TPD group has become increasingly popular amongst the research community.

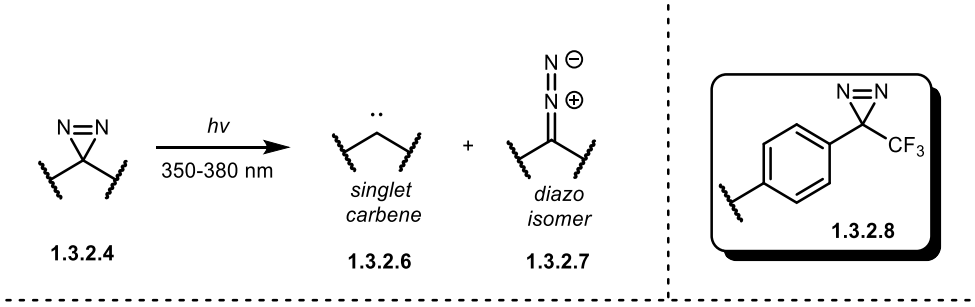

Figure 1.3.2.2 – Initial Products of Photolysis of Diazirines

After the loss of N_2, the singlet carbene **1.3.2.10** is an extremely short-lived species, having a half-life of ~ 1 ns, and can undergo intersystem crossing to generate the triplet carbene **1.3.2.12** (Figure 1.3.2.3). The singlet carbene itself is known to possess nucleophilic, electrophilic, and ambiphilic properties that are dependent on its neighbouring substituents. They rapidly undergo insertion reactions into nearby O-H, C-H, and N-H bonds in a non-discriminant manner to generate tagged complex, such as **1.3.2.11**. On the other hand, triplet carbenes behave like diradicals and will first undergo hydrogen abstraction from nearby X-H bonds, followed by recombination to form the same tagged species as the singlet carbene. However, after the initial H-atom abstraction, intermediate **1.3.2.13** can also extract a second hydrogen atom from an adjacent X-H bond, resulting in a formal reduction of the carbene species to generate **1.3.2.14**. Another potential undesired side reaction of the triplet carbene is oxidation with O_2 to generate the corresponding ketone **1.3.2.15**.[20]

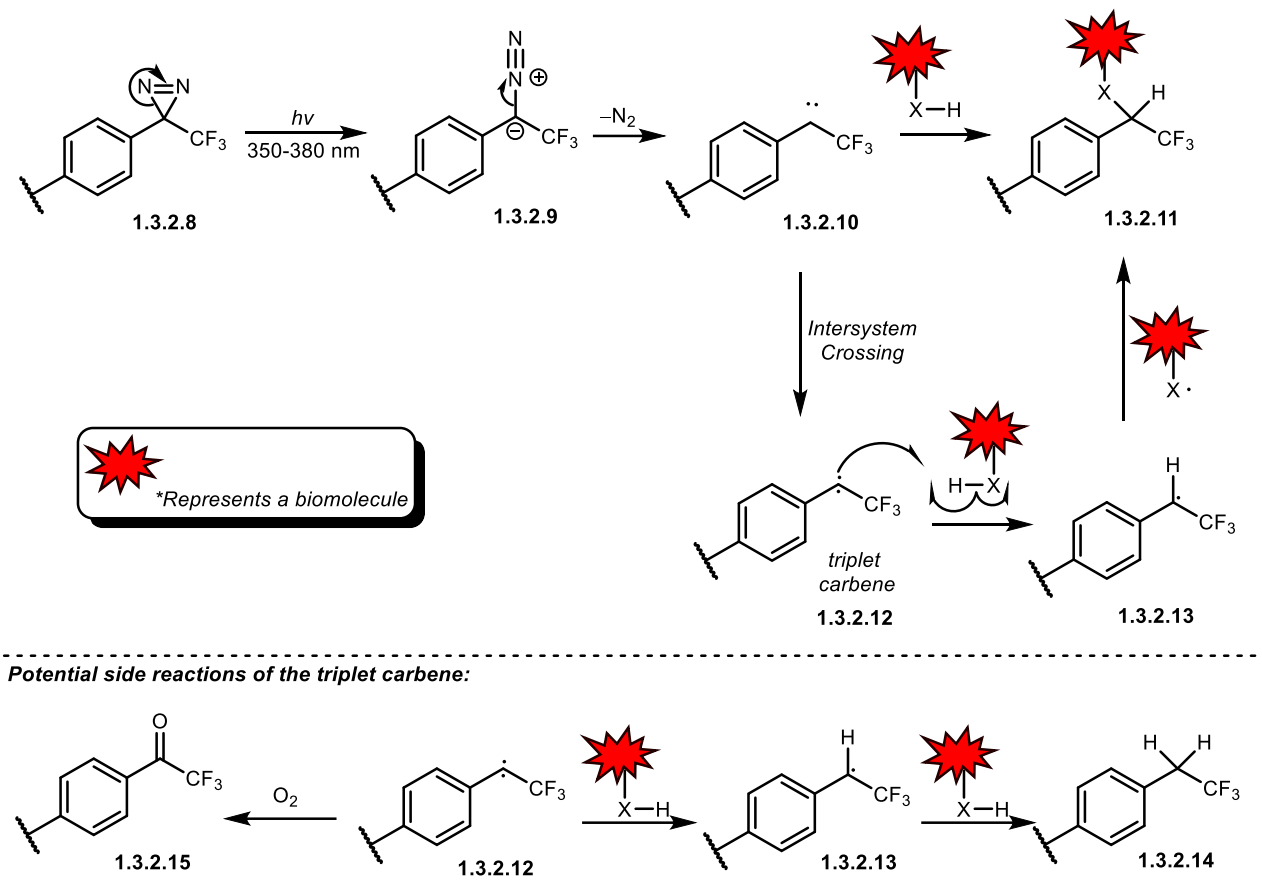

Figure 1.3.2.3 – Photolytic Pathway of Phenyldiazirines

In addition to their small size and long wavelengths required for activation, diazirines have become the most widely used photoreactive group in PAL studies due to their overall chemical inertness to a large variety of reaction conditions including strongly basic, strongly acidic, oxidizing and reducing; something that cannot be said about their arylazide counterparts. However, their use in PAL studies is limited by their ease of synthesis as it is more challenging and often requires multiple steps.[21]

1.3.3 – Reporter Tagging-Groups

In traditional PAL studies, the reporter group is directly installed onto the small molecule probe before it is administered into the cell culture. Commonly used groups include radioisotopes, fluorophores, and biotin affinity tags.[21] Reporter groups are used to facilitate the detection of the photo-crosslinked complex and to help in further isolation and purification of the tagged biomolecule. However, directly functionalizing the small molecule probe with the reporter group

often leads to reduced biological activity and significantly impacts the cell permeability due to their bulky size (Figure 1.3.3.1).[22]

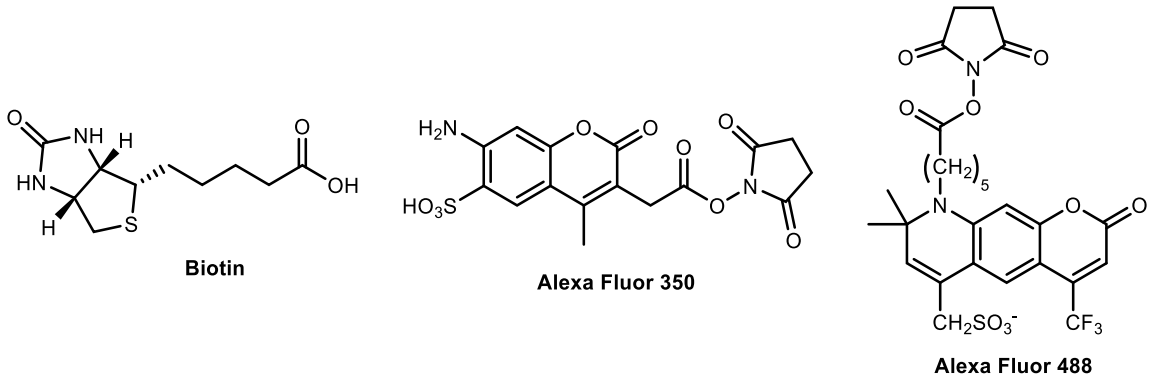

Figure 1.3.3.1 – Commonly Used Reporter Groups

For these reasons, an alternative method for reporter group tagging was developed in 2003 by Carolyn Bertozzi *et al*., wherein an appropriate functional handle is appended to the probe molecule that could be selectively ligated after photo-crosslinking through the addition of a reporter tag.[9] This approach, known as bioorthogonal chemistry, allows for chemical reactions to occur inside of a living system without interfering with any of the native biochemical processes (Figure 1.3.3.2).[23] This proved to be an extremely important method as it allowed for the capturing of biological targets in living cells; significantly expanding the scope of PAL studies.[10]

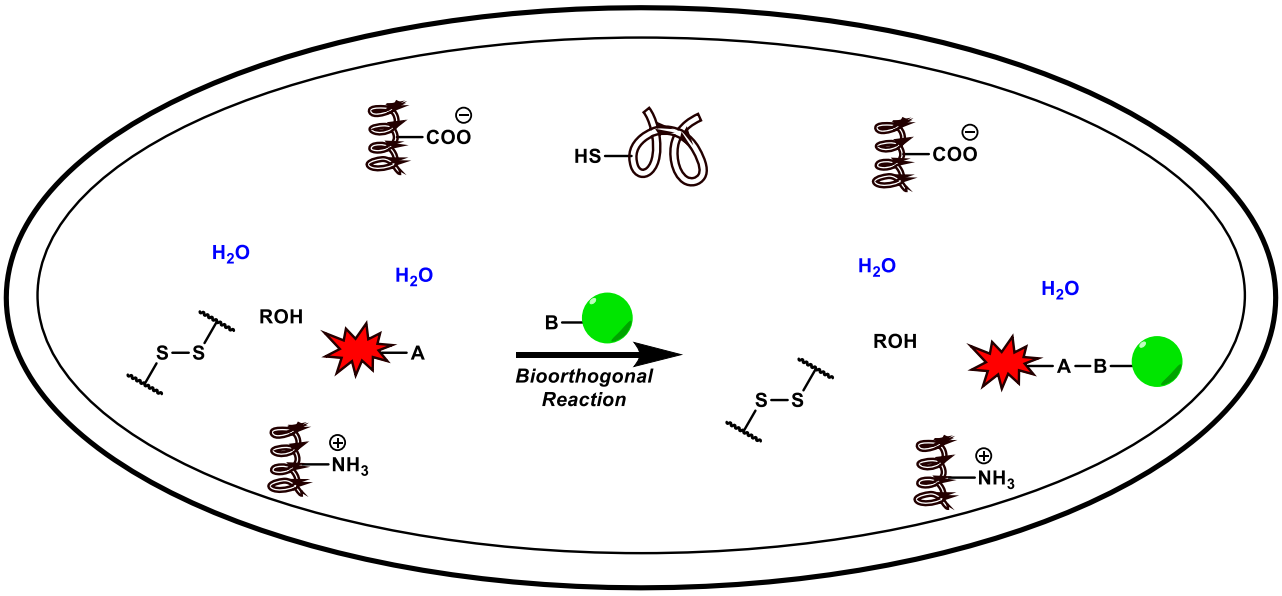

Figure 1.3.3.2 – A General Bioorthogonal Reaction. Bioorthogonal handles A and B selectively react in the presence of native biological molecules

One of the most important aspects of bioorthogonal chemistry is the design and development of appropriate reporter and ligation groups that will selectively react in a high yield, without the generation of toxic by-products.[24] Since 2003, several different bioorthogonal reactions have been developed including the Bertozzi-Staudinger ligation of triarylphosphines and azides,[25] the 1,3-dipolar cycloaddition between alkynes and azides,[26-27] the Diels-Alder cycloaddition between strained alkynes/alkenes and tetrazines,[28] and even Suzuki-Miyaura type coupling reactions.[29]

A classic Staudinger reaction involves the addition of a phosphine/phosphite to an azide to generate an aza-ylide intermediate, which is hydrolyzed to provide the amine (Figure 1.3.3.3). This reaction was modified by Carolyn Bertozzi and coworkers by introducing an electrophilic methyl ester trap *ortho* to the phosphorus atom. Upon formation of the aza-ylide, an amide bond is formed via and intramolecular cyclization instead of undergoing hydrolysis to form the amine. The 5-membered ring intermediate is then hydrolyzed to provide the ligation product.[25]

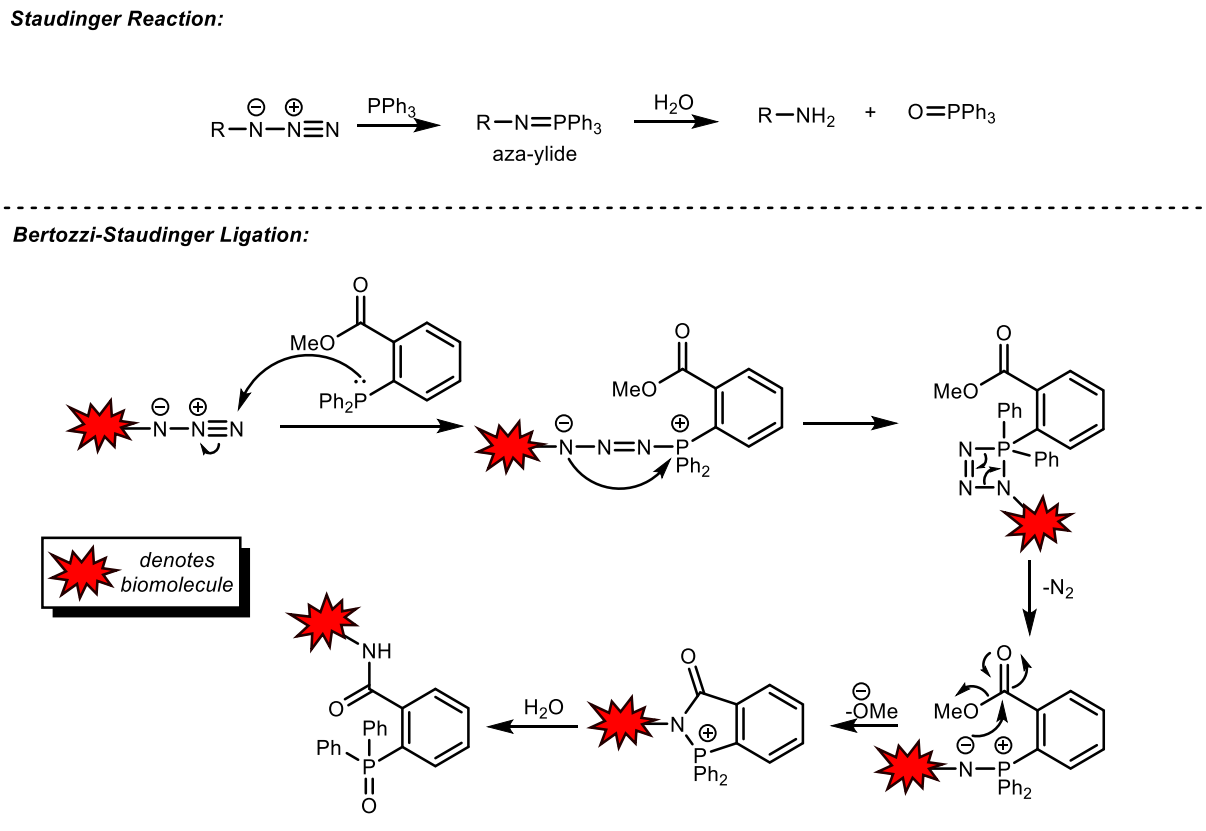

Figure 1.3.3.3 – General Mechanism of the Bertozzi-Staudinger Ligation

However, amongst these commonly employed ligation reactions, the most commonly used bioorthogonal reaction has been the 1,3-dipolar cycloaddition, or "click reaction".[27] This reaction, between an alkyne and an azide, has been widely used in bioorthogonal chemistry for several reasons. Firstly, both of these functional groups are small and therefore their incorporation into the probe can have negligible effects on its biological activity. Secondly, there are many well established methodologies to synthesize and install alkyne and azide substituents from relatively simple precursors.[30-31] The general workflow for a copper-catalyzed bioorthogonal reaction is depicted in Figure 1.3.3.4 and involves the installation of either an alkyne or an azide onto the probe molecule, which, after photo-crosslinking with its biological target, can be ligated by the addition of the reporter group containing the complimentary functional handle. In the presence of a copper catalyst, they will undergo a 1,3-dipolar cycloaddition (CuAAC) to provide the 1,4-disubstituted triazole containing the photo-labeled complex bound to the reporter group.

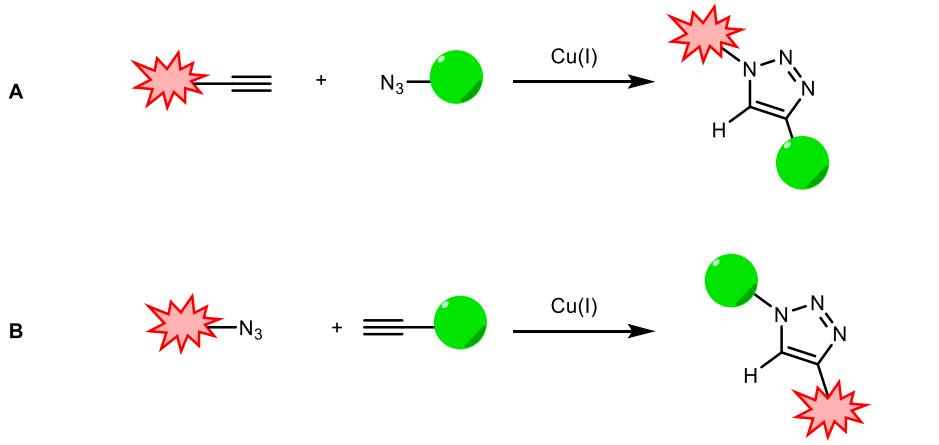

Figure 1.3.3.4 – Cu-catalyzed Bioorthogonal Click Reaction

The Cu-catalyzed 1,3-dipolar cycloaddition reaction has been studied extensively over the years along with its mechanism, which is known to involve dinuclear copper interactions.[32] Compared to the Bertozzi-Staudinger ligation, it has a much faster reaction rate, utilizes simple functional handles, and readily occurs in aqueous solutions; making it the most popular choice for bioorthogonal reactions for *in vivo* imaging.[33] However, the use of Cu(I) catalysts is known to be toxic to biological systems due to the formation of reactive oxygen species in the presence of O_2.[34] To alleviate this issue, several different approaches were taken. In 2004, Bertozzi and coworkers developed the copper-free click reaction by taking advantage of the ring strain found in

cyclooctynes. The ring strain found within the cyclooctyne promoted the [3+2] cycloaddition with an azide under physiological conditions without a Cu(I) catalyst to form the triazole (Figure 1.3.3.5).[35]

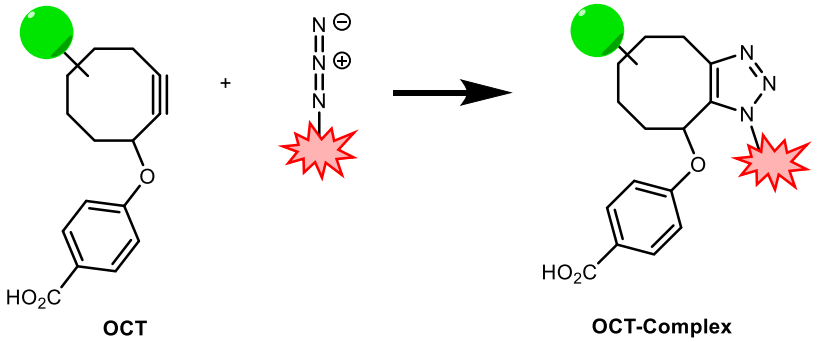

Figure 1.3.3.5 – Strain-Promoted Alkyne-Azide Bioorthogonal Cycloaddition

Although the use of strained cyclooctynes, such as OCT, have been proven to successfully label glycoproteins in living cells without any observed cytotoxicity,[35] they suffer from significantly lower reaction rates compared to the Cu-catalyzed counterpart, and OCT is poorly soluble in water. To address these issues, several different structurally distinct cyclooctynes have been developed wherein functional groups have been added to the cyclooctyne core to improve the reaction kinetics as well as its solubility profile in water. In an effort to further increase ring strain, a derivative of OCT was made where two benzene rings were fused to either side of the alkyne in place of the aryl ether, and an N-functionalized amide was introduced into the cyclooctyne scaffold (Figure 1.3.3.6). By making these structural modifications, the kinetics of the cycloaddition reaction were significantly improved from 0.0024 $M^{-1}S^{-1}$ with the parent compound OCT, to 0.96 $M^{-1}S^{-1}$ with the biarylazacylcooctynone analog (BARAC).[36]

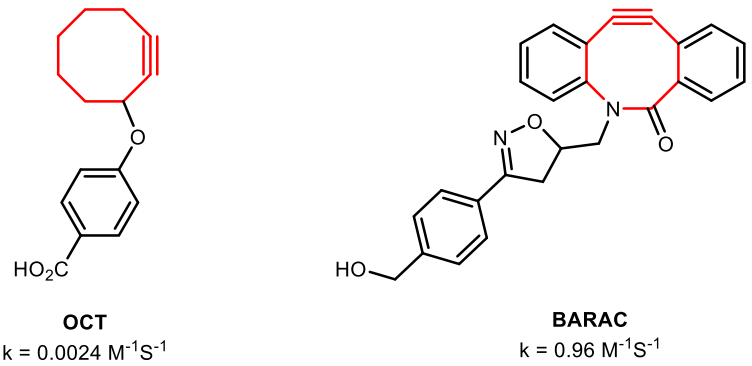

Figure 1.3.3.6 – Modified Cyclooctyne adduct BARAC leads to improved reaction kinetics

Although the structural modifications made to OCT led to a substantial increase in the kinetics of the bioorthogonal cycloaddition with the synthesis of BARAC, its reaction rate with azides was still ~10 times slower than that of a terminal alkyne in the presence of a Cu(I) catalyst.[37] This prompted further exploration into the development of a biocompatible Cu-mediated click reaction. In general, as the concentration of copper in the cell decreases, its cytotoxicity decreases; however, so does the rate of the reaction during the Cu-catalyzed azide-alkyne cycloaddition (CuAAC).[38] In 2012, Uttamapinant *et al.* demonstrated that an azide coupling partner containing a functional group capable of chelating to copper, significantly increased the kinetics of the cycloaddition reaction by increasing the concentration of copper at the reaction site (Figure 1.3.3.7).[39] They showed that the use of picolyl azide derivatives led to a 25-fold increase, compared to non-chelating azides, in specific protein labeling inside of living cells, even with a ten-fold decrease in the concentration of copper loading. To demonstrate the utility of this approach, they went on to successfully detect metabolically labeled proteins and RNAs in cells.

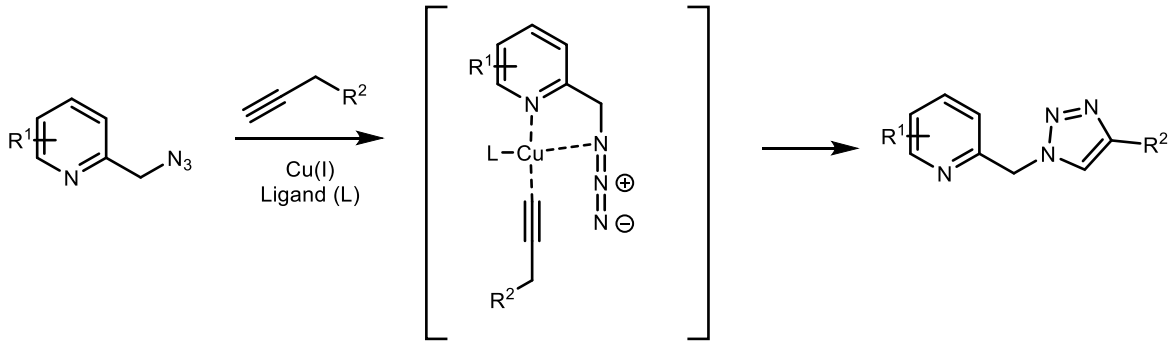

Figure 1.3.3.7 – Bioorthogonal CuAAC using copper-chelating Azides

In this section, the general mechanism of a PAL experiment has been described along with the requirements of designing a probe molecule to study protein-ligand interactions. Of utmost importance during the design of a PAL probe is that the derivations made to the parent scaffold do not interfere with the native biological activity of the parent compound. This poses several challenges, and oftentimes the effort required in optimizing the structure of a suitable probe is comparable to that of structure optimization studies in an early drug discovery program.[40]

1.4 - Synthetic Strategies to Install Diazirines

1.4.1 – General Synthesis of Diazirines

Since the popularity of utilizing diazirines in PAL studies has significantly increased over the past decade, several different groups have focused their attention on optimizing their synthesis. However, the scope of substrates can vary significantly, making it extremely difficult to develop a general set of conditions to prepare diazirines. For this reason, there have been several different synthetic routes adopted for the synthesis of diazirines that largely depend on the neighbouring substituents on the parent molecule. However, all synthetic pathways flow through the common diaziridine intermediate **1.4.1.1**, which upon treatment with an oxidant forms the desired diazirine **1.4.1.2** (Figure 1.4.1.1).[41] Since this transformation was reported by Schmitz and coworkers in 1961, it has become the most widely used method for the preparation of diazirines.[21]

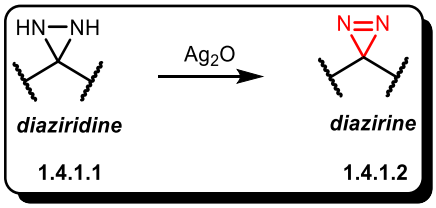

Figure 1.4.1.1 – Oxidation of Diaziridine to Diazirine by Schmitz et al.

As discussed in Section 1.3.2, a drawback to using diazirines in PAL studies is the formation of its diazo-isomer, which can lead to non-specific labeling. This prompted the search for a more suitable diazirine moiety that upon photo-excitation would provide a higher conversion to the carbene species, or would form a more stable diazo-isomer species that would not undergo subsequent off-target labeling; factors that are largely controlled by the neighbouring substituents to the diazirine. During the time of the development of the (trifluoromethyl)phenyldiazirine (TPD) photo-cross-linking group in 1980, the effectiveness of PAL studies were hindered by the availability of a photoactivatable group that was chemically stable, rapidly photoactivated, and generated a highly reactive species upon photolysis.[42] Although diazirines were being employed in PAL studies in the late 1970's, their efficiencies were limited by the formation of the unstable diazo-isomer species which led to non-specific labeling or hydroylsis.[43] By developing the TPD group, Brunner *et al.* more or less solved this problem, since the diazo-isomer generated upon photolysis was stabilized by the electron-withdrawing effects of the adjacent trifluoromethyl

moiety.[19] The synthesis of TPD was straightforward and commenced with oxime formation of commercially available 2,2,2-trifluoroacetophenone **1.4.1.3**, followed by tosylation to afford **1.4.1.4** in a 64% yield over two steps (Figure 1.4.1.2). Condensation onto the tosyl-oxime with liquid ammonia at -78°C provided the diaziridine **1.4.1.5**, which was then oxidized using freshly prepared Ag_2O to yield the diazirine **1.4.1.6** in a 95% yield after distillation. Since this initial report in 1980, a myriad of different conditions have been developed for the synthesis of TPD groups as well as aliphatic diazirines.

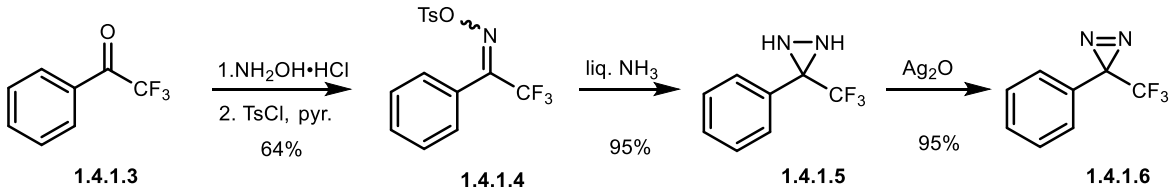

Figure 1.4.1.2 – Brunner's Synthesis of TPD

Aside from selected examples reporting the synthesis of diaziridines from the corresponding amidines,[44-45] they are usually prepared over a series of steps originating from the ketone starting material. The general pathway involves oxime formation of the ketone **1.4.1.7**, followed by either mesylation or tosylation to form the sulfonyl ketoxime **1.4.1.8** (Figure 1.4.1.3). Treatment of the sulfonyl ketoximes with liquid ammonia affords the diaziridine **1.4.1.1** which undergoes oxidation to generate the diazirine **1.4.1.2**.[21] However, since the chemical structure of each individual probe molecule varies significantly, different sets of reagents and conditions have been developed to arrive at these common intermediates.

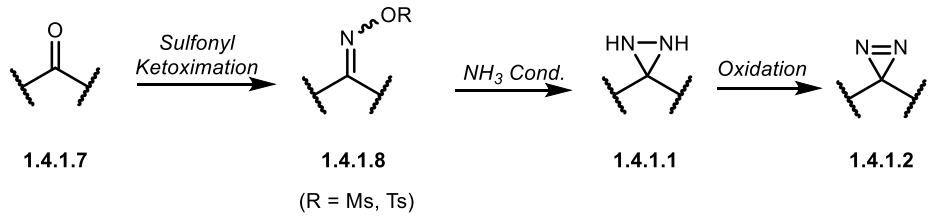

Figure 1.4.1.3 – General Synthesis of Diazirines

In 2012, Dubinsky *et al.* provided a comprehensive review of synthetic strategies used to construct diazirines, highlighting the methodologies reported between 2006-2012.[21] A general

scheme summarizing the syntheses is presented in Figure 1.4.1.4.[46-51] This chapter will therefore cover new literature examples from within the past 5 years.

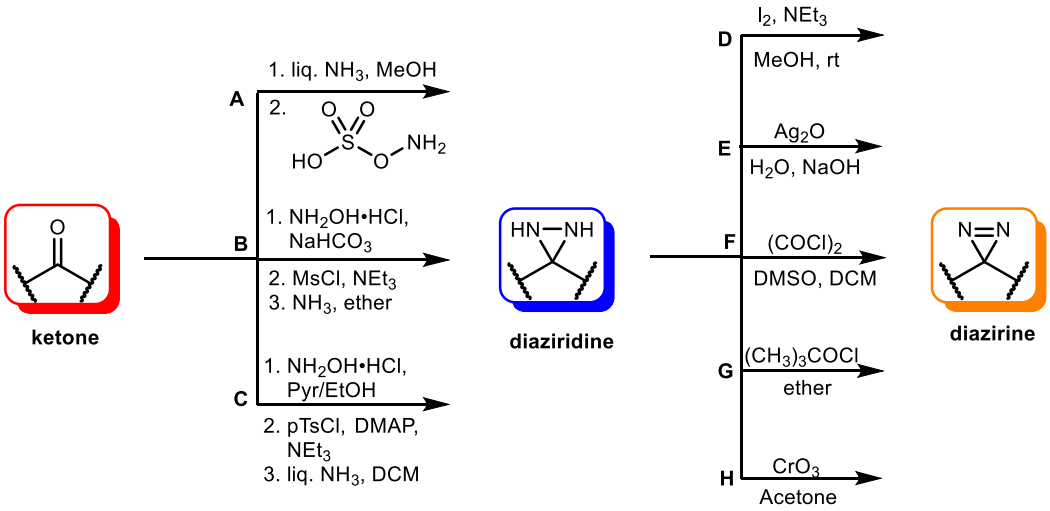

Figure 1.4.1.4 – Previous Syntheses of Diazirines

1.4.2 – Novel Methods of Diazirine Synthesis

Regardless of the other conditions being used, the key step in the synthesis of the diaziridine intermediate involves the addition of liquid ammonia onto either the ketone, or sulfonyl ketoxime, at -78°C. The use of liquid ammonia as a reagent poses several technical challenges as it requires proper experimental equipment for the setup and can be dangerous if not handled properly.[52] Other alternative protocols have been developed that describe the use of liquid ammonia as a solution dissolved in an organic solvent, such as ether, methanol or DCM, which helps to simplify the reaction setup.[53]

In 2017, Protasova *et al.* reported a novel method for the synthesis of TPDs using a solid-supported polystyrene sulfonyl-chloride as a polymer equivalent to mesyl/tosyl chlorides (Figure 1.4.2.1).[54] The oximes were prepared from the corresponding ketone starting materials using hydroxylamine hydrochloride, and then subsequently immobilized onto the polymer resin to afford the sulfonyl ketoxime **1.4.2.2** via reaction with the commercially available sulfonyl chloride linker **1.4.2.1**. Following treatment with an ammonia solution in dioxane, **1.4.2.2** underwent functional cleavage to provide the diaziridines **1.4.2.3**. Using this approach, they showed that the conditions were amenable to a variety of different functional groups to provide diaziridines in good to excellent yields.

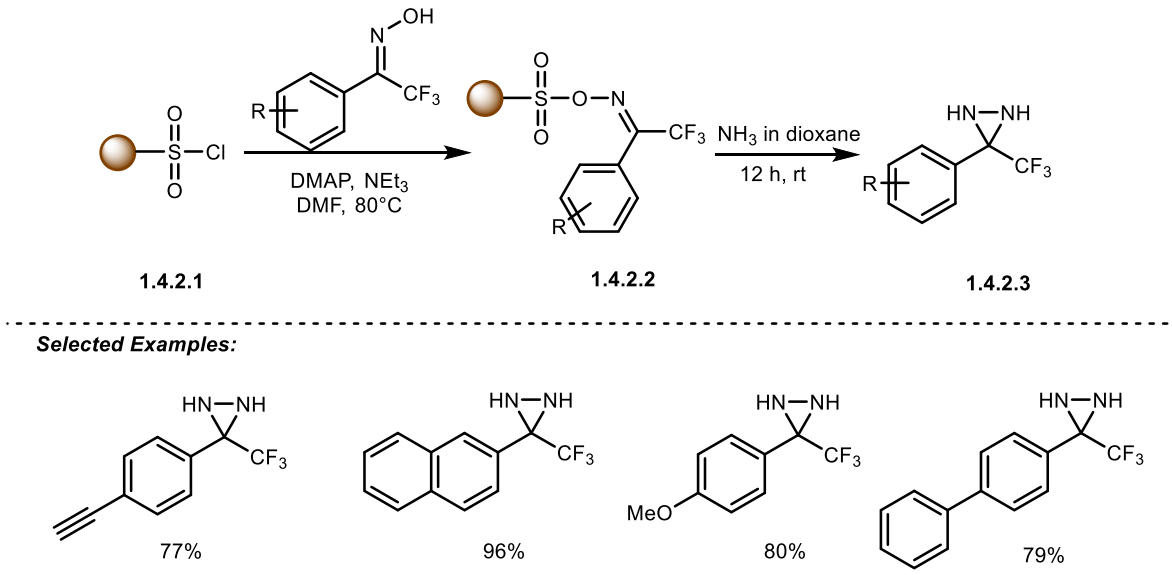

*Reported yields represent the isolated yields over the two step sequence

Figure 1.4.2.1 – Protasova's Solid-Supported Synthesis of Diaziridines

To expand the scope and increase the impact of the developed methodology, they wanted to showcase the ability to perform further modifications on the resin bound sulfonyl oximes **1.4.2.2**. Since there had been prior literature precedent for the CuAAC click reaction performed on solid-support,[55] they wanted to explore the reactivity of the alkyne substituted oxime **1.4.2.4** towards azides (Figure 1.4.2.2). Gratifyingly, they found that **1.4.2.4** was capable of undergoing cycloaddition reactions in the presence of a variety of azides with catalytic amounts of CuI to provide the triazole adducts **1.4.2.5**. In the same manner as above, they were treated with the ammonia solution in dioxane to afford the *para*-substituted diaziridines **1.4.2.6** in low to moderate yields.

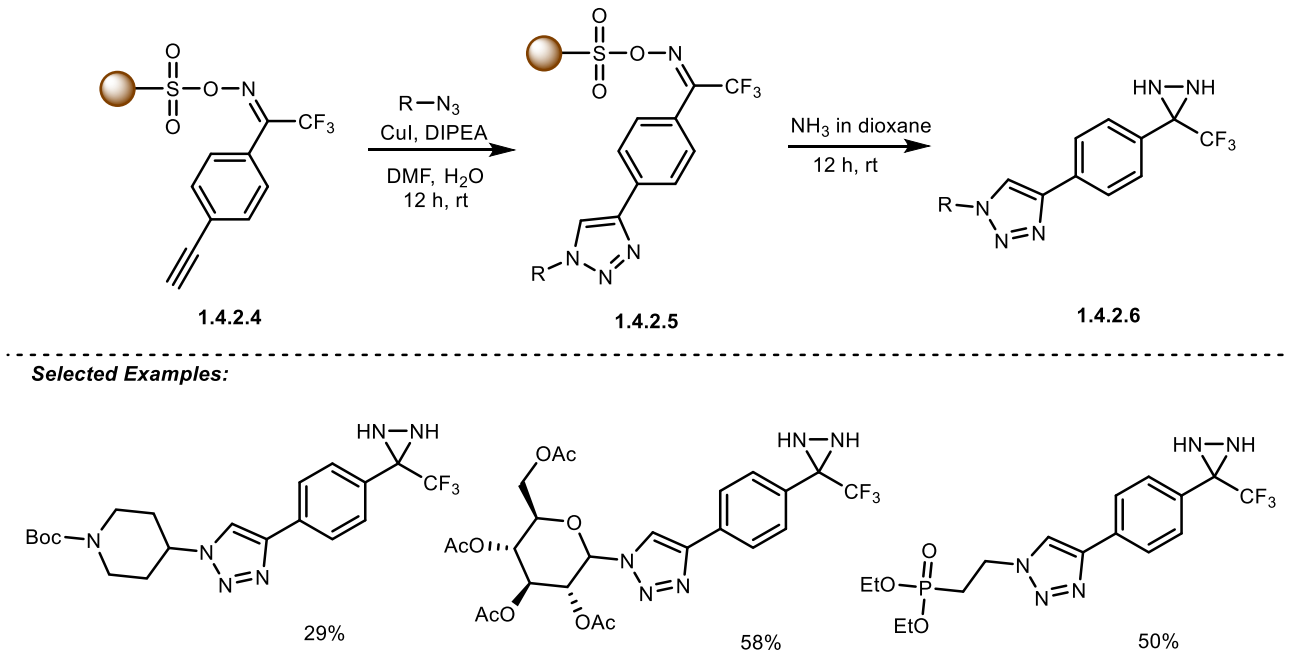

*Reported yields represent the isolated yields over the two step sequence

Figure 1.4.2.2 – CuAAC Click Reaction on Solid-Support Resin

To demonstrate that the diaziridines could be oxidized to the diazirines, they used standard conditions consisting of either I_2 with NEt_3 in DCM (conditions A), or MnO_2 in DCM (conditions B), on selected substrates (Figure 1.4.2.3). Oxidation proceeded smoothly to afford the diazirines in excellent yields. Therefore, this novel method is suitable for the synthesis of structurally diverse diazirines, and represented the first reported example of a solid-supported modification of sulfonyl oximes with CuAAC that conserved the sulfonyl oxime functionality.

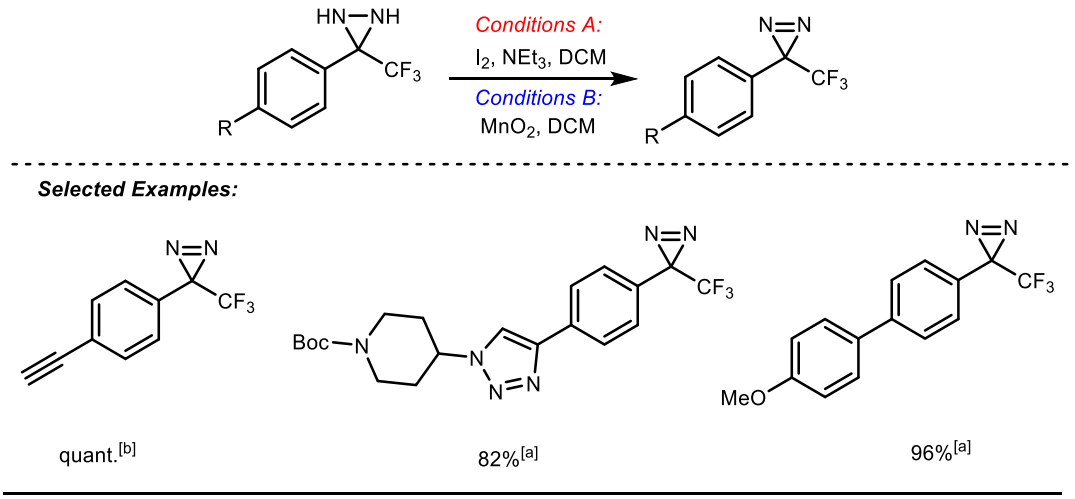

Figure 1.4.2.3 – Oxidation of Selected Substrates to Diazirines

In 2015, Lei Wang and coworkers reported a one-pot procedure for the synthesis of TPDs from their corresponding tosyloxime derivatives.[56] While synthesizing diaziridines using liquid ammonia under standard conditions, they observed small amounts of diazirine formation in the crude reaction mixture; hypothetically being derived from diaziridines. Further investigation and optimization provided two separate methods for the one-pot transformation (Figure 1.4.2.4). They found that heating the tosyloxime and liquid ammonia mixture to 80°C led to complete conversion of the starting material with the diazirine being the sole product obtained. To investigate the role of liquid ammonia in the formation of the diazirine, they treated the tosyloxime derivative with gaseous NH_3 at 80°C and found that the diaziridine was detected as the sole product, indicating that liquid ammonia was essential for this process. In line with these results, they postulated that the anionic NH_2^- species generated from liquid NH_3 may be responsible for the formation of the diazirine.[57] To probe this hypothesis, they screened different sources of NH_2^- using alkali amides. They found that 5 equivalents of lithium amide added to the liquid ammonia/tosyloxime mixture at 0°C led to complete conversion of the tosyloxime to the diazirine. With two optimized methods in hand, they explored the substrate scope of the one-pot transformation. They found that both methods readily produced the desired products in high yields, regardless of the electronic properties of the neighbouring substituents on the aromatic ring (Figure 1.4.2.5). As an application of their methodology, they synthesized a (trifluoromethyl)diazirinylphenylalanine derivative, which has previously been used as an important building block for the investigation of various

biological molecules.[58] Using their developed methodology, they synthesized the desired analog in a shorter sequence of steps in a significantly higher yield than previously reported.

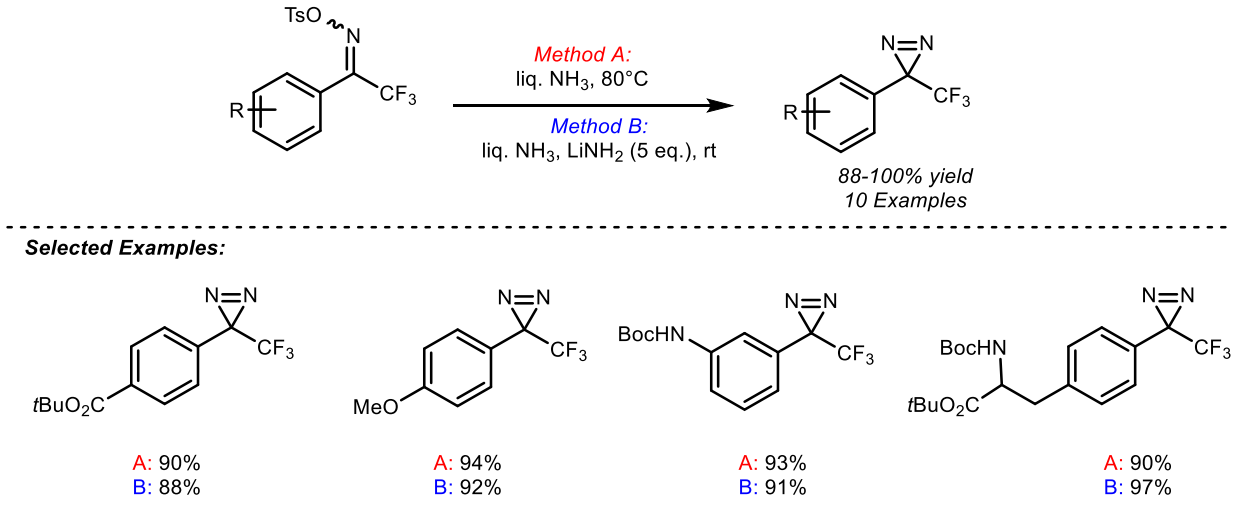

Figure 1.4.2.5 – Wang's One-Pot Procedure of Diazirines from Tosyloximes

To account for the observed formation of the diazirine, which requires oxidation, they proposed a mechanism in which NH_3 attacks the tosyloxime to form the aminal, which then expels TsOH to form the diaziridine. At an elevated temperature, liquid NH_3 undergoes self-ionization to form NH_2^- that deprotonates the diaziridine to form the anionic intermediate. This species then rearranges to the diazirine, generating H_2 gas and NH_3 in the process. When lithium amide is used as the NH_2^- source, the same sequence of deprotonation/rearrangement occurs, however LiH is generated as the by-product.

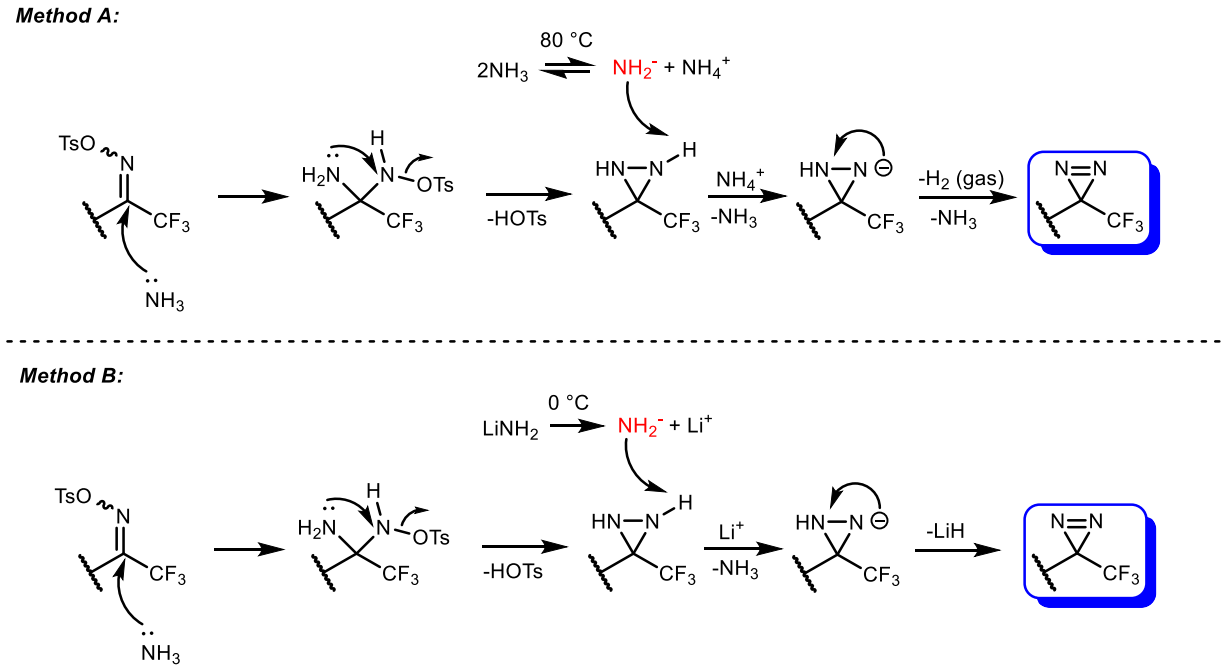

Figure 1.4.2.6 – Plausible Mechanism for the One-Pot Transformation

As mentioned in Section 1.3.2, one of the limiting factors to diazirines being employed in PAL studies is their often tedious, and lengthy synthesis. Recently, in conjunction with the development of a methodology to prepare azo-benzene derivatives, Wang and coworkers developed a one-pot procedure for the synthesis of aliphatic diazirines from their corresponding ketones.[59] Simultaneous treatment of the ketone with NH_2OSO_3H and liquid ammonia, followed by addition of *t*BuOK to dehydrogenate the diaziridine, afforded the aliphatic diazirines in moderate to excellent yields. Using this approach, they tested the scope of the reaction and found that these conditions were amenable to a variety of different substrates. Of particular interest, are the substrates containing carboxylic acids and hydroxyl groups, since these can serve as functional handles to append the diazirine tags to more complex substrates, making this methodology quite attractive for the synthesis of PAL probes.

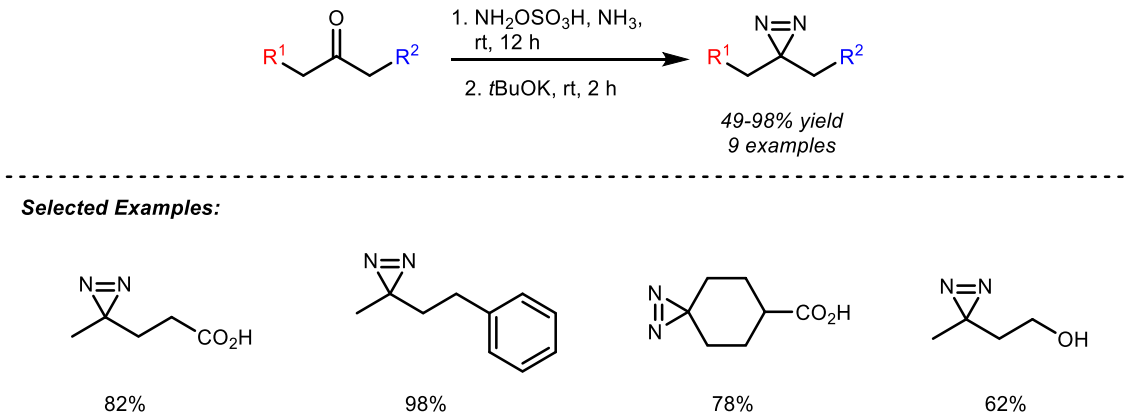

Figure 1.4.2.4 – Wang's One-Pot Synthesis of Aliphatic Diazirines

In this section, the general methods for the synthesis of diazirines have been discussed, along with several novel methods that have been published since 2012. Consistent throughout each methodology is the use of ketone starting materials that proceed through a diaziridine intermediate, followed by a formal oxidation to provide the diazirine. With the recent advancements in synthetic techniques to prepare diazirines, it is expected that their use in PAL studies will continue to flourish in the years to come.

1.5 – Diazirines in Target Identification

Over the past decade, the prevalence of diazirines in PAL studies has increased significantly.[21, 60] Whether to probe the binding sites of small molecules on known biological macromolecules, or to discover completely unknown cellular targets, they have become the most popular choice of photo-crosslinking groups amongst chemical biologists. In this section, the use of diazirines in recent PAL studies will discussed.

1.5.1 – Applications of Aryl Diazirines in PAL

The sirtuins represent a class of NAD^+ -dependent lysine deacylating enzymes that consist of seven isoforms (SIRT1−SIRT7).[61] The role of SIRT2 has been well characterized and it is known to be involved in several key cellular processes including apoptosis, metabolism, and bacterial infection.[62-64] However, its dysregulation has been implicated in many serious diseases, including cancer and several neurogenerative disorders,[65-67] therefore prompting the search for a suitable small molecule pharmaceutical agent that is capable of modulating this enzyme. Based off of previous work that identified a class of chromon-4-one derivatives that served to selectively

inhibit SIRT2,[68-69] the group of Kristina Luthman developed a diazirine-based PAL probe to identify the binding site of the chromone-derived inhibitors.[70]

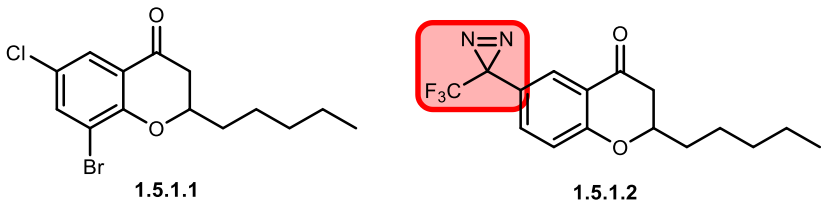

Figure 1.5.1.1 – Luthman's PAL Probe for SIRT2 Binding Site Identification

Their previous SAR work identified **1.5.1.1** as the most potent inhibitor of SIRT2 in their assays, which led them to construct the TPD derivative **1.5.1.2**, which demonstrated similar potency as the parent compound (Figure 1.5.1.1). Using short irradiation times, 3 x 10s, to avoid photoactivation of the diazo-isomer, **1.5.1.2** was cross-linked to SIRT2. Following trypsin digest and analysis by LC-MS/MS, they identified a tryptic peptide with the amino acid sequence ^{175}IAGLEQEDLVEAHGTFYTSHCVSASCRHEYPLSWMK^{210} displaying an increase in mass units of 298.11807 Da, corresponding to incorporation of the probe into this fragment (Figure 1.5.1.2).

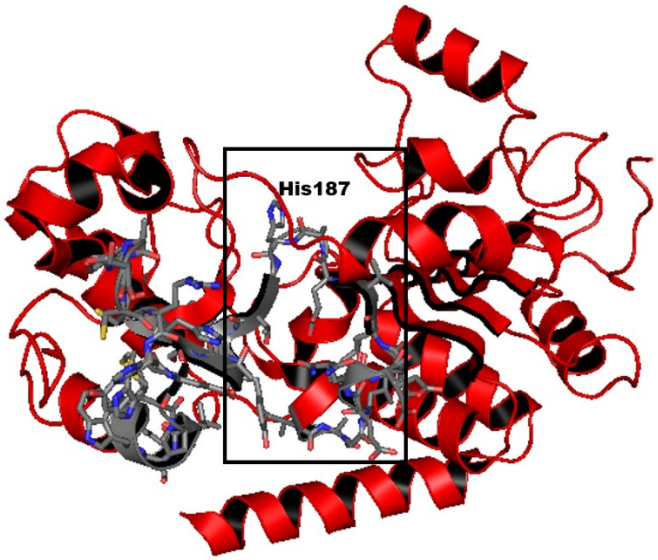

Figure 1.5.1.2 – SIRT2 Apo-Structure With the MS/MS Identified Amino Acid Sequence Highlighted. The Active Site is Framed

Further examination of the apo-structure of SIRT2 showed that this amino-acid sequence was in the region that had been previously hypothesized to contain the binding site of the chrom-4-one SIRT2 inhibitors. However, the precise amino acid residue that was modified by the cross-linked probe could not be identified. During MS/MS analysis they were unable to isolate the cross-linked complex and instead observed fragmentation of this species. Since it was evident from the initial MS/MS analysis that the probe was indeed covalently attached to this sequence, the fragmentation of the complex was attributed to the lability of the newly formed cross-linking bond between the probe and an amino acid residue, an issue that had been encountered previously in the literature.[71] Nevertheless, this report served as the first attempt at a PAL target identification study within the sirtuin family.

The G protein-coupled receptor (GPCR) family, consisting of five main classes, constitutes the largest group of membrane bound proteins that together make up more than 30% of marketed pharmaceutical drug targets.[2] The human adenosine receptors (AR) are a member of the largest class of GPCRs and are comprised of four subtypes: A_1, A_{2A}, A_{2B}, A_3.[72] Amongst these subtypes, A_{2A}AR antagonism has been exploited in the modulation of CNS stimulatory effects through elevated expression levels in the striatum. Numerous small molecule A_{2A}AR antagonists have been developed for the treatment of Parkinson's disease,[73] while several promising applications are currently under investigation, including those for Alzheimer's, ADHD, and cancer immunotherapy.[74] Significant efforts have been made to identify the binding sites of A_{2A}AR using the X-ray structure of the protein bound by the high affinity antagonists **1.5.1.3**[75] and **1.5.1.4**[76] which significantly bolstered our understanding of their mechanism of action (Figure 1.5.1.3). Recently, Muranaka and coworkers developed a diazirine-based PAL analog **1.5.1.5** based off the structure of **1.5.1.3** to further validate the antagonists binding site on A_{2A}AR using tandem MS analysis.[77]

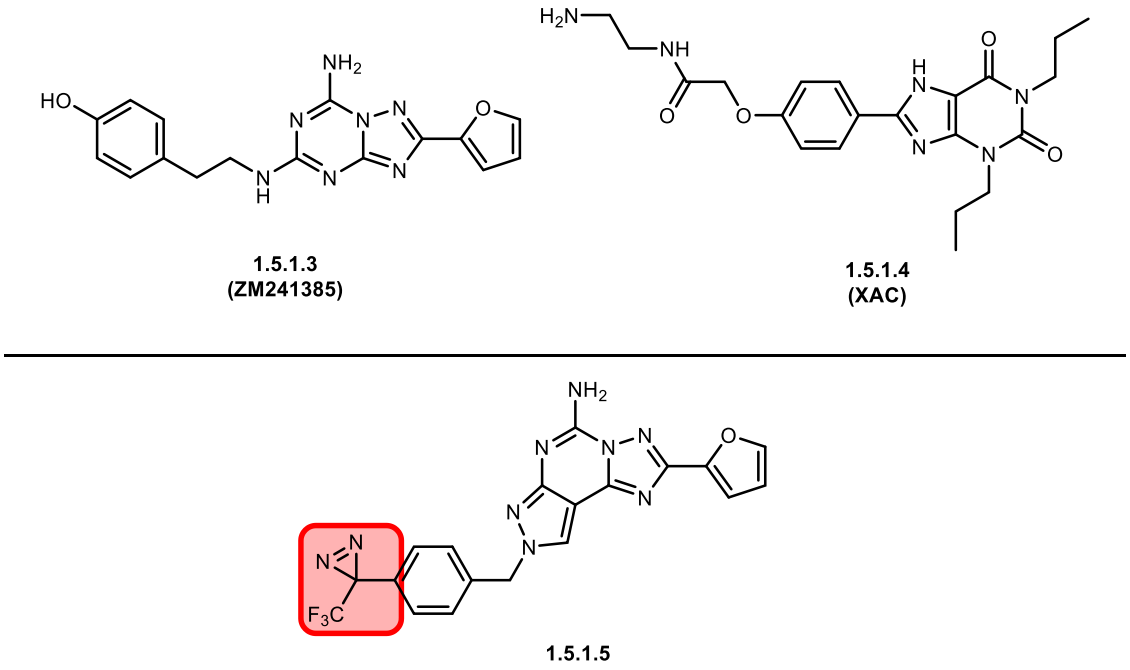

Figure 1.5.1.3 – Muranaka's PAL Probe for Antagonist Binding Site Identification

Using the human $A_{2A}AR$ ($hA_{2A}AR$), they found that **1.5.1.5** had been selectively cross-linked to the amino acid residue Tyr271 in TM7 (Figure 1.5.1.4). Subsequent docking studies confirmed that the diazirine moiety was in close proximity to this residue, further supporting their findings from the cross-linking experiment. This study represented the first reported example of PAL being used on human $A_{2A}AR$ for target identification studies.

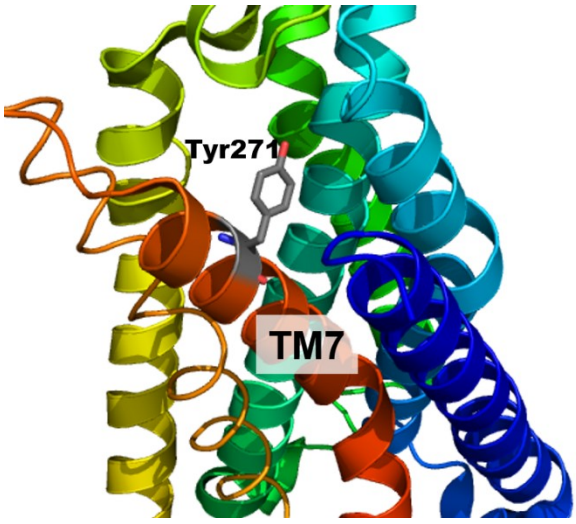

Figure 1.5.1.4 – Photolabeled Tyr271 in TM7 on $hA_{2A}AR$ Crystal Structure

In response to low levels of oxygen tension in the body, tumor angiogenesis and metastasis is regulated by the hypoxia inducible factor (HIF).[78] Under hypoxic conditions, HIF-1α dimerizes with HIF-1β, leading to the expression of genes involved in metastasis, angiogenesis, resistance to apoptosis, and cell proliferation of tumors.[79] Elevated expression levels of HIF-1α in solid tumors directly correlates with aggressive tumor growth and therapeutic resistance, which often leads to a poor clinical outcome. In 2010, Lee and coworkers reported the synthesis of LW6 (**1.5.1.6**),[80] which potently inhibited HIF-1α accumulation through its degradation, and has since been used in additional studies as an HIF-1α inhibitor.[81-82] Although proven effective as an inhibitor, the molecular target of LW6 was unknown, which significantly hindered the ability to perform structure optimization studies. To determine its cellular target, Lee further developed a bifunctional PAL analog (**1.5.1.8**) of LW6 containing a TPD group and a terminal alkyne reporter (Figure 1.5.1.5).[83] Additionally, they synthesized analog **1.5.1.7**, containing only the terminal alkyne to perform initial cellular localization experiments, and found that it was primarily situated in the mitochondria. Intracellular oxygen tension is controlled through the electron-transport chain (ETC) via mitochondrial respiration, and its pharmacological inhibition leads to an increase in intracellular oxygen concentration, inducing the degradation of HIF-1α.[84] Therefore the mitochondrial localization of **1.5.1.7** suggested that LW6 acted to inhibit mitochondrial respiration. Subsequent PAL was performed followed by ligation with a fluorescent dye and then lysate analysis using in-gel fluorescence. From this analysis, they identified malate dehydrogenase 2 (MDH2) as a protein that was bound to **1.5.1.8**. MDH2 is a key mitochondrial enzyme in the Krebs cycle, and is also involved in the mitochondrial ETC.[85] With this finding, they proposed that LW6 acted to bind to MDH2 to block the Krebs cycle, which inhibits mitochondrial respiration and therefore increases the local oxygen tension. These results not only allowed them to propose a mechanism of action of LW6, but will allow for further structure optimization studies to be performed on this scaffold.

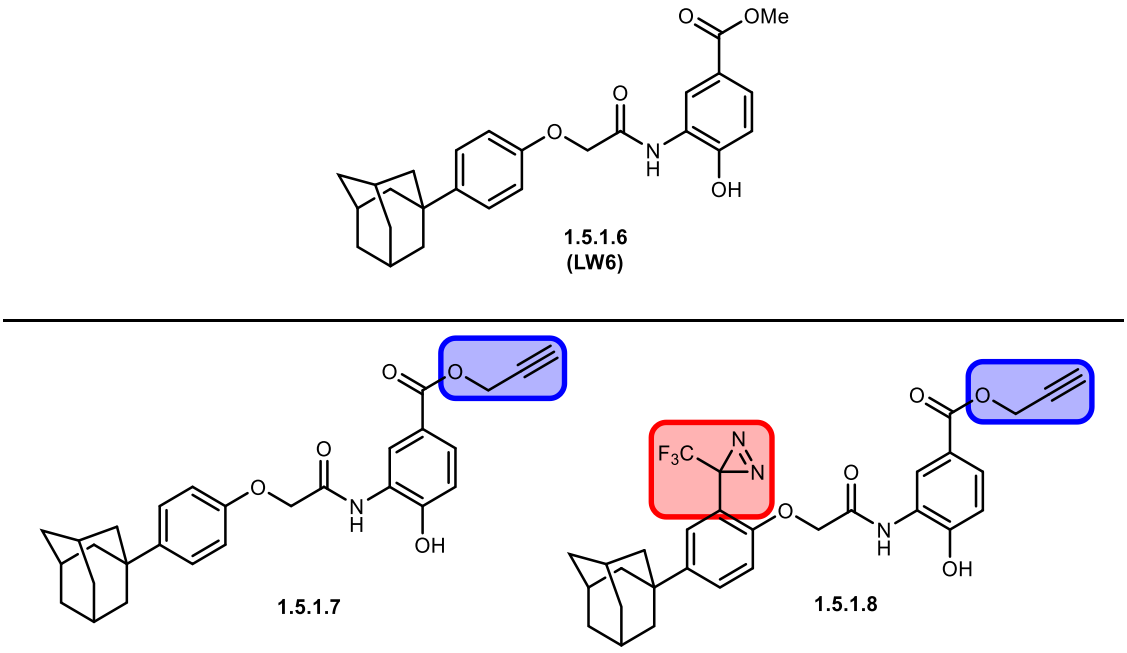

Figure 1.5.1.5 – Structure of HIF-1α Inhibitor LW6 and PAL Probes

Recently, Chicca and coworkers reported the design and synthesis of highly potent N-alkyl-2,4-dodecadienamide analogs for the inhibition of endocannabinoid (EC) uptake.[86] The endocannabinoid system (ECS) is a lipid signalling network responsible for modulating neurotransmission and the immune system, and its dysregulation has been implicated in many neurological disorders including anxiety, depression, and nociception.[87] Previous work demonstrated that pharmacological inhibition of selected endogenous agonists, mainly 2-arachidonoyl glycerol (2-AG) and N-arachidonoylethanolamine anandamide (AEA), was a viable method for the treatment of diseases related to the central nervous system.[88] However, existing inhibitors lack potency and selectivity,[89] hindering our understanding of the EC cellular uptake pathway. By performing a structure-activity relationship (SAR) study on the natural product (2*E*,4*E*)-N-isobutylamidedodeca-2,4-dienamide (**1.5.1.9**), they synthesized a panel of 634 analogs and screened their activity for the inhibition of AEA uptake (Figure 1.5.1.6). From these studies emerged a potent analog **1.5.1.10**, containing the bis-arylmethoxy group, that displayed activity to reversibly block the uptake of both AEA and 2-AG in the low nM range. Based off of the structure of **1.5.1.10**, they synthesized PAL analog **1.5.1.11** containing a TPD group to probe this biological pathway.

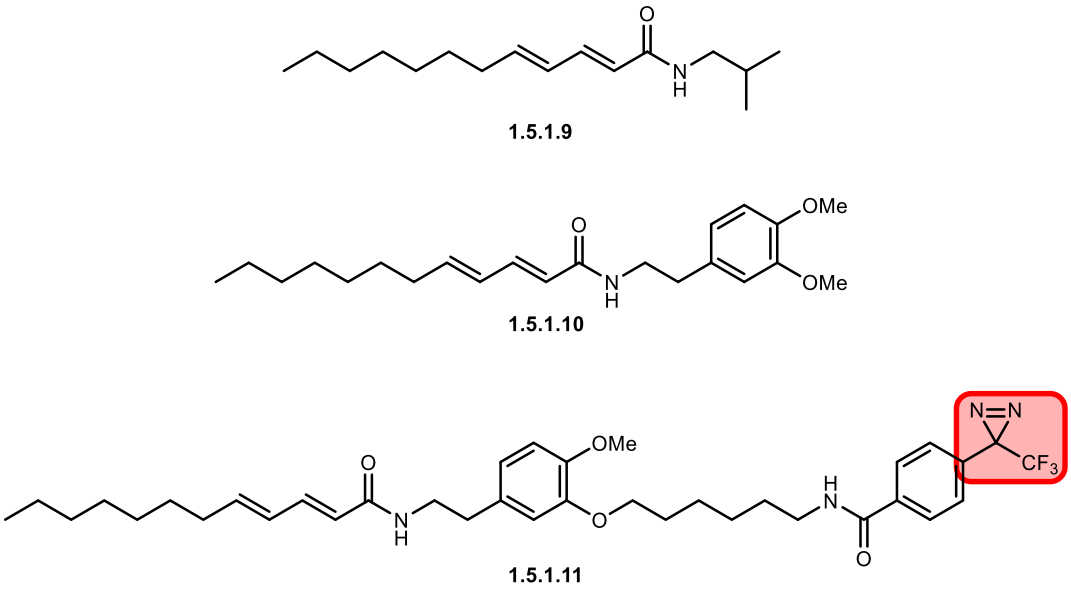

Figure 1.5.1.6 – Chicca's PAL Probe for EC Uptake Inhibition

To probe the mechanistic pathway of EC uptake inhibition, **1.5.1.11** was injected into the basolateral amygdala (BLA) of mice and subjected to *in situ* UV-irradiation. They found that **1.5.1.11** irreversibly blocked EC membrane transport from occurring upon photolysis and significantly reduced the anxiety levels in mice. This result demonstrated that the control of EC membrane trafficking plays a crucial role in the brain and demonstrated utility of this technique and probe **1.5.1.1** for the future study of lipid membrane transport and target identification studies.

1.5.2 – Applications of Aliphatic Diazirines in PAL

Histone deacetylases (HDACS) are a class of enzymes responsible for the deacetylation of ε-N-amino groups on lysine residues (Kac) on histones following post-translational modification (PTM).[90] The Kac modifications can be deacetylated by either epigenetic readers, such as bromodomains, or erasers, such as HDACs. Numerous reports have indicated that the dysregulation of HDACs is intimately associated with the progression and onset of several serious diseases including Alzheimer's,[91] neurodegenerative disorders,[92] and cancer.[93] Over the past several years, considerable efforts have been made to develop HDAC inhibitors as potential drugs,[94] as well as designing "one-step" fluorescent chemical probes to detect and monitor HDAC activity.[95-96] However, these methods can suffer from significant background fluorescence signals and only provide information on the enzymatic activity of HDACs, but do not provide insights

into their exact cellular targets. With these current limitations in mind, Xie and coworkers developed bifunctional probes that were capable of monitoring HDAC activity as well as identifying their cellular targets through tandem PAL.[97] They synthesized two HDAC inhibitor probes, **1.5.2.1** and **1.5.2.2**, which are one-step fluorescent activation probes to monitor HDAC activity in a continuous manner (Figure 1.5.2.1). In the presence of HDAC, the appendant *N*-acetyl group is deacetylated to form the free amine **1.5.2.3**, which undergoes an intramolecular substitution reaction with the *O*-Nitrobenzoxadiazole (NBD) to form the *N*-NBD **1.5.2.4** as a highly fluorescent species.[98]

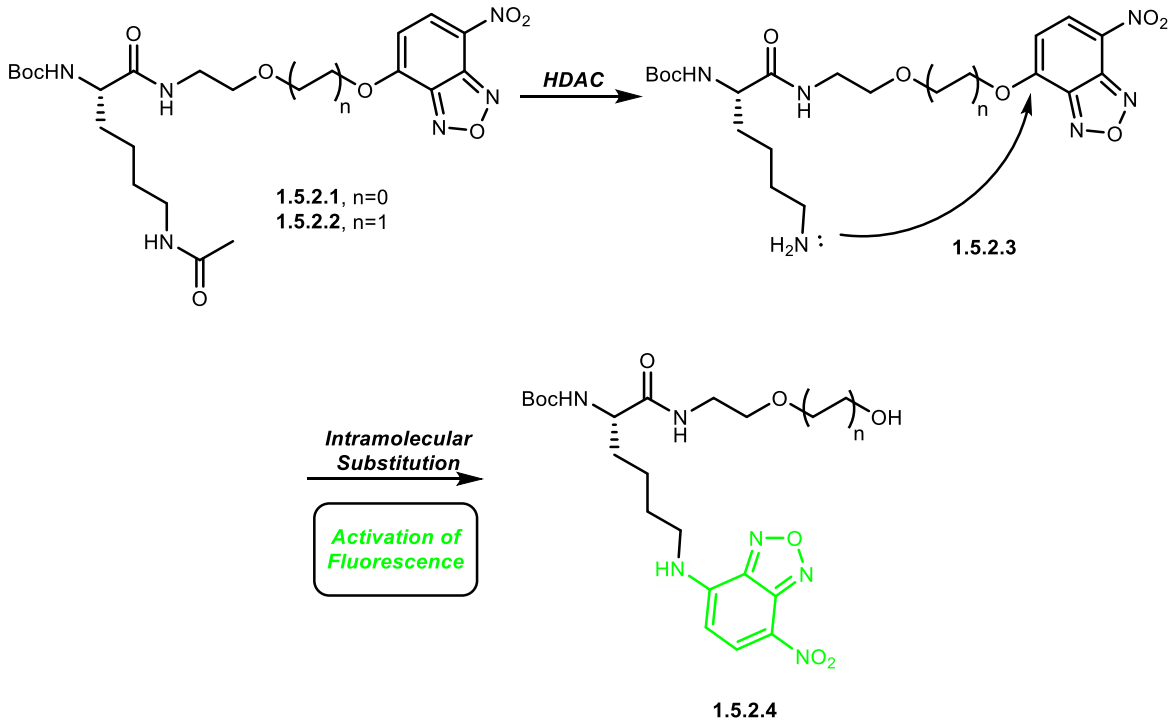

Figure 1.5.2.1 – Xie's HDAC Probes

After initial screening confirmed the ability of **1.5.2.1** and **1.5.2.2** to fluoresce when reacted with the HDACs, SIRT1 and SIRT2, they designed a bifunctional PAL probe **1.5.2.5**, consisting of an aliphatic diazirine and a terminal alkyne reporter group (Figure 1.5.2.2). To examine whether or not **1.5.2.5** was capable of labeling SIRT1 and SIRT2 in a complex proteomic environment, they subjected the probe to UV-irradiation in cell culture. Upon examination in a gel fluorescence assay, they were pleased to find clear fluorescent bands that corresponded to the molecular weights of the two HDACs, indicating that labeling was successful. In a follow-up experiment, they administered **1.5.2.5** to a mammalian cell culture overexpressing epigenetic eraser BRD4-1 and

reader SRT2 to determine if the probe was capable of differentiating between the two. Gratifyingly, they found that **1.5.2.5** could indeed differentiate between the two as a large fluorescence was observed selectively for SIRT2. In summary, this report displayed the ability to synthesize highly fluorescent HDAC probes capable of monitoring their activity in a continuous manner. Furthermore, the bifunctional probe **1.5.2.5** proved to be efficient for the selective labeling of epigenetic erasers in a complex cellular environment, displaying the potential of this probe for future proteomic profiling studies.

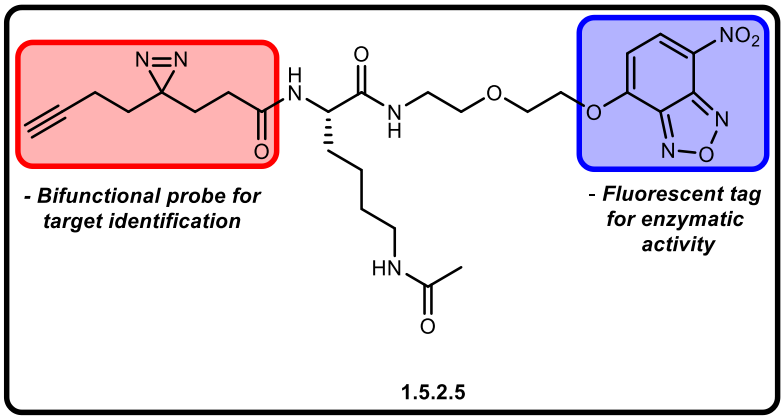

Figure 1.5.2.2 – Xie's bifunctional PAL Probe for HDAC Inhibitors

As mentioned in Section 1.3.3, considerable efforts have been made to develop copper-free methods for reporter ligation reactions for *in situ* live-cell imaging applications. However, the effectiveness of cyclooctyne derivatives is limited by their bulky size, and their synthesis can pose challenges. In 2014, Li and coworkers reported the design and synthesis of two alkyl diazirine minimalist linkers for *in situ* live-cell imaging applications, containing a cyclopropene moiety as a reporter group to allow for protein labeling via a Cu-free tetrazine-cyclopropene ligation reaction.[99] Based off of their previous work designing the terminal alkyne minimalist linker **1.5.2.6**,[14] they further modified this scaffold into linkers **1.5.2.7** and **1.5.2.8** (Figure 1.5.2.3). Although **1.5.2.6** proved to be effective to label a number of different kinases, the use of the terminal alkyne group required subsequent CuAAC conditions for ligation reactions and therefore could not be used for live-cell imaging.

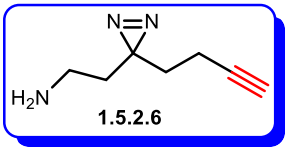

1.5.2.6

- First generation minimalist linker

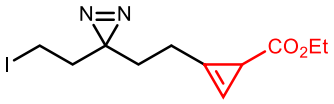

1.5.2.7

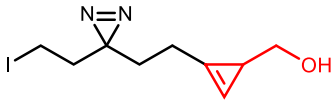

1.5.2.8

-Second generation minimalist linkers

Figure 1.5.2.3 – Li's Second-Generation Minimalist Probes

After the design and synthesis of the second-generation minimalist linkers, they wanted to test their efficacy in labeling experiments by synthesizing BRD-4 targeting probes. BRD-4 is an epigenetic reader and a member of the bromodomain that recognizes Kac residues located on histones which is involved in cell-cycle control, DNA damage pathways, and chromatin-remodeling.[100] Recent work has shown that benzodiazepine-derived compounds, such as (+)-JQ1, are nanomolar inhibitors of BRD-4,[101-104] while affinity-based pull-down experiments have confirmed BRD-4 to be their cellular targets.[105] However, their potential off-targets have not been identified *in situ* at the proteome level due to limitations in the ability of chemical probing techniques. Therefore, they synthesized two bifunctional probes (**1.5.2.9** and **1.5.2.10**) of (+)-JQ1 containing their novel cyclopropene handles (Figure 1.5.2.4). Additionally, they synthesized probe **1.5.2.11** containing their first-generation terminal alkyne linker for comparison in their assays. With the two cyclopropene probes in hand, they evaluated their efficiency to simultaneously image and covalently label the BRD-4 protein. Following UV-irradiation, the labeled samples were separated and visualized using in-gel fluorescence scanning. Strong fluorescent bands of **1.5.2.10**-BRD-4 complex labeling were observed after only one minute of cyclopropene-tetrazine ligation reaction time; however, the fluorescent signal of **1.5.2.9**-BRD-4 complex took 60 minutes to achieve comparable intensity. Comparably, the **1.5.2.11**-BRD-4 complex was detected after 5-60 minutes of click reaction time under CuACC conditions. Further *in situ* target identification studies using **1.5.2.10** confirmed its ability to label BRD-4 in live mammalian cells, even in the presence of a 10-fold amount of (+)-JQ1 as a competitor.

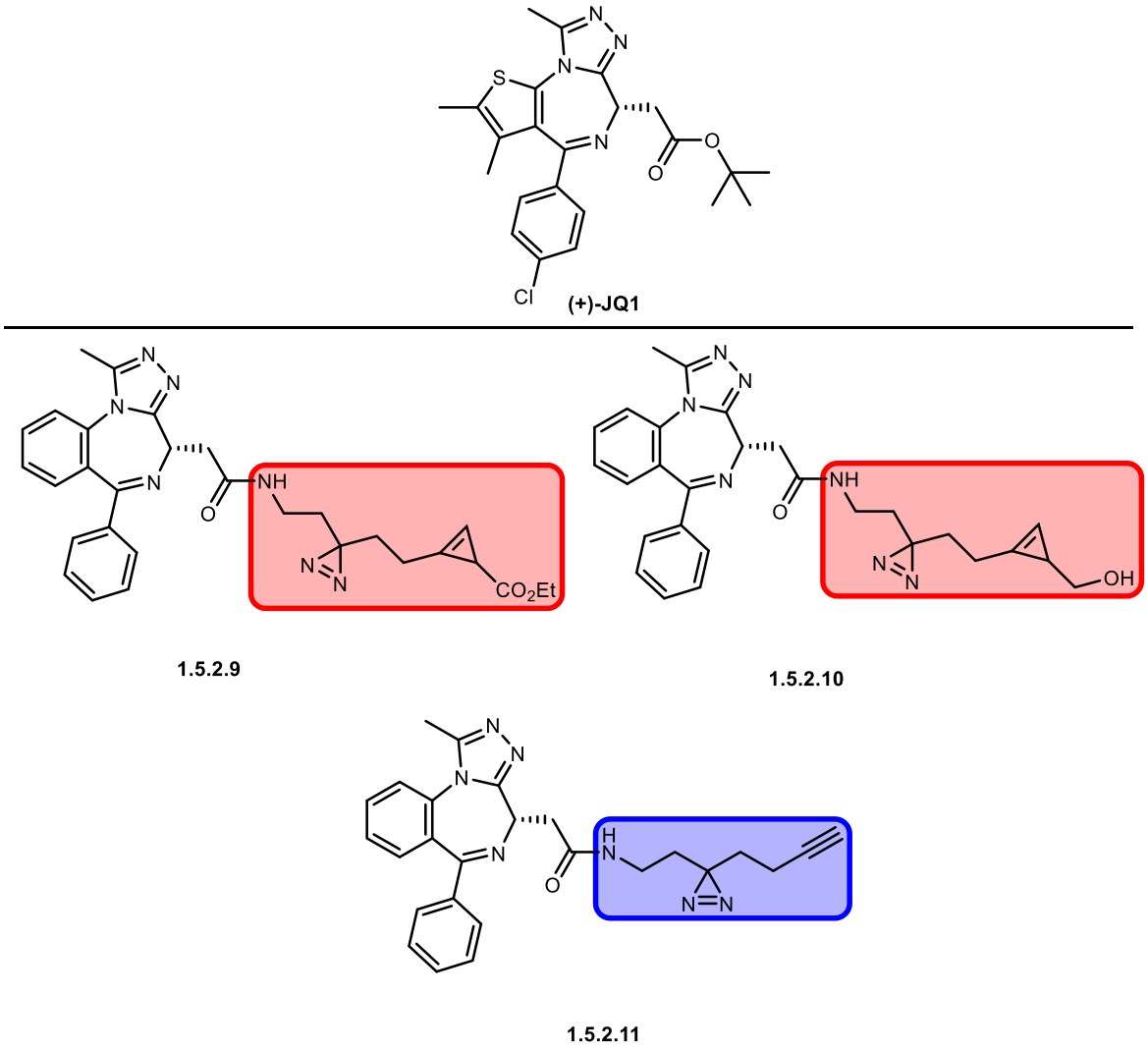

Figure 1.5.2.4 – Li's BRD-4 Targeting PAL Probes

Further large scale pull-down/MS-MS/MS analysis of the cell lysates was then performed to deconvolute any unknown targets of (+)-JQ1, as well as to compare the results obtained between **1.5.2.10** and **1.5.2.11**. From this, they initially identified several hundred different tagged proteins, but were able to narrow this down to a list of highly-probable off targets. To confirm that these were truly cellular targets of (+)-JQ1, two of that tagged proteins, DDB1 and RAD23B, were screened in additional target validation assays. Western-Blot analysis of HepG2 cell lysates enriched with *anti*-DDB1 and *anti*-RAD23B antibodies revealed that both proteins had been tagged by **1.5.1.9** and **1.5.1.10**, but not in the presence of a 10-fold amount of (+)-JQ1, indicating that these are truly cellular off-targets of (+)-JQ1. Through the development of cyclopropene-based probes capable of simultaneous live-cell imaging and proteomic profiling, Li and coworkers have

successfully identified several cellular off-targets of (+)-JQ1, and have set the stage for further target identification studies in this area.

The study and classification of complex glycolipids is essential for our understanding of the modulation of proteins, cell signaling transduction, and cellular recognition.[106] Fatty acid esters of monogalactosyldiacylglycerol (MGDG) constitute 80% of all membrane lipids found in green plant tissues, and have been shown to possess anti-tumor,[107] anti-viral,[108] and anti-inflammatory activities.[109] In 2003, Larsen and coworkers identified dilinolenoyl MGDG (**1.5.2.12**), which exhibited anti-inflammatory activity in human peripheral blood neutrophils;[110] however, its mechanism of action remained unknown (Figure 1.5.2.5). With this in mind, Liu *et al.* synthesized the bifunctional probe **1.5.2.13**,[111] by incorporating the aliphatic diazirine minimalist linker described by Li in 2013.[14] Endogenous proteomic labeling using **1.5.2.13**, followed by affinity pulldown/LC-MS/MS analysis identified the cross-linked target as toll-like receptor 4 (TLR4). Toll-like receptors are pattern recognition molecules that have been implicated in the pathology of inflammation.[112] In particular, TLR4 is responsible for the immunological response leading to the activation of downstream signaling pathways that induce systemic inflammation.[113] Therefore, the anti-inflammatory effects of MGDG were attributed to its ability to inhibit TLR4, resolving the longstanding question of its mode of action in the cell.

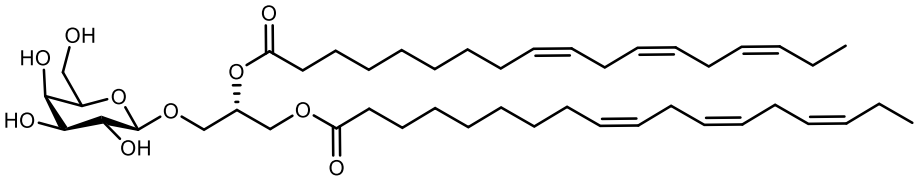

1.5.2.12
(dilinolenoyl MGDG)

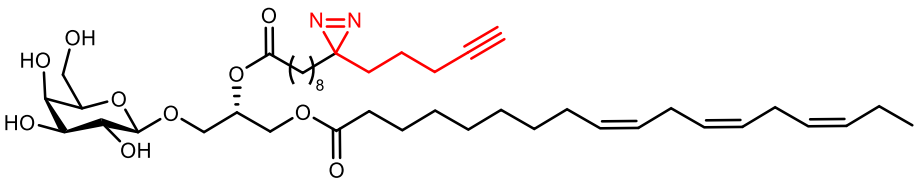

1.5.2.13

Figure 1.5.2.5 – MDGD and its Bifunctional PAL Probe

The dysregulation of protein kinases (PKs) has been implicated in the progression of cancer by modulating cell growth, angiogenesis, and metastasis.[114] Of the over 500 known PKs, many of them are considered promising therapeutic targets.[115] Dasatinib (**1.5.2.14**) is a promising FDA approved drug for the treatment of chronic myelogenous leukemia (CML) that acts as a dual Bcr-Abl and Src family tyrosine kinase inhibitor.[116] Although significant effort has been made in recent years, the majority of the kinase inhibitors developed thus far display non-selective inhibition. This is due to the highly conserved ATP-binding pocket shared amongst most kinases, resulting in poor discrimination between kinase sub-types.[117] To determine potential cellular off-targets of Dasatinib, Shi and coworkers developed PAL probe **1.5.2.15** containing a terminal alkyne reporter group and an aliphatic diazirine (Figure 1.5.2.6).[118] In the proteomic profiling study, they identified several new cellular targets through pull-down/LC-MS analysis. Most notably from this analysis was the identification of 6 serine/threonine kinases (PCTK3, STK25, eIF-2α, PIM3, PKA C-α, and PKN2) that were further validated by pull-down/immunoblotting experiments. Although these results were preliminary, and would require further investigation into Dasatinib's pharmacological effects on the newly cellular targets, they hypothesized that these kinases may be potential off-targets of Dasatinib.

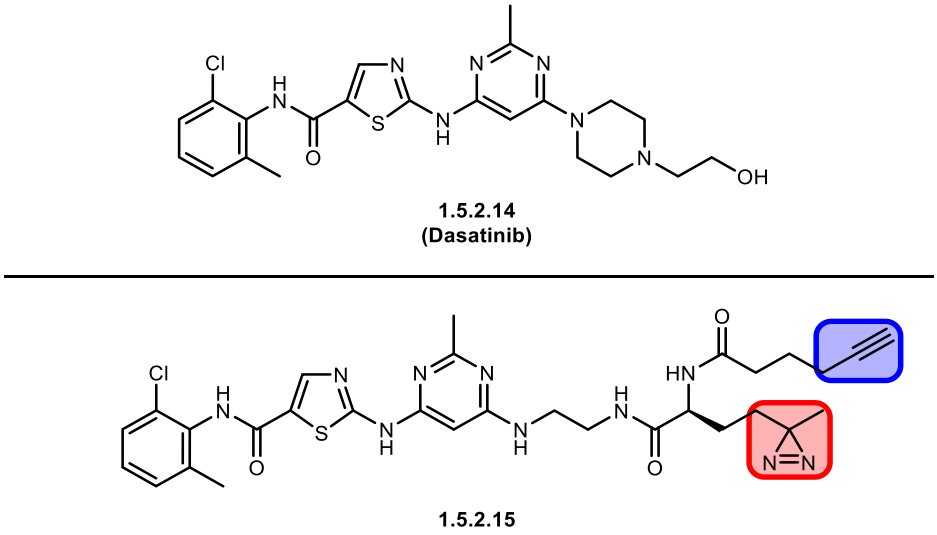

Figure 1.5.2.6 – Dasatinib and its PAL Probe for Off-site Target Identification

Voltage-dependent anion channel-1 (VDAC-1) is a β-barrel membrane protein responsible for ion transport between the mitochondria and cytosol, and is involved in apoptosis and mitochondrial respiration.[119] The effects of membrane lipids on VDAC-1 function have been

garnishing interest recently due to the observed changes in mitochondrial lipid composition during cellular apoptosis and neurogenerative diseases.[120-121] The binding of cholesterol to VDAC-1 has multiple pronounced effects on its voltage-dependent gating, oligomerization, and selectivity. NMR studies in conjunction with molecular modelling have identified five potential binding sites on VDAC-1 for cholesterol; however, experimental evidence confirming these interactions is lacking.[122-123] Recently, Budelier and coworkers developed two bifunctional PAL probes of cholesterol (**1.5.2.16** and **1.5.2.17**) to identify its binding sites on VDAC-1 (Figure 1.5.2.7).[124] Proteomic analysis of the cell lysates identified a binding pocket on VDAC-1 localized to the amino acid residues Thr^{83} and Glu^{73}. Further, mutation of the Glu^{73} residue to glutamine resulted in a shift of the cross-linked residue from Glu^{73} to Tyr^{62} within the same binding pocket, indicating that the cholesterol substrate is tightly held in the pocket in a very specific orientation. This led the authors to hypothesize that cholesterol regulation of VDAC-1 may be mediated by the specific binding site at Glu^{73}. This was the first reported example of using PAL to map a sterol binding site with such specificity.

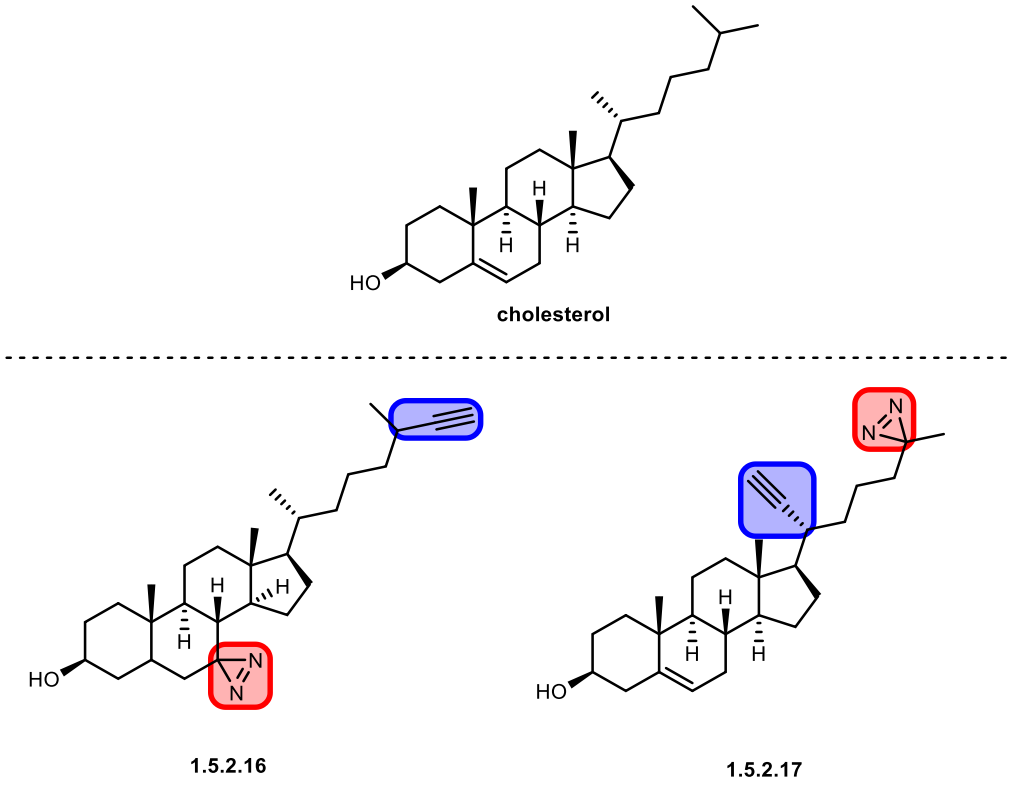

Figure 1.5.2.7 – Budelier's Bifunctional PAL Probes of Cholesterol for VDAC-1 Active Site Labeling

1.6 - Summary

As demonstrated in this chapter, PAL is an extremely powerful technique for the study of protein-ligand interactions that can be used to probe complex biological pathways or in target identification for the future development of active pharmaceutical agents. Through the combination of synthetic organic chemistry, chemical biology, and proteomic profiling, PAL has progressed into an all-encompassing strategy that enables the study of target-receptor complexes in their native biological settings. In recent years, there has been a significant increase in the use of diazirines as photoreactive agents owing to their small size and superior crosslinking ability. This, in combination with recent advances in synthetic methodologies to prepare diazirines, have accounted for their increased prevalence in PAL studies. Owing to the recent advancements in proteomic analysis and MS techniques, it is expected that the use of diazirines in PAL studies to probe protein-ligand interactions will continue to surge.

1.7 – References

1. van Dongen, M.; Weigelt, J.; Uppenberg, J.; Schultz, J.; Wikstrom, M., Structure-based screening and design in drug discovery. *Drug Discov. Today* **2002,** *7* (8), 471-8.
2. Rask-Andersen, M.; Almen, M. S.; Schioth, H. B., Trends in the exploitation of novel drug targets. *Nat. Rev. Drug Discov.* **2011,** *10* (8), 579-590.
3. Eder, J.; Sedrani, R.; Wiesmann, C., The discovery of first-in-class drugs: origins and evolution. *Nat. Rev. Drug Discov.* **2014,** *13* (8), 577-587.
4. Moffat, J. G.; Rudolph, J.; Bailey, D., Phenotypic screening in cancer drug discovery - past, present and future. *Nat. Rev. Drug Discov.* **2014,** *13* (8), 588-602.
5. Singh, A.; Westheimer, F. H.; Thornton, E. R., PHOTOLYSIS OF DIAZOACETYLCHYMOTRYPSIN. *J. Biol. Chem.* **1962,** *237* (9), 3006-&.
6. Lapinsky, D. J., Tandem photoaffinity labeling-bioorthogonal conjugation in medicinal chemistry. *Bioorg. Med. Chem.* **2012,** *20* (21), 6237-6247.
7. Lapinsky, D. J.; Johnson, D. S., Recent developments and applications of clickable photoprobes in medicinal chemistry and chemical biology. *Future Med. Chem.* **2015,** *7* (16), 2143-2171.
8. Vodovozova, E. L., Photoaffinity labeling and its application in structural biology. *Biochem. (Mosc)* **2007,** *72* (1), 1-20.
9. Hang, H. C.; Yu, C.; Kato, D. L.; Bertozzi, C. R., A metabolic labeling approach toward proteomic analysis of mucin-type O-linked glycosylation. *Proc. Natl. Acad. Sci. U.S.A.* **2003,** *100* (25), 14846-14851.
10. Smith, E.; Collins, I., Photoaffinity labeling in target- and binding-site identification. *Future Med. Chem.* **2015,** *7* (2), 159-183.
11. Schulke, J. P.; McAllister, L. A.; Geoghegan, K. F.; Parikh, V.; Chappie, T. A.; Verhoest, P. R.; Schmidt, C. J.; Johnson, D. S.; Brandon, N. J., Chemoproteornics Demonstrates Target Engagement and Exquisite Selectivity of the Clinical Phosphodiesterase 10A Inhibitor MP-10 in Its Native Environment. *ACS Chem. Biol.* **2014,** *9* (12), 2823-2832.
12. Battenberg, O. A.; Nodwell, M. B.; Sieber, S. A., Evaluation of alpha-Pyrones and Pyrimidones as Photoaffinity Probes for Affinity-Based Protein Profiling. *J. Org. Chem.* **2011,** *76* (15), 6075-6087.
13. Kempf, K.; Raja, A.; Sasse, F.; Schobert, R., Synthesis of Penicillenol C-1 and of a Bis-Azide Analogue for Photoaffinity Labeling. *J. Org. Chem.* **2013,** *78* (6), 2455-2461.
14. Li, Z.; Hao, P.; Li, L.; Tan, C. Y. J.; Cheng, X.; Chen, G. Y. J.; Sze, S. K.; Shen, H.-M.; Yao, S. Q., Design and Synthesis of Minimalist Terminal Alkyne-Containing Diazirine Photo-Crosslinkers and Their Incorporation into Kinase Inhibitors for Cell- and Tissue-Based Proteome Profiling. *Angew. Chem. Int. Ed.* **2013,** *52* (33), 8551-8556.
15. Li, Z. Q.; Qian, L. H.; Li, L.; Bernhammer, J. C.; Huynh, H. V.; Lee, J. S.; Yao, S. Q., Tetrazole Photoclick Chemistry: Reinvestigating Its Suitability as a Bioorthogonal Reaction and Potential Applications. *Angew. Chem. Int. Ed.* **2016,** *55* (6), 2002-2006.
16. Prestwich, G. D.; Dorman, G.; Elliott, J. T.; Marecak, D. M.; Chaudhary, A., Benzophenone photoprobes for phosphoinositides, peptides and drugs. *Photochem. Photobiol.* **1997,** *65* (2), 222-234.
17. Karney, W. L.; Borden, W. T., Why does o-fluorine substitution raise the barrier to ring expansion of phenylnitrene? *J. Am. Chem. Soc.* **1997,** *119* (14), 3347-3350.

18. Geurink, P. P.; Prely, L. M.; van der Marel, G. A.; Bischoff, R.; Overkleeft, H. S., Photoaffinity Labeling in Activity-Based Protein Profiling. *Activity-Based Protein Profiling* **2012,** *324*, 85-113.
19. Brunner, J.; Senn, H.; Richards, F. M., "3-TRIFLUOROMETHYL-3-PHENYLDIAZIRINE - A NEW CARBENE GENERATING GROUP FOR PHOTOLABELING REAGENTS. *J. Biol. Chem.* **1980,** *255* (8), 3313-3318.
20. Fleming, S. A., CHEMICAL REAGENTS IN PHOTOAFFINITY-LABELING. *Tetrahedron* **1995,** *51* (46), 12479-12520.
21. Dubinsky, L.; Krom, B. P.; Meijler, M. M., Diazirine based photoaffinity labeling. *Bioorg. Med. Chem.* **2012,** *20* (2), 554-570.
22. Sadaghiani, A. M.; Verhelst, S. H. L.; Bogyo, M., Tagging and detection strategies for activity-based proteomics. *Curr. Opin. Chem. Biol.* **2007,** *11* (1), 20-28.
23. Sletten, E. M.; Bertozzi, C. R., From Mechanism to Mouse: A Tale of Two Bioorthogonal Reactions. *Acc. Chem. Res.* **2011,** *44* (9), 666-676.
24. Patterson, D. M.; Nazarova, L. A.; Prescher, J. A., Finding the Right (Bioorthogonal) Chemistry. *ACS Chem. Biol.* **2014,** *9* (3), 592-605.
25. Saxon, E.; Bertozzi, C. R., Cell surface engineering by a modified Staudinger reaction. *Science* **2000,** *287* (5460), 2007-2010.
26. Baskin, J. M.; Prescher, J. A.; Laughlin, S. T.; Agard, N. J.; Chang, P. V.; Miller, I. A.; Lo, A.; Codelli, J. A.; Bertozzi, C. R., Copper-free click chemistry for dynamic in vivo imaging. *Proc. Natl. Acad. Sci. U.S.A.* **2007,** *104* (43), 16793-16797.
27. Kolb, H. C.; Finn, M. G.; Sharpless, K. B., Click chemistry: Diverse chemical function from a few good reactions. *Angew. Chem. Int. Ed.* **2001,** *40* (11), 2004-+.
28. Blackman, M. L.; Royzen, M.; Fox, J. M., Tetrazine ligation: Fast bioconjugation based on inverse-electron-demand Diels-Alder reactivity. *J. Am. Chem. Soc.* **2008,** *130* (41), 13518-+.
29. Chalker, J. M.; Wood, C. S. C.; Davis, B. G., A Convenient Catalyst for Aqueous and Protein Suzuki-Miyaura Cross-Coupling. *J. Am. Chem. Soc.* **2009,** *131* (45), 16346-+.
30. Habrant, D.; Rauhala, V.; Koskinen, A. M. P., Conversion of carbonyl compounds to alkynes: general overview and recent developments. *Chem. Soc. Rev.* **2010,** *39* (6), 2007-2017.
31. Scriven, E. F. V.; Turnbull, K., AZIDES - THEIR PREPARATION AND SYNTHETIC USES. *Chem. Rev.* **1988,** *88* (2), 297-368.
32. Worrell, B. T.; Malik, J. A.; Fokin, V. V., Direct Evidence of a Dinuclear Copper Intermediate in Cu(I)-Catalyzed Azide-Alkyne Cycloadditions. *Science* **2013,** *340* (6131), 457-460.
33. McKay, C. S.; Finn, M. G., Click Chemistry in Complex Mixtures: Bioorthogonal Bioconjugation. *Chem. Biol.* **2014,** *21* (9), 1075-1101.
34. Hong, V.; Steinmetz, N. F.; Manchester, M.; Finn, M. G., Labeling Live Cells by Copper-Catalyzed Alkyne-Azide Click Chemistry. *Bioconjugate Chem.* **2010,** *21* (10), 1912-1916.
35. Agard, N. J.; Prescher, J. A.; Bertozzi, C. R., A strain-promoted 3+2 azide-alkyne cycloaddition for covalent modification of biomolecules in living systems (vol 126, pg 15046, 2004). *J. Am. Chem. Soc.* **2005,** *127* (31), 11196-11196.
36. Jewett, J. C.; Sletten, E. M.; Bertozzi, C. R., Rapid Cu-Free Click Chemistry with Readily Synthesized Biarylazacyclooctynones. *J. Am. Chem. Soc.* **2010,** *132* (11), 3688-+.
37. Presolski, S. I.; Hong, V.; Cho, S. H.; Finn, M. G., Tailored Ligand Acceleration of the Cu-Catalyzed Azide-Alkyne Cycloaddition Reaction: Practical and Mechanistic Implications. *J. Am. Chem. Soc.* **2010,** *132* (41), 14570-14576.

38. Besanceney-Webler, C.; Jiang, H.; Zheng, T. Q.; Feng, L.; del Amo, D. S.; Wang, W.; Klivansky, L. M.; Marlow, F. L.; Liu, Y.; Wu, P., Increasing the Efficacy of Bioorthogonal Click Reactions for Bioconjugation: A Comparative Study. *Angew. Chem. Int. Ed.* **2011,** *50* (35), 8051-8056.
39. Uttamapinant, C.; Tangpeerachaikul, A.; Grecian, S.; Clarke, S.; Singh, U.; Slade, P.; Gee, K. R.; Ting, A. Y., Fast, Cell-Compatible Click Chemistry with Copper-Chelating Azides for Biomolecular Labeling. *Angew. Chem. Int. Ed.* **2012,** *51* (24), 5852-5856.
40. Hughes, J. P.; Rees, S.; Kalindjian, S. B.; Philpott, K. L., Principles of early drug discovery. *Br. J. Pharmacol.* **2011,** *162* (6), 1239-1249.
41. Schmitz, E.; Ohme, R., CYCLISCHE DIAZOVERBINDUNGEN .1. HERSTELLUNG UND UMSETZUNGEN VON DIAZIRINEN. *Chem. Ber.* **1961,** *94* (8), 2166-2173.
42. Chowdhry, V.; Westheimer, F. H., PHOTOAFFINITY-LABELING OF BIOLOGICAL-SYSTEMS. *Annu. Rev. Biochem.* **1979,** *48*, 293-325.
43. Bayley, H.; Knowles, J. R., PHOTOGENERATED REAGENTS FOR MEMBRANE LABELING .2. PHENYLCARBENE AND ADAMANTYLIDENE FORMED WITHIN LIPID BILAYER. *Biochemistry* **1978,** *17* (12), 2420-2423.
44. Graham, W. H., HALOGENATION OF AMIDINES .I. SYNTHESIS OF 3-HALO- AND OTHER NEGATIVELY SUBSTITUTED DIAZIRINES. *J. Am. Chem. Soc.* **1965,** *87* (19), 4396-&.
45. Moss, R. A., Diazirines: Carbene precursors par excellence. *Acc. Chem. Res.* **2006,** *39* (4), 267-272.
46. Al-Omari, M.; Banert, K.; Hagedorn, M., Bi-3H-diazirin-3-yls as precursors of highly strained cycloalkynes. *Angew. Chem. Int. Ed.* **2006,** *45* (2), 309-311.
47. Carrera, S. S.; Kerdelhue, J. L.; Langenwalter, K. J.; Brown, N.; Warmuth, R., Inner-phase reaction dynamics: The influence of hemicarcerand polarizability and shape on the potential energy surface of an inner-phase reaction. *Eur. J. Org. Chem.* **2005,** (11), 2239-2249.
48. Dubinsky, L.; Jarosz, L. M.; Amara, N.; Krief, P.; Kravchenko, V. V.; Krom, B. P.; Meijler, M. M., Synthesis and validation of a probe to identify quorum sensing receptors. *Chem. Commun.* **2009,** (47), 7378-7380.
49. Song, Z.; Zhang, Q., Fluorous Aryldiazirine Photoaffinity Labeling Reagents. *Org. Lett.* **2009,** *11* (21), 4882-4885.
50. Vedenyapina, M. D.; Kuznetsov, V. V.; Nizhnikovskii, E. A.; Strel'tsova, E. D.; Makhova, N. N.; Struchkova, M. I.; Vedenyapin, A. A., Electrochemical synthesis of pentamethylenediazirine. *Russ. Chem. Bull.* **2006,** *55* (11), 2013-2015.
51. Wagner, G.; Knoll, W.; Bobek, M. M.; Brecker, L.; van Herwijnen, H. W. G.; Brinker, U. H., Structure-Reactivity Relationships: Reactions of a 5-Substituted Aziadamantane in a Resorcin 4 arene-based Cavitand. *Org. Lett.* **2010,** *12* (2), 332-335.
52. Bond, M. R.; Zhang, H. C.; Vu, P. D.; Kohler, J. J., Photocrosslinking of glycoconjugates using metabolically incorporated diazirine-containing sugars. *Nat. Protoc.* **2009,** *4* (7), 1044-1063.
53. Savechenkov, P. Y.; Zhang, X.; Chiara, D. C.; Stewart, D. S.; Ge, R. L.; Zhou, X. J.; Raines, D. E.; Cohen, J. B.; Forman, S. A.; Miller, K. W.; Bruzik, K. S., Allyl m-Trifluoromethyldiazirine Mephobarbital: An Unusually Potent Enantioselective and Photoreactive Barbiturate General Anesthetic. *J. Med. Chem.* **2012,** *55* (14), 6554-6565.
54. Protasova, I.; Bulat, B.; Jung, N.; Brase, S., Synthesis of Diaziridines and Diazirines via Resin-Bound Sulfonyl Oximes. *Org. Lett.* **2017,** *19* (1), 34-37.

55. Castro, V.; Rodriguez, H.; Abericio, F., CuAAC: An Efficient Click Chemistry Reaction on Solid Phase. *ACS. Comb. Sci.* **2016,** *18* (1), 1-14.
56. Wang, L.; Murai, Y.; Yoshida, T.; Ishida, A.; Masuda, K.; Sakihama, Y.; Hashidoko, Y.; Hatanaka, Y.; Hashimoto, M., Alternative One-Pot Synthesis of (Trifluoromethyl)phenyldiazirines from Tosyloxime Derivatives: Application for New Synthesis of Optically Pure Diazirinylphenylalanines for Photoaffinity Labeling. *Org. Lett.* **2015,** *17* (3), 616-619.
57. Fernelius, W.; Bowman, G., Ammonolysis in Liquid Ammonia. *Chem. Rev.* **1940,** *26* (1), 3-48.
58. Nakashima, H.; Hashimoto, M.; Sadakane, Y.; Tomohiro, T.; Hatanaka, Y., Simple and versatile method for tagging phenyldiazirine photophores. *J. Am. Chem. Soc.* **2006,** *128* (47), 15092-15093.
59. Wang, L.; Ishida, A.; Hashidoko, Y.; Hashimoto, M., Dehydrogenation of the NH-NH Bond Triggered by Potassium tert-Butoxide in Liquid Ammonia. *Angew. Chem. Int. Ed.* **2017,** *56* (3), 870-873.
60. Ziegler, S.; Pries, V.; Hedberg, C.; Waldmann, H., Target identification for small bioactive molecules: finding the needle in the haystack. *Angew. Chem. Int. Ed.* **2013,** *52* (10), 2744-92.
61. Chen, B.; Zang, W.; Wang, J.; Huang, Y.; He, Y.; Yan, L.; Liu, J.; Zheng, W., The chemical biology of sirtuins. *Chem. Soc. Rev.* **2015,** *44* (15), 5246-5264.
62. Eskandarian, H. A.; Impens, F.; Nahori, M.-A.; Soubigou, G.; Coppee, J.-Y.; Cossart, P.; Hamon, M. A., A Role for SIRT2-Dependent Histone H3K18 Deacetylation in Bacterial Infection. *Science* **2013,** *341* (6145), 525-+.
63. Gomes, P.; Outeiro, T. F.; Cavadas, C., Emerging Role of Sirtuin 2 in the Regulation of Mammalian Metabolism. *Trends Pharmacol. Sci.* **2015,** *36* (11), 756-768.
64. Inoue, T.; Hiratsuka, M.; Osaki, M.; Oshimura, M., The molecular biology of mammalian SIRT proteins - SIRT2 in cell cycle regulation. *Cell Cycle* **2007,** *6* (9), 1011-1018.
65. de Oliveira, R. M.; Sarkander, J.; Kazantsev, A. G.; Outeiro, T. F., SIRT2 as a therapeutic target for age-related disorders. *Front. Pharmacol.* **2012,** *3*.
66. Donmez, G.; Outeiro, T. F., SIRT1 and SIRT2: emerging targets in neurodegeneration. *EMBO Mol. Med.* **2013,** *5* (3), 344-352.
67. Roth, M.; Chen, W. Y., Sorting out functions of sirtuins in cancer. *Oncogene* **2014,** *33* (13), 1609-1620.
68. Friden-Saxin, M.; Seifert, T.; Landergren, M. R.; Suuronen, T.; Lahtela-Kakkonen, M.; Jarho, E. M.; Luthman, K., Synthesis and Evaluation of Substituted Chroman-4-one and Chromone Derivatives as Sirtuin 2-Selective Inhibitors. *J. Med. Chem.* **2012,** *55* (16), 7104-7113.
69. Seifert, T.; Malo, M.; Kokkola, T.; Engen, K.; Friden-Saxin, M.; Wallen, E. A. A.; Lahtela-Kakkonen, M.; Jarho, E. M.; Luthman, K., Chroman-4-one- and Chromone-Based Sirtuin 2 Inhibitors with Antiproliferative Properties in Cancer Cells. *J. Med. Chem.* **2014,** *57* (23), 9870-9888.
70. Seifert, T.; Malo, M.; Lengqvist, J.; Sihlbom, C.; Jarho, E. M.; Luthman, K., Identification of the Binding Site of Chroman-4-one-Based Sirtuin 2-Selective Inhibitors using Photoaffinity Labeling in Combination with Tandem Mass Spectrometry. *J. Med. Chem.* **2016,** *59* (23), 10794-10799.
71. Ranade, A. R.; Higgins, L.; Markowski, T. W.; Glaser, N.; Kashin, D.; Bai, R. L.; Hong, K. H.; Hamel, E.; Hofle, G.; Georg, G. I., Characterizing the Epothilone Binding Site on beta-Tubulin by Photoaffinity Labeling: Identification of beta-Tubulin Peptides TARGSQQY and

TSRGSQQY as Targets of an Epothilone Photoprobe for Polymerized Tubulin. *J. Med. Chem.* **2016,** *59* (7), 3499-3514.
72. Fredholm, B. B.; Ijzerman, A. P.; Jacobson, K. A.; Linden, J.; Mueller, C. E., International Union of Basic and Clinical Pharmacology. LXXXI. Nomenclature and Classification of Adenosine Receptors-An Update. *Pharmacol. Rev.* **2011,** *63* (1), 1-34.
73. Shook, B. C.; Jackson, P. F., Adenosine A(2A) Receptor Antagonists and Parkinson's Disease. *ACS Chem. Neurosci.* **2011,** *2* (10), 555-567.
74. Muller-Haegele, S.; Muller, L.; Whiteside, T. L., Immunoregulatory activity of adenosine and its role in human cancer progression. *Expert Rev. Clin. Immunol.* **2014,** *10* (7), 897-914.
75. Jaakola, V. P.; Griffith, M. T.; Hanson, M. A.; Cherezov, V.; Chien, E. Y. T.; Lane, J. R.; Ijzerman, A. P.; Stevens, R. C., The 2.6 Angstrom Crystal Structure of a Human A(2A) Adenosine Receptor Bound to an Antagonist. *Science* **2008,** *322* (5905), 1211-1217.
76. Yuan, G. Y.; Gedeon, N. G.; Jankins, T. C.; Jones, G. B., Novel approaches for targeting the adenosine A(2A) receptor. *Exp. Op. Drug Disc.* **2015,** *10* (1), 63-80.
77. Muranaka, H.; Momose, T.; Handa, C.; Ozawa, T., Photoaffinity Labeling of the Human A(2A) Adenosine Receptor and Cross-link Position Analysis by Mass Spectrometry. *ACS Med. Chem. Lett.* **2017,** *8* (6), 660-665.
78. Wang, G. L.; Jiang, B. H.; Rue, E. A.; Semenza, G. L., HYPOXIA-INDUCIBLE FACTOR-1 IS A BASIC-HELIX-LOOP-HELIX-PAS HETERODIMER REGULATED BY CELLULAR O-2 TENSION. *Proc. Natl. Acad. Sci. U.S.A.* **1995,** *92* (12), 5510-5514.
79. Semenza, G. L., Targeting HIF-1 for cancer therapy. *Nat. Rev. Cancer* **2003,** *3* (10), 721-732.
80. Lee, K.; Kang, J. E.; Park, S.-K.; Jin, Y.; Chung, K.-S.; Kim, H.-M.; Lee, K.; Kang, M. R.; Lee, M. K.; Song, K. B.; Yang, E.-G.; Lee, J.-J.; Won, M., LW6, a novel HIF-1 inhibitor, promotes proteasomal degradation of HIF-1 alpha via upregulation of VHL in a colon cancer cell line. *Biochem. Pharmacol.* **2010,** *80* (7), 982-989.
81. Hashimoto, Y.; Tazawa, H.; Teraishi, F.; Kojima, T.; Watanabe, Y.; Uno, F.; Yano, S.; Urata, Y.; Kagawa, S.; Fujiwara, T., The hTERT Promoter Enhances the Antitumor Activity of an Oncolytic Adenovirus under a Hypoxic Microenvironment. *PLoS One.* **2012,** *7* (6).
82. Wang, L.; Son, Y.-O.; Ding, S.; Wang, X.; Hitron, J. A.; Budhraja, A.; Lee, J.-C.; Lin, Q.; Poyil, P.; Zhang, Z.; Luo, J.; Shi, X., Ethanol Enhances Tumor Angiogenesis In Vitro Induced by Low-Dose Arsenic in Colon Cancer Cells Through Hypoxia-Inducible Factor 1 Alpha Pathway. *Toxicol. Sci.* **2012,** *130* (2), 269-280.
83. Lee, K.; Ban, H. S.; Naik, R.; Hong, Y. S.; Son, S.; Kim, B. K.; Xia, Y.; Song, K. B.; Lee, H. S.; Won, M., Identification of Malate Dehydrogenase 2 as a Target Protein of the HIF-1 Inhibitor LW6 using Chemical Probes. *Angew. Chem. Int. Ed.* **2013,** *52* (39), 10286-10289.
84. Chua, Y. L.; Dufour, E.; Dassa, E. P.; Rustin, P.; Jacobs, H. T.; Taylor, C. T.; Hagen, T., Stabilization of Hypoxia-inducible Factor-1 alpha Protein in Hypoxia Occurs Independently of Mitochondrial Reactive Oxygen Species Production. *J. Biol. Chem.* **2010,** *285* (41), 31277-31284.
85. Goward, C. R.; Nicholls, D. J., MALATE-DEHYDROGENASE - A MODEL FOR STRUCTURE, EVOLUTION, AND CATALYSIS. *Protein Sci.* **1994,** *3* (10), 1883-1888.
86. Chicca, A.; Nicolussi, S.; Bartholomaus, R.; Blunder, M.; Rey, A. A.; Petrucci, V.; Reynoso-Moreno, I. D.; Viveros-Paredes, J. M.; Gens, M. D.; Lutz, B.; Schioth, H. B.; Soeberdt, M.; Abels, C.; Charles, R. P.; Altmann, K. H.; Gertsch, J., Chemical probes to potently and selectively inhibit endocannabinoid cellular reuptake. *Proc. Natl. Acad. Sci. U.S.A.* **2017,** *114* (25), E5006-E5015.

87. Maccarrone, M.; Bab, R.; Biro, T.; Cabral, G. A.; Dey, S. K.; Di Marzo, V.; Konje, J. C.; Kunos, G.; Mechoulam, R.; Pacher, P.; Sharkey, K. A.; Zimmer, A., Endocannabinoid signaling at the periphery: 50 years after THC. *Trends Pharmacol. Sci.* **2015,** *36* (5), 277-296.
88. Di Marzo, V., Targeting the endocannabinoid system: to enhance or reduce? *Nat. Rev. Drug Discov.* **2008,** *7* (5), 438-455.
89. Nicolussi, S.; Gertsch, J., Endocannabinoid Transport Revisited. *Hormones and Transport Systems* **2015,** *98*, 441-485.
90. Corminboeuf, C.; Hu, P.; Tuckerman, M. E.; Zhang, Y. K., Unexpected deacetylation mechanism suggested by a density functional theory QM/MM study of histone-deacetylase-like protein. *J. Am. Chem. Soc.* **2006,** *128* (14), 4530-4531.
91. Lu, X.; Wang, L.; Yu, C.; Yu, D.; Yu, G., Histone acetylation modifiers in the pathogenesis of Alzheimer's disease. *Front. Cell. Neurosci.* **2015,** *9*.
92. Steffan, J. S.; Bodai, L.; Pallos, J.; Poelman, M.; McCampbell, A.; Apostol, B. L.; Kazantsev, A.; Schmidt, E.; Zhu, Y. Z.; Greenwald, M.; Kurokawa, R.; Housman, D. E.; Jackson, G. R.; Marsh, J. L.; Thompson, L. M., Histone deacetylase inhibitors arrest polyglutamine-dependent neurodegeneration in Drosophila. *Nature* **2001,** *413* (6857), 739-743.
93. Komatsu, T.; Urano, Y., Evaluation of Enzymatic Activities in Living Systems with Small-molecular Fluorescent Substrate Probes. *Anal. Sci.* **2015,** *31* (4), 257-265.
94. Falkenberg, K. J.; Johnstone, R. W., Histone deacetylases and their inhibitors in cancer, neurological diseases and immune disorders. *Nat. Rev. Drug Discov.* **2014,** *13* (9), 673-691.
95. Baba, R.; Hori, Y.; Mizukami, S.; Kikuchi, K., Development of a Fluorogenic Probe with a Transesterification Switch for Detection of Histone Deacetylase Activity. *J. Am. Chem. Soc.* **2012,** *134* (35), 14310-14313.
96. Baba, R.; Hori, Y.; Kikuchi, K., Intramolecular Long-Distance Nucleophilic Reactions as a Rapid Fluorogenic Switch Applicable to the Detection of Enzymatic Activity. *Chem. Eur. J.* **2015,** *21* (12), 4695-4702.
97. Xie, Y. S.; Ge, J. Y.; Lei, H. P.; Peng, B.; Zhang, H. T.; Wang, D. Y.; Pan, S. J.; Chen, G. C.; Chen, L. F.; Wang, Y.; Hao, Q.; Yao, S. Q.; Sun, H. Y., Fluorescent Probes for Single-Step Detection and Proteomic Profiling of Histone Deacetylases. *J. Am. Chem. Soc.* **2016,** *138* (48), 15596-15604.
98. Yamaguchi, T.; Asanuma, M.; Nakanishi, S.; Saito, Y.; Okazaki, M.; Dodo, K.; Sodeoka, M., Turn-ON fluorescent affinity labeling using a small bifunctional O-nitrobenzoxadiazole unit. *Chem. Sci.* **2014,** *5* (3), 1021-1029.
99. Li, Z. Q.; Wang, D. Y.; Li, L.; Pan, S. J.; Na, Z. K.; Tan, C. Y. J.; Yao, S. Q., "Minimalist" Cyclopropene-Containing Photo-Cross-Linkers Suitable for Live-Cell Imaging and Affinity-Based Protein Labeling. *J. Am. Chem. Soc.* **2014,** *136* (28), 9990-9998.
100. Berger, S. L., The complex language of chromatin regulation during transcription. *Nature* **2007,** *447* (7143), 407-412.
101. Delmore, J. E.; Issa, G. C.; Lemieux, M. E.; Rahl, P. B.; Shi, J.; Jacobs, H. M.; Kastritis, E.; Gilpatrick, T.; Paranal, R. M.; Qi, J.; Chesi, M.; Schinzel, A. C.; McKeown, M. R.; Heffernan, T. P.; Vakoc, C. R.; Bergsagel, P. L.; Ghobrial, I. M.; Richardson, P. G.; Young, R. A.; Hahn, W. C.; Anderson, K. C.; Kung, A. L.; Bradner, J. E.; Mitsiades, C. S., BET Bromodomain Inhibition as a Therapeutic Strategy to Target c-Myc. *Cell* **2011,** *146* (6), 903-916.
102. Filippakopoulos, P.; Qi, J.; Picaud, S.; Shen, Y.; Smith, W. B.; Fedorov, O.; Morse, E. M.; Keates, T.; Hickman, T. T.; Felletar, I.; Philpott, M.; Munro, S.; McKeown, M. R.; Wang, Y.; Christie, A. L.; West, N.; Cameron, M. J.; Schwartz, B.; Heightman, T. D.; La Thangue, N.;

French, C. A.; Wiest, O.; Kung, A. L.; Knapp, S.; Bradner, J. E., Selective inhibition of BET bromodomains. *Nature* **2010,** *468* (7327), 1067-1073.
103. Floyd, S. R.; Pacold, M. E.; Huang, Q.; Clarke, S. M.; Lam, F. C.; Cannell, I. G.; Bryson, B. D.; Rameseder, J.; Lee, M. J.; Blake, E. J.; Fydrych, A.; Ho, R.; Greenberger, B. A.; Chen, G. C.; Maffa, A.; Del Rosario, A. M.; Root, D. E.; Carpenter, A. E.; Hahn, W. C.; Sabatini, D. M.; Chen, C. C.; White, F. M.; Bradner, J. E.; Yaffe, M. B., The bromodomain protein Brd4 insulates chromatin from DNA damage signalling. *Nature* **2013,** *498* (7453), 246-+.
104. Nicodeme, E.; Jeffrey, K. L.; Schaefer, U.; Beinke, S.; Dewell, S.; Chung, C.-w.; Chandwani, R.; Marazzi, I.; Wilson, P.; Coste, H.; White, J.; Kirilovsky, J.; Rice, C. M.; Lora, J. M.; Prinjha, R. K.; Lee, K.; Tarakhovsky, A., Suppression of inflammation by a synthetic histone mimic. *Nature* **2010,** *468* (7327), 1119-1123.
105. Chung, C.-w.; Coste, H.; White, J. H.; Mirguet, O.; Wilde, J.; Gosmini, R. L.; Delves, C.; Magny, S. M.; Woodward, R.; Hughes, S. A.; Boursier, E. V.; Flynn, H.; Bouillot, A. M.; Bamborough, P.; Brusq, J.-M. G.; Gellibert, F. J.; Jones, E. J.; Riou, A. M.; Homes, P.; Martin, S. L.; Uings, I. J.; Toum, J.; Clement, C. A.; Boullay, A.-B.; Grimley, R. L.; Blande, F. M.; Prinjha, R. K.; Lee, K.; Kirilovsky, J.; Nicodeme, E., Discovery and Characterizatlion of Small Molecule Inhibitors of the BET Family Bromodomains. *J. Med. Chem.* **2011,** *54* (11), 3827-3838.
106. Stocker, B. L.; Timmer, M. S. M., Chemical Tools for Studying the Biological Function of Glycolipids. *Chembiochem* **2013,** *14* (10), 1164-1184.
107. Andrianasolo, E. H.; Haramaty, L.; Vardi, A.; White, E.; Lutz, R.; Falkowski, P., Apoptosis-inducing galactolipids from a cultured, marine diatom, Phaeodactylum tricornutum. *J. Nat. Prod.* **2008,** *71* (7), 1197-1201.
108. Loya, S.; Reshef, V.; Mizrachi, F.; Silberstein, C.; Rachamim, Y.; Carmeli, S.; Hizi, A., The inhibition of the reverse transcriptase of HIV-1 by the natural sulfoglycolipids from cyanobacteria: Contribution of different moieties to their high potency. *J. Nat. Prod.* **1998,** *61* (7), 891-895.
109. Ulivi, V.; Lenti, M.; Gentili, C.; Marcolongo, G.; Cancedda, R.; Cancedda, F. D., Anti-inflammatory activity of monogalactosyldiacylglycerol in human articular cartilage in vitro: activation of an anti-inflammatory cyclooxygenase-2 (COX-2) pathway. *Arthritis Res. Ther.* **2011,** *13* (3).
110. Larsen, E.; Kharazmi, A.; Christensen, L. P.; Christensen, S. B., An antiinflammatory galactolipid from rose hip (Rosa canina) that inhibits chemotaxis of human peripheral blood neutrophils in vitro. *J. Nat. Prod.* **2003,** *66* (7), 994-995.
111. Liu, X. H.; Dong, T.; Zhou, Y.; Huang, N.; Lei, X. G., Exploring the Binding Proteins of Glycolipids with Bifunctional Chemical Probes. *Angew. Chem. Int. Ed.* **2016,** *55* (46), 14328-14332.
112. Hoshino, K.; Takeuchi, O.; Kawai, T.; Sanjo, H.; Ogawa, T.; Takeda, Y.; Takeda, K.; Akira, S., Cutting edge: Toll-like receptor 4 (TLR4)-deficient mice are hyporesponsive to lipopolysaccharide: Evidence for TLR4 as the Lps gene product. *J. Immunol.* **1999,** *162* (7), 3749-3752.
113. Palsson-McDermott, E. M.; O'Neill, L. A. J., Signal transduction by the lipopolysaccharide receptor, Toll-like receptor-4. *Immunology* **2004,** *113* (2), 153-162.
114. Cohen, P., Protein kinases - the major drug targets of the twenty-first century? *Nat. Rev. Drug Discov.* **2002,** *1* (4), 309-315.
115. Dancey, J.; Sausville, E. A., Issues and progress with protein kinase inhibitors for cancer treatment. *Nat. Rev. Drug Discov.* **2003,** *2* (4), 296-313.

116. Shah, N. P.; Tran, C.; Lee, F. Y.; Chen, P.; Norris, D.; Sawyers, C. L., Overriding imatinib resistance with a novel ABL kinase inhibitor. *Science* **2004,** *305* (5682), 399-401.
117. Capdeville, R.; Buchdunger, E.; Zimmermann, J.; Matter, A., Glivec (ST1571, Imatinib), a rationally developed, targeted anticancer drug. *Nat. Rev. Drug Discov.* **2002,** *1* (7), 493-502.
118. Shi, H. B.; Zhang, C. J.; Chen, G. Y. J.; Yao, S. Q., Cell-Based Proteome Profiling of Potential Dasatinib Targets by Use of Affinity-Based Probes. *J. Am. Chem. Soc.* **2012,** *134* (6), 3001-3014.
119. Colombini, M., VDAC structure, selectivity, and dynamics. *Biochim. Biophys. Acta* **2012,** *1818* (6), 1457-1465.
120. Aufschnaiter, A.; Kohler, V.; Diessl, J.; Peselj, C.; Carmona-Gutierrez, D.; Keller, W.; Buttner, S., Mitochondrial lipids in neurodegeneration. *Cell Tissue Res.* **2017,** *367* (1), 125-140.
121. Crimi, M.; Degli Esposti, M., Apoptosis-induced changes in mitochondrial lipids. *Biochim. Biophys. Acta* **2011,** *1813* (4), 551-557.
122. Hiller, S.; Garces, R. G.; Malia, T. J.; Orekhov, V. Y.; Colombini, M.; Wagner, G., Solution structure of the integral human membrane protein VDAC-1 in detergent micelles. *Science* **2008,** *321* (5893), 1206-1210.
123. Weiser, B. P.; Salari, R.; Eckenhoff, R. G.; Brannigan, G., Computational Investigation of Cholesterol Binding Sites on Mitochondrial VDAC. *J. Phys. Chem. B.* **2014,** *118* (33), 9852-9860.
124. Budelier, M. M.; Cheng, W. W. L.; Bergdoll, L.; Chen, Z. W.; Janetka, J. W.; Abramson, J.; Krishnan, K.; Mydock-McGrane, L.; Covey, D. F.; Whitelegge, J. P.; Evers, A. S., Photoaffinity labeling with cholesterol analogues precisely maps a cholesterol-binding site in voltage-dependent anion channel-1. *J. Biol. Chem.* **2017,** *292* (22), 9294-9304.

2 - Design and Synthesis of Inhibitors of eIF2α Phosphatase

2.1 - Introduction

Duchenne Muscular Dystrophy (DMD) is a lethal genetic disorder that afflicts 1 in 3600 males worldwide.[1] Characterized by progressive muscular degeneration and weakness, this disease is caused by an absence of dystrophin, a protein that is responsible for maintaining strength in muscle cells and protecting them from injury. In the absence of this protein, muscle cells become extremely fragile and susceptible to irreversible damage. Patients suffering from DMD can start to experience muscle weakness as early as age 3, first affecting the muscles in the pelvic area and thighs, and later moving onto the skeletal muscle in the arms and calves. Oftentimes, the child will require the use of a wheelchair by their 10th birthday, while the disease gradually progresses to affect the respiratory system as well as the myocardium of the heart, which leads to cardiomyopathy. Eventually, these muscles completely deteriorate, resulting in death at an early age. The severity and rapid onset of the symptoms create many challenges for children suffering from DMD as well as their loved ones since they eventually become fully dependent on their caregivers for survival. Current therapeutic treatments for DMD are extremely limited and are aimed solely at treating the symptoms of this disease to delay their progression and make day-to-day life easier.

The complex nature of the human genome makes the development of therapeutics aimed at curing or treating genetic diseases a very challenging feat. However, the ease in which a healthy human body can rapidly regenerate damaged skeletal muscle tissue after injury prompted biologists to closely examine this process at a cellular level. In 1961, while examining the peripheral region of the skeletal muscle fiber of a frog, Alexander Mauro discovered the presence of certain cells which were "intimately associated" with the muscle fiber.[2] As he was the pioneer behind this discovery, he chose to call the newly discovered cell line *satellite cells,* owing to their position underneath the basal lamina of the muscle fiber (Figure 2.1).[3] It was later discovered that this cell line was also present in higher vertebrates, including humans, and that they remained in a quiescent or quiet state until activated by injury.[4] It was also noted that repeated cycles of injury and regeneration did not cause a depletion in the number of satellite cells, suggesting that these cells have the capacity to self renew.

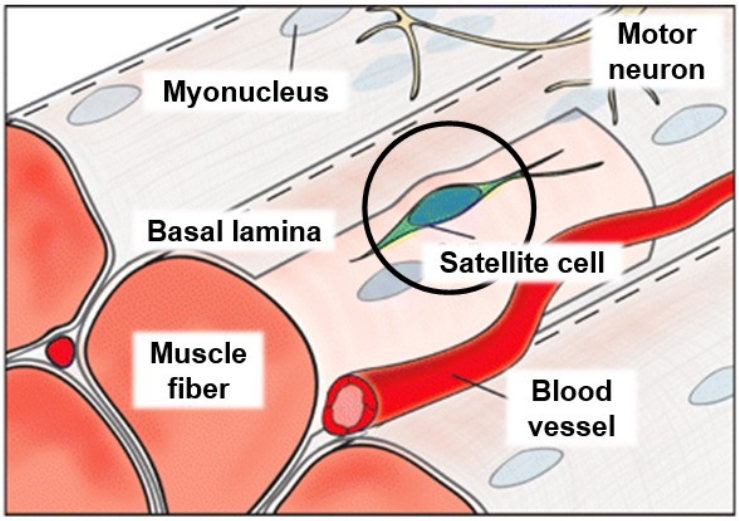

Figure 2.1.1 – Satellite Cell in its Niche Under the Basal Lamina

Since their discovery, researchers have been looking for ways of exploiting the regenerative capacity of satellite cells to treat skeletal muscle disorders. However, the relatively low-numbers of satellite cells in the human body complicate their use as donor cells. This has motivated considerable efforts to develop *ex vivo* culture conditions for their cultivation, which remains a desirable but challenging objective.[5] When taken out of the body, satellite cells exit quiescence, and enter into the myogenic program, thereby losing two innate features of adult stem cells: the ability to differentiate and self-renew.[5] By studying the molecular mechanisms that underlie satellite cell activation, a better understanding of how this pathway can be controlled for therapeutic benefit can be gained.

2.2 – Maintaining Quiescence in Skeletal Muscle Stem Cells

Owing to their fundamental importance for survival and their potential as therapeutic targets for skeletal muscle disorders, satellite cells have received considerable attention from researchers attempting to understand the molecular pathways leading to their maintenance and differentiation. Key contributions of Buckingham et al. have shown the involvement of the paired homeodomain family of transcription factors known as Pax3 and Pax7 during skeletal muscle development and repair. Pax3 and Pax7 are key regulators of satellite cell survival, and are responsible for the expression of myogenic determination genes *Myf5* and *MyoD*, whose expression leads to rapid muscle differentiation.[6] More specifically, the upregulation of Pax7 is responsible for the satellite cell's ability to self-renew, whereas the activation of *MyoD* leads to

satellite cell differentiation into muscle tissue, as it is one of the earliest markers of myogenic commitment.[6] In the quiescent state, Pax7 is upregulated while *MyoD* is downregulated (Figure 2.2.1). However, when skeletal muscle is damaged in the body, the satellite cell is activated, leading to the upregulation of *MyoD*. At this point, the satellite cell can either commit to differentiation to generate muscle tissue, or it can self-renew and return to the quiescent state.

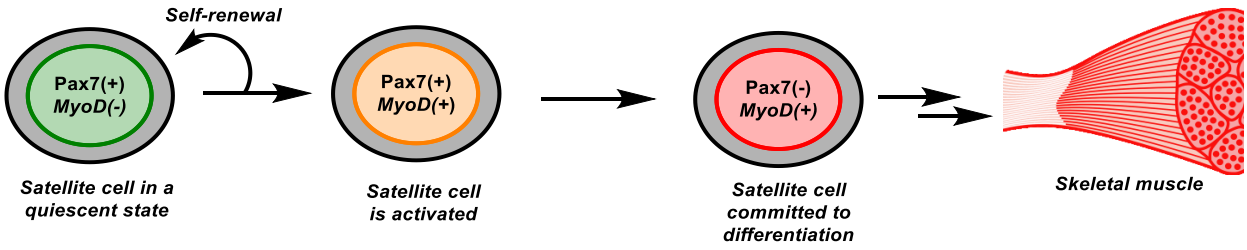

Figure 2.2.1 – Satellite Cell Activation Pathway

There are two, characteristic features of satellite cells that distinguish them from embryonic stem cells. Firstly, satellite cells remain in a quiescent state until activated in response to damage. Secondly, the majority of these cells already express *Myf5,* meaning they are primed for differentiation.[7] However, the cell prevents translation of *Myf5* through the microRNA pathway, thereby inhibiting the activation of the myogenic program.[8] Moreover, the transcripts for *Myf5* are sequestered in RNA granules in the quiescent satellite cell, further inhibiting their accumulation. During activation, they dissociate from the granules and the concentration of *Myf5* rapidly increases.[8] This process of suppression though aggregation of proteins into RNA granules is a conserved biological process that is also prevalent in cells that have been exposed to various forms of stress.[9] When a cell is under stress it stores mRNAs in stress granules and releases them only after the threat has been resolved. It is well known that this process can be mediated by phosphorylation of the alpha subunit of eukaryotic translation initiation factor 2 (eIF2α) at serine residue 51 (S51).[9] This molecular process has been studied extensively, since it has significant implications in many serious diseases including Alzheimer's and various forms of cancer.[10]

In 2015, Crist and coworkers questioned whether phosphorylation of eIF2α at S51 could dictate the assembly of RNA granules in quiescent satellite cells in a manner that could maintain quiescence *ex vivo*. Support for the feasibility of this hypothesis was provided by the isolation of single myofibers from the extensor digitorum longus (EDL) muscle of wild-type mice.[5] Using immunoblotting assays containing antibodies against Pax7 and phosphorylated-eIF2α (P- eIF2α),

they showed that levels of P-eIF2α were 5 times higher in freshly isolated satellite cells than in cells that had been cultured over a period of 3 days.[5] They also showed that satellite cells that had activated the myogenic program and were expressing *MyoD* had undetectable levels of P-eIF2α, strongly suggesting that this protein is intrinsically involved in the activation pathway.

In a very different biochemical cascade, known as the unfolded protein response (UPR), cells phosphorylate eIF2α in response to stress. This silences transcription to preserve energy until the stress has been addressed. In response to oxidative stress, appropriate genes are activated to trap reactive oxygen species (ROS).[7] In the context of the UPR, a kinase known as PERK is responsible for the phosphorylation of eIF2α in response to oxidative and ER stress. With this in mind, Crist and coworkers then went on to show that PERK is indeed activated in the quiescent satellite cell alongside *Atf4, Chop,* and *BiP*, three UPR target genes that are required to ensure cell survival during ER stress.[5] Given the breadth of life-threatening diseases linked to malfunctions in the molecular machinery responsible for the phosphorylation/dephosphorylation of eIF2α, a tremendous amount of research has been dedicated to finding ways to control this process using small-molecule pharmaceuticals. Therefore, it was further hypothesized that pharmacological inhibition of the eIF2α phosphatase would prevent the activation of satellite cells and promote self-renewal.

Crist and coworkers then examined whether the inhibition of eIF2α dephosphorylation would supress the activation of the myogenic program during an *ex vivo* culture. Satellite cells were isolated and cultured in the presence of 10μM sal003, a potent derivative of the small molecule salubrinal, which is hypothesized to interfere with the eIF2α phosphatase GADD34/PP1 (Figure 2.2.2).[11-12]

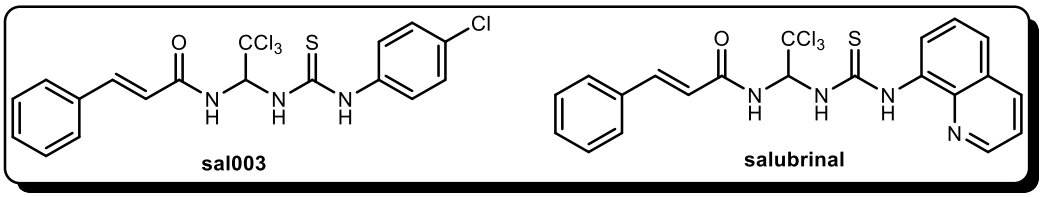

Figure 2.2.2 – Chemical Structures of sal003 and Salubrinal

After a 4 day culture the satellite cells were found to have a 3-fold increase in the numbers of $Pax7^{+}MyoD^{-}$ cells that retained their regenerative capacity.[5] Immunoblotting assays using

antibodies against Pax7 confirmed the positive effect of sal003 to suppress satellite cell entry into the myogenic program during an *ex vivo* culture. To test whether satellite cells cultured in the presence of sal003 would retain their stem cell properties to self-renew and regenerate damaged muscle tissue, they were engrafted into a mouse model of Duchene muscular dystrophy (Dmd^{mdx}). After a 4-day *ex vivo* culture period, the cells were engrafted into the Tibialis anterior muscle of the hindlimbs of Dmd^{mdx}. Using *in vivo* imaging to quantitatively measure over time the bioluminescence from the engrafted cells, they found that the sal003-treated satellite cells had a much more intense signal than the control.[5] Additionally, they found that the engrafted sal003-treated satellite cells gave rise to higher numbers of dystrophin$^+$ and Pax7$^+$ cells than freshly isolated cells, demonstrating that these engrafted cells retained the two key features of adult stem cells. Therefore, they were able to show that the small molecule, sal003, promoted the *ex vivo* expansion of satellite cells that retained their regenerative capacity, making sal003 a potential therapeutic to aid in stem cell transplantation.

Although these preliminary results were promising, there were still several major limitations to using sal003 as a pharmacological inhibitor of satellite cell activation. Firstly, sal003 must be administered at a 10 μM concentration to achieve the optimal effect. If this culture technique were to become a viable method for treatment of skeletal muscle disorders, a more potent analog would need to be developed that yields higher activity at a lower concentration. Secondly, although sal003 displayed activity to expand satellite cells in culture, its efficacy to do so remains an area of improvement, as over time the majority of the cells had entered the myogenic program (Figure 2.2.3). Ideally, the satellite cell culture would be expanded in size to nearly completely undifferentiated populations.

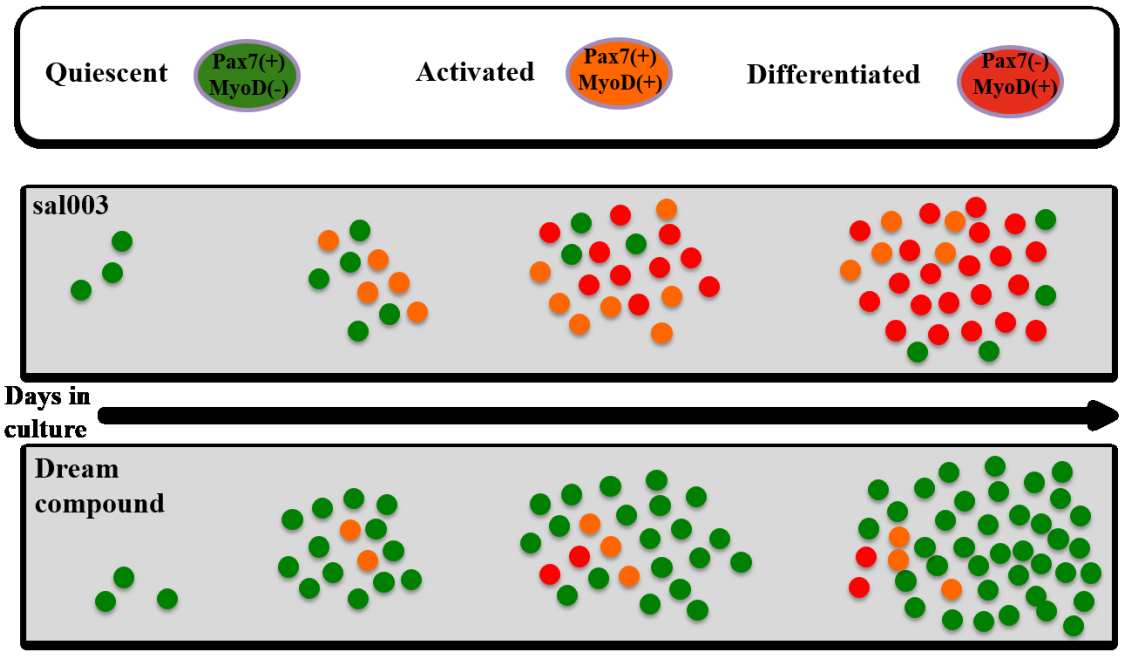

Figure 2.2.3 – The Ideal Compound Would Expand Satellite Cells That Maintain Their Ability to Self-Renew

These two points alone significantly hinder the likelihood of this technique ever becoming a suitable therapeutic method. Therefore, in order for this method to become a viable treatment option for stem cell transplantation, more potent analogs that are benchtop stable need to be developed and synthesized.

2.3 – Pharmacological Inhibition of eIF2α Phosphatase

2.3.1 – ER Stress-Induced Apoptosis and the UPR

All eukaryotic species respond to endoplasmic reticulum (ER) stress through a series of pathways collectively known as the unfolded protein response (UPR).[13] This pathway is essential for cellular homeostasis, and its malfunction is implicated in many serious diseases as well as viral infections. Therefore, this pathway has received considerable attention as a potential therapeutic target.[14-15]

Regular ER function can be disrupted by various forms of intracellular and extracellular stimuli, resulting in the induction of ER-stress. This can be triggered by a myriad of conditions including but not limited to, the reduction of disulfide bonds, the impairment of Golgi protein transport pathways, the expression of mutated ER proteins, the inhibition of ER-associated

degradation, or the depletion of ER calcium levels. Under stress, unfolded proteins accumulate in the ER lumen, resulting in the activation of the self-protective mechanism, the UPR. In mammalian cells, the UPR signaling pathway is mediated by three ER membrane associated sensors: RNA-dependent protein kinase (PKR)-like eukaryotic initiation factor 2α (eIF2α) kinase (PERK), inositol requiring transmembrane kinase/endoribonuclease 1 (IRE1), and activating transcription factor 6 (*Atf6*). These three sensors work in conjunction with one another to deal with the stress at hand; however, if the survival signal is inadequate to relieve cells from the stress, they may undergo apoptosis as a self-preservation mechanism to destroy the ER-stress damaged cells. In this Section, the UPR signalling pathway through PERK will be discussed.

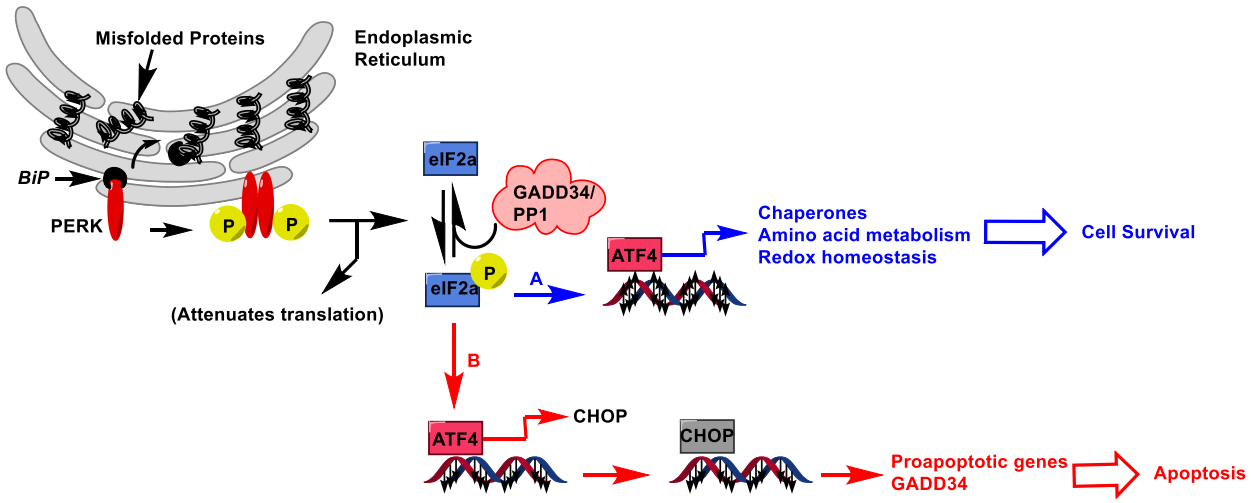

Figure 2.3.1.1 – Cellular Response to ER-Stress via PERK

PERK is a type-I ER transmembrane protein capable of recognizing the accumulation of misfolded proteins at its N-terminal luminal domain. Its activation is initiated by the dissociation of *BiP* from the luminal domain of PERK, which triggers its dimerization and autophosphorylation (Figure 2.3.1.1). Activated PERK then phosphorylates eIF2α at Serine reside 51, shutting down global protein translation in the cell to reduce the protein intake into the ER. Additionally, eIf2α phosphorylation leads to the specific translation of *Atf4* (eIF2α–activating transcription factor-4), which activates the transcription of several pro-survival genes such as those associated with the generation of molecular chaperones that serve to shuttle the misfolded proteins our of the ER lumen, amino-acid metabolism, and redox homeostasis. However, under severe or prolonged ER stress conditions, *Atf4* activates the transcription of proapoptotic factor CHOP. CHOP is a transcription factor that in turn upregulates several proapoptotic factors, none more significant than

GADD34. The CHOP mediated translation of GADD34 leads to the assembly of the GADD34/PP1 complex and ultimately the dephosphorylation of eIF2α, causing the recovery of protein translation in the ER.[16] However, if the dephosphorylation event, which is mediated by the GADD34/PP1 complex, occurs before the cell has dealt with the stress at hand, the cell will accumulate misfolded proteins in the ER lumen, leading to cellular apoptosis.

2.3.2 – A Small Molecule Inhibitor of ER Stress-Induced Apoptosis

Since it is well understood that the production of the GADD34/PP1 complex can lead to cellular apoptosis during ER stress, researchers have focused much of their attention on finding ways to inhibit this complex to promote cellular recovery and survival. In 2005, in a screen of over 19,000 compounds that protected rat PC12 cells from ER stress-induced apoptosis, Michael Boyce and coworkers identified a small molecule which they termed salubrinal (Figure 2.3.2.1).[11]

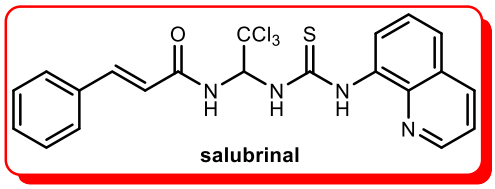

Figure 2.3.2.1 – Chemical Structure of Salubrinal

They found that salubrinal inhibited ER stress-induced apoptosis in a dose-dependent manner in cells that were treated with tunicamycin, a protein glycosylation inhibitor. To determine how salubrinal protects cells from apoptosis, they examined its effects on several known components of the UPR. Using an immunoblotting assay, salubrinal was found to rapidly promote the phosphorylation of eIF2α along with the production of several translational genes associated with the UPR.[11] Initially, they hypothesized that salubrinal was activating one of the protein kinases known to phosphorylate eIF2α. To examine this, they tested its effects on mouse embryos lacking the ability to produce the kinase PERK, and found that salubrinal retained its ability to induce eIF2α phosphorylation, indicating that salubrinal does not activate PERK. Furthermore, they investigated whether salubrinal acted to inhibit the dephosphorylation event from occurring. An in vitro dephosphorylation assay using lysates of cells that overexpressed an active fragment of GADD34 effectively dephosphorylated eIF2α, whereas the same cell lysates treated with salubrinal did not. Following several mechanistic studies and assays, they proposed that salubrinal

acted by disrupting the formation of the GADD34/PP1 complex, thereby preventing the dephosphorylation of eIF2α.

As a direct application of salubrinal's ability to act as a selective pharmacological inhibitor of eIF2α dephosphorylation, they selected the herpes simplex virus (HSV) to use as a disease model. During HSV infection, a protein kinase gets activated leading to the phosphorylation of eIF2α to slow down the viral protein synthesis and reproduction.[17] To negate this effect, HSV encodes ICP34.5, a protein homologous to GADD34, which then forms a complex with cellular PP1 and leads to eIF2α dephosphorylation.[18] Consistent with their earlier findings, they found that salubrinal acted to both induce the phosphorylation of eIF2α and inhibit the dephosphorylation of eIF2α in HSV-infected cell lysates.[11] Therefore, this pioneering work by Michael Boyce and coworkers brought to light the beneficial effects of inhibiting of the dephosphorylation of specific substrates in the context of the UPR, and set the stage for the further development of therapeutic agents in this field.

2.3.3 – Previous Structure Optimization Studies on Salubrinal

Since the initial discovery of salubrinal in 2005, there have been two structure optimization studies conducted in order to improve efficacy. The first study from Long *et al*. was published later in 2005, and biological assays were done in collaboration with Michael Boyce and coworkers. However, in the case of salubrinal, its biological target is unknown, posing several challenges and limiting the ability of the medicinal chemist to optimize its structure to achieve optimal potency. In the case of salubrinal, the general hypothesis is that it inhibits the GADD34/PP1 complex in some manner that prevents it from dephosphorylating eIF2α.[19] Whether this occurs through direct binding or through indirect binding causing a downstream signalling process remains unclear. Attempts have been made to synthesize biotinylated derivatives of salubrinal and use them for target identification; however, nothing has been reported regarding the success of these probes. Nonetheless, research groups have spent considerable amounts of time synthesizing derivatives of salubrinal in order to gain some insights into which functional groups are essential for compound activity and which groups can be modified.

In the initial cell-based activity assay in 2005, Long *et al*. report the synthesis and EC_{50} values of 26 novel derivatives and compare their activities to that of salubrinal for the protection

of ER stress-induced apoptosis brought upon by tunicamycin, in rat PC12 cells.[19] EC_{50} values in this instance are defined as the concentration of the compound that produces half of the maximal rescue from cell death. The synthesis of the analogs commenced by refluxing the appropriate amine in the presence of anhydrous chloral to give the chloralamides **2.3.3.1**, which were subsequently converted to the amines **2.3.3.2** via chlorination and quenching with an ammonia solution in ether. Addition of the amines to synthetically prepared isothiocyanates in refluxing THF resulted in the formation of thioureas **2.3.3.3**. Using this approach, derivatives were synthesized where the alkene was reduced to the alkane, as well as exchanging the aromatic rings on either side of the compounds for heterocyclic structures or even alkanes, without much loss in compound activity (Figure 2.3.3.1). Next, they explored the importance of the trichloromethyl moiety by substituting it for $-CF_3$, $-CBr_3$, $-CH_2Cl_2$, and $-CO_2Et$ groups. Only the $-CBr_3$ and the $-CH_2Cl_2$ derivatives retained any activity, albeit greatly reduced compared to that of the parent compound containing the $-CCl_3$ group. Therefore, they deemed the trichloromethyl moiety essential for compound activity. Furthermore, they reported the synthesis of a biotinylated derivative of salubrinal where they exchange the $-R^2$ group for biotin and show that it has similar activity to that of salubrinal. However, they claim that target identification studies are underway and that the results will be reported in due course. Unfortunately, nothing was ever published, which suggests that the affinity labelling experiment was unsuccessful.

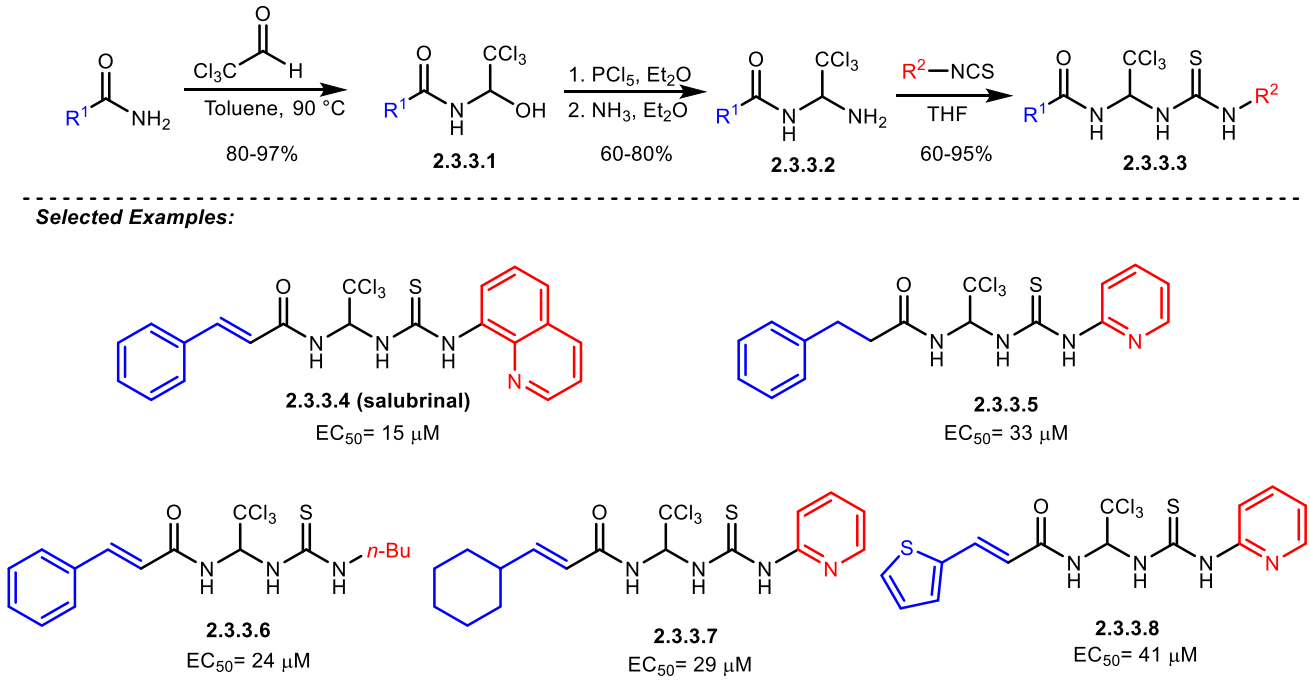

Figure 2.3.3.1 – Initial Cell-Based Activity Assay Study by Long et al.

Although they failed to synthesize any derivatives that were more potent than salubrinal, this initial study was beneficial since it showed that modifications to the external portions of the parent compound could be tolerated, whereas exchanging the -CCl_3 moiety resulted in a dramatic decrease in overall activity. Additionally, this was the first published synthetic route to this class of compounds, which paved the way for the second cell-based activity assay conducted by Liu *et al.* in 2012. In this study, 27 novel salubrinal derivatives were synthesized and tested for their ability to protect neonate rat cardiomyocytes from tunicamycin-induced apoptosis.[20] Using a slightly modified synthetic route, they were able to assemble a small compound library starting from aromatic aldehydes (Figure 2.3.3.2). Reacting the aldehyde with malonic acid in pyridine gave the unsaturated carboxylic acids **2.3.3.9**, which were converted to the cinnamamides **2.3.3.10** using thionyl chloride followed by quenching with aqueous ammonia. Refluxing in toluene with chloral hydrate provided the corresponding chloralamides **2.3.3.11** that were readily converted to the chlorides **2.3.3.12**, a key synthon throughout their study. Substitution of the chloride with potassium thiocyanate yielded the isothiocyanates **2.3.3.13**. Finally, refluxing in THF with commercially available anilines provided the desired products **2.3.3.14** that were isolated following column chromatography.

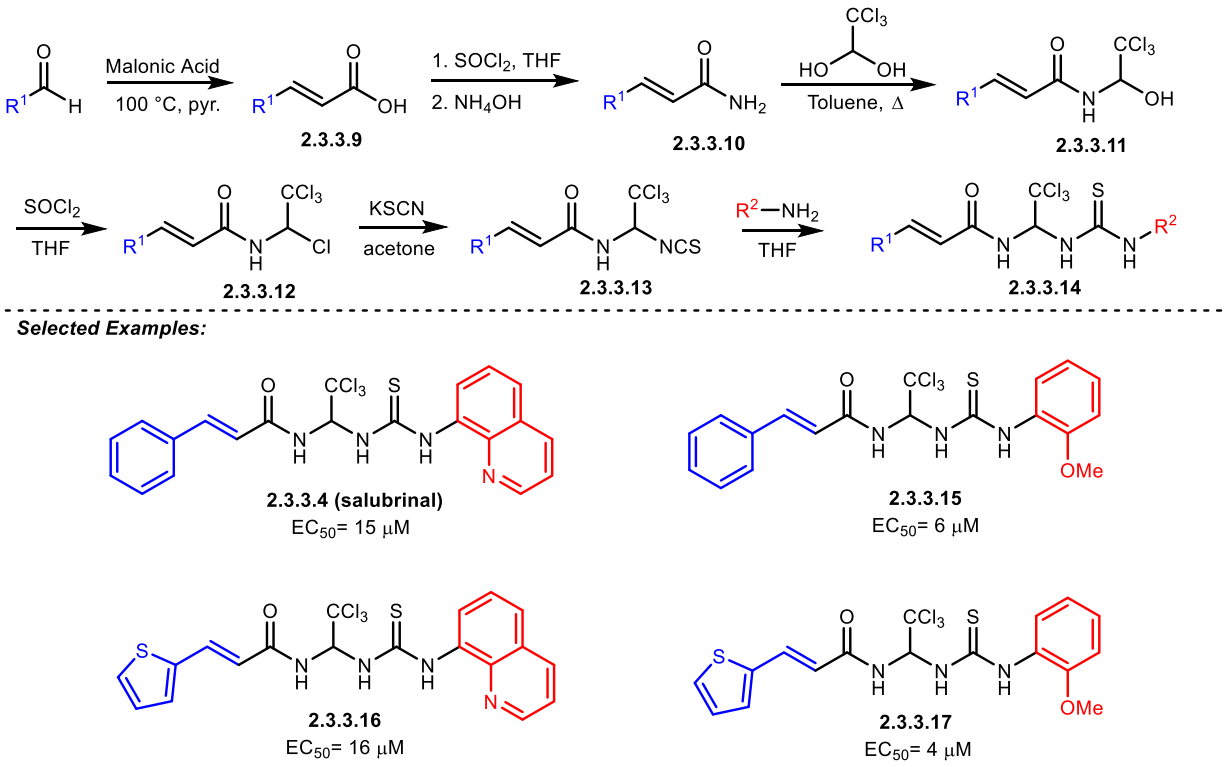

Figure 2.3.3.2 - Liu's Synthetic Route to Salubrinal Derivatives

The newly synthesized compounds were then screened for their ability to rescue cells from tunicamycin-induced ER stress using salubrinal as a positive control. Replacing the amino-quinoline ring with 2-methoxyaniline yielded substrate **2.3.3.15** which was roughly 3-fold more potent than salubrinal in their assay. Furthermore, replacing the phenyl substituent and the amino-quinoline moiety with thiophenyl, provided **2.3.3.17**, which had an even lower EC_{50} value of 4 μM.

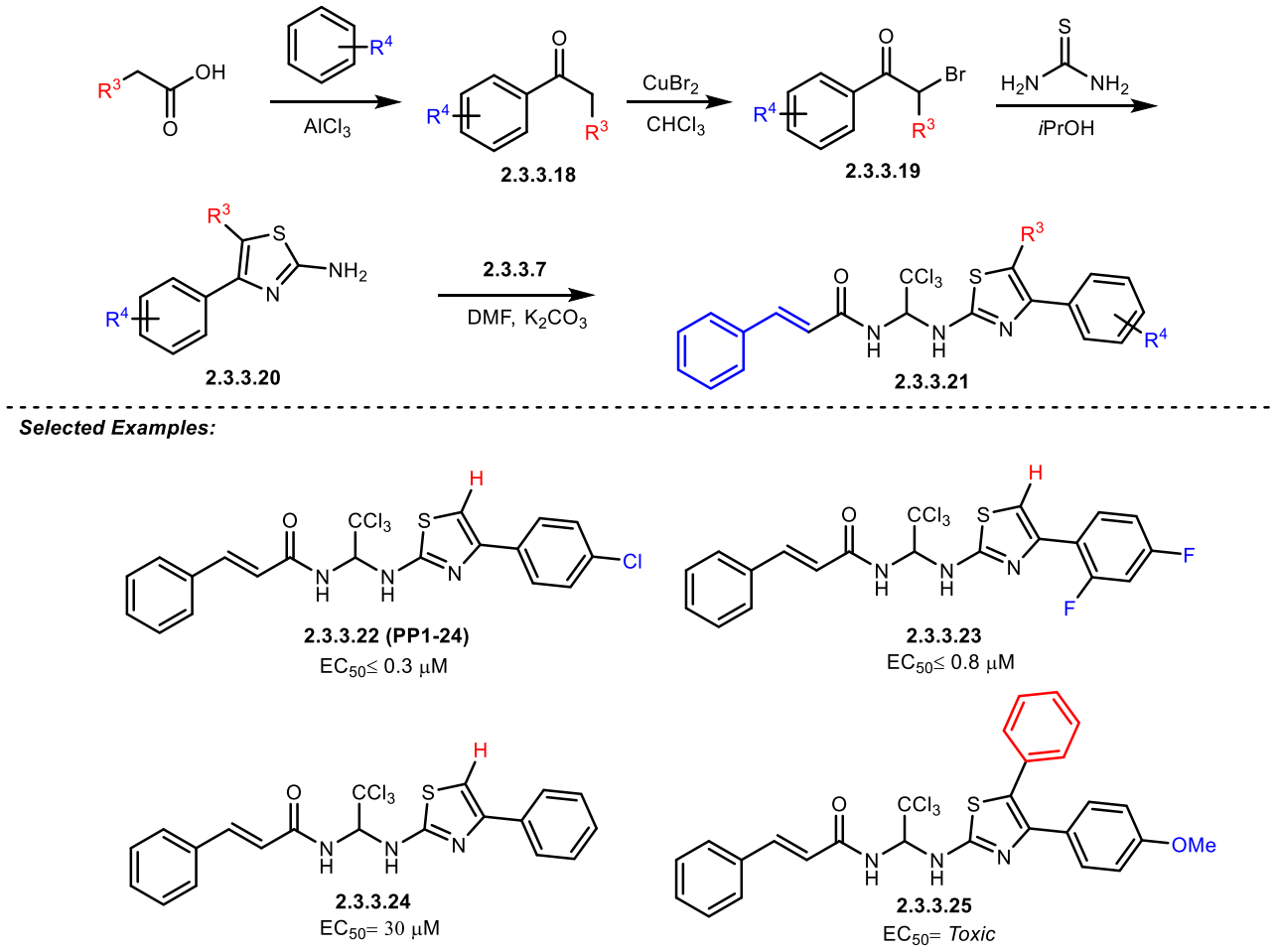

Figure 2.3.3.3 – Synthesis of Aminothiazole Derivatives

Based on these preliminary results, Liu *et al.* designed and synthesized several novel thiazole-based derivatives of salubrinal (Figure 2.3.3.3). Friedel-Crafts acylation of substituted acetic acids, followed by bromination, and finally thiazole cyclization with thiourea provided the aminothiazole derivatives **2.3.3.20**. When combined with the chloralamide derivative **2.3.3.7** in DMF in the presence of potassium carbonate, substitution occurred to yield to the desired thiazole derivatives **2.3.3.21**. In their biological assay, **2.3.3.22** (herein referred to as PP1-24) proved to be ~50-fold more potent than salubrinal with an $EC_{50} \leq 0.3$ μM. Interestingly, when they replaced the *para*-chloro on PP1-24 with a proton, a dramatic drop in activity was observed for **2.3.3.24**. Moreover, replacing the proton on the thiazole ring with a much larger substituent, such as a phenyl group, resulted in a cardiotoxic compound **2.3.3.25**. Regardless, they developed several analogs with markedly increased potency compared to that of salubrinal. With this preliminary assay data and the help of 3D-QSAR studies, the authors concluded that changing the steric and electronic

profile of the -R^2 substituent has the largest impact on the overall activity of the compound (Figure 2.3.3.4).

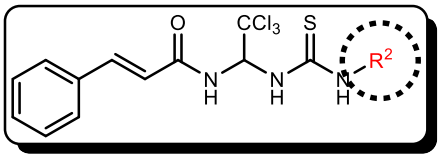

Figure 2.3.3.4 – Substitution of -R^2 Led to Most Prominent Changes in Compound Activity

Although they make no further progress determining the cellular target or biological mechanism of action of this class of compounds, they show that even minor chemical modifications to this scaffold can lead to the development of more potent analogs, therefore setting the stage for further work in this area.

2.3.4 – Structural and Functional Analysis of the GADD34/PP1 Complex

During the time that these two initial studies were conducted, the innate specificity of salubrinal to effect cellular eIF2α phosphorylation was thought to arise from its disruption of the GADD34/PP1 complex. Whether it prevented this complex from forming and subsequently recruiting and dephosphorylating eIF2α, or it targeted the complex after formation causing its dissociation, remained unknown. However, the exact molecular basis by which GADD34 initially recruits PP1 to form the complex, as well as how this complex binds to its substrate eIF2α, were not understood. This lack of understanding significantly hindered the ability to develop small molecule therapeutics aimed at inhibiting this holoenzyme.

In 2015, Meng Choy and coworkers provided a complete structural and functional analysis of the GADD34/PP1 complex wherein they elucidated the process of GADD34 mediated recruitment of PP1 and subsequent binding to its substrate eIF2α.[21] The GADD34 domain was found to consist of an ER-targeting helix, 4 central PEST repeats, and a C-terminal PP1-binding domain. Using the crystal structure of the holoenzyme, it was identified that GADD34 uses two specific motifs, RVxF and ΦΦ, to selectively bind PP1 to form the functional phosphatase (Figure 2.3.4.1). Two residues, Phe558 and Val556, that constitute the RVxF motif in GADD34, were found to bind the hydrophobic RVxF-binding pocket present on the surface of PP1. Additionally,

GADD34 binds to PP1 via the ΦΦ motif, with His565 forming a π-stacking interaction with Tyr78 in PP1.

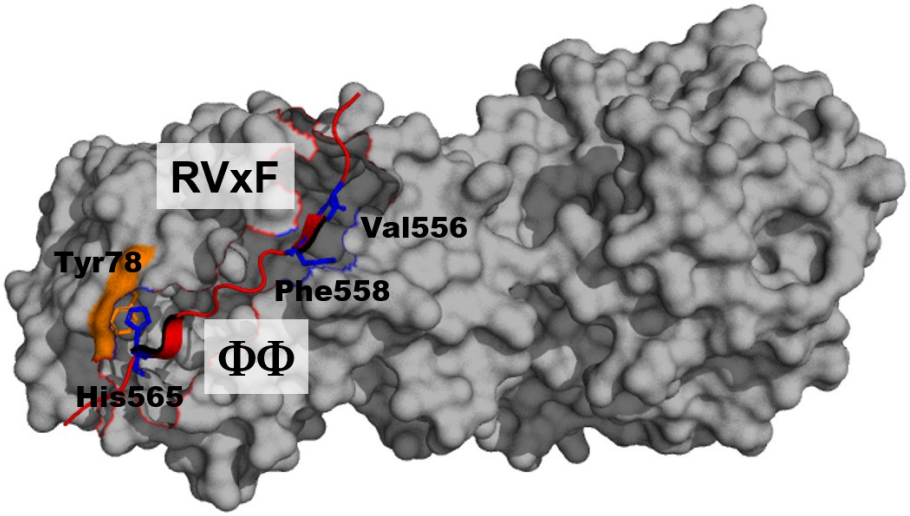

Figure 2.3.4.1 – GADD34/PP1-Binding Domain Highlighting the Two Primary Interaction Sites

Previously, it had been hypothesized that it was this activated complex that recruited eIF2α via a specific binding site within the C-terminal PP1-binding domain of GADD34. However, immunoprecipitation experiments confirmed that GADD34 recruitment of eIF2α is mediated by the GADD34 PEST domain and occurs independently of PP1. This study demonstrated that instead, GADD34 acts as a scaffold that brings PP1 close in proximity to the substrate eIF2α. With a better understanding of the molecular machinery responsible for the formation and recruitment of eIF2α by this holoenzyme, the authors wanted to probe the effects of salubrinal on this process. By reconstituting a purified GADD34/PP1 complex in vitro, they examined the ability of salubrinal to dissociate the holoenzyme. Surprisingly, no dissociation of the complex was observed. In fact, high concentrations of salubrinal seemed to enhance the binding of GADD34 to PP1. Additionally, the presence of salubrinal had no detectable effect on the binding of PP1 or eIF2α to GADD34. This information alone highlights the need for the understanding of the mechanism of action of this class of molecules. Moreover, the structural information of the GADD34/PP1 holoenzyme gained through this study may provide new avenues for the identification of small molecules that disrupt this complex.

2.3.5 – A Piperazine-Derived Compound Capable of Inactivating eIF2α

The development of salubrinal and its analogs have significantly impacted our ability to study the cell's response to ER stress and has therefore aided in our understanding of diseases that are implicated by the dysregulation of the eIF2α dephosphorylation pathway. However, salubrinal has a broad scope of working concentrations and its cellular target remains illusive, prompting the search for a new small molecule probe. In a high-throughput screen for compounds that inhibit ER stress-induced cell death, Hong *et al.* identified the small molecule AMC-01 and its derivatives (Figure 2.3.5.1).[22] Using thapsigargin, a UPR activator that raises cytosolic Ca^{2+} concentrations, over 50,000 compounds were screened for their cytoprotective effects, using salubrinal as a positive control. From this screen came 26 active compounds, 4 of which shared a benzyl-piperazine benzamide core.

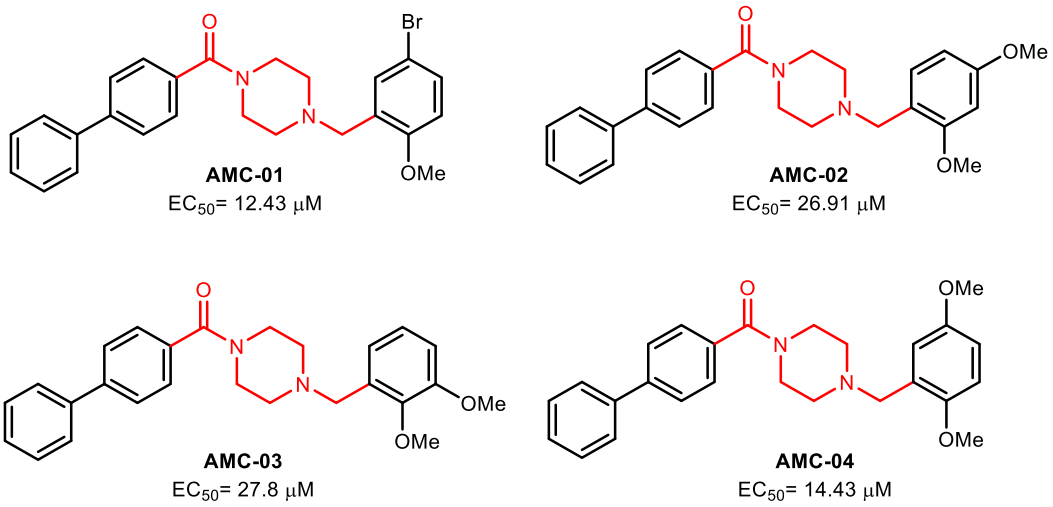

Figure 2.3.5.1 – AMC-01 and its Derivatives

In their assay, all 4 of the AMC compounds displayed lower EC_{50} values than salubrinal, with the most potent analog being AMC-01 having an EC_{50} value ~3-fold lower than that of salubrinal. Using immunoblotting, they showed that the AMC compounds are capable of inducing eIF2α phosphorylation in a dose-dependent manner at lower working concentrations than salubrinal. To determine the mechanism by which the AMC compounds were inducing eIF2α phosphorylation, they examined its effects on all four of the kinases that are known to

phosphorylate eIF2α under stress conditions once the UPR has been activated. They found that RNA-dependent protein kinase PKR was readily activated by pre-incubation with AMC-01, whereas it had no detectable effect on PERK. This suggests that AMC-01, in part, helps to activate PKR in response to stress leading to prolonged eIF2α phosphorylation. Another possible mechanism of action of AMC-01 could be the inhibition of eIF2α dephosphorylation via interactions with the GADD34/PP1 complex, a mechanistic hypothesis shared with that of salubrinal. However, they provide no evidence of this and state that mechanistic investigations are currently underway.

As detailed in this Section, a considerable amount of work has been devoted to the design and development of small molecules that rescue cells from ER stress-induced apoptosis. Through structure optimization studies it has been shown that modifications made to the salubrinal scaffold can lead to enhanced potency at lower administered concentrations. After the discovery of sal003's ability to expand skeletal muscle stems *ex vivo* by Crist and coworkers, we were approached and asked to solve the problem of synthesizing more potent compounds for their assays with the prospect of developing a therapeutic treatment to aid in stem cell transplantation.

2.4 Synthesis of sal003 and Analogs

2.4.1 – Synthesis of sal003 and Analogs

In collaboration with Dr. Colin Crist (McGill University, Lady Davis Institute for Medical Research) we planned to develop and synthesize more potent analogs of sal003, which enable *ex vivo* expansion of muscle stem cells that retain regenerative capacity. Furthermore, we set out to design a suitable PAL of sal003 to be used to identify its cellular target(s) and provide valuable information regarding its mechanism of action.

As a point of departure, we planned to synthesize a panel of salubrinal derivatives that had been previously reported by Liu and coworkers. Although the biological contexts are vastly different, it serves as a crucial point of comparison, since in both cases it is hypothesized that sal003 and its analogs suppress protein translation by inhibiting the dephosphorylation of eIF2α. But before any analogs could be made, of utmost importance was the ability to reproduce the synthesis of sal003 in our lab and ensure that its activity was consistent with that of material purchased from Sigma-Aldrich.

In the work published by Liu in 2012 they provide an extremely brief overview of the synthesis of this class of compounds wherein they state the reagents used in each step but provide no experimental/characterization data of any intermediates. Additional literature searches for any experimental details proved futile and any references found were patents containing very minimal information. Nevertheless, using the scheme provided by Liu as a rough guideline, commercially available benzaldehyde was converted to the unsaturated carboxylic acid **2.4.1.1** by refluxing in pyridine in the presence of malonic acid and catalytic amounts of piperidine (Scheme 2.4.1.1). Amidation proceeded smoothly via acid chloride formation followed by quenching with cold NH_4OH to yield **2.4.1.2**. A mixture of the cinnamamide and chloral hydrate were then heated to reflux in toluene for 12 hours using a Dean-Stark trap to yield the chloral amide **2.4.1.3**, which was isolated via vacuum filtration. It was found that using 2 equivalents of chloral hydrate was required in order to drive the reaction to completion. Subsequent chlorination of **2.4.1.3** using thionyl chloride with a catalytic amount of DMF provided **2.4.1.4** almost quantitatively as a light-yellow powder. The chloride was then converted to the isothiocyanate **2.4.1.5** using potassium thiocyanate in refluxing acetone. With compound **2.4.1.5** in hand, the last remaining step was the coupling of 4-chloroaniline with the isothiocyanate, a seemingly simple transformation that has been reported to proceed in 2 hours in refluxing THF.[20] Initial attempts to reproduce this were unsuccessful, and resulted in complete recovery of starting materials. Following the mechanochemical procedure reported in 2012 by the Friščić group,[23] **2.4.1.5** was combined with 4-chloroaniline in a mortar and ground manually with a pestle for 10 minutes to yield the coupled product **2.4.1.6** (sal003) in a 78% isolated yield as a white powder following column chromatography, with the remaining mass balance being unreacted starting material.

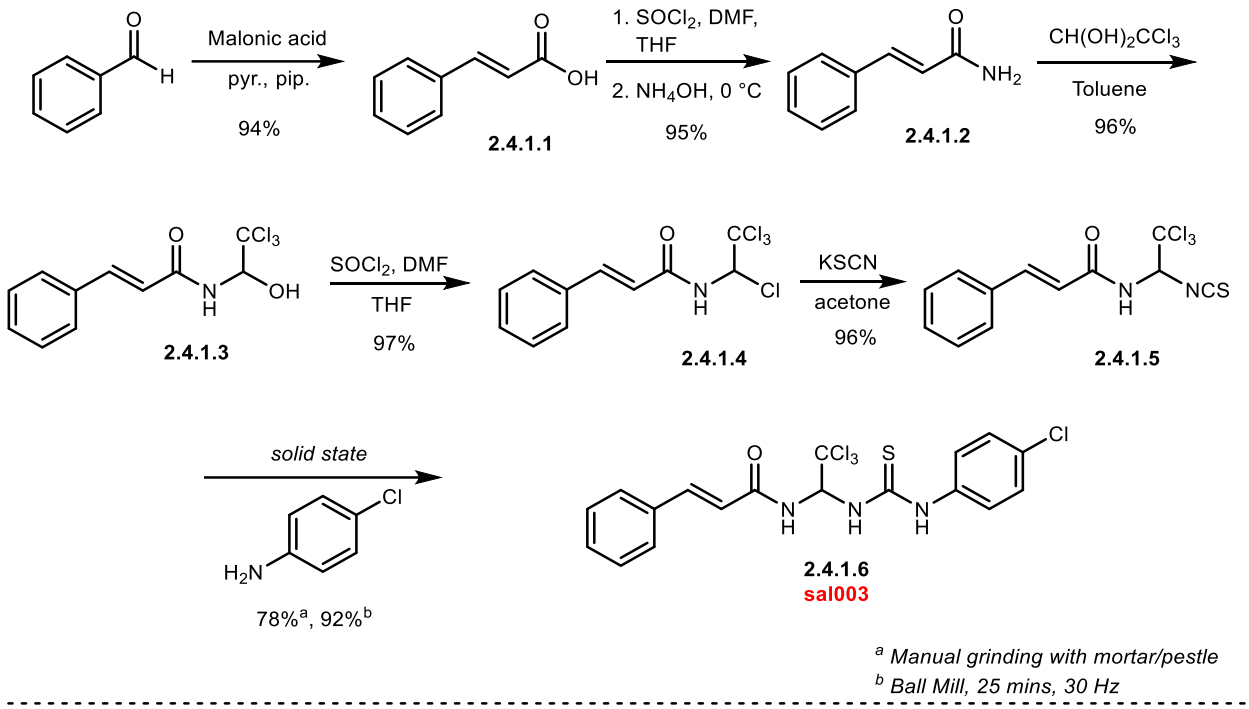

Scheme 2.4.1.1 Initial Synthesis of sal003

After obtaining this promising result, the coupling reaction was run in a Retsch MM200 mill for 25 minutes at 30 Hz, isolating **2.4.1.6** in a 92% yield following flash chromatography. Aside from ease in isolation/purification of the product, this solvent-free method provides a greener alternative to the synthesis of a class of biologically active compounds, an extremely attractive feature should these molecules ever become marketed pharmaceuticals. However, the limiting feature of the ball-milling reaction in the lab is the scalability, as the combined maximum mass of reagents placed into the Teflon jar cannot exceed 250 mg. However, for the purposes of preliminary biological screening, this provides more than ample amounts of material. In the cases where a compound exhibited a high potency, an alternative approach would have to be taken in order to synthesize larger quantities of these materials. It was hypothesized that refluxing in THF did not provide a sufficient amount of thermal energy to form the thiourea moiety, whereas the mechanical energy provided during ball-milling did. Therefore, in the interest of scalability, this process was investigated further. It was found that heating the isothiocyanate with the aniline in a sealed vessel at 80°C for 12 hours in THF, led to complete consumption of starting material and allowed for the gram-scale synthesis of analogs.

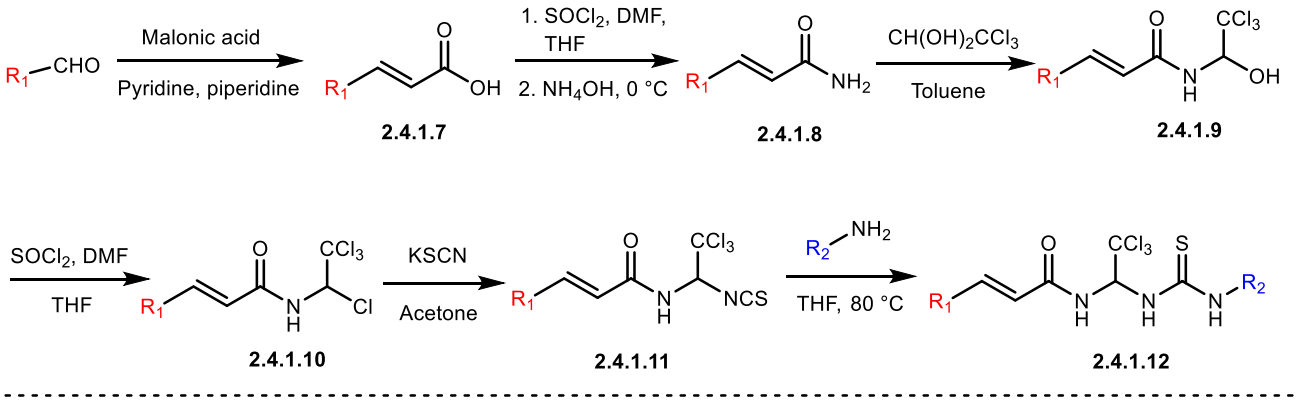

Scheme 2.4.1.2 – General Synthetic Pathway of sal003 Analogs

With an optimized synthetic procedure, we next assembled a library of compounds for our preliminary biological assays. Following the general synthetic pathway depicted in Scheme 2.4.1.2, a number of different anilines were coupled to isothiocyanate **2.4.1.11** to provide a panel of compounds with differing substituents on the aniline (Table 2.4.1.1). In the initial stages of the compound synthesis and development, we selected anilines containing electronically and sterically different functional groups at varying positions on the ring to gain some preliminary insight into how this effects the overall compound activity. In the case of analog **2.4.1.17**, 2-thiophenecarboxyaldehyde was carried through the synthetic pathway depicted in Scheme 2.4.1.2. Compound **2.4.1.33** was synthesized using benzyl protected 4-hydroxybenzaldehyde, which was subsequently deprotected to provide **2.4.1.35**. For compound **2.4.1.34**, 4-methoxybenzaldehyde was carried through the synthesis depicted above. The rationale behind the synthesis of these three compounds will be discussed in Section 2.5.

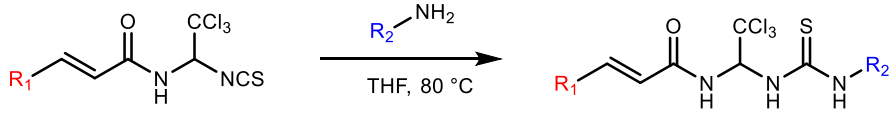

2.4.1.11 **2.4.1.12**

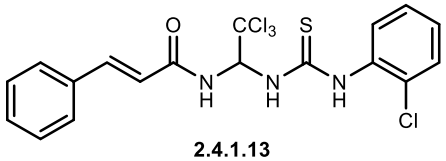

2.4.1.13

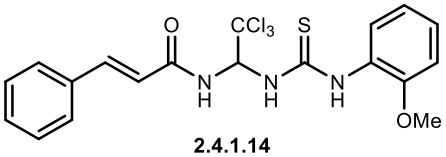

2.4.1.14

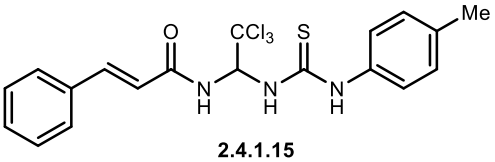

2.4.1.15

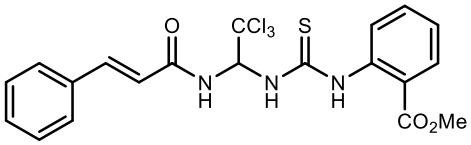

2.4.1.16

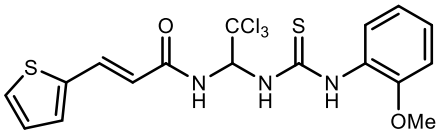

2.4.1.17

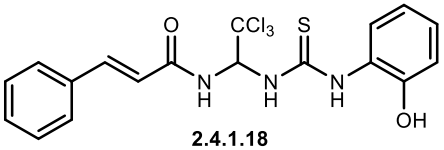

2.4.1.18

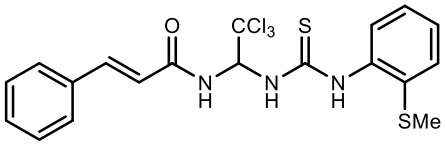

2.4.1.19

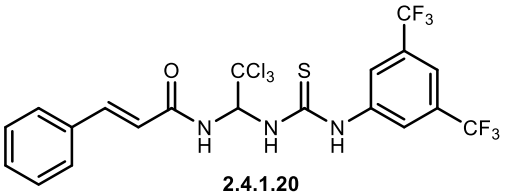

2.4.1.20

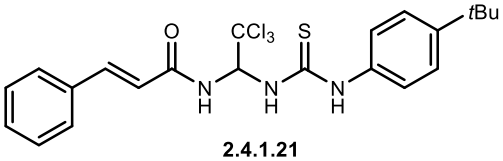

2.4.1.21

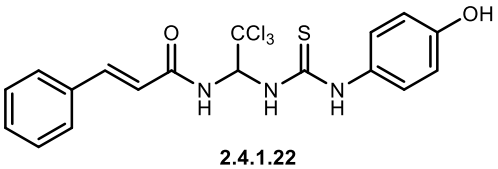

2.4.1.22

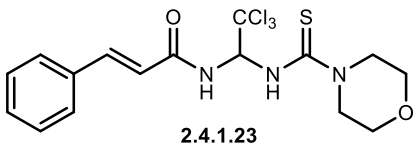

2.4.1.23

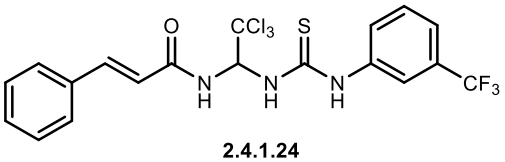

2.4.1.24

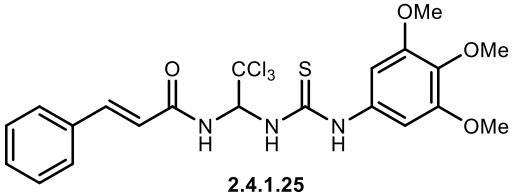

2.4.1.25

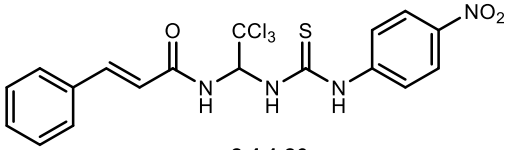

2.4.1.26

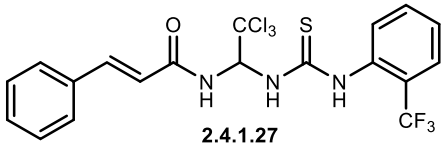

2.4.1.27

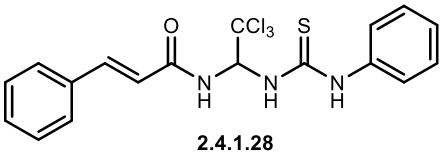

2.4.1.28

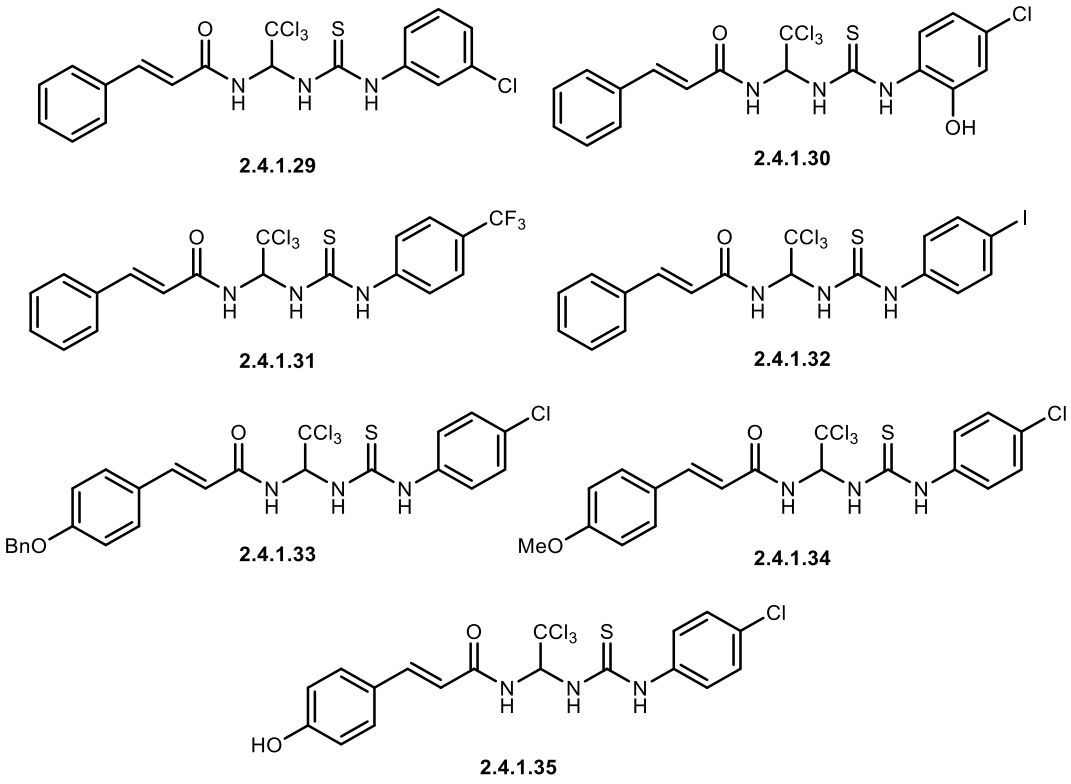

Table 2.4.1.1 – Synthetically Prepared sal003 Analogs

As discussed earlier in Section **2.3.3**, an extremely potent analogue from Liu's work was PP1-24, containing a thiazole ring in place of the thiourea group. The synthesis of the amino-thiazole ring started with the alpha-bromination of commercially available 4-chloroacetaphenone to yield **2.4.1.36** as a white crystalline solid. This was converted to the amino-thiazole through a substitution/condensation reaction under basic conditions using thiourea to obtain **2.4.1.37**. At first glance, the final substitution reaction between the amino-thiazole and chloride **2.4.1.4** seemed to be relatively straightforward, with Liu reporting conditions of K_2CO_3 in DMF at room temperature. Initial attempts to reproduce this result were not successful, and no reaction was observed even when the temperature was increased to 100 ºC.

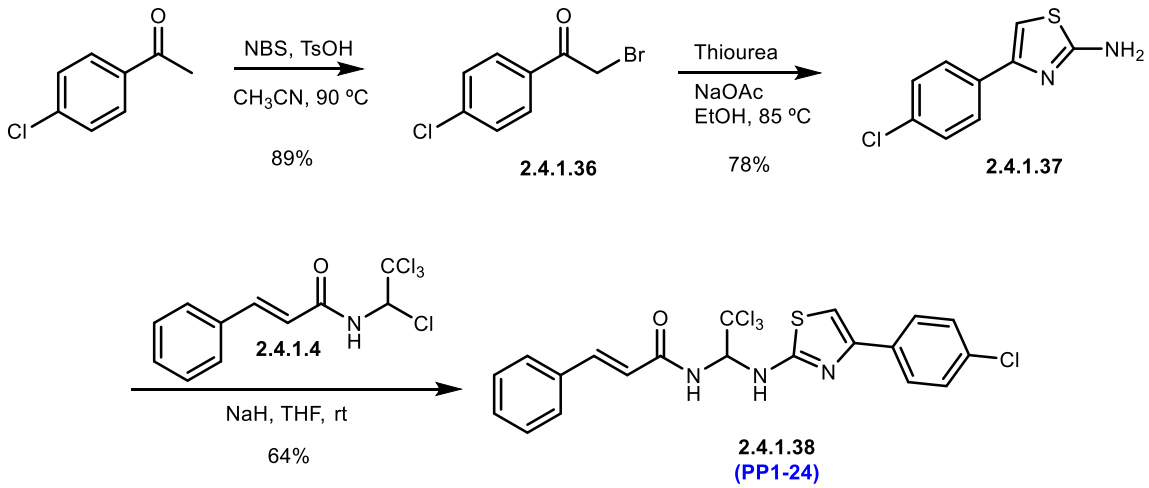

Scheme 2.4.1.3 – Synthesis of PP1-24

Owing to the earlier success of coupling the isothiocyanate with anilines in the solid state, this reaction was tested under the same set of conditions. Unfortunately, no reaction was observed and only starting material was recovered. Further investigation of this seemingly simple reaction prompted us to question the innate nucleophilicity and pKa of the amino-thiazole. If the amine was not acidic enough to be deprotonated by K_2CO_3, nor was it nucleophilic enough to undergo substitution as the neutral species, a much stronger base would need to be used. Satisfyingly, pre-mixing sodium hydride with **2.4.1.37**, followed by addition of the chloride **2.4.1.4** led to the desired coupled product **2.4.1.38** in a 64% isolated yield.

2.4.2 – Synthesis of AMC-01

As discussed in Section **2.3.5**, the AMC series of piperazine-based compounds proved to be more effective inhibitors of ER stress-induced apoptosis than salubrinal. In parallel with the design and synthesis of novel sal003 analogs, we wanted to synthesize AMC-01 for testing in our assay. However, no syntheses have been reported for this class of compounds in the literature, prompting us to develop a relatively straightforward and convergent approach (Figure 2.4.2.1).

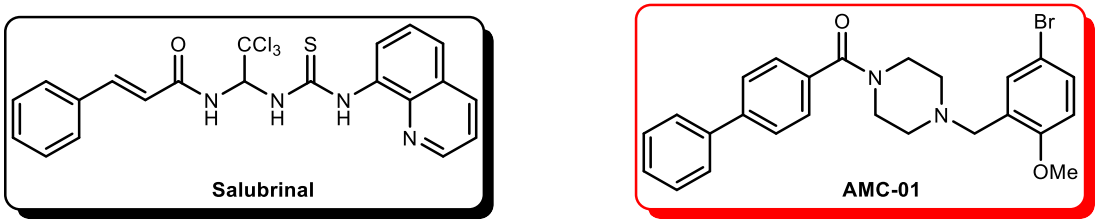

Figure 2.4.4.1 – Structures of Salubrinal and AMC-01

The synthesis began by reducing commercially available 5-bromo-2-methoxybenzaldehyde to the alcohol (**2.4.2.1**) using $NaBH_4$ in methanol, followed by conversion to the alkyl bromide coupling partner **2.4.2.2** using PBr_3 in DCM (Scheme 2.4.2.1). This was then coupled to Boc-protected piperazine **2.4.2.3** to generate the desired C-N linkage, which was subsequently Boc-deprotected using TFA in 1,2-dichloroethane to afford **2.4.2.4** in a 92% yield over two steps. The Boc-deprotection was problematic at first as no reaction was observed in DCM at room temperature, prompting further investigation. After refluxing the mixture in DCM, a small amount of the desired product spot became visible via TLC, which suggested that heating was necessary. The solvent was then switched to 1,2-DCE to allow the temperature to be increased further, and the reaction proceeded to completion after 2 hours to provide the desired free amine **2.4.2.4**. To synthesize the second coupling partner, commercially available 4-biphenylcarboxylic acid was converted to the acid chloride **2.4.2.5** using thionyl chloride in a 96% yield. The amine was then coupled with the prepared acid chloride **2.4.2.5** in DCM to afford AMC-01 (**2.4.2.6**) as an off-white solid in a 76% isolated yield.

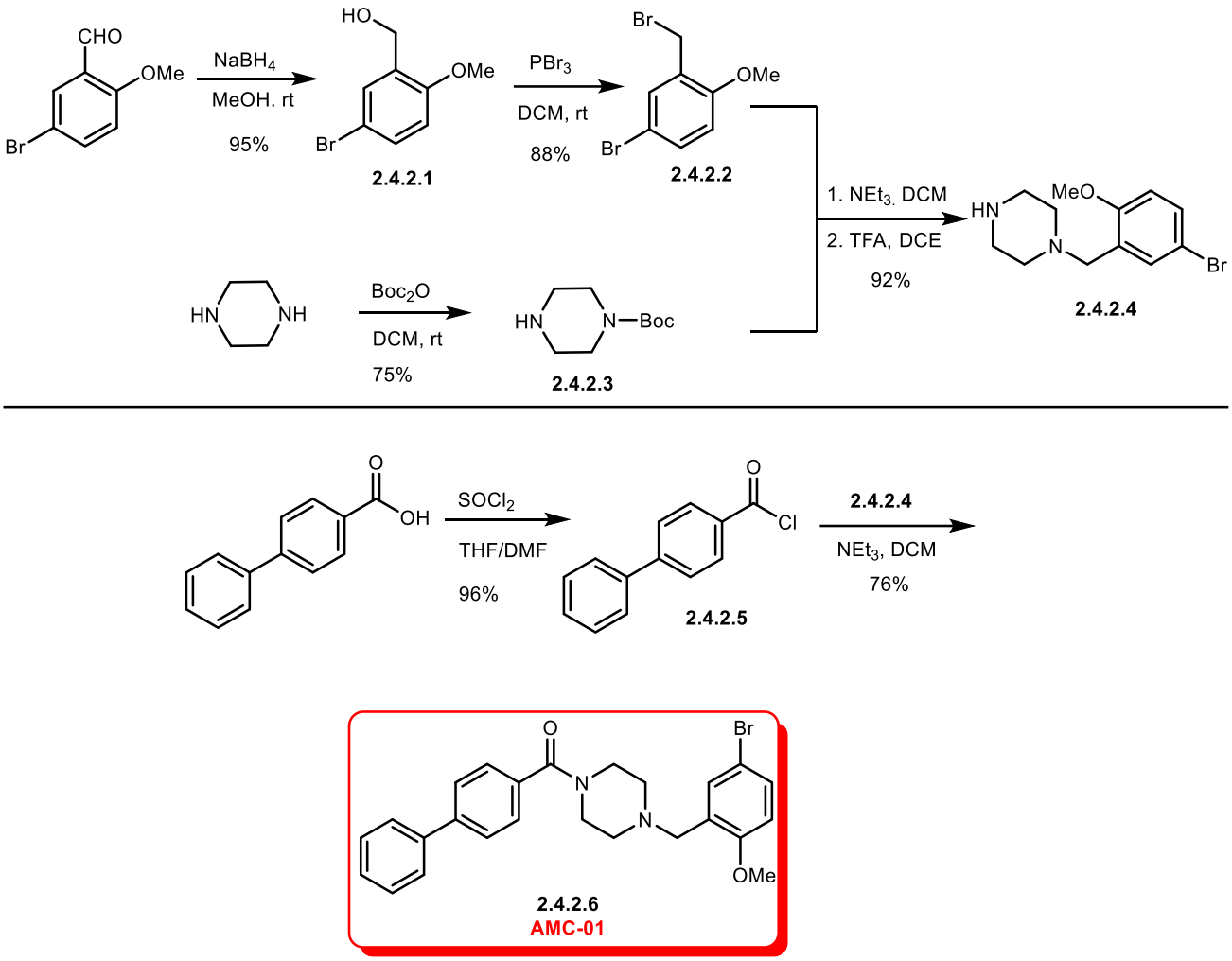

Scheme 2.4.2.1 – Convergent Synthesis of AMC-01

At this point, no further analogs have been synthesized; however, this is an avenue that we plan to pursue further in the future as well as synthesizing a PAL of AMC-01 to be used for target identification in the context of inhibiting ER stress-induced apoptosis.

2.4.3 – Design and Synthesis of Hybrid Compounds

At this point in the project we had two structurally diverse classes of small molecules, with two separate hypothesized mechanisms of action. In the case of sal003, it was believed that it acted to inhibit the dephosphorylation of eIF2α, whereas in the case of AMC-01, it was believed that it acted to promote the phosphorylation of eIF2α. Therefore, we hypothesized whether the combination of the potential active components of both classes of compounds would have a synergistic effect to maintain quiescence in satellite cells by simultaneously inhibiting

dephosphorylation, and promoting phosphorylation of eIF2α. With this in mind, we designed two distinct hybrid molecules as synthetic targets that are comprised of functional groups deemed essential from both classes of compounds (Figure 2.4.3.1). The rationale behind the design of these compounds was two-fold. Firstly, the components of both classes of compounds that had been deemed essential for activity from previous assays could be combined in a way that would be synthetically feasible and potentially provide highly potent compounds. Secondly, the hybrids were a completely novel class of compounds that would allow us access to brand new IP space, should they prove to be potent analogs.

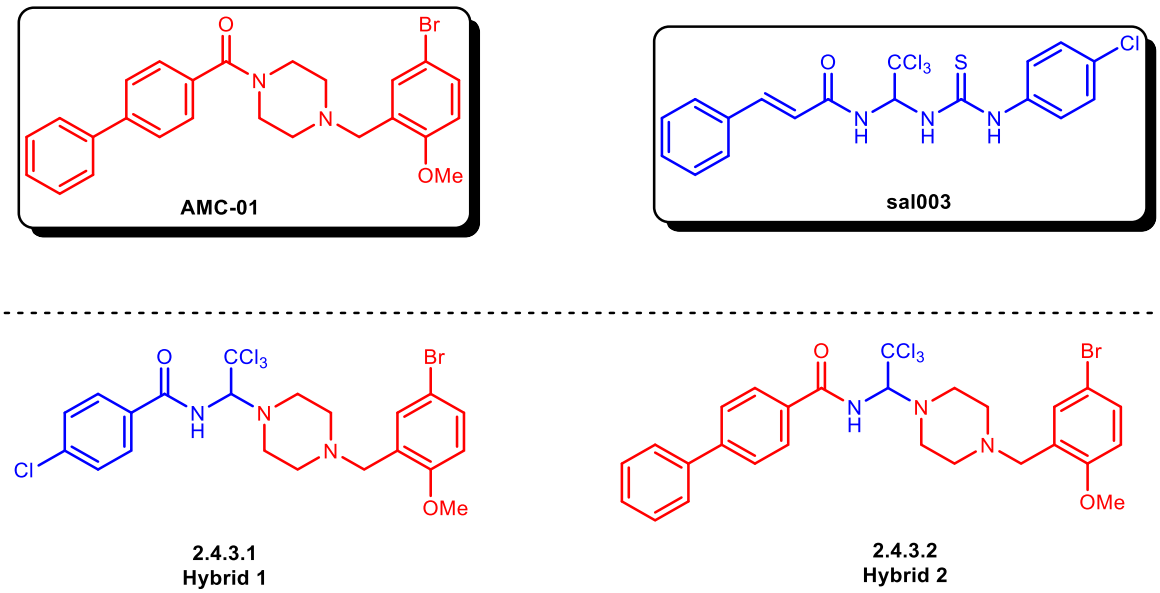

Figure 2.4.5.1 – Design and Structures of Hybrid Molecules

To prepare these compounds, a combination of procedures used to synthesize the sal003 analogs and AMC-01 were employed. The synthesis and characterization of these two novel compounds was conducted by undergraduate student Océane Marescal. The synthesis of **2.4.3.1** began by treating commercially available 4-chlorobenzamide with chloral hydrate in refluxing toluene to yield the chloralamide **2.4.3.3** that was then converted to the chloride coupling partner **2.4.3.4** with thionyl chloride (Scheme 2.4.3.1). The chloral amide **2.4.3.4** was then coupled with **2.4.2.4** in refluxing 1,2-DCE with NEt_3 to yield the desired compound **2.4.3.1** and the first hybrid compound in a 52% isolated yield.

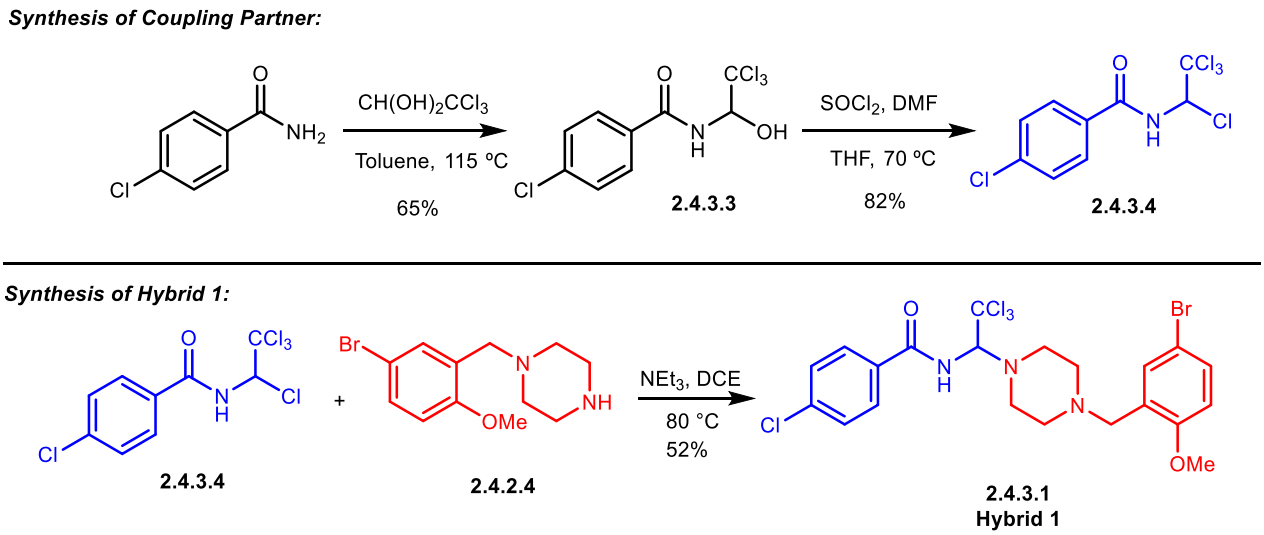

Scheme 2.4.5.1 – Synthesis of Hybrid Compound 1

The synthesis of hybrid compound 2 began by converting intermediate **2.4.2.5** into an amide by quenching the acid chloride with ammonium hydroxide to provide **2.4.3.5** quantitatively (Scheme 2.4.5.2). Heating the amide to reflux in toluene in the presence of chloral amide afforded chloral amide **2.4.3.6**, which was treated with thionyl chloride to afford the chlorinated coupling partner **2.4.3.7**. This was then combined with the free amine **2.4.4.4** in a similar fashion as above to undergo substitution and provide our second hybrid compound **2.4.3.2** in a 58% isolated yield.

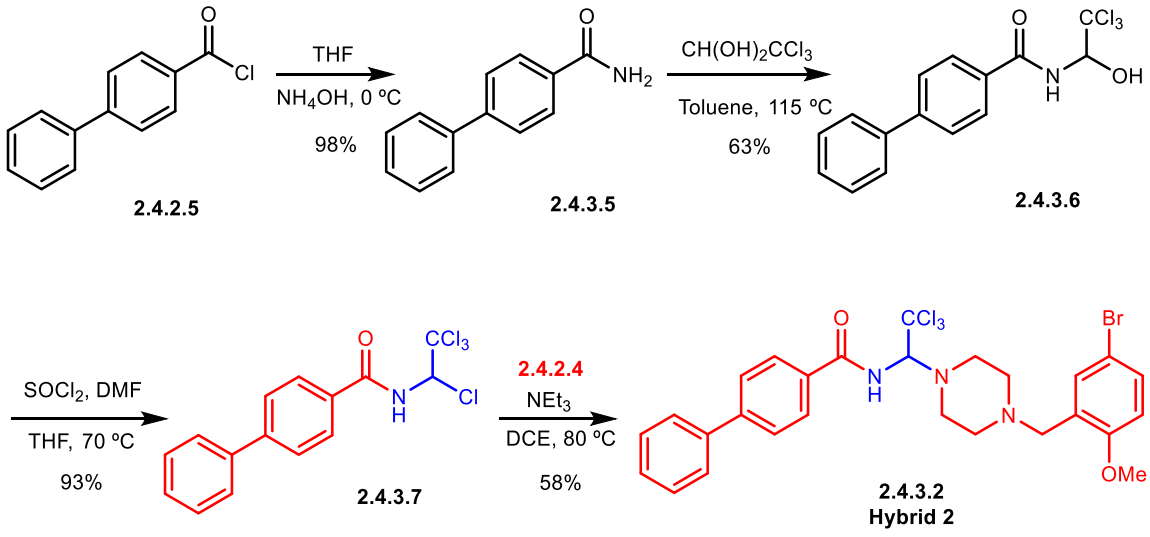

Scheme 2.4.3.2 – Synthesis of Hybrid Compound 2

In conjunction with the testing of these compounds in our preliminary biological assay, we would like to test the effects of co-administering sal003 and AMC-01 to see if any synergistic effects can be observed.

2.4.4 – Biological Activity of Analogs

All synthesized compounds were then tested in a bioluminescence assay for their ability to expand satellite cells at an administered concentration of 10 μM. Satellite cells isolated from *Pax3*$^{GFP/+}$*; tg(actb-luc)* mice were cultured in 96 well plates under normal conditions in the presence of sal003 and its analogs. At different culture times luciferase activity was analyzed by addition of D-luciferin to satellite cells and measured quantitatively using a bioluminometer. Proliferating satellite cells undergoing self-renewal show an increase in luciferase levels compared to the control (DMSO). Whereas cells that activate the myogenic program will begin to differentiate and therefore not self-renew, resulting in a plateau of luciferase levels. However, the preliminary assay only provides data on whether the cell culture has increased in size and does not identify if the cells have maintained their ability to self-renew, or if they have begun to differentiate. The analogs that display an increase in luciferase levels would then be tested in a secondary immunofluorescence screen containing antibodies against Pax7 and *MyoD* as well as an immunoblotting assay containing antibodies against total and phosphorylated eIF2α (P- eIF2α). In these assays, compounds are tested for their ability to upregulate Pax7 and maintain high levels of P-eIF2α. Top analogs from these two screens will then be evaluated for their effectiveness to expand satellite cells that retain their regenerative capacity in a preclinical mouse model of Duchenne muscular dystrophy.

The assays were performed in the laboratory of Dr. Colin Crist by MSc. Candidates Victor Chichkov and Graham Lean. The initial luminescence expansion assay was conducted to confirm that the sal003 being synthesized in the lab would perform as well as the sal003 being purchased from Sigma. It was found that this was in fact the case, as **2.4.1.6** had almost identical expansion numbers as the purchased material (Figure 2.4.4.1). In the same assay, four other synthesized compounds from Liu's work were screened to see if any trends were observed between the potency of compounds in their ability to protect cells from ER stress and expand skeletal muscle stem cells in culture. Satisfyingly, we observed similar trends with regards to potency as compounds **2.4.1.14**

and **2.4.1.17**, two potent compounds from Liu, had a greater ability to expand satellite cells than the parent compound sal003.

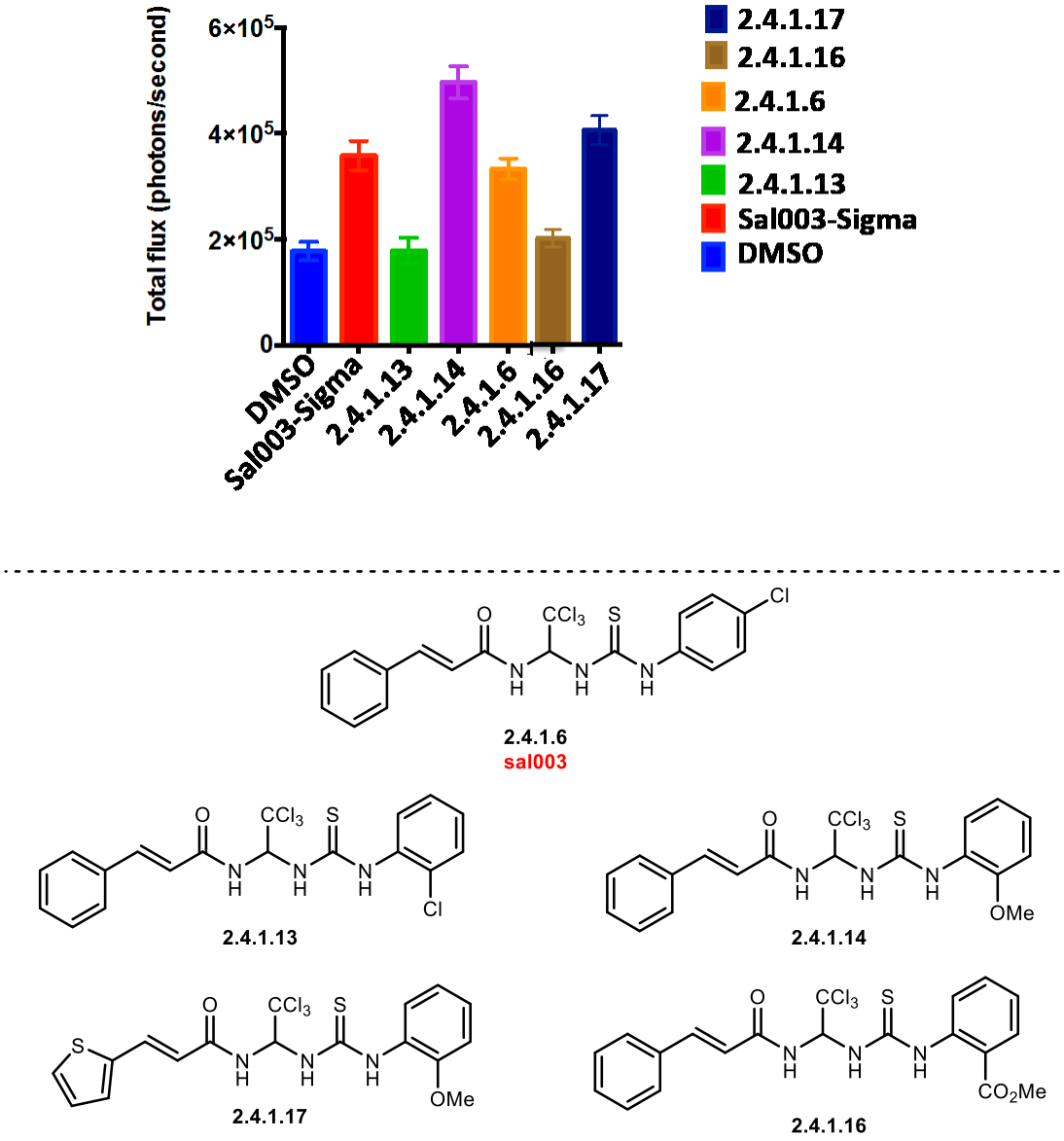

Figure 2.4.4.1 – Luminescence Assay Results at 4-day culture time with Corresponding Chemical Structures. Synthesized sal003 maintains identical activity to the purchased material.

We proceeded by screening another set of compounds in the luminescence assay to see if we could begin to understand how the minor structural modifications were changing the compounds activity. From this assay, it was found that over a culture period of 9 days, compound **2.4.1.18** bearing the meta hydroxyl group, had a greater ability to expand the satellite cell population in culture than sal003 (Figure 2.4.4.2). Additionally, compound **2.4.1.15** produced

almost identical results to that of sal003 and would therefore need to be investigated further. Also, compound **2.4.1.20**, containing bis-CF_3 groups in the meta positions, proved to be interesting as initially there was no expansion of cell numbers until day 5, when the luminescence signal began to rapidly increase. This observed lag of expansion, followed by rapid growth is an intriguing feature, which prompted us to examine compound **2.4.1.20** further.

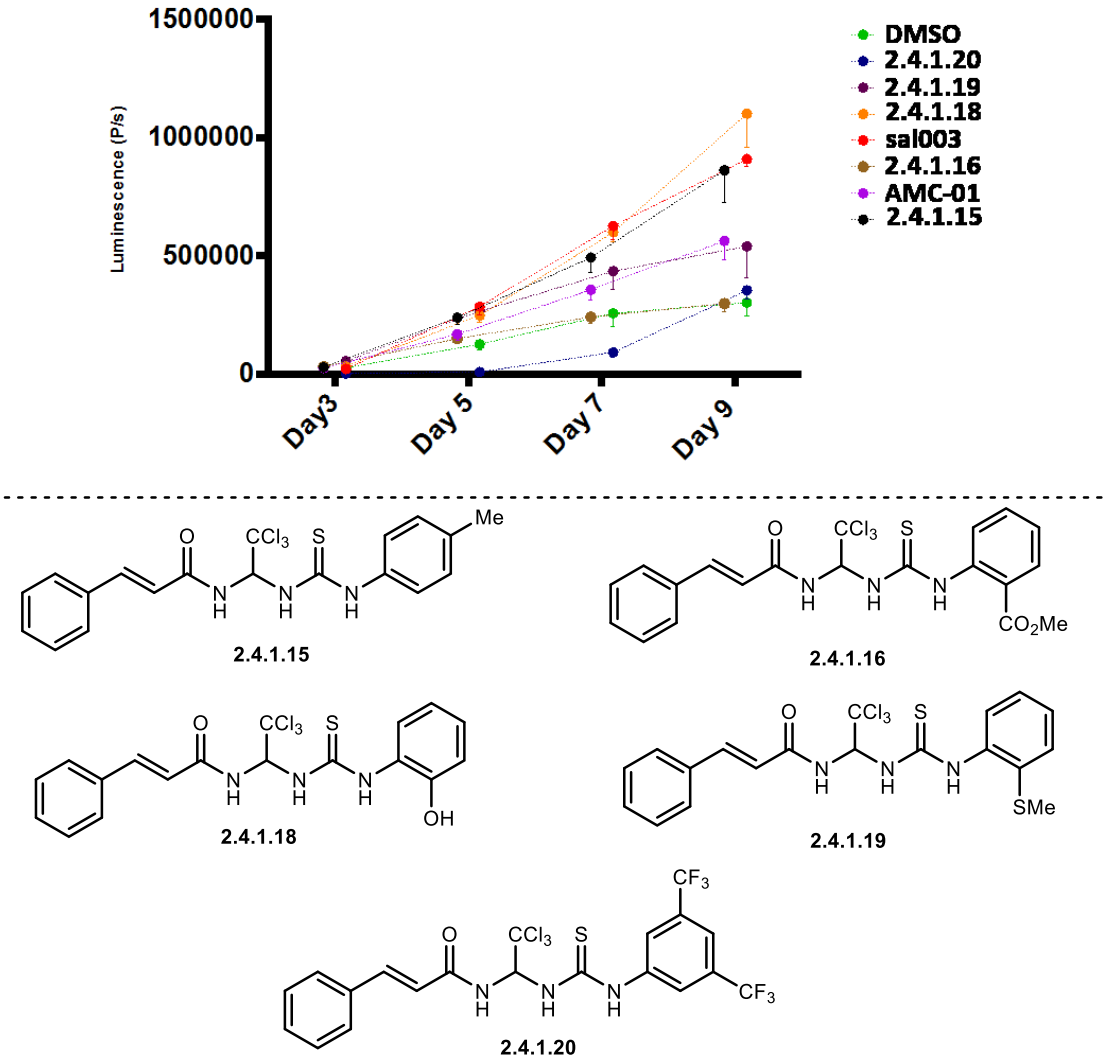

Figure 2.4.4.2 – Luminescence assay results of additional compounds after 9-day culture period

Further screening identified that compound **2.4.1.21**, bearing a *tert*-butyl group para to the thiourea, proved to be more efficacious to expand the population of satellite cells than sal003, while **2.4.1.22** and **2.4.1.23** exhibited no activity (Figure 2.4.4.3). Until day 7 of the assay, compound **2.4.1.21** displayed identical expansion kinetics to sal003. After this time period, the

expansion numbers with sal003 reached a plateau, whereas with **2.4.1.21** they continued to increase in size. This was a very interesting observation and we were interested to see if the expanded cell numbers maintained P-eIF2α in our secondary screen.

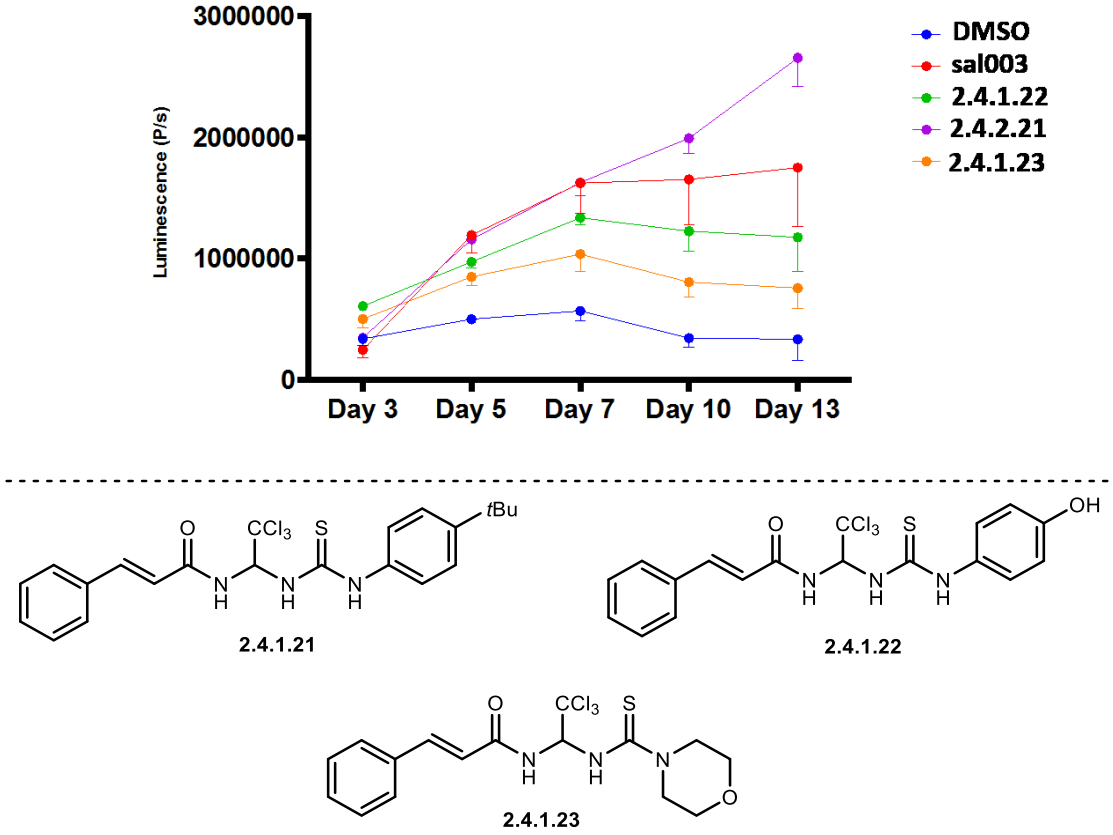

*Figure 2.4.4.3 – Compound **2.4.2.21** is more efficacious to expand satellite cells than sal003*

We next asked whether **2.4.1.20** could maintain its ability to expand skeletal muscle stem cells over a prolonged period of 13 days at a lower working concentration than sal003. If the dose of sal003 administered is less than 10 μM, it loses its activity in our assay. Therefore, we examined the effects of lowering the concentration of **2.4.1.20** to 5 μM and comparing its activity to that of sal003 at 5 μM (Figure 2.4.4.4). It was observed that **2.4.1.20** maintained its ability to expand satellite cells at 5 μM, while sal003 proved to be ineffective at this concentration. In fact, compound **2.4.1.20** administered at 5 μM is more potent in our assay than sal003 at 10 μM.

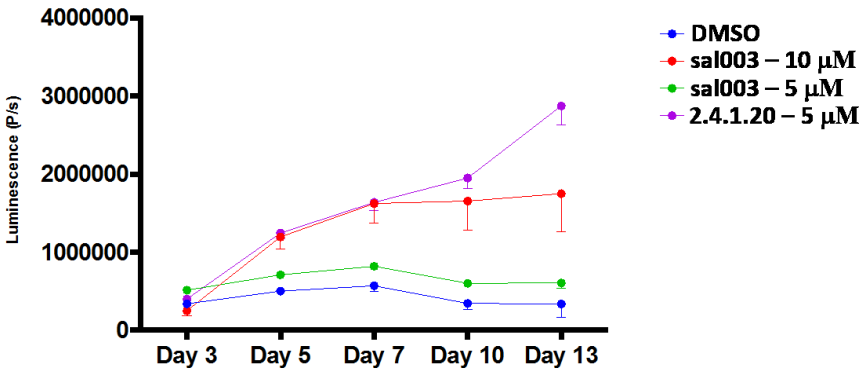

*Figure 2.4.4.4 – Compound **2.4.1.20** maintains its ability to expand muscle stem cells at 5 μM, the concentration at which sal003 loses activity*

As previously discussed, the luminescence assay only provides information on the ability of the compounds to expand the muscle stem cell culture and does not determine whether they have exited quiescence and activated the myogenic program. To determine this, the compounds were screened in the secondary Phospho-eIF2α assay for their ability to maintain phosphorylated eIF2α, thereby maintaining quiescence. They were screened relative to thapsigargin, which potently increases levels of P-eIF2α. From this assay, it was found that compound **2.4.1.20** was more efficient at maintaining P-eIF2α than sal003, demonstrating that it is capable of expanding skeletal muscle stem cells *ex vivo* that maintain P-eIF2α (Figure 2.4.4.5). Disappointingly, compounds **2.4.1.15** and **2.4.1.19**, which showed better expansion numbers than sal003 in our luminescence assay, were not efficient at maintaining P-eIF2α. That being said, we were very pleased with the results we had obtained using compound **2.4.1.20**. Not only did it outperform sal003 in both of our preliminary assays, but it also a novel compound itself, making these results even more exciting as it allows us to access new IP space.

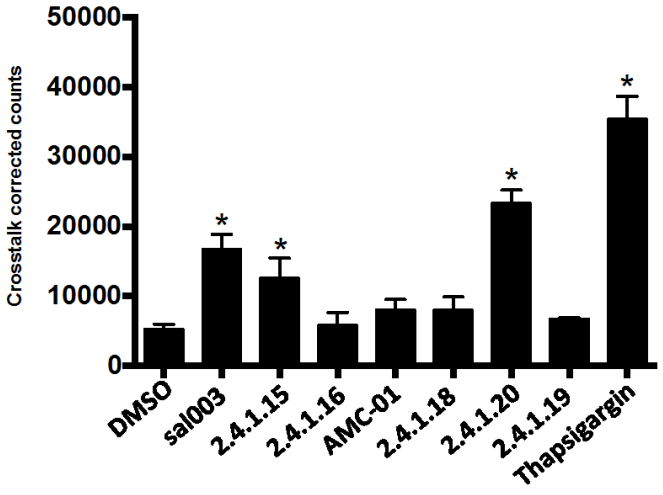

*Figure 2.4.4.5 – Compound **2.4.1.20** is more efficient than sal003 to maintain P-eIF2α*

With the preliminary results that we have obtained, we could begin to draw conclusions as to how the structural modifications impacted activity. The introduction of the Bis-CF_3 groups led to enhanced activity, as did the bulky *tert*-butyl group. It is well known that the introduction of CF_3 groups onto a drug scaffold can lead to a higher degree of lipophilicity and metabolic stability.[24] Whether the enhanced activity of compounds **2.4.1.20** and **2.4.1.21** is due to the enhanced lipophilicity remains unknown at this point and requires further investigation. However, it was quite apparent that even very minor modifications made to the scaffold of sal003 dramatically changed its ability to expand muscle stem cells. This of course draws attention to the longstanding question of what is the cellular target of sal003 and what is its mechanism of action in the cell. With the design and synthesis of a photoaffinity label (PAL) of sal003, we hope to identify this in the context of maintaining quiescence of satellite stem cells and then apply this knowledge to the broader scope of cells that have activated the UPR in response to ER stress.

Compound	MuSC Expansion	P-eIF2α
Sal003 (Sigma)	**Yes**	**Yes**
2.4.1.6 (sal003)	**Yes**	**Yes**
2.4.1.13	**No**	**tbd**
2.4.1.14	**No**	**tbd**
2.4.1.15	**Yes**	**<Sal003**
2.4.1.16	**No**	**No**
2.4.1.17	**No**	**tbd**
2.4.1.18	**Yes**	**No**
2.4.1.19	**No**	**No**
2.4.1.20	**Slow**	**>Sal003**
2.4.1.21	**Yes**	**tbd**
2.4.1.22	**No**	**No**
2.4.1.23	**No**	**No**
2.4.1.24	**tbd**	**tbd**
2.4.1.25	**tbd**	**tbd**
2.4.1.26	**tbd**	**tbd**
2.4.1.27	**tbd**	**tbd**
2.4.1.28	**tbd**	**tbd**
2.4.1.29	**tbd**	**tbd**
2.4.1.30	**tbd**	**tbd**
2.4.1.31	**tbd**	**tbd**
2.4.1.32	**tbd**	**tbd**

2.4.1.33	**tbd**	**tbd**
2.4.1.34	**tbd**	**tbd**
2.4.1.35	**tbd**	**tbd**
2.4.1.38	**Yes**	**tbd**
2.4.2.6 (AMC-01)	**No**	**tbd**
2.4.3.1 (Hybrid 1)	**No**	**No**
2.4.3.2 (Hybrid 2)	**No**	**No**

Table 2.4.4.2 – Summary and Screening Results of sal003 Analogs

One of the major challenges and limitations for us during the development of analogs was that we were receiving the results from the luminescence assay in several distinct pieces at different timepoints, which made it difficult for us to directly compare the activity of all our compounds. However, this did not deter us from assembling a library of sal003 analogs that were then screened in our biological assays for their ability to expand muscle stem cells and maintain P-eIF2α.

2.4.3 – Separation and Biological Activity of sal003's Enantiomers

It is well known that stereoisomeric compounds differ in their pharmacodynamic and pharmacokinetic properties.[25] In the case of enantiomers, these compounds will have identical chemical and physical properties, however the change in three-dimensional conformation can often have significant impacts on their pharmacological effects on the human body. Moreover, it is often the case that one of the enantiomers is responsible for the biological activity of the compound while the other is inactive or causes undesired side-effects.[25]

One of the numerous limitations preventing sal003 from becoming a marketable therapeutic aid for stem cell transplantations is that it is only active in concentrations of 10 μM and higher. However, the sal003 purchased from Sigma Aldrich, as well as the samples synthesized in our lab that have been used in the biological studies, have all been administered as a racemic mixture. Since its initial report in 2007, no one has drawn attention to the fact that sal003 contains

a center of chirality, and that every time it has been used in biological studies, it has been administered in racemic form (Figure 2.4.3.1).

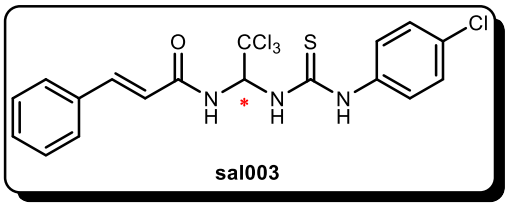

Figure 2.4.3.1 – Chiral Center of sal003 Indicated by Asterisk

Based on the reasons mentioned above, it would be of significant value if we were able to evaluate the biological activity of the individual enantiomers in our assay. However, before this could be accomplished, it needed to be determined first if the enantiomers could be separated using chiral HPLC, and secondly, whether or not they would be isolable and stable. Preliminary runs with sal003 using an analytical chiral HPLC column (Chiralpak IC 250 x 4.6, 5 µM) furnished promising results, as two distinct peaks were resolved (Figure 2.4.3.2).

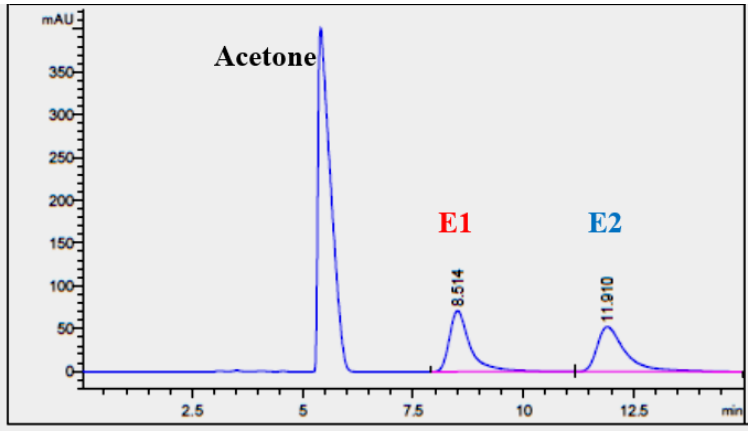

Figure 2.4.3.2 – Chiral HPLC Chromatogram Showing Resolution of sal003's Enantiomers

Subsequent scaling up to a semi-preparatory sized system using a Chiralpak IC 250 x 10, 20 µM column eluting 77:33 Hexanes/Isopropanol, allowed for milligram quantities of each enantiomer to be isolated, and then tested in our assay for their ability to expand satellite cells, using racemic sal003 as a positive control.

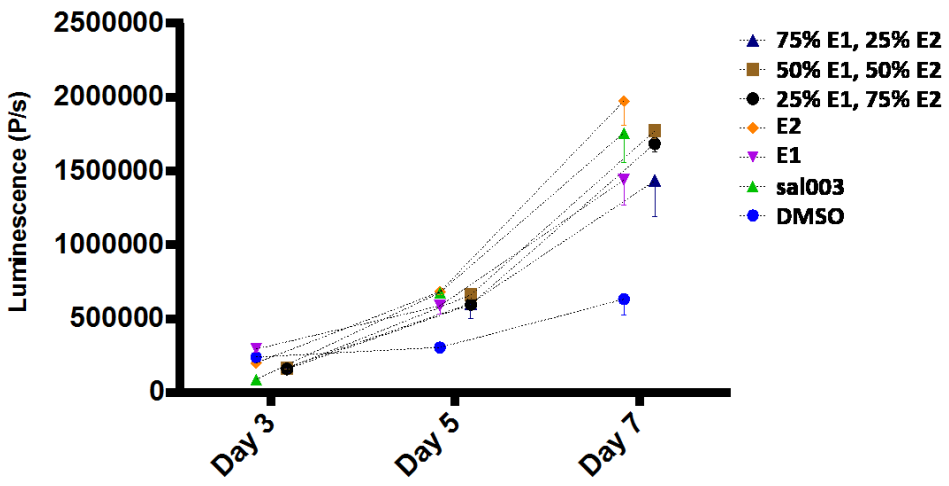

Figure 2.4.3.3 – Luciferase assay results for sal003 enantiomers (E1= enantiomer 1, E2= enantiomer 2)

Under our normal culture conditions, it was found that one of the enantiomers, termed E2, had a greater ability to expand satellite cells than the other (Figure 2.4.3.3). To confirm that these results were not an anomaly, different concentrations of each enantiomer were combined and evaluated. The rationale behind this is that a 50-50 mixture of each enantiomer should perform similarly to the racemic sal003, whereas a 75-25 mixture of E2/E1 should produce better results than the 75-25 mixture of E1/E2. Satisfyingly, this was precisely what we saw as the 50-50 mixture resulted in almost identical expansion numbers as racemic sal003. Although preliminary, these results support our initial hypothesis that the individual enantiomers have different abilities to expand satellite cells *ex vivo*. Moving forward, they will be tested in our secondary screen for their ability to maintain P-eIF2α. Additionally, we would like to determine the absolute configurations of the enantiomers for characterization purposes as well as to provide us with some insight into the three-dimensional structure of the binding pocket of the cellular target.

2.5 – Design and Synthesis of a sal003 PAL

Although we have shown that it is feasible to synthesize novel derivatives that are more potent than sal003 by making only minor modifications to its scaffold, the longstanding questions of its exact cellular target and mechanism of action remain unanswered. We planned to address this issue by designing and synthesizing a PAL of sal003 to be used for target identification in the context of *ex vivo* expansion of skeletal muscle stem cells. As discussed in Chapter 1, one of the biggest challenges in designing a functional PAL is ensuring that the probe maintains similar biological activity to that of the parent compound. Oftentimes, this is accomplished through initial

screening of compounds wherein functional groups are interchanged at different positions on the molecule to determine which aspects of the molecule are essential for activity, and which can be altered without noticeable change. We planned to follow this approach by appending a diazirine moiety to the sal003 scaffold to allow for cellular labelling.

Our first strategy was to synthesize derivatives of sal003 containing a trifluoromethyl-diazirine moiety owing to their success in other PAL studies in the recent literature. The most feasible way to append this to sal003 would be to synthesize an aniline derivative containing the CF_3-diazirine, and then couple this aniline to isothiocyanate **2.4.1.5**. Inspired by the success of compound **2.4.1.20** to expand muscle stem cells that maintained high P-eIF2α levels, we wanted to mimic its structural features by installing the CF_3-diazirine in the meta position on the aniline (Figure 2.5.1).

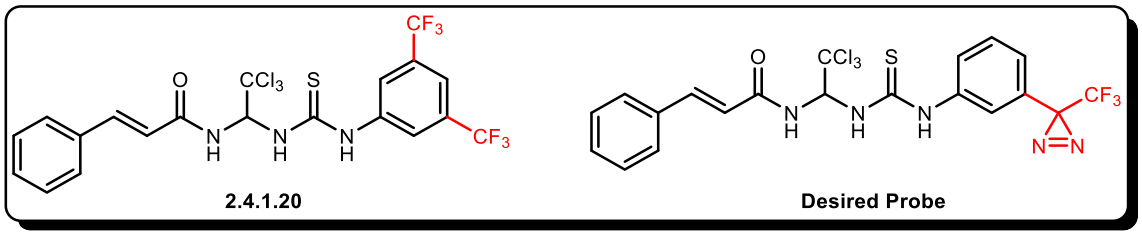

*Figure 2.5.1 – Desired Probe Based off of the Structure of Compound **2.4.1.20***

Using a combination of modified procedures, the desired aniline was prepared in 8 steps from commercially available 2,2,2-trifluoroacetophenone.[26-27] Using classic nitration conditions, 200 mmol of 2,2,2-trifluoroacetophenone was treated with a mixture of sulfuric and fuming nitric acid to obtain the single addition product **2.5.1** in a 77% yield (Scheme 2.5.1). Iron-mediated reduction of the nitro group to the amine, followed by Boc-protection provided **2.5.2** in an 80% yield over two steps. The formation of the tosyl-oxime proceeded smoothly as the ketone was first treated with hydroxylamine hydrochloride to give the oxime, which was then protected with tosyl chloride to provide **2.5.3** as a mixture of E/Z isomers. Condensation with liquid ammonia provided the diaziridine **2.5.4** as a yellow oil in a 66% isolated yield after purification. Finally, oxidation to the diazirine under standard conditions followed by Boc-deprotection in TFA, provided the desired aniline coupling partner **2.5.5** as a dark orange oil. Using the standard conditions, the coupling reaction with isothiocyanate **2.4.1.5** in THF was successful to provide our initial sal003 probe **2.5.6**. A yield of 45% was obtained for this as the reaction was stopped prematurely once the

product spot became visible through TLC because the stability of the diazirine compound in solution at 80°C is unknown. Following the standard work-up procedure, **2.5.6** was purified and isolated using column chromatography to yield the desired compound as a yellow powder.

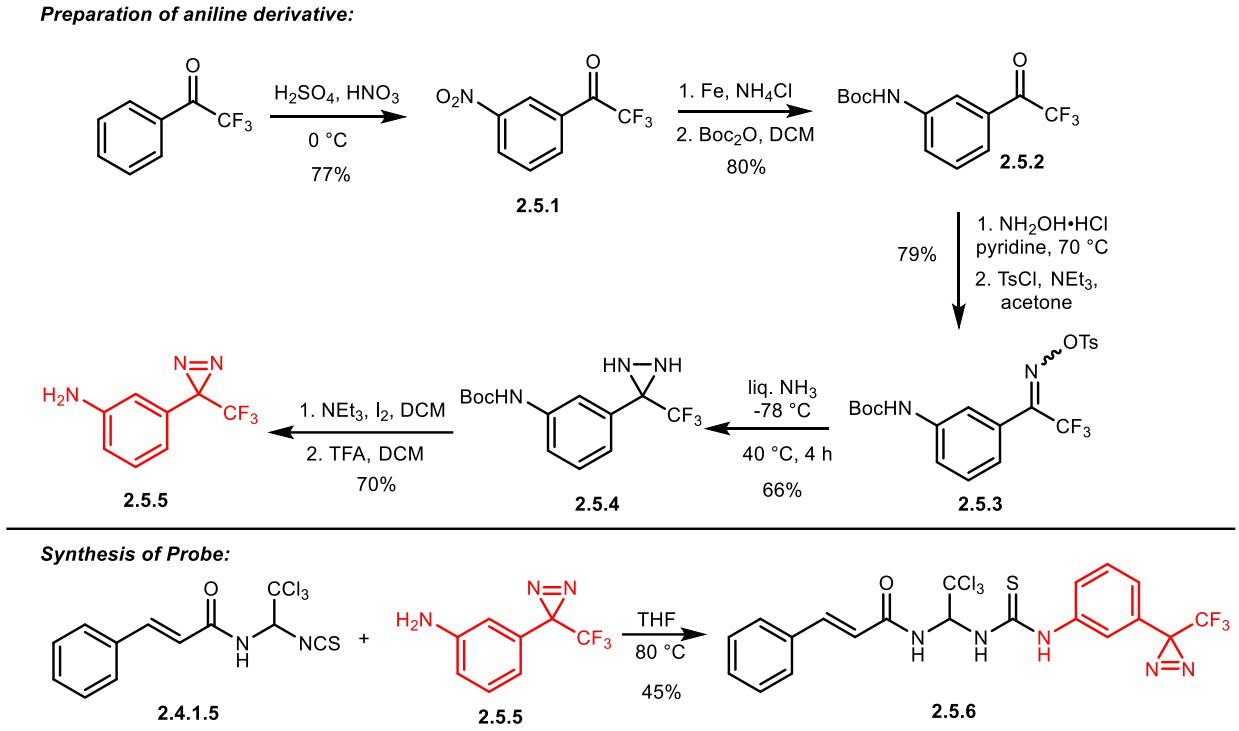

*Scheme 2.5.1 – Synthesis of Probe **2.5.6***

After completing the synthesis of **2.5.6**, it was of utmost importance to ensure that the diazirine was photoactive. The most direct way to assess this was to dissolve the probe in methanol and irradiate the sample with long-wave UV light.[28] If the diazirine is photoreactive, it should undergo a formal -OH insertion with methanol to provide the methyl ether (Scheme 2.5.2). When this experiment was run in the lab, complex reaction mixtures were obtained with no evidence for the formation of **2.5.7**. This is something that will be investigated further.

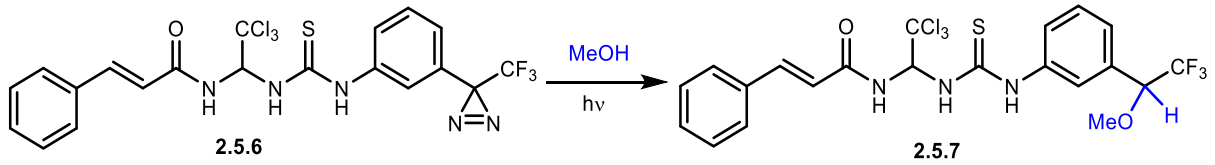

*Scheme 2.5.2 – Photolysis of Probe **2.5.6***

Moving forward, **2.5.6** needs to be further tested for its photoactivity, as well as its activity in our assays to ensure that it maintains the ability to expand skeletal muscle stem cells that retain P-eIF2α. These are experiments that are currently underway.

In parallel with the synthesis of **2.5.6**, we wanted to prepare probe analogs of sal003 containing both a diazirine unit and an alkyne group to perform pull-down/MS analysis of the cell lysates for target identification experiments. From our initial investigative studies, it seemed as though modifications made to the Region B on the compound had the largest impact on overall activity, whereas Region A tolerated changes without noticeable effects (Figure 2.5.2). Therefore, we identified that Region A was potentially modifiable whereas Region B would tolerate only minor structural modifications. With these preliminary results, we proposed to synthesize a derivative containing a diazirine and alkyne units to Region B on the molecule in hopes that it would have a negligible effect on the biological activity compared to the parent compound sal003.

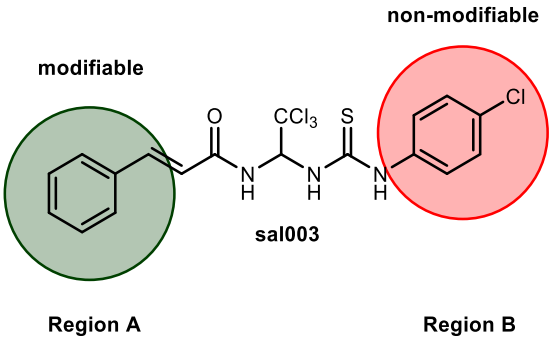

Figure 2.5.2 – Potentially Modifiable Regions of sal003

The most traditional approach to append these functional groups to sal003 would involve a cross-coupling reaction to install the terminal alkyne and a Grignard reaction to append the ketone pre-cursor for the diazirine. However, the most direct approach to a bifunctional probe would be to replicate the work reported by Li *et al.* in 2013 wherein they report the synthesis of a minimalist linker unit that contained both a diazirine and a terminal alkyne.[29] This is beneficial from a synthetic standpoint since depending on the complexity of the parent compound, it can be a difficult task to install the diazirine and alkyne separately, and in a selective manner. To avoid this complication, they developed 3 linker probes with different functional handles at the terminal sites to allow them to be appended to the parent compounds through simple substitution or coupling reactions (Figure 2.5.3).

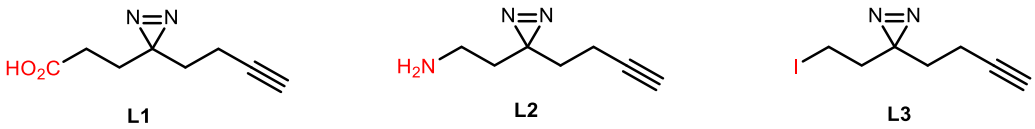

Figure 2.5.3 – Li's Minimalist Terminal Alkyne Linkers

Our plan was to synthesize **L3** and append it to the left-hand side of sal003 by incorporating a phenol onto the aromatic ring as a functional handle. Following the procedure reported by Li, ethyl acetoacetate was alkylated with propargyl bromide to yield **2.5.8** (Scheme 2.5.3). After ketone protection under standard conditions, the ester was reduced with $LiAlH_4$ to give **2.5.9** in an 85% yield over two steps. The acetal was then hydrolyzed under acidic conditions to provide the free ketone **2.5.10**, a key intermediate in the synthesis of all 3 linker probes. The ketone was treated with neat liquid NH_3 at -78°C, slowly warmed to room temperature, and then heated at 40°C to yield the N-H imine. This was treated with hydroxylamine-*o*-sulfonic acid to provide the diaziridine, which was oxidized using I_2 to yield the diazirine **2.5.11** in a 65% yield over three steps. The free alcohol was then converted to the alkyl iodide under standard Appel conditions to yield the desired compound **2.5.12**.

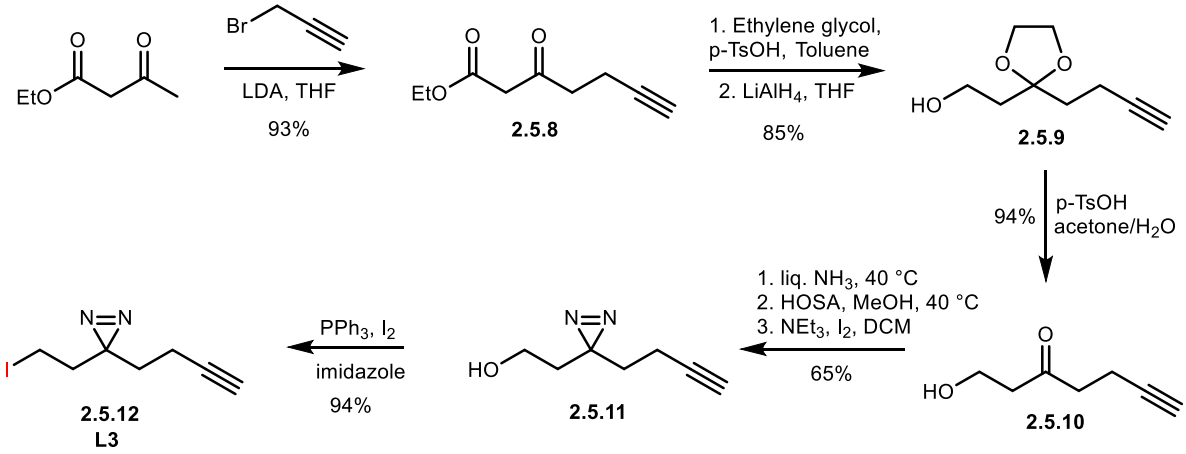

*Scheme 2.5.3 – Synthesis of **L3***

Before **L3** could be appended, the proper derivative of sal003 had to be synthesized containing a phenolic handle on the left-hand side. In order to simplify the purification in between steps, methyl and benzyl protected phenols were carried through the general synthesis of sal003 analogs to yield compounds **2.4.1.33** and **2.1.34**, which could then be deprotected to provide the desired free phenol (Figure 2.5.3). However, attempts to deprotect **2.4.1.34** using BBr_3 were met

with failure and led to decomposition of starting material. Therefore, hydrogenation conditions were employed to deprotect **2.4.1.33**. This quickly proved to be problematic as **2.4.1.33** is insoluble in traditional organic solvents used for hydrogenation; prompting us to seek an alternative approach. Gratifyingly, when **2.4.1.33** was treated with an excess of BBr_3 in DCM at -78 °C, the free phenol **2.4.1.35** was obtained in an 56% isolated yield following column chromatography. With the phenolic handle installed onto sal003, we wanted to first test the efficacy of these three compounds in our preliminary biological assay to ensure that they maintained similar activity to that of sal003 before the actual probe was synthesized. The three test probes were then tested for their ability to expand satellite cells in an *ex vivo* culture using sal003 as a positive control.

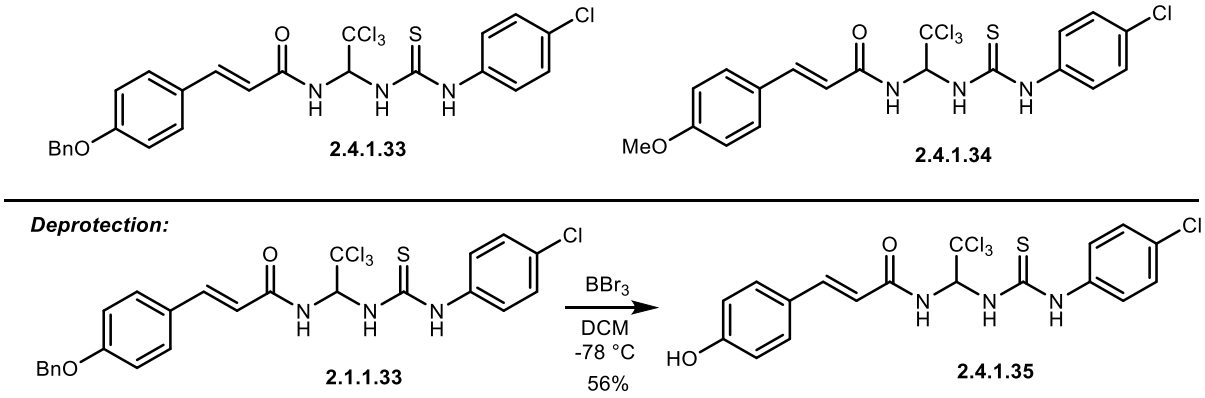

Figure 2.5.4 – Synthesis of Test Probes

Unfortunately, all three compounds showed a significant decrease in their ability to expand skeletal muscle stems compared to sal003 (Figure 2.5.5). In the case of the benzyl derivative **2.4.1.33**, it led to cell death after 3 days in culture. The introduction of the phenol in the para position, whether protected or not, changes the overall electronic properties of the compound, which can lead to adverse changes in its biological activities. We believed that the electron-donating capability of the phenol in the para position could potentially lead to a fragmentation of the compound in culture, which could account for the loss of activity. After obtaining these disappointing results from the assays, we set out to synthesize derivatives wherein the phenol is in the meta position. Placing this in the meta position will change the electronics of the compound, and we hypothesize that eliminating the electron-donating ability of the phenol will allow for retention of activity. The synthesis of the meta-protected and free phenol are currently underway.

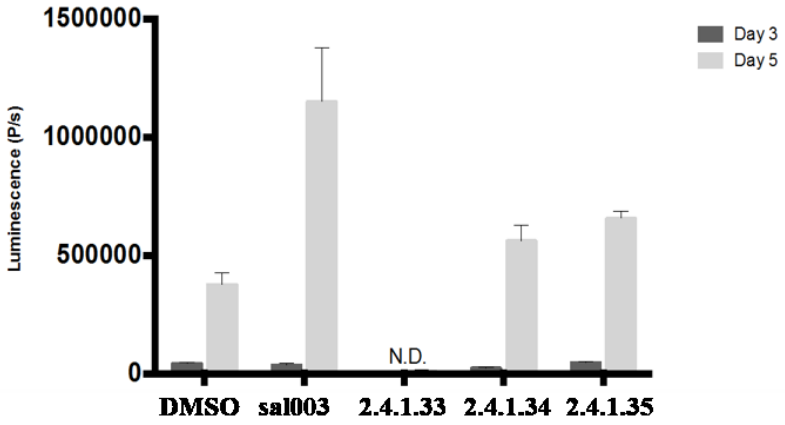

Figure 2.5.5 – Luminescence Assay results displaying poor activity from test probes

2.6 - ISRIB

Through our initial assays, we have shown that pharmacological inhibition of eIF2α phosphatase permits the *ex vivo* expansion of skeletal muscle stem cells that maintain P-eIF2α. When the cell expresses elevated levels of P-eIF2α, general translation initiation is hindered; however, certain mRNAs get selectively translated under these conditions with the exemplary transcript being the *Atf4* gene. To quantify the expression levels of *Atf4* in the quiescent satellite cell, Crist and coworkers replicated a previous assay and replaced the *Atf4* coding region with the luciferase gene, which produces light through an enzymatic reaction and allows the expression level to be quantified based on how much light is produced.[30] Next, to determine if *Atf4* expression is increased independently of mRNA levels, they cultured cells in the presence of a small molecule ISRIB (Figure 2.6.1), which is known to reverse the effects of P-eIF2α at nM concentrations.[31] Therefore, by comparing the expression levels of the *Atf4*-luciferase construct when cultured with ISRIB to the control group, they can determine to what extent *Atf4* is unregulated at the protein level independent of mRNA level.

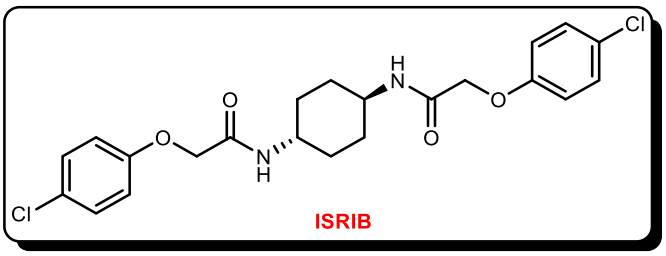

Figure 2.6.1 – Symmetrical structure of ISRIB

However, purchasing even small quantities of ISRIB from chemical suppliers is extremely expensive and therefore we wanted to be able to synthesize ample quantities in the lab. The synthesis of ISRIB is simple and required the mixing of two cheap, commercially available reagents, trans-1,4-diaminocyclohexane and 4-chlorophenoxyacetyl chloride, with triethylamine to afford **2.6.1** in a 97% isolated yield. This facile one-step synthesis allowed for the preparation of gram-scale quantities of ISRIB.

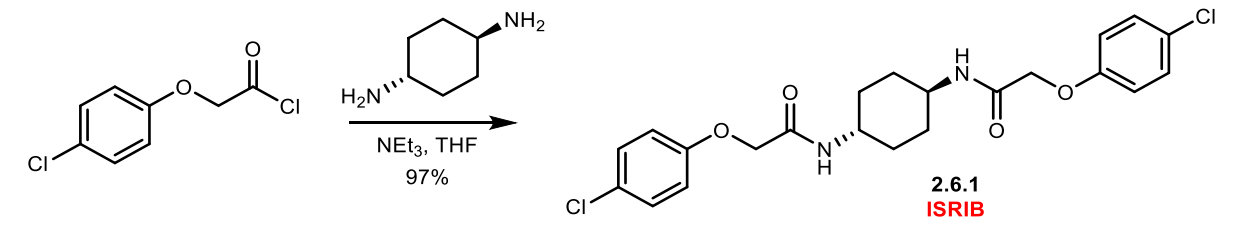

Scheme 2.6.1 – Synthesis of ISRIB

Additionally, a SAR study was conducted with ISRIB by Sidrauski *et al.* in 2015 wherein they synthesized an analog improving the EC_{50} value to 600 pM in cell culture.[32] Following their reported procedure as a rough guideline, commercially available 4-chloro-3-fluorophenol was reacted with *tert*-butyl bromoacetate to afford **2.6.2** which was readily saponified to yield **2.6.3** as white solid (Scheme 2.6.2). This was then converted to the acid chloride **2.6.4** under standard conditions. In similar fashion as above, the acid chloride was reacted with the diamine to provide the desired ISRIB analog **2.6.5** in an 88% yield.

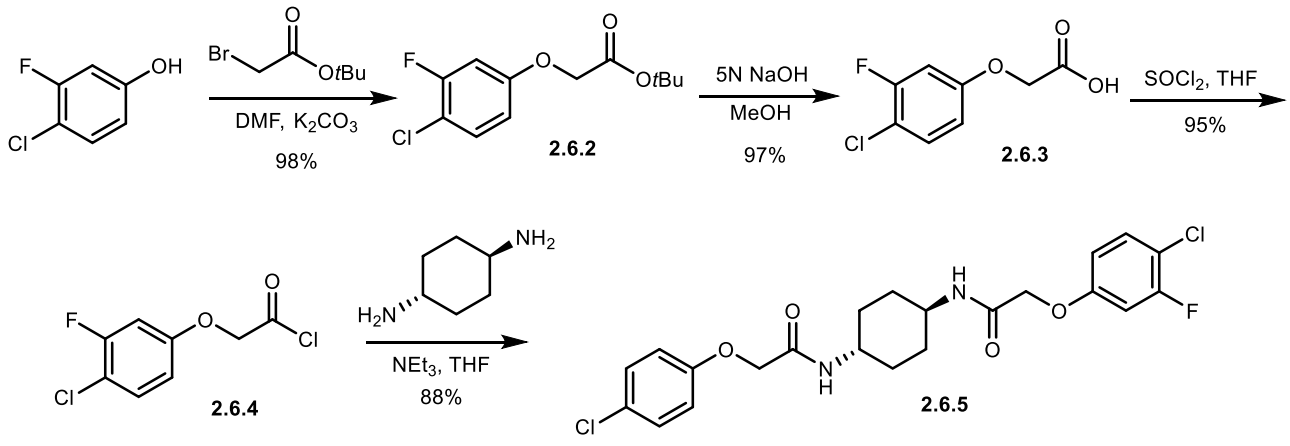

Scheme 2.6.2 – Synthesis of ISRIB Derivative

With the two compounds in hand, they were tested for their ability to reduce P-eIF2a translation, and mediate the expression levels of *Atf4*. It was found that satellite cells cultured in the presence of **2.6.1** and **2.6.5** displayed significantly lower levels of *Atf4* expression compared to the control, or cells cultured with sal003 (Figure 2.6.2).

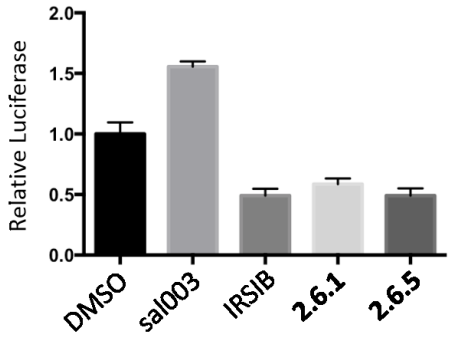

Figure 2.6.2 – Atf4-Luciferase Assay

Furthermore, they went on to show that satellite cells treated with 200 nm of ISRIB led to an overall decrease in the number of cells that had not activated the myogenic program (Figure 2.6.3). This was confirmed using an immunoblotting assay using antibodies for Pax7 and *MyoD*. Further investigations are currently underway to examine the effects of ISRIB on skeletal stem cell activation in live mice.

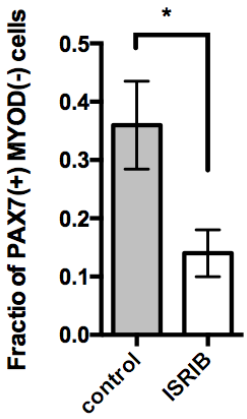

Figure 2.6.3 - ISRIB decreases numbers of satellite cells that have not activated the myogenic program after 3-hour culture

2.7 – Conclusion and Future Work

In this chapter, we have discussed the importance of eIF2α Phosphatase in maintaining quiescence in satellite cells, and how its pharmacological manipulation is a potentially viable

approach to developing therapeutics for the treatment of skeletal muscle disorders. Currently, the use of satellite cells as a treatment option is limited by their rarity in the human body, encouraging their cultivation *ex vivo*. However, *ex vivo* culture of satellite cells is extremely challenging as once they are taken out of their niche in the body, they immediately differentiate and activate the myogenic program. By studying the molecular mechanisms that underlie satellite cell activation, Colin Crist and coworkers identified the dephosphorylation of eIF2α to be a key event in this process and that by treating freshly isolated satellite cells with a small molecule known to inhibit this pathway, sal003, they were able to culture stem cells *ex vivo* that maintained P-eIF2α.

By performing a structure optimization study on sal003, we synthesized several novel compounds that were more potent at a lower effective concentration. However, our ability to develop more potent analogs was significantly hindered by our lack of understanding of their cellular targets or biological mechanism of action. We planned to address this issue by designing and synthesizing PAL probes of sal003 to be used in target identification. An initial probe containing a diazirine photoactivable group has been synthesized and will be tested for activity in preliminary assays.

The future endeavours of this project are three-fold. Firstly, additional sal003 analogs need to be synthesized and tested in the interim to allow us to gain a better understanding of which positions on the molecule are amenable to modification. Secondly, the enantiomers of sal003 need to be tested further to determine if one stereoisomer is in fact more active than the other. If this proves to be the case, this could prompt the investigation of an enantioselective synthesis. In parallel with this, the enantiomers of our more potent analogs need to be resolved on the chiral HPLC and screened in our assays for activity. Finally, the number one priority of this project is to identify the cellular target and mechanism of action of sal003 in the quiescent satellite cell. The identification of its cellular target would allow for rapid structure optimization studies to develop highly potent analogs based off of the binding site on its biological target. Furthermore, we would like to extend our sal003 PAL studies to a more widespread application and use them for target identification in cells that have activated the UPR in response to ER stress. Owing to the prevalence of the dysregulation of the eIF2α dephosphorylation pathway in many life-threatening diseases, the ability to manipulate and control this by small-molecule intervention would have serious implications in the pharmaceutical industry.

2.8 – References

1. Theadom, A.; Rodrigues, M.; Roxburgh, R.; Balalla, S.; Higgins, C.; Bhattacharjee, R.; Jones, K.; Krishnamurthi, R.; Feigin, V., Prevalence of Muscular Dystrophies: A Systematic Literature Review. *Neuroepidemiology* **2014,** *43* (3-4), 259-268.
2. Mauro, A., SATELLITE CELL OF SKELETAL MUSCLE FIBERS. *J. Biophys. Biochem. Cytol.* **1961,** *9* (2), 493-&.
3. Bentzinger, C. F.; Wang, Y. X.; Rudnicki, M. A., Building Muscle: Molecular Regulation of Myogenesis. *Cold Spring Harb. Perspect. Biol.* **2012,** *4* (2).
4. Cardasis, C. A.; Cooper, G. W., ANALYSIS OF NUCLEAR NUMBERS IN INDIVIDUAL MUSCLE-FIBERS DURING DIFFERENTIATION AND GROWTH - SATELLITE CELL MUSCLE FIBER GROWTH UNIT. *J. Exp. Zool.* **1975,** *191* (3), 347-357.
5. Zismanov, V.; Chichkov, V.; Colangelo, V.; Jamet, S.; Wang, S.; Syme, A.; Koromilas, A. E.; Crist, C., Phosphorylation of eIF2 alpha Is a Translational Control Mechanism Regulating Muscle Stem Cell Quiescence and Self-Renewal. *Cell Stem Cell* **2016,** *18* (1), 79-90.
6. Relaix, F.; Montarras, D.; Zaffran, S.; Gayraud-Morel, B.; Rocancourt, D.; Tajbakhsh, S.; Mansouri, A.; Cumano, A.; Buckingham, M., Pax3 and Pax7 have distinct and overlapping functions in adult muscle progenitor cells. *J. Cell Biol.* **2006,** *172* (1), 91-102.
7. Pallafacchina, G.; Francois, S.; Regnault, B.; Czarny, B.; Dive, V.; Cumano, A.; Montarras, D.; Buckingham, M., An adult tissue-specific stem cell in its niche: A gene profiling analysis of in vivo quiescent and activated muscle satellite cells. *Stem Cell Res.* **2010,** *4* (2), 77-91.
8. Crist, C. G.; Montarras, D.; Buckingham, M., Muscle Satellite Cells Are Primed for Myogenesis but Maintain Quiescence with Sequestration of Myf5 mRNA Targeted by microRNA-31 in mRNP Granules. *Cell Stem Cell* **2012,** *11* (1), 118-126.
9. Buchan, J. R.; Parker, R., Eukaryotic Stress Granules: The Ins and Outs of Translation. *Mol. Cell* **2009,** *36* (6), 932-941.
10. Fullwood, M. J.; Zhou, W.; Shenolikar, S., Targeting Phosphorylation of Eukaryotic Initiation Factor-2 alpha to Treat Human Disease. In *Protein Phosphorylation in Health and Disease*, Shenolikar, S., Ed. 2012; Vol. 106, pp 75-106.
11. Boyce, M.; Bryant, K. F.; Jousse, C.; Long, K.; Harding, H. P.; Scheuner, D.; Kaufman, R. J.; Ma, D. W.; Coen, D. M.; Ron, D.; Yuan, J. Y., A selective inhibitor-of eIF2 alpha dephosphorylation protects cells from ER stress. *Science* **2005,** *307* (5711), 935-939.
12. Costa-Mattioli, M.; Gobert, D.; Stern, E.; Gamache, K.; Colina, R.; Cuello, C.; Sossin, W.; Kaufman, R.; Pelletier, J.; Rosenblum, K.; Krnjevic, K.; Lacaille, J. C.; Nader, K.; Sonenberg, N., eIF2 alpha phosphorylation bidirectionally regulates the switch from short- to long-term synaptic plasticity and memory. *Cell* **2007,** *129* (1), 195-206.
13. Kaufman, R. J., Stress signaling from the lumen of the endoplasmic reticulum: coordination of gene transcriptional and translational controls (vol 13, pg 1211, 1999). *Genes Dev.* **1999,** *13* (14), 1898-1898.
14. Hetz, C., The unfolded protein response: controlling cell fate decisions under ER stress and beyond. *Nat. Rev. Mol. Cell Biol.* **2012,** *13* (2), 89-102.
15. Hetz, C.; Chevet, E.; Harding, H. P., Targeting the unfolded protein response in disease. *Nat. Rev. Drug Discov.* **2013,** *12* (9), 703-719.
16. Kadowaki, H.; Nishitoh, H., Signaling Pathways from the Endoplasmic Reticulum and Their Roles in Disease. *Genes* **2013,** *4* (3), 306-333.
17. Chou, J.; Chen, J. J.; Gross, M.; Roizman, B., ASSOCIATION OF A M(R)-90,000 PHOSPHOPROTEIN WITH PROTEIN-KINASE PKR IN CELLS EXHIBITING ENHANCED

PHOSPHORYLATION OF TRANSLATION INITIATION-FACTOR EIF-2-ALPHA AND PREMATURE SHUTOFF OF PROTEIN-SYNTHESIS AFTER INFECTION WITH GAMMA(1)34.5(-) MUTANTS OF HERPES-SIMPLEX-VIRUS-1. *Proc. Natl. Acad. Sci. U.S.A.* **1995,** *92* (23), 10516-10520.
18. Chou, J.; Roizman, B., HERPES-SIMPLEX VIRUS-1 GAMMA(1)34.5-GENE FUNCTION, WHICH BLOCKS THE HOST RESPONSE TO INFECTION, MAPS IN THE HOMOLOGOUS DOMAIN OF THE GENES EXPRESSED DURING GROWTH ARREST AND DNA-DAMAGE. *Proc. Natl. Acad. Sci. U.S.A.* **1994,** *91* (12), 5247-5251.
19. Long, K.; Boyce, M.; Lin, H.; Yuan, J. Y.; Ma, D. W., Structure-activity relationship studies of salubrinal lead to its active biotinylated derivative. *Bioorg. Med. Chem. Lett.* **2005,** *15* (17), 3849-3852.
20. Liu, J.; He, K. L.; Li, X.; Li, R. J.; Liu, C. L.; Zhong, W.; Li, S., SAR, Cardiac Myocytes Protection Activity and 3D-QSAR Studies of Salubrinal and its Potent Derivatives. *Curr. Med. Chem.* **2012,** *19* (35), 6072-6079.
21. Choy, M. S.; Yusoff, P.; Lee, I. C.; Newton, J. C.; Goh, C. W.; Page, R.; Shenolikar, S.; Peti, W., Structural and Functional Analysis of the GADD34:PP1 eIF2 alpha Phosphatase. *Cell Rep.* **2015,** *11* (12), 1885-1891.
22. Hong, M. N.; Nam, K. Y.; Kim, K. K.; Kim, S. Y.; Kim, I., The small molecule '1-(4-biphenylylcarbonyl)-4-(5-bromo-2-methoxybenzyl) piperazine oxalate' and its derivatives regulate global protein synthesis by inactivating eukaryotic translation initiation factor 2-alpha. *Cell Stress Chaperones* **2016,** *21* (3), 485-497.
23. Strukil, V.; Igrc, M. D.; Fabian, L.; Eckert-Maksic, M.; Childs, S. L.; Reid, D. G.; Duer, M. J.; Halasz, I.; Mottillo, C.; Friscic, T., A model for a solvent-free synthetic organic research laboratory: click-mechanosynthesis and structural characterization of thioureas without bulk solvents. *Green Chem.* **2012,** *14* (9), 2462-2473.
24. Purser, S.; Moore, P. R.; Swallow, S.; Gouverneur, V., Fluorine in medicinal chemistry. *Chem. Soc. Rev.* **2008,** *37* (2), 320-330.
25. Chhabra, N.; Aseri, M. L.; Padmanabhan, D., A review of drug isomerism and its significance. *Int. J. Appl. Basic. Med. Res.* **2013,** *3* (1), 16-8.
26. Biasotti, B.; Dallavalle, S.; Merlini, L.; Farina, C.; Gagliardi, S.; Parini, C.; Belfiore, P., Synthesis of photoactivable inhibitors of osteoclast vacuolar ATPase. *Bioorg. Med. Chem.* **2003,** *11* (10), 2247-2254.
27. Stewart, R.; Vanderlinden, R., THE ACIDITY OF SOME AROMATIC FLUORO ALCOHOLS AND KETONES. *Can. J. Chem.* **1960,** *38* (3), 399-406.
28. Brunner, J.; Senn, H.; Richards, F. M., "3-TRIFLUOROMETHYL-3-PHENYLDIAZIRINE - A NEW CARBENE GENERATING GROUP FOR PHOTOLABELING REAGENTS. *J. Biol. Chem.* **1980,** *255* (8), 3313-3318.
29. Li, Z. Q.; Hao, P. L.; Li, L.; Tan, C. Y. J.; Cheng, X. M.; Chen, G. Y. J.; Sze, S. K.; Shen, H. M.; Yao, S. Q., Design and Synthesis of Minimalist Terminal Alkyne-Containing Diazirine Photo-Crosslinkers and Their Incorporation into Kinase Inhibitors for Cell- and Tissue-Based Proteome Profiling. *Angew. Chem. Int. Ed.* **2013,** *52* (33), 8551-8556.
30. Vattem, K. M.; Wek, R. C., Reinitiation involving upstream ORFs regulates ATF4 mRNA translation in mammalian cells. *Proc. Natl. Acad. Sci. U.S.A.* **2004,** *101* (31), 11269-11274.
31. Sidrauski, C.; Acosta-Alvear, D.; Khoutorsky, A.; Vedantham, P.; Hearn, B. R.; Li, H.; Gamache, K.; Gallagher, C. M.; Ang, K. K. H.; Wilson, C.; Okreglak, V.; Ashkenazi, A.; Hann,

B.; Nader, K.; Arkin, M. R.; Renslo, A. R.; Sonenberg, N.; Walter, P., Pharmacological brake-release of mRNA translation enhances cognitive memory. *eLife* **2013,** *2*.
32. Sidrauski, C.; Tsai, J. C.; Kampmann, M.; Hearn, B. R.; Vedantham, P.; Jaishankar, P.; Sokabe, M.; Mendez, A. S.; Newton, B. W.; Tang, E. L.; Verschueren, E.; Johnson, J. R.; Krogan, N. J.; Fraser, C. S.; Weissman, J. S.; Renslo, A. R.; Walter, P., Pharmacological dimerization and activation of the exchange factor eIF2B antagonizes the integrated stress response. *eLife* **2015,** *4*.

3. Benzothiazine Synthesis

3.1 – Introduction

Benzothiazines are a privileged class of heterocycles with wide ranging applications as pigments and pharmacophores.[1-2] 1,4-Benzothiazines have attracted particular interest, due to their antibiotic, antiemetic, and antipsychotic activities (Figure 3.1).[3] This heterocyclic scaffold is also found in nature, and is a key component of pheomelanin, a particular form of the ubiquitous bio-polymer melanin, which has a red-hue. The efficiency of melanogenesis, coupled with the prevalence and importance of 1,4-benzothiazines in materials and medicinal chemistry motivated us to develop an efficient, easily diversifiable and scalable synthesis that was inspired by pheomelanogenesis. These efforts are complementary to more traditional cross-coupling strategies, which include annulation reactions of 2-aminobenzenethiols with diketones or halides at elevated temperatures. Although effective, these methods suffer from significant drawbacks including pre-functionalization of starting materials, limited substrate scope, and poor control over regioselectivity. Transition-metal catalyzed cross-coupling reactions have been developed for the synthesis of 1,4-benzothiazines, but these transformations also require substrate prefunctionalization, and employ transition metals. Therefore, a transition metal free synthesis of 1,4-benzothiazines that retains a broad substrate scope while using readily available feedstock chemicals under mild reaction conditions would be attractive. This chapter details my efforts towards this goal, and builds upon preliminary work conducted by Ms. Elizabeth Li (M.Sc. Lumb Group), Mr. Zheng Huang (Ph.D. Candidate, Lumb Group) and Dr. Kenneth V. N. Esguerra (Ph.D. Lumb Group).

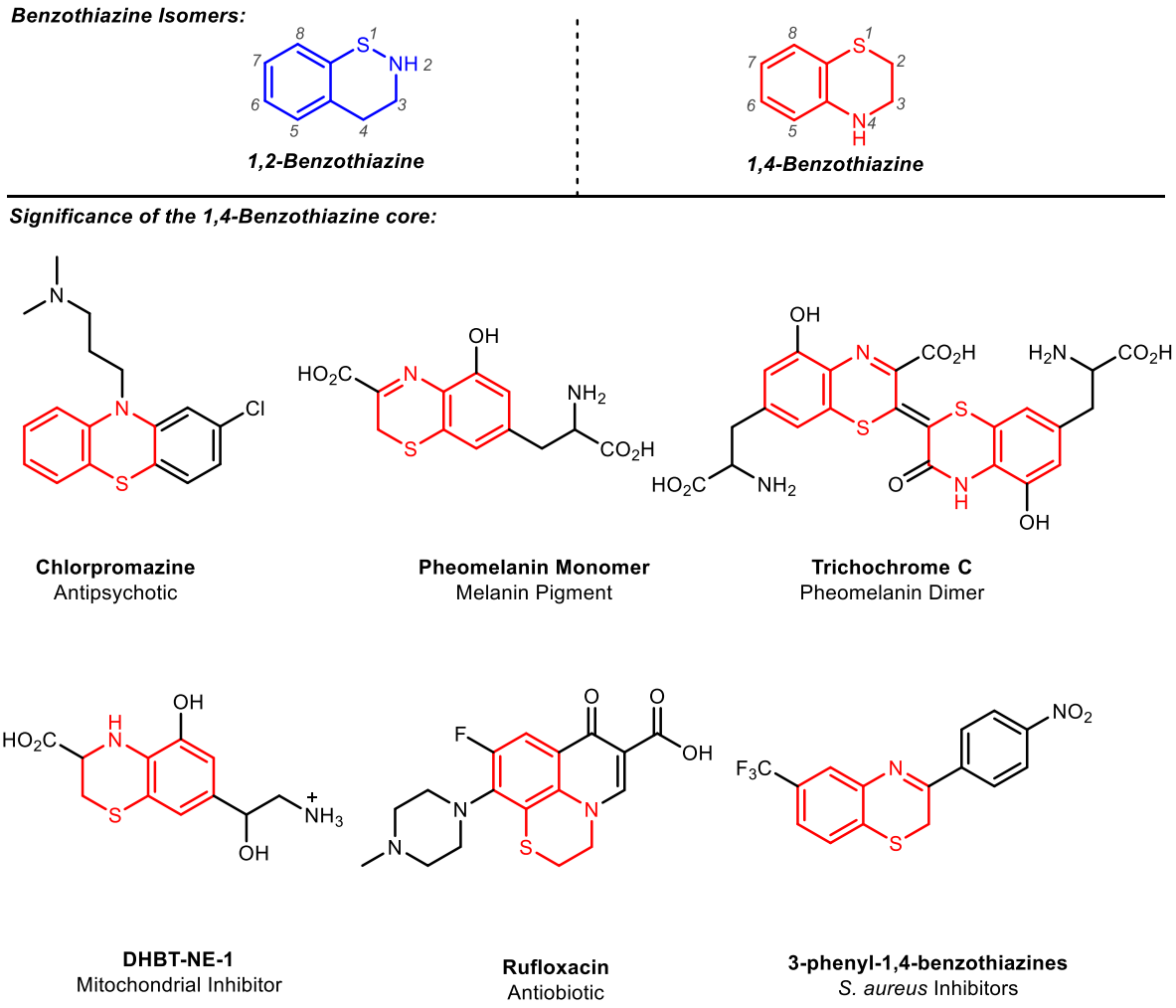

Figure 3.1 – Relevance of the 1,4-benzothiazine core

3.2 – Overview of Chapter 3

In section 3.3 the 1,4-benzothiazine heterocycle will be discussed in the context of pheomelanogenesis (i.e. the biosynthesis of red pigments). Current methodologies for the synthesis of benzothiazines will be then be discussed in Section 3.4. In Section 3.5, our bio-inspired methodology for the selective installment of aryl C-S bonds through the nucleophilic addition of thiols to *ortho*-quinones will be discussed, in order to create the context for our synthesis of 1,4-benzothiazines. This synthesis is discussed in Section 3.6, which discusses the optimization and scope of our bio-inspired approach to 1,4-benzothiazines.

3.3 – 1,4-Benzothiazines in the Production of Pheomelanin

Melanogenesis is a complex biological process that is conserved throughout nature, and is responsible for the pigmentation of skin, the browning of fruits, and the colouring of hair.[4] Early studies into this process identified that it results in the production of pigment polymers that can be classified as either: eumelanin (black), or pheomelanin (red). Extensive investigations have been conducted in order to characterize eumelanin intermediates from its starting material building block tyrosine **3.3.1**, and what is known about its biosynthetic pathway, whose first steps are abbreviated in Scheme 3.3.1. Initially, **3.3.1** is oxidized by the enzyme tyrosinase to generate dopaquinone **3.3.2**, which can undergo an intramolecular cyclization reaction with the appendant amine to arrive at cyclodopa **3.3.3**. At this point, cyclodopa **3.3.3** is susceptible to undergo a redox exchange process with dopaquinone **3.3.2** to generate the corresponding oxidized dopachrome **3.3.5**, and the reduced dopa **3.3.4**. Dopachrome is a highly reactive species that can then undergo a series of complex polymerization reactions to generate the pigment eumelanin. The process of redox exchange is essential in the production of melanin pigments and occurs because the product generated after the intramolecular cyclization (**3.3.3**) is a highly electron-rich species that can reduce the electron-poor species (**3.3.2**) in a facile manner to generate **3.3.4** and **3.3.5**, respectively.

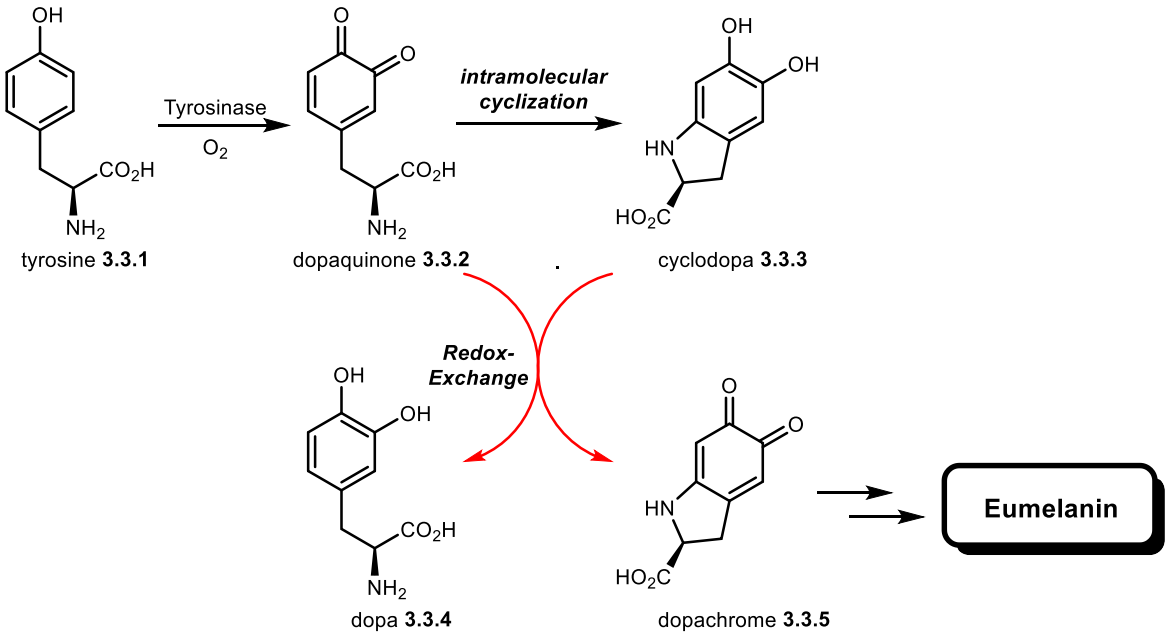

Scheme 3.3.1 - The First Steps of the Biosynthetic Pathway of Eumelanin in Melanogenesis

Significant efforts have been made to study and characterize the intermediates in the eumelanin process. However, structurally speaking, little was known about its complimentary pheomelanin process until the 1960s. In 1964, degradative studies confirmed the presence of nitrogen and sulfur atoms in pheomelanin structures. Subsequently, it was observed that the enzymatic oxidation of dopa **3.3.4** in the presence of cysteine **3.3.6** gave rise to the same pheomelanin trichochrome compounds **3.3.7** and **3.3.8** that were observed from isolation of feathers from New Hampshire hens (*gallus gallus*) (Scheme 3.3.2).[5-6] Further investigations identified that regioisomers 5S- and 2S- cysteinyldopa were intermediates in the biosynthesis of these trichochrome products.[7] It was then hypothesized that these intermediates arose first from oxidation of dopa **3.3.4** to dopaquinone **3.3.2**, followed by addition of cysteine **3.3.6** to generate the regioisomers **3.3.9** and **3.3.10** (Scheme 3.3.2).[8]

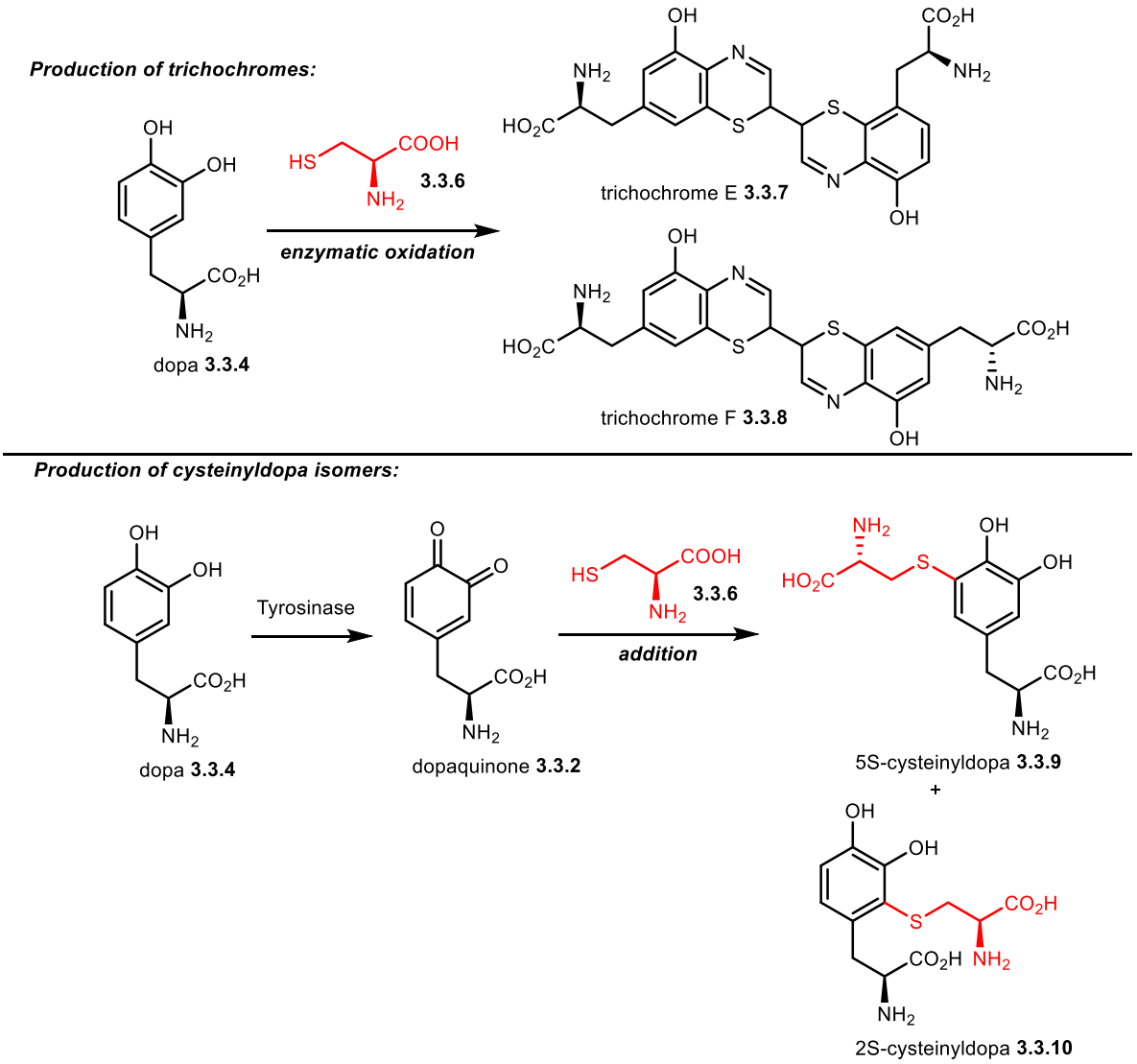

Scheme 3.3.2 - Early Isolation of Trichochromes and Proposed Incorporation of Cysteine into Pheomelanin Pigments by Prota et al.

Interest into the synthesis of the cysteinyldopas increased when it was discovered that 5S-cysteinyldopa **3.3.9** was present in elevated levels in the urine samples of individuals afflicted with Harding-Passey melanoma, while levels in healthy patients are almost undetectable.[9] This prompted Itoh and Prota to apply a biomimetic strategy to the direct synthesis of these cysteinyldopa compounds (Scheme 3.3.3).[10] By mixing dopa **3.3.4** and L-cysteine **3.3.6** in a pH 6.8 phosphate buffer in the presence of mushroom tyrosinase, they reported the one-step synthesis of 5S-cysteinyldopa **3.3.6**, along with its regioisomer 2S-cysteinyldopa **3.3.7**, and the double addition product **3.3.8**. The isolation of the di-thiol adduct **3.3.11** was a clear indication of redox

exchange. This marked this first reported synthesis and isolation of these compounds, which were characterized by UV-Vis and ^{1}H-NMR analysis.

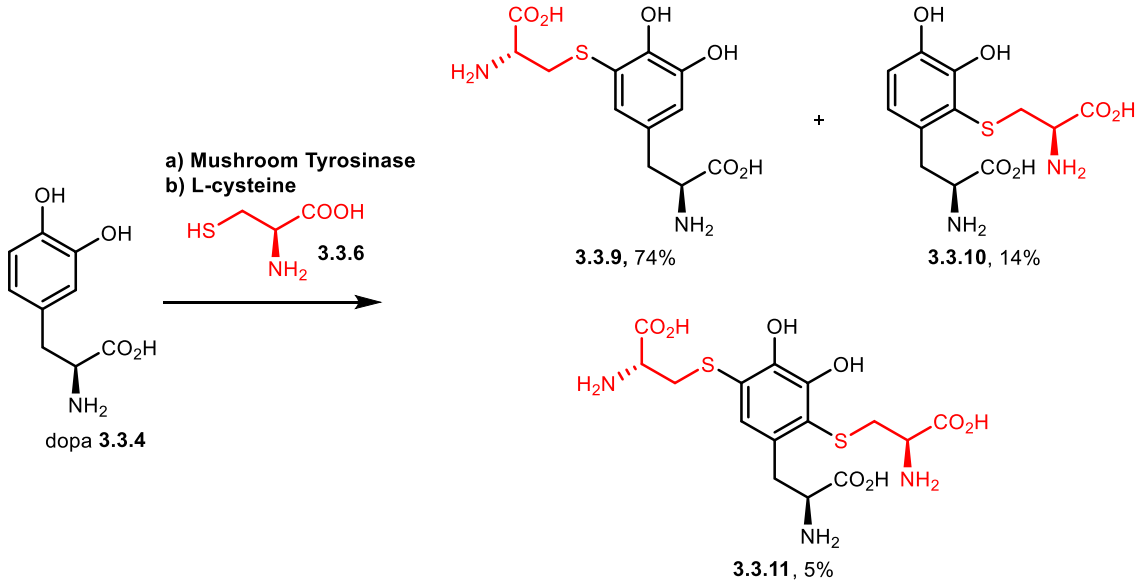

Scheme 3.3.3 – Itoh's Synthesis of Cysteinyldopas using Mushroom Tyrosinase

In another context, Novellino and coworkers reported a one-step synthesis of the cysteinyldopas using ceric ammonium nitrate (CAN) under acidic conditions and a large excess of cysteine.[11] In this case, the 5S isomer was also obtained as the major product along with trace amounts of 2S- and di-thiolated adducts. To our knowledge, these are the only two reported syntheses of these compounds utilizing a thiol addition to quinones. This can be attributed to the difficulty of working with *ortho*-quinones owing to their tendency to undergo redox-exchange. While this process is important in melanogenesis, it complicates more general reactions between *ortho*-quinones and sulfur nucleophiles as it leads to the formation of undesired di-thiol adducts. There are currently no strategies to supress redox-exchange, and factors governing this process remain poorly understood.

It was later reported by Thompson *et al.* that the rate constant for the thiol addition of cysteine **3.3.6** to dopaquinone **3.3.2** was 3 x 10^{7} $M^{-1}sec^{-1}$, to generate regioisomers **3.3.9** and **3.3.10** (Scheme 3.3.4).[12] The same authors later reported an additional rate constant of 8.8 x 10^{5} $M^{-1}sec^{-1}$ for the redox exchange process between dopaquinone **3.3.2** and the cysteinyldopas, a rate constant ~30 times less than the thiol addition. As previously discussed in this section, the biosynthetic pathway

of the black pigment eumelanin involves the nitrogen cyclization of dopaquinone **3.3.2**, bearing a rate constant of 7.6 sec^{-1}. Therefore, it was concluded that production of pheomelanin occurs only if there is a large concentration of cysteine present, *i.e.* if it is higher than 1 μM. These results, calculated via pulse radiolysis, are consistent with the belief that the dictating factor of the pathway dopaquinone takes in melanogenesis, *i.e.* whether it undergoes cyclization to form dopachrome, or whether it undergoes thiol addition to form the isomeric cysteinyldopa compounds **3.3.9** and **3.3.10**, is the concentration of cysteine present in the melanosomal compartments of the cell.

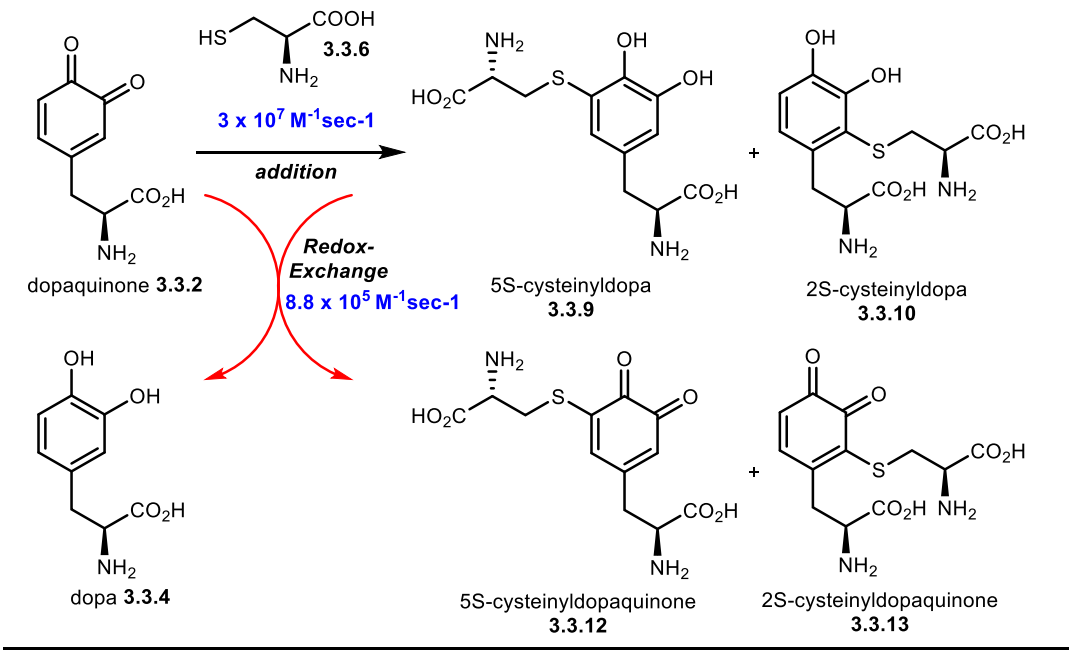

Scheme 3.3.4 - Calculated Rate Constants for the Thiol Addition of Cysteine to Dopaquinone, and for the Redox Exchange between dopaquinone and Cysteinyldopa Products

Our understanding of the early stages of melanogenesis are summarized in Scheme 3.3.5, including the key step of the cysteine sulfur addition to the *ortho*-quinone dopaquinone **3.3.2**.[13] This step has been defined as the branch point in the pathways of the production of eumelanin (black pigment) and pheomelanin (red pigment). First, tyrosine **3.3.1** is oxygenated to dopaquinone **3.3.2** by the enzyme tyrosinase. In the absence of cysteine, **3.3.2** undergoes intramolecular cyclization to provide cyclodopa **3.3.3**, a highly electron-rich species that is prone to undergo redox exchange with dopaquinone **3.3.2** to generate dopachrome **3.3.4**. After a series of oxidation/polymerization reactions, eumelanin is produced. However, in the presence of cysteine (**3.3.6**), it will add to dopaquinone **3.3.2** via the thiol moiety to generate the 5S- (**3.3.9**) and 2S-

(**3.3.10**) cysteinyldopa regioisomers. These intermediates then undergo a subsequent oxidation reaction to give 5S- **3.3.12** and 2S- **3.3.13** cysteinyldopaquinones, which then are then attacked in an intramolecular fashion by the appendant amine followed by condensation and tautomerization to generate the 1,4-benzothiazine intermediates **3.3.14** and **3.3.15**. Following the production of benzothiazines **3.3.14** and **3.3.15**, a series of more complex oxidative processes ensue in the presence of O_2 to generate the pheomelanin pigment in a rapid and uncontrolled fashion; steps that are not well understood at this point.

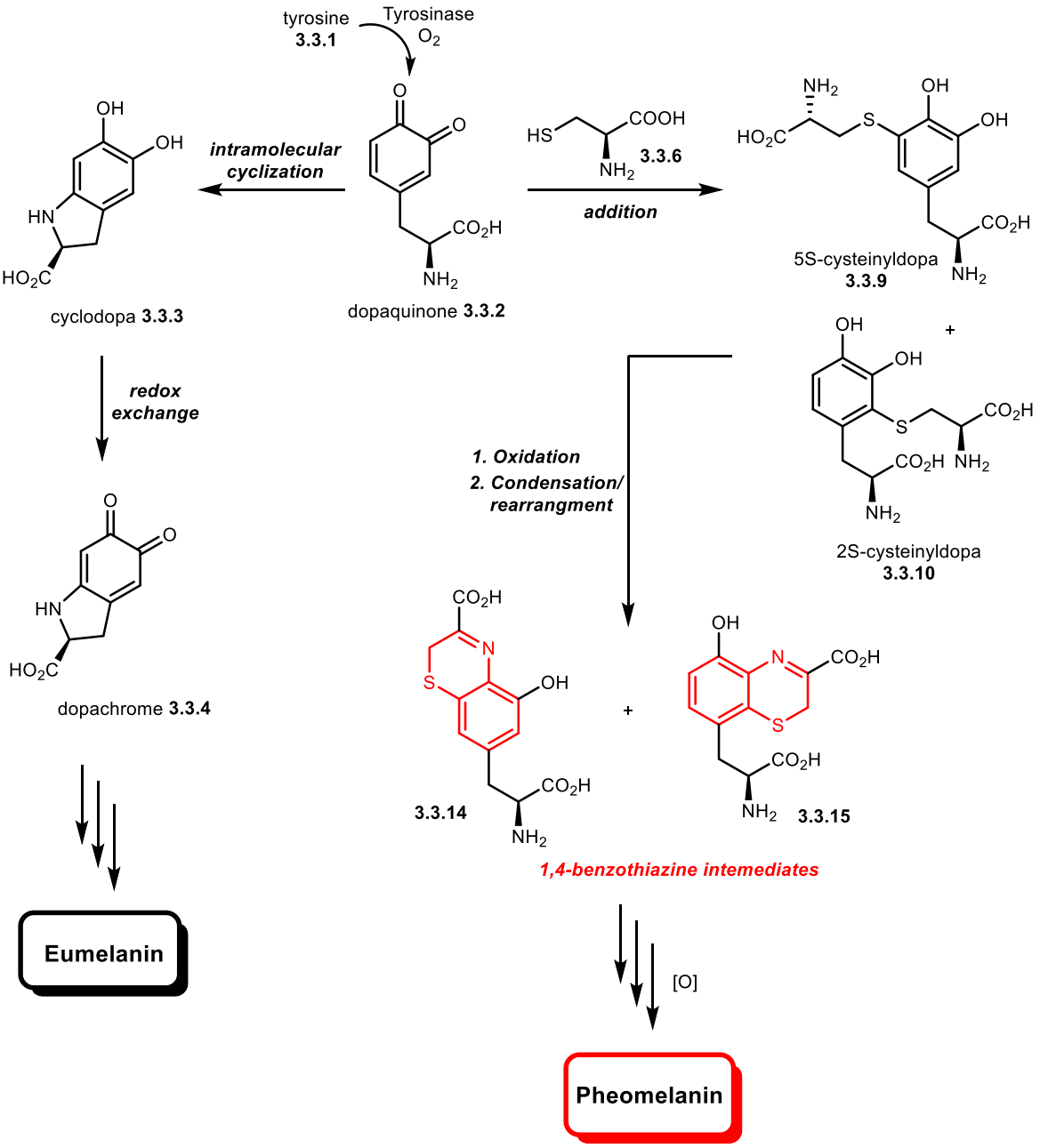

Scheme 3.3.5 – Biosynthetic pathway displaying the branch point in Melanogenesis

The exact feedback mechanism by which cysteine concentrations are regulated is still unclear, but it is hypothesized to be regulated by the specific transcription of enzymes in the melanosome.[14] It is known that the enzymes melanocyte stimulating hormone (MSH) and agouti signalling protein (ASP) play a large role in the regulation process. When the MSH receptor is activated, eumelanin production is initiated through an increase in tyrosinase production.

However, if the MSH receptor is blocked or ASP is overexpressed, pheomelanin production will occur in place of eumelanin.[15]

3.4 – Previous Syntheses of Benzothiazines

The ubiquity of the benzothiazine scaffold in pharmaceutical agents and materials chemistry has prompted synthetic chemists to develop methodologies that will allow them to access this heterocyclic core in a simple fashion.[1] The challenges in developing a diversifiable synthesis stem from the synthetic limitations of installing aryl C-S and C-N bonds in a mild, selective manner. Herein, current methods for the synthesis of 1,4-benzothiazines will be discussed.

3.4.1 – Transition Metal-Free Condensation Reactions

Of the methods that will be discussed in this section, transition metal-free condensations between β-diketones/organic halides and 2-aminobenzenethiols is the most traditional and straightforward approach. A simple, yet elegant example of using this strategy was reported by Munde and coworkers wherein they developed a solvent free approach to the oxidative cyclocondensation of 2-aminobenzenethiols and 1,3-dicarbonyls using a catalytic amount of hydrazine hydrate and air (Figure 3.4.1.1).[16] Although the scope was narrow, they obtained the 1,4-benzothiazine in excellent yields.

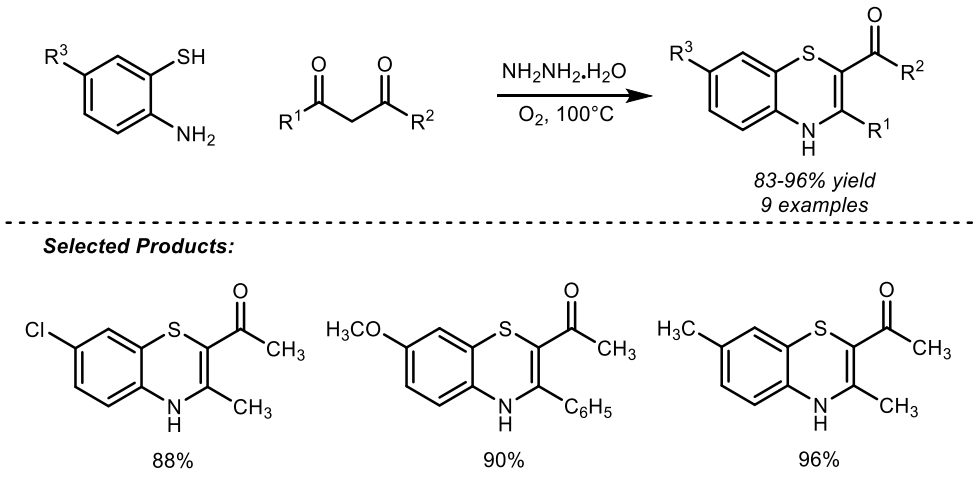

Figure 3.4.1.1 – Munde's Preparation of 1,4-benzothiazines

They reasoned that hydrazine hydrate is used to first oxidize the thiol to the disulfide, followed by condensation of the amine onto one of the carbonyls. This then triggers a cyclization

event, breaking the disulfide bond and releasing the desired 2,3-disubstituted benzothiazine after rearrangement (Figure 3.4.1.2). Their mechanistic proposal for the formation of the disulfide bond is based on previous work by Iyengar *et al.* who reported the use of catalytic amounts of hydrazine hydrate to convert thiols to disulfides.[17]

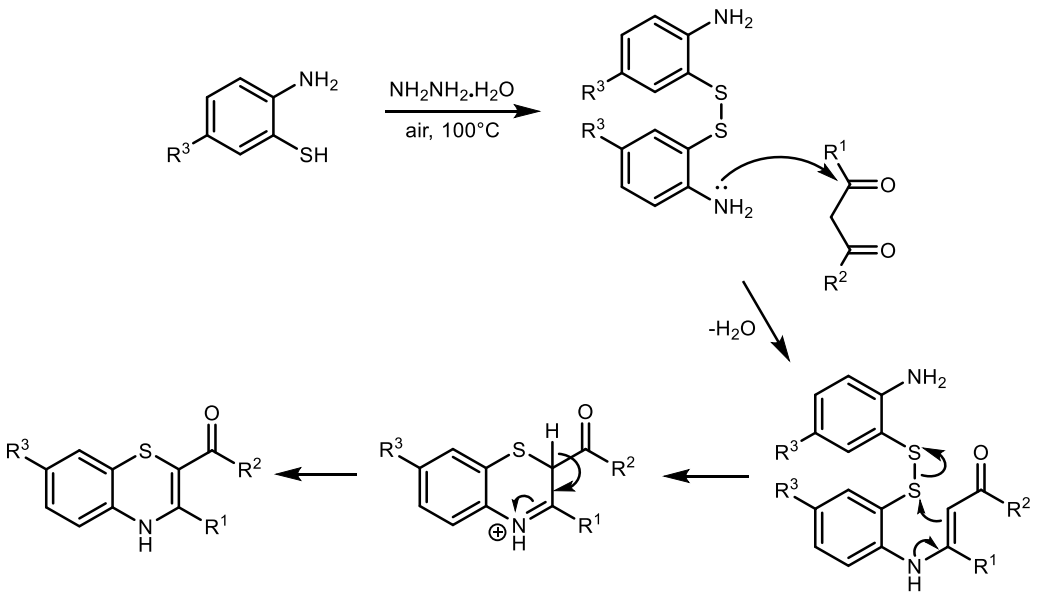

Figure 3.4.1.2 – Mechanistic Proposal for the Hydrazine Hydrate Catalyzed 1,4-Benzothioazine Synthesis

In 2008, Sabatini *et al.* reported the synthesis of a small library of 3-phenyl-1,4-benzothiazine derivatives utilizing the condensation between 2-aminobenzenethiols and α-bromo acetophenones in DMF at room temperature (Figure 3.4.1.3).[18] The reported substrate scope is relatively narrow, with only 20 compounds being reported, and much of the variability stemming from the α-bromo acetophenone coupling partners. They attributed the drop in yields to the spontaneous oxidative dimerization at the C2 position, a side reaction that is known to occur when using polar solvents (Figure 3.4.1.4).[19]

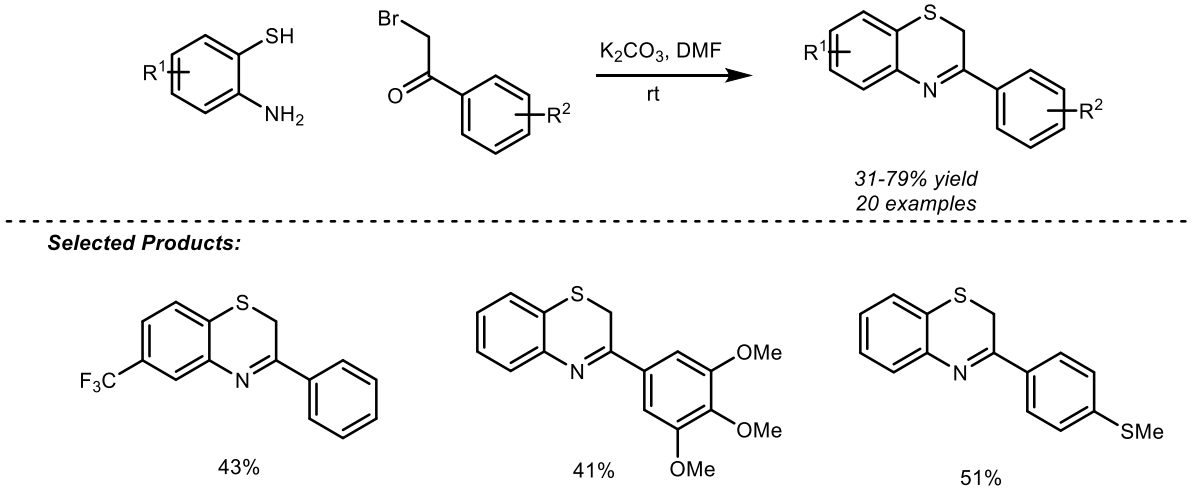

Figure 3.4.1.3 – Sabatini's Method for 3-phenyl-1,4-benzothiazines

Although the α-bromo acetophenones need to be prepared prior to use, they provide much better regioselective control than the 1,3-dicarbonyls, since the thiol will preferentially undergo substitution at the α position before the amine. Additionally, the use of potassium carbonate in DMF at room temperature provides a very mild set of conditions to access the 1,4-benzothiazine heterocyclic core in a convergent, selective manner.

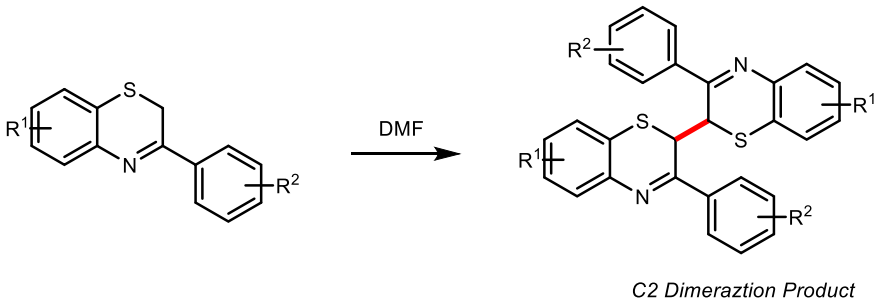

Figure 3.4.1.4 – Observed C2 Dimerization Leading to Diminished Yields

Recently, Yi *et al.* reported a radical based route to the synthesis of substituted 1,4-benzothiazines from 2-aminobenzenethiols and a variety of ketones (Figure 3.4.1.5).[20] They show that these conditions are tolerant of a variety of different ketones including α,β-unsaturated, cyclic, linear, and fluoroalkyl, allowing them access to several novel benzothiazine derivatives. Additionally, they performed a variety of control experiments in order to probe the mechanism of the reaction and they found that all four reactions were inhibited by the presence of TEMPO, supporting their initial hypothesis that the reaction proceeded through radical intermediates.

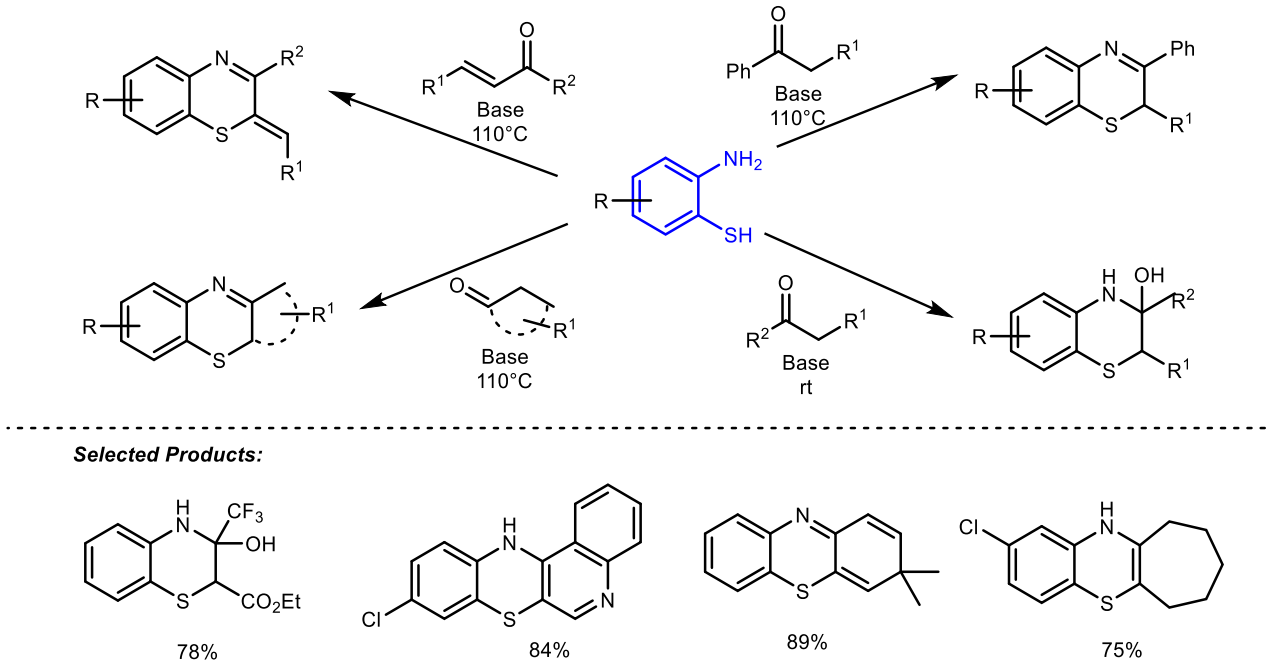

Figure 3.4.1.5 – Yi's Radical Route to 1,4-benzothiazines

Mechanistically, they proposed the *in situ* formation of a thiyl radical when the thiol is heated under an air atmosphere (Figure 3.4.1.6). The thiyl oxidatively couples to the enol, which is generated from the treatment of the ketone with base, to form the carbon centered radical species. This species subsequently undergoes a single electron transfer process to generate the ketone, which upon further heating in the presence of base, will undergo intramolecular condensation with the appendant amine to provide the desired 1,4-benzothiazine product.

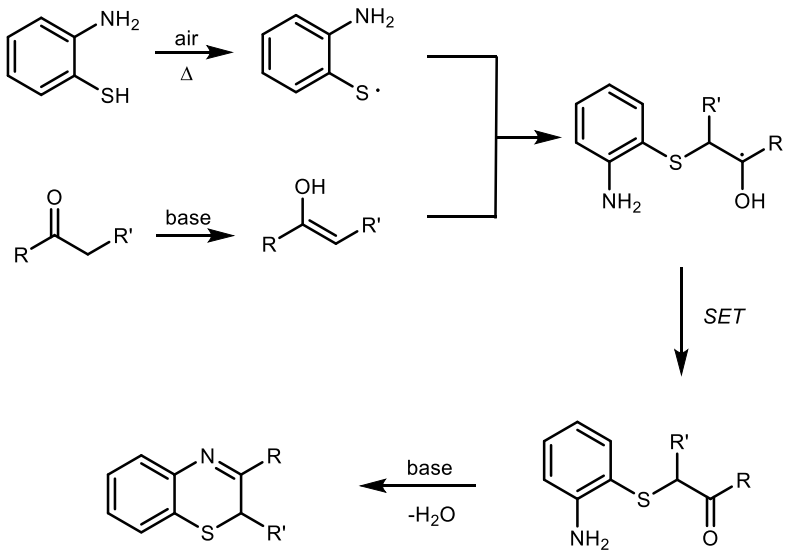

Figure 3.4.1.6 – Mechanistic Proposal for the Radical Formation of 1,4-benzothiazines

Consistent between literature examples that use this transition-metal-free approach is the issue of pre-functionalization of starting materials and narrow substrate scope that is significantly hindered by the requirement of 2-aminobenzenethiol starting materials. To overcome these limitations, numerous transition-metal catalyzed methods have been developed for the construction of the 1,4-benzothiazine core.

3.4.2 – Transition-Metal Catalyzed Cross-Coupling Approaches

The use of transition-metal catalysis for the synthesis of 1,4-benzothiazines has become increasingly popular. In 2016, Zhang and coworkers reported the copper-catalyzed coupling of cyanamide and an isothiocyanates (Figure 3.4.2.1).[21] Mechanistically, they proposed the initial generation of a thiourea intermediate via the addition of ammonia onto the isothiocyanate, followed by C-S bond formation in the presence of CuTC and K_2CO_3 to form a Cu-S species that immediately undergoes another cross-coupling reaction with the alkyne. Finally, a Cu-mediated intramolecular hydroamination reaction affords the desired 1,4-benzothiazine. They then go on to show that these conditions are tolerant of electron-withdrawing and donating substituents on both coupling partners, and assemble a library of 24 compounds that includes heteroaromatics and aryl halides. Nevertheless, the substrate scope is still relatively limited by the commercial availability of the aryl-isothiocyanates as well as the substituted terminal alkynes.

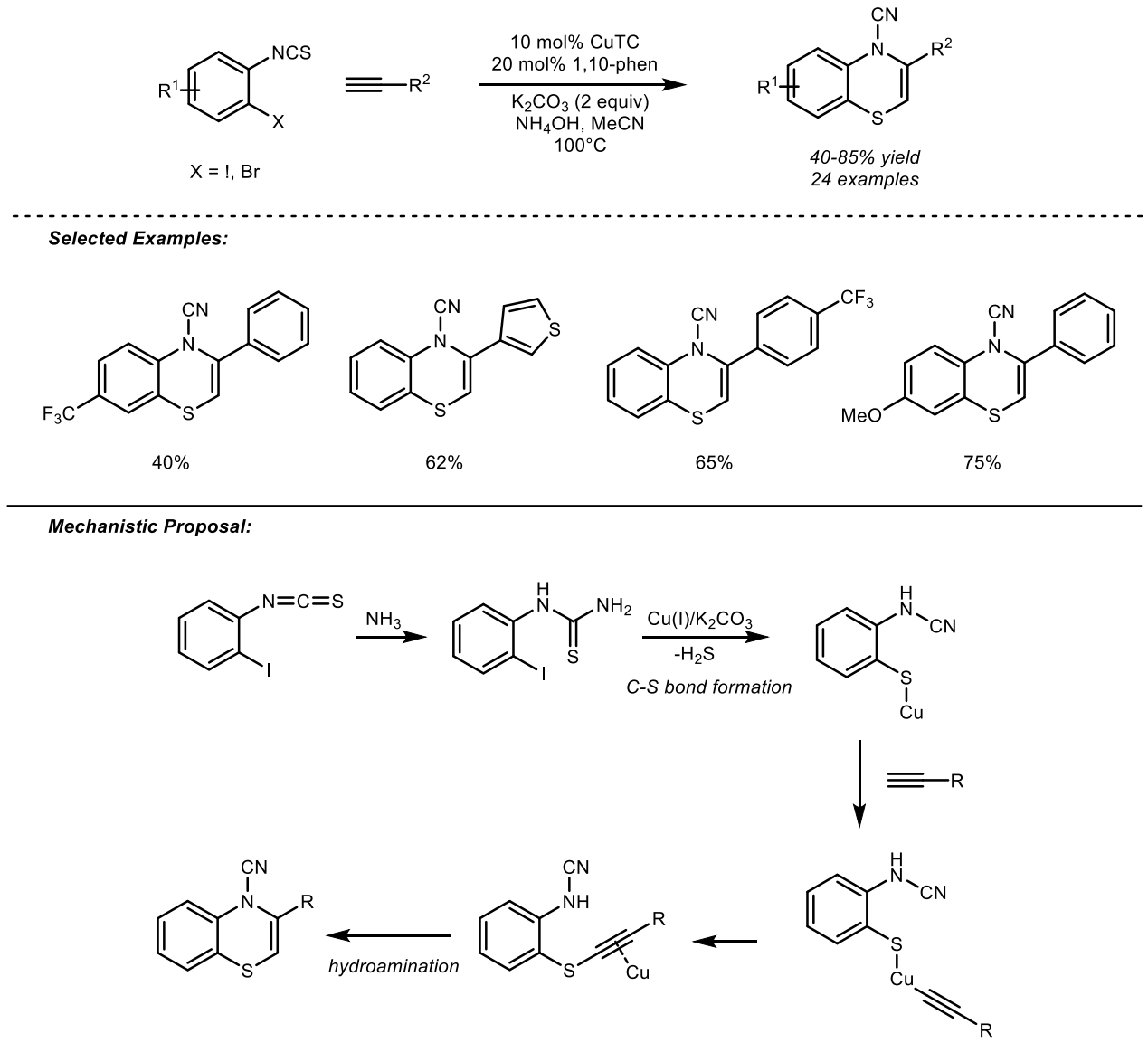

Figure 3.4.2.1 – Zhang's Cu-Catalyzed Tandem Cyclization Strategy

Another example of a transition metal catalyzed synthesis comes from Jiang and coworkers, who developed novel conditions for the palladium-catalyzed double C-S bond formation coupling reaction using $Na_2S_2O_3$ as the sulfur source (Figure 3.4.2.2).[22] They show that these conditions are tolerant to several differentially substituted aryl-halide starting materials including unprotected alcohols as well as the presence of additional sulfur atoms without affecting the coupling reaction. Noteworthy from this example is the use of $Na_2S_2O_3$ as the sulfur source. Compared to free thiols, sodium dithionite is a cheap, benchtop stable salt that is relatively odour-free, greatly simplifying the reaction setup. The obvious drawback to this methodology is the need

for the preparation of the N-tosylated aryl-halide starting materials, which requires two-steps from commercially available 2-iodoanilines.

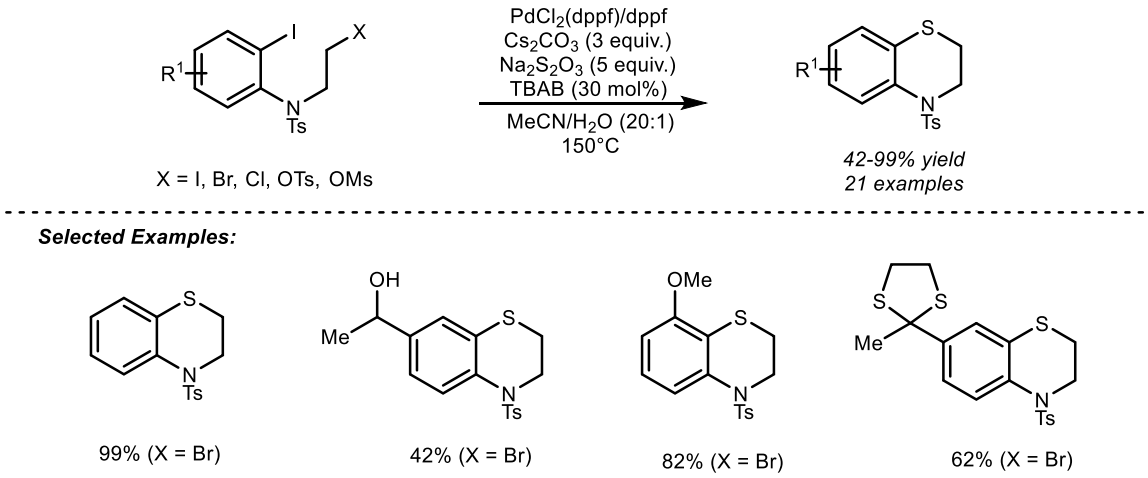

Figure 3.4.2.2 – Jiang's Pd-catalyzed Synthesis of 1,4-benzothiazines

As mentioned in Section 3.1, the development of transition-metal catalyzed approaches to the synthesis of 1,4-benzothiazines has solved many of the issues relating to regioselectivity and limited substrate scope that are commonly encountered in the more traditional metal-free methods. However, current metal-catalyzed methodologies still suffer from significant drawbacks; most notably being the limited substrate scope that they can access. Owing to the importance of this heterocyclic scaffold, the need for a diversifiable synthesis of substituted 1,4-benzothiazines providing access to a large substrate scope is highly desirable.

3.5 – Sulfur Addition to *ortho*-Quinones: A Mild Synthesis of Aryl C-S Bonds

In our group, we have often drawn inspiration from chemical processes that occur in nature, with the objective of adapting these processes into a laboratory setting. Over the past several years we have been examining the addition of sulfur nucleophiles to *ortho*-quinones using a biomimetic approach. As a more general methodology for aryl C-S bond formation, thiol addition to *ortho*-quinones has been severely underexploited, most likely due to the difficulty of working with *ortho*-quinones as reagents.

This work has origin in an initial experiment performed by Dr. Kenneth Esguerra, who investigated the reaction of *ortho*-quinone **3.5.1** and ethanethiol using N,N-diisopropylethylamine as a Brønsted base (Scheme 3.5.1). Using these conditions, catechol **3.5.2** was isolated as a single

regioisomer with C-S bond formation occurring exclusively at C6 in 85% isolated yield. This result demonstrated aromatic C-S bond formation under remarkably mild reaction conditions, which motivated our work to develop this transformation into a more general methodology.

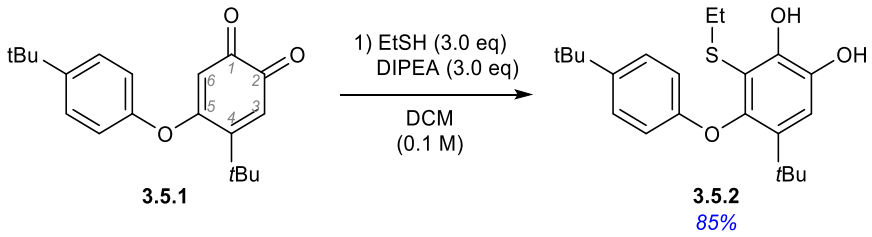

Scheme 3.5.1 - Initial Experiment Investigating the Addition of Sulfur Nucleophiles to ortho-Quinones

Following this initial investigative experiment, the project was undertaken by Ms. Elizabeth Li who screened reaction conditions for C-S bond formation using 3,5-di-*tert*-butyl-*ortho*-quinone **3.5.3** as a model substrate, due to its commercial availability and stability (Table 3.5.1). Crude reaction mixtures were treated with acetic anhydride (3.0 equiv.) and catalytic amounts of 4-dimethylaminopyridine (DMAP), to generate the bis-acetate, which is redox stable, and avoids complications of air-oxidation during isolation and purification. Initially, the reaction conditions developed by Dr. Kenneth Esguerra were compared with those previously reported in the literature. A slight change made to the procedure by lowering the equivalents of ethanethiol to 1.5 lead to the generation of **3.5.4** in 88% yield (Entry 1). Degassing the solvent by purging with N_2 immediately prior to use increased the reaction yield to 99% (Entry 2). Previous methodologies employing sulfur addition to *ortho*-quinones reported the use of acidic conditions, ranging from strongly acidic (2M sulfuric acid),[11] to mildly acidic (3:3:10 acetic acid/water/CH_3CN).[23] Therefore, the addition of ethanethiol to quinone **3.5.3** under acidic conditions was examined next, employing *para*-toluene sulfonic acid (p-TsOH) as a Brønsted acid to obtain **3.5.4** in a 63% yield (Entry 3). Finally, strongly basic conditions were evaluated by using sodium thiolate, returning **3.5.3** in a 79% yield (Entry 4). These preliminary reactions demonstrated that the conditions using DIPEA as a mild Brønsted base were the most efficient, meriting further investigation.

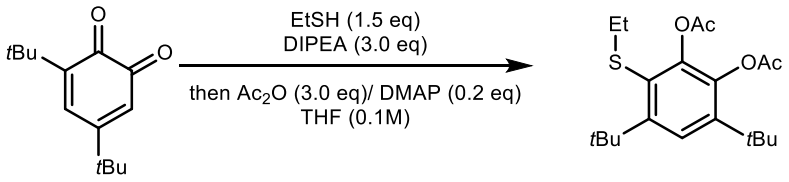

3.5.3 **3.5.4**

Entry	Thiol	Conditions	Yield
1	Et	Basic (DIPEA)	88
2[a]	Et	Basic (DIPEA)	99
3[b]	Et	Acidic (pTSOH)	63
4[c]	Et	Strongly Basic (Sodium Thiolate)	79

[a]Solvent was degassed
[b]Sodium Thiolate used as nucleophile
[c]pTsOH (1.0 eq), no DIPEA

Table 3.5.1 - Initial Experiments with ortho-Quinone 3.2.3

Further examination of the reaction scope using *ortho*-quinone **3.5.5** and thiophenol provided a mixture of products, including the desired thiol adduct **3.5.6**, the di-thiol adduct **3.5.7**, and the reduced bis-acetylated catechol **3.5.8** (Figure 3.5.1A). The isolation of the di-thiol adduct **3.5.7** was a clear indication of redox exchange, *i.e.* that the thiol adduct **3.5.6** catechol was oxidizing to the quinone, and allowing for a second thiol addition to occur at C6. The bis-acetylated catechol **3.5.8** isolated is the product generated from the redox-exchange of starting material quinone **3.5.5**, and product **3.5.6**. As previously discussed in this section, redox-exchange is a process that is known to occur between electron-rich catechols and electron-poor quinones. To further investigate the effects of redox exchange on *ortho*-quinone **3.5.5**, its ethanethiol adduct was generated in solution, and instead of bis-acetylation of the product catechol, another equivalent of starting material quinone was added. This mixture was stirred for 1.5h, upon which acetic anhydride/DMAP was added. This lead to the generation of complex mixtures, from which **3.5.9**, **3.5.10**, and **3.5.11**, were isolated (Figure 3.5.1B). The remaining mass balance also could not be accounted for, verifying our hypothesis that redox-exchange was a deleterious process occurring during the thiol additions performed with *ortho*-quinone **3.5.5**.

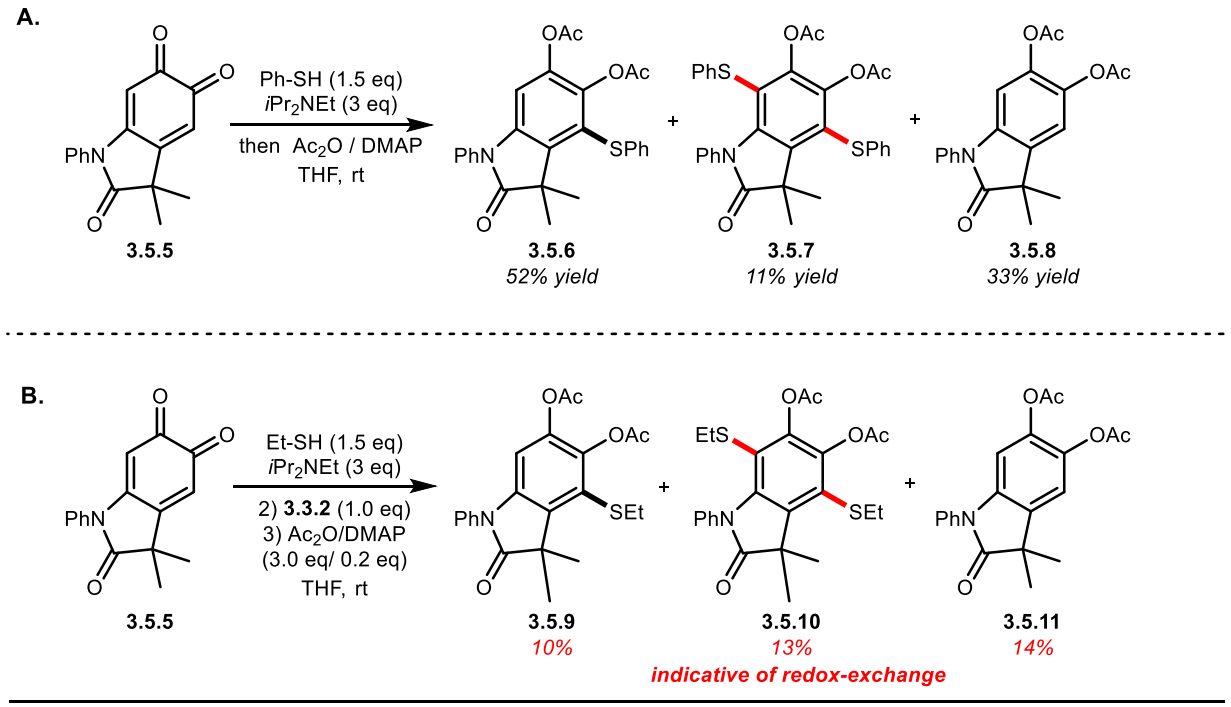

Figure 3.5.1 - Experiments Probing Redox-Exchange

Further optimization studies were carried using *ortho*-quinone **3.5.1** and 2-propanethiol, in an effort to promote thiol addition and prevent redox exchange from occurring. Numerous different additives were screened for their ability to enhance the sulfur addition step, including a variety of Lewis acids. From this screen, magnesium bromide diethyl etherate ($MgBr_2 \cdot Et_2O$) was identified as the optimal additive, with the hypothesis being that it acted as a Lewis acid to enhance the electrophilicity of C6 and therefore promote sulfur addition. The fully optimized conditions are provided in Scheme 3.1.2 and involve using 1.5 equiv. of thiol, 3 equiv. of DIPEA, 0.25 equiv. of $MgBr_2 \cdot Et_2O$ in a 0.05 M solution of 1,4-dioxane. These conditions provided the desired C6 sulfur adduct **3.5.12** in a 96% yield along with the reduced/acylated catechol **3.5.13** in a 3% yield. For a full explanation of the optimization procedure see Elizabeth Li's thesis.[24]

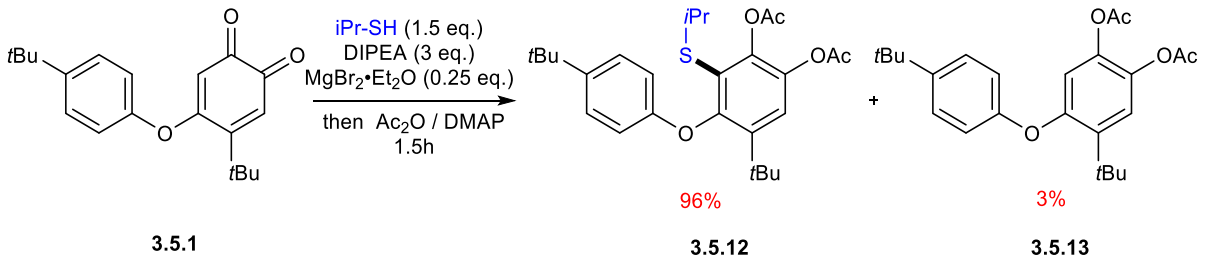

*Scheme 3.5.2 – Optimized reactions conditions for the addition of 2-propanethiol to ortho-quinone **3.1.1***

With optimized conditions in hand, a variety of 4,5-substituted quinones were then evaluated using ethanethiol, thiophenol, and 2-propanethiol (Table 3.5.1). Sulfur addition remains efficient across a range of 4,5-substituted quinones (entries **3.5.14**-**3.5.22**), with coupling occurring exclusively at C6. In order to explore the regiochemistry of the reaction further, a variety of 4-*mono*-substituted quinones bearing electron-rich/poor substituents (entries **3.5.23**-**3.5.34**) were tested. In all cases, 1,6-addition products were observed. The diminished yields of adducts **3.5.32**-**3.5.34** can be attributed to the overall stability of the *ortho*-quinone starting material, as it is prone to undergo decomposition when exposed to air.[24] When 1,2-napthoquinone and 1,2-*ortho*-quinone were examined, addition was observed exclusively at C3 and C4 respectively. The crude reaction mixtures were treated with Ac_2O/DMAP to simplify purification by protecting the catechol. Upon examination of the substrate scope in Figure 3.4.1, it is evident that under these conditions, the reaction preferentially undergoes a 1,6-addition as demonstrated with the 4,5-substituted and *mono*-substituted quinones. The only outliers were observed for when *ortho*-quinone was used as the coupling partner (entries **3.5.38**-**3.5.40**), in which case 1,4-addition was the only observable product.

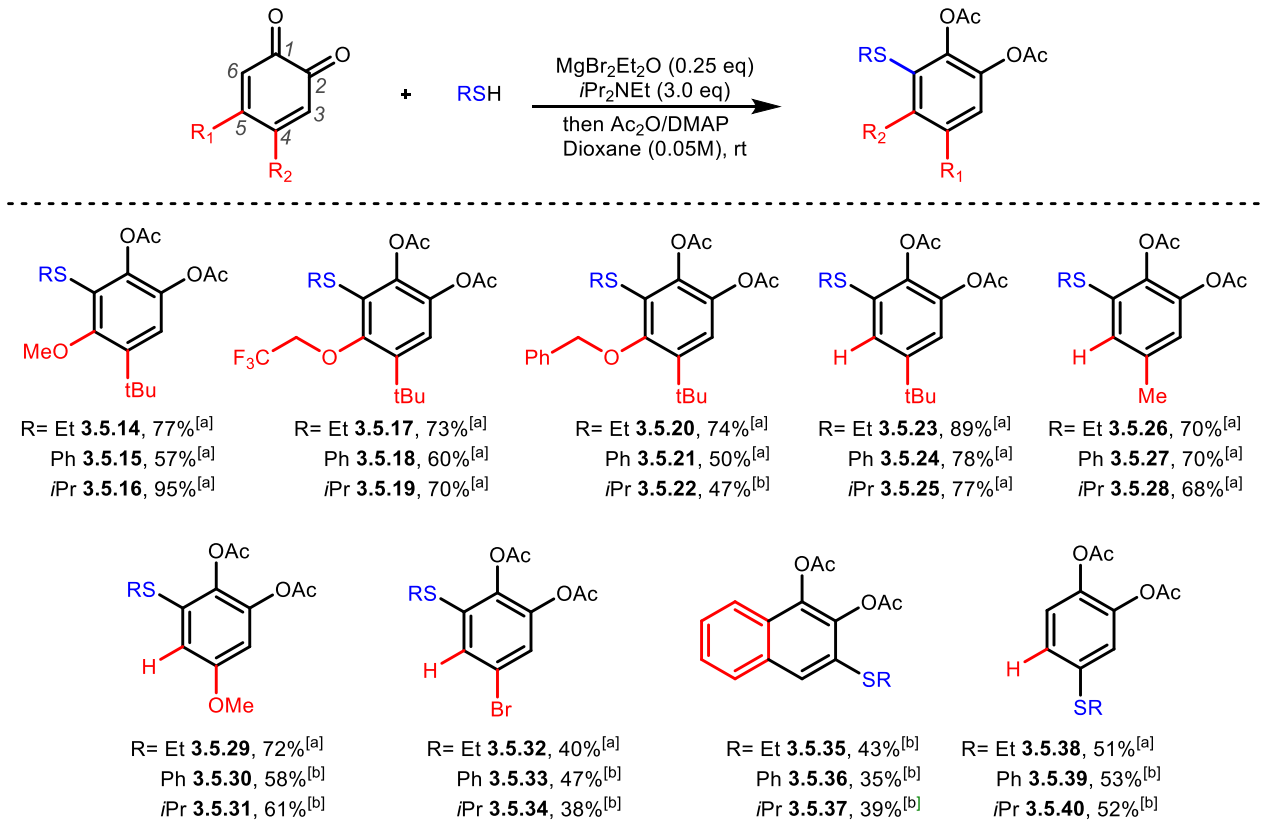

[a] Corresponds to substrates synthesized by Ms. Elizabeth Li
[b] Corresponds to substrates synthesized by the author

Table 3.5.1 – ortho-Quinone substrate scope

After examining the completed substrate scope, it was evident that our developed conditions were amenable to a broad range of quinones and provided a highly selective and mild procedure for the installation of aryl C-S bonds. Drawing inspiration from the biosynthetic pathway for the production of pheomelanin, we planned to show synthetic utility of our developed methodology by showing its direct application for the synthesis of novel 1,4-benzothiazines.

3.6 – Synthesis of Benzothiazines

3.6.1 – Scope of *ortho*-Quinones with L-cysteine

As previously mentioned in Section 3.4, the challenges in developing a diversifiable synthesis of benzothiazines stem from the synthetic limitations of installing aryl C-S and C-N bonds in a mild, selective manner. By taking advantage of the regioselectivity that our aryl C-S bond methodology provides, we sought to apply this to a synthesis of benzothiazines. This idea

originates from an initial experiment conducted by Dr. Kenneth Esguerra, wherein sulfur adduct **3.6.1.1** was prepared by the addition of L-cysteine ethyl ester to *ortho*-quinone **3.5.1** under non-optimized conditions (Figure 3.6.1.1). The addition proceeded smoothly and yielded the desired aryl C-S bond adduct that now contained an appendant nitrogen nucleophile that could be used as a functional handle. Catechol **3.6.1.1** was then oxidized by the addition of phenyliodine diacetate (PIDA) to generate the *ortho*-quinone *in-situ*, which immediately underwent a condensation/rearrangement reaction with the appendant nitrogen, generating benzothiazine **3.6.1.2** in a 90% isolated yield. Noteworthy features of this method are the generation of the benzothiazine with complete regiocontrol, using a transition metal-free process that readily occurs at room temperature. Moreover, benzothiazine heterocycle contains a free phenol as well as an ester that can be used as functional handles for additional synthetic manipulation.

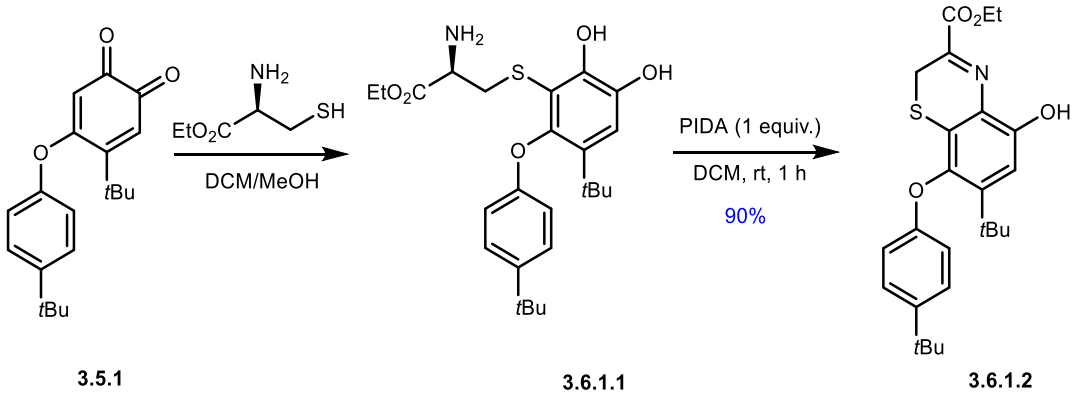

Scheme 3.6.1.1 – Initial synthesis of benzothiazine from L-cysteine ethyl ester

After obtaining these promising results, we wanted to apply this methodology to the synthesis of the functionalized pheomelanin monomer unit **3.6.1.4** (Figure 3.6.1.2). However, using our optimized C-S coupling additions to couple **3.6.1.6** to *ortho*-quinone **3.6.1.5** lead to the generation of complex reaction mixtures, which we attributed to the free amine moiety on the thiol when used in conjunction with less stable *ortho*-quinones than **3.5.1**. This prompted us to use the N-Boc protected cysteine analog, which could be subsequently deprotected after the C-S coupling.

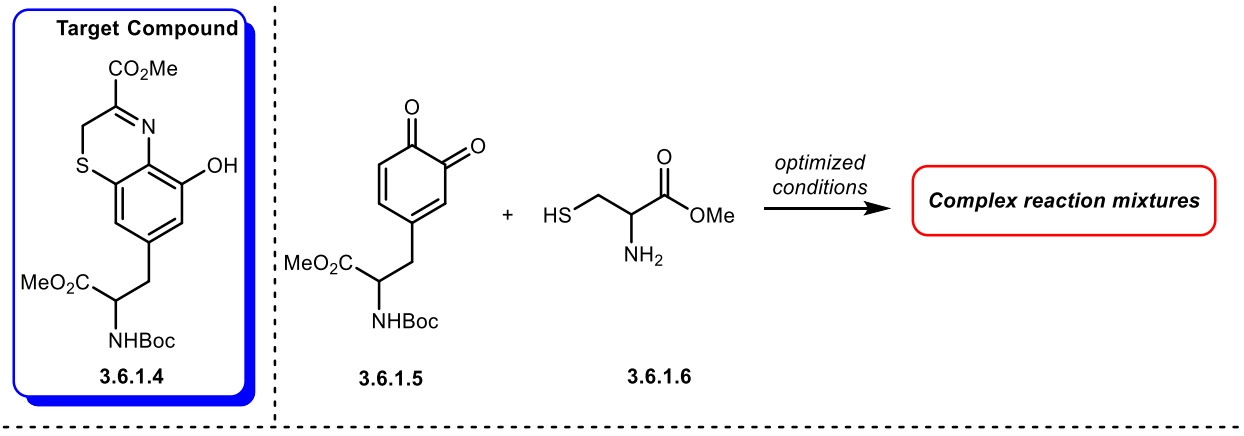

Figure 3.6.1.2 – Complex Reaction Mixtures Obtained using the Free Amine with More Complex Substrates

Using the commercially available N-Boc-L-cysteine methyl ester as the thiol source, the scope of the *ortho*-quinone was then evaluated (Table 3.6.1.1). Under our optimized conditions for C-S bond formation, the cysteine analog was added to the *ortho*-quinone to generate the catechol-sulfur adduct (C-S adduct). Gratifyingly, ^{1}H-NMR analysis of the crude reaction mixtures always displayed the C-S adduct as the major product obtained, which allowed us to proceed with the Boc-deprotection without any purification. Subsequent Boc-deprotection using a DCM/TFA (1:1) mixture at room temperature provided the free amine adducts (FA adducts) in near-quantitative yields. It was found that a large excess of TFA was needed in order to drive the reaction to completion. Using identical conditions as Dr. Kenneth Esguerra (1 equivalent of PIDA in DCM at room temperature), the FA adducts were oxidized to the *ortho*-quinones *in situ*, which then underwent condensation/rearrangement to afford the 1,4-benzothiazine derivatives. This reaction sequence was then applied to a variety of *ortho*-quinones to test their scope.

As discussed in Section 3.4, the substituents on the *ortho*-quinone starting material play a large role in determining its overall stability in the reaction media. To that end, several 4-*mono*-substitued quinones were evaluated (Table 3.6.1.1), recognizing that these are challenging substrates. The addition of protected cysteine **3.6.1.7** proceeded smoothly in almost all cases to provide the C-S adducts in good yields. Not surprisingly, the yields decreased slightly for the 4-bromo adduct as the quinone itself is noticeably unstable. Nevertheless, the material was carried through and the benzothiazines were isolated in moderate to excellent yields. The use of 4-bromo-

ortho-quinone to provide benzothiazine **3.6.1.9** is notable for its complementarity to more traditional cross-coupling reactions.

Following these promising results, more highly substituted *ortho*-quinones were then examined. Consistent with the results seen in Section 3.4, sulfur addition occurred selectively at C6 for all substrates, even when a 3,5-disubstituted quinone is used (**3.6.1.11**). It was also found that these conditions tolerated the presence of additional heteroatoms (entries **3.6.1.13** and **3.6.1.14**). Compound **3.6.1.14** is particularly interesting, not only because it is a highly-functionalized substrate, but also because it is a synthetic, unnatural amino-acid that could potentially be interesting for peptide chemists. Additionally, **3.6.1.14** is the N-Cbz protected, methyl ester derivative of the pheomelanin monomer described in Section 3.3 and to our knowledge is only the third reported synthesis of this monomer unit. The use of the protecting groups is crucial as it simplifies isolation during the purification procedure and allowed us to scale up the synthesis of **3.6.1.14** to 5 mmol, providing the first example of a scalable synthesis of this pheomelanin monomer unit.

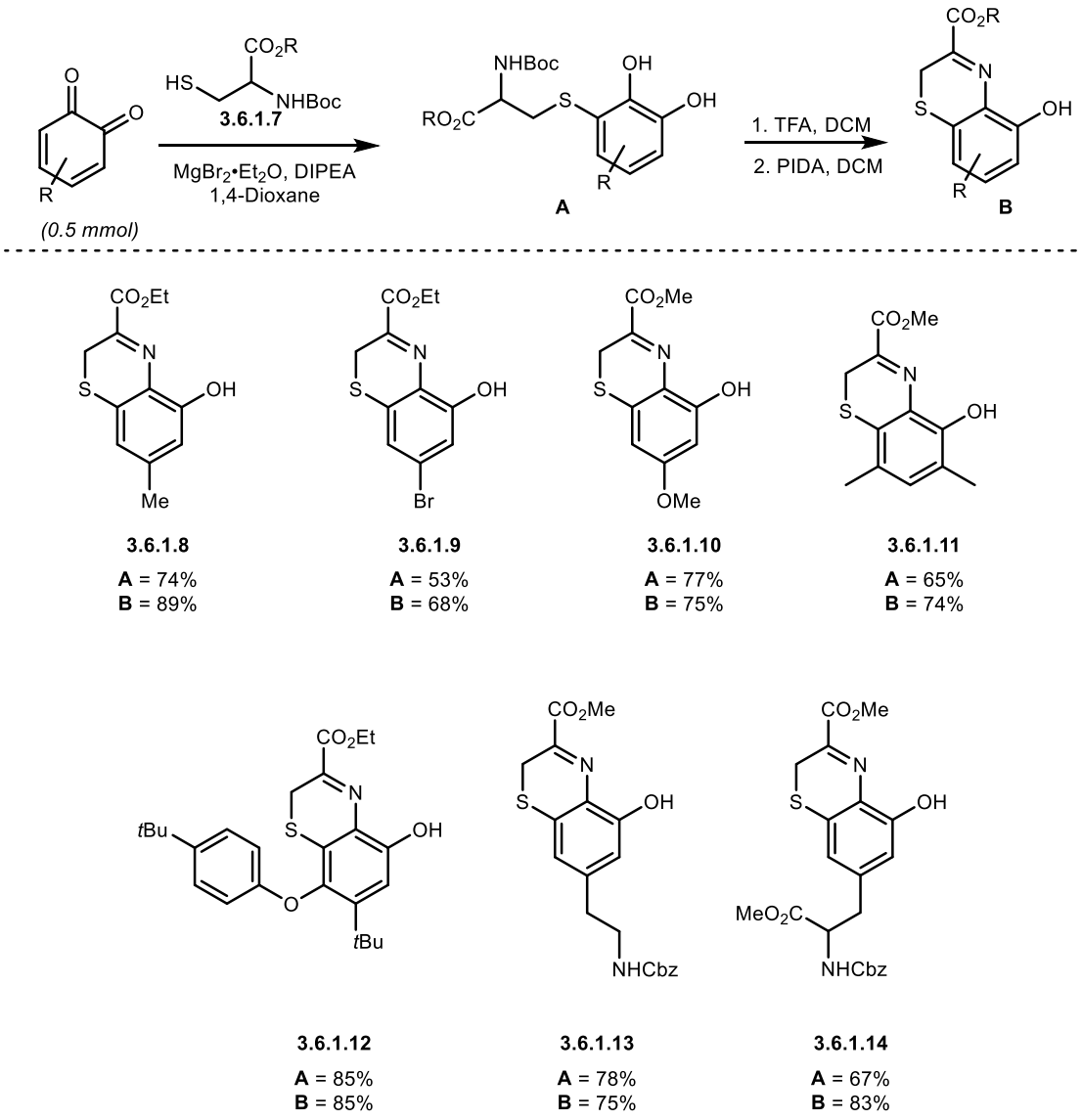

*The yields that are given next to (A) correspond to the initial sulfur addition step and represent ^{1}H-NMR yields obtained on crude reaction mixtures. The yields next to (B) correspond to the isolated yield of the benzothiazine.

Table 3.6.1.1 – Scope of ortho-Quinone with N-Boc-L-cysteine ester

3.6.2 – Scope of 2-aminothiols with L-dopaquinone

Next, we investigated the scope of the 2-aminothiol. L-dopaquinone derivative **3.6.2.6** was selected as the coupling partner since the benzothiazine products generated would constitute a new class of unnatural amino-acids. Unfortunately, the commercial availability of 2-aminothiols is limited, requiring that we prepare a small family of derivatives following the procedure of Mercey *et al*. (Figure 3.6.2.1).[25]

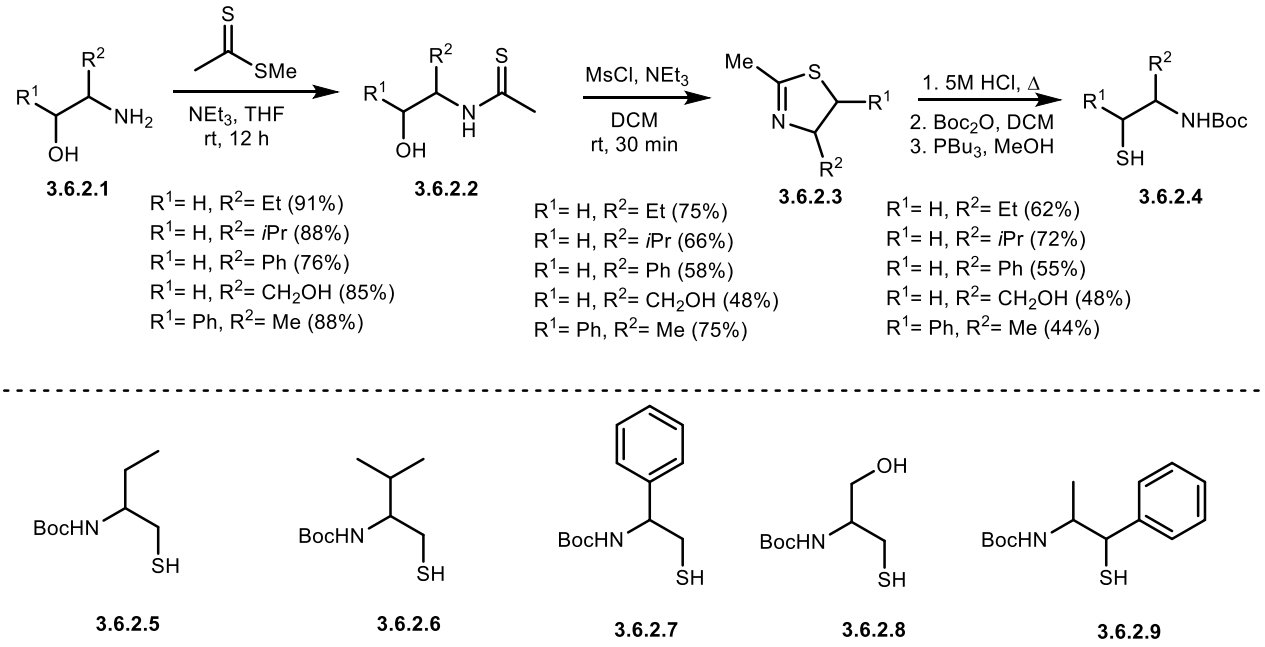

Table 3.6.2.1 – Synthesis of 2-aminothiol compounds

The synthesis begins by the conversion of commercially available 2-aminoalcohols (**3.6.2.1**) into their thioamide derivatives using methyldithioacetate, which acted as both a latent protecting group for both nitrogen and sulfur. The thioamides were then treated with methanesulfonylchloride and NEt_3 to provide thiazoles after purification on a silica gel column (**3.6.2.3**). The thiazoles were then heated to reflux in 5M HCl to generate the HCl salts of the 2-aminothiols in their disulfide forms, which were then protected with Boc-anhydride, and then reduced with tributylphosphine to provide the desired 2-aminothiol compounds. It was found that the stability of these compounds varied significantly and therefore they needed to be stored in the freezer under an inert atmosphere to prevent disulfide bond formation.

With the desired thiol-coupling partners in hand, the next step was to couple them with L-dopaquinone derivative **3.6.2.6** using our optimized conditions. These reactions proceeded smoothly using aminothiols **3.6.2.5**, **3.6.2.6**, and **3.6.2.7** to provide the desired aryl C-S product in moderate yields (Table 3.6.2.2). The remaining mass balance can be attributed to the reduced catechol product, which was observed in all three cases. This was not an unexpected result as working with quinone **3.6.2.6** is not a trivial task since it needs to be prepared immediately before use and starts to decompose if exposed to air. Unfortunately, when aminothiols **3.6.2.8** and **3.6.2.9**

were used as coupling partners the reaction failed to take place and only the reduced catechol was observed in the crude ^{1}H-NMRs.

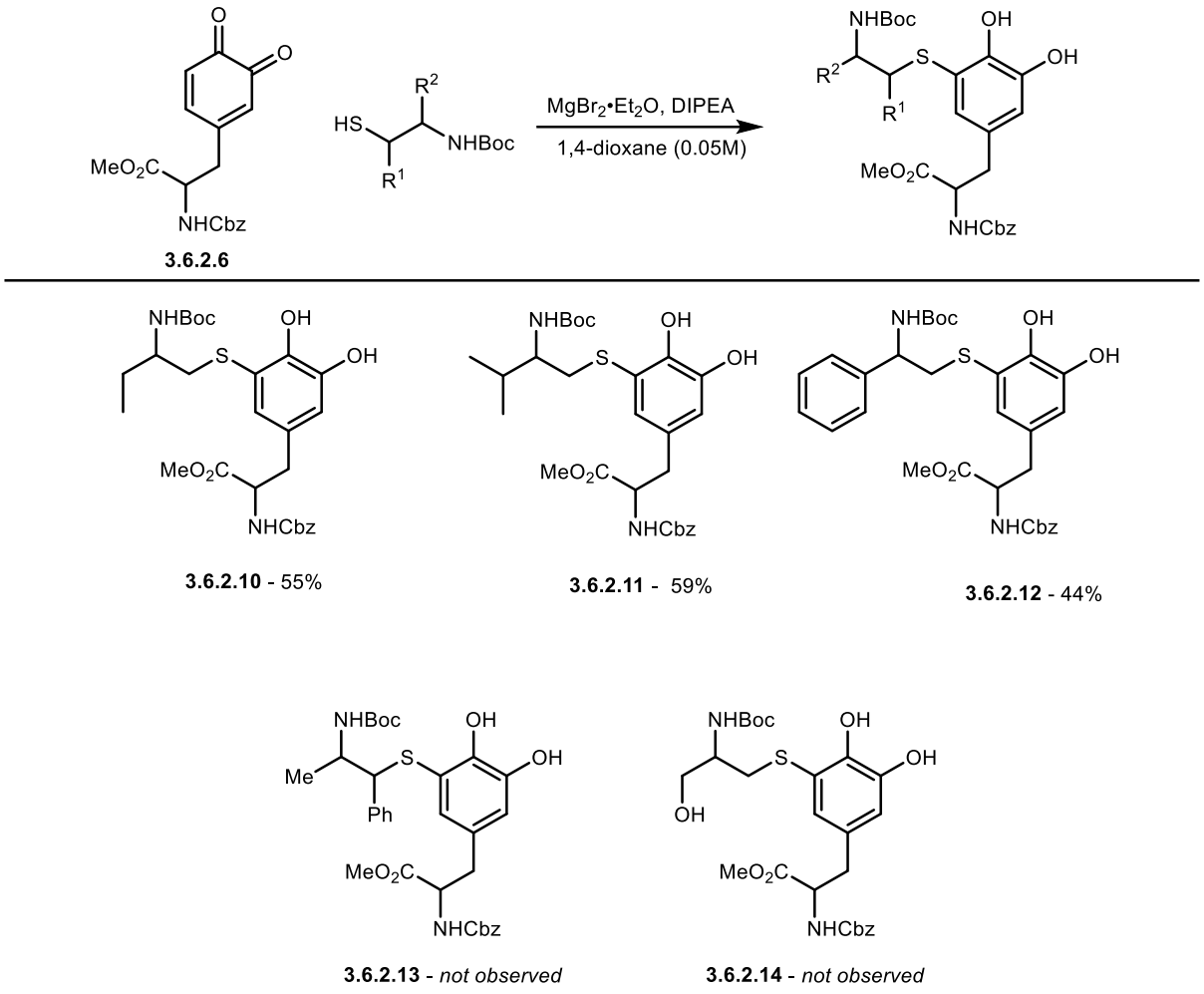

Table 3.6.2.2 – Scope of 2-aminothiols with L-Dopaquinone

Compounds **3.6.2.10**-**3.6.2.12** were then treated with TFA in DCM to successfully liberate the free amines (Figure 3.6.2.3). When these compounds were subjected to our original reaction conditions for oxidative cyclization, it was evident that the *ortho*-quinone was being generated *in situ* since the reaction mixture turned from yellow to bright orange. But it appeared as though the subsequent condensation/rearrangement failed to take place as over a period of ten minutes the mixture turned to dark purple/brown and then finally black. Attempts to monitor the reaction progress by TLC suggested complex reaction mixtures, which where further observed by crude ^{1}H-NMRs. In each case, complete decomposition of starting materials was observed without detectable quantities of the desired products.

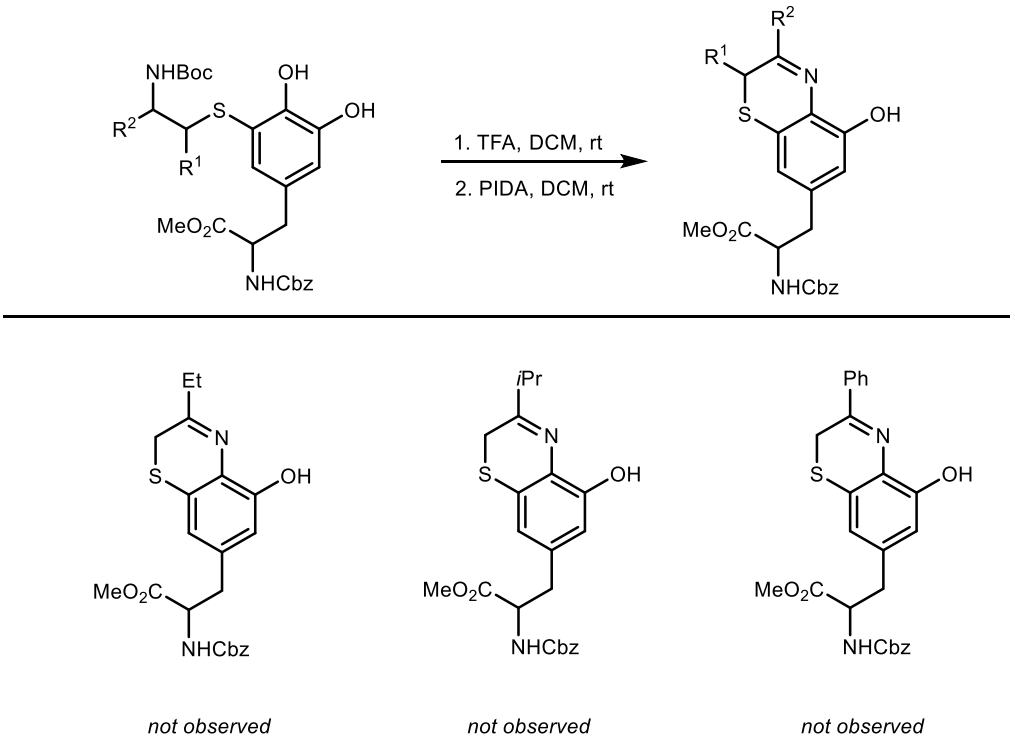

Figure 3.6.2.3 – Unsuccessful benzothiazine syntheses leading to complex reaction mixtures

To rationalize these results, we considered our proposed reaction mechanism. After the formation of *ortho*-quinone **3.6.2.15**, the appendant amine condenses to form intermediate **3.6.2.16** (Figure 3.6.2.4). From here, a formal 1,5-H shift, consisting most likely of a proton transfer mediated by acetate, is required for the formation of **3.6.2.17**. We suspect that amino-thiols possessing an ester at C2 have sufficiently acidic hydrogen atoms at C2 to allow for rapid proton transfer under the mild reaction conditions. For thiols lacking this electron withdrawing group, the corresponding C-H bond is less acidic, preventing the formal 1,5-H shift from occurring. Under these circumstances, imine **3.6.2.16** could be hydrolyzed to regenerate *ortho*-quinone **3.6.2.15**, which would be susceptible to nucleophilic attack by nitrogen nucleophiles in an intermolecular fashion. This remains our working hypothesis, since additional mechanistic insights were precluded by the complexity of the reaction mixtures.

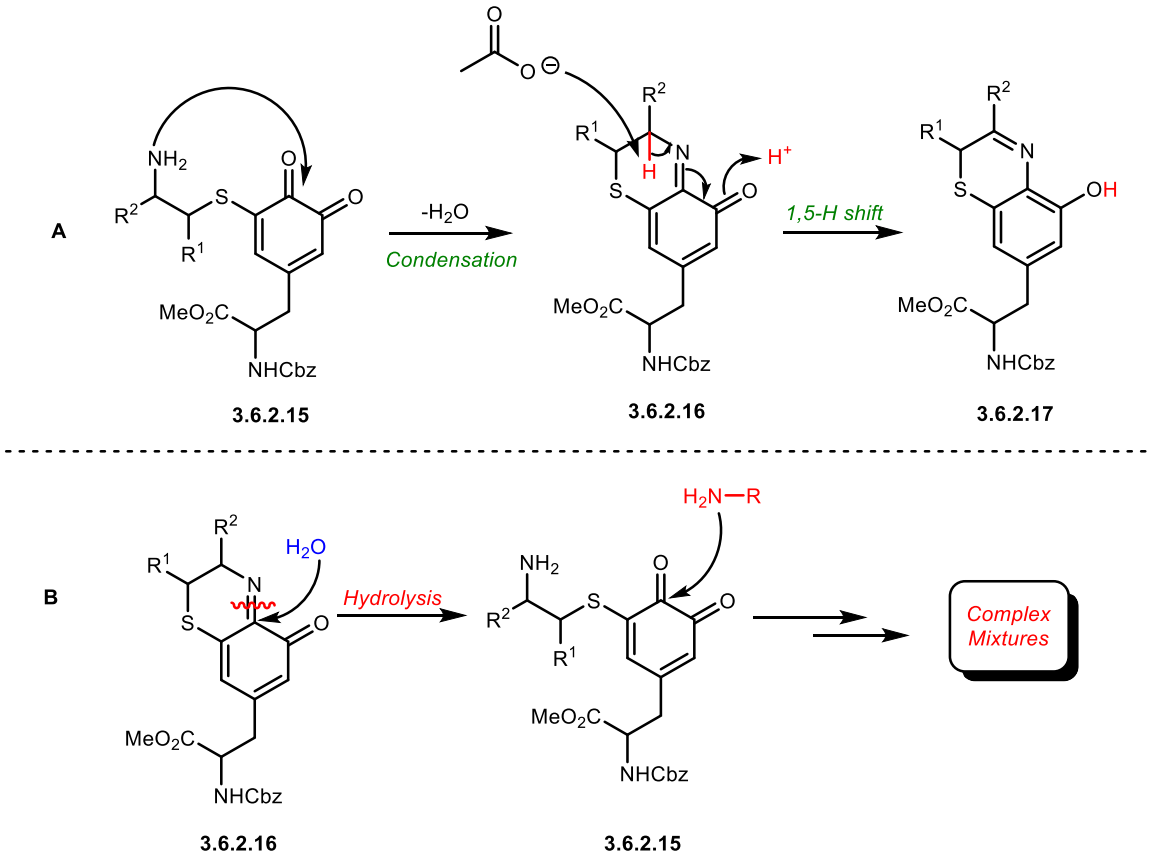

Figure 3.6.2.4 – Necessary 1,5-H Shift Required for Benzothiazine Synthesis

Since we hypothesized that the problematic step in the formation of **3.6.2.17** was the deprotonation at C3 which caused the reaction to stall at the imine intermediate **3.6.2.16**, we wondered whether the addition of a non-nucleophilic base to the reaction mixture would facilitate the formal 1,5-H shift. To this end, NEt_3, DIPEA, and pyridine were screened for their ability to facilitate this process using **3.6.2.18** as the model substrate (Table 3.6.2.1). Bases were added either at the start of the reaction or after a 10 minute time period. In all cases, the starting material was completely consumed; however, there was no detectable trace of benzothiazine **3.6.2.19** in the crude ^{1}H-NMRs. This led us to conclude that our oxidation conditions using PIDA would not be amenable to this transformation, prompting us to consider an alternative approach.

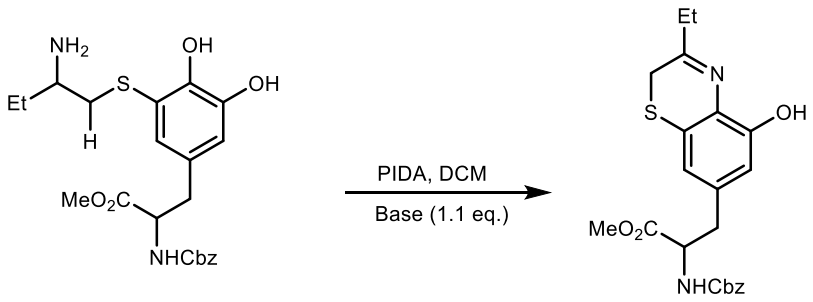

3.6.2.18 **3.6.2.19**

Entry	Base	Conversion	Yield
1[a]	NEt_3	100	0
2[b]	NEt_3	100	0
3[a]	DIPEA	100	0
4[b]	DIPEA	100	0
5[a]	Pyridine	100	0
6[b]	Pyridine	100	0

[a] Base was added at the start of the reaction
[b] Base was added after 10 minutes of reaction time

Table 3.6.2.1 – Screening of bases to facilitate 1,5-H Shift

In our search for alternative conditions to prepare the benzothiazines in Figure 3.6.2.3, we came across the work of Katherine Franz and coworkers, who reported the synthesis and isolation of benzothiazine-metal complexes through a similar oxidation/condensation route originating from the C-S adduct **3.6.2.20** (Scheme 3.6.2.5).[26-27] Under an air atmosphere, **3.6.2.20** is oxidized using either $CuCl_2 \cdot H_2O$ or $Ni(OAc)_2$ and NEt_3, to afford a stable, isolable benzothiazine-metal complex (**3.6.2.21**). Noteworthy from this example is the formation of the benzothiazine in the absence of an ester on C2 of the amino-thiol chain, suggesting that the relative acidity of the proton at C2 is not a factor under these conditions. Therefore, we hypothesized whether we could apply these conditions to prepare analogous benzothiazine-metal complexes which could be hydrolyzed upon work-up to provide our desired substrates. Under identical conditions reported by Franz, **3.6.2.18** was treated with either $CuCl_2 \cdot H_2O$ or $Ni(OAc)_2$ and NEt_3 under an air atmosphere. However, no reaction was observed in either case.

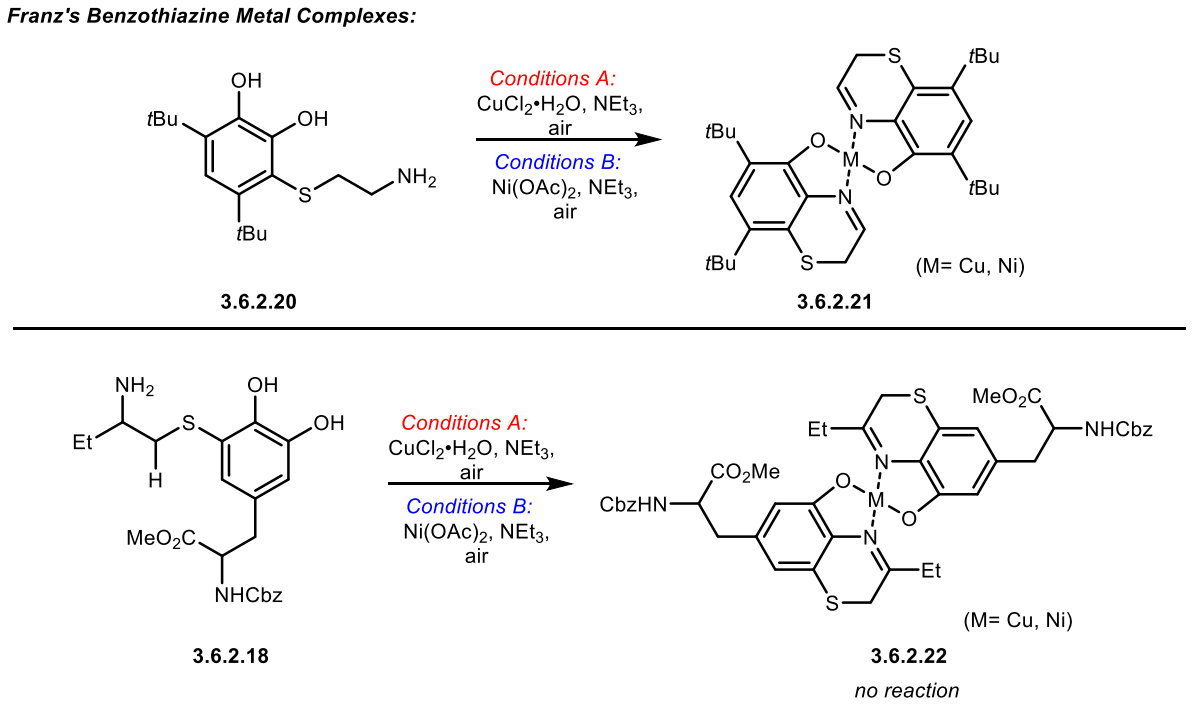

*Scheme 3.6.2.5 – Franz's Synthesis of Benzothiazine Metal Complexes and our Efforts to Prepare Metal Complex **3.6.2.20***

3.7 – Conclusion and Future Work

Building off of previous work conducted by Dr. Kenneth Esguerra, Mr. Zheng Huang, and Ms. Elizabeth Li who demonstrated the utility of aromatic C-S bond formation through the nucleophilic addition of thiols to *ortho*-quinones, the methodology was applied to a novel synthesis of 1,4-benothiazine derivatives. Under mild reaction conditions, a small library of 1,4-benzothiazine analogs were synthesized via a three-step sequence entailing the nucleophilic addition of cysteine to *ortho*-quinones under our optimized conditions, followed by Boc-deprotection, and finally oxidation of this C-S adduct which underwent a subsequent condensation/rearrangement reaction with the appendant amine to generate the benzothiazines. This sequence was used to synthesize compound **3.6.1.17**, which is a synthetic, unnatural amino-acid, as well as the N-Cbz protected, ethyl ester derivative of the pheomelanin monomer described in Section 3.3. The scope of the 2-aminothiols was then investigated, and it was found that substrates lacking an ester at C2 on the aminothiol were unable to undergo the formal 1,5-H shift, causing the reaction to stall at the unstable imine species **3.6.2.16**, which underwent decomposition. With this as our mechanistic hypothesis, we screened the addition of several non-

nucleophilic bases to facilitate the 1,5-H shift; however, this too resulted in decomposition of starting material.

Future endeavours for this project involve the further diversification of benzothiazine **3.6.1.17**, by manipulating the functional handles on the scaffold to synthesize a library of non-natural amino acids. This includes triflating the free phenol to perform cross coupling reactions (**3.7.1**), as well as saponifying the ester on the thiazole ring (**3.7.2**) for decarboxylative cross coupling purposes (Figure 3.7.1). Since we were unable to show scope on the 2-aminothiol end, this approach would still provide access to a diverse array of non-natural amino acids.

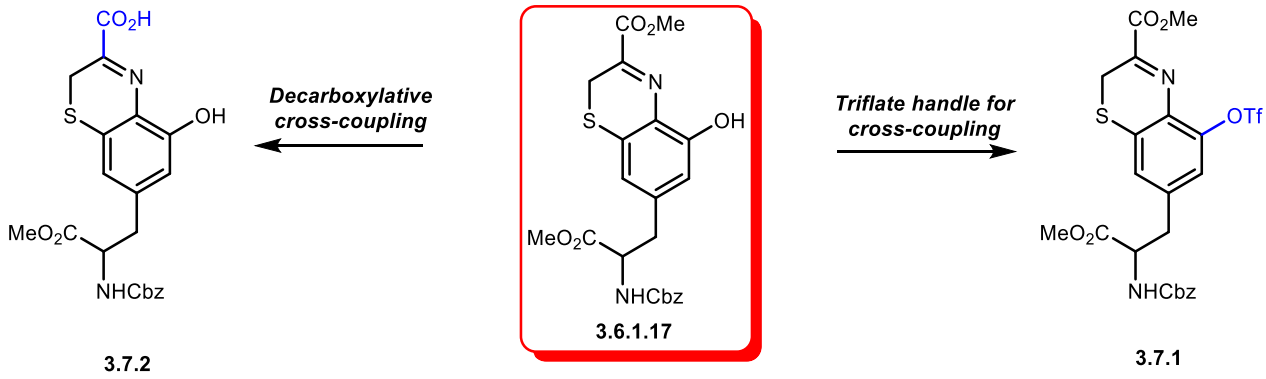

*Figure 3.7.1 – Future Endeavours for the Diversification of **3.6.1.17***

3.8 - References

1. Badshah, S. L.; Naeem, A., Bioactive Thiazine and Benzothiazine Derivatives: Green Synthesis Methods and Their Medicinal Importance. *Molecules* **2016,** *21* (8).
2. Napolitano, A.; Panzella, L.; Leone, L.; D'Ischia, M., Red Hair Benzothiazines and Benzothiazoles: Mutation-Inspired Chemistry in the Quest for Functionality. *Accounts of Chemical Research* **2013,** *46* (2), 519-528.
3. Ajani, O. O., Functionalized 1,4-Benzothiazine: A Versatile Scaffold with Diverse Biological Properties. *Archiv Der Pharmazie* **2012,** *345* (11), 841-851.
4. D'Mello, S. A. N.; Finlay, G. J.; Baguley, B. C.; Askarian-Amiri, M. E., Signaling Pathways in Melanogenesis. *International Journal of Molecular Sciences* **2016,** *17* (7).
5. Prota, G.; Nicolaus, R. A., *Gazzetta chimica Italiana* **1967,** *97*, 665.
6. Thomson, R. H., The pigments of reddish hair and feathers. *Angew Chem Int Ed Engl* **1974,** *13* (5), 305-12.
7. Prota, G.; Petrillo, O.; Nicolaus, R. A., *Gazzetta chimica Italiana* **1969,** *99*, 1193.
8. Prota, G.; Nicolaus, R. A., *Gazzetta chimica Italiana* **1968,** *98*, 495.
9. Rorsman, H.; Rosengren, A. M.; Rosengren, E., DETERMINATION OF 5-S-CYSTEINYLDOPA IN MELANOMAS WITH A FLUORIMETRIC METHOD. *Yale Journal of Biology and Medicine* **1973,** *46* (5), 516-522.

10. Ito, S.; Prota, G., FACILE ONE-STEP SYNTHESIS OF CYSTEINYLDOPAS USING MUSHROOM TYROSINASE. *Experientia* **1977,** *33* (8), 1118-1119.
11. Chioccara, F.; Novellino, E., A CONVENIENT ONE-STEP SYNTHESIS OF 5-CYSTEIN-S-YLDOPA USING CERIC AMMONIUM-NITRATE. *Synthetic Communications* **1986,** *16* (8), 967-971.
12. Thompson, A.; Land, E. J.; Chedekel, M. R.; Subbarao, K. V.; Truscott, T. G., A pulse radiolysis investigation of the oxidation of the melanin precursors 3,4-dihydroxyphenylalanine (dopa) and the cysteinyldopas. *Biochim. Biophys. Acta* **1985,** *843* (1), 49-57.
13. Simon, J. D.; Peles, D. N., The Red and the Black. *Accounts of Chemical Research* **2010,** *43* (11), 1452-1460.
14. Hearing, V. J., Biochemical control of melanogenesis and melanosomal organization. *Journal of Investigative Dermatology Symposium Proceedings* **1999,** *4* (1), 24-28.
15. Hida, T.; Wakamatsu, K.; Sviderskaya, E. V.; Donkin, A. J.; Montoliu, L.; Lamoreux, M. L.; Yu, B.; Millhauser, G. L.; Ito, S.; Barsh, G. S.; Jimbow, K.; Bennett, D. C., Agouti protein, mahogunin, and attractin in pheomelanogenesis and melanoblast-like alteration of melanocytes: a cAMP-independent pathway. *Pigment Cell & Melanoma Research* **2009,** *22* (5), 623-634.
16. Munde, S. B.; Bondge, S. P.; Bhingolikar, V. E.; Mane, R. A., A facile synthesis of 1,4-benzothiazines under solvent free conditions. *Green Chemistry* **2003,** *5* (2), 278-279.
17. Rajaram, S.; Reddy, G. S.; Iyengar, D. S., *Ind. J. Chem., Sect. B* **1999,** *38*, 639–640.
18. Sabatini, S.; Kaatz, G. W.; Rossolini, G. M.; Brandini, D.; Fravolini, A., From phenothiazine to 3-phenyl-1,4-benzothiazine derivatives as inhibitors of the Staphylococcus aureus NorA multidrug efflux pump. *Journal of Medicinal Chemistry* **2008,** *51* (14), 4321-4330.
19. Wilhelm, M.; Schmidt, P., A STUDY OF SYNTHESIS AND SOME REACTIONS OF 3-PHENYL-1,4-BENZOTHIAZINES. *Journal of Heterocyclic Chemistry* **1969,** *6* (5), 635-&.
20. Lin, Y. M.; Lu, G. P.; Wang, R. K.; Yi, W. B., Radical Route to 1,4-Benzothiazine Derivatives from 2-Aminobenzenethiols and Ketones under Transition-Metal-Free Conditions. *Organic Letters* **2016,** *18* (24), 6424-6427.
21. Chu, J. J.; Hu, B. L.; Liao, Z. Y.; Zhang, X. G., Copper-Catalyzed Three-Component Tandem Cyclization for One-Pot Synthesis of 1,4-Benzothiazines. *Journal of Organic Chemistry* **2016,** *81* (18), 8647-8652.
22. Qiao, Z. J.; Liu, H.; Xiao, X.; Fu, Y. N.; Wei, J. P.; Li, Y. X.; Jiang, X. F., Efficient Access to 1,4-Benzothiazine: Palladium-Catalyzed Double C-S Bond Formation Using Na2S2O3 as Sulfurating Reagent. *Organic Letters* **2013,** *15* (11), 2594-2597.
23. Cao, K.; Stack, D. E.; Ramanathan, R.; Gross, M. L.; Rogan, E. G.; Cavalieri, E. L., Synthesis and structure elucidation of estrogen quinones conjugated with cysteine, N-acetylcysteine, and glutathione. *Chemical Research in Toxicology* **1998,** *11* (8), 909-916.
24. Li, E.; Lumb, J.-P. An alternative synthesis of aromatic carbon-sulfur bonds: thiol addition to ortho-quinones. McGill, Montreal, QC, 2016.
25. Mercey, G.; Bregeon, D.; Gaumont, A. C.; Levillain, J.; Gulea, M., Efficient synthesis of primary 2-aminothiols from 2-aminoalcohols and methyldithioacetate. *Tetrahedron Letters* **2008,** *49* (46), 6553-6555.
26. Tesema, Y. T.; Pham, D. M.; Franz, K. J., Synthesis and characterization of copper(II) complexes of cysteinyldopa and benzothiazine model ligands related to pheomelanin. *Inorg Chem* **2006,** *45* (16), 6102-4.
27. Tesema, Y. T.; Pham, D. M.; Franz, K. J., Counterions influence reactivity of metal ions with cysteinyldopa model compounds. *Inorg Chem* **2008,** *47* (3), 1087-95.

Appendix
Experimental Procedures and Spectral Data
Table of Contents

1. General Experimental

All chemicals and solvents were purchased from Sigma Aldrich, Alfa Aesar, TCI, or Oakwood Chemicals. All solvents were dried and purified using an MBraun MB SPS 800 or Innovative Technology PureSolv MD 7. Unless otherwise stated, reactions were performed in flame-dried glassware under a nitrogen or argon atmosphere. Column chromatography was conducted using 200-400 mesh silica gel from Silicycle. ^{1}H-NMR spectra were acquired using Bruker Ascend 500 MHz, Bruker Ascend 400 MHz, and Varian Inova 400 MHz spectrometers. Chemical shifts (δ) are reported in parts per million (ppm) and are calibrated to the residual solvent peak. Coupling constants (*J*) are reported in Hz. Multiplicities are reported using the following abbreviations: s = singlet; d = doublet; t = triplet; q = quartet; m = multiplet (range of multiplet is given). ^{13}C-NMR spectra were acquired using Bruker Ascend 125 MHz, Bruker Ascend 100 MHz, and Varian Inova 100 MHz spectrometers. Chemical shifts (δ) are reported in parts per million (ppm) and are calibrated to the residual solvent peak. High resolution mass spectrometry was performed by Dr. Nadim Saade and Dr. Alexander Wahba in the Mass Spectrometry Facility at McGill University. High resolution mass spectra (HRMS) were recorded using a Bruker maXis Impact TOF mass spectrometer by electrospray ionization time of flight reflectron experiments. Low resolution mass spectra were recorded in the Lumb Group laboratory using an Agilent 5975C TAD Series GC/MSD EI-quadrupole mass spectrometer. All infrared spectra were recorded in the Integrated Laboratory Facility (Rm. 121) on a Bruker ALPHA FT-IR spectrometer. Analytical thin-layer chromatography was performed on pre-coated 250 mm layer thickness silica gel 60 F254 plates (EMD Chemicals Inc.). Solid state experiments were carried out in a Retsch MM200 mill at a frequency of 30 Hz using a 10 cm^3 teflon grinding jar and 2 stainless steel balls of 12 mm diameter.

Unless otherwise stated, all reactions proceeded to complete conversion. All NMR Yields were calculated from crude reaction mixture NMRs acquired with 30μL of nitromethane as an internal standard.

2. General Procedures for sal003 Derivatives:

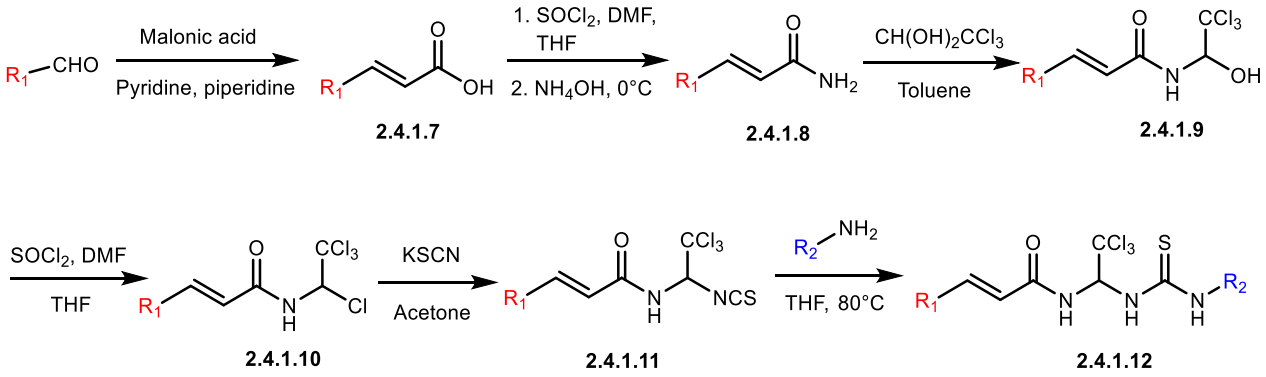

a) General Procedure A

In accordance with a previously described method, a flame-dried round bottom flask the appropriate aromatic aldehyde (1 equiv.) was combined with malonic acid (2 equiv.) and piperidine (0.1 equiv.) in anhydrous pyridine (0.5 M) and heated at 100˚C for 8h.[1] The reaction mixture was cooled to room temperature, quenched with 2M HCl, extracted with DCM, dried with $MgSO_4$ and concentrated *in vacuo*. The obtained solid was then washed with water and collected via vacuum filtration to afford **2.4.1.7**.

b) General Procedure B

In a flame-dried round bottom flask equipped with a Teflon-coated stir bar, **2.4.1.7** (1 equiv.) was added to a mixture of $SOCl_2$ (3 equiv.) and DMF (0.05 equiv.) in anhydrous THF (0.3 M) and heated at reflux for 2h. The reaction mixture was cooled to room temperature, the solvent removed *in vacuo*, and the residue was *carefully* added dropwise to a cooled solution of NH_4OH (5 equiv.). The obtained solid was then vacuum filtered and washed with water to yield the amide **2.4.1.8**.

c) General Procedure C

In a round bottom flask equipped with a Teflon-coated stir bar, **2.4.1.8** (1 equiv.) was combined with chloral hydrate (2 equiv.) in Toluene (0.5 M) and heated at reflux for 12h. The reaction mixture was allowed to cool to room temperature, placed into an ice bath, and the obtained solid was collected via vacuum filtration and washed with cold toluene to yield the chloral derivatives **2.4.1.9**.

d) General Procedure D

In a flame-dried round bottom flask equipped with a Teflon-coated stir bar, **2.4.1.9** (1 equiv.) was added to a mixture of $SOCl_2$ (3 equiv.) and DMF (0.05 equiv.) in anhydrous THF (0.3 M) and heated at reflux for 2h. The reaction mixture was cooled to room temperature, the solvent removed *in vacuo*, and the obtained solid was washed with cold hexanes and dried under vacuum to yield the chlorinated compounds **2.4.1.10** as solids.

e) General Procedure E

In a round bottom flask equipped with a Teflon-coated stir bar, potassium thiocyanate (1 equiv.) was combined with **2.4.1.10** (1 equiv.) and refluxed in acetone (0.5 M) for 1h. The reaction was cooled to room temperature, the white solid was filtered off and the filtrate was concentrated under reduced pressure to afford the isothiocyanates **2.4.1.11**.

f) General Procedure F

In a pressure vial equipped with a Teflon-coated stir bar, **2.4.1.11** (1 equiv.) was combined with the appropriate aniline and dissolved in THF (0.2 M). The pressure vial was sealed with the screwcap and heated at 85ºC for 8h. The mixture was cooled to room temperature, the vial was opened, the white solid was vacuum filtered and washed with cold EtOAc to afford the analogs **2.4.1.12.** In the case where there was no precipitate formed, the solvent was removed *in vacuo* and the solid was suspended in cold EtOAc and vacuum filtered to obtain **2.4.1.12**.

3. Synthesis and Characterization of Compounds in Chapter 2

a) Synthesis of Starting Materials

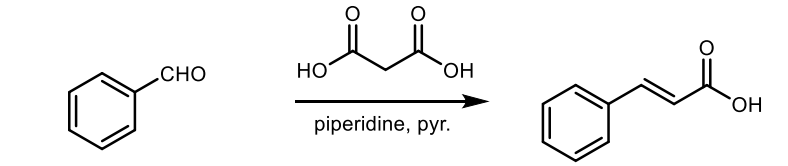

Chemical Formula: C_7H_6O
Molecular Weight: 106.1240

Chemical Formula: $C_9H_8O_2$
Molecular Weight: 148.1610
2.4.1.1

The reaction was carried out according to general procedure A using benzaldehyde (5.31 g, 50.0 mmol, 1 equiv.), malonic acid (10.41 g, 100.0 mmol, 2 equiv.), piperidine (0.49 mL, 5 mmol, 0.1

equiv.), and pyridine (100 mL, 0.5 M). Compound **2.4.1.1** (6.96 g, 47.0 mmol) was obtained as a white solid in 94% isolated yield.

^{1}H NMR (300 MHz, Acetone-d_6) δ 10.78 (bs, 1H), 7.75 – 7.65 (m, 3H), 7.48 – 7.40 (m, 3H), 6.55 (d, J = 16.1 Hz, 1H) ppm; **^{13}C NMR** (75 MHz, Acetone-d_6) δ 167.0, 144.6, 134.6, 130.2, 128.9, 128.1, 118.3 ppm. *Analytical data matches that reported in the literature.*[2]

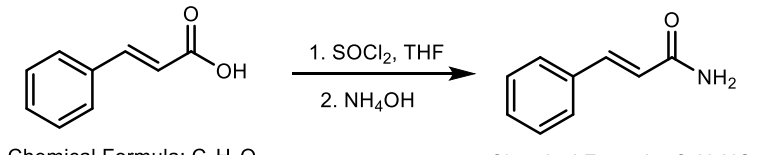

Chemical Formula: $C_9H_8O_2$
Molecular Weight: 148.1610
2.4.1.1

Chemical Formula: C_9H_9NO
Molecular Weight: 147.1770
2.4.1.2

The reaction was carried out according to general procedure B using **2.4.1.1** (100.0 g. 0.675 mol, 1 equiv.), $SOCl_2$ (146.8 mL, 2.025 mol, 3 equiv.), DMF (2.61 mL, 33.75 mmol, 0.05 equiv), THF (675 mL, 1 M), and then NH_4OH (120 mL, 5 equiv.) to afford **2.4.1.2** (87.42 g, 0.594 mol) as a white powder in 88% isolated yield.

^{1}H NMR (300 MHz, Acetone-d_6) δ 7.62 – 7.54 (m, 3H), 7.43 – 7.31 (m, 3H), 7.12 (bs, 1H), 6.75 (d, J = 15.8 Hz, 1H), 6.74 (bs, 1H) ppm; **^{13}C NMR** (75 MHz, Acetone-d_6) δ 167.0, 140.1, 135.3, 129.4, 128.8, 127.6, 121.7 ppm. *Analytical data matches that reported in the literature.*

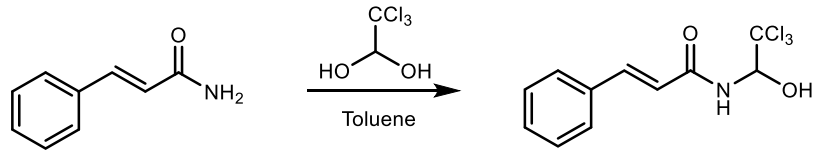

Chemical Formula: C_9H_9NO
Molecular Weight: 147.1770
2.4.1.2

Chemical Formula: $C_{11}H_{10}Cl_3NO_2$
Molecular Weight: 294.5560
2.4.1.3

The reaction was carried out according to general procedure C using **2.4.1.2** (87.42 g, 0.594 mol, 1 equiv.), chloral hydrate (196.49 g, 1.19 mol, 2 equiv.) and toluene (600 mL, 1 M) to obtain **2.4.1.3** (148.72 g, 0.505 mol) as white crystals in 85% isolated yield.

^{1}H NMR (500 MHz, Acetone-d_6) δ 8.06 (d, J = 9.4 Hz, 1H), 7.68 (d, J = 15.7 Hz, 1H), 7.63 (dd, J = 7.8, 1.8 Hz, 2H), 7.47 – 7.37 (m, 3H), 6.94 (d, J = 15.7 Hz, 1H), 6.78 – 6.69 (m, 1H), 6.18 –

6.08 (m, 1H) ppm; **^{13}C-NMR:** (125 MHz, $(CD_3)_2CO$): 165.1, 141,7, 135.0, 129.8, 128.9, 127.8, 120.7, 102.2, 81.1 ppm. *Analytical data matches that reported in the literature.*[3]

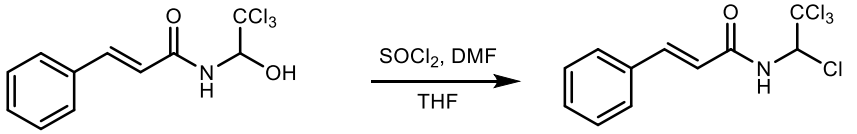

Chemical Formula: $C_{11}H_{10}Cl_3NO_2$
Molecular Weight: 294.5560
2.4.1.3

Chemical Formula: $C_{11}H_9Cl_4NO$
Molecular Weight: 312.9990
2.4.1.4

The reaction was carried out according to general procedure D using **2.4.1.3** (148.72 g, 0.505 mol, 1 equiv.), $SOCl_2$ (110 mL, 1.515 mol, 3 equiv.), DMF (1.96 mL, 25.25 mmol, 0.05 equiv.), and THF (505 mL, 1 M) to afford **2.4.1.4** (150.16 g, 0.480 mol) as a light yellow powder in 95% isolated yield.

^{1}H-NMR: (500 MHz, $(CD_3)_2CO$): 8.78 (d, *J*= 10.8 Hz, 1H), 7.75 (d, *J*= 15.4 Hz, 1H), 7.64 (m, 2H), 7.43 (m, 3H), 6.92 (d, *J*= 15.4 Hz, 1H), 6.82 (d, *J*= 10.8 Hz, 1H) ppm; ^{13}**C-NMR:** (125 MHz, $(CD_3)_2CO$): 164.8, 143.5, 134.6, 130.3, 129.0, 128.1, 119.2, 99.6, 75.0 ppm. *Analytical data matches that reported in the literature.*[3]

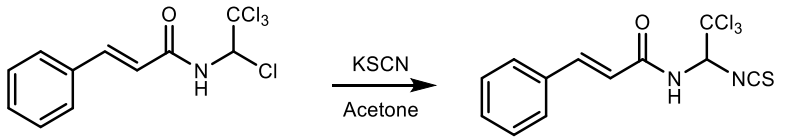

Chemical Formula: $C_{11}H_9Cl_4NO$
Molecular Weight: 312.9990
2.4.1.4

Chemical Formula: $C_{12}H_9Cl_3N_2OS$
Molecular Weight: 335.6270
2.4.1.5

The reaction was carried out according to general procedure E using **2.4.1.4** (150.16 g, 0.48 mol, 1 equiv.), potassium thiocyanate (46.65 g, 0.48 mol), and acetone (480 mL, 1 M) to afford **2.4.1.5** (153.05 g, 0.456 mol) as a yellow solid in 95% isolated yield.

^{1}H-NMR: (500 MHz, $(CD_3)_2CO$): 8.80 (d, *J*= 9 Hz, 1H), 7.76 (d, *J*= 16.1 Hz, 1H), 7.65 (m, 2H), 7.45 (m, 3H), 6.91 (d, *J*= 16.6 Hz, 1H), 6.61 (d, *J*= 9 Hz, 1H) ppm; **^{13}C-NMR:** (125 MHz, $(CD_3)_2CO$): 165.2, 143.4, 142.1, 134.6, 130.3, 129.0, 128.1, 119.2, 99.3, 73.0 ppm. *Analytical data matches that reported in the literature.*[3]

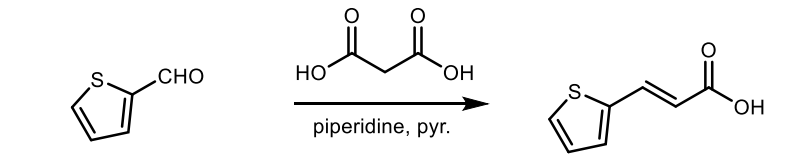

Chemical Formula: C_5H_4OS
Molecular Weight: 112.1460

Chemical Formula: $C_7H_6O_2S$
Molecular Weight: 154.1830
S3.1

The reaction was carried out according to general procedure A using 2-thiophenecarboxaldehyde (4.67 mL, 50.0 mmol, 1 equiv.), malonic acid (10.41 g, 100.0 mmol, 2 equiv.), piperidine (0.49 mL, 5 mmol, 0.1 equiv.), and pyridine (100 mL, 0.5 M). Compound **S3.1** (6.47 g, 42.0 mmol) was obtained as a beige solid in 84% isolated yield.

^{1}H-NMR: (500 MHz, $CDCl_3$): δ 7.91 (d, *J*=15.6 Hz, 1H), 7.45 (d, *J*= 5.0 Hz, 1H), 7.33 (d, *J*= 3.5 Hz, 1H), 7.11 (dd, *J*= 5.0, 3.6 Hz, 1H), 6.27 (d, *J*= 15.6 Hz, 1H) ppm. *Analytical data matches that reported in the literature.*

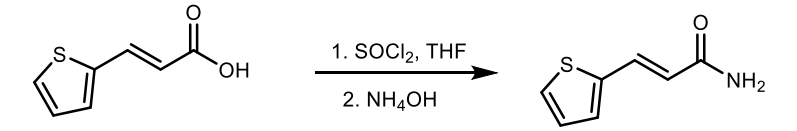

Chemical Formula: $C_7H_6O_2S$
Molecular Weight: 154.1830
S3.1

Chemical Formula: C_7H_7NOS
Molecular Weight: 153.1990
S3.2

The reaction was carried out according to general procedure B using **S3.1** (4.63 g, 30.0 mmol, 1equiv.), $SOCl_2$ (6.53 mL, 90.0 mmol, 3 equiv.), DMF (116 µL, 1.5 mmol, 0.05 equiv.), THF (100 mL, 0.3 M), and then NH_4OH (53 mL, 5 equiv.) to afford **S3.2** (4.04 g, 26.4 mmol) in 88% isolated yield.

^{1}H-NMR: (300 MHz, $(CD_3)_2CO$): δ 7.66 (d, *J*= 15.6 Hz, 1H), 7.51 (d, *J*= 5.2 Hz, 1H), 7.33 (d, *J*= 3.7 Hz, 1H), 7.10 (dd, *J*= 5.1, 3.6 Hz, 1H), 6.97 (bs, 1H), 6.47 (d, *J*= 15.1 Hz, 1H), 6.38 (bs, 1H) ppm. *Analytical data matches that reported in the literature.*

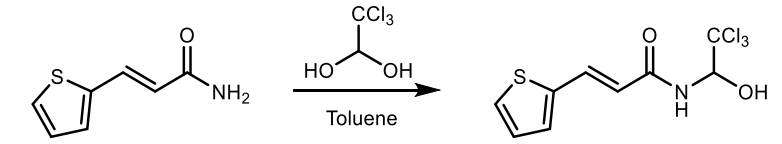

Chemical Formula: C_7H_7NOS
Molecular Weight: 153.1990
S3.2

Chemical Formula: $C_9H_8Cl_3NO_2S$
Molecular Weight: 300.5780
S3.3

The reaction was carried out according to general procedure C using **S3.2** (3.06 g, 20 mmol, 1 equiv.), chloral hydrate (6.62 g, 40 mmol, 2 equiv.), and Toluene (40 mL, 0.5 M) to afford **S3.3** (5.53 g, 18.4 mmol) in 92% isolated yield.

^{1}H-NMR: (300 MHz, $(CD_3)_2CO$): δ 8.08 (d, *J*= 9.1 Hz, 1H), 7.79 (d, *J*= 15.6 Hz, 1H), 7.56 (d, *J*= 5.2 Hz, 1H), 7.39 (d, *J*= 3.5 Hz, 1H), 7.12 (dd, *J*= 5.0, 3.7 Hz, 1H), 6.70 (d, *J*= 6.3 Hz, 1H), 6.67 (d, *J*= 15.6 Hz, 1H), 6.10 (dd, *J*= 9.3, 5.3 Hz, 1H) ppm. *Analytical data matches that reported in the literature.*

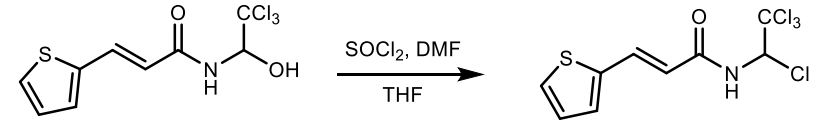

Chemical Formula: $C_9H_8Cl_3NO_2S$
Molecular Weight: 300.5780
S3.3

Chemical Formula: $C_9H_7Cl_4NOS$
Molecular Weight: 319.0210
S3.4

The reaction was carried out according to general procedure D using **S3.3** (4.51 g, 15 mmol, 1 equiv.), $SOCl_2$ (3.26 mL, 45 mmol, 3 equiv.), DMF (58 μL, 0.75 mmol, 0.05 equiv.), and THF (50 mL, 0.3 M) to afford **S3.4** (4.54 g, 14.25 mmol) in 95% isolated yield.

^{1}H-NMR: (300 MHz, $(CD_3)_2CO$): δ 8.77 (d, *J*= 10.5 Hz, 1H), 7.89 (d, *J*= 15.0 Hz, 1H), 7.61 (d, *J*= 5.2 Hz, 1H), 7.46 (d, *J*= 3.5 Hz, 1H), 7.14 (dd, *J*= 5.2, 3.7 Hz, 1H), 6.80 (d, *J*= 10.7 Hz, 1H), 6.65 (d, *J*= 15.2 Hz, 1H) ppm. *Analytical data matches that reported in the literature.*

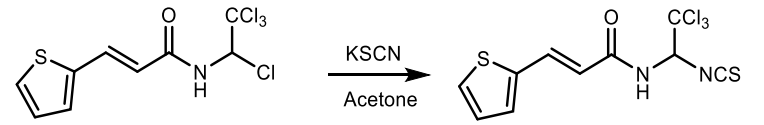

Chemical Formula: $C_9H_7Cl_4NOS$
Molecular Weight: 319.0210
S3.4

Chemical Formula: $C_{10}H_7Cl_3N_2OS_2$
Molecular Weight: 341.6490
S3.5

The reaction was carried out according general procedure E using **S3.4** (3.19 g, 10 mmol, 1 equiv.), KSCN (972 mg, 10 mmol, 1 equiv.), and acetone (20 mL, 0.5 M) to afford **S3.5** (3.25 g, 9.5 mmol) in a 95% isolated yield.

^{1}H-NMR: (500 MHz, $(CD_3)_2CO$): δ 8.77 (d, *J*= 9.2 Hz, 1H), 7.89 (d, *J*= 14.5 Hz, 1H), 7.62 (d, *J*= 5.1 Hz, 1H), 7.47 (d, *J*= 3.4 Hz, 1H), 7.16 (dd, *J*= 5.1, 3.8 Hz, 1H), 6.65 (d, *J*= 15.4 Hz, 1H), 6.57 (d, *J*= 9.6 Hz, 1H) ppm. *Analytical data matches that reported in the literature.*

b) Synthesis of sal003 Analogs in Table 2.4.1.1

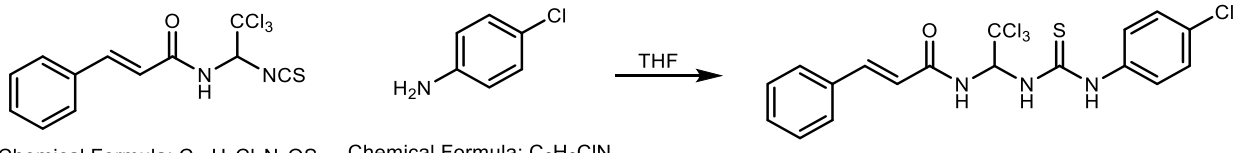

Chemical Formula: $C_{12}H_9Cl_3N_2OS$
Molecular Weight: 335.6270
2.4.1.5

Chemical Formula: C_6H_6ClN
Molecular Weight: 127.5710

Chemical Formula: $C_{18}H_{15}Cl_4N_3OS$
Molecular Weight: 463.1980
2.4.1.6

The reaction was carried out according to general procedure F using **2.4.1.5** (1.58 g, 4.0 mmol, 1 equiv.), 4-chloroaniline (510 mg, 4.0 mmol, 1 equiv.), and THF (20 mL, 0.2 M) to afford **2.4.1.6** (1.67 g, 3.6 mmol) as a white powder in 90% isolated yield.

^{1}H-NMR (400 MHz, DMSO-d_6) δ 10.38 (s, 1H), 8.99 (d, *J* = 8.7 Hz, 1H), 8.27 (d, *J* = 9.5 Hz, 1H), 7.68 – 7.53 (m, 5H), 7.48 – 7.38 (m, 6H), 6.79 (d, *J* = 15.8 Hz, 1H) ppm; **^{13}C-NMR:** (125 MHz, DMSO-d_6) δ 181.2, 164.8, 141.6, 138.3, 135.0, 130.4, 129.5, 129.1, 129.0, 128.3, 125.2, 121.3, 101.9, 70.1 ppm. *Analytical data matches that reported in the literature.*[4]

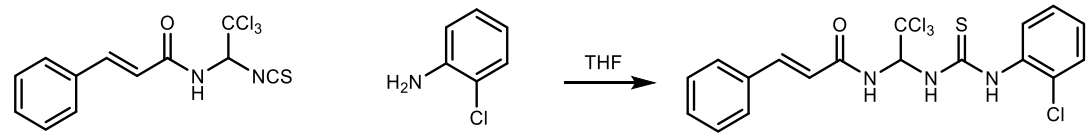

Chemical Formula: $C_{12}H_9Cl_3N_2OS$
Molecular Weight: 335.6270
2.4.1.5

Chemical Formula: C_6H_6ClN
Molecular Weight: 127.5710

Chemical Formula: $C_{18}H_{15}Cl_4N_3OS$
Molecular Weight: 463.1980
2.4.1.13

The reaction was carried out according to general procedure F using **2.4.1.5** (1.58 g, 4.0 mmol, 1 equiv.), 2-chloroaniline (410 μL, 4.0 mmol, 1 equiv.), and THF (20 mL, 0.2 M) to afford **2.4.1.13** (1.72 g, 3.7 mmol) as a white powder in 93% isolated yield.

^{1}H-NMR (400 MHz, DMSO-d_6) δ 9.97 (s, 1H), 9.08 (d, J = 8.8 Hz, 1H), 8.60 (d, J = 9.5 Hz, 1H), 7.74 (dd, J = 8.1, 1.6 Hz, 1H), 7.67 – 7.38 (m, 8H), 7.35 (td, J = 7.7, 1.5 Hz, 1H), 7.26 (td, J = 7.7, 1.7 Hz, 1H), 6.83 (d, J = 15.8 Hz, 1H) ppm; **^{13}C NMR** (101 MHz, DMSO-d_6) δ 182.8, 164.8, 141.5, 136.3, 135.0, 130.4, 129.9, 129.9, 129.5, 129.3, 128.2, 128.0, 127.5, 121.3, 102.0, 70.5 ppm. *Analytical data matches that reported in the literature.*[4]

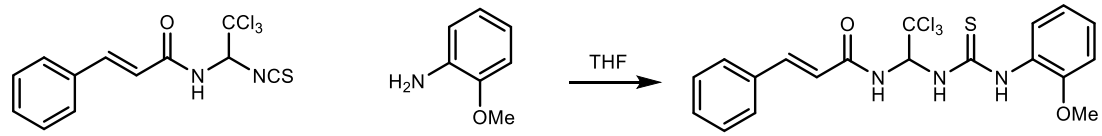

Chemical Formula: $C_{12}H_9Cl_3N_2OS$
Molecular Weight: 335.6270
2.4.1.5

Chemical Formula: C_7H_9NO
Molecular Weight: 123.1550

Chemical Formula: $C_{19}H_{18}Cl_3N_3O_2S$
Molecular Weight: 458.7820
2.4.1.14

The reaction was carried out according to general procedure F using **2.4.1.5** (1.58 g, 4.0 mmol, 1 equiv.), 2-methoxyaniline (451 μL, 4.0 mmol, 1 equiv.), and THF (20 mL, 0.2 M) to afford **2.4.1.14** (1.65 g, 3.6 mmol) as a white powder in 90% isolated yield.

^{1}H-NMR (400 MHz, DMSO-d_6) δ 9.82 (s, 1H), 9.02 (d, J = 8.7 Hz, 1H), 8.47 (bs, 1H), 8.00 – 7.83 (m, 1H), 7.66 – 7.38 (m, 7H), 7.22 – 7.12 (m, 1H), 7.07 (dd, J = 8.3, 1.4 Hz, 1H), 6.94 (td, J = 7.6, 1.4 Hz, 1H), 6.82 (d, J = 15.8 Hz, 1H), 3.84 (s, 3H) ppm; **^{13}C NMR** (101 MHz, DMSO-d_6) δ 181.6, 164.7, 152.2, 141.4, 135.0, 130.3, 129.5, 128.2, 127.6, 126.6, 126.4, 121.4, 120.2, 111.9, 102.1, 70.3, 56.1 ppm. *Analytical data matches that reported in the literature.*[4]

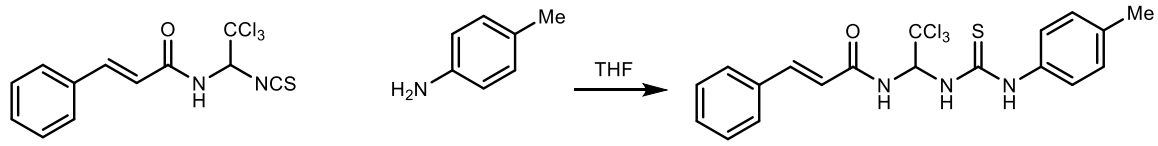

Chemical Formula: $C_{12}H_9Cl_3N_2OS$
Molecular Weight: 335.6270
2.4.1.5

Chemical Formula: C_7H_9N
Molecular Weight: 107.1560

Chemical Formula: $C_{19}H_{18}Cl_3N_3OS$
Molecular Weight: 442.7830
2.4.1.15

The reaction was carried out according to general procedure F using **2.4.1.5** (1.58 g, 4.0 mmol, 1 equiv.), 4-methylaniline (429 mg, 4.0 mmol, 1 equiv.), and THF (20 mL, 0.2 M) to afford **2.4.1.15** (1.56 g, 3.5 mmol) in 88% isolated yield.

^{1}H-NMR (400 MHz, DMSO-d_6) δ 10.25 (s, 1H), 8.97 (d, J = 8.6 Hz, 1H), 8.14 – 7.90 (m, 1H),

7.66 – 7.53 (m, 3H), 7.49 – 7.35 (m, 6H), 7.18 (d, *J* = 8.2 Hz, 2H), 6.76 (d, *J* = 15.8 Hz, 1H), 2.29 (s, 3H) ppm; **^{13}C NMR** (101 MHz, DMSO-d_6) δ 181.1, 164.7, 141.5, 136.5, 135.0, 134.8, 130.4, 129.7, 129.5, 128.2, 124.0, 121.3, 102.2, 70.2, 21.0 ppm. *Analytical data matches that reported in the literature.*[4]

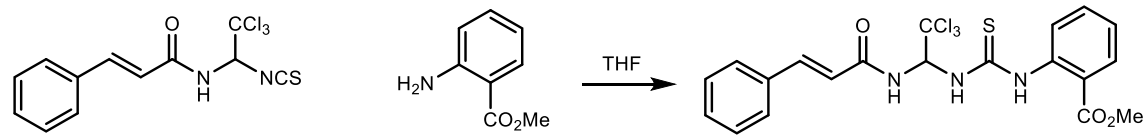

Chemical Formula: $C_{12}H_9Cl_3N_2OS$
Molecular Weight: 335.6270
2.4.1.5

Chemical Formula: $C_8H_9NO_2$
Molecular Weight: 151.1650

Chemical Formula: $C_{20}H_{18}Cl_3N_3O_3S$
Molecular Weight: 486.7920
2.4.1.16

The reaction was carried out according to general procedure F using **2.4.1.5** (1.58 g, 4.0 mmol, 1 equiv.), methyl 2-aminobenzoate (518 μL, 4.0 mmol, 1 equiv.), and THF (20 mL, 0.2 M) to afford **2.4.1.16** (1.79 g, 3.7 mmol) in 92% isolated yield.

^{1}H-NMR (400 MHz, DMSO-d_6) δ 10.33 (s, 1H), 9.02 (d, *J* = 8.9 Hz, 1H), 8.92 (d, *J* = 9.4 Hz, 1H), 7.83 (ddd, *J* = 23.9, 8.0, 1.4 Hz, 2H), 7.67 – 7.37 (m, 8H), 7.31 (td, *J* = 7.6, 1.2 Hz, 1H), 6.88 (d, *J* = 15.8 Hz, 1H), 3.81 (s, 3H) ppm; **^{13}C NMR** (101 MHz, DMSO-d_6) δ 182.8, 166.7, 164.8, 141.5, 139.6, 135.1, 132.8, 130.6, 130.4, 129.5, 128.3, 128.2, 125.8, 124.5, 121.4, 101.9, 70.5, 52.8 ppm. *Analytical data matches that reported in the literature.*[4]

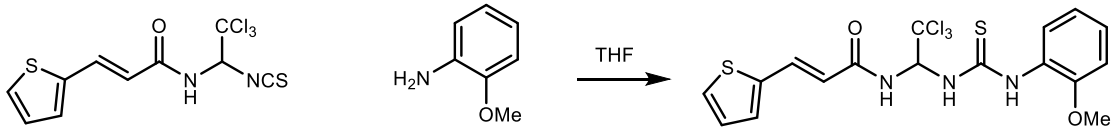

Chemical Formula: $C_{10}H_7Cl_3N_2OS_2$
Molecular Weight: 341.6490
2.7.5

Chemical Formula: C_7H_9NO
Molecular Weight: 123.1550

Chemical Formula: $C_{17}H_{16}Cl_3N_3O_2S_2$
Molecular Weight: 464.8040
2.4.1.17

The reaction was carried out according to general procedure F using **2.7.5** (1.37 g, 4 mmol, 1 equiv.), 2-methoxylaniline (451 μL, 4.0 mmol, 1 equiv.), and THF (20 mL, 0.2 M) to afford **2.4.1.17** (1.67 g, 3.6 mmol) as a white powder in 91% isolated yield.

^{1}H-NMR (500 MHz, DMSO-d_6) δ 9.81 (s, 1H), 9.00 (d, *J* = 8.8 Hz, 1H), 8.49 (s, 1H), 7.90 (d, *J* = 7.7 Hz, 1H), 7.70 (d, *J* = 15.5 Hz, 1H), 7.64 (d, *J* = 5.1 Hz, 1H), 7.49 – 7.41 (m, 2H), 7.18 – 7.10 (m, 2H), 7.05 (dd, *J* = 8.4, 1.3 Hz, 1H), 6.92 (td, *J* = 7.7, 1.3 Hz, 1H), 6.56 (d, *J* = 15.5 Hz, 1H),

3.82 (s, 3H) ppm; **^{13}C NMR** (126 MHz, DMSO-d_6) δ 181.6, 164.5, 152.1, 140.0, 134.4, 131.9, 129.1, 128.9, 127.6, 126.6, 126.4, 120.2, 119.9, 111.9, 102.1, 70.2, 56.1 ppm. *Analytical data matches that reported in the literature.*[4]

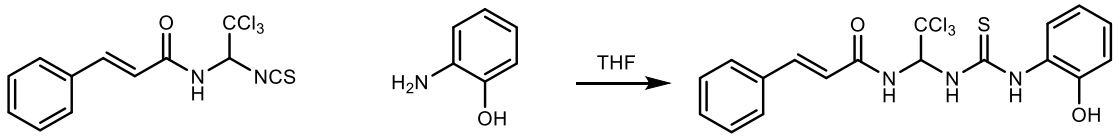

Chemical Formula: $C_{12}H_9Cl_3N_2OS$
Molecular Weight: 335.6270
2.4.1.5

Chemical Formula: C_6H_7NO
Molecular Weight: 109.1280

Chemical Formula: $C_{18}H_{16}Cl_3N_3O_2S$
Molecular Weight: 444.7550
2.4.1.18

The reaction was carried out according to general procedure F using **2.4.1.5** (1.58 g, 4.0 mmol, 1 equiv.), 2-aminophenol (437 mg, 4.0 mmol, 1 equiv.), and THF (20 mL, 0.2 M) to afford **2.4.1.18** (1.51 g, 3.4 mmol) in 85% isolated yield.

R_f = (EtOAc/hexanes 1:1): 0.24; **IR** (neat) v = 3287.4, 3210.6, 3083.0, 3026.1, 2955.5, 1494.7, 1452.0, 1342.6, 1206.4, 1136.0, 742.0 cm^{-1}; **^{1}H NMR** (400 MHz, DMSO-d_6) δ 9.93 (s, 1H), 9.78 (s, 1H), 9.02 (d, J = 8.8 Hz, 1H), 8.55 (bs, 1H), 8.02 – 7.81 (m, 1H), 7.66 – 7.35 (m, 7H), 7.08 – 6.72 (m, 4H) ppm; **^{13}C NMR** (101 MHz, DMSO-d_6) δ 181.4, 164.7, 150.1, 141.4, 135.1, 130.3, 129.5, 128.2, 126.7, 126.0, 121.4, 118.8, 115.8, 102.1, 70.3 ppm; **HRMS:** Calcd. for $C_{18}H_{16}Cl_3N_3NaO_2S$: $[M+Na]^+$: 465.9921 m/z, found 465.9920 m/z.

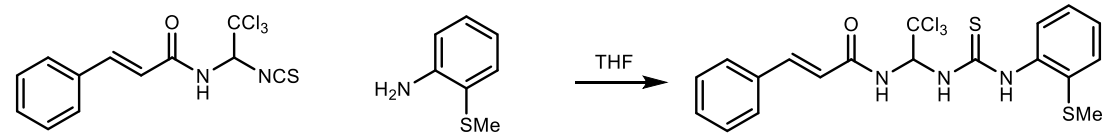

Chemical Formula: $C_{12}H_9Cl_3N_2OS$
Molecular Weight: 335.6270
2.4.1.5

Chemical Formula: C_7H_9NS
Molecular Weight: 139.2160

Chemical Formula: $C_{19}H_{18}Cl_3N_3OS_2$
Molecular Weight: 474.8430
2.4.1.19

The reaction was carried out according to general procedure F using **2.4.1.5** (1.58 g, 4.0 mmol, 1 equiv.), 2-(methylthio)aniline (501 μL, 4.0 mmol, 1 equiv.), and THF (20 mL, 0.2 M) to afford **2.4.1.19** (1.80 g, 3.8 mmol) in 95% isolated yield.

R_f = (EtOAc/hexanes 1:1): 0.36; **IR** (neat) v = 3311.1, 3250.4, 3033.9, 1654.4, 1608.8, 1492.0, 1274.5, 1090.5, 1072.1, 992.0, 887.1, 766.7, 711.5, 686.8, 602.5, 513.4, 480.3 cm^{-1}; **^{1}H NMR**

(400 MHz, DMSO-d_6) δ 9.76 (s, 1H), 9.07 (d, J = 8.8 Hz, 1H), 8.35 (s, 1H), 7.66 – 7.53 (m, 3H), 7.52 – 7.38 (m, 5H), 7.35 – 7.24 (m, 2H), 7.18 (td, J = 7.5, 1.6 Hz, 1H), 6.83 (d, J = 15.8 Hz, 1H), 2.42 (s, 3H) ppm; **^{13}C NMR** (101 MHz, DMSO-d_6) δ 183.0, 164.7, 141.5, 136.4, 136.0, 135.0, 130.4, 129.5, 129.3, 128.2, 127.7, 126.6, 125.3, 121.4, 102.2, 70.5, 15.1 ppm; **HRMS:** Calcd. for $C_{19}H_{18}Cl_3N_3NaOS_2$: $[M+Na]^+$: 495.9849 m/z, found 495.9862 m/z.

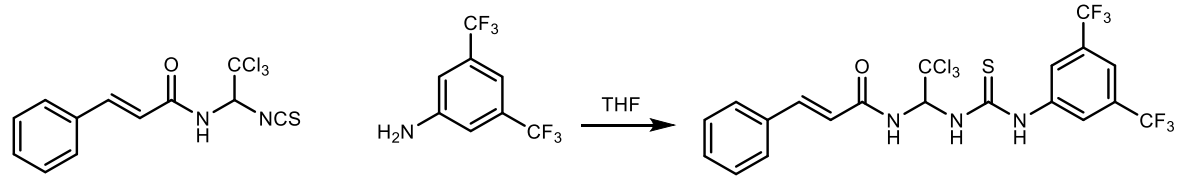

Chemical Formula: $C_{12}H_9Cl_3N_2OS$
Molecular Weight: 335.6270
2.4.1.5

Chemical Formula: $C_8H_5F_6N$
Molecular Weight: 229.1254

Chemical Formula: $C_{20}H_{14}Cl_3F_6N_3OS$
Molecular Weight: 564.7524
2.4.1.20

The reaction was carried out according to general procedure F using **2.4.1.5** (1.58 g, 4.0 mmol, 1 equiv.), 3,5-Bis(trifluoromethyl)aniline (625 μL, 4.0 mmol, 1 equiv.), and THF (20 mL, 0.2 M) to afford **2.4.1.20** (2.10 g, 3.7 mmol) in 93% isolated yield.

R_f = (EtOAc/hexanes 1:1): 0.51; **IR** (neat) v = 3232.1, 3070.2, 2998.7, 2945.5, 1656.0, 1621.6, 1503.4, 1376.5, 1274.3, 1174.9, 1131.1, 954.8, 896.3, 837.2, 811.3, 767.7, 681.1, 490.1 cm^{-1}; **^{1}H-NMR** (400 MHz, DMSO-d_6) δ 10.79 (s, 1H), 9.03 (d, J = 8.8 Hz, 1H), 8.62 (d, J = 9.4 Hz, 1H), 8.33 (s, 2H), 7.84 (s, 1H), 7.68 – 7.53 (m, 3H), 7.43 (q, J = 8.1, 7.3 Hz, 4H), 6.84 (d, J = 15.8 Hz, 1H) ppm; **^{13}C NMR** (101 MHz, DMSO-d_6) δ 181.6, 164.9, 141.7, 141.6, 135.0, 131.3, 131.0, 130.7, 130.4, 129.5, 128.3, 127.6, 124.9, 123.1, 122.2, 121.2, 119.5, 117.9, 101.7, 70.0 ppm; **HRMS:** Calcd. for $C_{20}H_{14}Cl_3F_6N_3NaOS$: $[M+Na]^+$: 585.9720 m/z, found 585.9712 m/z.

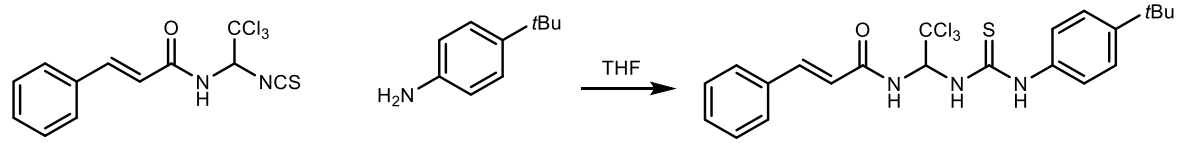

Chemical Formula: $C_{12}H_9Cl_3N_2OS$
Molecular Weight: 335.6270
2.4.1.5

Chemical Formula: $C_{10}H_{15}N$
Molecular Weight: 149.2370

Chemical Formula: $C_{22}H_{24}Cl_3N_3OS$
Molecular Weight: 484.8640
2.4.1.21

The reaction was carried out according to general procedure F using **2.4.1.5** (1.58 g, 4.0 mmol, 1 equiv.), 4-*tert*-butylaniline (637 μL, 4.0 mmol, 1 equiv.), and THF (20 mL, 0.2 M) to afford

2.4.1.21 (1.82 g, 3.76 mmol) in 94% isolated yield.

R_f = (EtOAc/hexanes 1:1): 0.54; **IR** (neat) v = 3233.6, 2962.3, 1659.8, 1625.4, 1550.5, 1450.6, 1289.5, 1037.7, 986.7, 834.4, 827.6, 805.1, 739.4, 633.3, 520.3, 490.3 cm^{-1}; **^{1}H NMR** (400 MHz, DMSO-d_6) δ 10.25 (s, 1H), 8.97 (d, J = 8.7 Hz, 1H), 8.10 (s, 1H), 7.65 – 7.54 (m, 3H), 7.43 (m, 8H), 6.77 (d, J = 15.8 Hz, 1H), 1.28 (s, 9H) ppm; **^{13}C NMR** (101 MHz, DMSO-d_6) δ 181.1, 164.7, 147.9, 141.5, 136.5, 135.0, 130.4, 129.5, 128.2, 125.9, 123.5, 121.3, 102.2, 70.2, 34.6, 31.6 ppm; **HRMS:** Calcd. for $C_{22}H_{24}Cl_3N_3NaOS$: $[M+Na]^+$: 506.0598 m/z, found 506.0601 m/z.

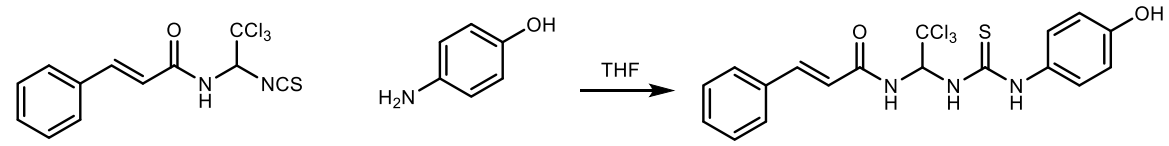

Chemical Formula: $C_{12}H_9Cl_3N_2OS$
Molecular Weight: 335.6270
2.4.1.5

Chemical Formula: C_6H_7NO
Molecular Weight: 109.1280

Chemical Formula: $C_{18}H_{16}Cl_3N_3O_2S$
Molecular Weight: 444.7550
2.4.1.22

The reaction was carried out according to general procedure F using **2.4.1.5** (1.58 g, 4.0 mmol, 1 equiv.), 4-aminophenol (437 mg, 4.0 mmol, 1 equiv.), and THF (20 mL, 0.2 M) to afford **2.4.1.22** (1.51 g, 3.4 mmol) in 85% isolated yield.

R_f = (EtOAc/hexanes 1:1): 0.16; **IR** (neat) v = 3197.9, 3083.5, 3025.7, 2957.1, 1654.9, 1617.1, 1500.8, 1341.2, 1203.5, 1030.9, 887.7, 792.4, 764.0, 682.6, 554.1 cm^{-1}; **^{1}H NMR** (500 MHz, DMSO-d_6) δ 10.06 (s, 1H), 9.49 (s, 1H), 8.95 (d, J = 8.7 Hz, 1H), 8.19 – 7.49 (m, 4H), 7.49 – 7.36 (m, 4H), 7.20 (d, J = 8.0 Hz, 2H), 6.75 (dd, J = 22.7, 11.9 Hz, 3H) ppm; **^{13}C NMR** (101 MHz, DMSO-d_6) δ 181.3, 164.6, 155.8, 141.5, 135.0, 134.9, 130.4, 129.5, 128.3, 126.4, 121.3, 115.8, 102.3, 70.3 ppm; **HRMS:** Calcd. for $C_{18}H_{16}Cl_3N_3NaO_2S$: $[M+Na]^+$: 465.9921 m/z, found 465.9911 m/z.

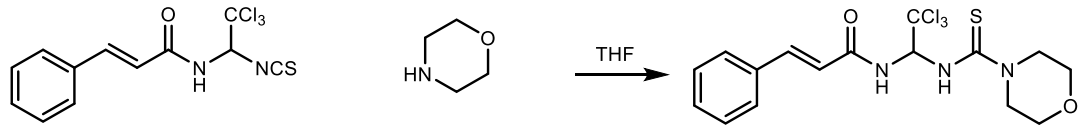

Chemical Formula: $C_{12}H_9Cl_3N_2OS$
Molecular Weight: 335.6270
2.4.1.5

Chemical Formula: C_4H_9NO
Molecular Weight: 87.1220

Chemical Formula: $C_{16}H_{18}Cl_3N_3O_2S$
Molecular Weight: 422.7490
2.4.1.23

The reaction was carried out according to general procedure F using **2.4.1.5** (1.58 g, 4.0 mmol, 1 equiv.), morpholine (345 μL, 4.0 mmol, 1 equiv.), and THF (20 mL, 0.2 M) to afford **2.4.1.23**

(1.62 g, 3.84 mmol) in 96% isolated yield.

^{1}H NMR (500 MHz, DMSO-d_6) δ 8.36 (d, J = 8.9 Hz, 1H), 7.89 (d, J = 8.7 Hz, 1H), 7.68 – 7.63 (m, 2H), 7.61 (t, J = 8.8 Hz, 1H), 7.56 (d, J = 15.8 Hz, 1H), 7.47 – 7.39 (m, 3H), 6.80 (d, J = 15.7 Hz, 1H), 3.93 – 3.82 (m, 2H), 3.83 – 3.73 (m, 2H), 3.64 (pt, J = 6.5, 3.6 Hz, 4H) ppm; **^{13}C NMR** (126 MHz, DMSO-d_6) δ 182.7, 164.6, 141.7, 134.9, 130.4, 129.4, 128.4, 121.4, 102.7, 71.6, 66.1, 49.0 ppm. *Analytical data matches that reported in the literature.*[4]

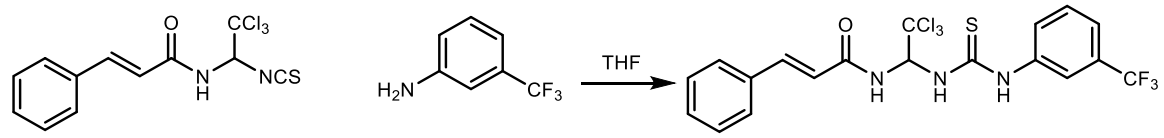

Chemical Formula: $C_{12}H_9Cl_3N_2OS$
Molecular Weight: 335.6270
2.4.1.5

Chemical Formula: $C_7H_6F_3N$
Molecular Weight: 161.1272

Chemical Formula: $C_{19}H_{15}Cl_3F_3N_3OS$
Molecular Weight: 496.7542
2.4.1.24

The reaction was carried out according to general procedure F using **2.4.1.5** (1.58 g, 4.0 mmol, 1 equiv.), 3-(trifluoromethyl)aniline (494 μL, 4.0 mmol, 1 equiv.), and THF (20 mL, 0.2 M) to afford **2.4.1.24** (1.82 g, 3.76 mmol) in 94% isolated yield.

R_f = (EtOAc/hexanes 1:1): 0.40; **IR** (neat) ν = 3195.7, 3092.7, 1654.3, 1617.5, 1505.2, 1328.6, 1164.4, 1127.9, 1040.4, 967.4, 931.5, 831.5, 770.5, 716.1, 619.4, 560.3 cm^{-1}; **^{1}H NMR** (500 MHz, DMSO-d_6) δ 10.57 (s, 1H), 9.01 (d, J = 8.8 Hz, 1H), 8.42 (d, J = 9.5 Hz, 1H), 8.14 (d, J = 1.9 Hz, 1H), 7.77 (dd, J = 8.1, 2.0 Hz, 1H), 7.64 – 7.38 (m, 9H), 6.81 (d, J = 15.8 Hz, 1H) ppm; **^{13}C NMR** (126 MHz, DMSO-d_6) δ 181.0, 164.8, 141.6, 140.3, 135.0, 130.4, 130.3, 129.8, 129.5, 129.5, 128.3, 127.0, 125.5, 123.4, 121.5, 121.2, 119.5, 101.9, 70.0 ppm; **HRMS:** Calcd. for $C_{19}H_{15}Cl_3F_3N_3NaOS$: $[M+Na]^+$: 517.9846 m/z, found 517.9856 m/z.

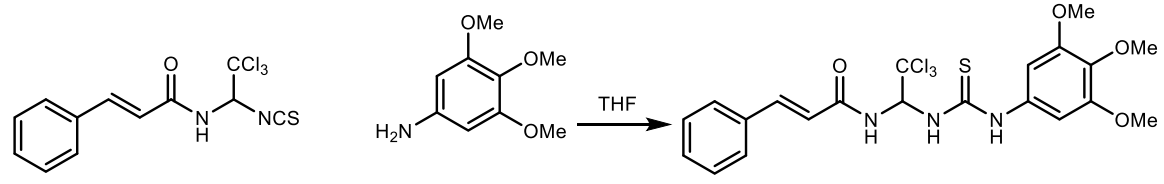

Chemical Formula: $C_{12}H_9Cl_3N_2OS$
Molecular Weight: 335.6270
2.4.1.5

Chemical Formula: $C_9H_{13}NO_3$
Molecular Weight: 183.2070

Chemical Formula: $C_{21}H_{22}Cl_3N_3O_4S$
Molecular Weight: 518.8340
2.4.1.25

The reaction was carried out according to general procedure F using **2.4.1.5** (1.58 g, 4.0 mmol, 1 equiv.), 3,4,5-trimethoxyaniline (733 mg, 4.0 mmol, 1 equiv.), and THF (20 mL, 0.2 M) to afford

2.4.1.25 (1.86 g, 3.6 mmol) in 90% isolated yield.

R_f = (EtOAc/hexanes 1:1): 0.23; **IR** (neat) v = 3220.7, 3067.5, 2942.2, 2830.4, 1502.5, 1334.3, 1229.1, 1167.4, 1129.9, 1097.9, 1043.0, 1007.6, 840.7, 811.5, 718.1, 690.7 cm^{-1}; **^{1}H NMR** (400 MHz, DMSO-d_6) δ 10.31 (s, 1H), 8.91 (d, J = 8.7 Hz, 1H), 8.04 (d, J = 8.9 Hz, 1H), 7.66 – 7.59 (m, 2H), 7.56 (d, J = 15.8 Hz, 1H), 7.49 – 7.37 (m, 4H), 6.83 (s, 2H), 6.74 (d, J = 15.8 Hz, 1H), 3.77 (s, 6H), 3.66 (s, 3H) ppm; **^{13}C NMR** (101 MHz, DMSO-d_6) δ 180.7, 164.6, 153.2, 141.5, 135.3, 134.9, 134.6, 130.4, 129.5, 128.3, 121.3, 102.2, 101.6, 70.2, 60.5, 56.3 ppm; **HRMS:** Calcd. for $C_{21}H_{22}Cl_3N_3NaO_4S$: $[M+Na]^+$: 540.0289 m/z, found 540.0286 m/z.

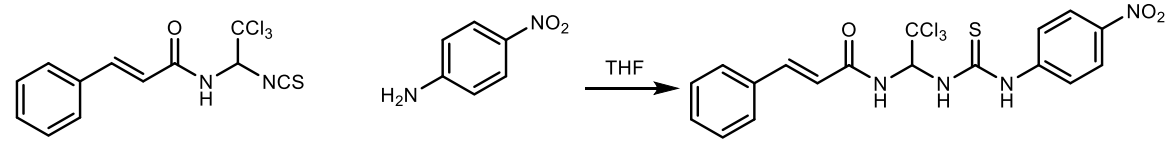

Chemical Formula: $C_{12}H_9Cl_3N_2OS$
Molecular Weight: 335.6270
2.4.1.5

Chemical Formula: $C_6H_6N_2O_2$
Molecular Weight: 138.1260

Chemical Formula: $C_{18}H_{15}Cl_3N_4O_3S$
Molecular Weight: 473.7530
2.4.1.26

The reaction was carried out according to general procedure F using **2.4.1.5** (1.58 g, 4.0 mmol, 1 equiv.), 4-nitroaniline (552 mg, 4.0 mmol, 1 equiv.), and THF (20 mL, 0.2 M) to afford **2.4.1.26** (1.68 g, 3.52 mmol) in 88% isolated yield.

R_f = (EtOAc/hexanes 1:1): 0.26; **IR** (neat) v = 3283.5, 3196.7, 3080.9, 3025.9, 2938.4, 1661.1, 1629.3, 1492.5, 1330.7, 1202.7, 1111.6, 969.3, 892.4, 802.0, 765.1, 703.5, 545.9 cm^{-1}; **^{1}H NMR** (400 MHz, DMSO-d_6) δ 10.86 (s, 1H), 9.07 (d, J = 9.4 Hz, 1H), 8.65 (d, J = 9.4 Hz, 1H), 8.23 (d, J = 9.2 Hz, 2H), 8.01 (d, J = 9.2 Hz, 2H), 7.67 – 7.53 (m, 3H), 7.53 – 7.34 (m, 4H), 6.82 (d, J = 15.8 Hz, 1H) ppm; **^{13}C NMR** (101 MHz, DMSO-d_6) δ 180.8, 164.9, 145.9, 143.2, 141.7, 135.0, 130.4, 129.5, 128.3, 125.0, 121.8, 121.2, 101.6, 69.9 ppm; **HRMS:** Calcd. for $C_{18}H_{15}Cl_3N_4NaO_3S$: $[M+Na]^+$: 494.9823 m/z, found 494.9804 m/z.

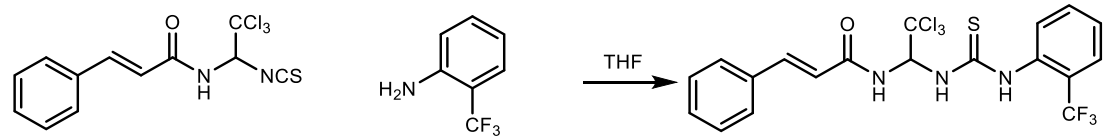

Chemical Formula: $C_{12}H_9Cl_3N_2OS$
Molecular Weight: 335.6270
2.4.1.5

Chemical Formula: $C_7H_6F_3N$
Molecular Weight: 161.1272

Chemical Formula: $C_{19}H_{15}Cl_3F_3N_3OS$
Molecular Weight: 496.7542
2.4.1.27

The reaction was carried out according to general procedure F using **2.4.1.5** (335.6 mg, 1.0 mmol,

1 equiv.), 2-(trifluoromethyl)aniline (126 μL, 1.0 mmol, 1 equiv.), and THF (20 mL, 0.2 M) to afford **2.4.1.27** (407 mg, 0.82 mmol) in 82% isolated yield.

R_f = (EtOAc/hexanes 1:1): 0.42; **IR** (neat) v = 3204.4, 3101.3, 3013.1, 1660.0, 1627.4, 1520.6, 1319.4, 1206.5, 1171.5, 1121.8, 1055.8, 1023.4, 991.0, 814.2, 768.3, 722.0, 669.7, 555.6 cm^{-1}; **^{1}H NMR** (500 MHz, DMSO-d_6) δ 9.86 (s, 1H), 9.11 (d, J = 8.9 Hz, 1H), 8.65 (d, J = 9.6 Hz, 1H), 7.74 (d, J = 7.7 Hz, 1H), 7.68 (t, J = 7.6 Hz, 1H), 7.65 – 7.55 (m, 4H), 7.51 – 7.39 (m, 5H), 6.85 (d, J = 15.8 Hz, 1H) ppm; **^{13}C NMR** (126 MHz, DMSO-d_6) δ 184.1, 164.7, 141.5, 137.3, 135.0, 133.1, 132.7, 130.4, 129.5, 128.2, 127.7, 126.5, 126.5, 125.8, 125.6, 125.1, 122.9, 121.4, 102.1, 70.6 ppm;**HRMS** Calc. for $C_{19}H_{15}Cl_3F_3N_3NaOS$ $[M+Na]^+$ = 517.9846 m/z, found $[M+Na]^+$ = 517.9832 m/z.

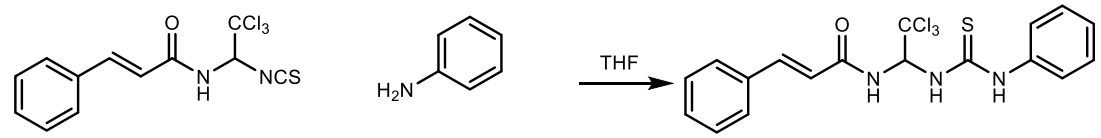

Chemical Formula: $C_{12}H_9Cl_3N_2OS$
Molecular Weight: 335.6270
2.4.1.5

Chemical Formula: C_6H_7N
Molecular Weight: 93.1290

Chemical Formula: $C_{18}H_{16}Cl_3N_3OS$
Molecular Weight: 428.7560
2.4.1.28

The reaction was carried out according to general procedure F using **2.4.1.5** (1.58 g, 4.0 mmol, 1 equiv.), aniline (365 μL, 4.0 mmol, 1 equiv.), and THF (20 mL, 0.2 M) to afford **2.4.1.28** (1.66 g, 3.88 mmol) in 97% isolated yield.

R_f = (EtOAc/hexanes 1:1): 0.44; **IR** (neat) v = 3280.6, 3193.4, 3081.2, 1656.6, 1615.6, 1504.0, 1449.6, 1337.2, 1126.7, 1098.0, 1036.1, 987.9, 883.6, 763.8, 657.4, 605.4, 559.9, 477.8 cm^{-1}; **^{1}H NMR** (500 MHz, DMSO-d_6) δ 10.33 (s, 1H), 8.99 (d, J = 8.7 Hz, 1H), 8.16 (d, J = 9.5 Hz, 1H), 7.65 – 7.51 (m, 5H), 7.50 – 7.33 (m, 6H), 7.18 (t, J = 7.4 Hz, 1H), 6.78 (d, J = 15.8 Hz, 1H) ppm; **^{13}C NMR** (126 MHz, DMSO-d_6) δ 181.1, 164.7, 141.5, 139.2, 135.0, 130.4, 129.5, 129.2, 128.3, 125.4, 123.7, 121.3, 102.1, 70.2 ppm; **HRMS:** Calcd. for $C_{18}H_{16}Cl_3N_3NaOS$: $[M+Na]^+$: 449.9972 m/z, found 449.9964 m/z.

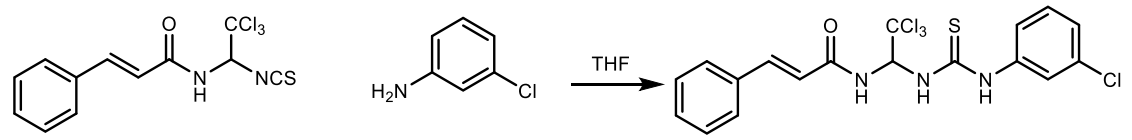

Chemical Formula: $C_{12}H_9Cl_3N_2OS$
Molecular Weight: 335.6270
2.4.1.5

Chemical Formula: C_6H_6ClN
Molecular Weight: 127.5710

Chemical Formula: $C_{18}H_{15}Cl_4N_3OS$
Molecular Weight: 463.1980
2.4.1.29

The reaction was carried out according to general procedure F using **2.4.1.5** (1.58 g, 4.0 mmol, 1 equiv.), 3-chloroaniline (423 µL, 4.0 mmol, 1 equiv.), and THF (20 mL, 0.2 M) to afford **2.4.1.29** (1.77 g, 3.84 mmol) in 96% isolated yield.

R_f = (EtOAc/hexanes 1:1): 0.45; **IR** (neat) v = 3260.8, 3190.9, 3089.4, 3057.0, 2993.5, 1654.1, 1618.3, 1502.1, 1337.1, 1206.9, 1131.2, 1103.7, 1040.0, 966.7, 827.5, 806.9, 764.7, 706.6, 559.5 cm^{-1}; **^{1}H NMR** (400 MHz, DMSO-d_6) δ 10.44 (s, 1H), 9.00 (d, *J* = 8.7 Hz, 1H), 8.35 (d, *J* = 9.4 Hz, 1H), 7.88 (s, 1H), 7.66 – 7.54 (m, 3H), 7.42 (dt, *J* = 14.4, 7.9 Hz, 6H), 7.22 (d, *J* = 6.9 Hz, 1H), 6.80 (d, *J* = 15.8 Hz, 1H) ppm; **^{13}C NMR** (101 MHz, DMSO-d_6) δ 181.2, 164.8, 141.6, 140.9, 135.0, 133.2, 130.8, 130.4, 129.5, 128.3, 125.0, 122.8, 121.8, 121.3, 101.9, 70.1 ppm; **HRMS:** Calcd. for $C_{18}H_{15}Cl_4N_3NaOS$: $[M+Na]^+$: 483.9582 m/z, found 483.9576 m/z.

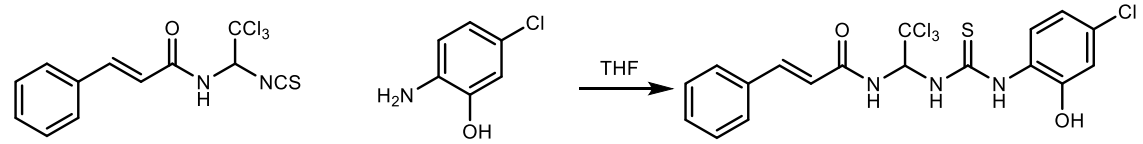

Chemical Formula: $C_{12}H_9Cl_3N_2OS$
Molecular Weight: 335.6270
2.4.1.5

Chemical Formula: C_6H_6ClNO
Molecular Weight: 143.5700

Chemical Formula: $C_{18}H_{15}Cl_4N_3O_2S$
Molecular Weight: 479.1970
2.4.1.30

The reaction was carried out according to general procedure F using **2.4.1.5** (1.58 g, 4.0 mmol, 1 equiv.), 2-amino-4-chlorophenol (574 mg, 4.0 mmol, 1 equiv.), and THF (20 mL, 0.2 M) to afford **2.4.1.30** (1.26 g, 2.64 mmol) in 66% isolated yield as a brown solid following purification using silica gel chromatography eluting EtOAc/Hexanes (1:1).

R_f = (EtOAc/hexanes 1:1): 0.27; **IR** (neat) v = 3219.8, 1657.9, 1600.83, 1505.0, 1341.7, 1193.8, 1036.6, 823.5, 719.5, 510.3 cm^{-1}; **^{1}H NMR** (400 MHz, DMSO-d_6) δ 10.48 (s, 1H), 9.79 (s, 1H), 9.02 (d, *J* = 8.8 Hz, 1H), 8.67 (bs, 1H), 8.00 (d, *J* = 8.4 Hz, 1H), 7.65 – 7.53 (m, 3H), 7.44 (dp, *J* = 15.3, 8.1, 7.2 Hz, 4H), 6.92 (d, *J* = 2.4 Hz, 1H), 6.88 – 6.78 (m, 2H) ppm; **^{13}C NMR** (101 MHz, DMSO-d_6) δ 181.5, 164.7, 151.0, 141.4, 135.1, 130.3, 129.5, 129.3, 128.2, 127.0, 126.1, 121.4,

118.6, 115.4, 102.0, 70.2 ppm; **HRMS:** Calcd. for $C_{18}H_{15}Cl_4N_3NaO_2S$: $[M+Na]^+$: 499.9531 m/z, found 499.9518 m/z.

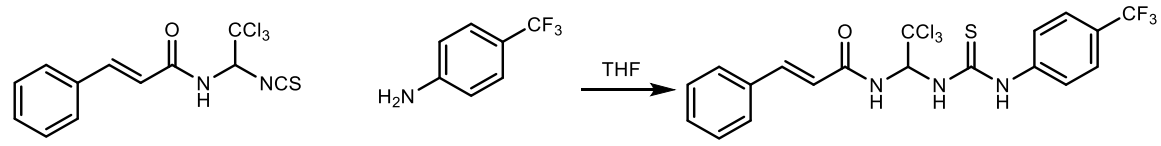

Chemical Formula: $C_{12}H_9Cl_3N_2OS$
Molecular Weight: 335.6270
2.4.1.5

Chemical Formula: $C_7H_6F_3N$
Molecular Weight: 161.1272

Chemical Formula: $C_{19}H_{15}Cl_3F_3N_3OS$
Molecular Weight: 496.7542
2.4.1.31

The reaction was carried out according to general procedure F using **2.4.1.5** (1.58 g, 4.0 mmol, 1 equiv.), 4-(trifluoromethyl)aniline (502 µL, 4.0 mmol, 1 equiv.), and THF (20 mL, 0.2 M) to afford **2.4.1.31** (1.78 g, 3.6 mmol) in 90% isolated yield.

R_f = (EtOAc/hexanes 1:1): 0.45; **IR** (neat) v = 3027.2, 1662.1, 1627.0, 1549.0, 1493.8, 1319.7, 1166.7, 1108.0, 1063.9, 1015.8, 971.4, 892.1, 806.7, 705.7, 679.8, 540.7 cm^{-1}; **^{1}H NMR** (500 MHz, DMSO-d_6) δ 10.63 (s, 1H), 9.03 (d, J = 8.7 Hz, 1H), 8.47 (d, J = 9.4 Hz, 1H), 7.88 (d, J = 8.5 Hz, 2H), 7.72 (d, J = 8.7 Hz, 2H), 7.66 – 7.54 (m, 3H), 7.43 (td, J = 10.5, 6.4 Hz, 4H), 6.81 (d, J = 15.8 Hz, 1H) ppm; **^{13}C NMR** (126 MHz, DMSO-d_6) δ 181.1, 164.8, 143.2, 141.6, 135.0, 130.4, 129.5, 128.2, 126.3, 125.8, 125.0, 124.8, 123.6, 122.8, 121.2, 101.8, 70.0 ppm; **HRMS** Calc. for $C_{19}H_{15}Cl_3F_3N_3NaOS$ $[M+Na]^+$ = 517.9846 m/z, found $[M+Na]^+$ = 517.9842 m/z.

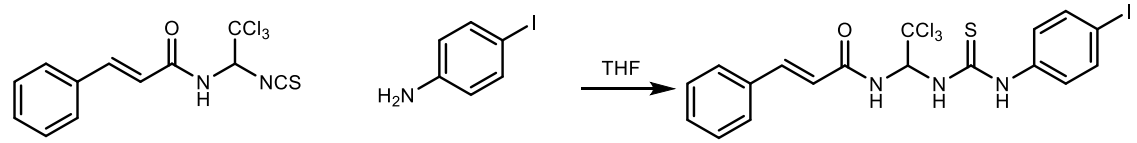

Chemical Formula: $C_{12}H_9Cl_3N_2OS$
Molecular Weight: 335.6270
2.4.1.5

Chemical Formula: C_6H_6IN
Molecular Weight: 219.0255

Chemical Formula: $C_{18}H_{15}Cl_3IN_3OS$
Molecular Weight: 554.6525
2.4.1.32

The reaction was carried out according to general procedure F using **2.4.1.5** (1.58 g, 4.0 mmol, 1 equiv.), 4-iodoaniline (876 mg, 4.0 mmol, 1 equiv.), and THF (20 mL, 0.2 M) to afford **2.4.1.32** (1.93 g, 3.48 mmol) in 87% isolated yield.

R_f = (EtOAc/hexanes 1:1): 0.45; **IR** (neat) v = 3334.0, 3305.8, 3025.5, 2951.1, 1661.3, 1609.1, 1548.3, 1491.5, 1303.6, 1202.9, 1071.0, 1056.2, 973.1, 888.5, 762.2, 748.1, 722.6, 651.1, 576.7, 538.1, 501.1 cm^{-1}; **^{1}H NMR** (400 MHz, DMSO-d_6) δ 10.36 (s, 1H), 8.99 (d, J = 8.7 Hz, 1H), 8.26

(d, J = 9.4 Hz, 1H), 7.70 (d, J = 8.7 Hz, 2H), 7.66 – 7.52 (m, 3H), 7.49 – 7.37 (m, 6H), 6.78 (d, J = 15.8 Hz, 1H) ppm; **^{13}C NMR** (101 MHz, DMSO-d_6) δ 181.0, 164.7, 141.5, 139.2, 137.8, 135.0, 130.4, 129.5, 128.3, 125.6, 121.3, 101.9, 89.5, 70.1 ppm; **HRMS:** Calcd. for $C_{18}H_{15}Cl_3IN_3NaOS$: $[M+Na]^+$: 575.8938 m/z, found 575.8913 m/z.

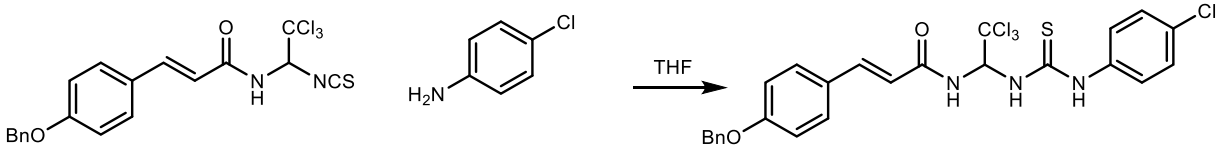

Chemical Formula: $C_{19}H_{15}Cl_3N_2O_2S$
Molecular Weight: 441.7510
S3.6

Chemical Formula: C_6H_6ClN
Molecular Weight: 127.5710

Chemical Formula: $C_{25}H_{21}Cl_4N_3O_2S$
Molecular Weight: 569.3220
2.4.1.33

The reaction was carried out according to general procedure F using **S3.6** (1.76 g, 4.0 mmol, 1 equiv.), 4-chloroaniline (510 mg, 4.0 mmol, 1 equiv.), and THF (20 mL, 0.2 M) to afford **2.4.1.33** (1.93 g, 3.44 mmol) in 86% isolated yield.

R_f = (EtOAc/hexanes 1:1): 0.52; **IR** (neat) v = 3195.6, 3066.4, 3010.1, 2947.9, 1655.0, 1600.3, 1507.0, 1200.1, 1170.5, 1014.2, 889.1, 823.3, 723.4, 510.8 cm^{-1}; **^{1}H NMR** (500 MHz, DMSO-d_6) δ 10.38 (s, 1H), 8.89 (d, J = 8.7 Hz, 1H), 8.25 (d, J = 9.5 Hz, 1H), 7.59 (dd, J = 18.9, 8.8 Hz, 4H), 7.52 (d, J = 15.7 Hz, 1H), 7.48 – 7.36 (m, 7H), 7.37 – 7.31 (m, 1H), 7.08 (d, J = 8.8 Hz, 2H), 6.64 (d, J = 15.8 Hz, 1H), 5.16 (s, 2H) ppm; **^{13}C NMR** (126 MHz, DMSO-d_6) δ 181.2, 165.0, 160.2, 141.2, 138.3, 137.2, 129.9, 129.1, 129.0, 128.9, 128.4, 128.2, 127.8, 125.2, 118.8, 115.8, 102.1, 70.1, 69.8 ppm; **HRMS:** Calcd. for $C_{25}H_{21}Cl_4N_3NaO_2S$: $[M+Na]^+$: 590.0001 m/z, found 589.9983 m/z.

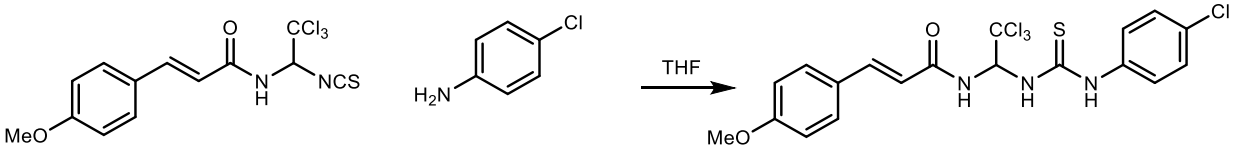

Chemical Formula: $C_{13}H_{11}Cl_3N_2O_2S$
Molecular Weight: 365.6530
S3.7

Chemical Formula: C_6H_6ClN
Molecular Weight: 127.5710

Chemical Formula: $C_{19}H_{17}Cl_4N_3O_2S$
Molecular Weight: 493.2240
2.4.1.34

The reaction was carried out according to general procedure F using **S3.7** (1.46 g, 4.0 mmol, 1 equiv.), 4-chloroaniline (510 mg, 4.0 mmol, 1 equiv.), and THF (20 mL, 0.2 M) to afford **2.4.1.34** (1.74 g, 3.52 mmol) in 88% isolated yield.

R_f = (EtOAc/hexanes 1:1): 0.35; **IR** (neat) v = 3256.1, 1660.6, 1600.0, 1501.9, 1343.8, 1260.3, 1201.2, 1170.6, 1142.4, 1016.3, 979.4 825.4, 727.7, 526.4 cm^{-1}; **^{1}H NMR** (400 MHz, DMSO-d_6) δ 10.40 (s, 1H), 8.89 (d, *J* = 8.7 Hz, 1H), 8.26 (d, *J* = 9.5 Hz, 1H), 7.65 – 7.48 (m, 5H), 7.42 (t, *J* = 9.7 Hz, 3H), 6.99 (d, *J* = 8.8 Hz, 2H), 6.64 (d, *J* = 15.8 Hz, 1H), 3.80 (s, 3H) ppm; **^{13}C NMR** (101 MHz, DMSO-d_6) δ 181.2, 165.0, 161.1, 141.3, 138.3, 129.9, 129.1, 129.0, 127.6, 125.1, 118.7, 114.9, 102.1, 70.1, 55.8 ppm; **HRMS:** Calcd. for $C_{19}H_{17}Cl_4N_3NaO_2S$: $[M+Na]^+$: 513.9688 m/z, found 513.9681 m/z.

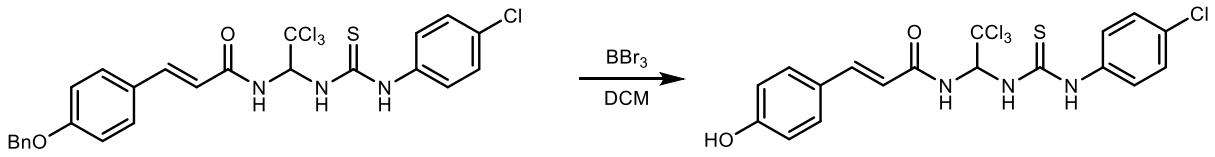

Chemical Formula: $C_{25}H_{21}Cl_4N_3O_2S$
Molecular Weight: 569.3220
2.4.1.33

Chemical Formula: $C_{18}H_{15}Cl_4N_3O_2S$
Molecular Weight: 479.1970
2.4.1.35

Compound **2.4.1.33** (1.14 g, 2 mmol, 1 equiv.) was suspended in dry DCM (50 mL) and cooled to -78°C under an N_2 atmosphere. BBr_3 (1 M in DCM, 5 equiv.) was added and the reaction mixture was stirred at room temperature for 2 hours. The reaction mixture was quenched by the slow addition of methanol (10 mL), concentrated *in vacuo* and then purified using silica gel chromatography (7:3 EtOAc/Hexanes) to afford **2.4.1.35** (537 mg, 1.12 mmol) as an off-white solid in a 56% yield.

R_f = (EtOAc/hexanes 1:1): 0.16; **IR** (neat) v = 3206.0, 1657.3, 1601.6, 1490.2, 1338.6, 1192.6, 1167.0, 1014.2, 887.5, 824.1, 791.1, 725.8, 508.8 cm^{-1}; **^{1}H NMR** (400 MHz, DMSO-d_6) δ 10.36 (s, 1H), 9.93 (s, 1H), 8.84 (d, *J* = 8.7 Hz, 1H), 8.23 (d, *J* = 9.5 Hz, 1H), 7.60 (d, *J* = 8.5 Hz, 2H), 7.50 – 7.36 (m, 6H), 6.82 (d, *J* = 8.2 Hz, 2H), 6.56 (d, *J* = 15.7 Hz, 1H) ppm; **^{13}C NMR** (126 MHz, DMSO-d_6) δ 181.2, 165.2, 159.8, 141.7, 138.3, 130.1, 129.1, 129.0, 126.0, 125.2, 117.6, 116.3, 102.1, 70.1 ppm; **HRMS:** Calcd. for $C_{18}H_{15}Cl_4N_3NaO_2S$: $[M+Na]^+$: 499.9531 m/z, found 499.9519 m/z.

c) Synthesis of Compound 2.4.1.38

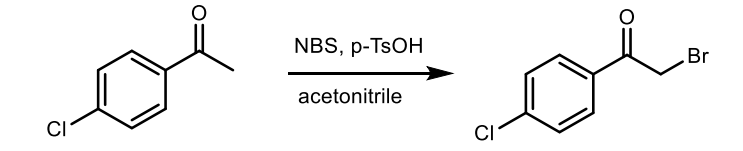

Chemical Formula: C_8H_7ClO
Molecular Weight: 154.5930

Chemical Formula: C_8H_6BrClO
Molecular Weight: 233.4890
2.4.1.36

Compound **2.4.1.36** was prepared according to a known procedure.[5] A 50 mL round-bottom flask equipped with a Teflon coated stir-bar was charged with 1-(4-chlorophenyl)ethan-1-one (10 mmol, 1.0 eq), NBS (10 mmol, 1.0 eq), p-TsOH (15 mmol, 1.5 eq), and CH_3CN (20 mL). The resulting mixture was refluxed for 12 hours before cooling to room temperature and adding water (20 mL). The reaction mixture was then extracted with EtOAc (3 x 30 mL), dried over $MgSO_4$, filtered, and concentrated *in vacuo*. The crude product was purified by recrystallization with hexanes to obtain **2.4.1.36** (2.08 g, 8.9 mmol) as white needles in 89% yield.

^{1}H NMR (300 MHz, $CDCl_3$) δ 7.93 (d, *J* = 8 Hz, 2H), 7.48 (d, *J* = 8 Hz, 2H), 4.41 (s, 2H) ppm; **^{13}C NMR** (125 MHz, $CDCl_3$) δ 190.2, 140.5, 132.2, 130.4, 129.2, 30.6 ppm. *Analytical data matches that reported in the literature.*[5]

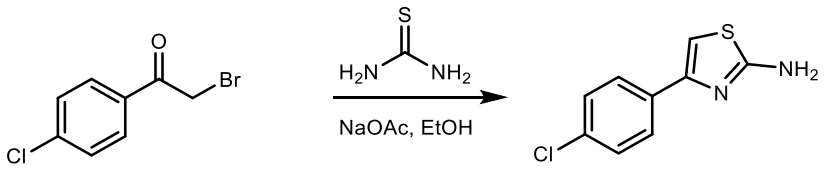

Chemical Formula: C_8H_6BrClO
Molecular Weight: 233.4890
2.4.1.36

Chemical Formula: $C_9H_7ClN_2S$
Molecular Weight: 210.6790
2.4.1.37

In a 100 mL round-bottom flask equipped with a Teflon coated stir-bar, **2.4.1.36** (999 mg, 4.3 mmol, 1.1 eq), thiourea (296 mg, 3.9 mmol, 1.0 eq) and NaOAc (7.79 mmol, 2.0 eq) were dissolved in EtOH (45 mL) and refluxed for 12 hours. The mixture was cooled to room temperature, poured over ice, and the resulting precipitate was vacuumed filtered and washed with water (50 mL) to afford **2.4.1.37** (707 mg, 3.35 mmol) as a yellow solid in 78%.

^{1}H NMR (300 MHz, DMSO-d_6) δ 7.79 (d, *J* = 8.7 Hz, 2H), 7.39 (d, *J* = 8.7 Hz, 2H), 7.07 (s, 2H), 7.05 (s, 1H) ppm; **^{13}C NMR** (125 MHz, DMSO-d_6) δ 168.8, 149.1, 134.2, 132.0, 128.9, 127.7, 102.8 ppm. *Analytical data matches that reported in the literature.*[6]

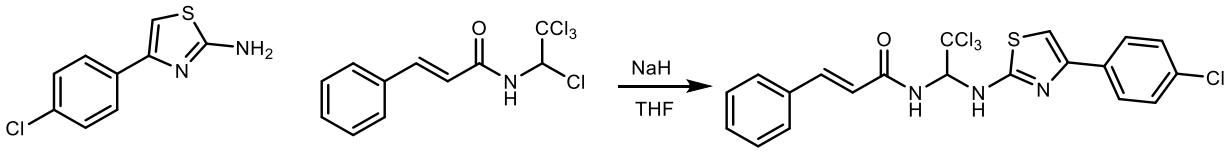

Chemical Formula: $C_9H_7ClN_2S$
Molecular Weight: 210.6790
2.4.1.37

Chemical Formula: $C_{11}H_9Cl_4NO$
Molecular Weight: 312.9990
2.4.1.4

Chemical Formula: $C_{20}H_{15}Cl_4N_3OS$
Molecular Weight: 487.2200
2.4.1.38

In a flame-dried 25 mL round bottom flask equipped with a Teflon-coated stir bar, **2.4.1.37** (464 mg, 2.2 mmol, 1.1 eq.) was dissolved in anhydrous THF (8 mL) and cooled in an ice-bath. NaH (60% dispersion in mineral oil, 92 mg, 2.4 mmol, 1.2 eq.) was added slowly and the mixture was stirred for 15 minutes. Chloral amide **2.4.1.4** (626 mg, 2 mmol, 1 eq.) was dissolved in anhydrous THF (7 mL) and added rapidly to the reaction mixture, which was then stirred for 1 hour at rt. The solvent was removed *in vacuo* and the crude mixture was purified using silica gel chromatography (9:1 DCM/hexanes) to yield **2.4.1.38** (633 mg, 1.3 mmol) as a white solid in 65%.

^{1}H NMR (500 MHz, DMSO-d_6) δ 8.99 (d, J = 9.1 Hz, 1H), 8.70 (d, J = 9.0 Hz, 1H), 7.88 (d, J = 8.6 Hz, 2H), 7.62 – 7.55 (m, 3H), 7.51 – 7.36 (m, 5H), 7.29 (s, 1H), 7.01 – 6.90 (m, 2H) ppm; **^{13}C NMR** (125 MHz, DMSO-d_6) δ 166.4, 165.3, 148.5, 141.4, 135.1, 133.8, 132.3, 130.3, 129.5, 129.0, 128.2, 127.8, 121.4, 104.7, 101, 7, 70.5 ppm. *Analytical data matches that reported in the literature.*[4]

d) Synthesis of Compound 2.4.2.6

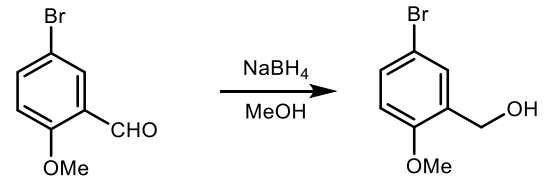

Chemical Formula: $C_8H_7BrO_2$
Molecular Weight: 215.0460

Chemical Formula: $C_8H_9BrO_2$
Molecular Weight: 217.0620
2.4.2.1

In a 250 mL round bottom flask equipped with a Teflon coated stir bar, 5-bromo-2-methoxybenzaldehyde (2.15g, 10 mmol, 1 eq.) was dissolved in MeOH (50 mL) and cooled in an ice bath. $NaBH_4$ (95 mg, 2.5 mmol, 0.25 eq.) was added slowly and the mixture was stirred at rt for 1 hour. The reaction mixture was diluted with 1M HCl (10 mL) and extracted with DCM (3 x 50 mL). The organic layers were combined, washed with brine (50 mL), dried over $MgSO_4$, filtered, and concentrated *in vacuo* to yield **2.4.2.1** (2.06 g, 9.5 mmol) as a white solid in 95% that was used without further purification.

^{1}H NMR (300 MHz, $CDCl_3$) δ 7.42 (d, *J* = 2.5 Hz, 1H), 7.37 (dd, *J* = 2.5 Hz, 8.7 Hz, 1H), 6.75 (d, *J* = 8.7 Hz, 1H), 4.64 (s, 2H), 3.84 (s, 3H), 1.87 (s, 2H) ppm; **^{13}C NMR** (125 MHz, $CDCl_3$) δ 188.5, 156.3, 138.3, 131.3, 112.9, 111.8, 61.1, 55.6 ppm. *Analytical data matches that reported in the literature.*[7]

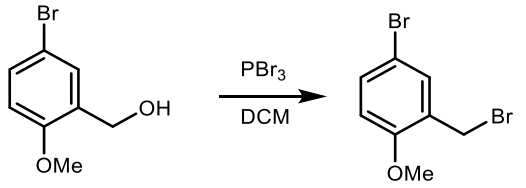

Chemical Formula: $C_8H_9BrO_2$
Molecular Weight: 217.0620
2.4.2.1

Chemical Formula: $C_8H_8Br_2O$
Molecular Weight: 279.9590
2.4.2.2

In a 250 mL round-bottom flask equipped with a Teflon coated stir-bar, **2.4.2.1** (2.06 g, 9.5 mmol, 1.0 eq) was dissolved in DCM (100 mL) and cooled to 0°C in an ice bath. In a separate 50 mL round bottom flask, PBr_3 (1.79 mL, 19 mmol, 2.0 eq) was dissolved in DCM (10 mL) and slowly added to the cooled solution, and then stirred at rt for 15 minutes. The reaction mixture was then concentrated *in vacuo* and the resulting slurry was carefully quenched with a cold, saturated $NaHCO_3$ solution (100 mL). The reaction mixture was then extracted with DCM (3 x 30 mL), dried over $MgSO_4$, filtered, and concentrated *in vacuo* to obtain the alkyl bromide **2.4.2.2** (2.34 g, 8.36 mmol) in 88% which was used without further purification.

^{1}H NMR (300 MHz, $CDCl_3$) δ 7.47 (d, *J* = 2.5 Hz, 1H), 7.41 (dd, *J* = 2.5 Hz, 8.7 Hz, 1H), 6.78 (d, *J* = 8.7 Hz, 1H), 4.50 (s, 2H), 3.90 (s, 3H) ppm; **^{13}C NMR** (125 MHz, $CDCl_3$) δ 156.5, 133.4, 132.7, 128.2, 112.7, 112.5, 55.9, 27.6 ppm. *Analytical data matches that reported in the literature.*[8]

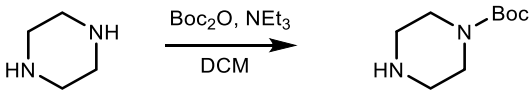

Chemical Formula: $C_4H_{10}N_2$
Molecular Weight: 86.1380

Chemical Formula: $C_9H_{18}N_2O_2$
Molecular Weight: 186.2550
2.4.2.3

In a 500 mL round-bottom flask equipped with a Teflon coated stir-bar, piperazine (92.87 mmol, 2.0 eq) was dissolved in DCM (210 mL) and cooled to 0°C in an ice-bath. Boc_2O (46.43 mmol, 1.0 eq) was dissolved in DCM (20 mL), then added to reaction mixture dropwise and stirred for 1

hour. The reaction mixture was gravity-filtered, washed with cold DCM (2 x 30 mL), and concentrated *in vacuo*. Water (75 mL) was then added, and the resulting mixture was gravity filtered. The solution was saturated with K_2CO_3 before being extracted with EtOAc (3 x 30mL), dried over $MgSO_4$, filtered, and concentrated *in vacuo* to yield the Boc-protected piperazine **2.4.2.3** (12.97 g, 69.65 mmol) in 75% as a white solid.

^{1}H NMR (300 MHz, $CDCl_3$) δ 3.38 (m, 4H), 2.79 (m, 4H), 1.80 (s, 1H), 1.45 (s, 9H). *Analytical data matches that reported in the literature.*

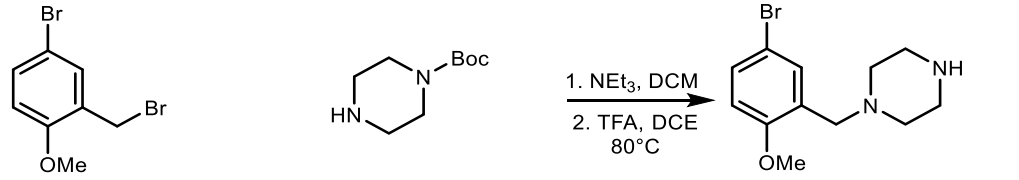

Chemical Formula: $C_8H_8Br_2O$
Molecular Weight: 279.9590
2.4.2.2

Chemical Formula: $C_9H_{18}N_2O_2$
Molecular Weight: 186.2550
2.4.2.3

Chemical Formula: $C_{12}H_{17}BrN_2O$
Molecular Weight: 285.1850
2.4.2.4

In a 250 mL round-bottom flask equipped with a Teflon coated stir-bar, **xx** (9.07 mmol, 1.0 eq), **xx** (9.07 mmol, 1.0 eq), and NEt_3 (8.841 mmol, 1.0 eq) were dissolved in 1,2-dichloroethane (90 mL) and refluxed for 18 hours at 85°C. The mixture was then washed with water (3 x 30 mL), dried over $MgSO_4$, filtered, and concentrated *in vacuo*. The crude mixture was then dissolved in a 1,2-dichloroethane/TFA (1:1) mixture (20 mL) and heated at 80°C for 12 hours. After cooling to rt, the mixture was carefully washed with sat. $NaHCO_3$ (50 mL) and brine (50 mL), dried over $MgSO_4$, filtered and concentrated *in vacuo* to yield **2.4.2.4** (2.38 g, 8.34 mmol) in 92% as a white powder which was used without further purification.

^{1}H NMR (300 MHz, DMSO-d_6) δ 7.46-7.36 (m, 2H), 6.95 (d, J = 8.6 Hz, 1H), 3.75 (s, 3H), 3.48 (s, 2H), 3.30 (s, 4H), 2.98 (m, 4H), 1.36 (s, 1H) ppm.

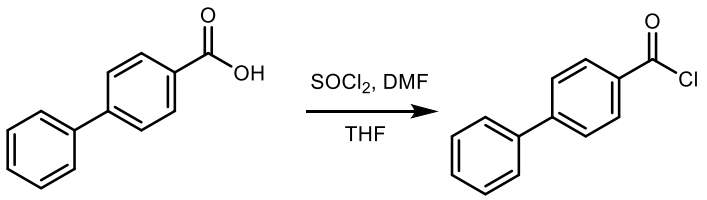

Chemical Formula: $C_{13}H_{10}O_2$
Molecular Weight: 198.2210

Chemical Formula: $C_{13}H_9ClO$
Molecular Weight: 216.6640
2.4.2.5

Was prepared according to the procedure for compound **2.4.1.4**. Biphenyl-4-carboxylic acid (1.98 g, 10 mmol, 1 eq.) was dissolved in anhydrous THF (50 mL), followed by the addition of DMF and $SOCl_2$ (2.2 ml, 30 mmol, 3 eq.). The mixture was heated at reflux for 2 hours, cooled to rt and the solvent removed *in vacuo* to yield the acid chloride **2.4.2.5** (2.06 g, 9.5 mmol) which was used in the next step without purification.

^{1}H NMR (500 MHz, Acetone-d_6) δ 8.27 – 8.23 (m, 2H), 7.99 – 7.93 (m, 2H), 7.83 – 7.79 (m, 2H), 7.58 – 7.54 (m, 2H), 7.52 – 7.48 (m, 1H) ppm. *Analytical data matches that reported in the literature.*

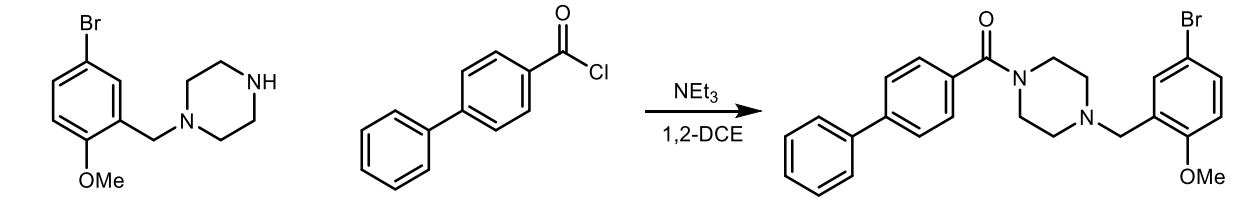

Chemical Formula: $C_{12}H_{17}BrN_2O$
Molecular Weight: 285.1850
2.4.2.4

Chemical Formula: $C_{13}H_9ClO$
Molecular Weight: 216.6640
2.4.2.5

Chemical Formula: $C_{25}H_{25}BrN_2O_2$
Molecular Weight: 465.3910
2.4.2.6

In a flame-dried 250 mL round bottom flask equipped with a Teflon coated stir bar, **2.4.2.4** (570 mg, 2 mmol, 1 eq.) was dissolved in anhydrous 1,2-dichloroethane (20 mL), NEt_3 (0.51 mL, 4 mmol, 2 eq.) was added and the mixture was stirred at 60ºC for 30 minutes. The mixture was cooled to rt, **2.4.2.5** (433 mg, 2 mmol, 1 eq.) was added and the reaction was stirred and heated at reflux for 6 hours. After cooling to rt, the mixture was washed with 1M HCl (20 mL), dried with $MgSO_4$, filtered and concentrated *in vacuo*. The crude mixture was purified using silica gel chromatography to yield **2.4.2.6** (707 mg, 1.52 mmol) as a yellow solid in 76%.

^{1}H NMR (500 MHz, Acetone-d_6) δ 7.72 (dd, J = 12.6, 7.8 Hz, 4H), 7.60 – 7.46 (m, 5H), 7.44 – 7.36 (m, 2H), 6.96 (d, J = 8.7 Hz, 1H), 3.85 (s, 3H), 3.66 (bs, 2H), 3.58 (s, 2H), 2.52 (s, 4H), 1.30 (s, 2H) ppm; **^{13}C NMR** (126 MHz, Acetone-d_6) δ 169.0, 157.1, 142.0, 140.1, 135.5, 132.2, 130.6, 128.9, 128.9, 127.9, 127.7, 126.9, 126.7, 112.7, 112.2, 55.3, 55.0, 53.0 ppm. *Analytical data matches that reported in the literature.*[9]

e) Synthesis of Compounds 2.4.3.1 and 2.4.3.2

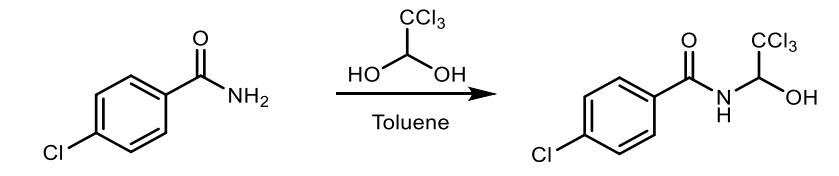

Chemical Formula: C_7H_6ClNO
Molecular Weight: 155.5810

Chemical Formula: $C_9H_7Cl_4NO_2$
Molecular Weight: 302.9600
2.4.3.3

Compound **2.4.3.3** was prepared according to the procedure for **2.4.1.3** using 4-chlorobenzamide (1.56 g, 10 mmol, 1.0 eq), chloral hydrate (3.31 g, 20 mmol, 2.0 eq), and toluene (100 mL) to obtain **2.4.3.3** (1.97 g, 6.5 mmol) as white crystals in 65%.

^{1}H NMR (300 MHz, $(CD_3)_2CO$) δ 8.33 (d, *J* = 8.3 Hz, 1H), 7.98 (d, *J* = 8.6 Hz, 2H), 7.53 (d, *J* = 8.8 Hz, 2H), 6.85 (s, 1H), 6.21 (d, *J* = 9 Hz, 1H). **^{13}C NMR** (125 MHz, $(CD_3)_2CO$) δ 165.8, 132.5, 129.5, 128.8, 128.6, 102.1, 81.7.

Chemical Formula: $C_9H_7Cl_4NO_2$
Molecular Weight: 302.9600
2.4.3.3

Chemical Formula: $C_9H_6Cl_5NO$
Molecular Weight: 321.4030
2.4.3.4

Was prepared according to the procedure for **2.4.1.4** using **2.4.3.3** (1.42 g, 4.70 mmol, 1.0 eq), $SOCl_2$ (1.02 mL, 14.11 mmol, 3.0 eq), DMF (catalytic amount, 1 mol%), and THF (50 mL) to obtain **2.4.3.4** (1.24 g, 3.85 mmol) as a yellow powder in 82%.

^{1}H NMR (300 MHz, $(CD_3)_2CO$) δ 9.07 (d, *J* = 9.8 Hz, 1H), 7.98 (d, *J* = 8.8Hz, 2H), 7.57 (d, *J* = 8.8 Hz, 2H), 6.89 (d, *J* = 10.2 Hz, 1H). **^{13}C NMR** (125 MHz, $(CD_3)_2CO$) δ 165.7, 138.3, 131.3, 129.9, 128.7, 99.7, 74.8.

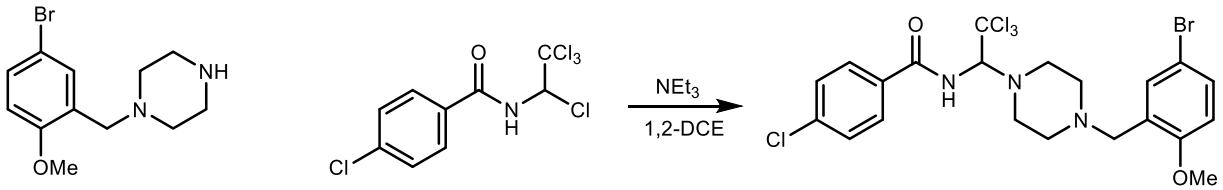

Chemical Formula: $C_{12}H_{17}BrN_2O$
Molecular Weight: 285.1850
2.4.2.4

Chemical Formula: $C_9H_6Cl_5NO$
Molecular Weight: 321.4030
2.4.3.4

Chemical Formula: $C_{21}H_{22}BrCl_4N_3O_2$
Molecular Weight: 570.1300
2.4.3.1

Was prepared according to the procedure for **2.4.2.6** using **2.4.2.4** (200 mg, 0.70 mmol, 1.0 eq), **2.4.3.4** (225 mg, 0.70 mmol, 1.0 eq), NEt_3 (89 µL, 0.70 mmol, 1.0 eq), and DCE (10 mL) to obtain The crude product was purified using a column of 1:1 EtOAc:Hexanes and concentrated *in vacuo*.

Rf = (EtOAc/hexanes 1:1) 0.6; **^{1}H NMR** (500 MHz, $(CD_3)_2CO$) δ 8.23 (d, *J* = 9.5 Hz, 1H), 7.96 (d, *J* = 8.5 Hz, 2H), 7.54 (m, 3H), 7.37 (dd, *J* = 8.7, 2.5 Hz, 1H), 6.94 (d, *J* = 8.7 Hz, 1H), 5.63 (d, *J* = 9.6 Hz, 1H), 3.84 (s, 3H), 3.55 (s, 2H), 3.21 (s, 2H), 2.91 (s, 2H), 2.59 (s, 4H) ppm; **^{13}C NMR** (125 MHz, $(CD_3)_2CO$) δ 166.8, 157.2, 137.4, 132.5, 130.8, 129.7, 128.5, 112.7, 112.2, 102.6, 79.7, 55.3, 54.7, 52.9, 29.7 ppm; **HRMS**: Calcd for $C_{21}H_{23}BrCl_4N_3O_2$ $(M+H)^+$: 567.97278 m/z, found 567.97223 m/z.

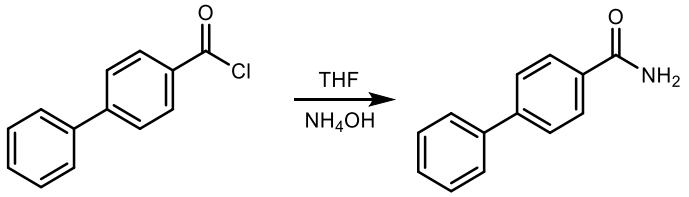

Chemical Formula: $C_{13}H_9ClO$
Molecular Weight: 216.6640
2.4.2.5

Chemical Formula: $C_{13}H_{11}NO$
Molecular Weight: 197.2370
2.4.3.5

A flame-dried 50 mL round-bottom flask was charged with **2.4.2.5** (1.36 g, 6.29 mmol, 1.0 eq). Dry, degassed THF (20 mL) was added dropwise until the compound dissolved. In a separate 100 mL round-bottom flask equipped with a Teflon coated stir-bar, NH_4OH (50 mL, excess) was cooled to 0˚C in an ice bath. While stirring, **2.4.2.5** dissolved in THF was added dropwise to the NH_4OH. Water was then added. The resulting mixture was stirred for one hour before being vacuum filtered to afford **2.4.3.5** (1.22 g, 6.16 mmol) in a 98% isolated yield.

^{1}H NMR (300 MHz, $CDCl_3$) δ 7.89 (d, *J* = 8.2 Hz, 2H), 7.68 (d, *J* = 8.3 Hz, 2H), 7.62 (d, *J* = 7.0, 2H), 7.51-7.35 (m, 3H), 5.88, (d, *J* = 128.5 Hz, 1H) ppm; **^{13}C NMR** (125 MHz, $CDCl_3$) δ 168.0, 143.2, 139.7, 133.6, 129.5, 128.5, 127.3, 126.9 ppm.

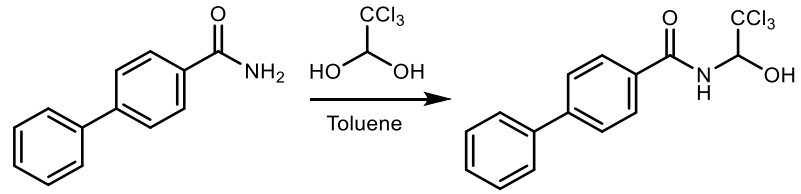

Chemical Formula: $C_{13}H_{11}NO$
Molecular Weight: 197.2370
2.4.3.5

Chemical Formula: $C_{15}H_{12}Cl_3NO_2$
Molecular Weight: 344.6160
2.4.3.6

Was prepared according to the procedure for **2.4.1.3** using **2.4.3.5** (1.18g, 6.0 mmol, 1.0 eq), chloral hydrate (1.99 g, 12.0 mmol, 2.0 eq), and toluene (50 mL) to afford **2.4.3.6** (1.30 g, 3.78 mmol) as white crystals in 63% isolated yield.

^{1}H NMR (300 MHz, $(CD_3)_2CO$) δ 8.25 (d, *J* = 9.2 Hz, 1H), 8.06 (d, *J* = 8.5 Hz, 2H), 7.80 (d, *J* = 8.5 Hz, 2H), 7.73 (d, *J* = 7.1 Hz, 2H), 7.55-7.38 (m, 3H), 6.81 (d, *J* = 6.0, 1H), 6.29-6.21 (m, 1H) ppm; **^{13}C NMR** (125 MHz, $(CD_3)_2CO$) δ 166.5, 144.5, 139.8, 132.5, 129.0, 128.4, 128.1, 127.1, 126.9, 102.3, 81.7 ppm.

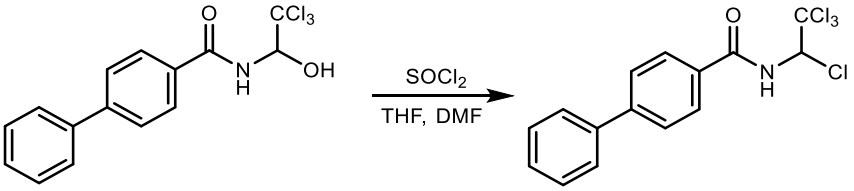

Chemical Formula: $C_{15}H_{12}Cl_3NO_2$
Molecular Weight: 344.6160
2.4.3.6

Chemical Formula: $C_{15}H_{11}Cl_4NO$
Molecular Weight: 363.0590
2.4.3.7

Was prepared according to the procedure for **2.4.1.4** using **2.4.3.6** (1.03 g, 3.0 mmol, 1.0 eq) and $SOCl_2$ (0.65 mL, 9 mmol, 3.0 eq), DMF (catalytic), and THF (40mL) to afford **2.4.3.7** (1.01 g, 2.79 mmol) in a 93% yield.

^{1}H NMR (300 MHz, $(CD_3)_2CO$) δ 9.01 (d, *J* = 10.4 Hz, 1H), 8.06 (d, *J* = 8.6 Hz, 2H), 7.8 (d, *J* = 8.6 Hz, 2H), 7.73 (d, *J* = 7.0 Hz, 2H), 7.56- 7.40 (m, 3H), 6.94 (d, *J* = 10.4 Hz, 1H) ppm; **^{13}C NMR** (125 MHz, $(CD_3)_2CO$) δ 166.3, 145.1, 139.6, 131.3, 129.0, 128.7, 128.3, 127.1, 126.9, 99.9, 75.0 ppm.

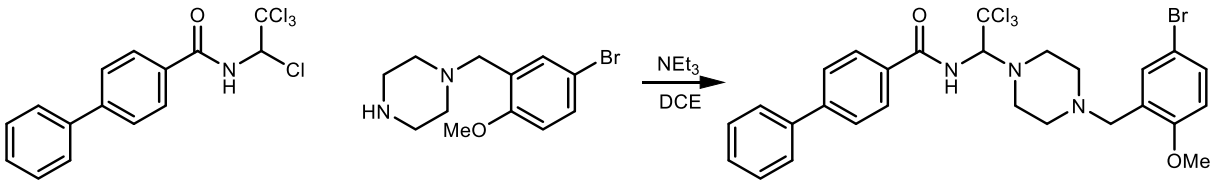

Chemical Formula: $C_{15}H_{11}Cl_4NO$
Molecular Weight: 363.0590
2.4.3.7

Chemical Formula: $C_{12}H_{17}BrN_2O$
Molecular Weight: 285.1850
2.4.2.4

Chemical Formula: $C_{27}H_{27}BrCl_3N_3O_2$
Molecular Weight: 611.7860
2.4.3.2

In a 50 mL round bottom flask equipped with a Teflon-coated stir bar, **2.4.3.7** (635 mg, 1.75 mmol, 1.0 eq), **2.4.2.4** (499 mg, 1.75 mmol, 1.0 eq), and NEt_3 (366 µL, 2.63 mmol, 1.5 eq) were dissolved in DCE (20mL) and refluxed at 80˚C for 4 hours. The resulting mixture was then gravity filtered and concentrated *in vacuo*. The crude product was purified using a column eluting 6:4 Hexanes:Ethyl Acetate to afford **2.4.3.2** (621 mg, 1.02 mmol) in 58% yield.

Rf = (60:40 Hexanes/Ethyl acetate) 0.65; **^{1}H NMR** (500 MHz, $(CD_3)_2CO$) δ 8.15 (d, *J* = 9.6 Hz, 1H), 8.03 (d, *J* = 8.5 Hz, 2H), 7.78 (d, *J* = 8.6 Hz, 2H), 7.72 (d, *J* = 7.0 Hz, 2H), 7.54-7.38 (m, 4H), 7.35 (dd, *J* = 8.7, 2.6 Hz, 1H), 5.65 (d, *J* = 9.6 Hz, 1H), 3.82 (s, 3H), 3.52 (s, 2H), 3.20 (s, 2H), 2.92 (s, 2H), 2.58 (s, 4H) ppm; **^{13}C NMR** (125 MHz, $(CD_3)_2CO$) δ 167.4, 157.1, 144.4, 139.8, 132.6, 129.0, 128.5, 128.1, 127.1, 126.8, 112.6, 112.2, 102.9, 79.7, 55.2, 53.1 ppm; **HRMS**: Calcd for $C_{27}H_{28}BrCl_3N_3O_2$ $(M+H)^+$ = 610.043047 m/z , found 610.0425 m/z.

f) Synthesis of Compound 2.5.6

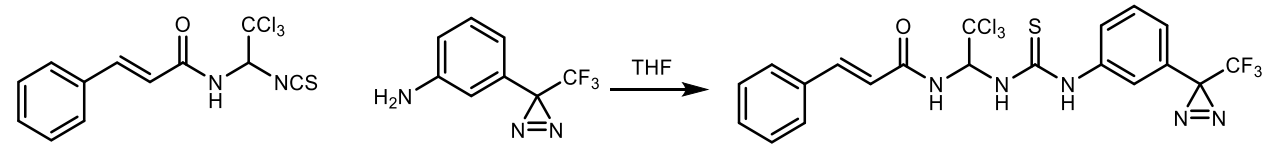

Chemical Formula: $C_{12}H_9Cl_3N_2OS$
Molecular Weight: 335.6270
2.4.1.5

Chemical Formula: $C_8H_6F_3N_3$
Molecular Weight: 201.1522
2.5.5

Chemical Formula: $C_{20}H_{15}Cl_3F_3N_5OS$
Molecular Weight: 536.7792
2.5.6

The reaction was carried out according to general procedure F using **2.4.1.5** (335.6 mg, 1.0 mmol, 1 equiv.), **2.5.5** (201 mg, 1.0 mmol, 1 equiv.), and THF (5 mL, 0.2 M) to afford **2.5.6** (242 mg, 0.45 mmol) in 45% isolated yield following purification on a silica gel column eluting EtOAc/hexanes (4:6).

R_f = (EtOAc/hexane 4:6): 0.28; **IR** (neat) ν = 3271.2, 3196.2, 3086.6, 2995.5, 1655.9, 1617.3, 1502.6, 1339.8, 1262.2, 1155.1, 972.0, 809.3, 764.8, 682.7, 558.4, 486.3 cm^{-1}; **^{1}H NMR** (400

MHz, DMSO-d_6): δ = 10.50 (s, 1H), 8.98 (d, J = 8.7 Hz, 1H), 8.34 (d, J = 9.4 Hz, 1H), 8.03 – 7.13 (m, 10H), 7.02 (d, J = 7.9 Hz, 1H), 6.79 (d, J = 15.8 Hz, 1H) ppm; **^{13}C NMR** (101 MHz, DMSO-d_6) δ 181.2, 164.8, 141.6, 140.4, 135.0, 130.4, 129.5, 128.4, 128.3, 124.7, 123.7, 122.7, 121.2, 120.9, 120.5, 101.8, 70.0, 28.7, 28.3 ppm; **HRMS** Calc. for $C_{20}H_{15}Cl_3F_3N_5NaOS$ $[M+Na]^+$ = 557.9907 m/z, found $[M+Na]^+$ = 557.9897 m/z.

4. General Procedures for the Synthesis of Compounds in Chapter 3

a) General Procedure for Thiol/Quinone C-S Coupling for Compounds in Table 3.5.1

A flame-dried 10 mL round bottom flask equipped with a Teflon coated stir-bar and a rubber septum was charged with *ortho*-quinone (0.5 mmol, 1 eq), magnesium bromide ethyl etherate ($MgBr_2 \cdot Et_2O$) (0.125 mmol, 0.25 eq), and dry, degassed dioxane (5 mL). In a separate, flame dried 10 mL round bottom flask, thiol (0.75 mmol, 1.5 eq) and DIPEA (1.5 mmol, 3 eq) were dissolved in dry, degassed dioxane (5 mL). Using a syringe, the resulting solution was rapidly added to the test tube containing the quinone, and the reaction mixture was stirred at rt for 1.5 hours. Ac_2O (3 eq) and DMAP (12.217 mg, 0.10 mmol, 0.20 eq) were then added sequentially, and the reaction mixture was stirred for another 2 hours at rt. The reaction mixture was then extracted with EtOAc (3 x 10 mL), washed with 2M HCl, dried over $MgSO_4$, filtered and concentrated *in vacuo*. The residue was then purified on silica gel to afford the C-S coupled product.

5. Procedures for the Synthesis of Starting Materials

a) General Procedure for the Generation of quinone 3.2.1

Quinone **3.5.1** was generated according to a procedure previously reported by our group.[10]

b) General Procedure for the Generation of *mono*-substituted *ortho*-quinone coupling partners

A 25 mL round bottom flask was charged with a Teflon coated stir-bar, catechol (0.5 mmol, 1 eq), and sodium *meta*-periodate (0.55 mmol, 1.1 eq). Dichloromethane (DCM) (10 mL) was then added to dissolve the flask contents, upon dissolution, deionized water (5 mL) was added, upon which the clear mixture turned dark orange. The flask was then equipped

with a rubber septum and stirred for 45 minutes. The reaction mixture was then diluted with DCM and H_2O, and extracted with DCM (3 x 25 mL). The mixture was then concentrated *in vacuo* and then used immediately in the next reaction.

c) General Procedure for the Generation of 4,5-substituted *ortho*-quinone coupling partners

All 4,5-substituted *ortho*-quinones were synthesized according to a procedure previously reported by our group.[11]

d) General Procedures for the Synthesis of 1,4-benzothiazines from *ortho*-quinone

i. General Procedure for the L-Cysteine/Quinone C-S Coupling

A flame-dried 10 mL round bottom flask equipped with a Teflon coated stir-bar and a rubber septum was charged with *ortho*-quinone (0.5 mmol, 1 eq), magnesium bromide ethyl etherate ($MgBr_2 \cdot Et_2O$) (0.125 mmol, 0.25 eq), and dry, degassed dioxane (5 mL). In a separate, flame dried 10 mL round bottom flask, N-Boc-L-cysteine ester (0.75 mmol, 1.5 eq) and DIPEA (1.5 mmol, 3 eq) were dissolved in dry, degassed dioxane (5 mL). Using a syringe, the resulting solution was rapidly added to the test tube containing the quinone, and the reaction mixture was stirred at rt for 1.5 hours. The reaction mixture was then extracted with EtOAc (3 x 10 mL), washed with 2M HCl, dried over $MgSO_4$, filtered and concentrated *in vacuo* to yield the sulfur-catechol adduct as crude material.

ii. Boc-Deprotection/PIDA Oxidation – General Procedure

The crude reaction mixture was then dissolved in a 1:1 mixture of DCM/TFA (10 mL) and stirred for 6 hours at rt. After disappearance of the starting material indicated by TLC analysis, the reaction was washed with sat. $NaHCO_3$ (20 mL), brine (20 mL), dried over $MgSO_4$, filtered and concentrated *in vacuo* to yield the free amine. This material was then transferred into a flame-dried 50 mL round bottom flask that was equipped with a Teflon coated stir-bar and a rubber septum and dissolved in dry, degassed DCM (20 mL). PIDA (1 eq.) was then added to this mixture and the reaction was stirred for a further 1.5 hours at rt. The reaction mixture was then washed with brine (20 mL), dried over $MgSO_4$, filtered and concentrated *in vacuo.* The residue was then purified on silica gel to afford the 1,4-benzothiazine product.

6. Synthesis and Characterization of Compounds

a) Compounds in Table 3.5.1

Compound 3.5.22

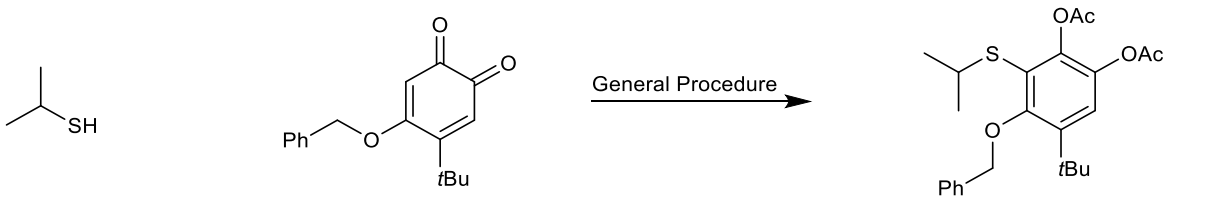

Chemical Formula: C_3H_8S
Molecular Weight: 76.1570

Chemical Formula: $C_{17}H_{18}O_3$
Molecular Weight: 270.3280

Chemical Formula: $C_{24}H_{30}O_5S$
Molecular Weight: 430.5590

Procedure: The reaction was carried out according to general procedure 1.

Amounts of Reagents:

2-propanethiol (70 μL, 0.75 mmol)

Quinone (135.2 mg, 0.5 mmol)

$MgBr_2 \cdot Et_2O$ (32.3 mg, 0.125 mmol, 25 mol%)

DIPEA (245 μL, 1.5 mmol)

Acetic Anhydride (142 μL, 1.5 mmol)

DMAP (12.3 mg, 0.1 mmol)

1,4-Dioxane (10 mL, 0.05 M)

Purification: 5% EtOAc in Toluene

Yield of Product:

3.5.22: 101 mg, 0.24 mmol, 47%

Characterization:

$\mathbf{R_f}$ = (5% EtOAc in toluene): 0.4; **IR** (neat) v = 2958.0, 1762.3, 1457.0, 1437.0, 1364.1, 1294.6, 1237.1, 1207.0, 1156.0, 1067.9, 1050.9, 1030.9, 1007.6, 939.0, 901.6, 730.8, 694.8 cm^{-1}; **^{1}H NMR** (500 MHz, $CDCl_3$) δ 7.55 (d, *J*=7.4 Hz, 2H), 7.42 (t, *J*= 6.9 Hz, 2H), 7.35 (m, 1H), 7.15 (s, 1H),

5.31 (s, 2H), 3.46 (hep, *J*= 6.8 Hz, 1H), 2.35 (s, 3H), 2.31 (s, 3H), 1.42 (s, 9H), 1.10 (d, *J*=6.8Hz, 6H); **^{13}C NMR** (125 MHz, $CDCl_3$) δ 168.5, 168.0, 157.7, 143.1, 142.2, 138.2, 137.9, 128.4, 127.6, 127.2, 124.4, 121.7, 74.3, 38.5, 35.4, 30.6, 23.1, 20.7, 20.6; **HRMS:** Calc. for $C_{24}H_{31}O_5S$: $[M+H]^+$: 431.1887 m/z, found 431.1887 m/z.

Compound 3.5.30

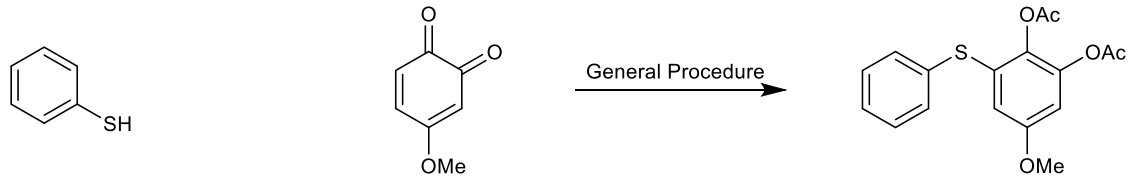

Chemical Formula: C_6H_6S
Molecular Weight: 110.1740

Chemical Formula: $C_7H_6O_3$
Molecular Weight: 138.1220

Chemical Formula: $C_{17}H_{16}O_5S$
Molecular Weight: 332.3700

Procedure: The reaction was carried out according to the general procedure 1.

Amounts of Reagents:

Thiophenol (77 μL, 0.75 mmol)

Quinone (69.1 mg, 0.5 mmol)

$MgBr_2 \cdot Et_2O$ (32.3 mg, 0.125 mmol, 25 mol%)

DIPEA (245 μL, 1.5 mmol)

Acetic Anhydride (142 μL, 1.5 mmol)

DMAP (12.3 mg, 0.1 mmol)

1,4-Dioxane (10 mL, 0.05 M)

Purification: 9:1 Toluene/EtOAc

Yield of Product:

3.5.30: 103 mg, 0.31 mmol, 62%

Characterization:

R_f = (toluene/ethyl acetate 9:1): 0.6 **IR** (neat) v = 3059.9, 2936.8, 2838.8, 1767.8, 1472.1, 1368.2, 1192.9, 1168.5, 1040.9, 1012.4, 883.9, 746.0, 691.0 cm^{-1}; **^{1}H NMR** (500 MHz, $CDCl_3$) δ 6.77 (d, *J*= 2.9 Hz, 1H), 6.59 (d, *J*= 2.9 Hz,1H), 3.80 (s, 3H), 2.92 (q, *J*= 7.4 Hz, 2H), 2.33 (s, 3H), 2.29 (s, 3H), 1.33 (t, *J*= 7.4 Hz, 3H); **^{13}C NMR** (125 MHz, $CDCl_3$) δ 168.1, 168.0, 157.4, 143.5, 134.5, 133.0, 132.4, 132.3, 129.4, 128.0, 114.0, 107.9, 55.7, 20.7, 20.2; **HRMS:** Calcd. for $C_{17}H_{16}NaO_5S$: $[M+Na]^+$: 355.0611 m/z, found 355.0597 m/z.

Compound 3.5.31

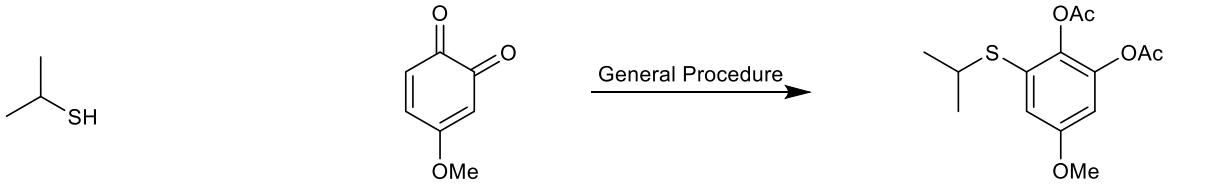

Chemical Formula: C_3H_8S
Molecular Weight: 76.1570

Chemical Formula: $C_7H_6O_3$
Molecular Weight: 138.1220

Chemical Formula: $C_{14}H_{18}O_5S$
Molecular Weight: 298.3530

Procedure: The reaction was carried out according to general procedure 1.

Amounts of Reagents:

2-propanethiol (70 μL, 0.75 mmol)

Quinone (69.1 mg, 0.5 mmol)

$MgBr_2 \cdot Et_2O$ (32.3 mg, 0.125 mmol, 25 mol%)

DIPEA (245 μL, 1.5 mmol)

Acetic Anhydride (142 μL, 1.5 mmol)

DMAP (12.3 mg, 0.1 mmol)

1,4-Dioxane (10 mL, 0.05 M)

Purification: 9:1 Toluene/EtOAc

Yield of Product:

3.5.31: 101 mg, 0.34 mmol, 68%

Characterization:

R_f = (toluene/ethyl acetate 9:1): 0.6 **IR** (neat) v = 2965.4, 2929.6, 2866.7, 1767.3, 1437.0, 1367.7, 1192.8, 1168.9, 1120.4, 1039.7, 1011.2, 882.5 cm^{-1}; **^{1}H NMR** (500 MHz, $CDCl_3$): δ 6.86 (d, *J*= 2.9 Hz, 1H), 6.63 (d, *J*= 2.9 Hz, 1H), 3.78 (s, 3H), 3.37 (hep, *J*= 6.7 Hz, 1H), 2.31 (s, 3H), 2.27 (s, 3H), 1.29 (d, *J*= 6.7 Hz, 6H); **^{13}C NMR** (125 MHz, $CDCl_3$) δ 168.2, 168.1, 157.2, 143.3, 135.7, 131.4, 115.2, 107.5, 55.8, 37.9, 23.1, 20.7, 20.3; **HRMS:** Calcd. for $C_{14}H_{18}NaO_5S$: $[M+Na]^+$: 321.0767 m/z, found 321.0761 m/z.

Compound 3.5.33

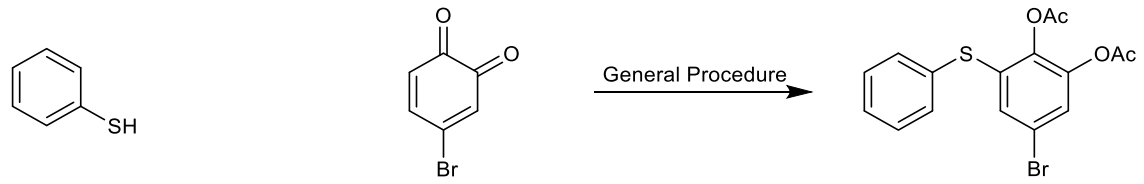

Chemical Formula: C_6H_6S
Molecular Weight: 110.1740

Chemical Formula: $C_6H_3BrO_2$
Molecular Weight: 186.9920

Chemical Formula: $C_{16}H_{13}BrO_4S$
Molecular Weight: 381.2400

Procedure: The reaction was carried out according to general procedure 1.

Amounts of Reagents:

Thiophenol (77 μL, 0.75 mmol)

Quinone (93.5 mg, 0.5 mmol)

$MgBr_2 \cdot Et_2O$ (32.3 mg, 0.125 mmol, 25 mol%)

DIPEA (245 μL, 1.5 mmol)

Acetic Anhydride (142 μL, 1.5 mmol)

DMAP (12.3 mg, 0.1 mmol)

1,4-Dioxane (10 mL, 0.05 M)

Purification: 95:5 Toluene/EtOAc

Yield of Product:

3.5.33: 76 mg, 0.2 mmol, 40%

Characterization:

R_f = (toluene/ethyl acetate 95:5): 0.5 **IR** (neat) v = 1770.3, 1572.1, 1450.5, 1367.3, 1243.6, 1186.1, 1148.9, 1009.2, 946.0, 896.6, 747.8, 690.0, 615.5 cm^{-1}; **^{1}H NMR** (500 MHz, $CDCl_3$): δ 7.42 (m, 2H), 7.37 (m, 3H), 7.23 (d, *J*= 2.2 Hz, 1H), 7.03 (d, *J*= 2.2 Hz, 1H), 2.30 (s, 6H); **^{13}C NMR** (125 MHz, $CDCl_3$) δ 167.7, 167.4, 143.4, 139.6, 134.5, 133.1, 131.7, 130.2, 129.7, 128.7, 124.9, 119.0, 20.6, 20.2; **HRMS:** Calcd. for $C_{16}H_{13}BrNaO_4S$: $[M+Na]^+$: 402.9610 m/z, found 402.9592 m/z.

Compound 3.5.34

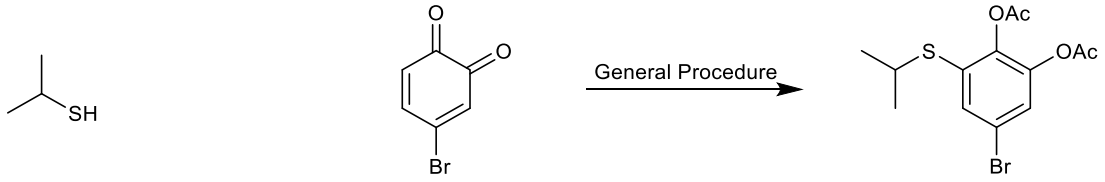

Chemical Formula: C_3H_8S
Molecular Weight: 76.1570

Chemical Formula: $C_6H_3BrO_2$
Molecular Weight: 186.9920

Chemical Formula: $C_{13}H_{15}BrO_4S$
Molecular Weight: 347.2230

Procedure: The reaction was carried out according to general procedure 1.

Amounts of Reagents:

2-propanethiol (70 μL, 0.75 mmol)

Quinone (93.5 mg, 0.5 mmol)

$MgBr_2 \cdot Et_2O$ (32.3 mg, 0.125 mmol, 25 mol%)

DIPEA (245 μL, 1.5 mmol)

Acetic Anhydride (142 μL, 1.5 mmol)

DMAP (12.3 mg, 0.1 mmol)

1,4-Dioxane (10 mL, 0.05 M)

Purification: 4:1 Hexanes/EtOAc

Yield of Product:

3.5.34: 66 mg, 0.19 mmol, 38%

Characterization:

R_f = (hexanes/ethyl acetate 4:1): 0.3; **IR** (neat) v = 2978.8, 2925.1, 2865.5, 1761.6, 1402.9, 1366.3, 1184.7, 1150.5, 944.9, 859.0, 768.5, 686.8 cm^{-1}; **^{1}H NMR** (500 MHz, $CDCl_3$): δ 7.41 (d, *J*= 2.2 Hz, 1H), 7.24 (d, *J*= 2.2 Hz, 1H), 3.39 (hep, *J*= 6.7 Hz, 1H), 2.32 (s, 3H), 2.27 (s, 3H), 1.31 (d, *J*= 6.7 Hz, 6H); **^{13}C NMR** (125 MHz, $CDCl_3$) δ 167.7, 167.5, 143.4, 141.1, 133.4, 131.3, 124.8, 118.6, 37.9, 23.1, 20.6, 20.3; **HRMS:** Calcd. for $C_{13}H_{15}BrNaO_4S$: $[M+Na]^+$: 368.9797 m/z, found 368.9754 m/z.

Compound 3.5.35

Chemical Formula: C_2H_6S
Molecular Weight: 62.1300

Chemical Formula: $C_{10}H_6O_2$
Molecular Weight: 158.1560

Chemical Formula: $C_{16}H_{16}O_4S$
Molecular Weight: 304.3600

Procedure: The reaction was carried out according to general procedure 1.

Amounts of Reagents:

Ethanethiol (56 μL, 0.75 mmol)

Quinone (79.1 mg, 0.5 mmol)

$MgBr_2{\cdot}Et_2O$ (32.3 mg, 0.125 mmol, 25 mol%)

DIPEA (245 μL, 1.5 mmol)

Acetic Anhydride (142 μL, 1.5 mmol)

DMAP (12.3 mg, 0.1 mmol)

1,4-Dioxane (10 mL, 0.05 M)

Purification: 1:1 Hexanes/EtOAc

Yield of Product:

3.5.35: 65 mg, 0.22 mmol, 43%

Characterization:

R_f = (hexanes/ethyl acetate 1:1): 0.6; **IR** (neat) v = 2968.9, 2934.3, 1763.4, 1367.6, 1179.9, 1091.5, 1005.5, 767.0, 739.4, 584.4 cm^{-1}; **^{1}H NMR** (500 MHz, $CDCl_3$): δ 8.36 (m, 1H), 7.84 (m, 1H), 7.56 (m, 2H), 7.36 (s, 1H), 3.01 (q, *J*= 7.4 Hz, 2H), 2.45 (s, 3H), 2.35 (s, 3H), 1.36 (t, *J*= 7.4 Hz, 3H); **^{13}C NMR** (125 MHz, $CDCl_3$) δ 168.3, 168.1, 138.7, 135.7, 133.4, 131.5, 128.0, 127.3, 126.5, 125.3, 122.5, 121.7, 28.2, 20.8, 20.4, 14.2; **HRMS:** Calcd. for $C_{16}H_{16}NaO_4S$: $[M+Na]^+$: 327.0662 m/z, found 327.0653 m/z.

Compound 3.5.36

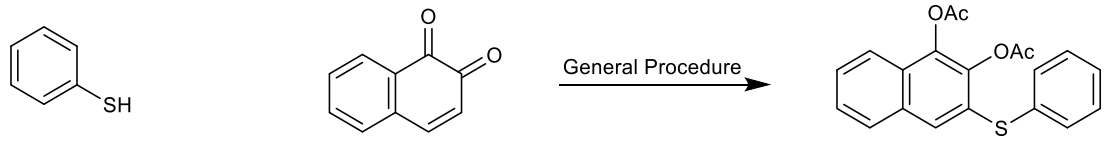

Chemical Formula: C_6H_6S
Molecular Weight: 110.1740

Chemical Formula: $C_{10}H_6O_2$
Molecular Weight: 158.1560

Chemical Formula: $C_{20}H_{16}O_4S$
Molecular Weight: 352.4040

Procedure: The reaction was carried out according to general procedure 1.

Amounts of Reagents:

Thiophenol (77 μL, 0.75 mmol)

Quinone (79.1 mg, 0.5 mmol)

$MgBr_2 \cdot Et_2O$ (32.3 mg, 0.125 mmol, 25 mol%)

DIPEA (245 μL, 1.5 mmol)

Acetic Anhydride (142 μL, 1.5 mmol)

DMAP (12.3 mg, 0.1 mmol)

1,4-Dioxane (10 mL, 0.05 M)

Purification: 5% DCM in Toluene

Yield of Product:

3.5.36: 62 mg, 0.18 mmol, 35%

Characterization:

$\mathbf{R_f}$ = (5% DCM in toluene): 0.3; **IR** (neat) v = 2994.0, 1762.3, 1367.4, 1205.0, 1179.7, 1154.1, 1091.7, 1005.6, 986.9, 739.3, 584.7 cm^{-1}; **^{1}H NMR** (500 MHz, $CDCl_3$): δ 8.37 (d, *J*= 8.1 Hz, 1H), 7.88 (d, *J*= 8.1, 1H), 7.55 (m, 2H), 7.42 (s, 1H), 7.29 (m, 4H), 7.22 (m, 1H), 2.47 (s, 3H), 2.30 (s, 3H); **^{13}C NMR** (125 MHz, $CDCl_3$) δ 168.1, 168.0, 138.8, 137.3, 135.3, 132.0, 131.2, 130.1, 129.4, 128.3, 127.5, 127.1, 127.0, 126.8, 125.8, 121.8, 20.7, 20.5; **HRMS:** Calcd. for $C_{20}H_{16}NaO_4S$: $[M+Na]^+$: 375.0662 m/z, found 375.0656 m/z.

Compound 3.5.37

Chemical Formula: C_3H_8S
Molecular Weight: 76.1570

Chemical Formula: $C_{10}H_6O_2$
Molecular Weight: 158.1560

Chemical Formula: $C_{17}H_{18}O_4S$
Molecular Weight: 318.3870

Procedure: The reaction was carried out according to general procedure 1.

Amounts of Reagents:

2-propanethiol (70 μL, 0.75 mmol)

Quinone (79.1 mg, 0.5 mmol)

$MgBr_2{\cdot}Et_2O$ (32.3 mg, 0.125 mmol, 25 mol%)

DIPEA (245 μL, 1.5 mmol)

Acetic Anhydride (142 μL, 1.5 mmol)

DMAP (12.3 mg, 0.1 mmol)

1,4-Dioxane (10 mL, 0.05 M)

Purification: 1:1 Hexanes/EtOAc

Yield of Product:

3.5.37: 62 mg, 0.20 mmol, 39%

Characterization:

R_f = (hexanes/ethyl acetate 1:1): 0.6; **IR** (neat) v = 3070.7, 2963.4, 2926.5, 2865.8, 1769.2, 1364.7, 1153.5, 1089.5, 1012.1, 764.0 cm^{-1}; **^{1}H NMR** (500 MHz, $CDCl_3$) δ: 8.48 (m, 1H), 7.85 (m, 1H), 7.56 (m, 2H), 7.51 (s, 1H), 3.40 (hep, *J*= 6.8 Hz, 1H), 2.46 (s, 3H), 2.35 (s, 3H), 1.33 (d, *J*= 6.8 Hz, 6H); **^{13}C NMR** (125 MHz, $CDCl_3$) δ: 168.3, 168.0, 138.5, 136.6, 133.0, 132.1, 128.1, 127.2, 126.6, 126.2, 121.7, 39.1, 23.3, 20.8, 20.4; **HRMS:** Calcd. for $C_{17}H_{18}NaO_4S$: $[M+Na]^+$: 341.0818 m/z, found 341.0810 m/z.

Compound 3.5.39

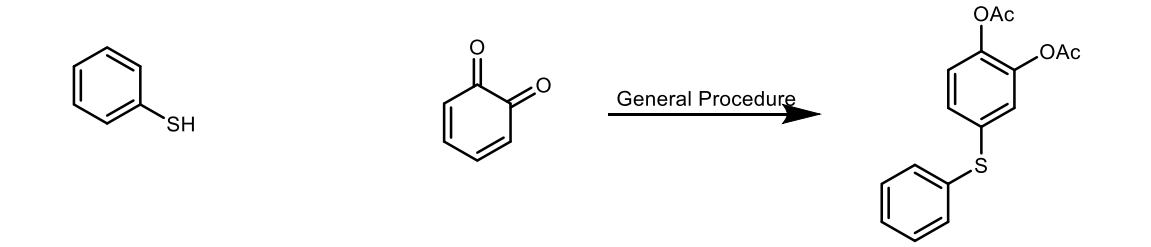

Chemical Formula: C_6H_6S
Molecular Weight: 110.1740

Chemical Formula: $C_6H_4O_2$
Molecular Weight: 108.0960

Chemical Formula: $C_{16}H_{14}O_4S$
Molecular Weight: 302.3440

Procedure: The reaction was carried out according to general procedure 1.

Amounts of Reagents:

Thiophenol (77 μL, 0.75 mmol)

Quinone (51 mg, 0.5 mmol)

$MgBr_2 \cdot Et_2O$ (32.3 mg, 0.125 mmol, 25 mol%)

DIPEA (245 μL, 1.5 mmol)

Acetic Anhydride (142 μL, 1.5 mmol)

DMAP (12.3 mg, 0.1 mmol)

1,4-Dioxane (10 mL, 0.05 M)

Purification: 5% EtOAc in Toluene

Yield of Product:

3.5.39: 81.6 mg, 0.27 mmol, 54%

Characterization:

R_f = (5% EtOAc in toluene): 0.4; **IR** (neat) v = 2968.4, 2934.2, 1762.3, 1367.9, 1180.5, 1154.7, 1145.2, 1092.0, 1006.2, 767.2, 739.5, 686.9, 584.7 cm^{-1}; **^{1}H NMR** (500 MHz, $CDCl_3$): δ 7.38 (m, 2H), 7.31 (m, 3H), 7.12 (m, 2H), 7.05 (dd, *J*= 7.6, 1.8 Hz, 1H), 2.28 (s, 3H), 2.27 (s, 3H); **^{13}C NMR** (125 MHz, $CDCl_3$) δ = 168.2, 167.71, 143.2, 141.1, 133.4, 132.1, 131.8, 129.4, 129.0, 127.9, 126.6, 122.1, 20.7, 20.2 ppm; Calcd. for $C_{16}H_{14}NaO_4S$: $[M+Na]^+$: 325.0505 m/z, found 325.0511 m/z.

Compound 3.5.40

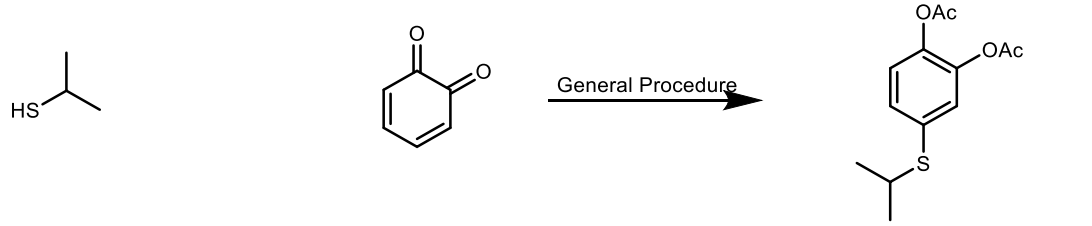

Chemical Formula: C_3H_8S
Molecular Weight: 76.1570

Chemical Formula: $C_6H_4O_2$
Molecular Weight: 108.0960

Chemical Formula: $C_{13}H_{16}O_4S$
Molecular Weight: 268.3270

Procedure: The reaction was carried out according to general procedure 1.

Amounts of Reagents:

2-propanethiol (70 µL, 0.75 mmol)

Quinone (54 mg, 0.5 mmol)

$MgBr_2 \cdot Et_2O$ (32.3 mg, 0.125 mmol, 25 mol%)

DIPEA (245 µL, 1.5 mmol)

Acetic Anhydride (142 µL, 1.5 mmol)

DMAP (12.3 mg, 0.1 mmol)

1,4-Dioxane (10 mL, 0.05 M)

Purification: 95:5 Toluene/EtOAc

Yield of Product:

3.5.40: 76.5 mg, 0.29 mmol, 57%

Characterization:

R_f = (toluene/ethyl acetate 95:5): 0.4; **IR** (neat) v = 2966.3, 2927.9, 2866.9, 1767.7, 1446.5, 1367.7, 1190.4, 1159.3, 1141.2, 1008.4 cm^{-1}; **^{1}H NMR** (500 MHz, $CDCl_3$): δ): 7.33 (dd, *J*= 7.9, 1.5 Hz, 1H), 7.21 (t, *J*= 8.1 Hz, 1H), 7.09 (dd, *J*= 8.1, 1.5 Hz, 1H), 3.37 (hep, *J*= 6.7 Hz, 1H), 2.33 (s, 3H), 2.28 (s, 3H), 1.29 (d, *J*= 6.7 Hz, 6H); **^{13}C NMR** (125 MHz, $CDCl_3$) δ: 168.2, 167.8, 143.1, 142.3, 131.1, 130.0, 126.3, 122.0, 38.0, 23.2, 20.7, 20.4; **HRMS:** Calcd. for $C_{13}H_{16}NaO_4S$: $[M+Na]^+$: 291.0662 m/z, found 291.0662 m/z.

b) Compounds in Table 3.6.1.1

Compound 3.6.1.8

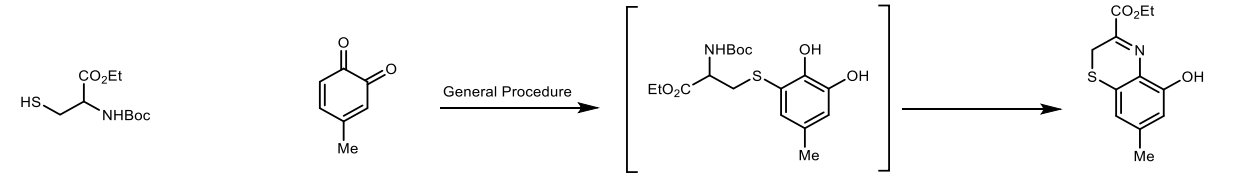

Chemical Formula: $C_{10}H_{19}NO_4S$
Molecular Weight: 249.3250

Chemical Formula: $C_7H_6O_2$
Molecular Weight: 122.1230

Chemical Formula: $C_{12}H_{13}NO_3S$
Molecular Weight: 251.3000

Procedure: The reaction was carried out according to the General Procedure described above.

Amounts of Reagents:

A. N-Boc-L-cysteine ethyl ester (186 mg, 0.75 mmol)
Quinone (61.1 mg, 0.5 mmol)
$MgBr_2 \cdot Et_2O$ (32.3 mg, 0.125 mmol, 25 mol%)
DIPEA (245 μL, 1.5 mmol)
1,4-Dioxane (10 mL, 0.05 M)

B. TFA/DCM (10 mL, 1:1)
PIDA (161 mg, 0.5 mmol)
DCM (20 mL)

Purification: 50:50 Hexanes/EtOAc

Yield of Product:

3.6.1.8: 78 mg, 0.33 mmol, 66% *over 3 steps*

Characterization:

R_f = (hexanes/ethyl acetate 50:50): 0.68; **IR** (neat) v = 3393.9, 3269.6, 3215.9, 2980.7, 1708.7, 1558.5, 1448.9, 1368.6, 1212.1, 1162.4, 1081.6, 1013.9, 833.0, 712.4, 590.4 cm^{-1}; **^{1}H NMR** (500 MHz, $CDCl_3$) δ 7.34 (s, 1H), 6.62 (d, *J* = 1.7 Hz, 1H), 6.59 (d, *J* = 1.8 Hz, 1H), 4.39 (q, *J* = 7.1 Hz, 2H), 3.65 (s, 2H), 2.28 (s, 3H), 1.40 (t, *J* = 7.1 Hz, 3H) ppm; **^{13}C NMR** (126 MHz, $CDCl_3$) δ 163.4, 154.1, 144.2, 142.5, 127.7, 125.0, 118.8, 113.3, 62.5, 22.6, 21.8, 14.2 ppm; **HRMS:** Calcd. for $C_{12}H_{13}NNaO_3S$: $[M+Na]^+$: 274.0508 m/z, found 274.0501 m/z.

Compound 3.6.1.9

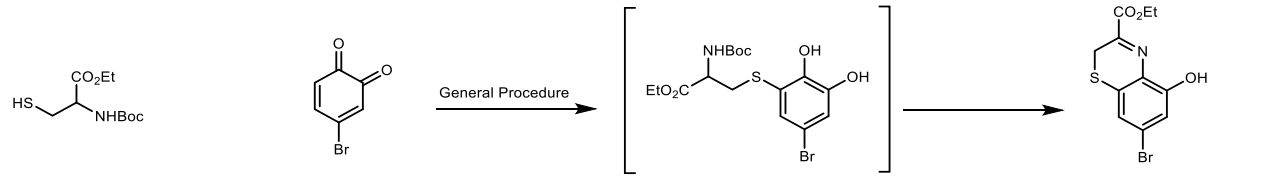

Chemical Formula: $C_{10}H_{19}NO_4S$
Molecular Weight: 249.3250

Chemical Formula: $C_6H_3BrO_2$
Molecular Weight: 186.9920

Chemical Formula: $C_{11}H_{10}BrNO_3S$
Molecular Weight: 316.1690

Procedure: The reaction was carried out according to the General Procedure described above.

Amounts of Reagents:

A. N-Boc-L-cysteine ethyl ester (186 mg, 0.75 mmol)
Quinone (93.5 mg, 0.5 mmol)
$MgBr_2 \cdot Et_2O$ (32.3 mg, 0.125 mmol, 25 mol%)
DIPEA (245 μL, 1.5 mmol)
1,4-Dioxane (10 mL, 0.05 M)

B. TFA/DCM (10 mL, 1:1)
PIDA (161 mg, 0.5 mmol)
DCM (20 mL)

Purification: 50:50 Hexanes/EtOAc

Yield of Product:

3.6.1.9: 54 mg, 0.18 mmol, 36% *over 3 steps*

Characterization:

R_f = (hexanes/ethyl acetate 50:50): 0.44; **IR** (neat) v = 3374.9, 3305.5, 3076.4, 2980.8, 1709.9, 1550.8, 1410.1, 1368.6, 1301.8, 1207.7, 1159.3, 1071.2, 1014.8, 960.2, 909.5, 833.3, 729.9, 583.0 cm^{-1}; **^{1}H NMR** (400 MHz, $CDCl_3$) δ 7.00 (s, 1H), 6.96 (s, 1H), 4.43 (q, *J* = 7.1 Hz, 2H), 3.68 (s, 2H), 1.44 (t, *J* = 7.1 Hz, 3H) ppm; **^{13}C NMR** (101 MHz, $CDCl_3$) δ 163.1, 154.6, 145.5, 128.7, 127.0, 124.8, 120.8, 116.1, 62.8, 22.5, 14.2 ppm; **HRMS:** Calcd. for $C_{11}H_9BrNO_3S$: $[M-H]^+$: 313.94920 m/z, found 313.94921 m/z.

Compound 3.6.1.10

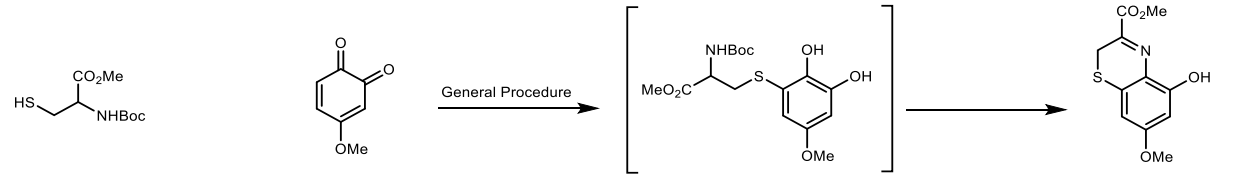

Chemical Formula: $C_9H_{17}NO_4S$
Molecular Weight: 235.2980

Chemical Formula: $C_7H_6O_3$
Molecular Weight: 138.1220

Chemical Formula: $C_{11}H_{11}NO_4S$
Molecular Weight: 253.2720

Procedure: The reaction was carried out according to the General Procedure described above.

Amounts of Reagents:

A. N-Boc-L-cysteine methyl ester (154 μL, 0.75 mmol)
Quinone (69.1 mg, 0.5 mmol)
$MgBr_2 \cdot Et_2O$ (32.3 mg, 0.125 mmol, 25 mol%)
DIPEA (245 μL, 1.5 mmol)
1,4-Dioxane (10 mL, 0.05 M)

B. TFA/DCM (10 mL, 1:1)
PIDA (161 mg, 0.5 mmol)
DCM (20 mL)

Purification: 50:50 Hexanes/EtOAc

Yield of Product:

3.6.1.10: 73 mg, 0.29 mmol, 58% *over 3 steps*

Characterization:

R_f = (hexanes/ethyl acetate 50:50): 0.43; **IR** (neat) v = 3384.0, 3289.3, 3003.8, 2951.0, 2839.4, 1711.1, 1615.5, 1559.6, 1434.1, 1293.6, 1211.2, 1136.7, 1085.2, 1033.7, 989.8, 906.4, 828.3, 727.9, 570.3 cm^{-1}; **^{1}H NMR** (500 MHz, $CDCl_3$) δ 7.43 (bs, 1H), 6.35 (d, *J* = 2.6 Hz, 1H), 6.32 (d, *J* = 2.6 Hz, 1H), 3.92 (s, 3H), 3.79 (s, 3H), 3.68 (s, 2H) ppm; **^{13}C NMR** (125 MHz, $CDCl_3$) δ 164.1, 162.3, 156.1, 141.3, 126.8, 124.2, 104.4, 98.4, 55.6, 53.1, 22.6 ppm; **HRMS:** Calcd. for $C_{11}H_{11}NNaO_4S$: $[M+Na]^+$: 276.0301 m/z, found 276.0304 m/z.

Compound 3.6.1.11

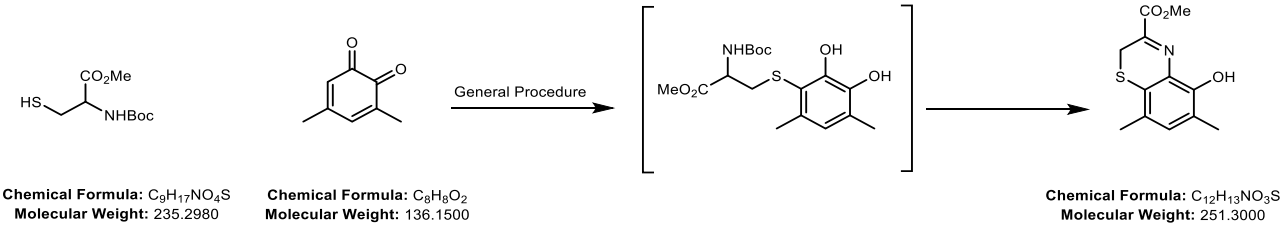

Chemical Formula: $C_9H_{17}NO_4S$
Molecular Weight: 235.2980

Chemical Formula: $C_8H_8O_2$
Molecular Weight: 136.1500

Chemical Formula: $C_{12}H_{13}NO_3S$
Molecular Weight: 251.3000

Procedure: The reaction was carried out according to the General Procedure described above.

Amounts of Reagents:

A. N-Boc-L-cysteine methyl ester (154 μL, 0.75 mmol)
Quinone (68.1 mg, 0.5 mmol)
$MgBr_2 \cdot Et_2O$ (32.3 mg, 0.125 mmol, 25 mol%)
DIPEA (245 μL, 1.5 mmol)
1,4-Dioxane (10 mL, 0.05 M)

B. TFA/DCM (10 mL, 1:1)
PIDA (161 mg, 0.5 mmol)
DCM (20 mL)

Purification: 60:40 Hexanes/EtOAc

Yield of Product:

3.6.1.11: 60.4 mg, 0.24 mmol, 48% *over 3 steps*

Characterization:

R_f = (hexanes/ethyl acetate 60:40): 0.57; **IR** (neat) v = 3368.3, 3005.2, 2946.3, 2920.1, 2856.6, 1709.5, 1565.1, 1435.6, 1321.3, 1285.7, 1232.4, 1098.4, 1021.9, 879.6, 791.2, 721.4, 616.1 cm^{-1}; **^{1}H NMR** (500 MHz, $CDCl_3$): δ = 7.23 (bs, 1H), 6.91 (s, 1H), 3.94 (s, 3H), 3.61 (s, 2H), 2.21 (d, *J* = 5.7 Hz, 6H) ppm; **^{13}C NMR** (125 MHz, $CDCl_3$) δ = 163.9, 150.6, 144.4, 134.2, 129.1, 125.2, 121.4, 120.8, 53.1, 22.1, 19.1, 15.3 ppm; **HRMS:** Calcd. for $C_{12}H_{13}NNaO_3S$: $[M+Na]^+$: 274.0508 m/z, found 274.0497 m/z.

Compound 3.6.1.12

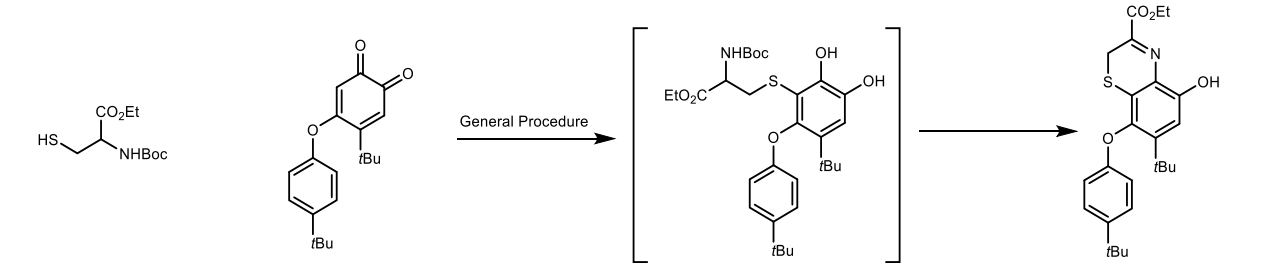

Chemical Formula: $C_{10}H_{19}NO_4S$ **Molecular Weight:** 249.3250

Chemical Formula: $C_{20}H_{24}O_3$ **Molecular Weight:** 312.4090

Chemical Formula: $C_{25}H_{31}NO_4S$ **Molecular Weight:** 441.5860

Procedure: The reaction was carried out according to the General Procedure described above.

Amounts of Reagents:

A. N-Boc-L-cysteine ethyl ester (186 mg, 0.75 mmol)
Quinone (156.2 mg, 0.5 mmol)
$MgBr_2 \cdot Et_2O$ (32.3 mg, 0.125 mmol, 25 mol%)
DIPEA (245 μL, 1.5 mmol)
1,4-Dioxane (10 mL, 0.05 M)

B. TFA/DCM (10 mL, 1:1)
PIDA (161 mg, 0.5 mmol)
DCM (20 mL)

Purification: 60:40 Hexanes/EtOAc

Yield of Product:

3.6.1.12: 159 mg, 0.36 mmol, 73% *over 3 steps*

Characterization:

$\mathbf{R_f}$ = (hexanes/ethyl acetate 60:40): 0.55; **IR** (neat) v = 3384.1, 2960.7 2906.7, 2870.1, 1713.2, 1581.4, 1506.4, 1431.5, 1221.1, 1169.3, 1093.6, 1011.5, 952.3, 907.5, 863.4, 828.2, 728.8, 549.0 cm^{-1}; **^{1}H NMR** (400 MHz, $CDCl_3$): 7.24 (d, J = 8.8 Hz, 2H), 6.94 (s, 1H), 6.67 (d, J = 8.8 Hz, 2H), 4.37 (q, J = 7.1 Hz, 2H), 3.48 (s, 2H), 1.38 (t, J = 7.2 Hz, 4H), 1.33 (s, 9H), 1.28 (s, 9H); **^{13}C NMR** (101 MHz, $CDCl_3$) δ 163.2, 155.6, 150.6, 147.5, 145.5, 144.6, 142.2, 128.7, 126.4, 120.7, 115.0, 110.8, 62.5, 35.7, 34.2, 31.5, 30.5, 22.4, 14.2 ppm; **HRMS:** Calcd. for $C_{25}H_{31}NNaO_4S$: $[M+Na]^+$: 464.1866 m/z, found 464.1873 m/z.

Compound 3.6.1.13

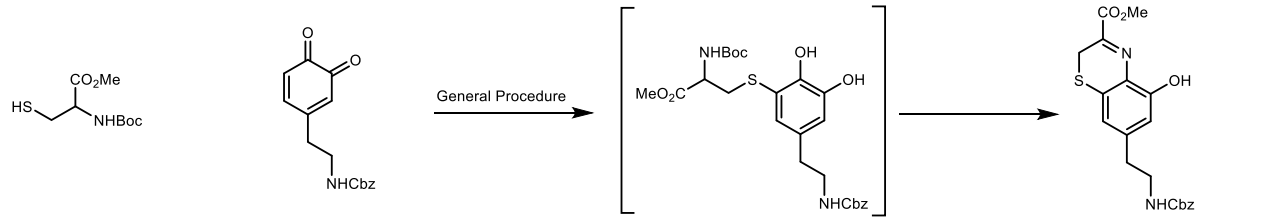

Chemical Formula: $C_9H_{17}NO_4S$
Molecular Weight: 235.2980

Chemical Formula: $C_{16}H_{15}NO_4$
Molecular Weight: 285.2990

Chemical Formula: $C_{20}H_{20}N_2O_5S$
Molecular Weight: 400.4490

Procedure: The reaction was carried out according to the General Procedure described above.

Amounts of Reagents:

A. N-Boc-L-cysteine methyl ester (154 μL, 0.75 mmol)
Quinone (142.6 mg, 0.5 mmol)
$MgBr_2 \cdot Et_2O$ (32.3 mg, 0.125 mmol, 25 mol%)
DIPEA (245 μL, 1.5 mmol)
1,4-Dioxane (10 mL, 0.05 M)

B. TFA/DCM (10 mL, 1:1)
PIDA (161 mg, 0.5 mmol)
DCM (20 mL)

Purification: 40:60 Hexanes/EtOAc

Yield of Product:

3.6.1.13: 117 mg, 0.29 mmol, 59% *over 3 steps*

Characterization:

$\mathbf{R_f}$ = (hexanes/ethyl acetate 4:6): 0.40; **IR** (neat) ν = 3332.0, 3032.8, 2951.2, 1703.3, 1516.8, 1438.1, 1217.0, 1085.0, 1001.0, 907.9, 727.6, 696.6, 573.5 cm^{-1}; **^{1}H NMR** (500 MHz, $CDCl_3$): δ 7.35 (m, 5H), 6.62 (d, *J* = 11.2 Hz, 2H), 5.10 (s, 2H), 4.90 (s, 1H), 3.93 (s, 3H), 3.65 (s, 2H), 3.47 – 3.38 (m, 2H), 2.73 (t, *J* = 7.0 Hz, 2H) ppm; **^{13}C NMR** (125 MHz, $CDCl_3$) δ 163.8, 156.3, 154.3, 144.5, 143.1, 136.4, 128.6, 128.4, 128.2, 128.1, 125.6, 118.4, 113.0, 66.8, 53.2, 41.7, 36.2, 22.5 ppm; **HRMS:** Calcd. for $C_{20}H_{20}N_2NaO_5S$: $[M+Na]^+$: 423.0985 m/z, found 423.0981 m/z.

Compound 3.6.1.14

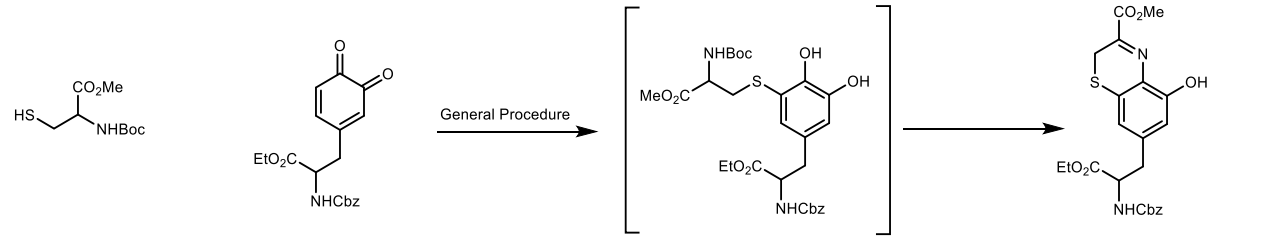

Chemical Formula: $C_9H_{17}NO_4S$
Molecular Weight: 235.2980

Chemical Formula: $C_{19}H_{19}NO_6$
Molecular Weight: 357.3620

Chemical Formula: $C_{23}H_{24}N_2O_7S$
Molecular Weight: 472.5120

Procedure: The reaction was carried out according to the General Procedure described above.

Amounts of Reagents:

A. N-Boc-L-cysteine methyl ester (154 μL, 0.75 mmol)
Quinone (171.7 mg, 0.5 mmol)
$MgBr_2 \cdot Et_2O$ (32.3 mg, 0.125 mmol, 25 mol%)
DIPEA (245 μL, 1.5 mmol)
1,4-Dioxane (10 mL, 0.05 M)

B. TFA/DCM (10 mL, 1:1)
PIDA (161 mg, 0.5 mmol)
DCM (20 mL)

Purification: 50:50 Hexanes/EtOAc

Yield of Product:

3.6.1.14: 128.4 mg, 0.28 mmol, 56% *over 3 steps*

Characterization:

R_f = (hexanes/ethyl acetate 50:50): 0.37; **IR** (neat) v = 3341.3, 2954.4, 2926.3, 1706.5, 1499.2, 1438.8, 1212.9, 1021.9, 735.4, 696.7, 576.4 cm^{-1}; **^{1}H NMR** (500 MHz, $CDCl_3$) δ 7.48 (s, 1H), 7.33 (d, *J* = 11.3 Hz, 5H), 6.56 (d, *J* = 12.7 Hz, 2H), 5.38 (d, *J* = 8.4 Hz, 1H), 5.10 (s, 2H), 4.61 (d, *J* = 6.9 Hz, 1H), 4.18 (q, *J* = 7.3 Hz, 2H), 3.93 (s, 3H), 3.63 (s, 2H), 3.02 (qd, *J* = 13.9, 5.5 Hz, 2H), 1.25 (t, *J* = 6.9 Hz, 3H) ppm;**^{13}C NMR** (125 MHz, $(CD_3)_2CO$)): δ 171.3, 163.7, 156.0, 154.7, 145.5, 141.0, 129.0, 128.3, 127.7, 127.6, 125.4, 118.5, 114.0, 65.9, 60.8, 55.3, 52.3, 37.3, 21.9, 13.6 ppm; **HRMS:** Calcd. for $C_{23}H_{24}N_2NaO_7S$: $[M+Na]^+$: 495.1196 m/z, found 495.1202 m/z.

7. References

1. Mao, J. G.; Bao, W. L., Palladium(0)-Catalyzed Methylenecyclopropanation of Norbornenes with Vinyl Bromides. *Org. Lett.* **2014,** *16* (10), 2646-2649.
2. Yu, H.; Ru, S.; Dai, G. Y.; Zhai, Y. Y.; Lin, H. L.; Han, S.; Wei, Y. G., An Efficient Iron(III)-Catalyzed Aerobic Oxidation of Aldehydes in Water for the Green Preparation of Carboxylic Acids. *Angew. Chem. Int. Ed.* **2017,** *56* (14), 3867-3871.
3. Li, S. THIAZOLE COMPOUND AND USE THEREOF. 2013.
4. Liu, J.; He, K. L.; Li, X.; Li, R. J.; Liu, C. L.; Zhong, W.; Li, S., SAR, Cardiac Myocytes Protection Activity and 3D-QSAR Studies of Salubrinal and its Potent Derivatives. *Curr. Med. Chem.* **2012,** *19* (35), 6072-6079.
5. Chundawat, T. S.; Kumari, P.; Sharma, N.; Bhagat, S., Strategic synthesis and in vitro antimicrobial evaluation of novel difluoromethylated 1-(1, 3-diphenyl-1H-pyrazol-4-yl)-3, 3-difluoro-1, 3-dihydro-indol-2-ones. *Med. Chem. Res.* **2016,** *25* (10), 2335-2348.
6. Saravanan, K.; Elancheran, R.; Divakar, S.; Anand, S. A. A.; Ramanathan, M.; Kotoky, J.; Lokanath, N. K.; Kabilan, S., Design, synthesis and biological evaluation of 2-(4-phenylthiazol-2-yl) isoindoline-1,3-dione derivatives as anti-prostate cancer agents. *Bioorg. Med. Chem. Lett.* **2017,** *27* (5), 1199-1204.
7. Nambo, M.; Keske, E. C.; Rygus, J. P. G.; Yim, J. C. H.; Crudden, C. M., Development of Versatile Sulfone Electrophiles for Suzuki-Miyaura Cross-Coupling Reactions. *ACS Catal.* **2017,** *7* (2), 1108-1112.
8. Denton, R. M.; Scragg, J. T.; Saska, J., A concise synthesis of 4 '-O-methyl honokiol. *Tetrahedron Lett.* **2011,** *52* (20), 2554-2556.
9. Hong, M. N.; Nam, K. Y.; Kim, K. K.; Kim, S. Y.; Kim, I., The small molecule '1-(4-biphenylylcarbonyl)-4-(5-bromo-2-methoxybenzyl) piperazine oxalate' and its derivatives regulate global protein synthesis by inactivating eukaryotic translation initiation factor 2-alpha. *Cell Stress Chaperones* **2016,** *21* (3), 485-497.
10. Esguerra, K. V. N.; Fall, Y.; Lumb, J.-P., A Biomimetic Catalytic Aerobic Functionalization of Phenols. *Angew. Chem.* **2014,** *126* (23), 5987-5991.
11. Huang, Z.; Kwon, O.; Esguerra, K. V. N.; Lumb, J.-P., A divergent and selective synthesis of ortho- and para-quinones from phenols. *Tetrahedron* **2015,** *71* (35), 5871-5885.

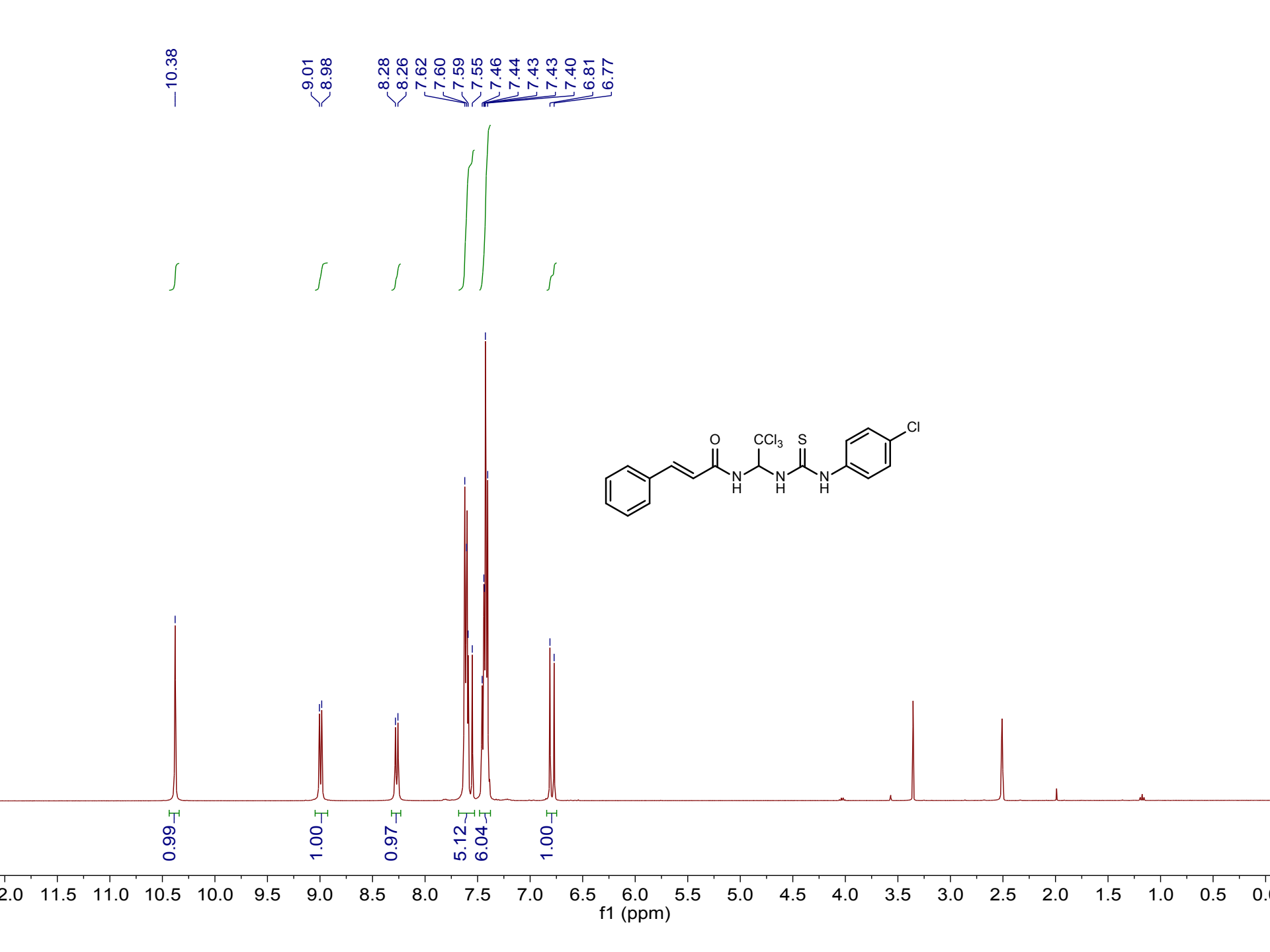
10.38
9.01
8.98
8.28
8.26
7.62
7.60
7.59
7.55
7.46
7.44
7.43
7.43
7.40
6.81
6.77
O
CCl3
S
N
H
N
H
N
H
Cl
0.99
1.00
0.97
5.12
6.04
1.00
f1 (ppm)

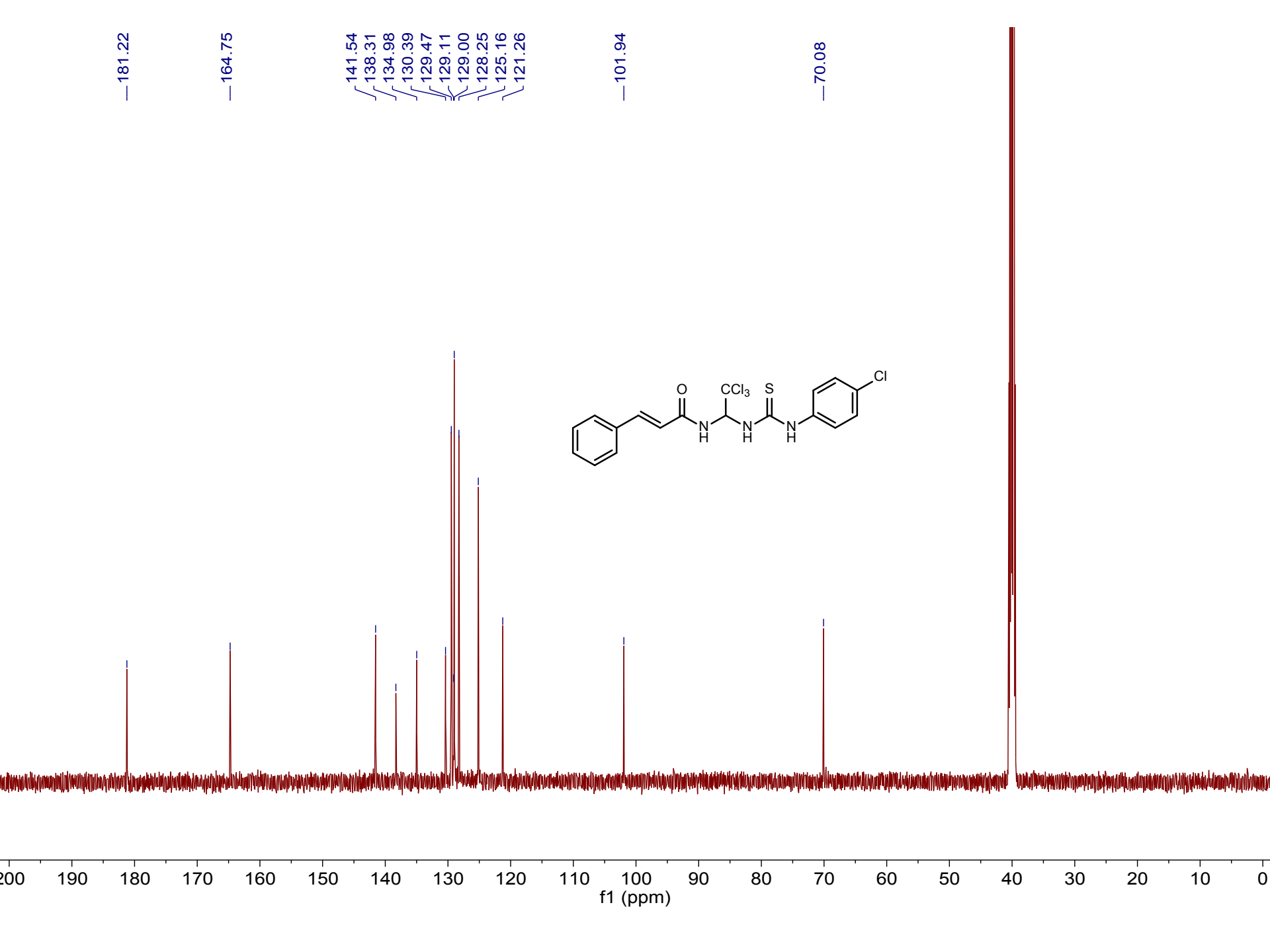
181.22
164.75
141.54
138.31
134.98
130.39
129.47
129.11
129.00
128.25
125.16
121.26
101.94
70.08
O
CCl3
S
N
H
N
H
N
H
Cl
200
190
180
170
160
150
140
130
120
110
100
90
80
70
60
50
40
30
20
10
0
f1 (ppm)

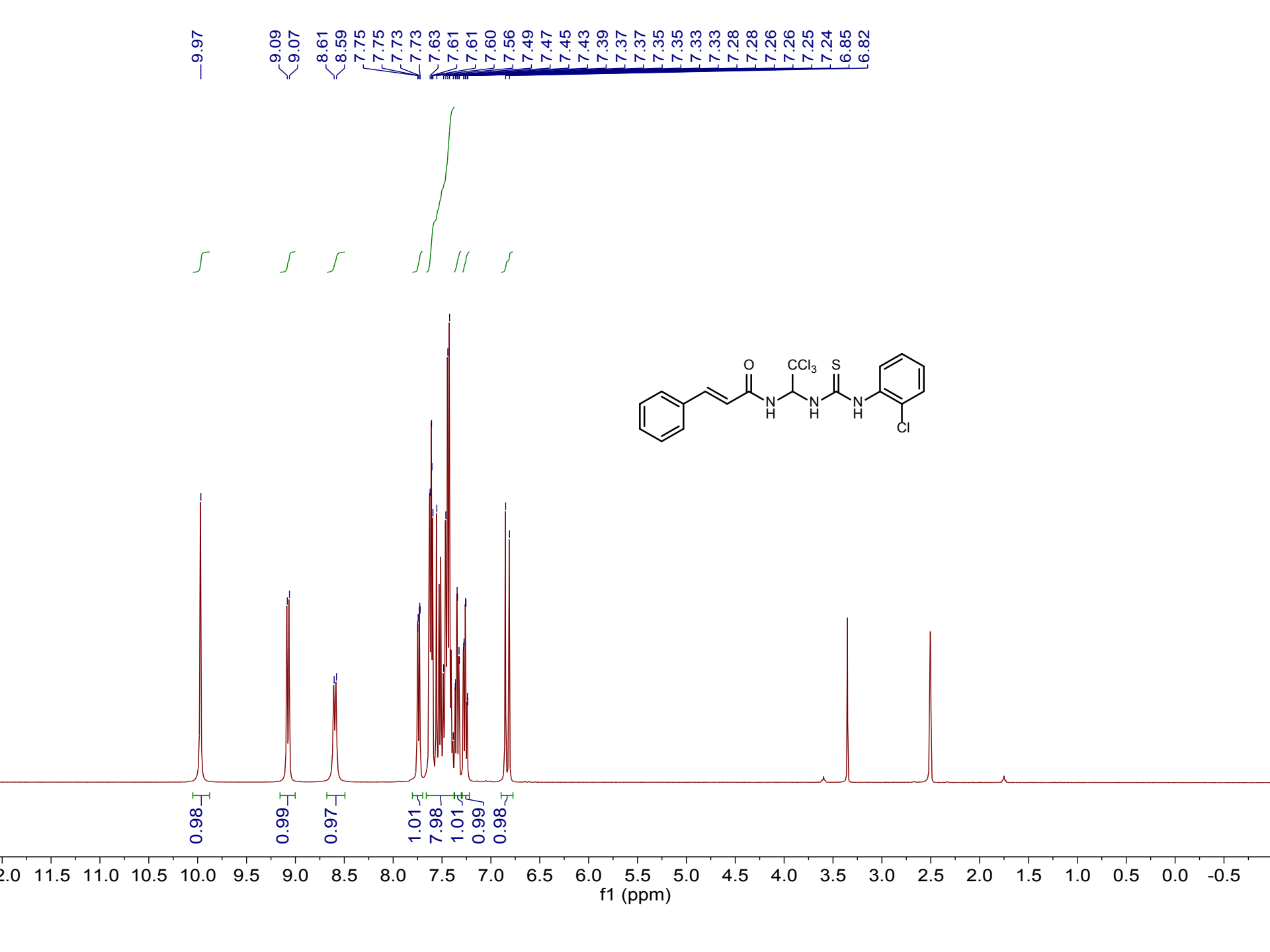
9.97
9.09
9.07
8.61
8.59
7.75
7.75
7.73
7.73
7.63
7.61
7.61
7.60
7.56
7.49
7.47
7.45
7.43
7.39
7.37
7.37
7.35
7.35
7.33
7.33
7.28
7.28
7.26
7.26
7.25
7.24
6.85
6.82
O
CCl3
S
N
H
N
H
N
H
Cl
0.98
0.99
0.97
1.01
7.98
1.01
0.99
0.98
f1 (ppm)

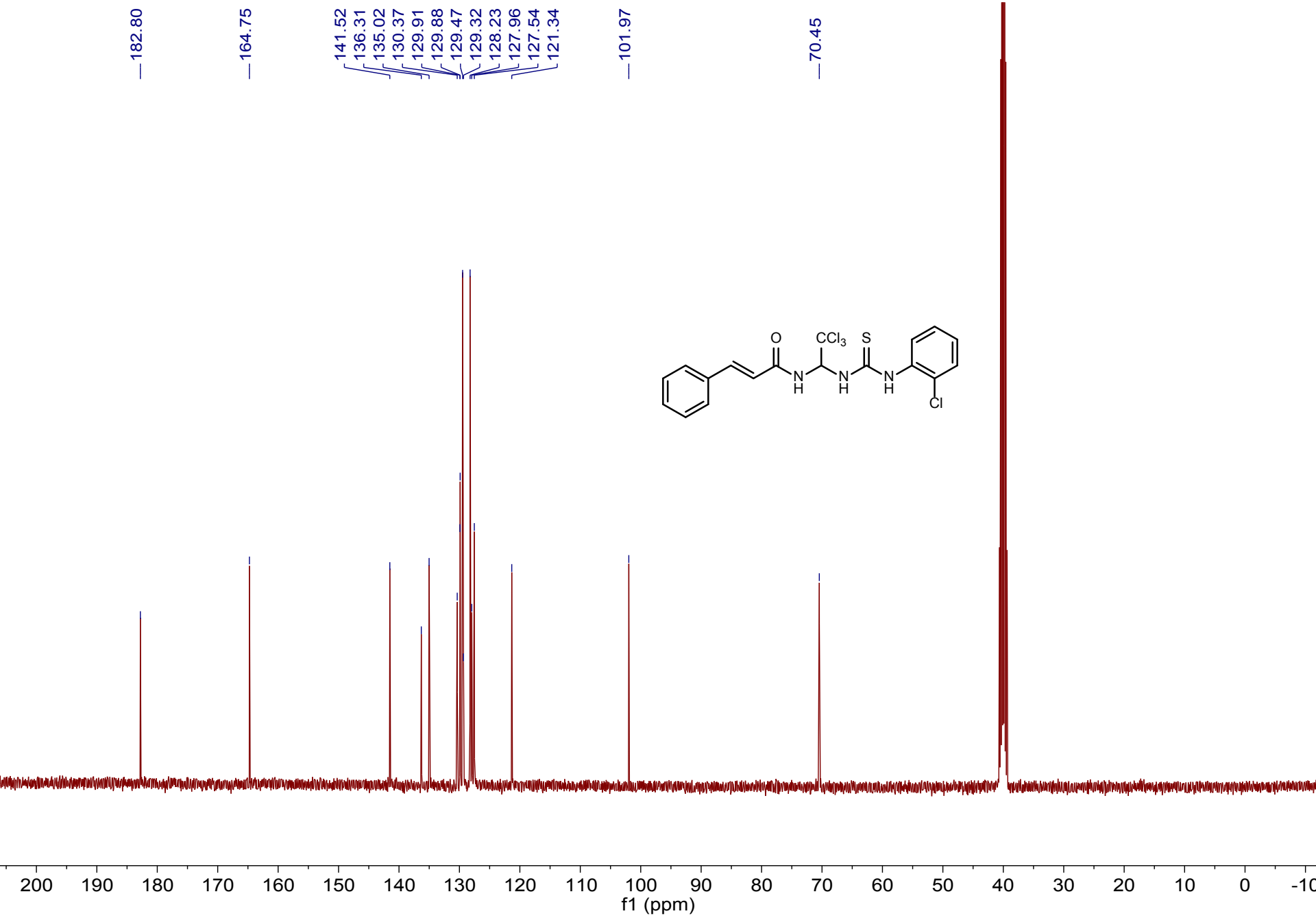
182.80
164.75
141.52
136.31
135.02
130.37
129.91
129.88
129.47
129.32
128.23
127.96
127.54
121.34
101.97
70.45
O
CCl3
S
N
H
N
H
N
H
Cl
200
190
180
170
160
150
140
130
120
110
100
90
80
70
60
50
40
30
20
10
0
-10
f1 (ppm)

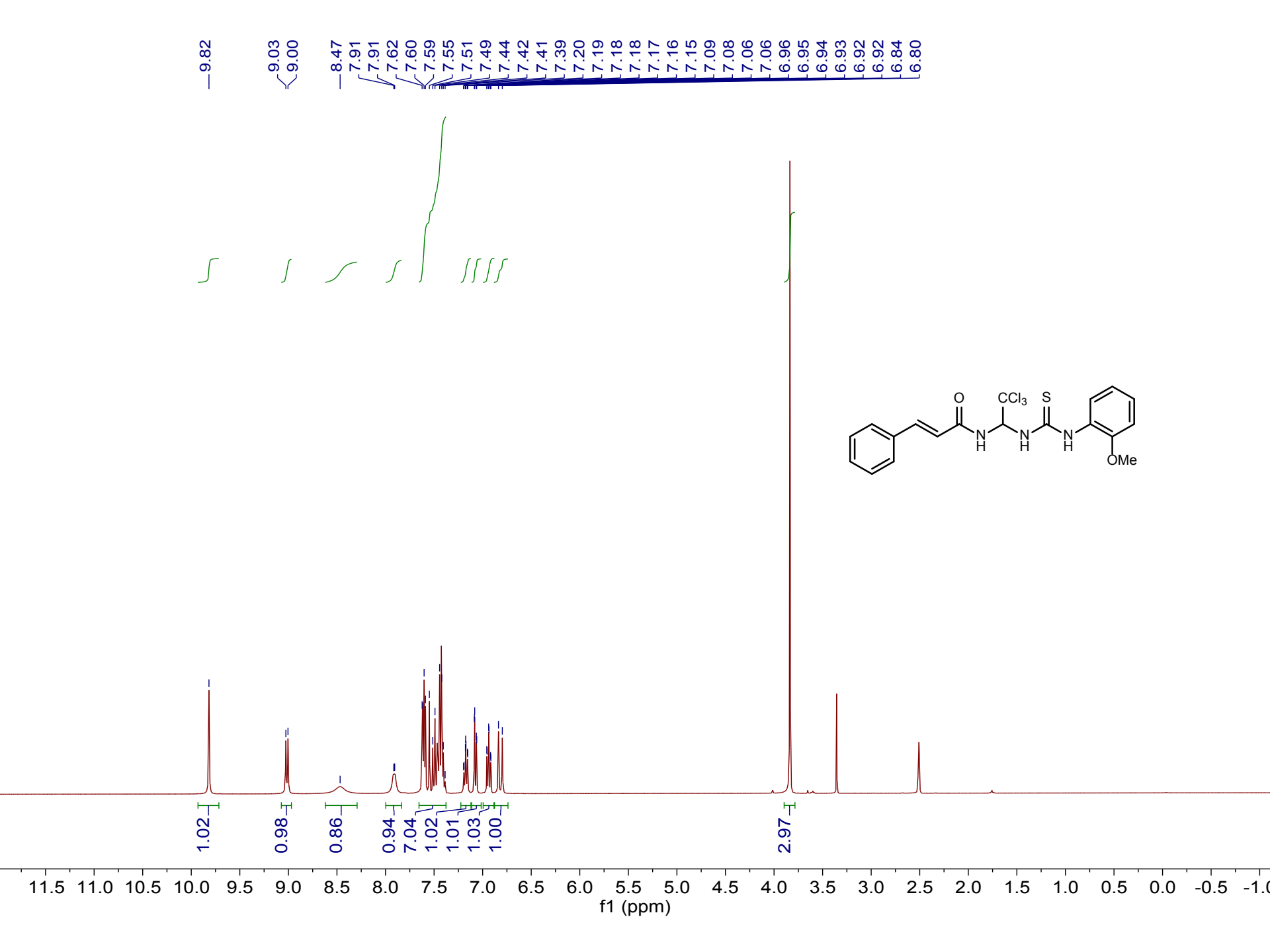
9.82
9.03
9.00
8.47
7.91
7.91
7.62
7.60
7.59
7.55
7.51
7.49
7.44
7.42
7.41
7.39
7.20
7.19
7.18
7.18
7.17
7.16
7.15
7.09
7.08
7.06
7.06
6.96
6.95
6.94
6.93
6.92
6.92
6.84
6.80
O
CCl3
S
N
H
N
H
N
H
OMe
1.02
0.98
0.86
0.94
7.04
1.02
1.01
1.03
1.00
2.97
11.5 11.0 10.5 10.0 9.5 9.0 8.5 8.0 7.5 7.0 6.5 6.0 5.5 5.0 4.5 4.0 3.5 3.0 2.5 2.0 1.5 1.0 0.5 0.0 -0.5 -1.0
f1 (ppm)

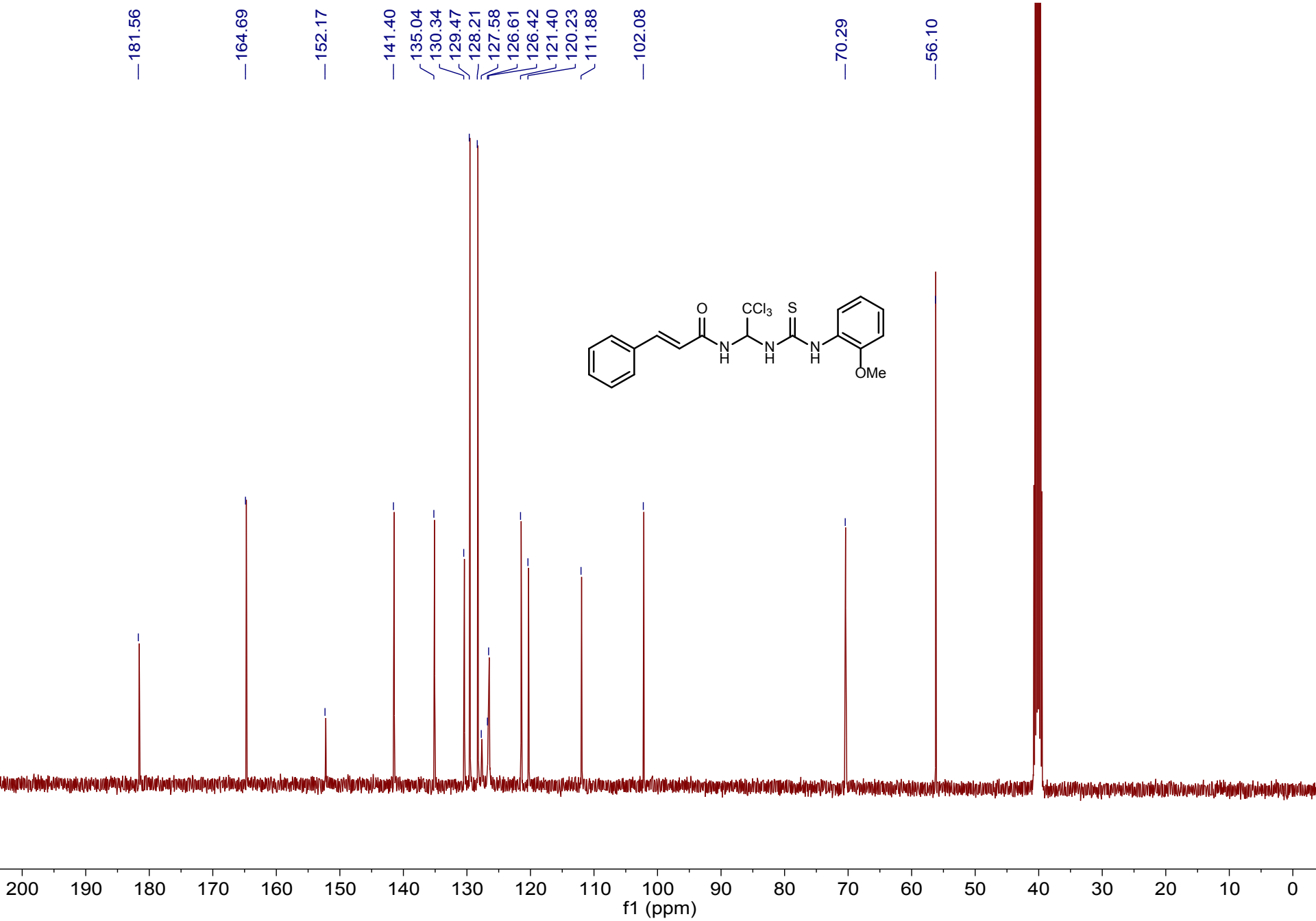
181.56
164.69
152.17
141.40
135.04
130.34
129.47
128.21
127.58
126.61
126.42
121.40
120.23
111.88
102.08
70.29
56.10
O
CCl3
S
N
H
N
H
N
H
OMe
200
190
180
170
160
150
140
130
120
110
100
90
80
70
60
50
40
30
20
10
0
f1 (ppm)

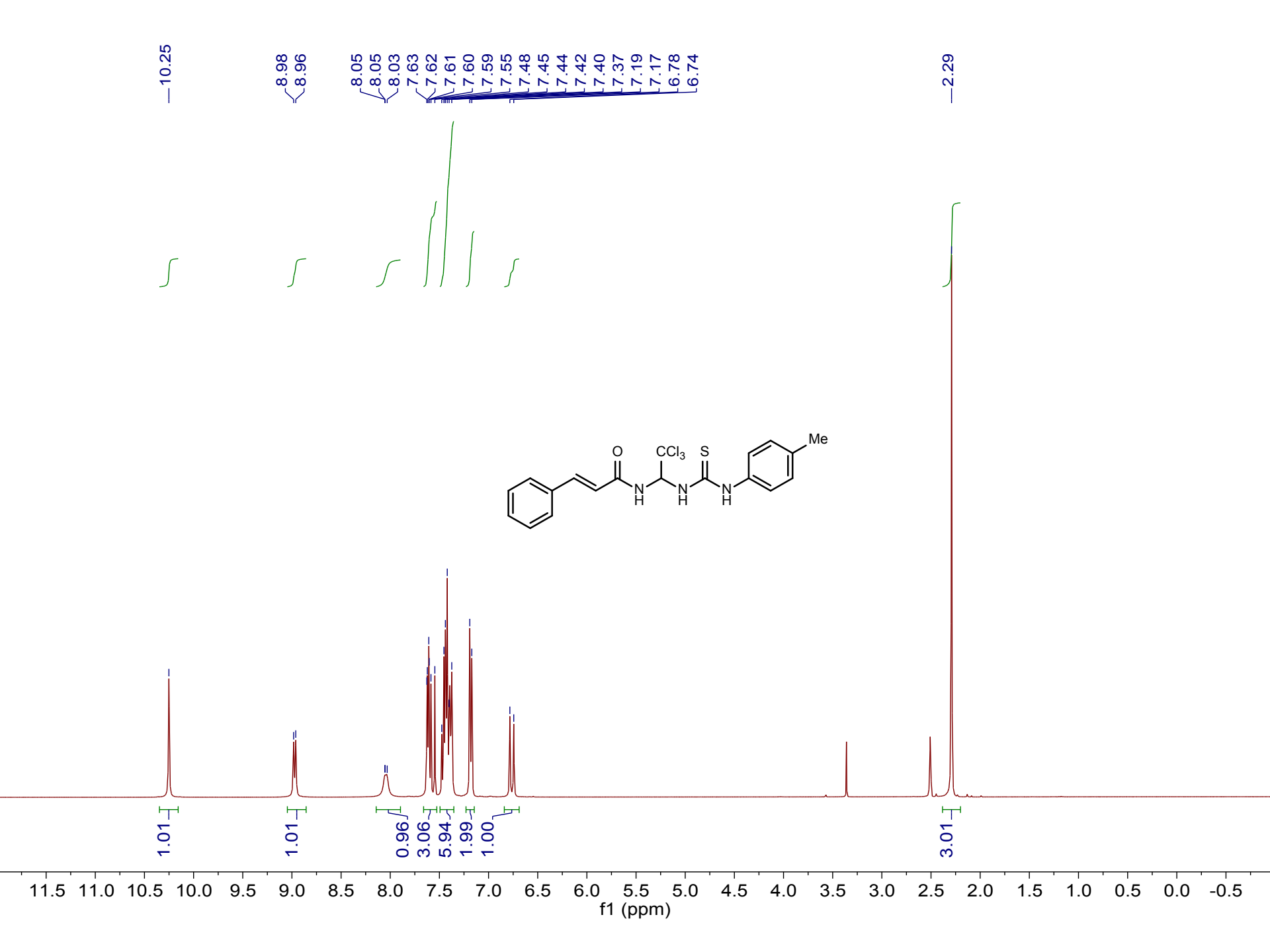
10.25
8.98
8.96
8.05
8.05
8.03
7.63
7.62
7.61
7.60
7.59
7.55
7.48
7.45
7.44
7.42
7.40
7.37
7.19
7.17
6.78
6.74
2.29
O
CCl3
S
Me
N
H
N
H
N
H
1.01
1.01
0.96
3.06
5.94
1.99
1.00
3.01
11.5 11.0 10.5 10.0 9.5 9.0 8.5 8.0 7.5 7.0 6.5 6.0 5.5 5.0 4.5 4.0 3.5 3.0 2.5 2.0 1.5 1.0 0.5 0.0 -0.5
f1 (ppm)

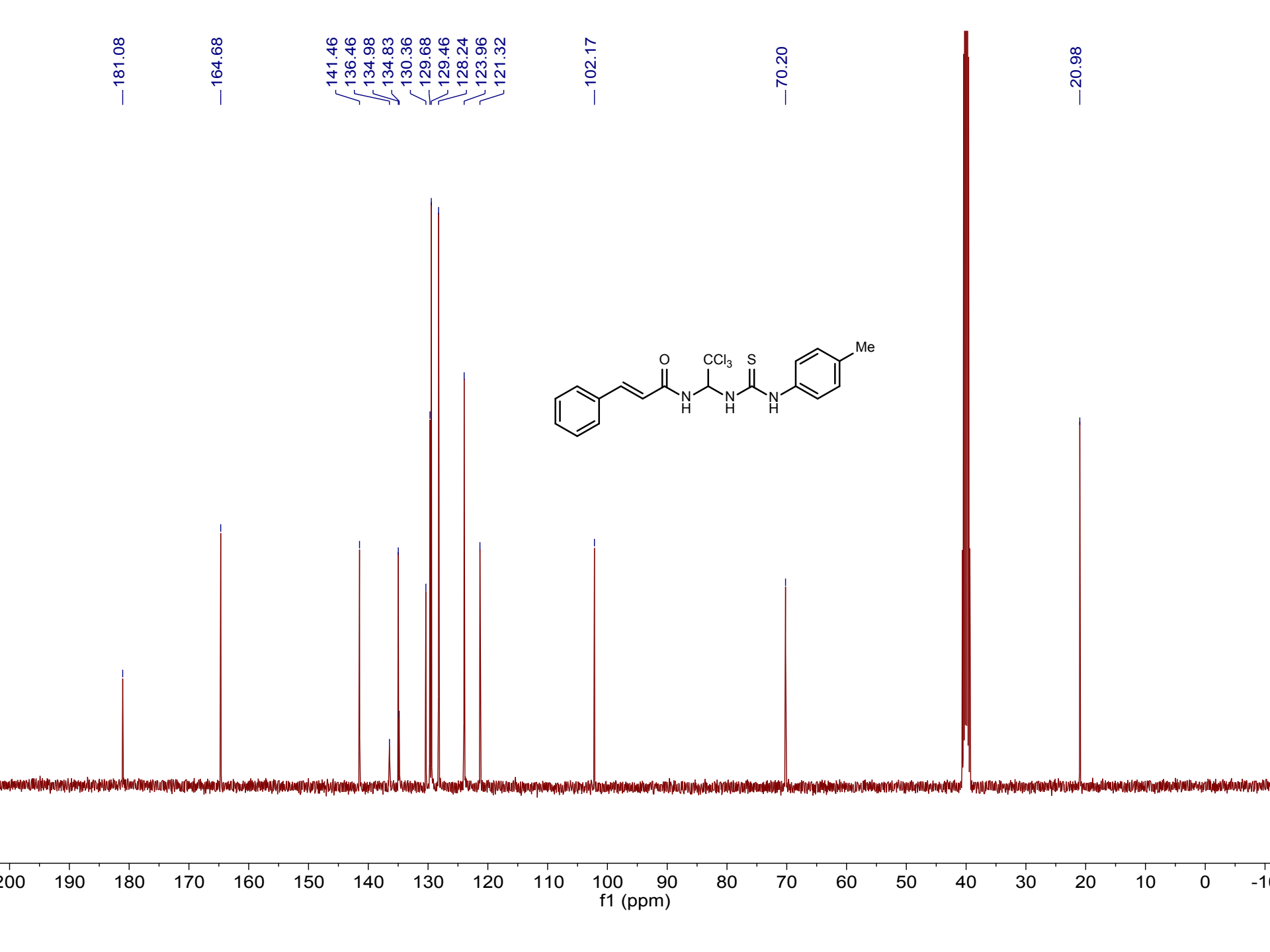
181.08
164.68
141.46
136.46
134.98
134.83
130.36
129.68
129.46
128.24
123.96
121.32
102.17
70.20
20.98
O
CCl3
S
Me
N
H
N
H
N
H
f1 (ppm)

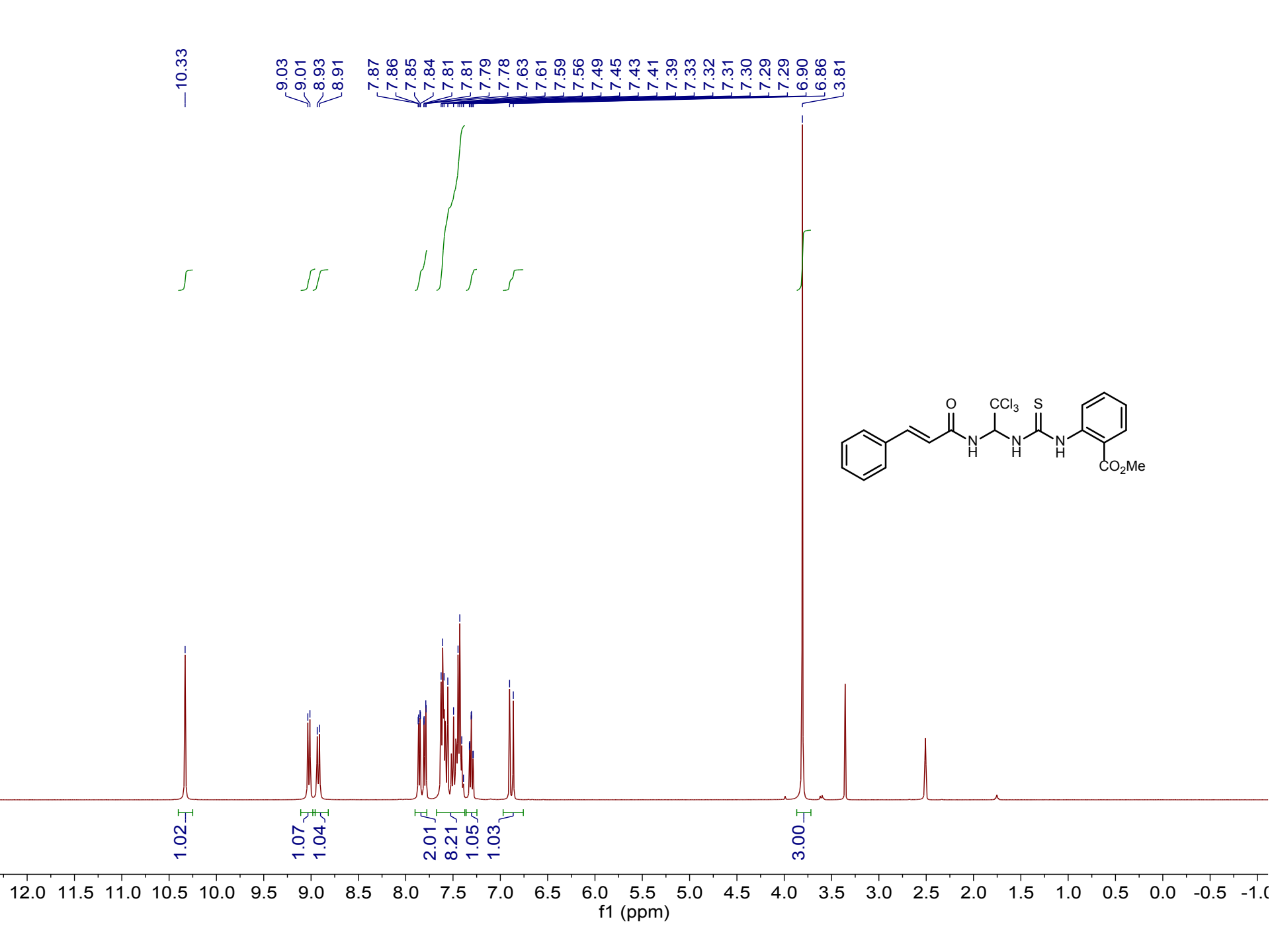
10.33
9.03
9.01
8.93
8.91
7.87
7.86
7.85
7.84
7.81
7.81
7.79
7.78
7.63
7.61
7.59
7.56
7.49
7.45
7.43
7.41
7.39
7.33
7.32
7.31
7.30
7.29
7.29
6.90
6.86
3.81
O
CCl3
S
N
H
N
H
N
H
CO2Me
1.02
1.07
1.04
2.01
8.21
1.05
1.03
3.00
12.0 11.5 11.0 10.5 10.0 9.5 9.0 8.5 8.0 7.5 7.0 6.5 6.0 5.5 5.0 4.5 4.0 3.5 3.0 2.5 2.0 1.5 1.0 0.5 0.0 -0.5 -1.0
f1 (ppm)

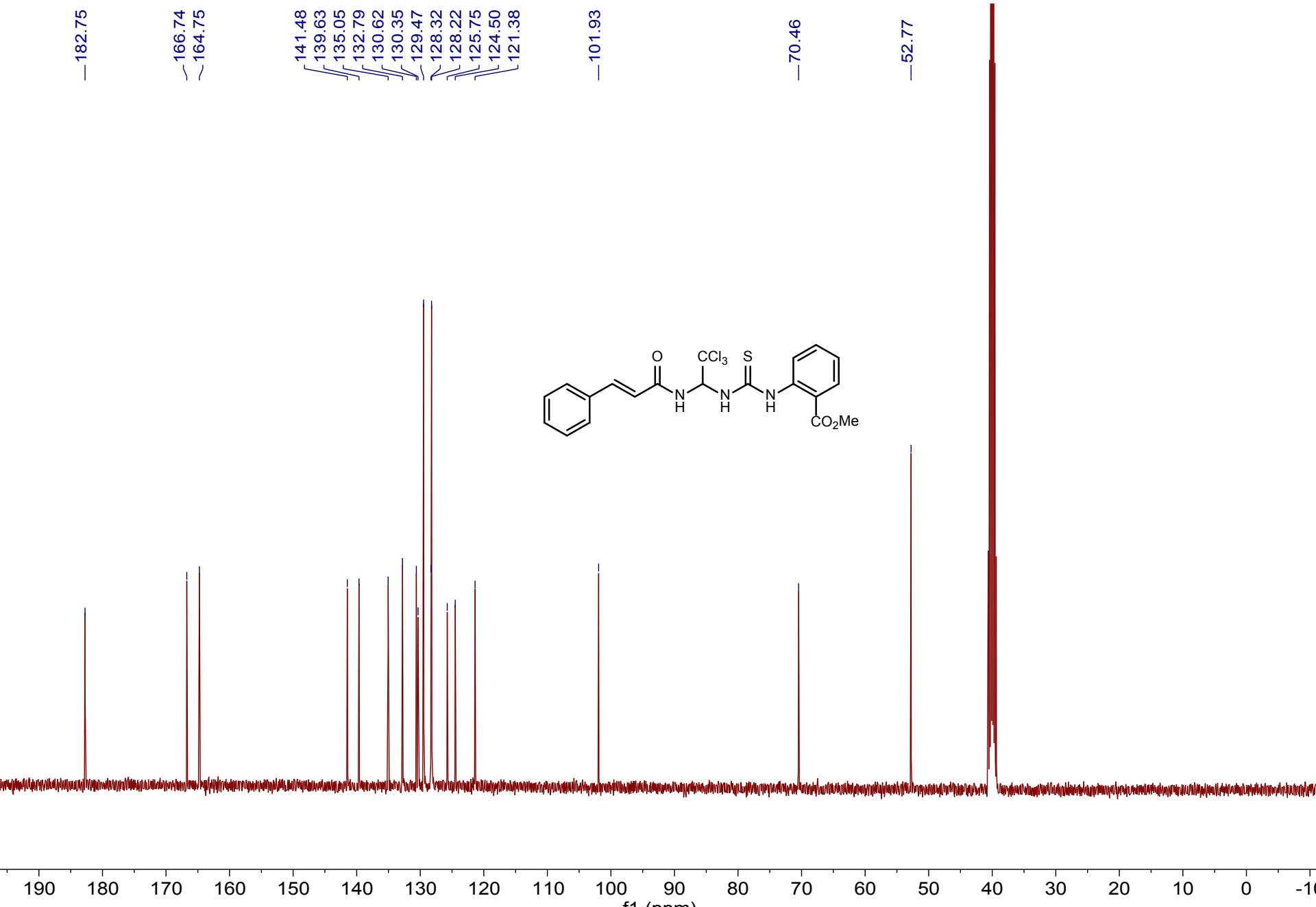
182.75
166.74
164.75
141.48
139.63
135.05
132.79
130.62
130.35
129.47
128.32
128.22
125.75
124.50
121.38
101.93
70.46
52.77
O
CCl3
S
N
H
N
H
N
H
CO2Me
190
180
170
160
150
140
130
120
110
100
90
80
70
60
50
40
30
20
10
0
f1 (ppm)

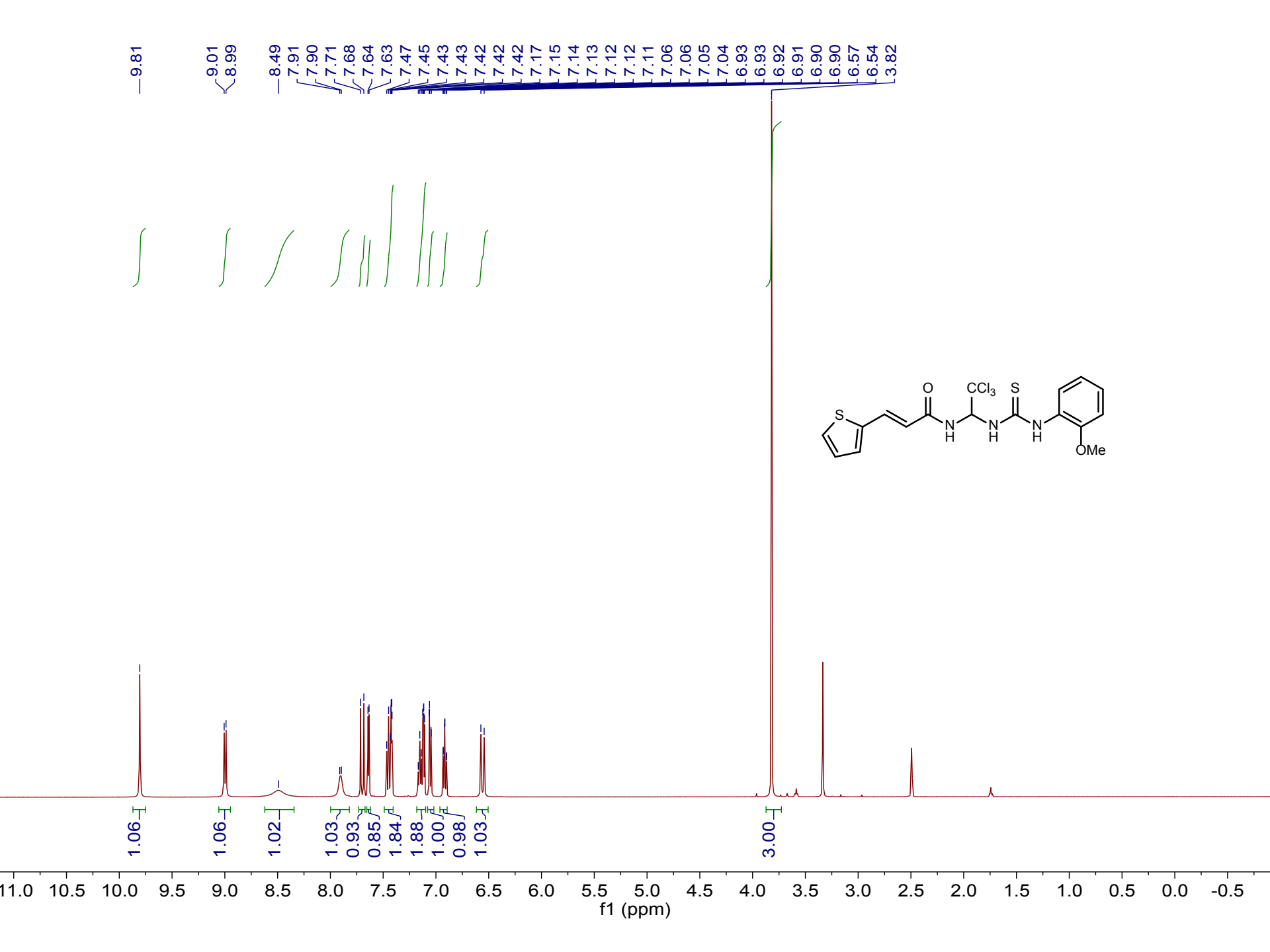
9.81
9.01
8.99
8.49
7.91
7.90
7.71
7.68
7.64
7.63
7.47
7.45
7.43
7.43
7.42
7.42
7.42
7.17
7.15
7.14
7.13
7.12
7.12
7.11
7.06
7.06
7.05
7.04
6.93
6.93
6.92
6.91
6.90
6.90
6.57
6.54
3.82
O
CCl3
S
S
N
H
N
H
N
H
OMe
1.06
1.06
1.02
1.03
0.93
0.85
1.84
1.88
1.00
0.98
1.03
3.00
11.0
10.5
10.0
9.5
9.0
8.5
8.0
7.5
7.0
6.5
6.0
5.5
5.0
4.5
4.0
3.5
3.0
2.5
2.0
1.5
1.0
0.5
0.0
-0.5
f1 (ppm)

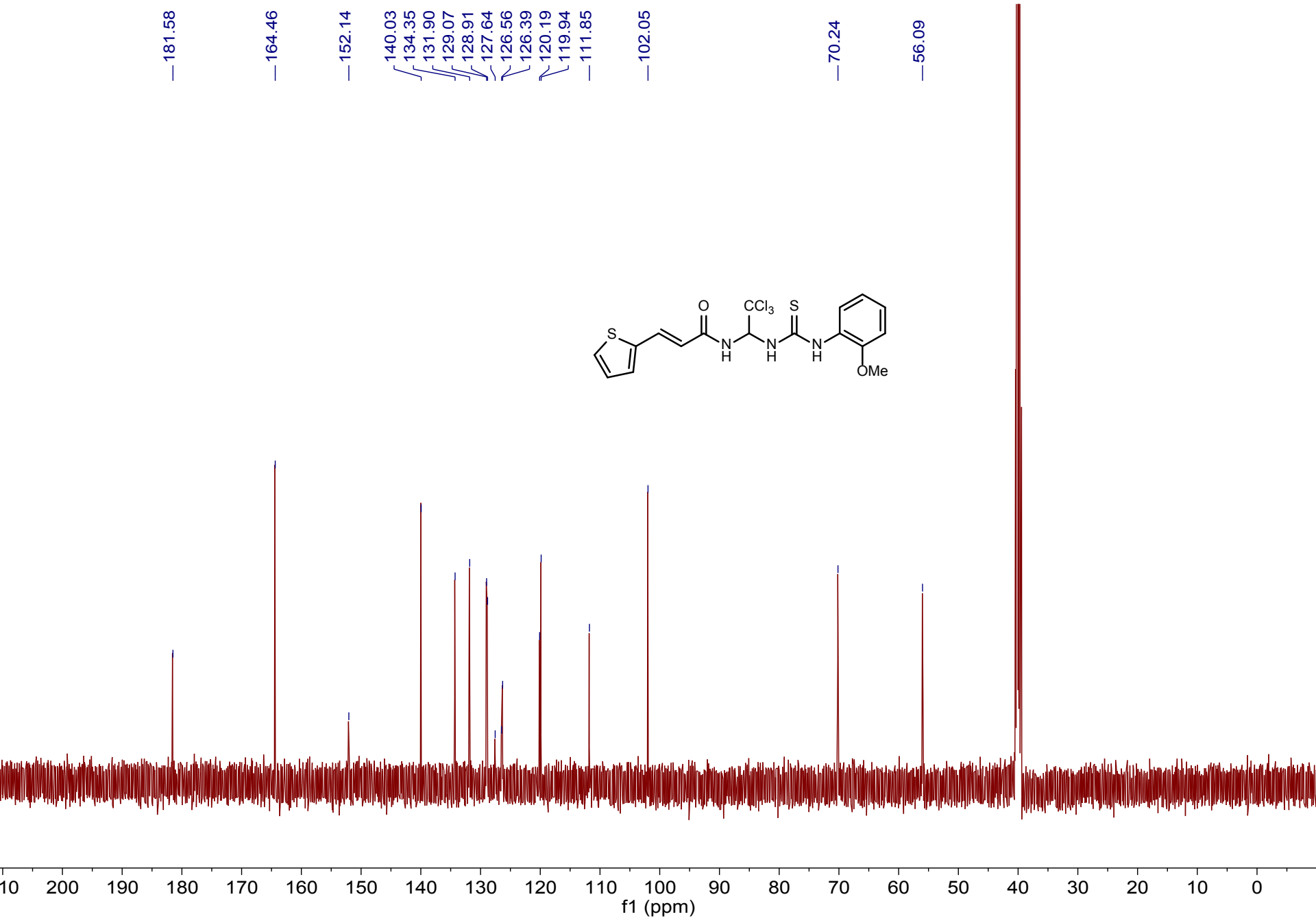
181.58
164.46
152.14
140.03
134.35
131.90
129.07
128.91
127.64
126.56
126.39
120.19
119.94
111.85
102.05
70.24
56.09
O
CCl3
S
S
N
H
N
H
N
H
OMe
10
200
190
180
170
160
150
140
130
120
110
100
90
80
70
60
50
40
30
20
10
0
f1 (ppm)

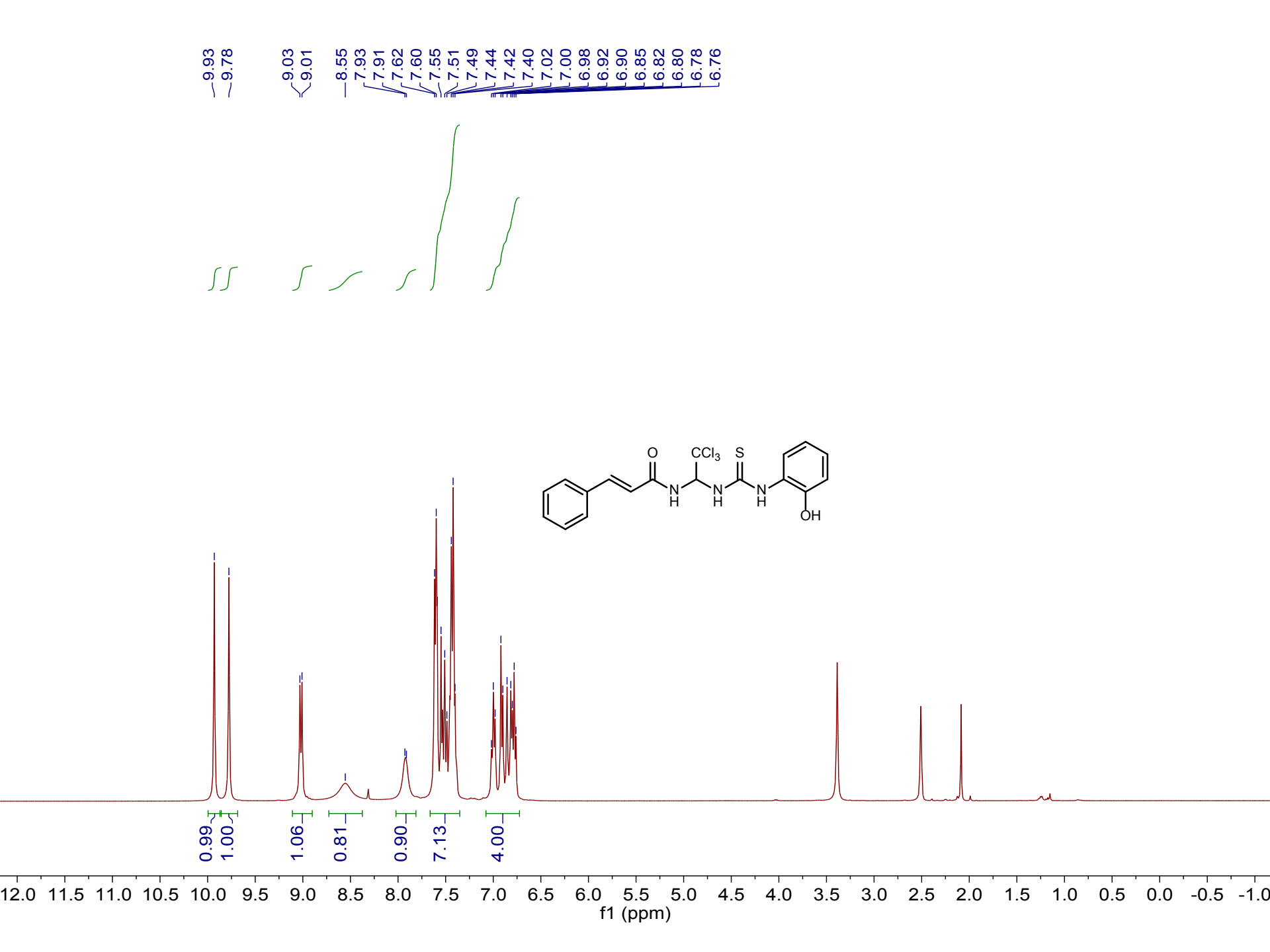
9.93
9.78
9.03
9.01
8.55
7.93
7.91
7.62
7.60
7.55
7.51
7.49
7.44
7.42
7.40
7.02
7.00
6.98
6.92
6.90
6.85
6.82
6.80
6.78
6.76
O
CCl3
S
N
H
N
H
N
H
OH
0.99
1.00
1.06
0.81
0.90
7.13
4.00
12.0 11.5 11.0 10.5 10.0 9.5 9.0 8.5 8.0 7.5 7.0 6.5 6.0 5.5 5.0 4.5 4.0 3.5 3.0 2.5 2.0 1.5 1.0 0.5 0.0 -0.5 -1.0
f1 (ppm)

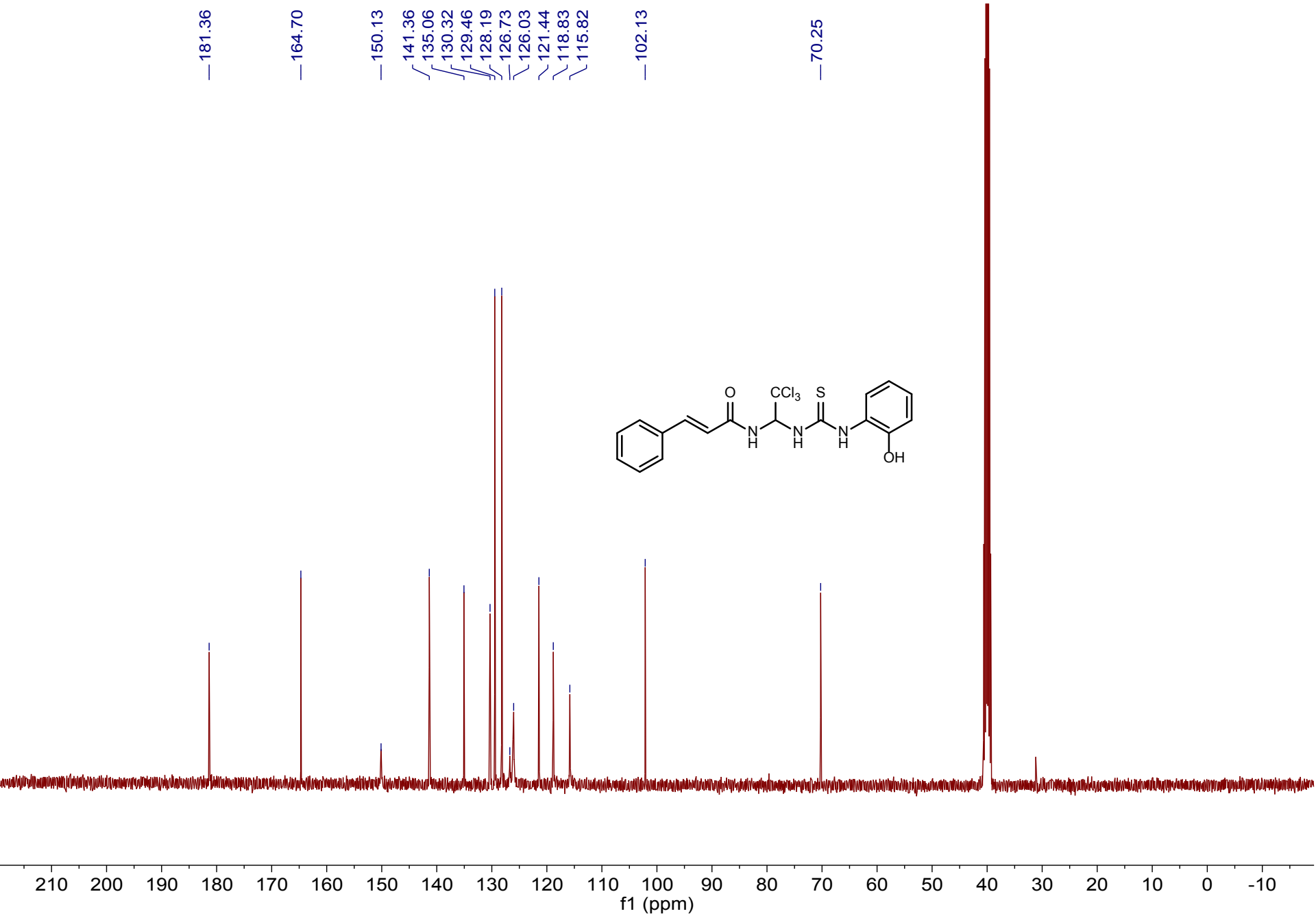
181.36
164.70
150.13
141.36
135.06
130.32
129.46
128.19
126.73
126.03
121.44
118.83
115.82
102.13
70.25
O
CCl3
S
N
H
N
H
N
H
OH
210
200
190
180
170
160
150
140
130
120
110
100
90
80
70
60
50
40
30
20
10
0
-10
f1 (ppm)

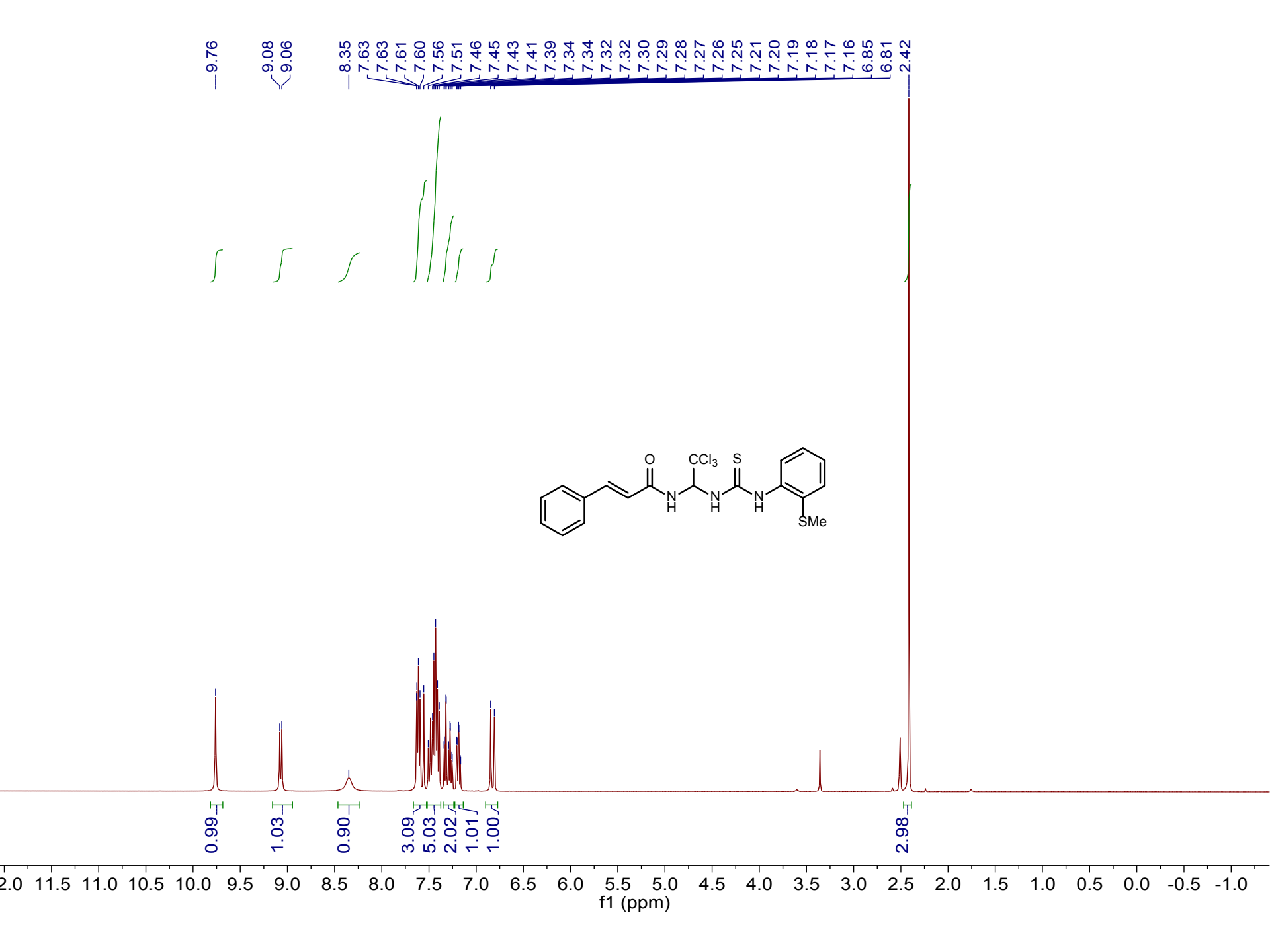
9.76
9.08
9.06
8.35
7.63
7.63
7.61
7.60
7.56
7.51
7.46
7.45
7.43
7.41
7.39
7.34
7.34
7.32
7.32
7.30
7.29
7.28
7.27
7.26
7.25
7.21
7.20
7.19
7.18
7.17
7.16
6.85
6.81
2.42
O
CCl3
S
N
H
N
H
N
H
SMe
0.99
1.03
0.90
3.09
5.03
2.02
1.01
1.00
2.98
f1 (ppm)

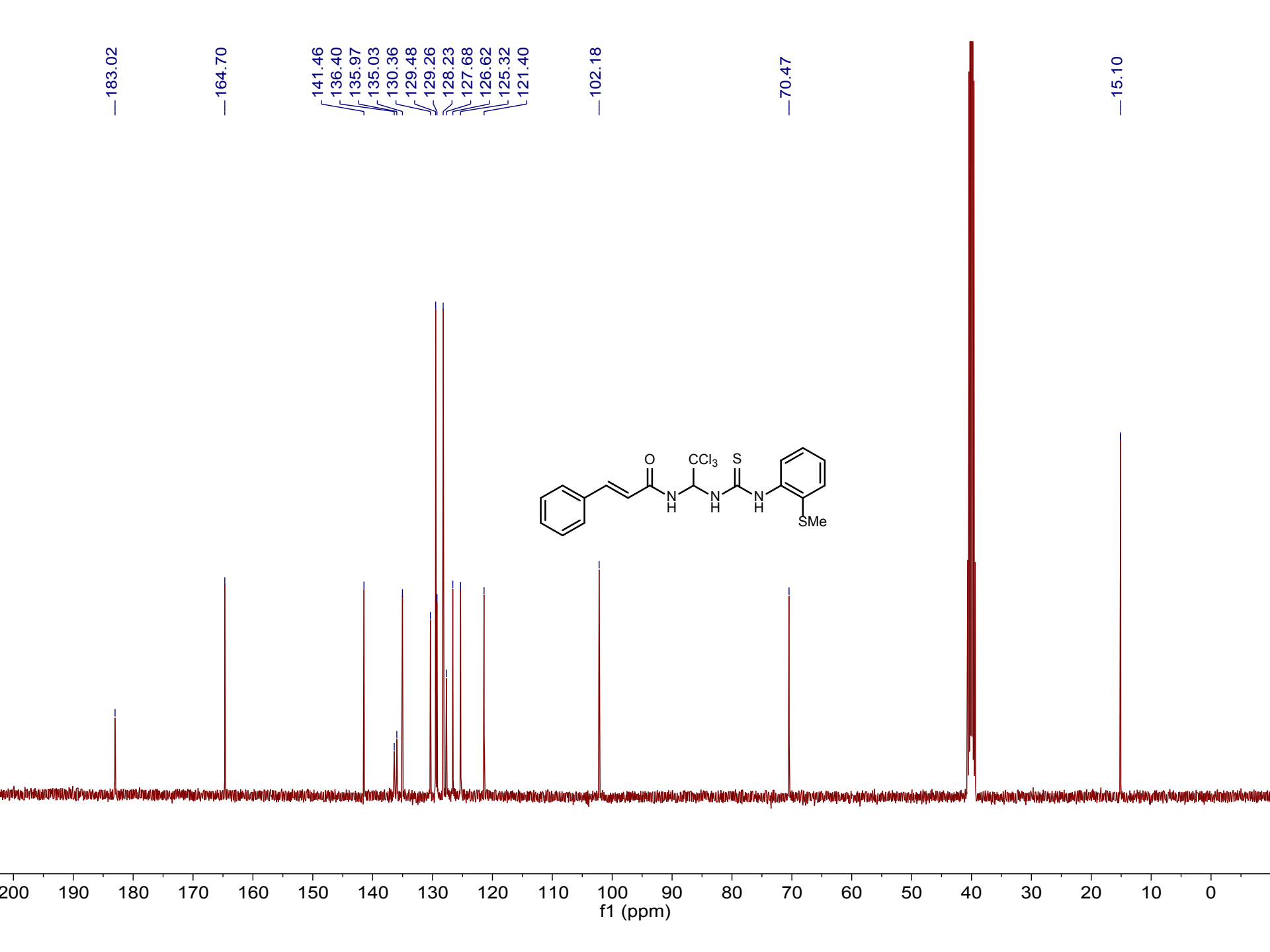
183.02
164.70
141.46
136.40
135.97
135.03
130.36
129.48
129.26
128.23
127.68
126.62
125.32
121.40
102.18
70.47
15.10
O
CCl3
S
N
H
N
H
N
H
SMe
200
190
180
170
160
150
140
130
120
110
100
90
80
70
60
50
40
30
20
10
0
f1 (ppm)

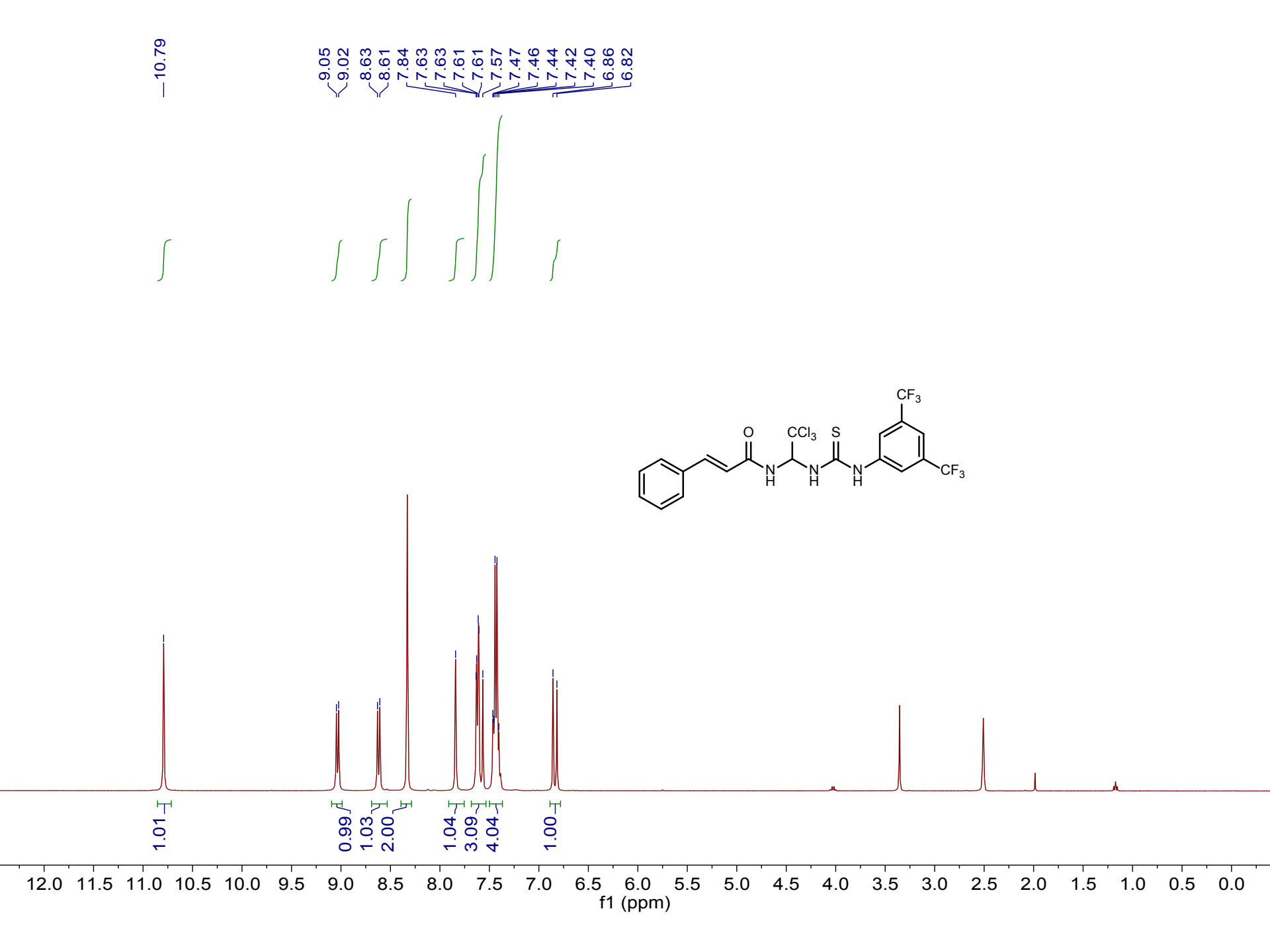
10.79
9.05
9.02
8.63
8.61
7.84
7.63
7.63
7.61
7.61
7.57
7.47
7.46
7.44
7.42
7.40
6.86
6.82
CF3
O
CCl3
S
N
H
N
H
N
H
CF3
1.01
0.99
1.03
2.00
1.04
3.09
4.04
1.00
12.0 11.5 11.0 10.5 10.0 9.5 9.0 8.5 8.0 7.5 7.0 6.5 6.0 5.5 5.0 4.5 4.0 3.5 3.0 2.5 2.0 1.5 1.0 0.5 0.0
f1 (ppm)

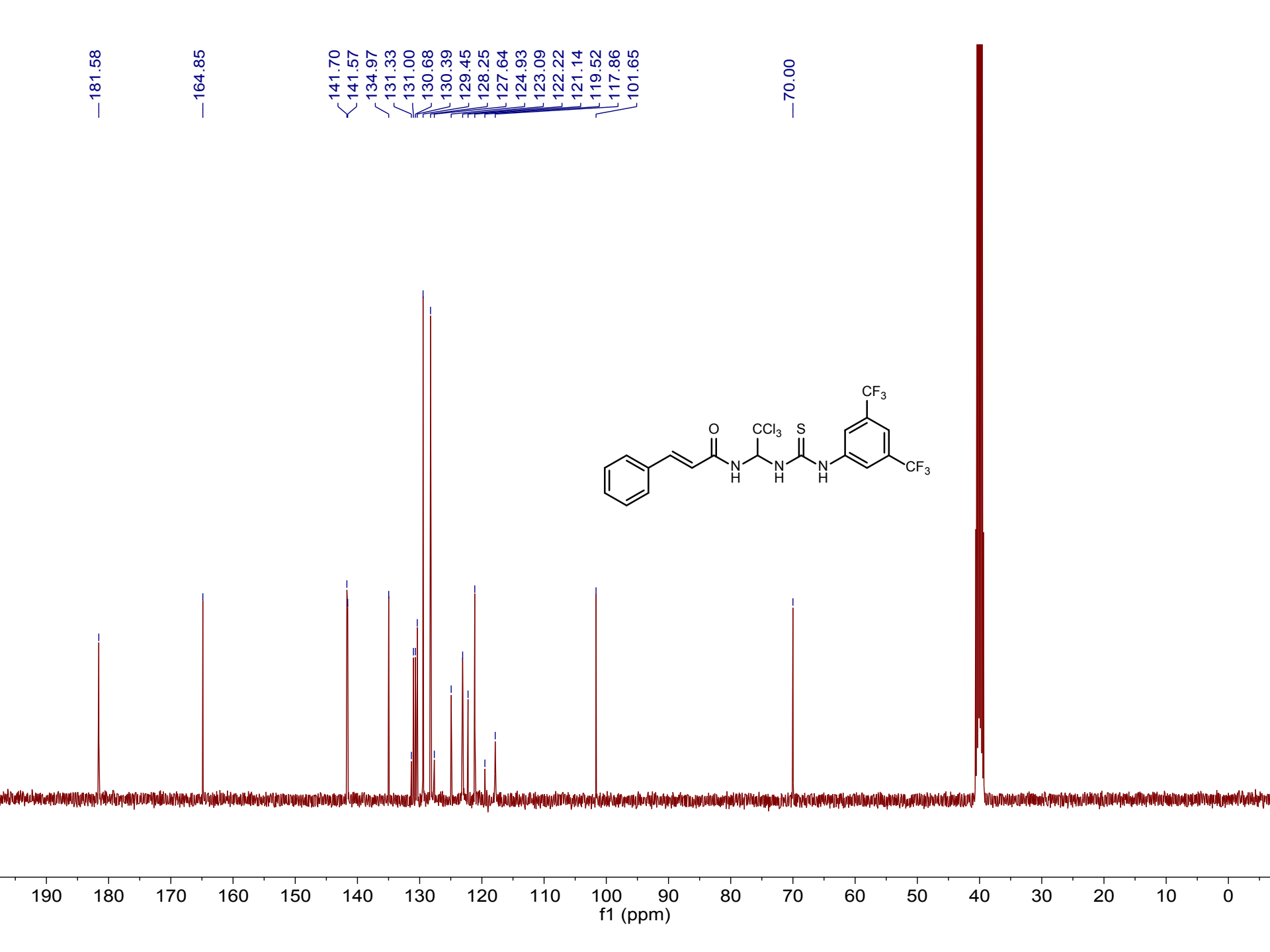
181.58
164.85
141.70
141.57
134.97
131.33
131.00
130.68
130.39
129.45
128.25
127.64
124.93
123.09
122.22
121.14
119.52
117.86
101.65
70.00
O
CCl3
S
N
H
N
H
N
H
CF3
CF3
190
180
170
160
150
140
130
120
110
100
90
80
70
60
50
40
30
20
10
0
f1 (ppm)

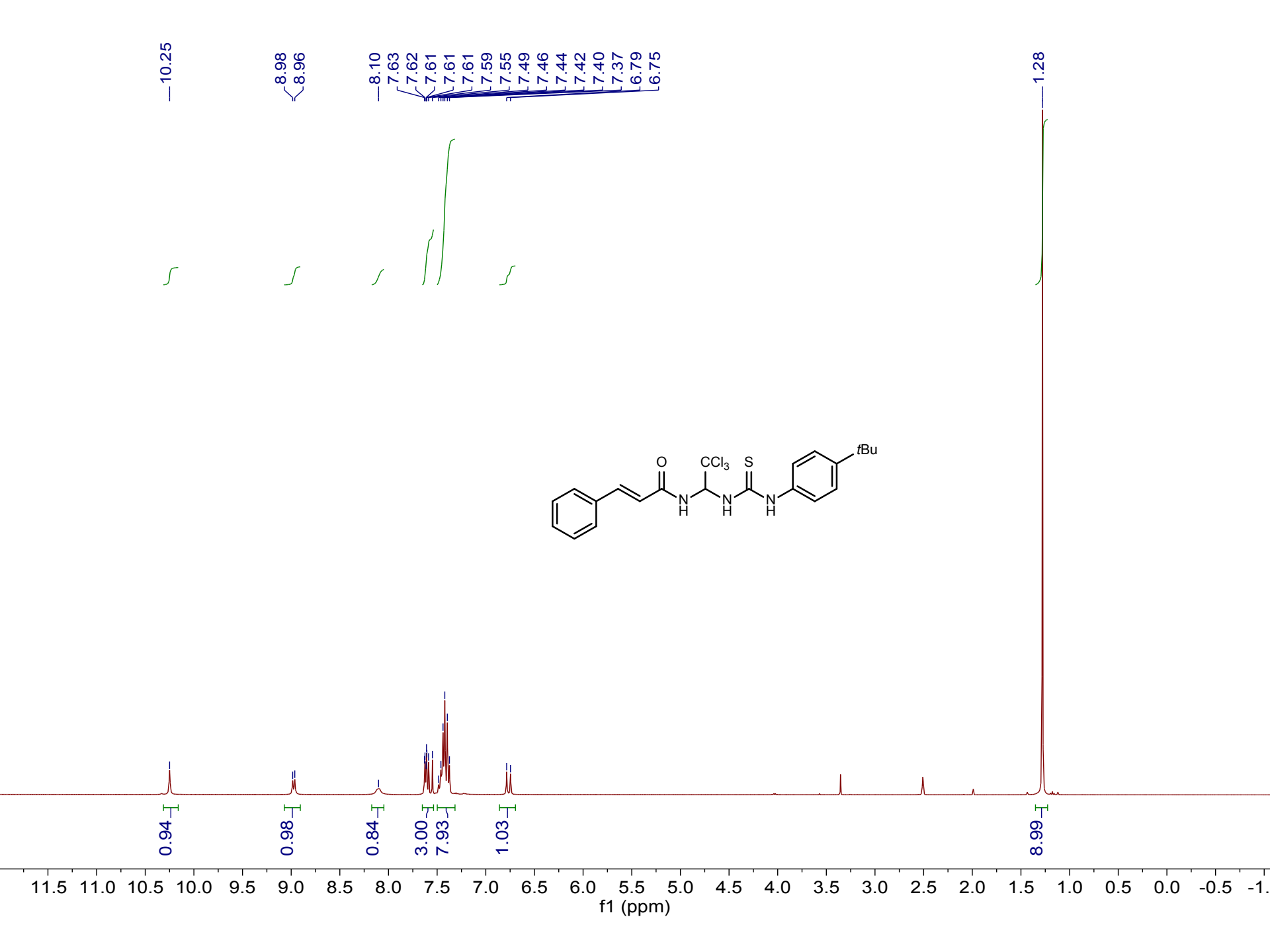
10.25
8.98
8.96
8.10
7.63
7.62
7.61
7.61
7.61
7.59
7.55
7.49
7.46
7.44
7.42
7.40
7.37
6.79
6.75
1.28
O
CCl3
S
N
H
N
H
N
H
tBu
0.94
0.98
0.84
3.00
7.93
1.03
8.99
11.5 11.0 10.5 10.0 9.5 9.0 8.5 8.0 7.5 7.0 6.5 6.0 5.5 5.0 4.5 4.0 3.5 3.0 2.5 2.0 1.5 1.0 0.5 0.0 -0.5 -1.
f1 (ppm)

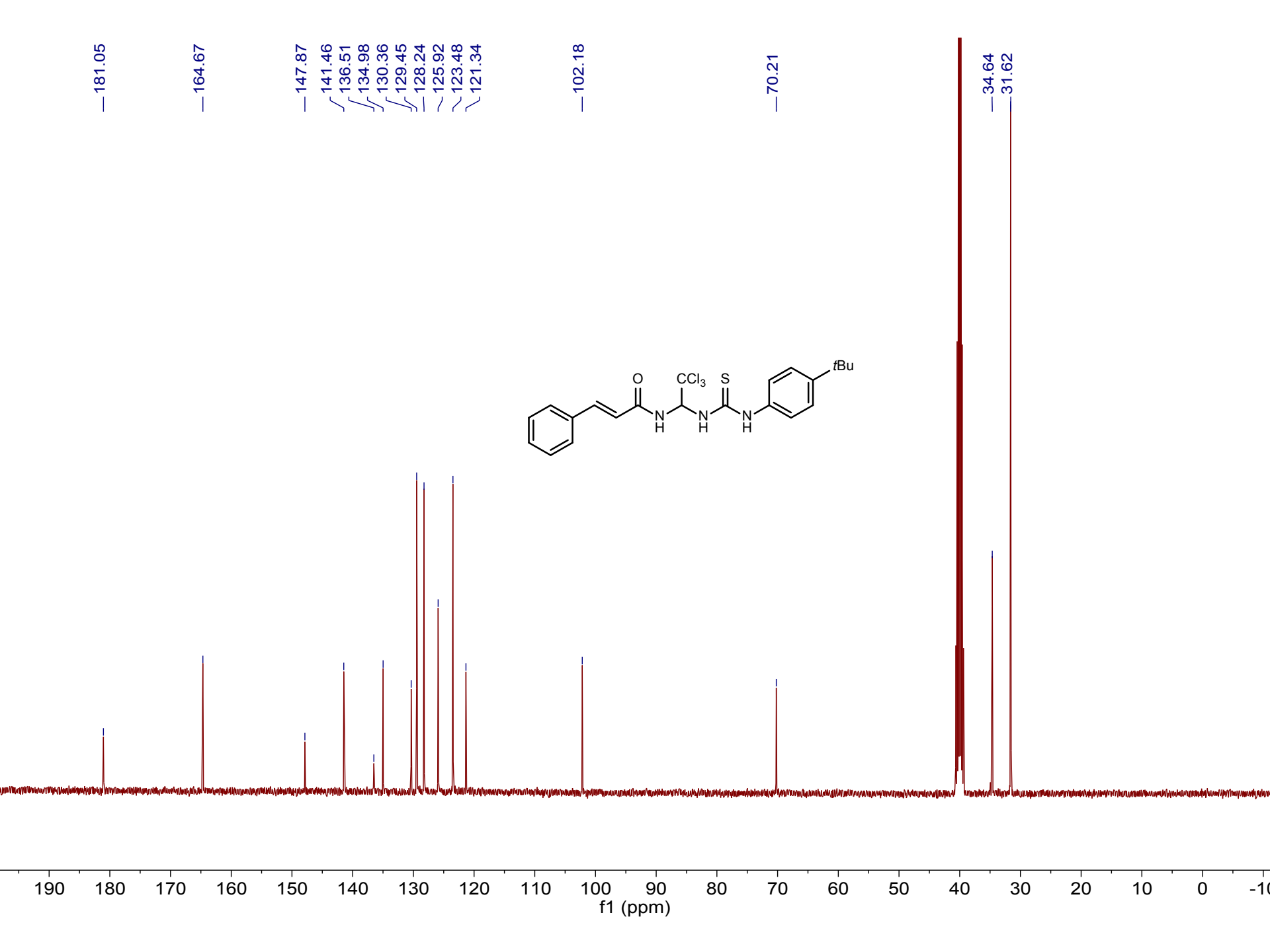
181.05
164.67
147.87
141.46
136.51
134.98
130.36
129.45
128.24
125.92
123.48
121.34
102.18
70.21
34.64
31.62
O
CCl3
S
N
H
N
H
N
H
tBu
190
180
170
160
150
140
130
120
110
100
90
80
70
60
50
40
30
20
10
0
-10
f1 (ppm)

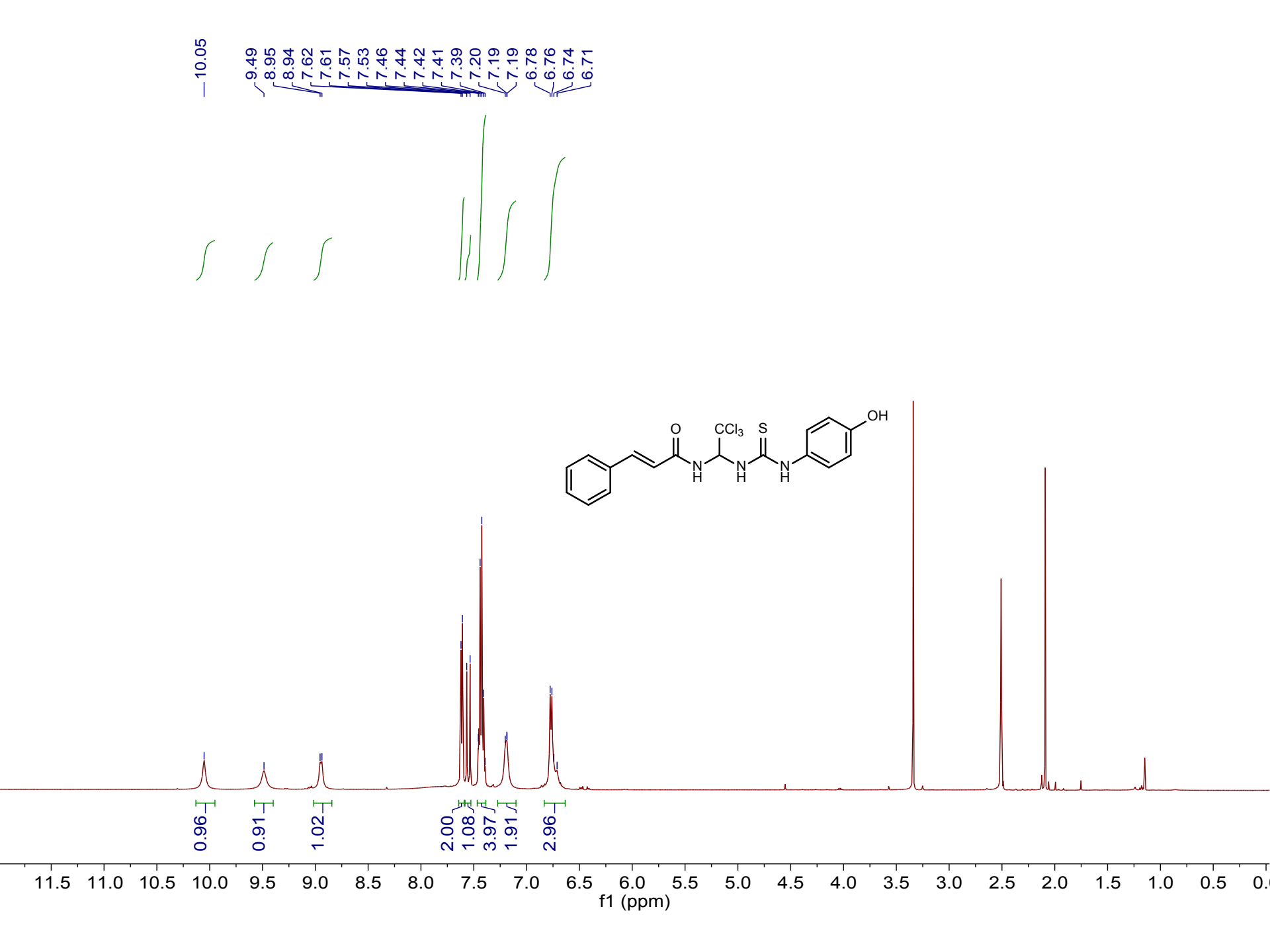
10.05
9.49
8.95
8.94
7.62
7.61
7.57
7.53
7.46
7.44
7.42
7.41
7.39
7.20
7.19
7.19
6.78
6.76
6.74
6.71
O
CCl3
S
N
H
N
H
N
H
OH
0.96
0.91
1.02
2.00
1.08
3.97
1.91
2.96
11.5
11.0
10.5
10.0
9.5
9.0
8.5
8.0
7.5
7.0
6.5
6.0
5.5
5.0
4.5
4.0
3.5
3.0
2.5
2.0
1.5
1.0
0.5
f1 (ppm)

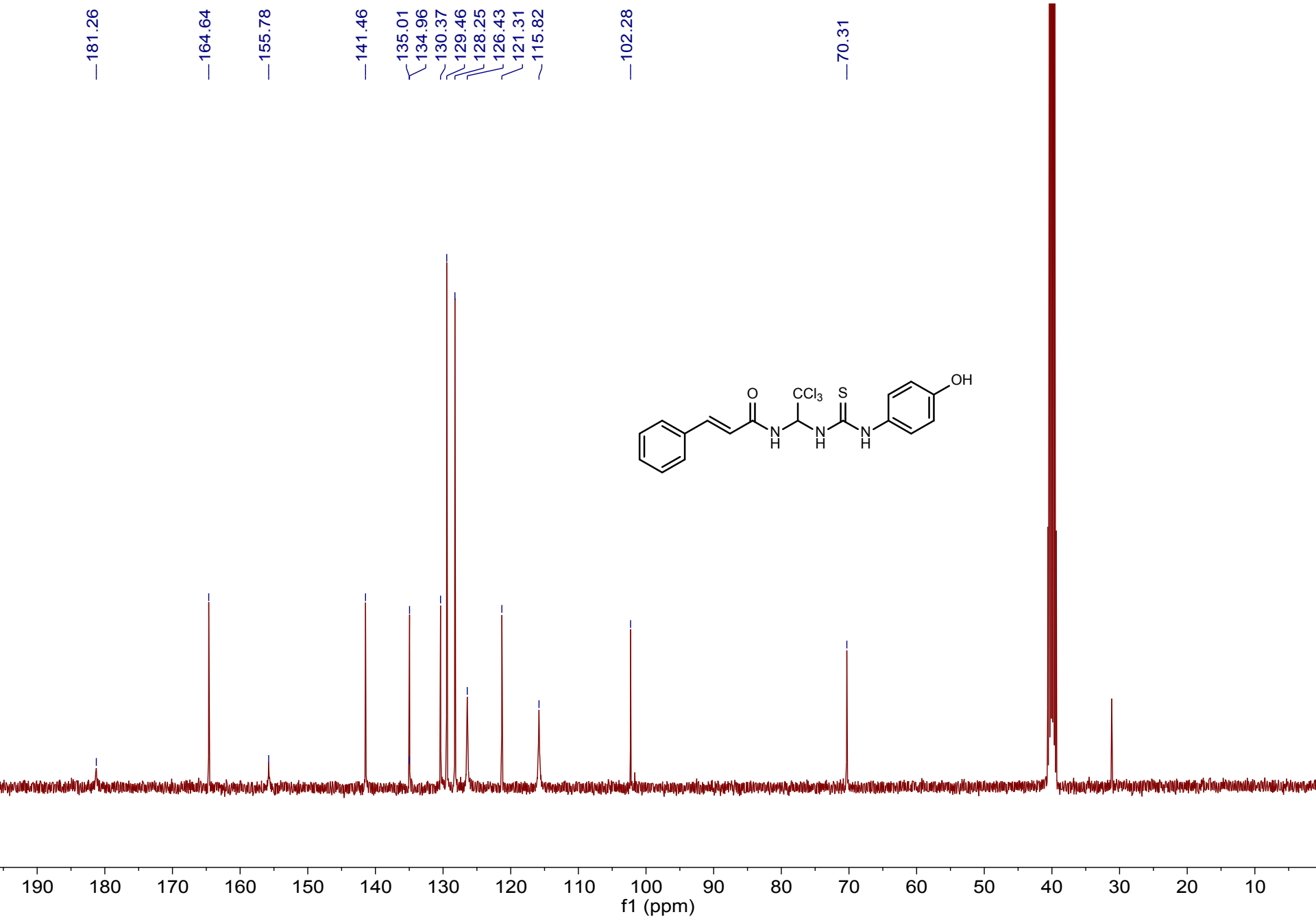
181.26
164.64
155.78
141.46
135.01
134.96
130.37
129.46
128.25
126.43
121.31
115.82
102.28
70.31
O
CCl3
S
OH
N
H
N
H
N
H
190
180
170
160
150
140
130
120
110
100
90
80
70
60
50
40
30
20
10
f1 (ppm)

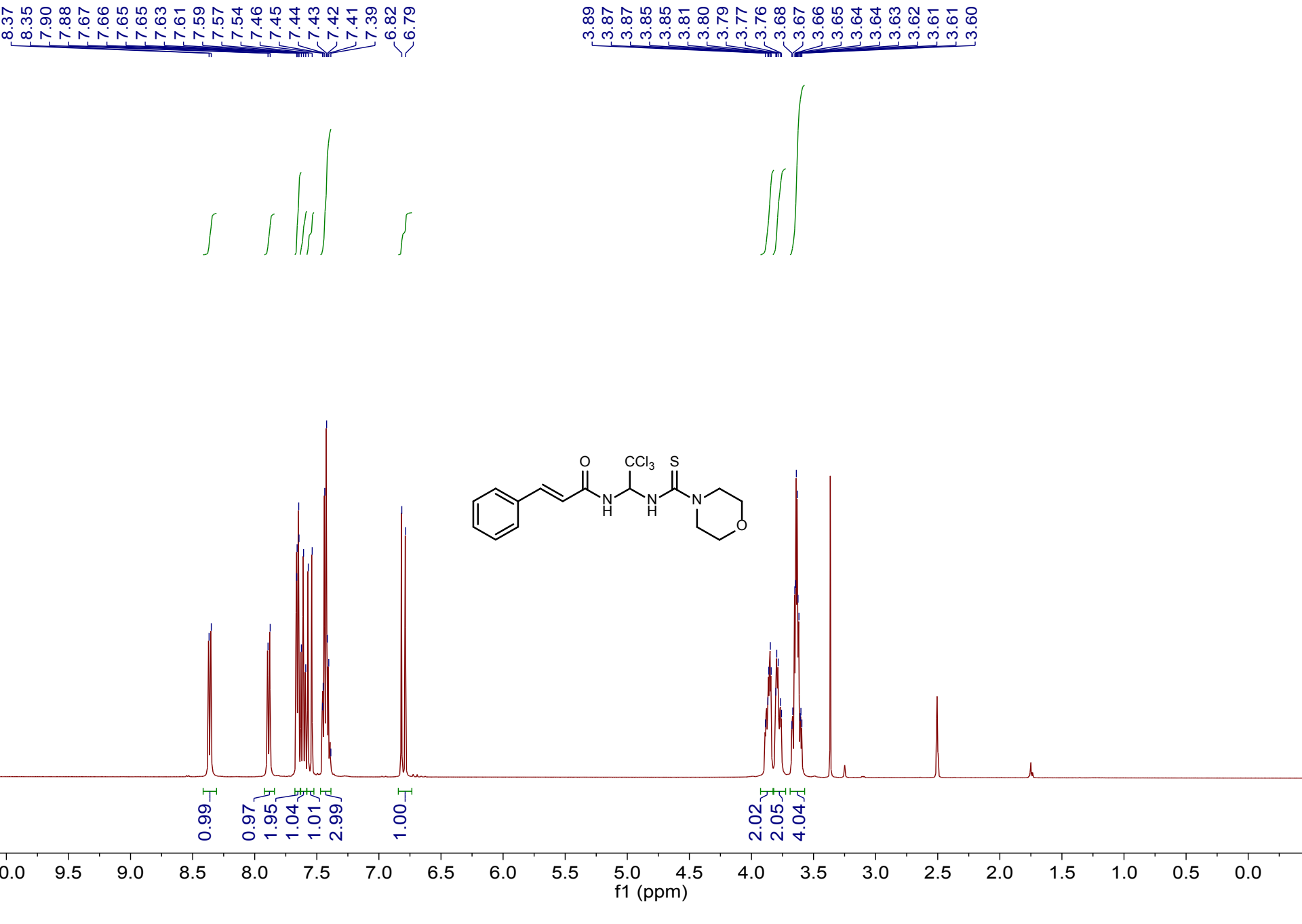
8.37
8.35
7.90
7.88
7.67
7.66
7.65
7.65
7.63
7.61
7.59
7.57
7.54
7.46
7.45
7.44
7.43
7.42
7.41
7.39
6.82
6.79
3.89
3.87
3.87
3.85
3.85
3.81
3.80
3.79
3.77
3.76
3.68
3.67
3.66
3.65
3.64
3.64
3.63
3.62
3.61
3.61
3.60
O
CCl3
S
N
H
N
H
N
O
0.99
0.97
1.95
1.04
1.01
2.99
1.00
2.02
2.05
4.04
0.0
9.5
9.0
8.5
8.0
7.5
7.0
6.5
6.0
5.5
5.0
4.5
4.0
3.5
3.0
2.5
2.0
1.5
1.0
0.5
0.0
f1 (ppm)

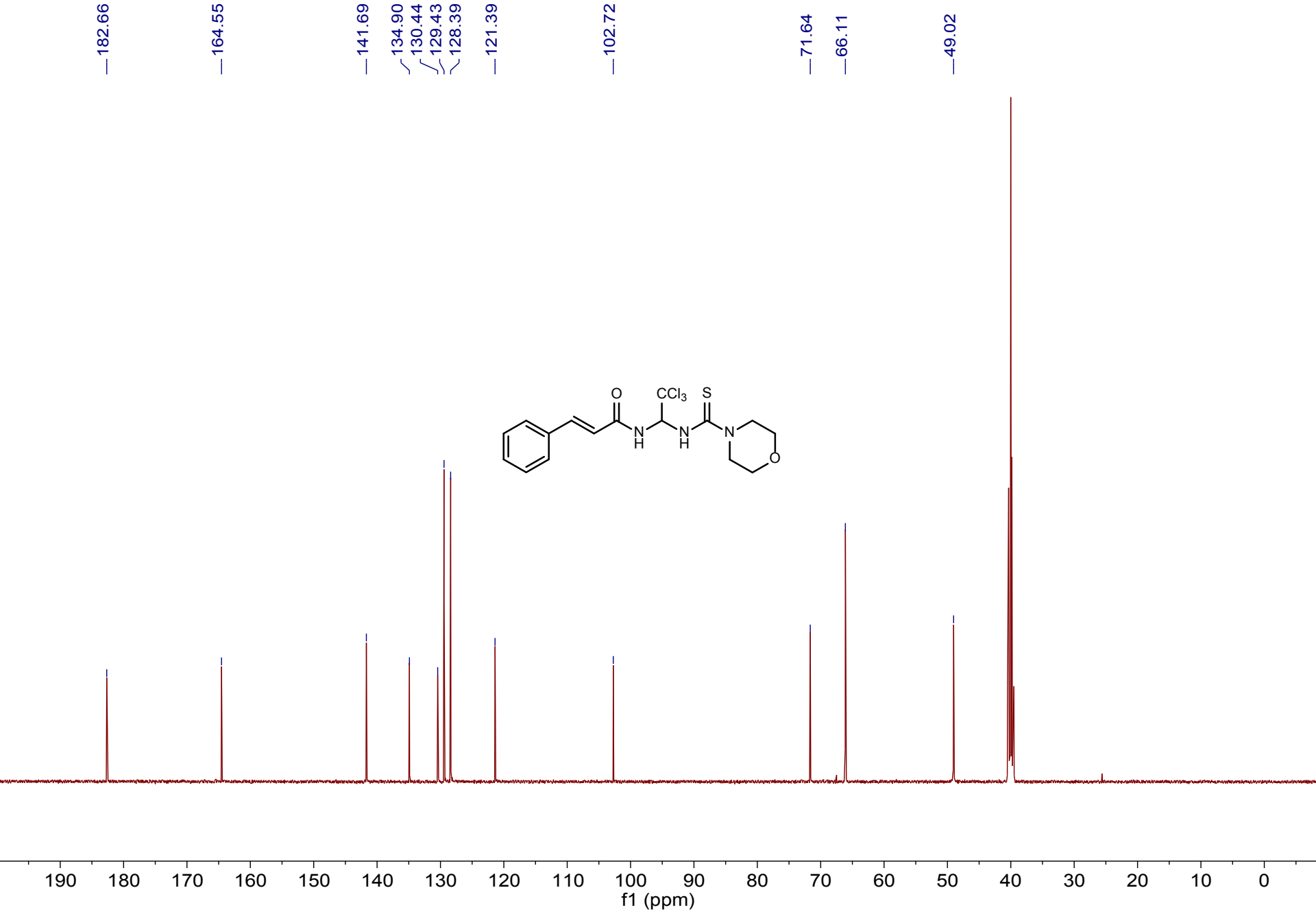
182.66
164.55
141.69
134.90
130.44
129.43
128.39
121.39
102.72
71.64
66.11
49.02
O
CCl3
S
N
H
N
H
N
O
190
180
170
160
150
140
130
120
110
100
90
80
70
60
50
40
30
20
10
0
f1 (ppm)

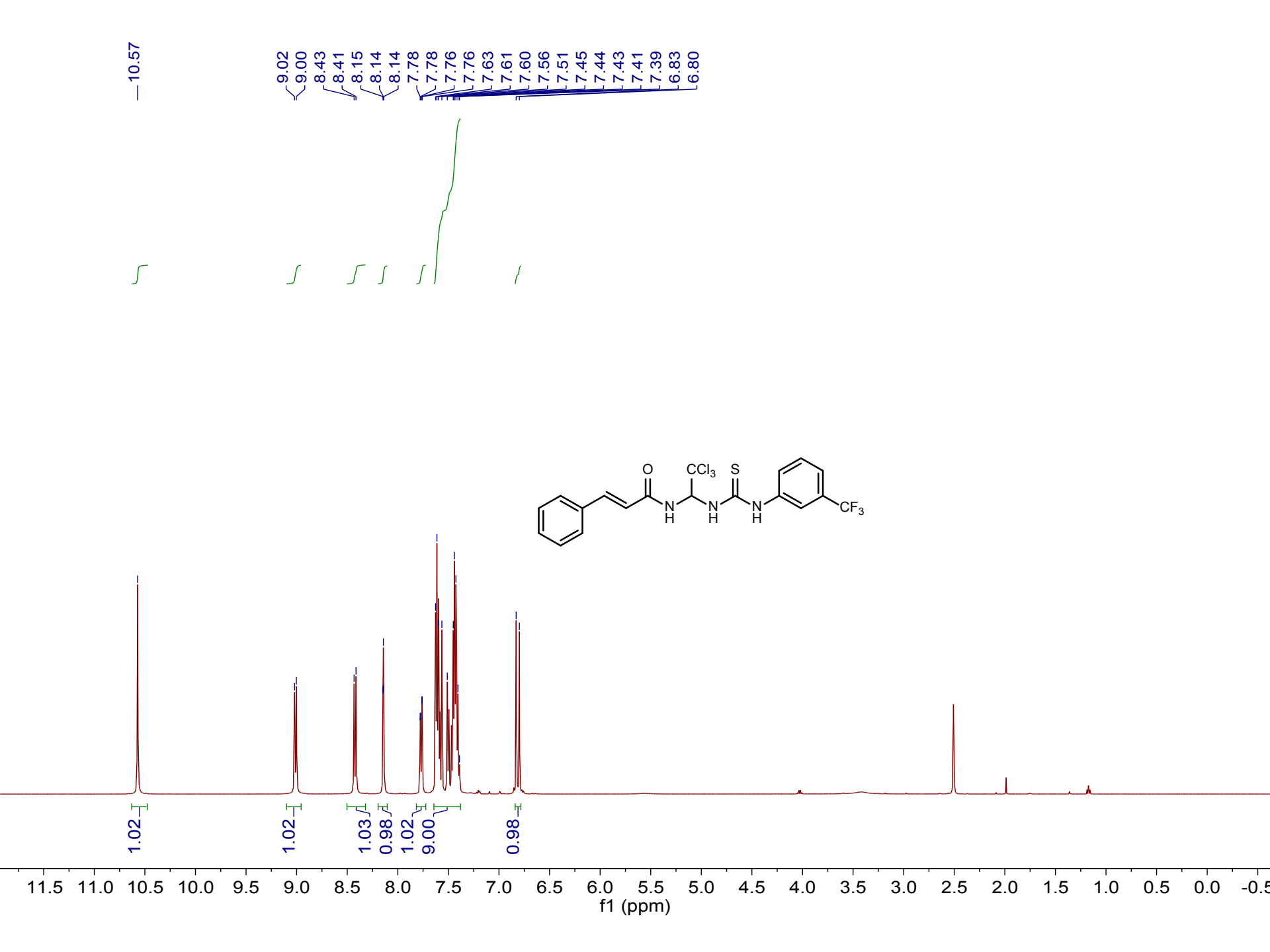
10.57
9.02
9.00
8.43
8.41
8.15
8.14
8.14
7.78
7.78
7.76
7.76
7.63
7.61
7.60
7.56
7.51
7.45
7.44
7.43
7.41
7.39
6.83
6.80
O
CCl3
S
N
H
N
H
N
H
CF3
1.02
1.02
1.03
0.98
1.02
9.00
0.98
11.5
11.0
10.5
10.0
9.5
9.0
8.5
8.0
7.5
7.0
6.5
6.0
5.5
5.0
4.5
4.0
3.5
3.0
2.5
2.0
1.5
1.0
0.5
0.0
-0.5
f1 (ppm)

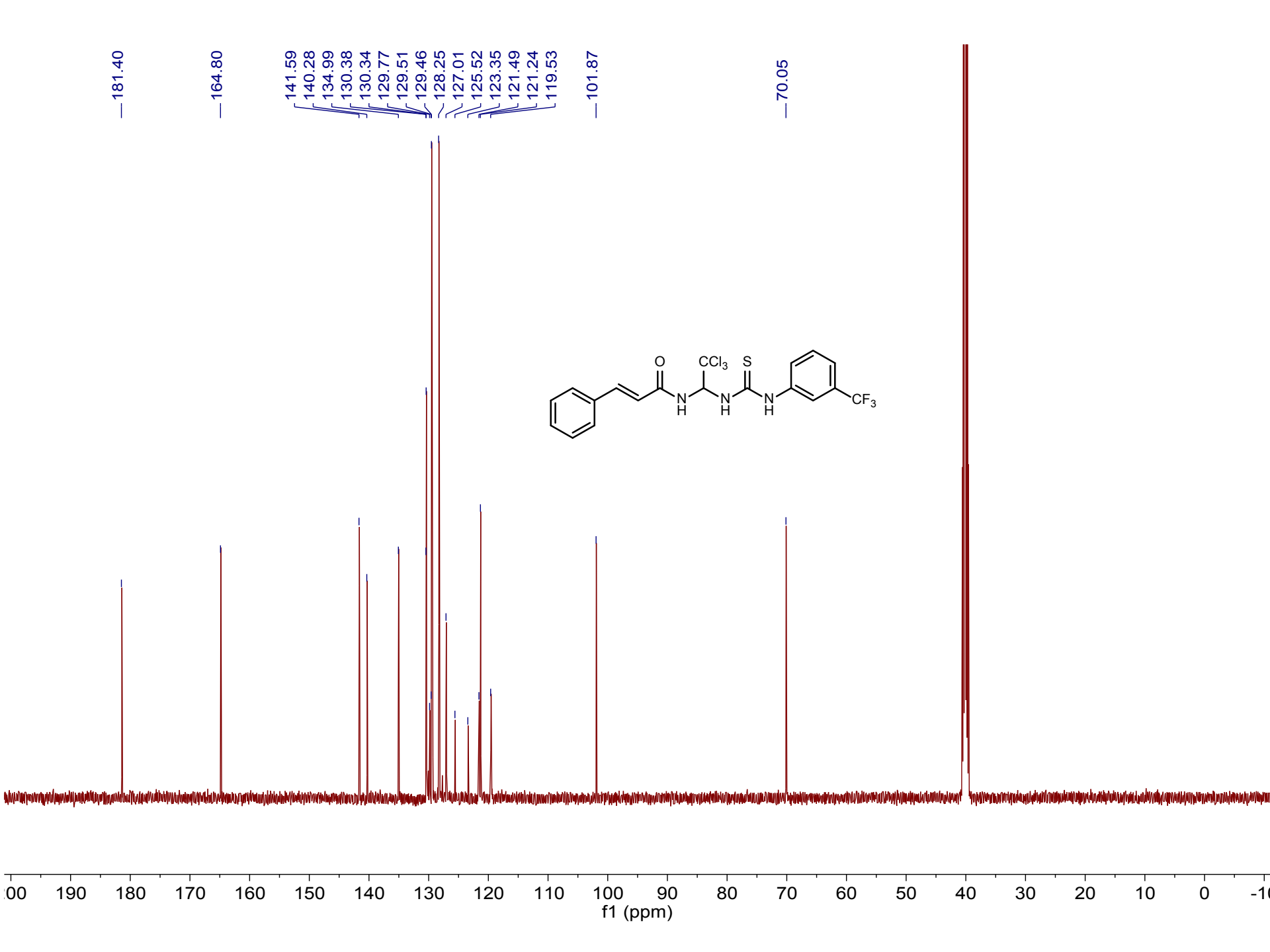
181.40
164.80
141.59
140.28
134.99
130.38
130.34
129.77
129.51
129.46
128.25
127.01
125.52
123.35
121.49
121.24
119.53
101.87
70.05
O
CCl3
S
N
H
N
H
N
H
CF3
f1 (ppm)

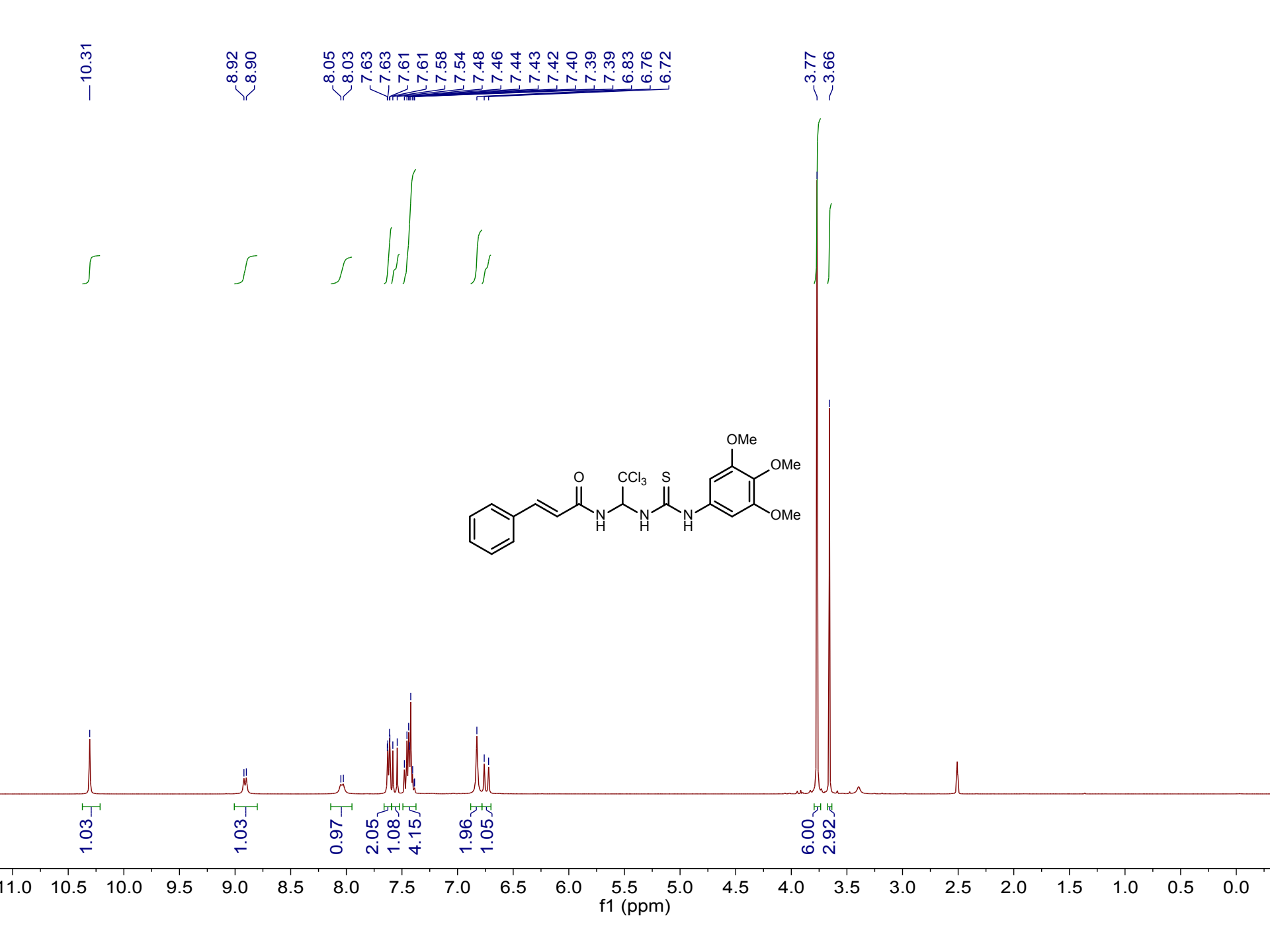
10.31
8.92
8.90
8.05
8.03
7.63
7.63
7.61
7.61
7.58
7.54
7.48
7.46
7.44
7.43
7.42
7.40
7.39
7.39
6.83
6.76
6.72
3.77
3.66
OMe
OMe
OMe
O
CCl3
S
N
H
N
H
N
H
1.03
1.03
0.97
2.05
1.08
4.15
1.96
1.05
6.00
2.92
11.0
10.5
10.0
9.5
9.0
8.5
8.0
7.5
7.0
6.5
6.0
5.5
5.0
4.5
4.0
3.5
3.0
2.5
2.0
1.5
1.0
0.5
0.0
f1 (ppm)

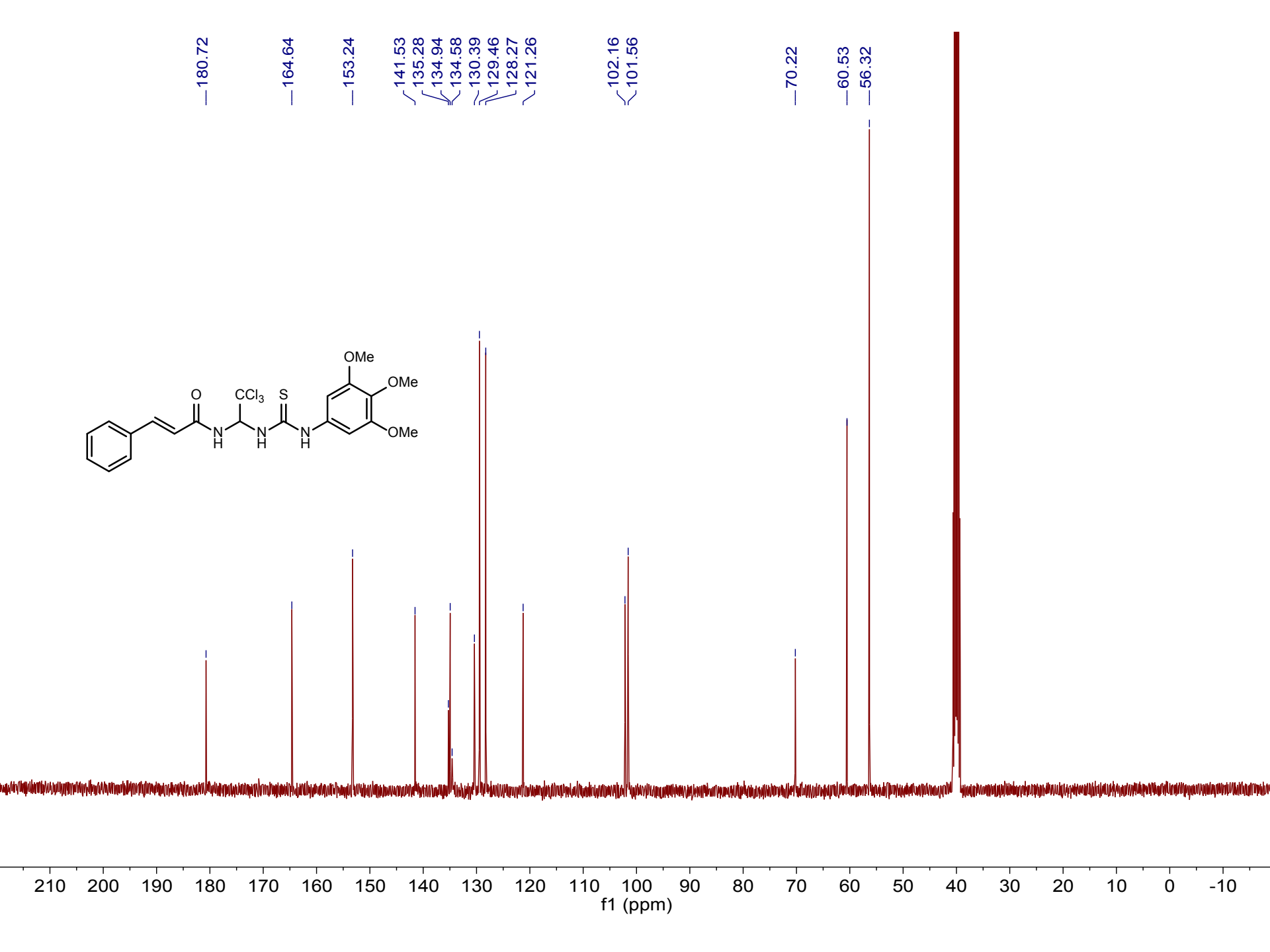
180.72
164.64
153.24
141.53
135.28
134.94
134.58
130.39
129.46
128.27
121.26
102.16
101.56
70.22
60.53
56.32
OMe
OMe
OMe
O
CCl3
S
N
H
N
H
N
H
210 200 190 180 170 160 150 140 130 120 110 100 90 80 70 60 50 40 30 20 10 0 -10
f1 (ppm)

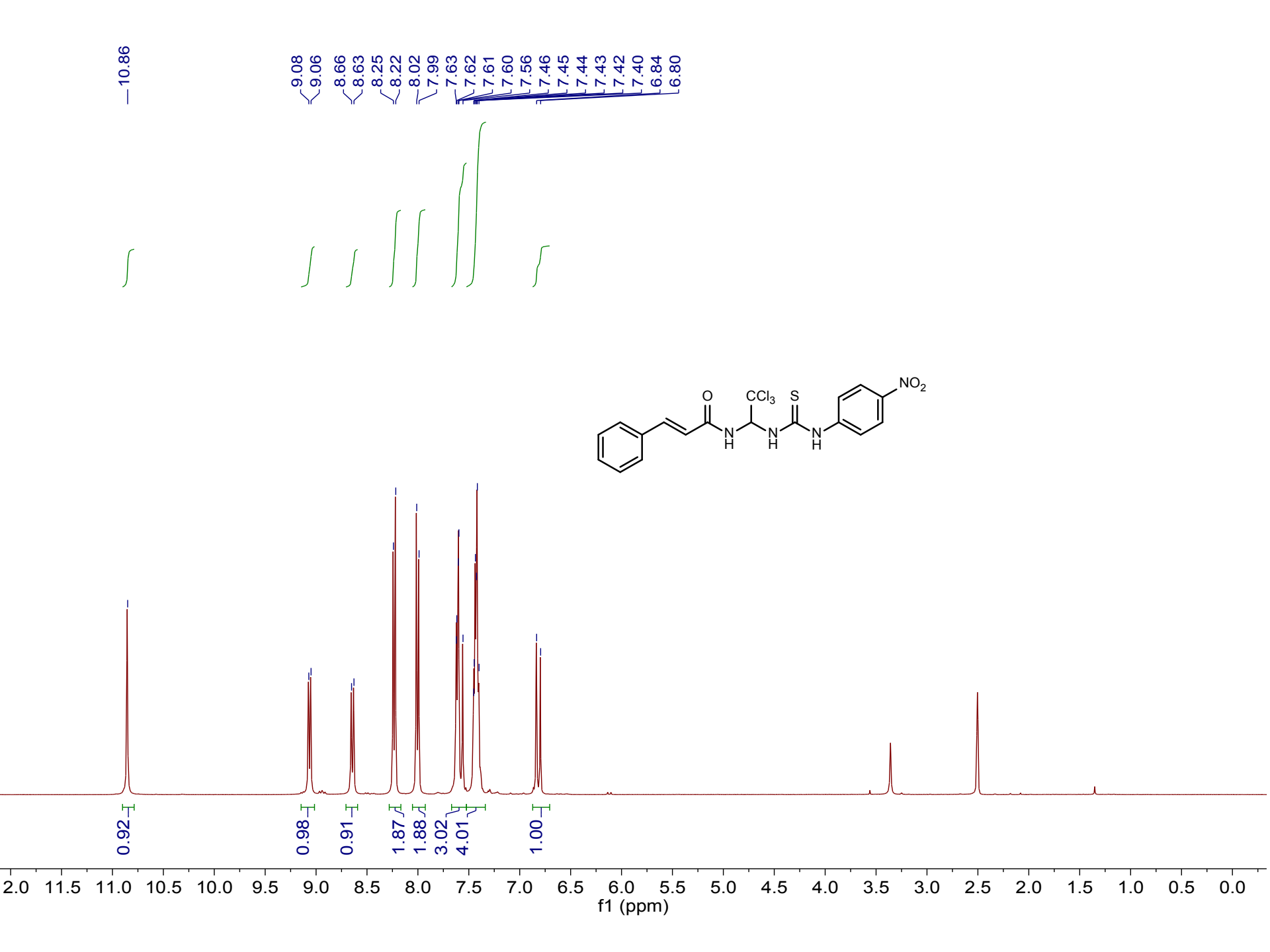
10.86
9.08
9.06
8.66
8.63
8.25
8.22
8.02
7.99
7.63
7.62
7.61
7.60
7.56
7.46
7.45
7.44
7.43
7.42
7.40
6.84
6.80
O
CCl3
S
NO2
N
H
N
H
N
H
0.92
0.98
0.91
1.87
1.88
3.02
4.01
1.00
2.0
11.5
11.0
10.5
10.0
9.5
9.0
8.5
8.0
7.5
7.0
6.5
6.0
5.5
5.0
4.5
4.0
3.5
3.0
2.5
2.0
1.5
1.0
0.5
0.0
f1 (ppm)

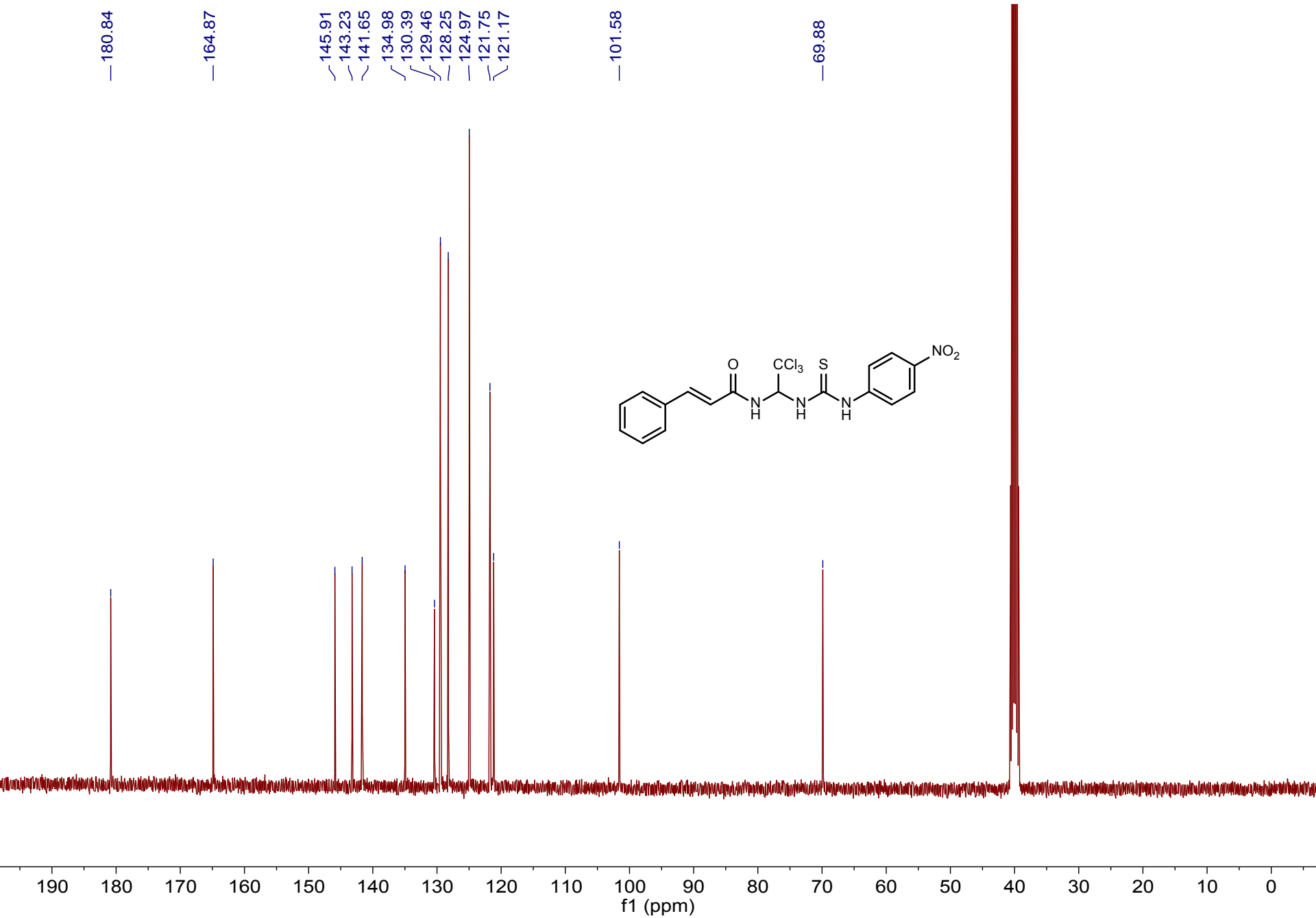
180.84
164.87
145.91
143.23
141.65
134.98
130.39
129.46
128.25
124.97
121.75
121.17
101.58
69.88
O
CCl3
S
NO2
N
H
N
H
N
H
190
180
170
160
150
140
130
120
110
100
90
80
70
60
50
40
30
20
10
0
f1 (ppm)

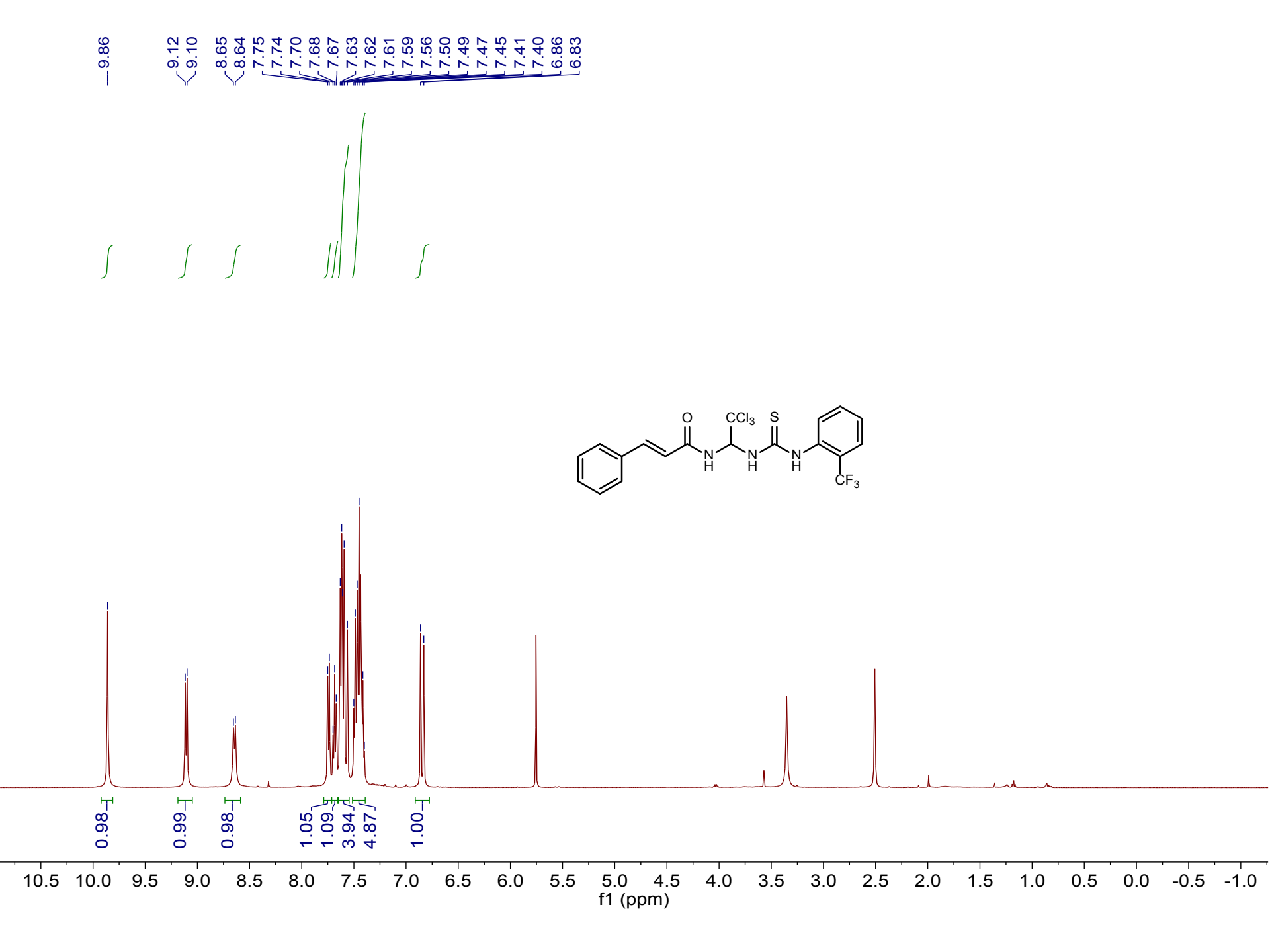
9.86
9.12
9.10
8.65
8.64
7.75
7.74
7.70
7.68
7.67
7.63
7.62
7.61
7.59
7.56
7.50
7.49
7.47
7.45
7.41
7.40
6.86
6.83
O
CCl3
S
N
H
N
H
N
H
CF3
0.98
0.99
0.98
1.05
1.09
3.94
4.87
1.00
10.5 10.0 9.5 9.0 8.5 8.0 7.5 7.0 6.5 6.0 5.5 5.0 4.5 4.0 3.5 3.0 2.5 2.0 1.5 1.0 0.5 0.0 -0.5 -1.0
f1 (ppm)

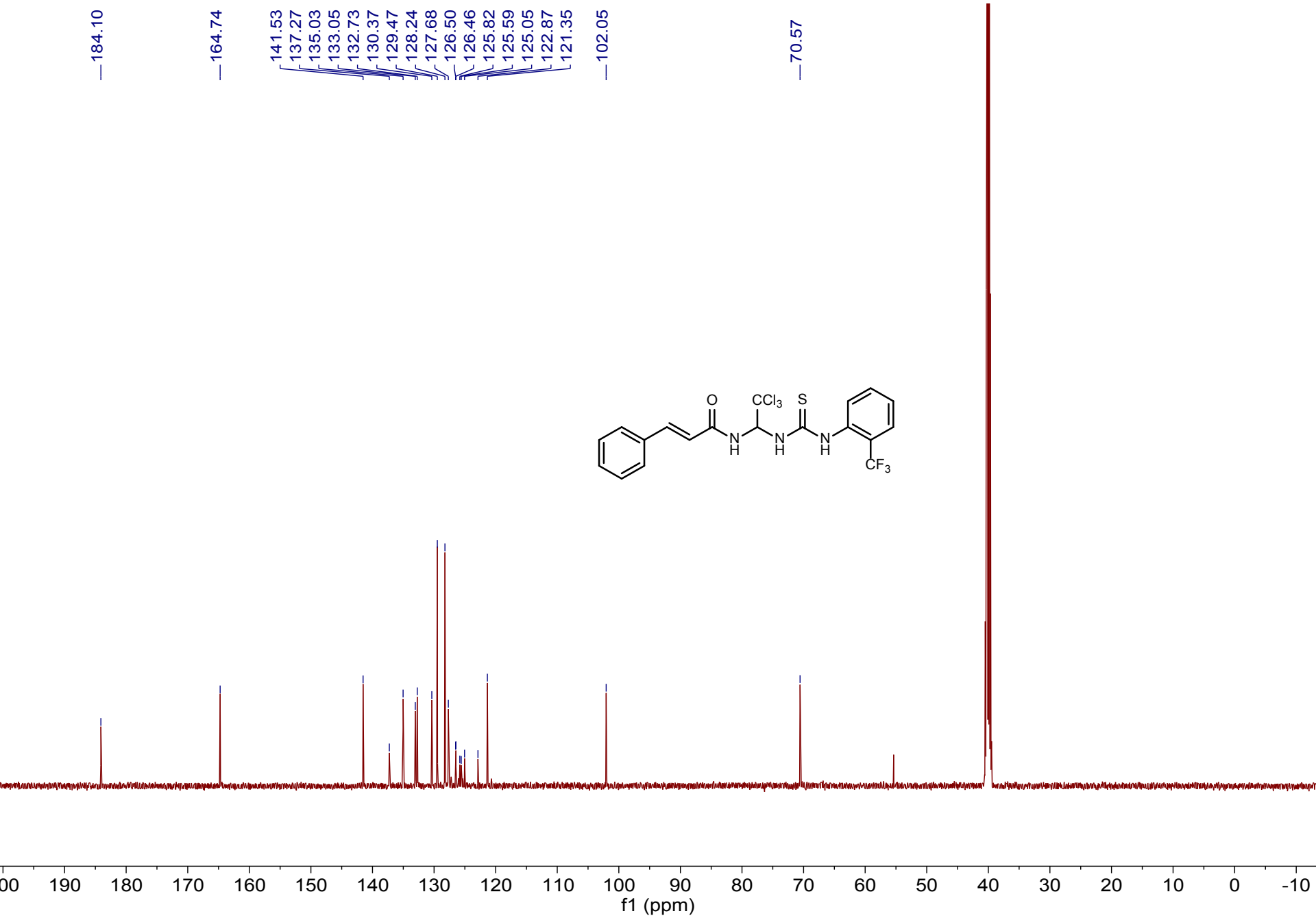
184.10
164.74
141.53
137.27
135.03
133.05
132.73
130.37
129.47
128.24
127.68
126.50
126.46
125.82
125.59
125.05
122.87
121.35
102.05
70.57
O
CCl3
S
N
H
N
H
N
H
CF3
f1 (ppm)

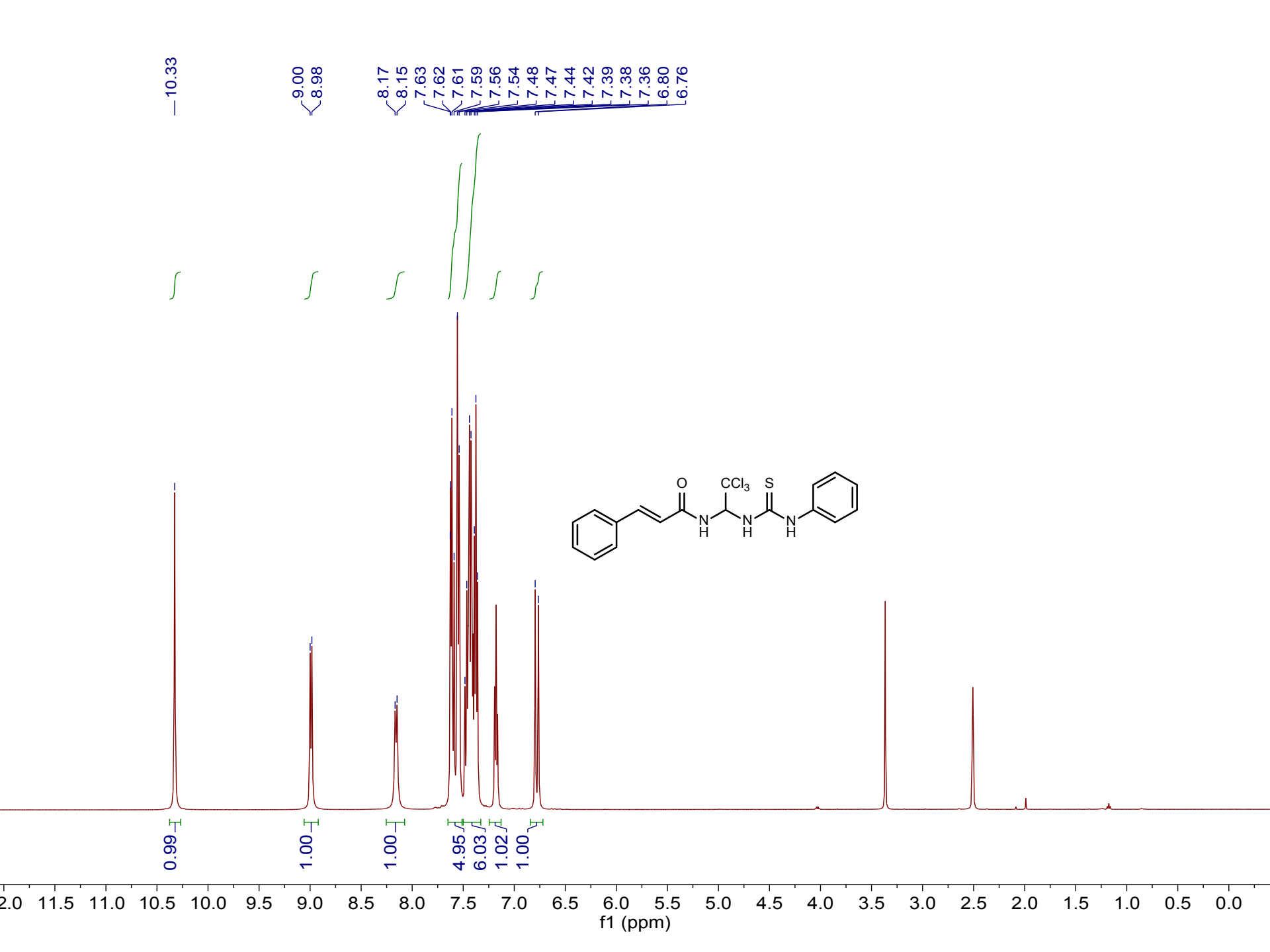
10.33
9.00
8.98
8.17
8.15
7.63
7.62
7.61
7.59
7.56
7.54
7.48
7.47
7.44
7.42
7.39
7.38
7.36
6.80
6.76
O
CCl3
S
N
H
N
H
N
H
0.99
1.00
1.00
4.95
6.03
1.02
1.00
f1 (ppm)

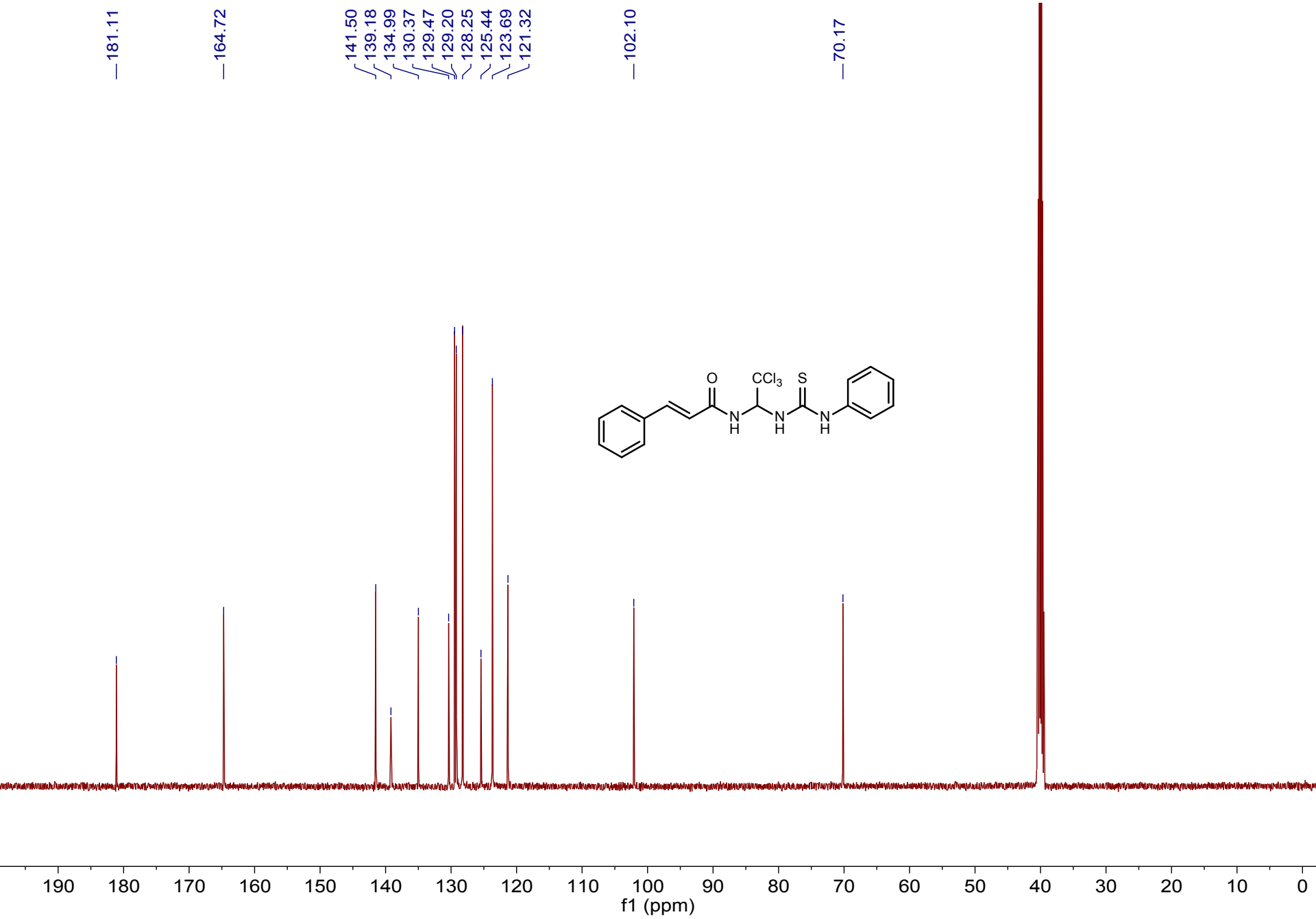
181.11
164.72
141.50
139.18
134.99
130.37
129.47
129.20
128.25
125.44
123.69
121.32
102.10
70.17
O
CCl3
S
N
H
N
H
N
H
190
180
170
160
150
140
130
120
110
100
90
80
70
60
50
40
30
20
10
0
f1 (ppm)

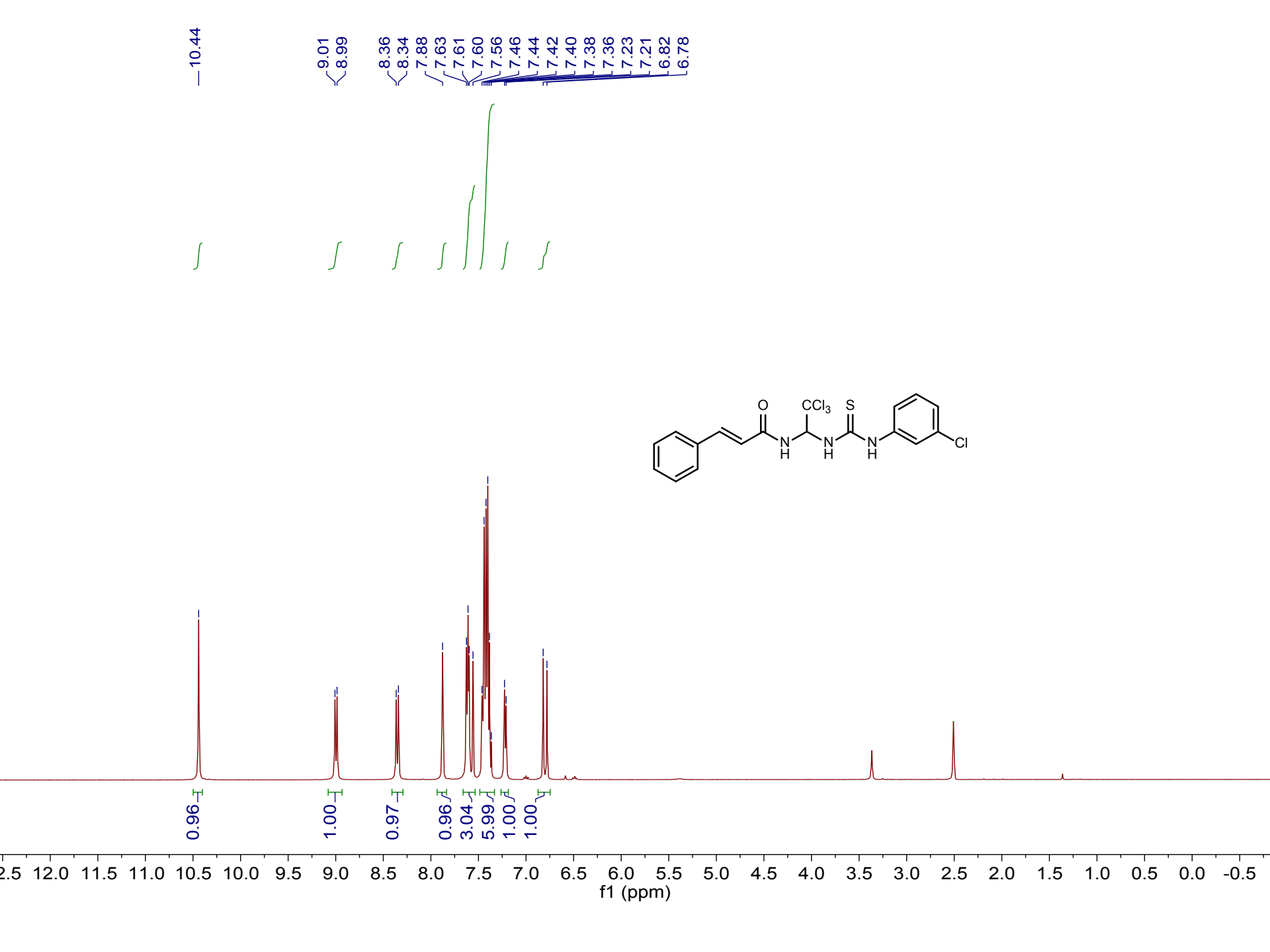
10.44
9.01
8.99
8.36
8.34
7.88
7.63
7.61
7.60
7.56
7.46
7.44
7.42
7.40
7.38
7.36
7.23
7.21
6.82
6.78
O
CCl3
S
N
H
N
H
N
H
Cl
0.96
1.00
0.97
0.96
3.04
5.99
1.00
1.00
f1 (ppm)

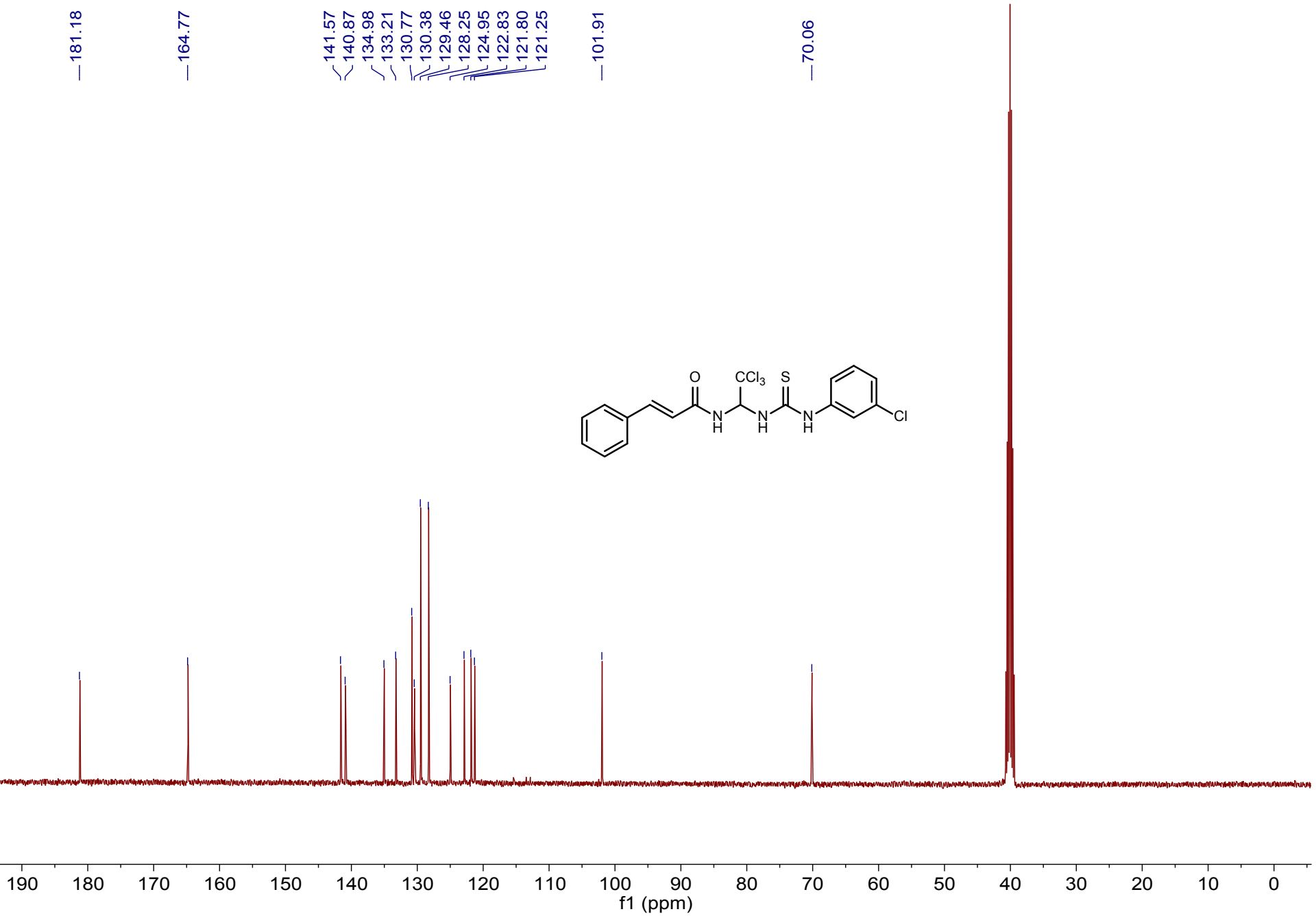
181.18
164.77
141.57
140.87
134.98
133.21
130.77
130.38
129.46
128.25
124.95
122.83
121.80
121.25
101.91
70.06
O
CCl3
S
N
H
N
H
N
H
Cl
190
180
170
160
150
140
130
120
110
100
90
80
70
60
50
40
30
20
10
0
f1 (ppm)

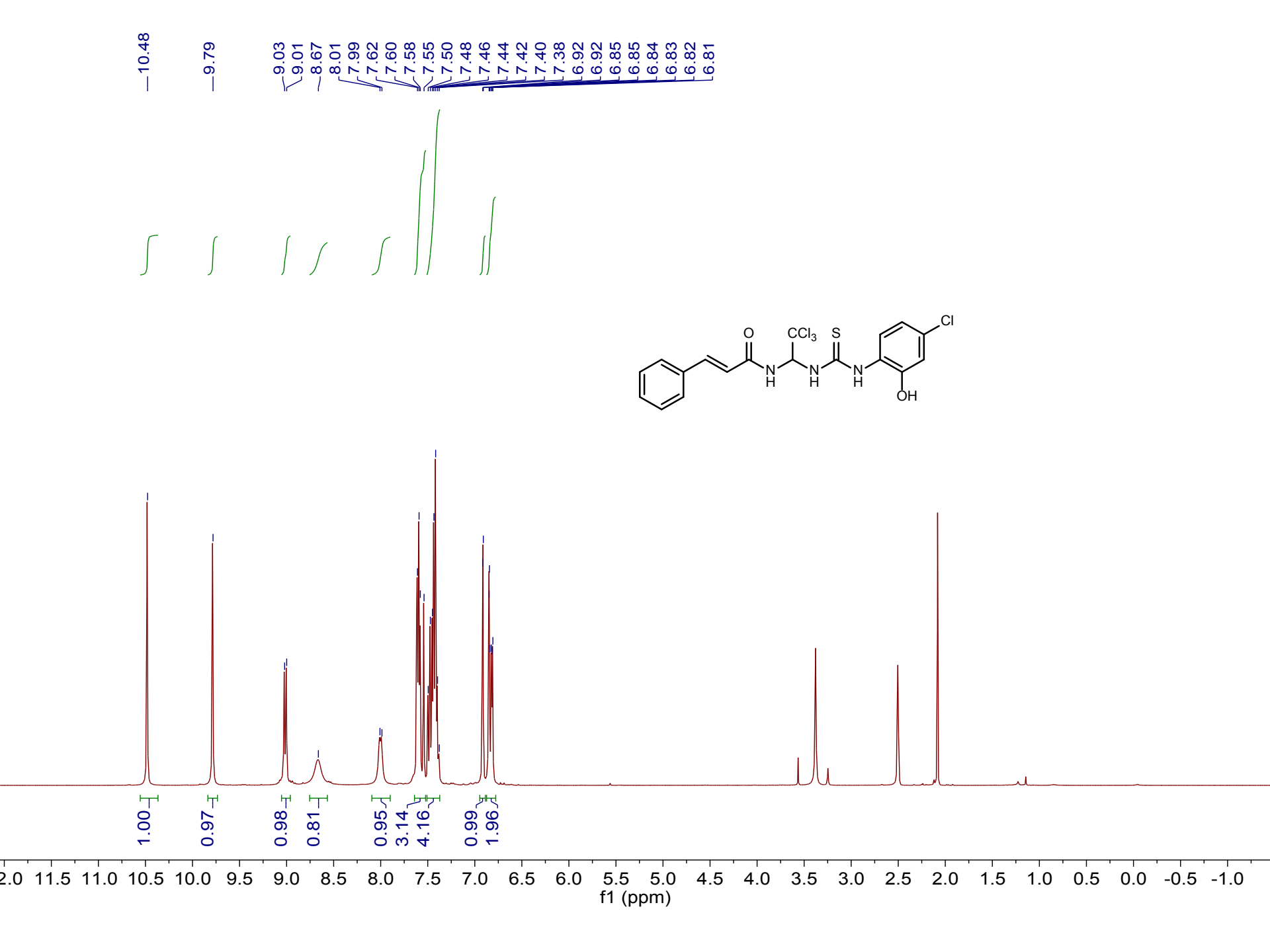
10.48
9.79
9.03
9.01
8.67
8.01
7.99
7.62
7.60
7.58
7.55
7.50
7.48
7.46
7.44
7.42
7.40
7.38
6.92
6.92
6.85
6.85
6.84
6.83
6.82
6.81
O
CCl3
S
N
H
N
H
N
H
Cl
OH
1.00
0.97
0.98
0.81
0.95
3.14
4.16
0.99
1.96
f1 (ppm)

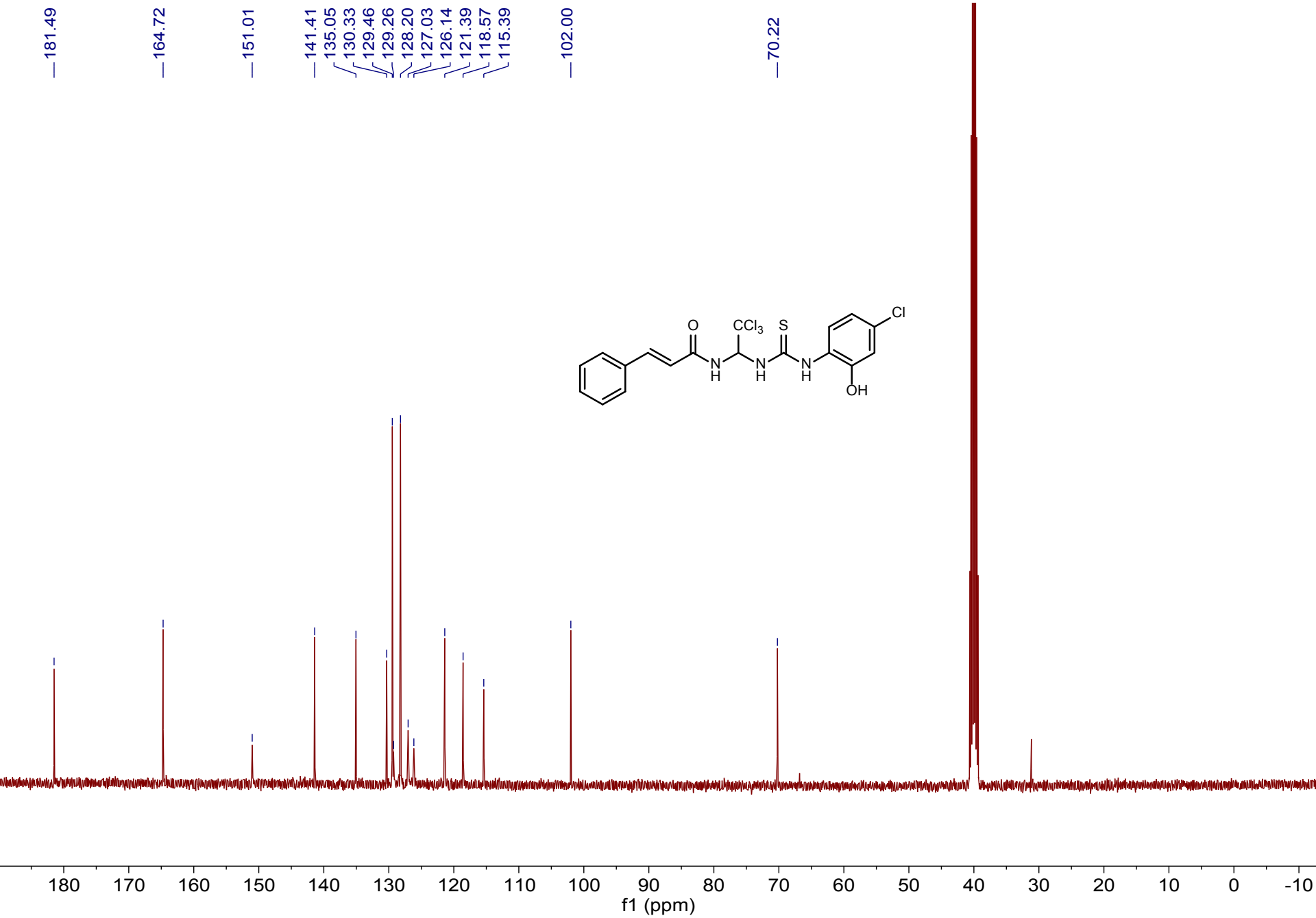
181.49
164.72
151.01
141.41
135.05
130.33
129.46
129.26
128.20
127.03
126.14
121.39
118.57
115.39
102.00
70.22
O
CCl3
S
N
H
N
H
N
H
Cl
OH
180
170
160
150
140
130
120
110
100
90
80
70
60
50
40
30
20
10
0
-10
f1 (ppm)

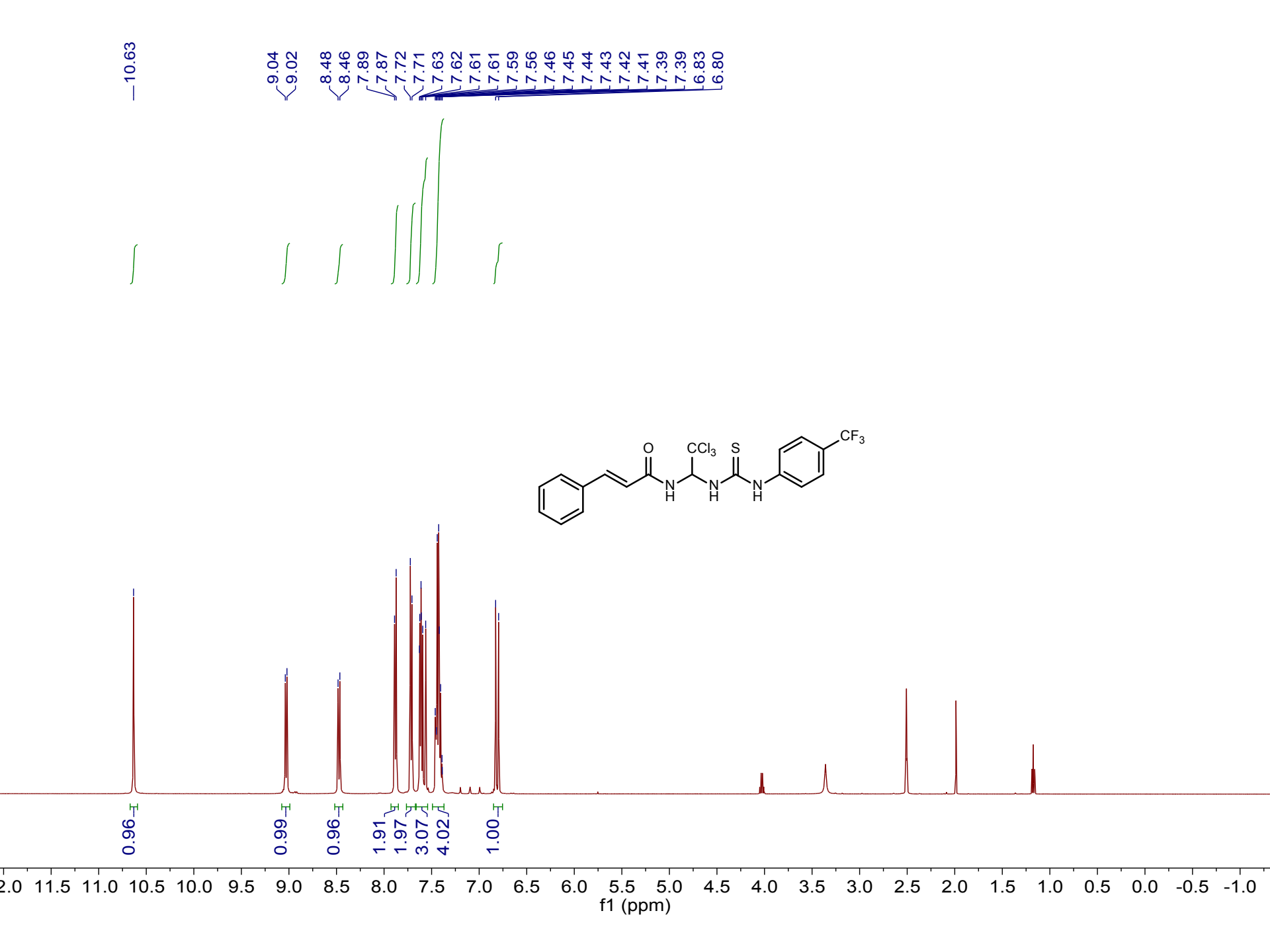
10.63
9.04
9.02
8.48
8.46
7.89
7.87
7.72
7.71
7.63
7.62
7.61
7.61
7.59
7.56
7.46
7.45
7.44
7.43
7.42
7.41
7.39
7.39
6.83
6.80
O
CCl3
S
CF3
N
H
N
H
N
H
0.96
0.99
0.96
1.91
1.97
3.07
4.02
1.00
f1 (ppm)

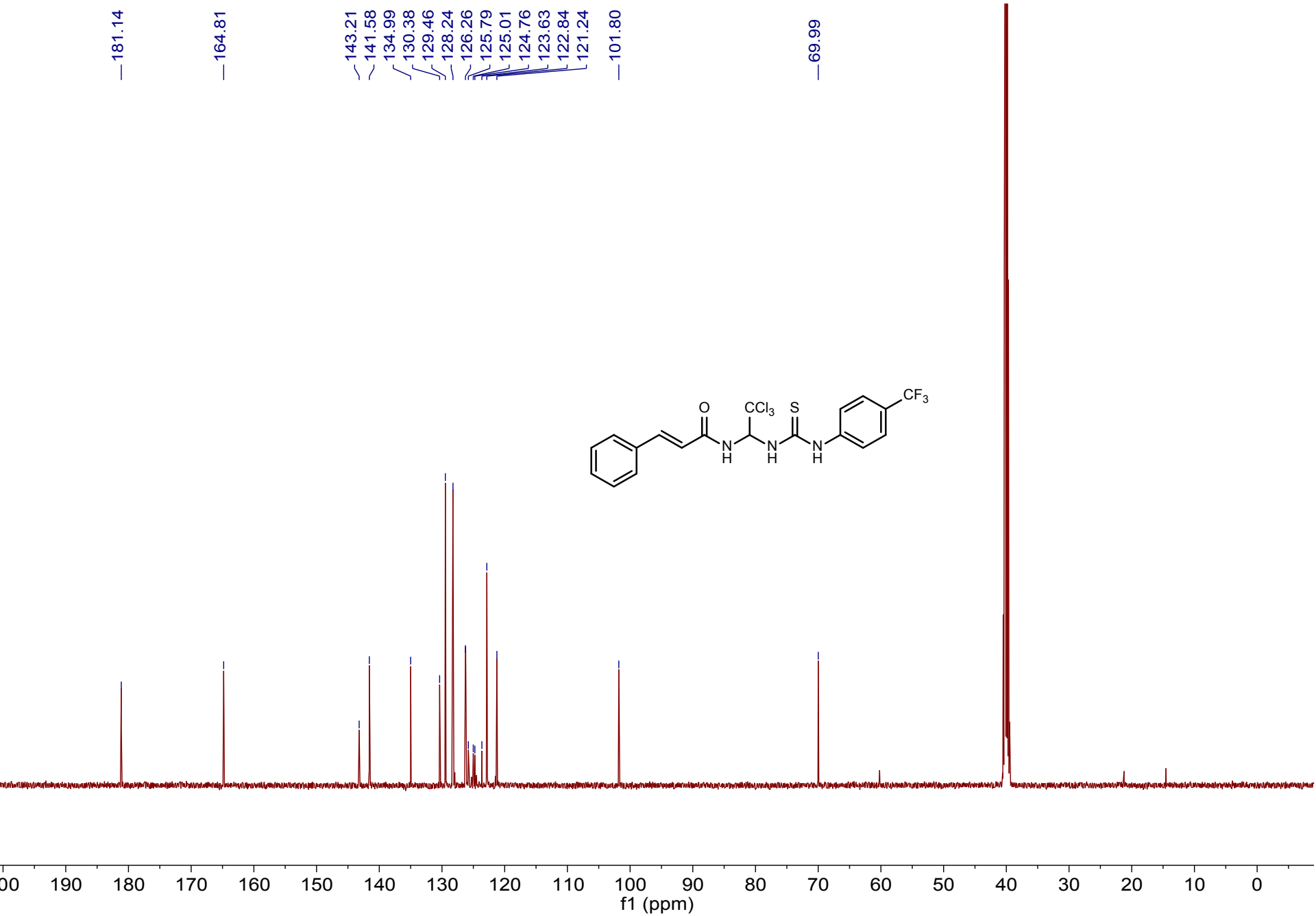
181.14
164.81
143.21
141.58
134.99
130.38
129.46
128.24
126.26
125.79
125.01
124.76
123.63
122.84
121.24
101.80
69.99
O
CCl3
S
CF3
N
H
N
H
N
H
f1 (ppm)

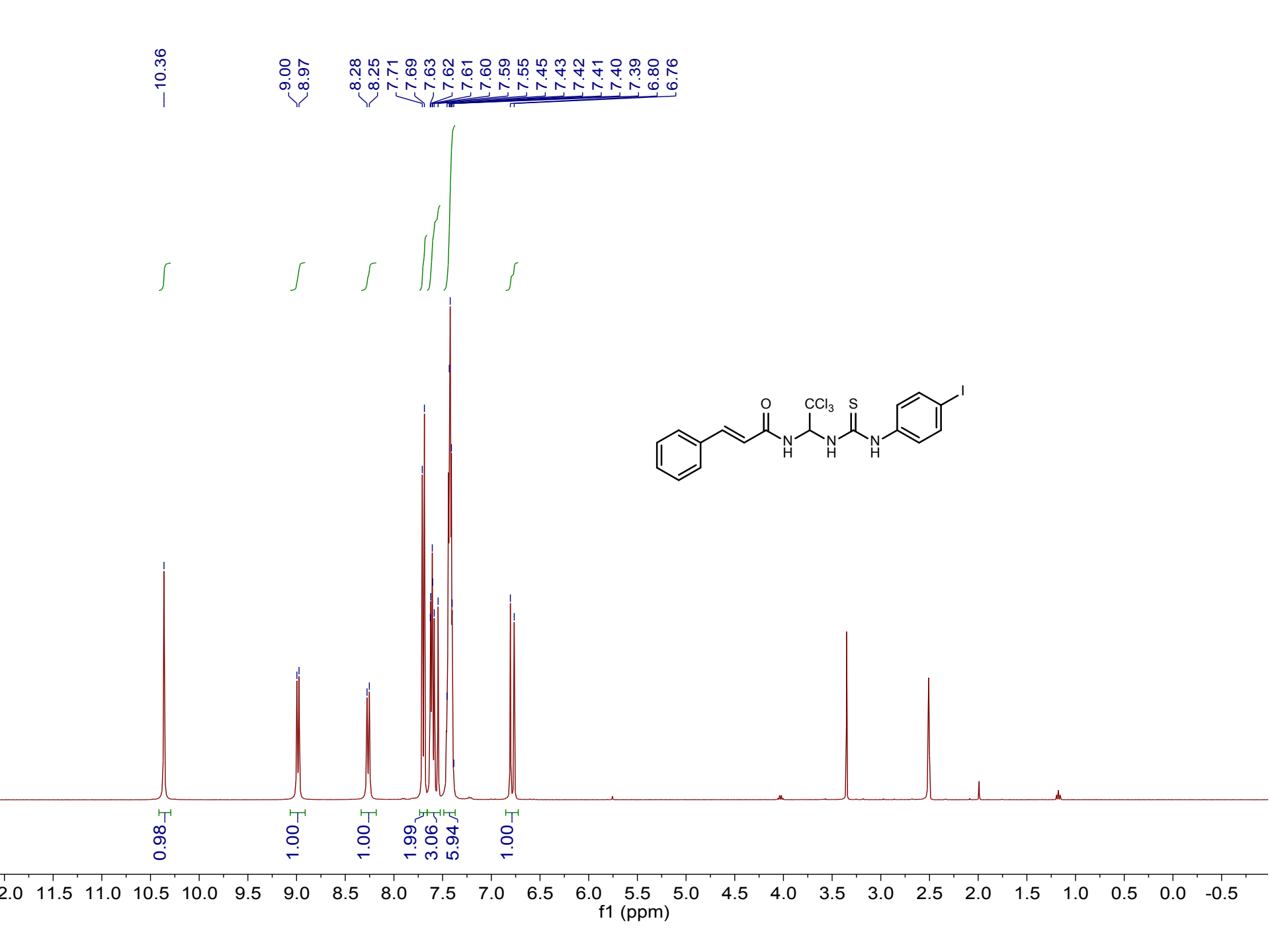
10.36
9.00
8.97
8.28
8.25
7.71
7.69
7.63
7.62
7.61
7.60
7.59
7.55
7.45
7.43
7.42
7.41
7.40
7.39
6.80
6.76
O
CCl3
S
N
H
N
H
N
H
I
0.98
1.00
1.00
1.99
3.06
5.94
1.00
f1 (ppm)

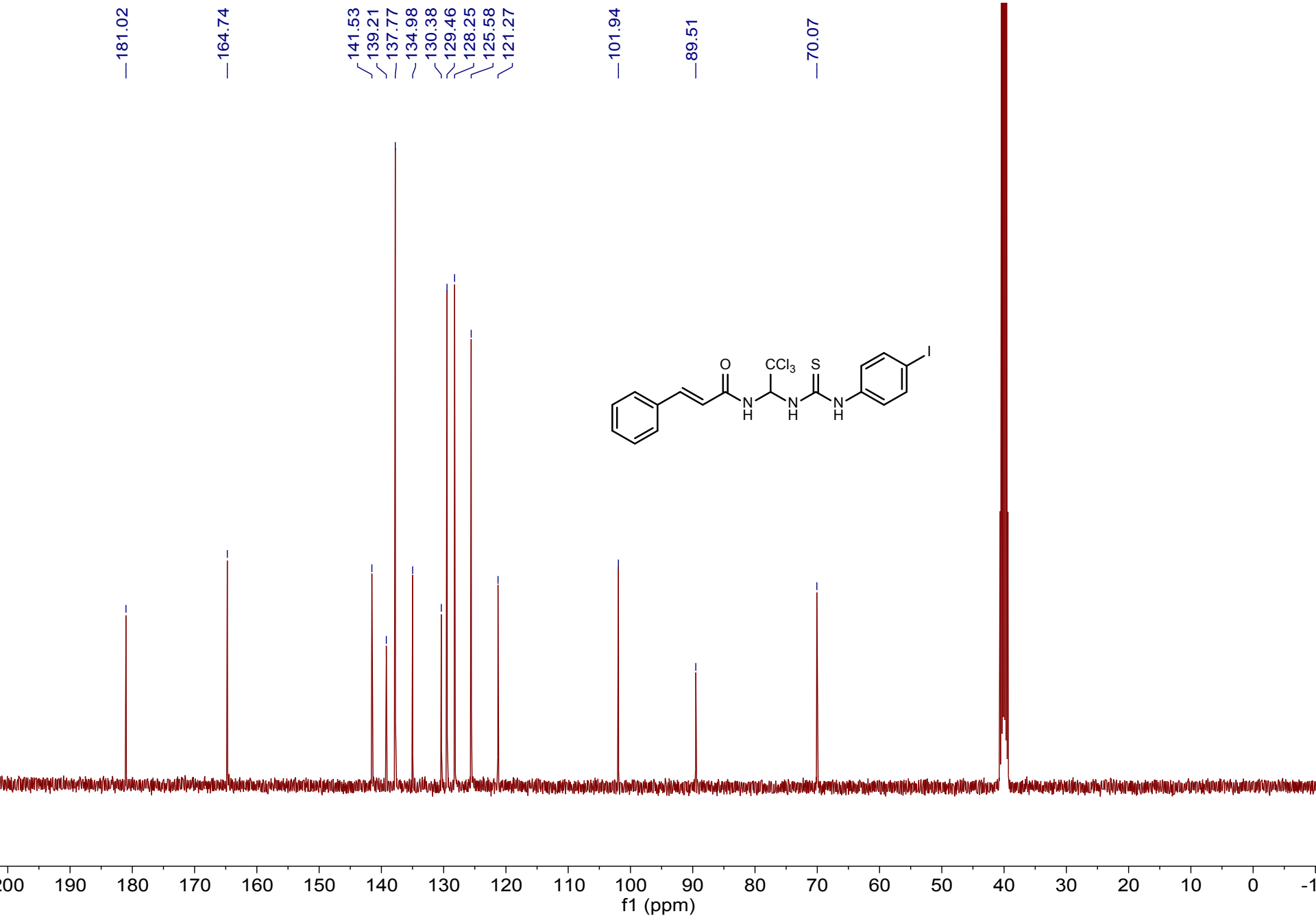
181.02
164.74
141.53
139.21
137.77
134.98
130.38
129.46
128.25
125.58
121.27
101.94
89.51
70.07
O
CCl3
S
N
H
N
H
N
H
I
200
190
180
170
160
150
140
130
120
110
100
90
80
70
60
50
40
30
20
10
0
-1
f1 (ppm)

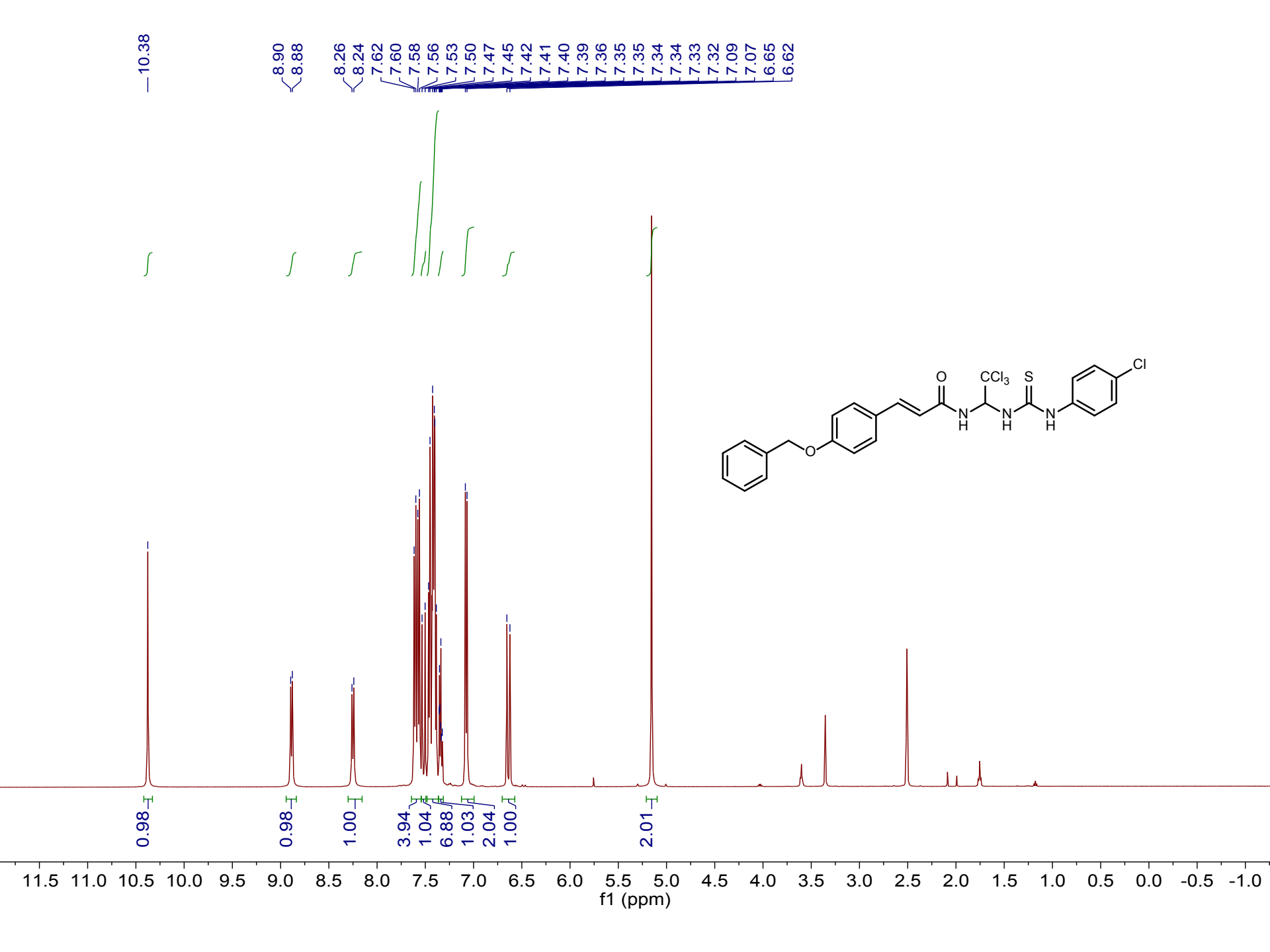
10.38
8.90
8.88
8.26
8.24
7.62
7.60
7.58
7.56
7.53
7.50
7.47
7.45
7.42
7.41
7.40
7.39
7.36
7.35
7.35
7.34
7.34
7.33
7.32
7.09
7.07
6.65
6.62
O
CCl3
S
Cl
N
H
N
H
N
H
O
0.98
0.98
1.00
3.94
1.04
6.88
1.03
2.04
1.00
2.01
11.5 11.0 10.5 10.0 9.5 9.0 8.5 8.0 7.5 7.0 6.5 6.0 5.5 5.0 4.5 4.0 3.5 3.0 2.5 2.0 1.5 1.0 0.5 0.0 -0.5 -1.0
f1 (ppm)

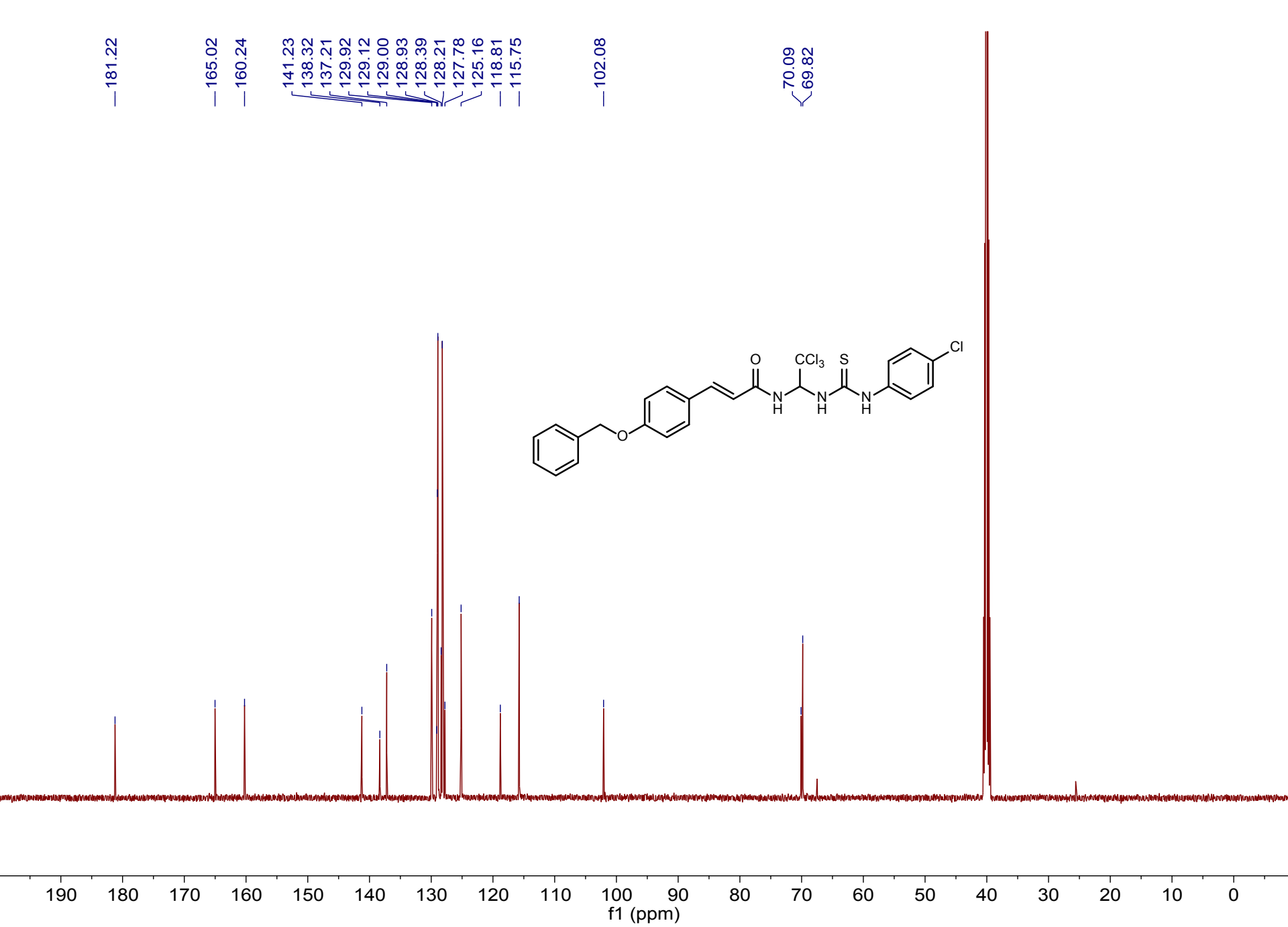
181.22
165.02
160.24
141.23
138.32
137.21
129.92
129.12
129.00
128.93
128.39
128.21
127.78
125.16
118.81
115.75
102.08
70.09
69.82
O
CCl3
S
N
H
N
H
N
H
Cl
O
190
180
170
160
150
140
130
120
110
100
90
80
70
60
50
40
30
20
10
0
f1 (ppm)

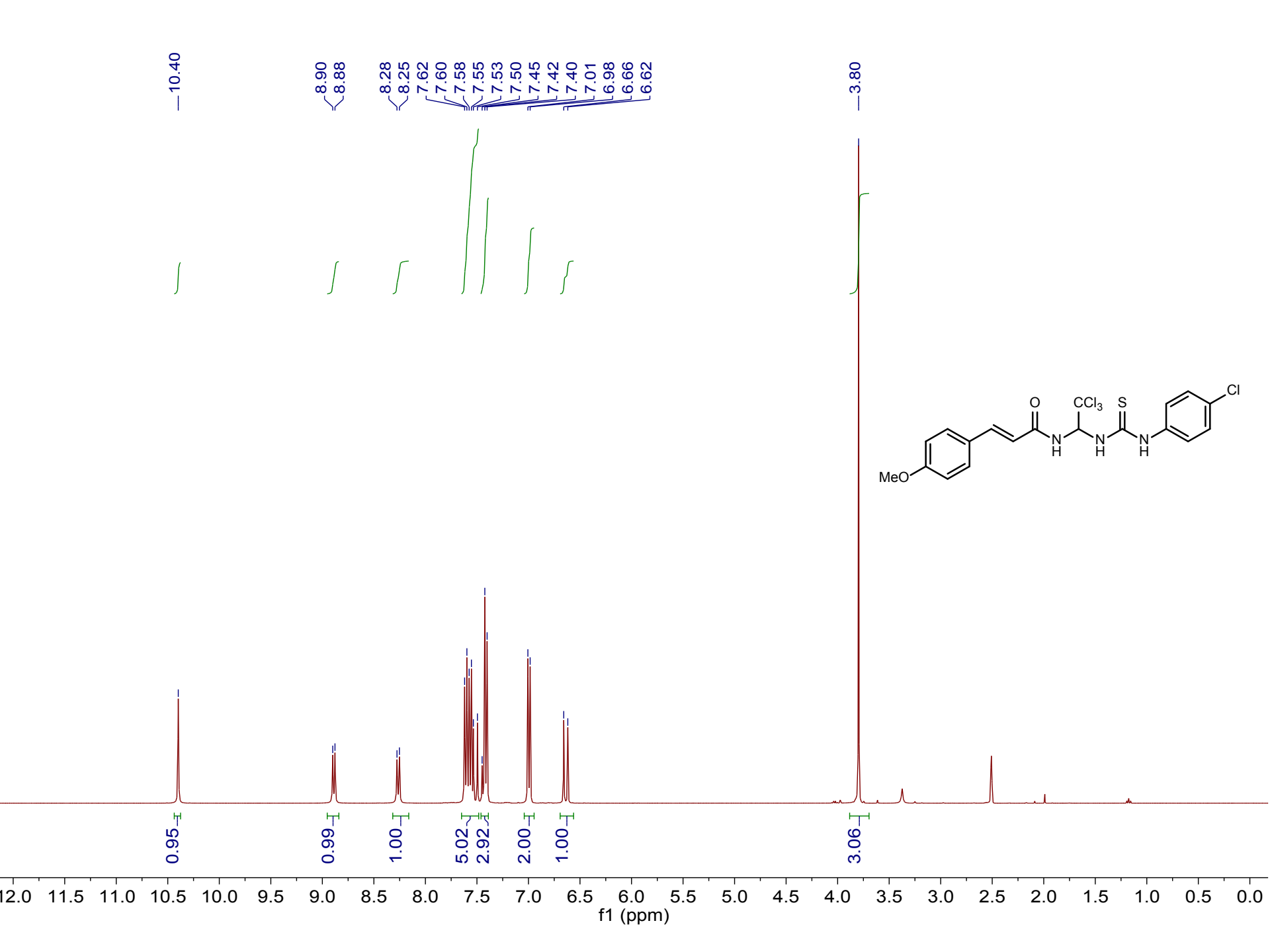
10.40
8.90
8.88
8.28
8.25
7.62
7.60
7.58
7.55
7.53
7.50
7.45
7.42
7.40
7.01
6.98
6.66
6.62
3.80
O
CCl3
S
N
H
N
H
N
H
Cl
MeO
0.95
0.99
1.00
5.02
2.92
2.00
1.00
3.06
12.0 11.5 11.0 10.5 10.0 9.5 9.0 8.5 8.0 7.5 7.0 6.5 6.0 5.5 5.0 4.5 4.0 3.5 3.0 2.5 2.0 1.5 1.0 0.5 0.0
f1 (ppm)

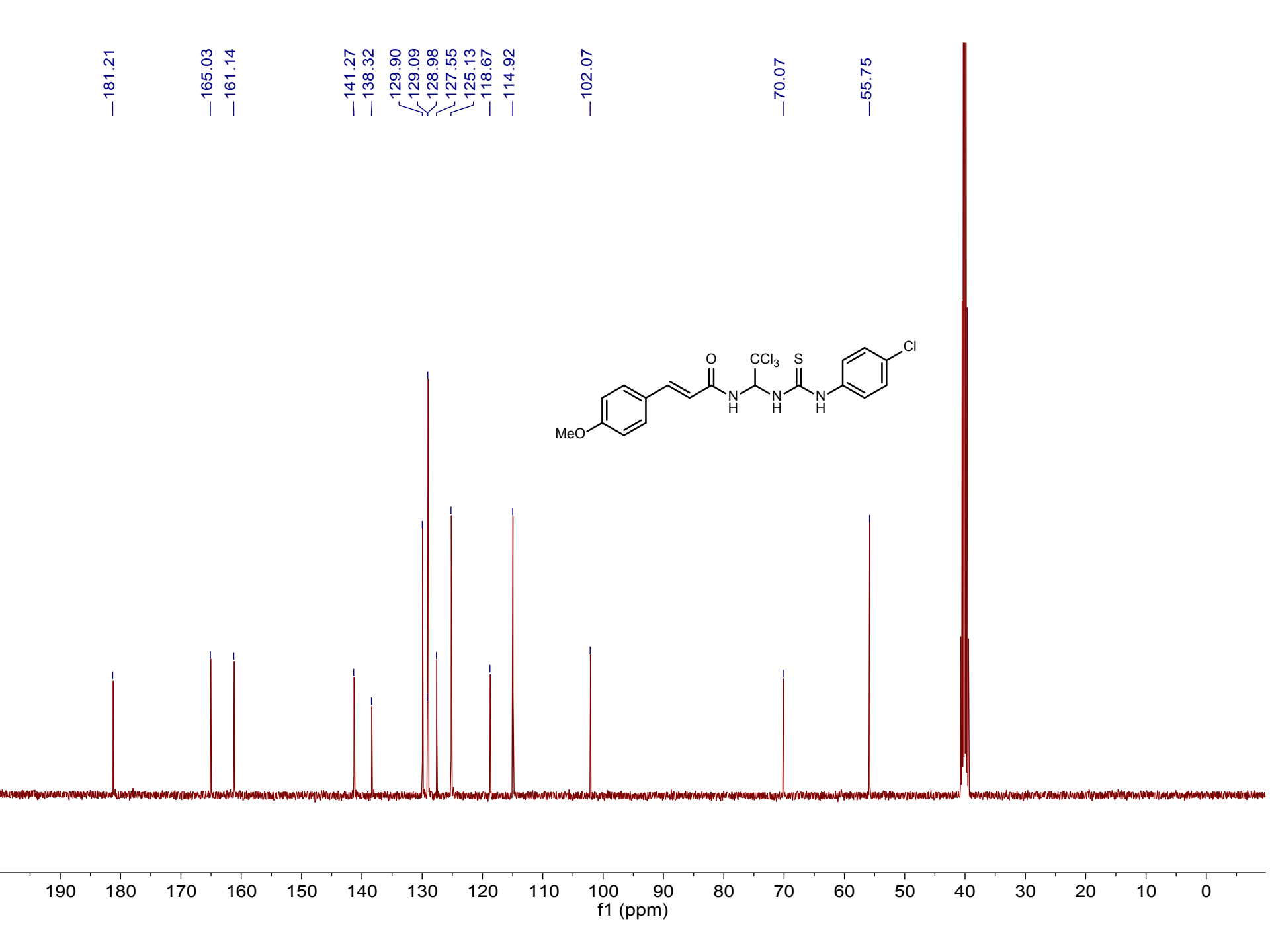
181.21
165.03
161.14
141.27
138.32
129.90
129.09
128.98
127.55
125.13
118.67
114.92
102.07
70.07
55.75
O
CCl3
S
Cl
N
H
N
H
N
H
MeO
190
180
170
160
150
140
130
120
110
100
90
80
70
60
50
40
30
20
10
0
f1 (ppm)

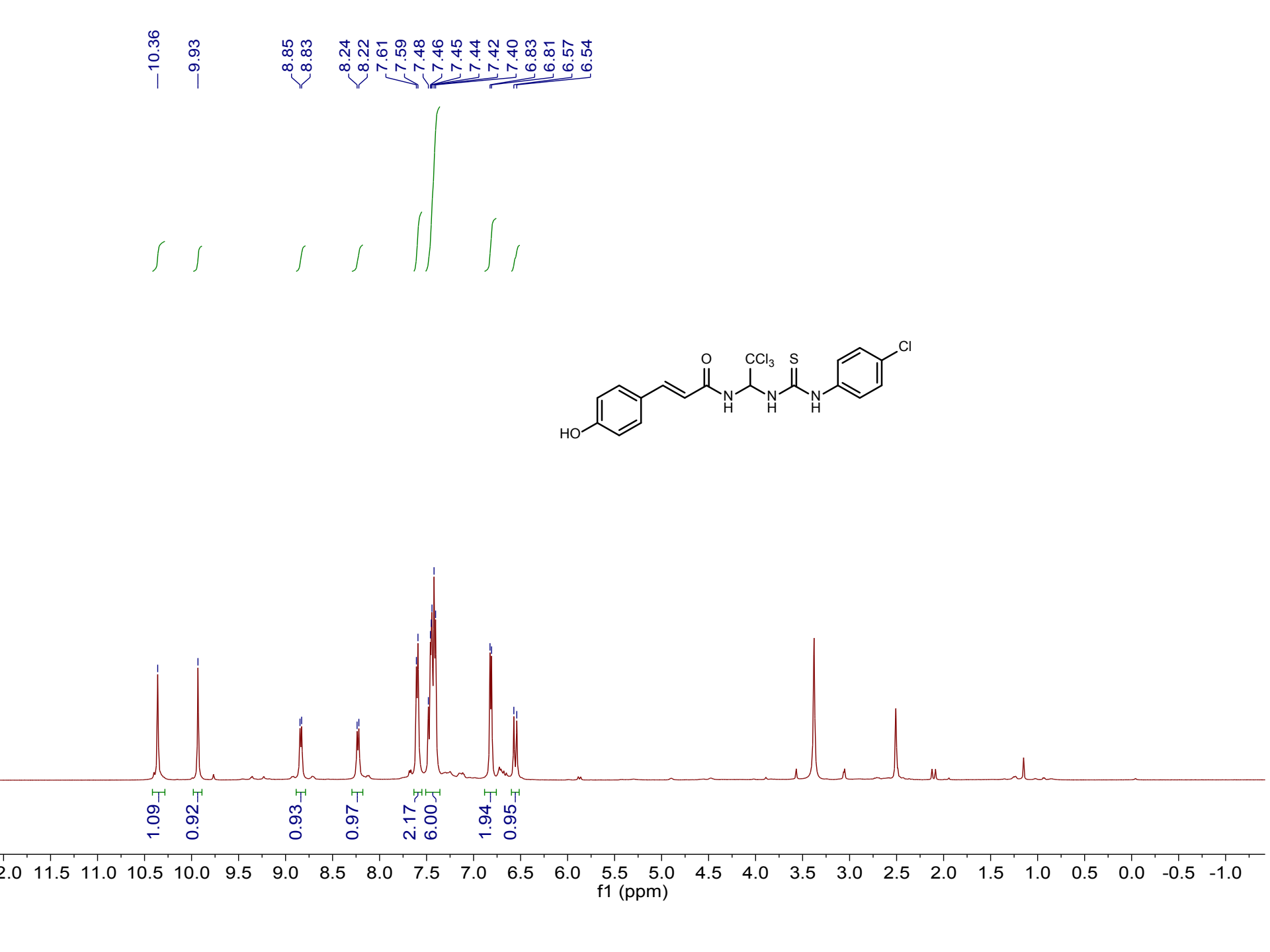
10.36
9.93
8.85
8.83
8.24
8.22
7.61
7.59
7.48
7.46
7.45
7.44
7.42
7.40
6.83
6.81
6.57
6.54
O
CCl3
S
Cl
N
H
N
H
N
H
HO
1.09
0.92
0.93
0.97
2.17
6.00
1.94
0.95
f1 (ppm)

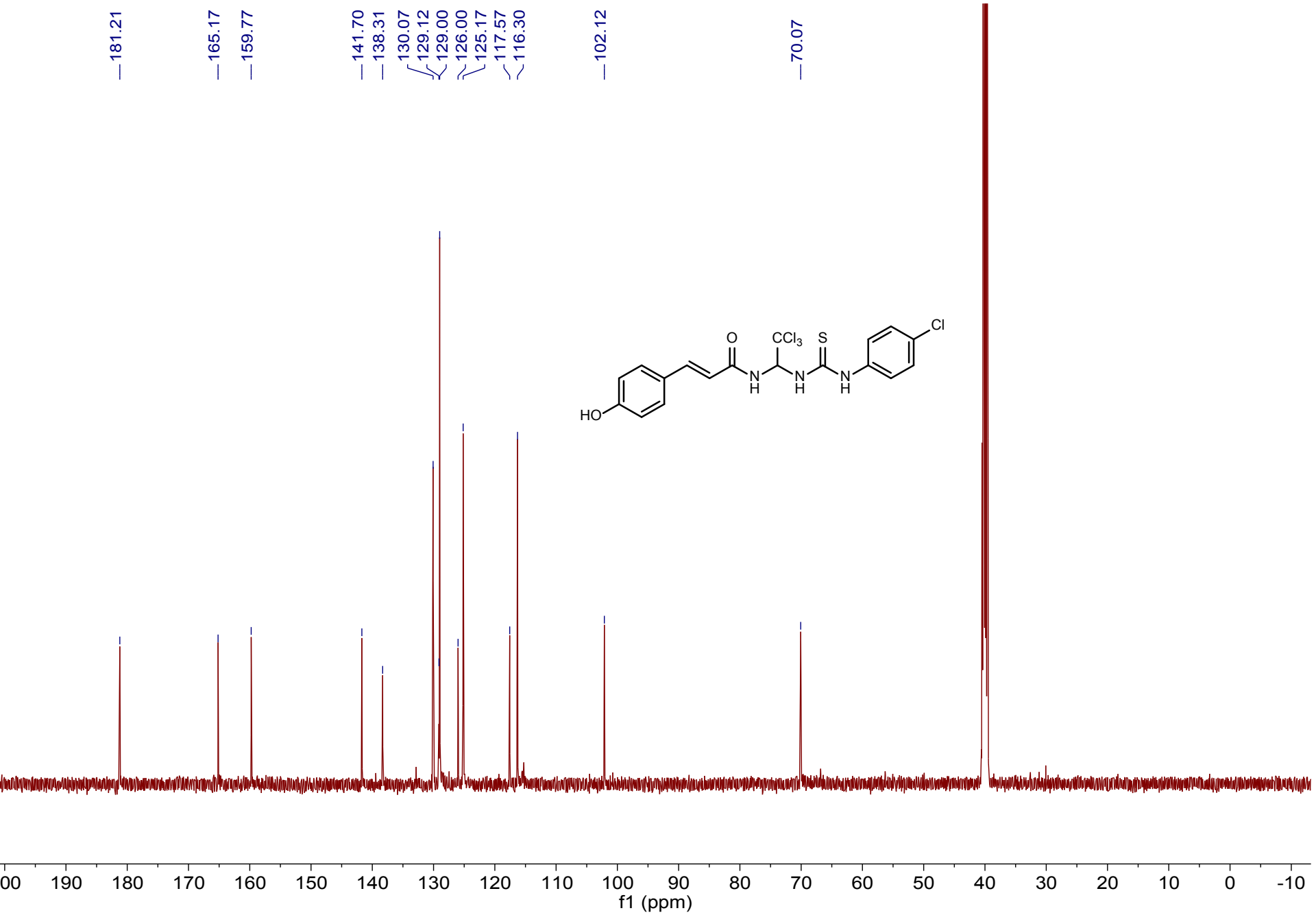
181.21
165.17
159.77
141.70
138.31
130.07
129.12
129.00
126.00
125.17
117.57
116.30
102.12
70.07
O
CCl3
S
Cl
HO
N
H
N
H
N
H
f1 (ppm)

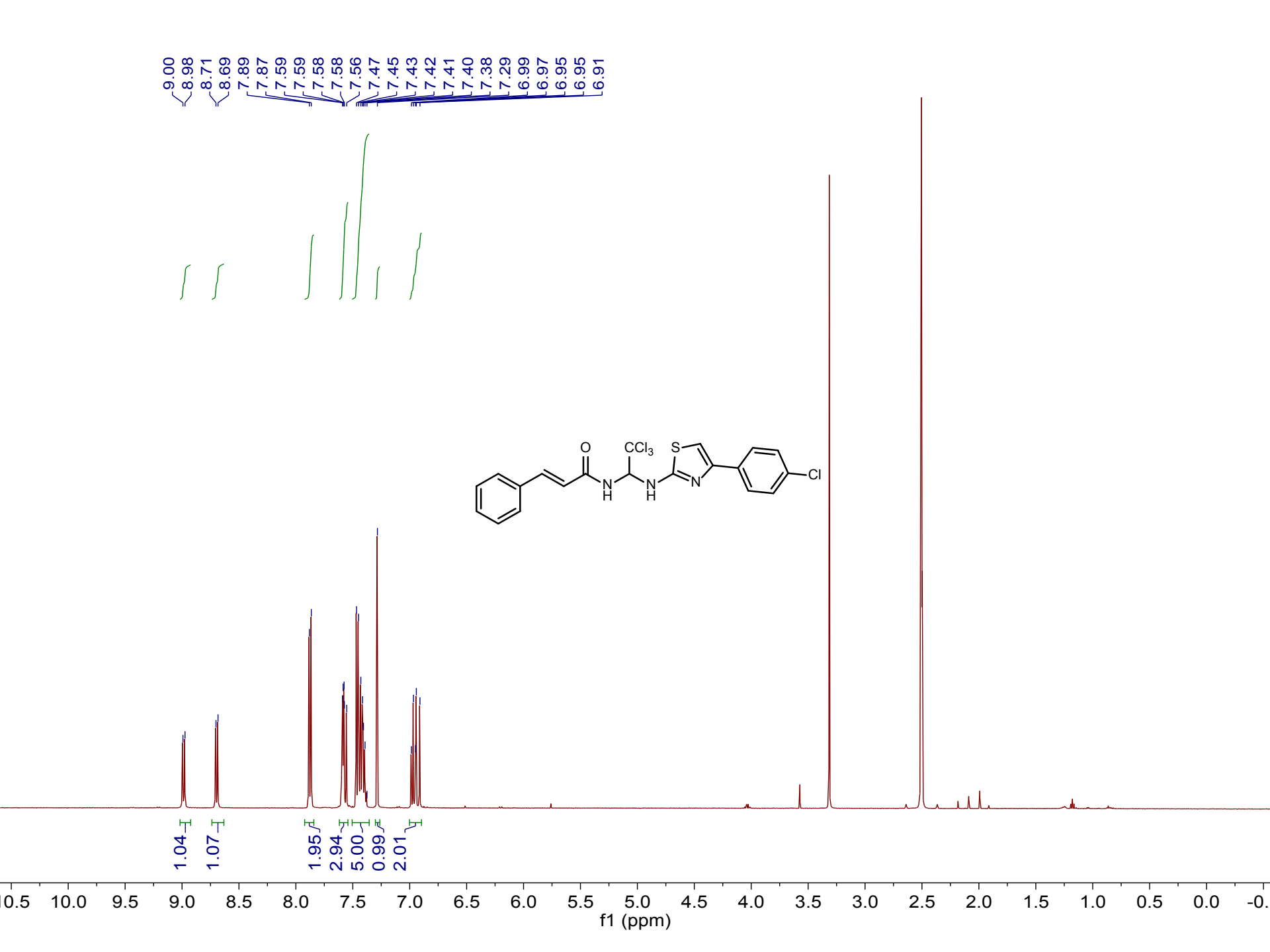
9.00
8.98
8.71
8.69
7.89
7.87
7.59
7.59
7.58
7.58
7.56
7.47
7.45
7.43
7.42
7.41
7.40
7.38
7.29
6.99
6.97
6.95
6.95
6.91
O
CCl3
S
N
H
N
H
N
Cl
1.04
1.07
1.95
2.94
5.00
0.99
2.01
10.5
10.0
9.5
9.0
8.5
8.0
7.5
7.0
6.5
6.0
5.5
5.0
4.5
4.0
3.5
3.0
2.5
2.0
1.5
1.0
0.5
0.0
-0.
f1 (ppm)

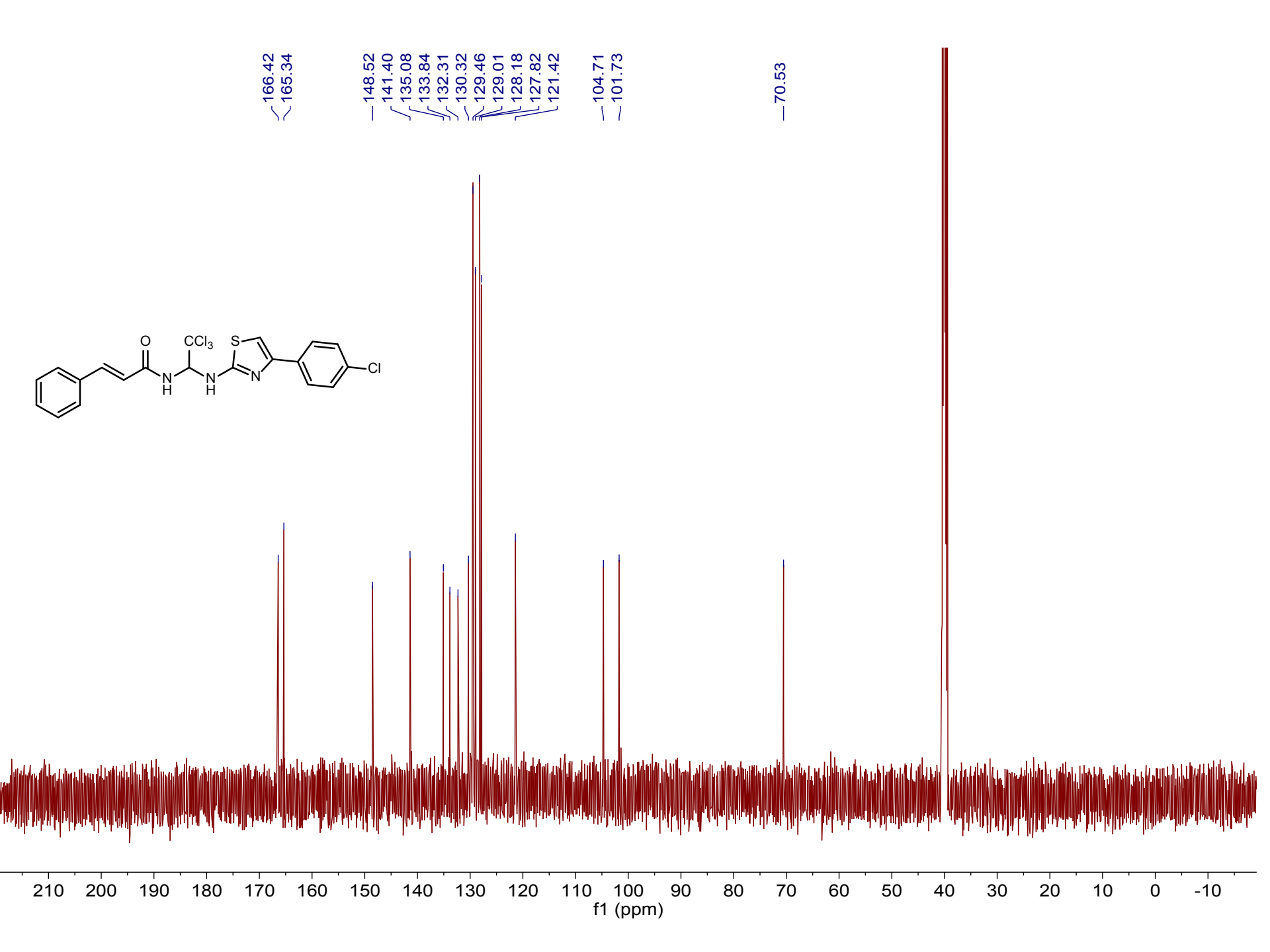
166.42
165.34
148.52
141.40
135.08
133.84
132.31
130.32
129.46
129.01
128.18
127.82
121.42
104.71
101.73
70.53
O
CCl3
S
N
H
N
H
N
Cl
210
200
190
180
170
160
150
140
130
120
110
100
90
80
70
60
50
40
30
20
10
0
-10
f1 (ppm)

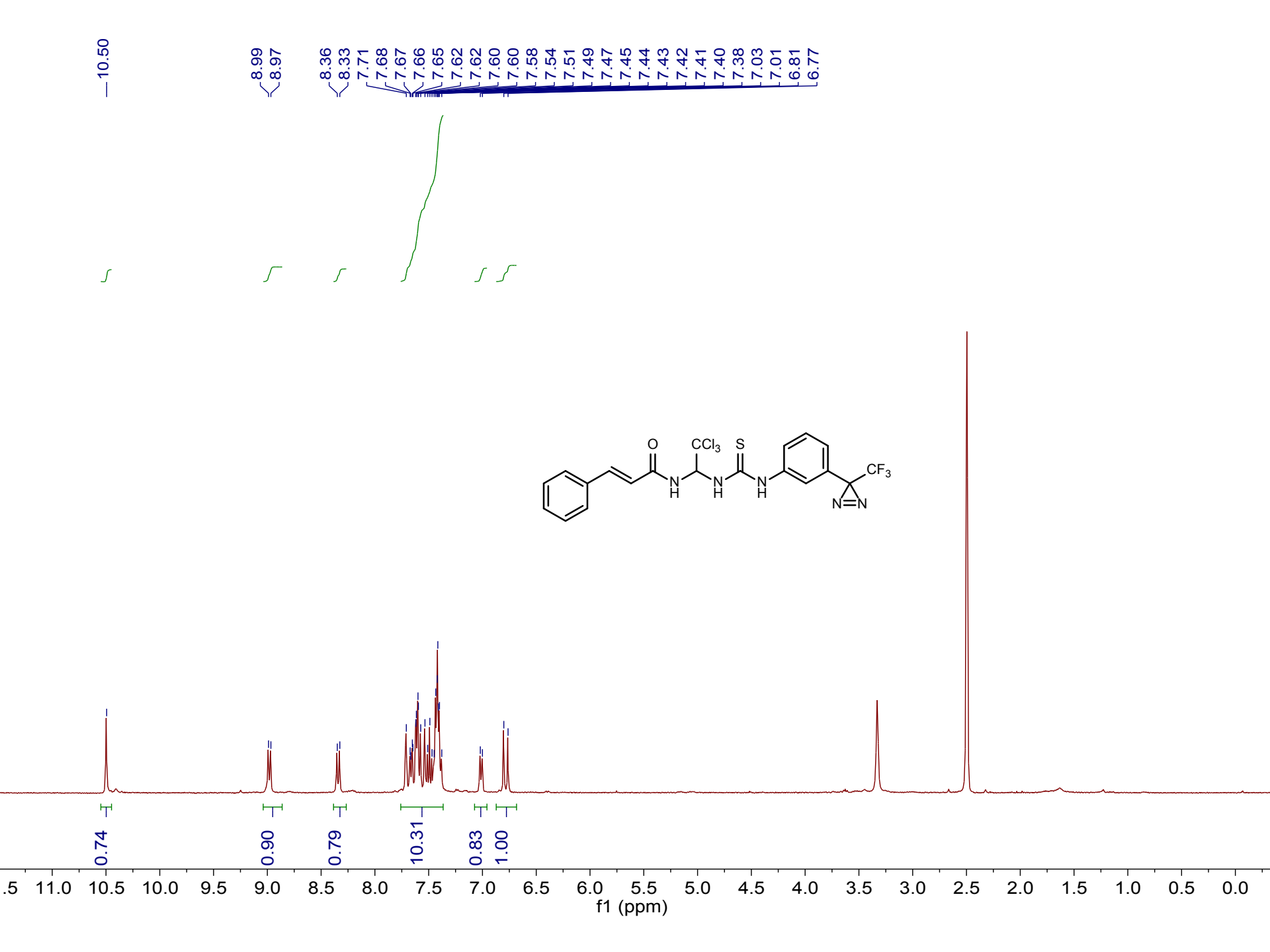
10.50
8.99
8.97
8.36
8.33
7.71
7.68
7.67
7.66
7.65
7.62
7.62
7.60
7.60
7.58
7.54
7.51
7.49
7.47
7.45
7.44
7.43
7.42
7.41
7.40
7.38
7.03
7.01
6.81
6.77
O
CCl3
S
N
H
N
H
N
H
CF3
N=N
0.74
0.90
0.79
10.31
0.83
1.00
f1 (ppm)

^{19}F NMR

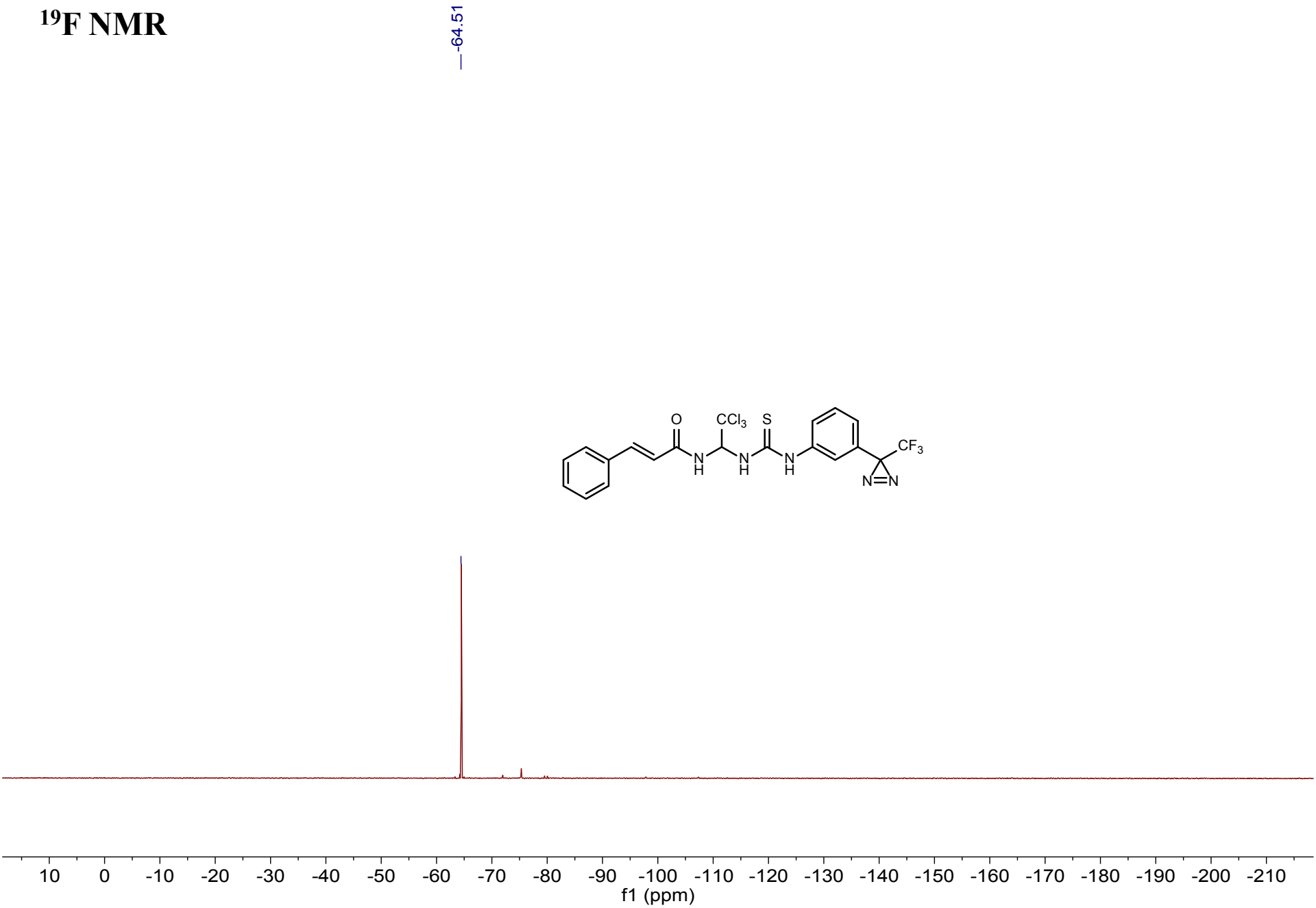
-64.51
O
CCl3
S
N
H
N
H
N
H
CF3
N=N
10
0
-10
-20
-30
-40
-50
-60
-70
-80
-90
-100
-110
-120
-130
-140
-150
-160
-170
-180
-190
-200
-210
f1 (ppm)

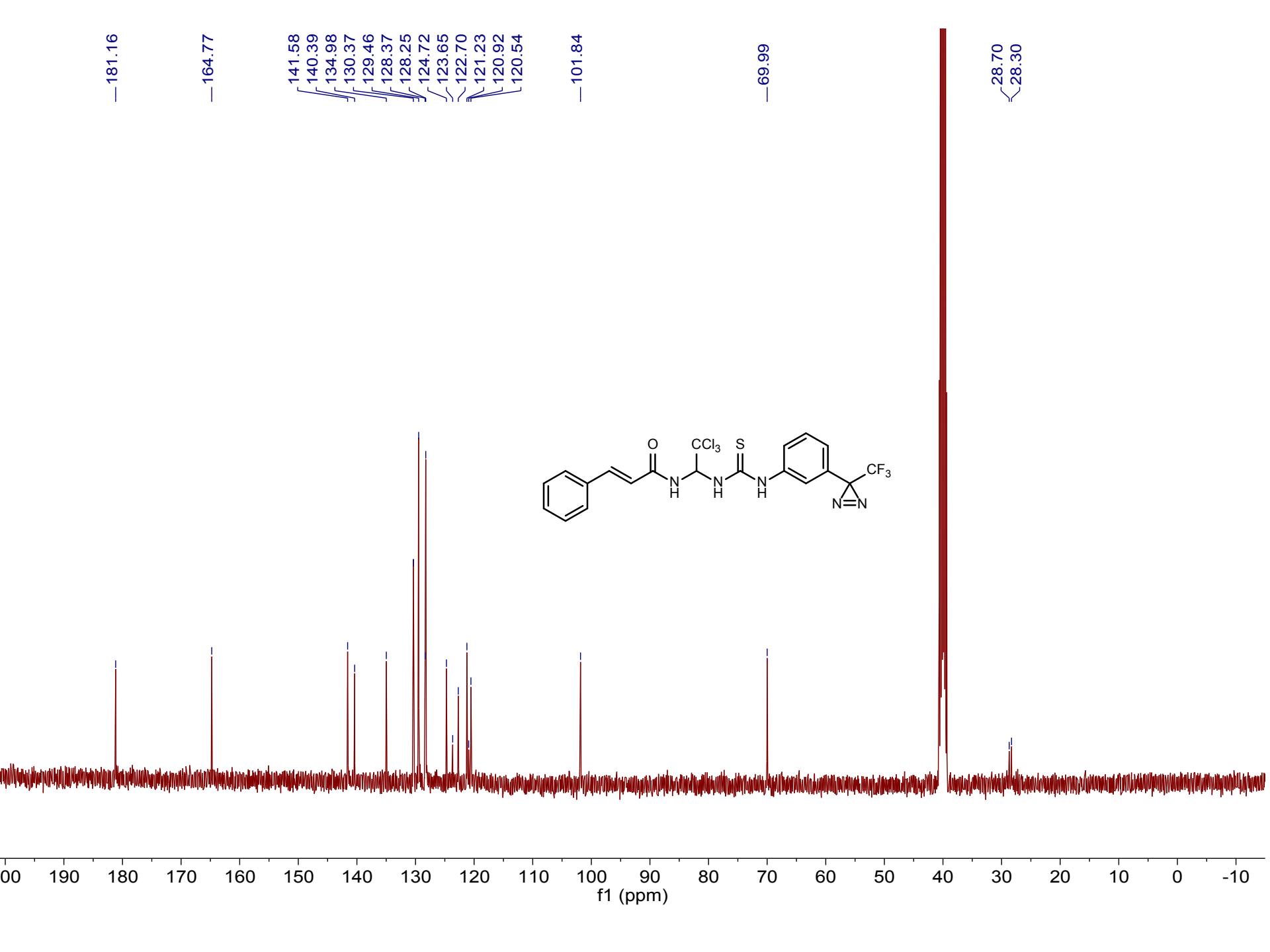
181.16
164.77
141.58
140.39
134.98
130.37
129.46
128.37
128.25
124.72
123.65
122.70
121.23
120.92
120.54
101.84
69.99
28.70
28.30
O
CCl3
S
N
H
N
H
N
H
CF3
N=N
f1 (ppm)

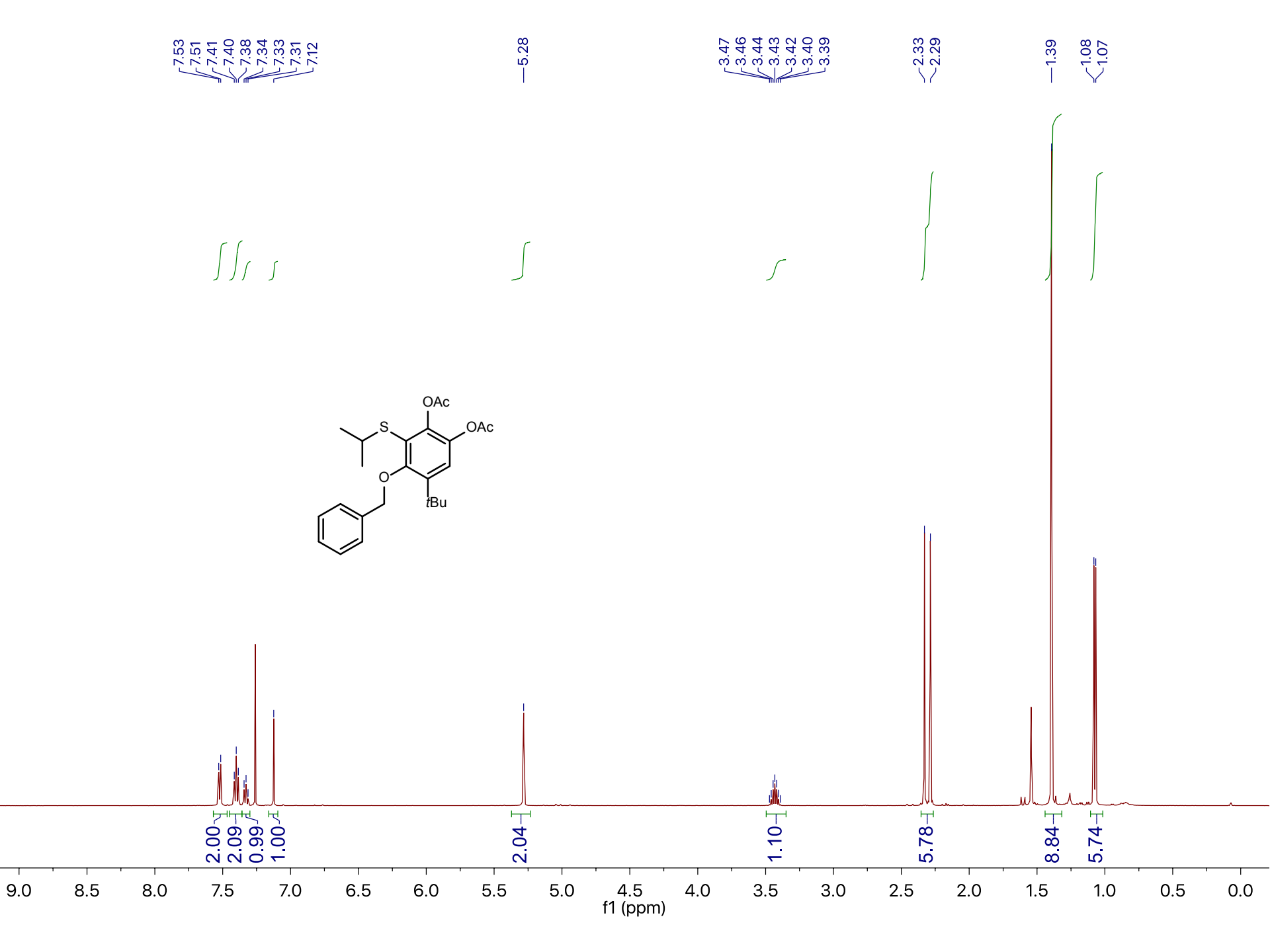
7.53
7.51
7.41
7.40
7.38
7.34
7.33
7.31
7.12
5.28
3.47
3.46
3.44
3.43
3.42
3.40
3.39
2.33
2.29
1.39
1.08
1.07
OAc
OAc
S
O
tBu
2.00
2.09
0.99
1.00
2.04
1.10
5.78
8.84
5.74
9.0
8.5
8.0
7.5
7.0
6.5
6.0
5.5
5.0
4.5
4.0
3.5
3.0
2.5
2.0
1.5
1.0
0.5
0.0
f1 (ppm)

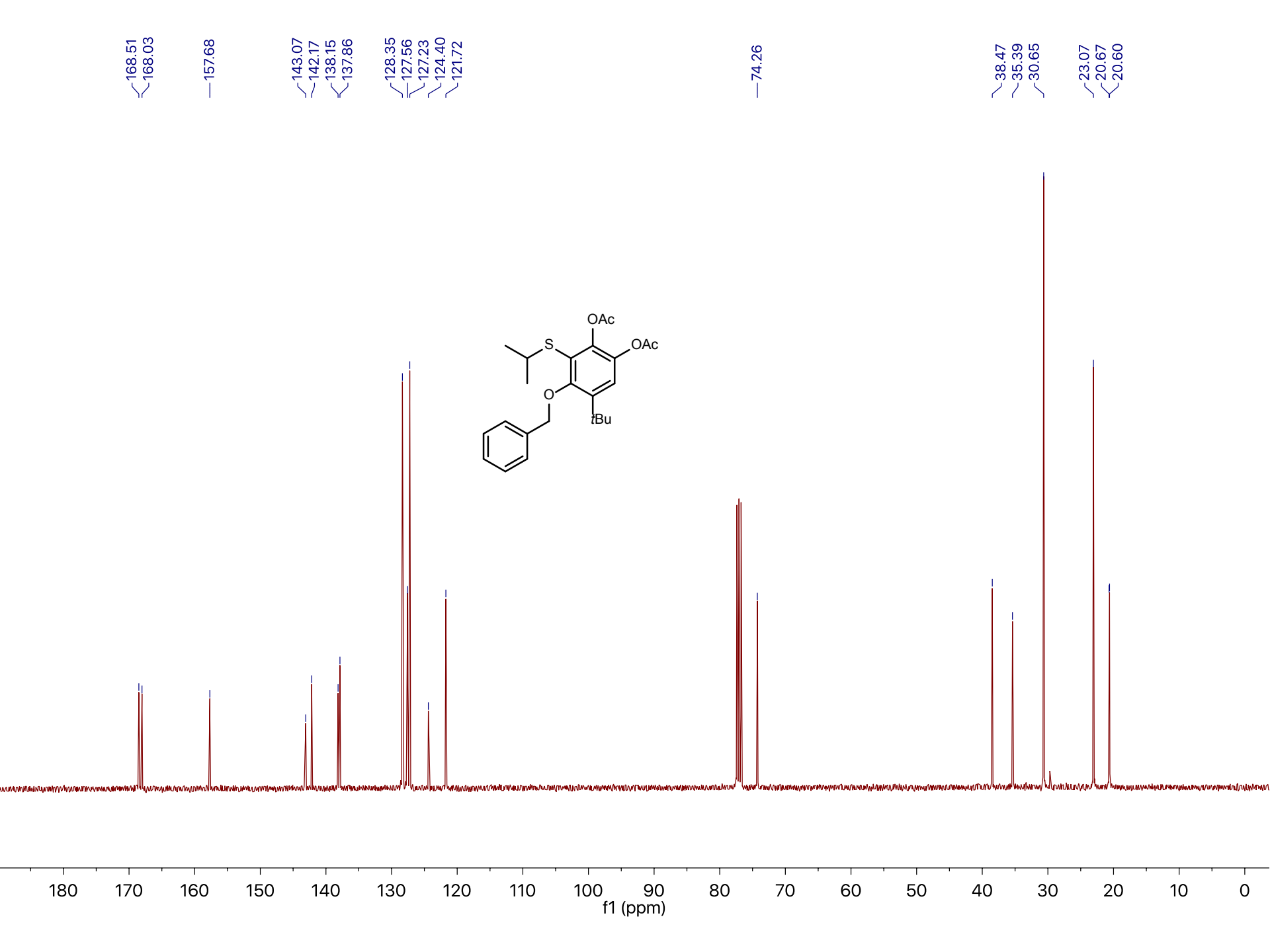
168.51
168.03
157.68
143.07
142.17
138.15
137.86
128.35
127.56
127.23
124.40
121.72
74.26
38.47
35.39
30.65
23.07
20.67
20.60
OAc
OAc
S
O
tBu
180
170
160
150
140
130
120
110
100
90
80
70
60
50
40
30
20
10
0
f1 (ppm)

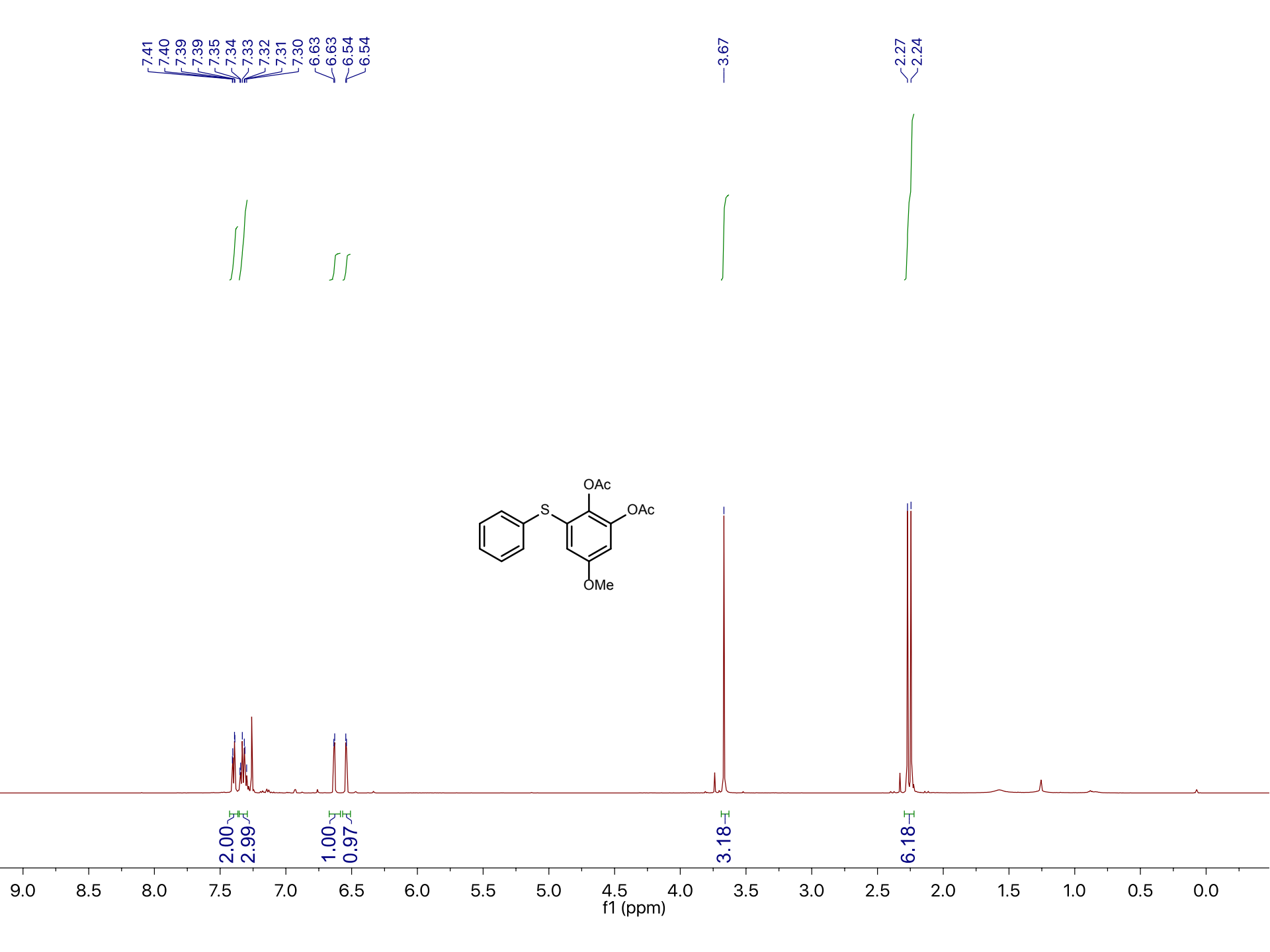
7.41
7.40
7.39
7.39
7.35
7.34
7.33
7.32
7.31
7.30
6.63
6.63
6.54
6.54
3.67
2.27
2.24
OAc
OAc
S
OMe
2.00
2.99
1.00
0.97
3.18
6.18
9.0
8.5
8.0
7.5
7.0
6.5
6.0
5.5
5.0
4.5
4.0
3.5
3.0
2.5
2.0
1.5
1.0
0.5
0.0
f1 (ppm)

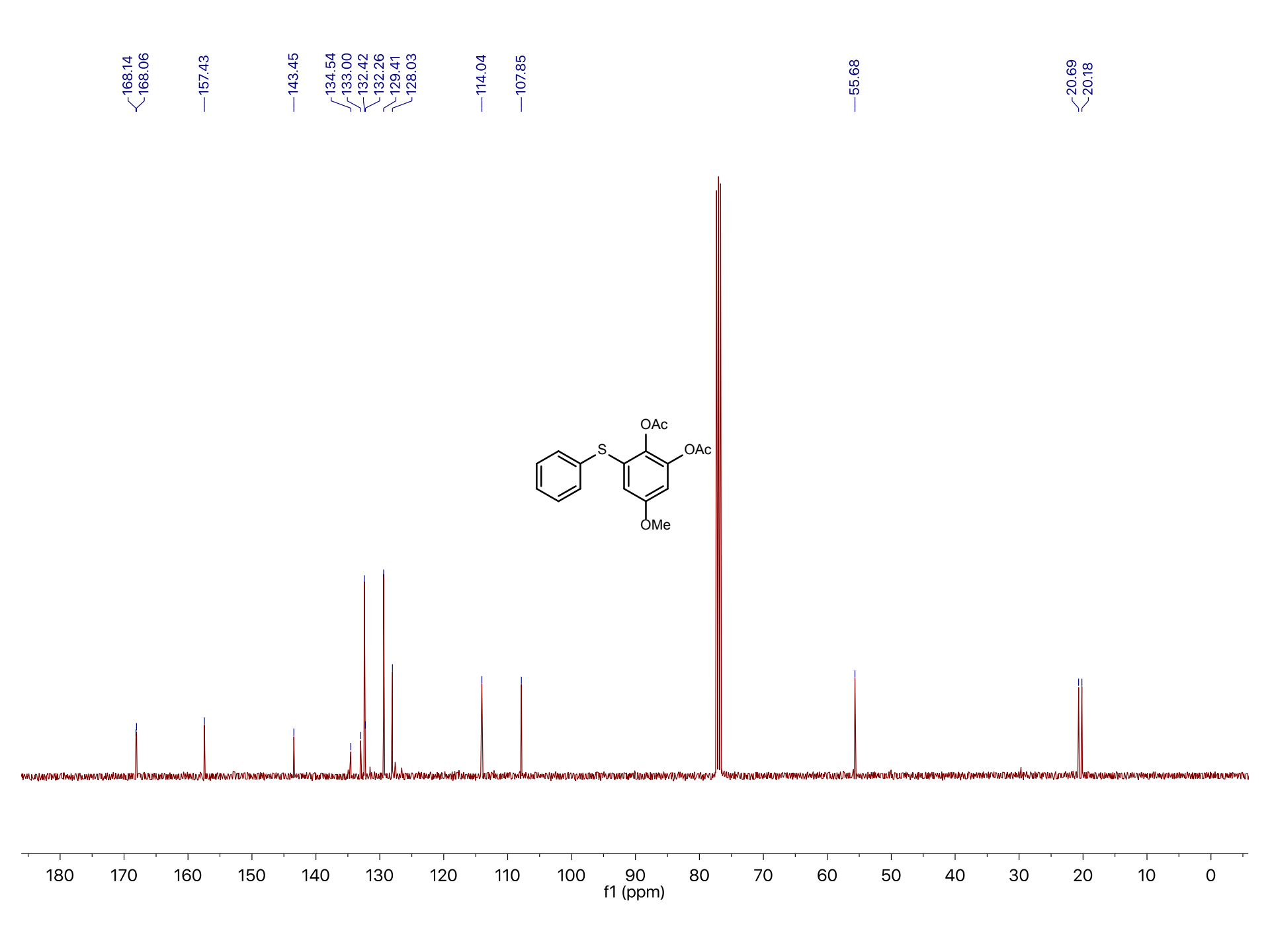
168.14
168.06
157.43
143.45
134.54
133.00
132.42
132.26
129.41
128.03
114.04
107.85
55.68
20.69
20.18
OAc
OAc
S
OMe
180
170
160
150
140
130
120
110
100
90
80
70
60
50
40
30
20
10
0
f1 (ppm)

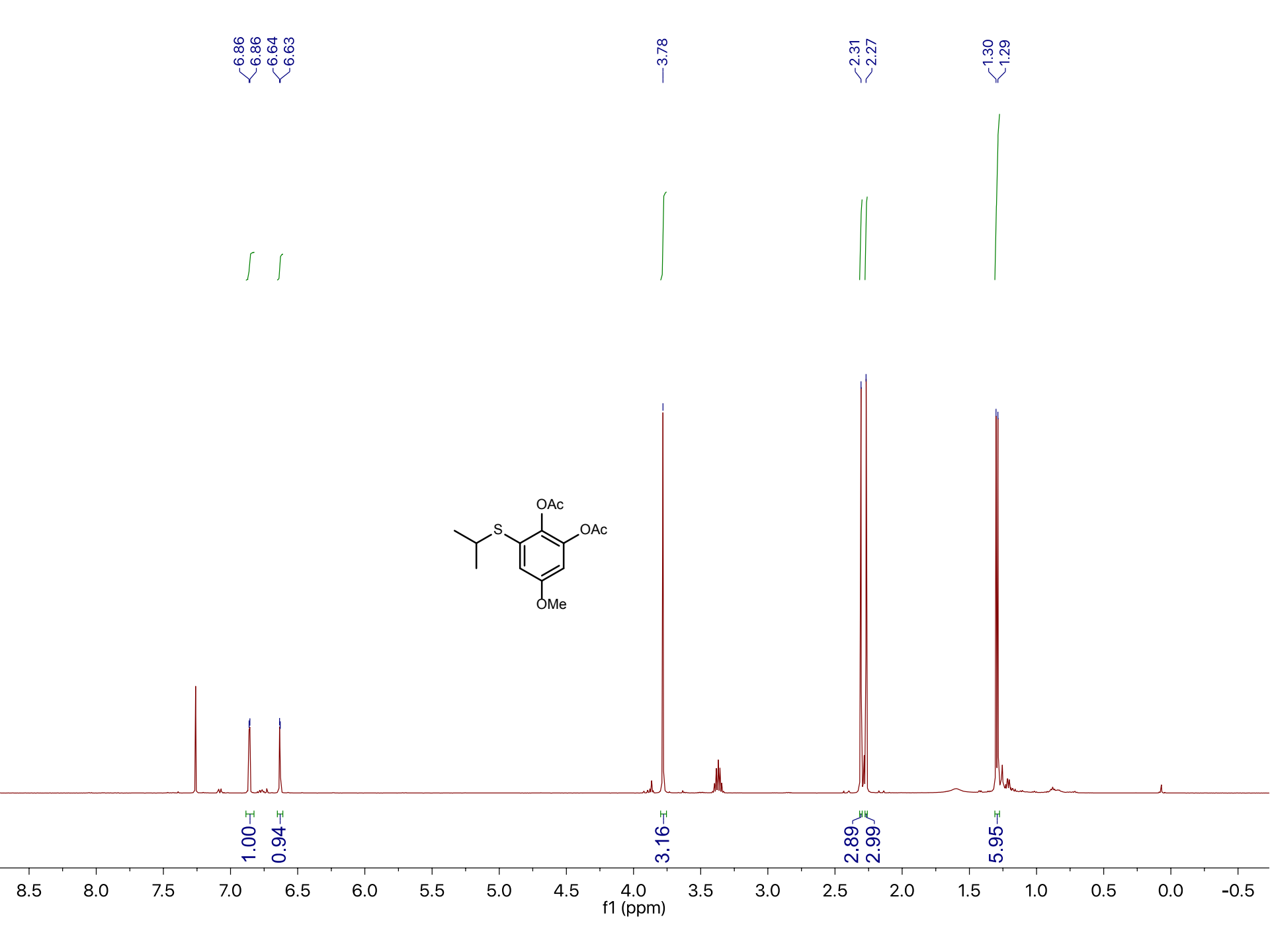
6.86
6.86
6.64
6.63
3.78
2.31
2.27
1.30
1.29
OAc
OAc
S
OMe
1.00
0.94
3.16
2.89
2.99
5.95
8.5
8.0
7.5
7.0
6.5
6.0
5.5
5.0
4.5
4.0
3.5
3.0
2.5
2.0
1.5
1.0
0.5
0.0
-0.5
f1 (ppm)

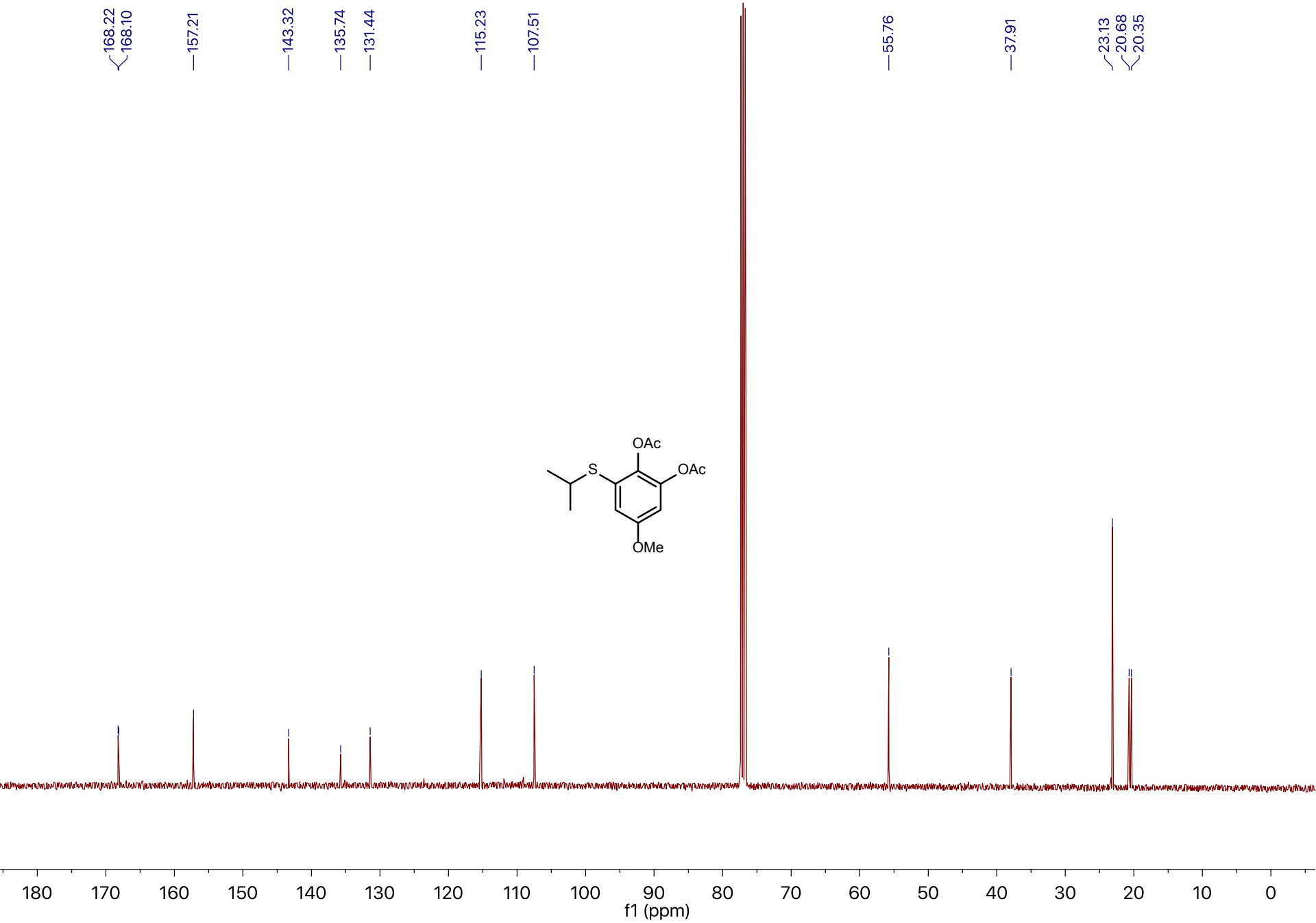
168.22
168.10
157.21
143.32
135.74
131.44
115.23
107.51
55.76
37.91
23.13
20.68
20.35
OAc
S
OAc
OMe
180
170
160
150
140
130
120
110
100
90
80
70
60
50
40
30
20
10
0
f1 (ppm)

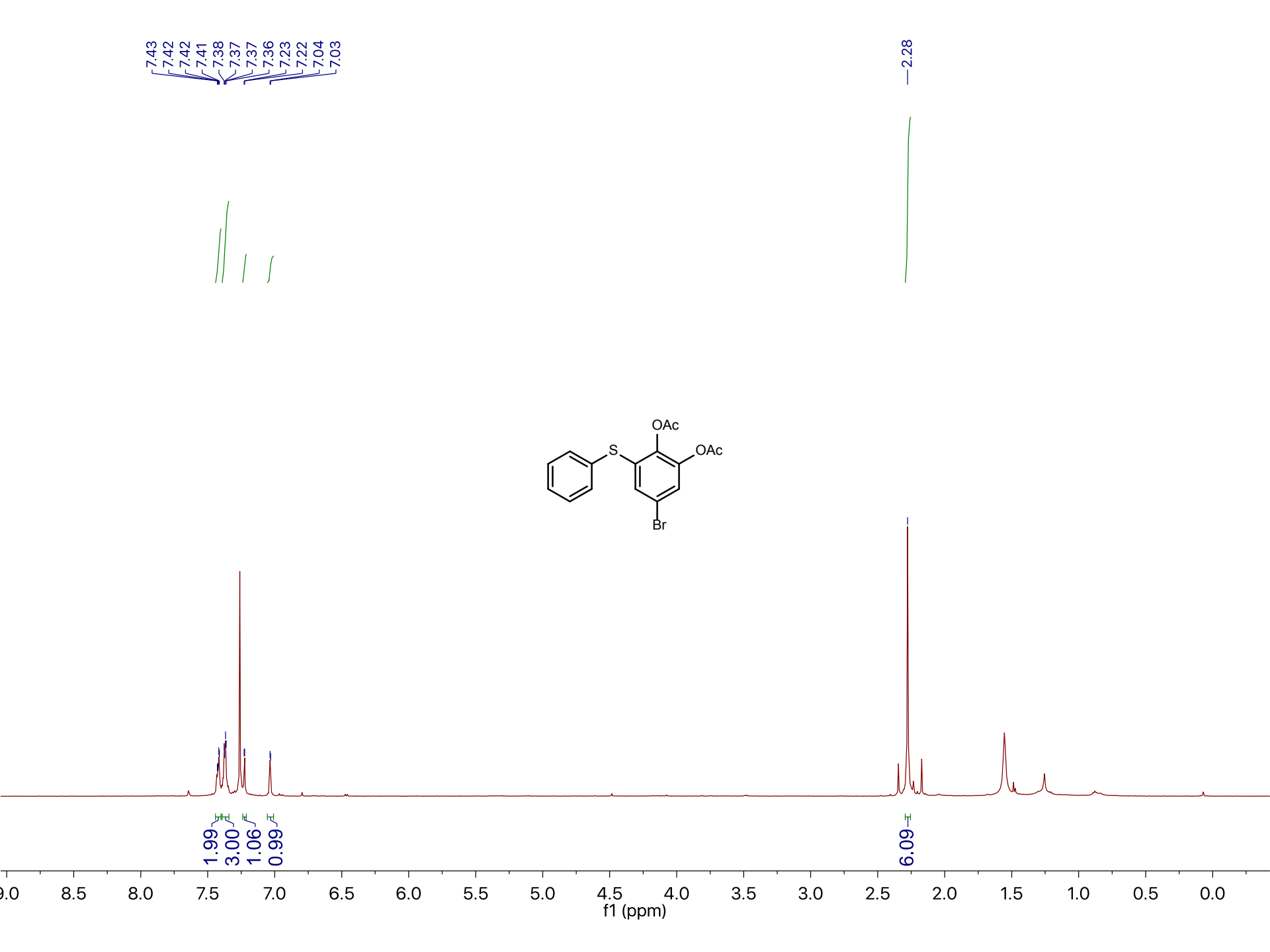
7.43
7.42
7.42
7.41
7.38
7.37
7.37
7.36
7.23
7.22
7.04
7.03
2.28
OAc
OAc
S
Br
1.99
3.00
1.06
0.99
6.09
9.0
8.5
8.0
7.5
7.0
6.5
6.0
5.5
5.0
4.5
4.0
3.5
3.0
2.5
2.0
1.5
1.0
0.5
0.0
f1 (ppm)

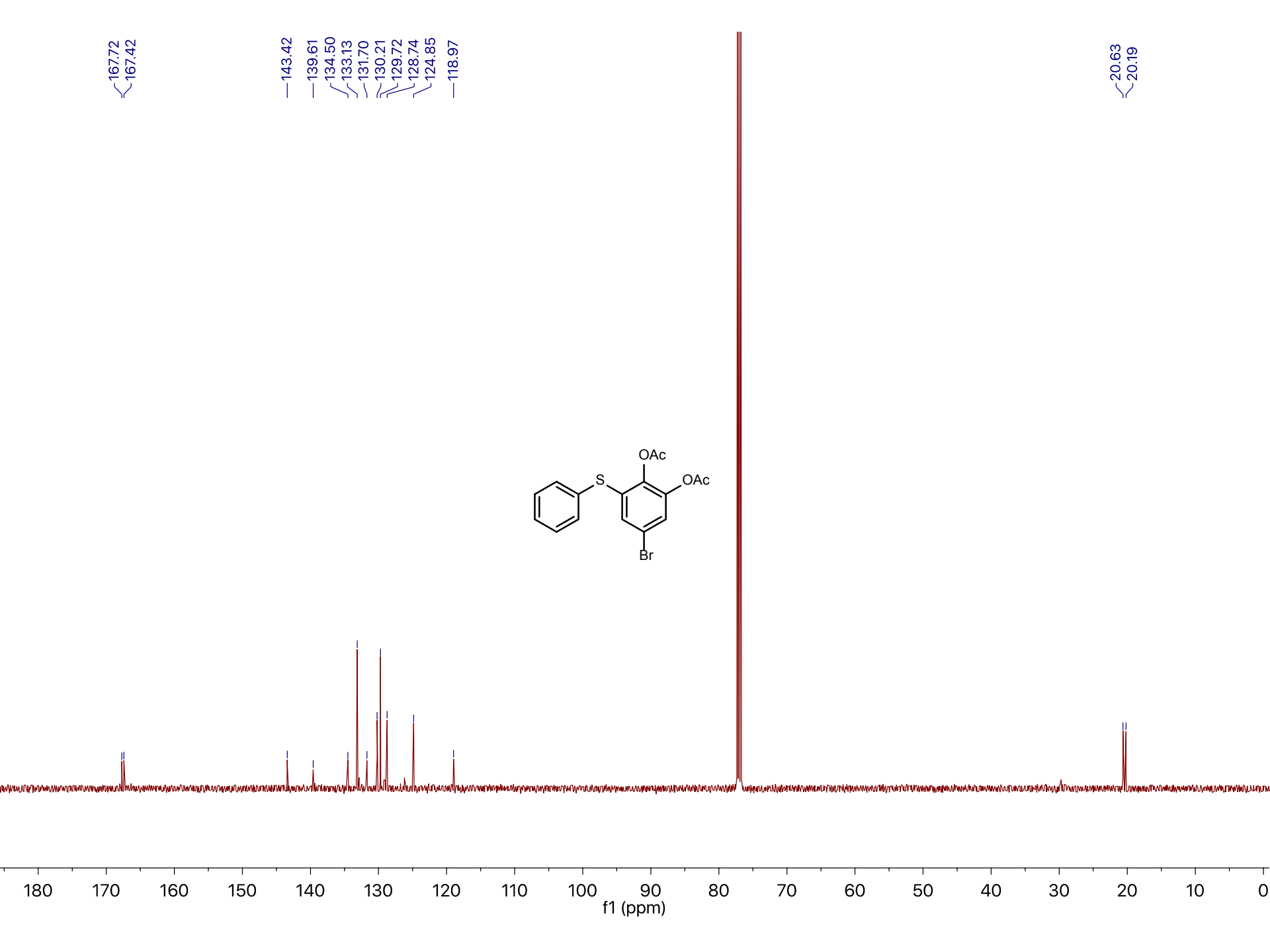
167.72
167.42
143.42
139.61
134.50
133.13
131.70
130.21
129.72
128.74
124.85
118.97
20.63
20.19
OAc
OAc
S
Br
180
170
160
150
140
130
120
110
100
90
80
70
60
50
40
30
20
10
0
f1 (ppm)

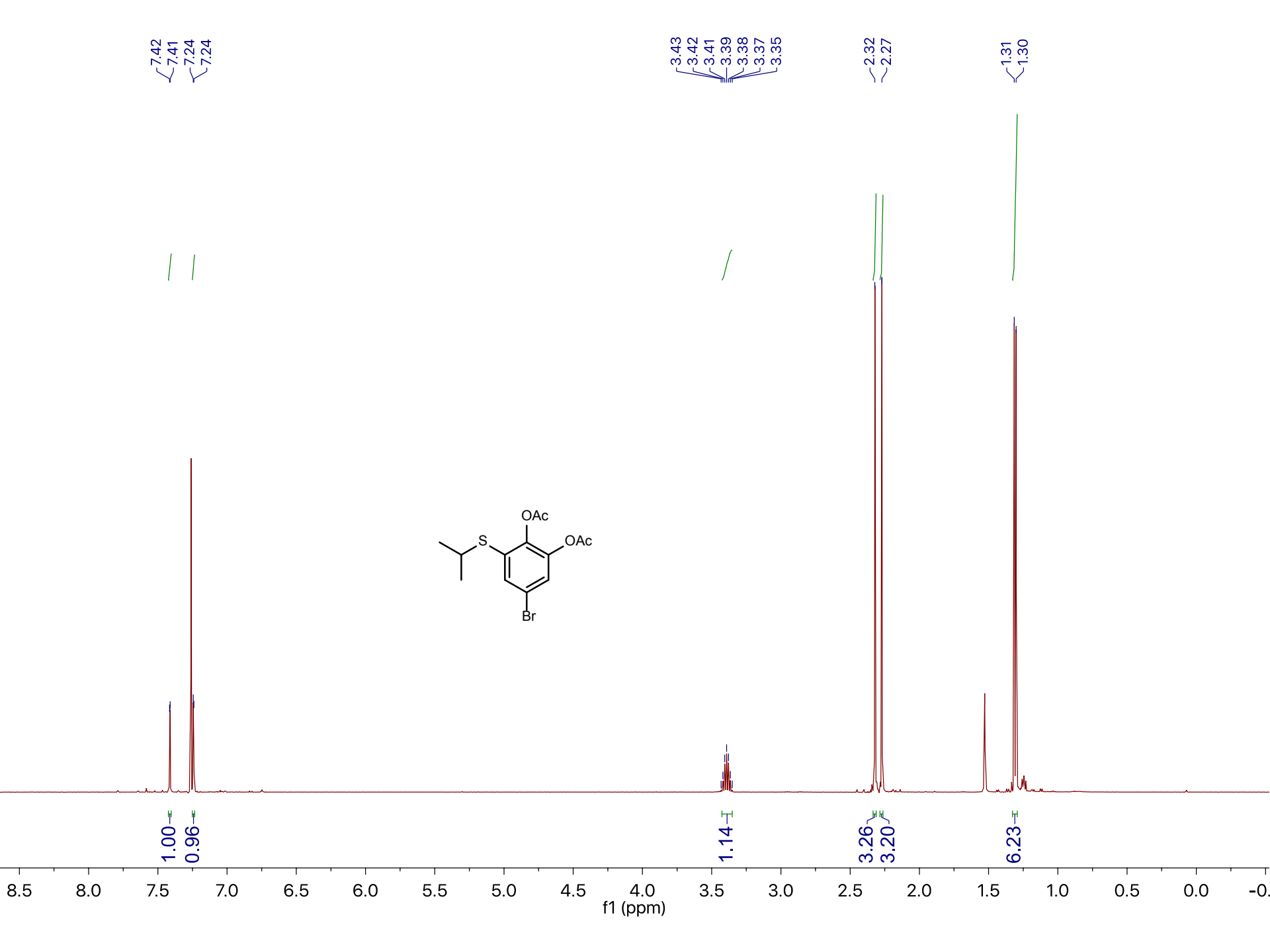
7.42
7.41
7.24
7.24
3.43
3.42
3.41
3.39
3.38
3.37
3.35
2.32
2.27
1.31
1.30
OAc
OAc
S
Br
1.00
0.96
1.14
3.26
3.20
6.23
8.5
8.0
7.5
7.0
6.5
6.0
5.5
5.0
4.5
4.0
3.5
3.0
2.5
2.0
1.5
1.0
0.5
0.0
f1 (ppm)

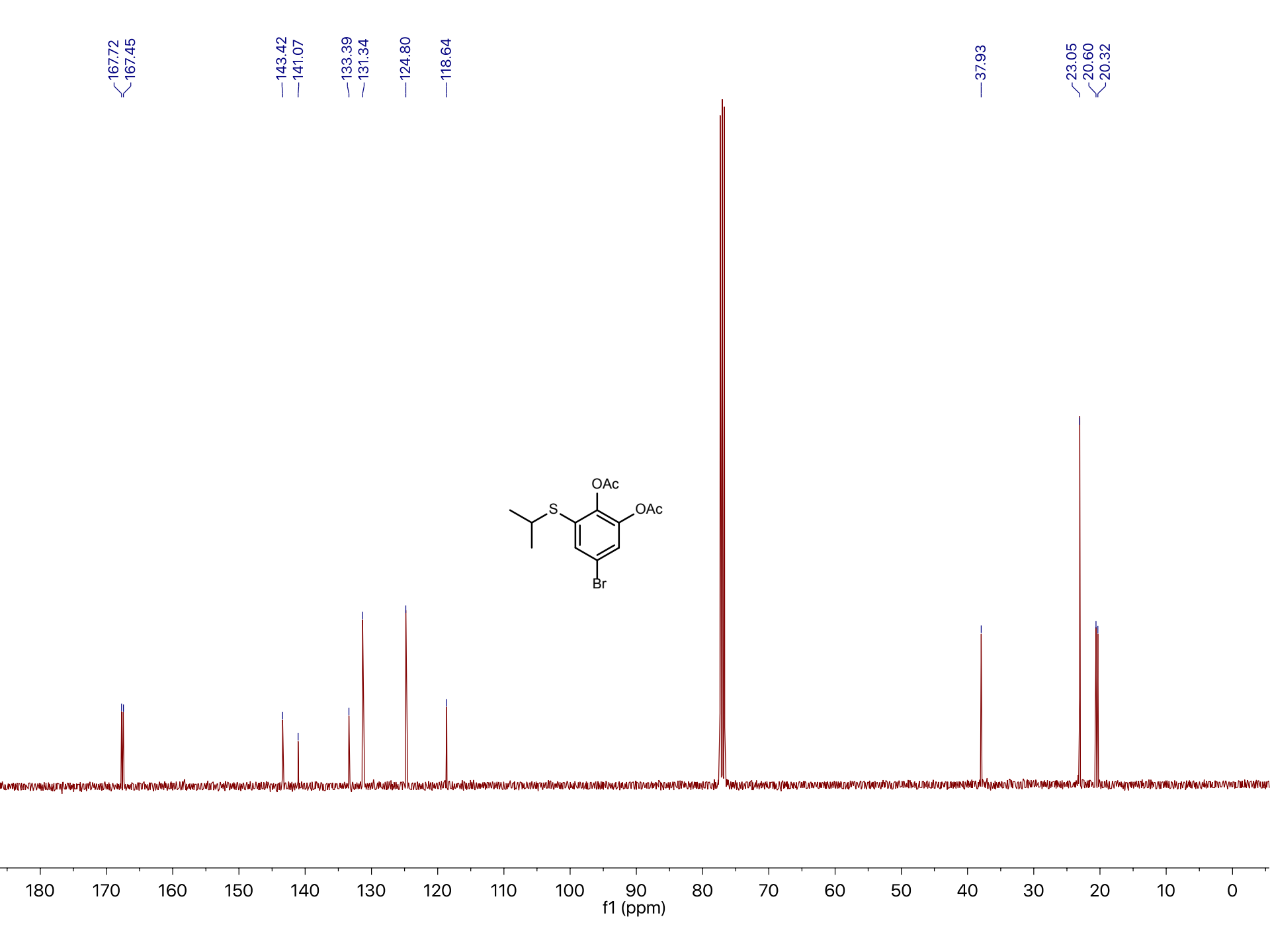
167.72
167.45
143.42
141.07
133.39
131.34
124.80
118.64
37.93
23.05
20.60
20.32
OAc
OAc
S
Br
180
170
160
150
140
130
120
110
100
90
80
70
60
50
40
30
20
10
0
f1 (ppm)

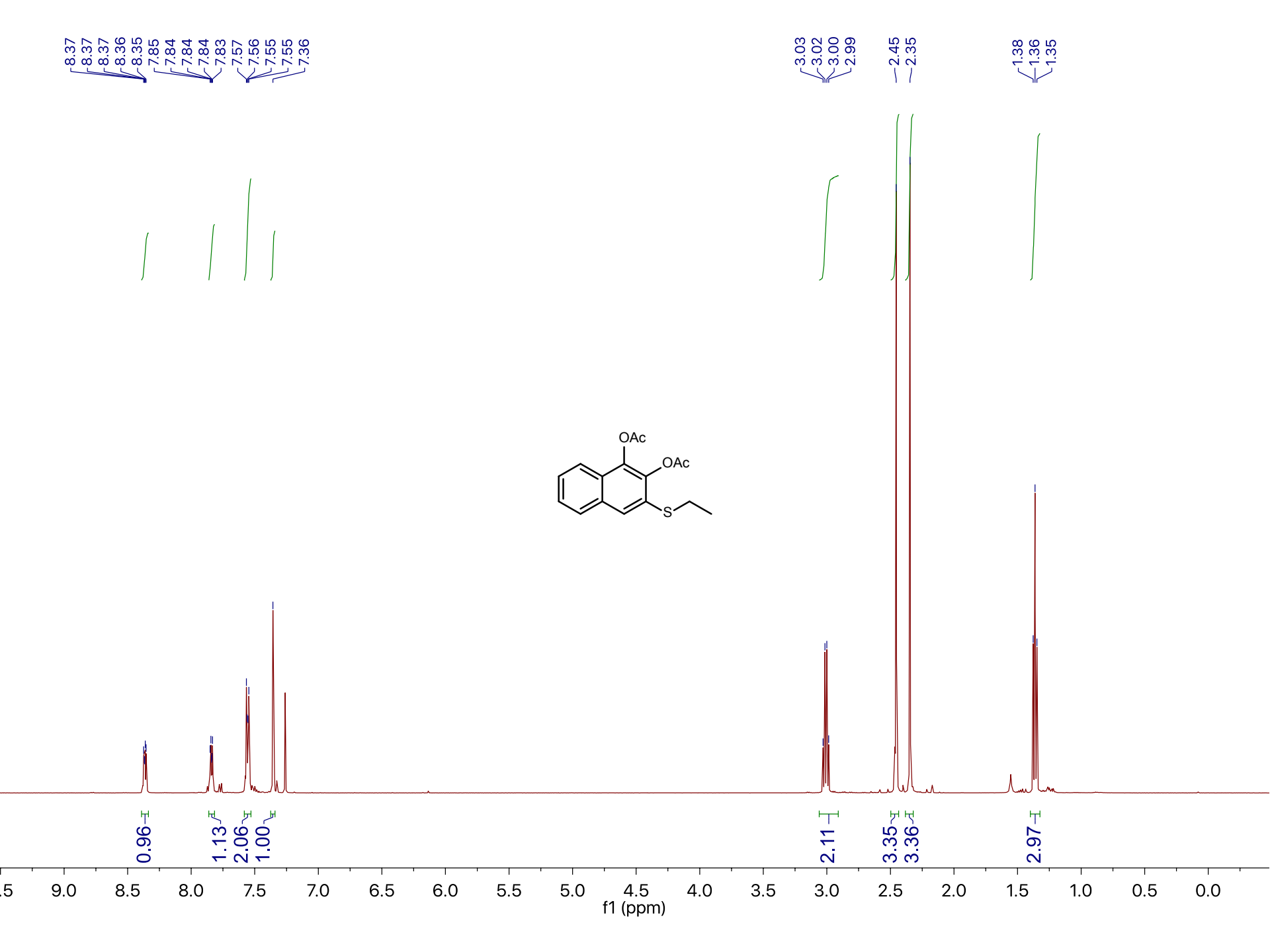
8.37
8.37
8.37
8.36
8.35
7.85
7.84
7.84
7.84
7.83
7.57
7.56
7.55
7.55
7.36
3.03
3.02
3.00
2.99
2.45
2.35
1.38
1.36
1.35
OAc
OAc
S
0.96
1.13
2.06
1.00
2.11
3.35
3.36
2.97
9.0
8.5
8.0
7.5
7.0
6.5
6.0
5.5
5.0
4.5
4.0
3.5
3.0
2.5
2.0
1.5
1.0
0.5
0.0
f1 (ppm)

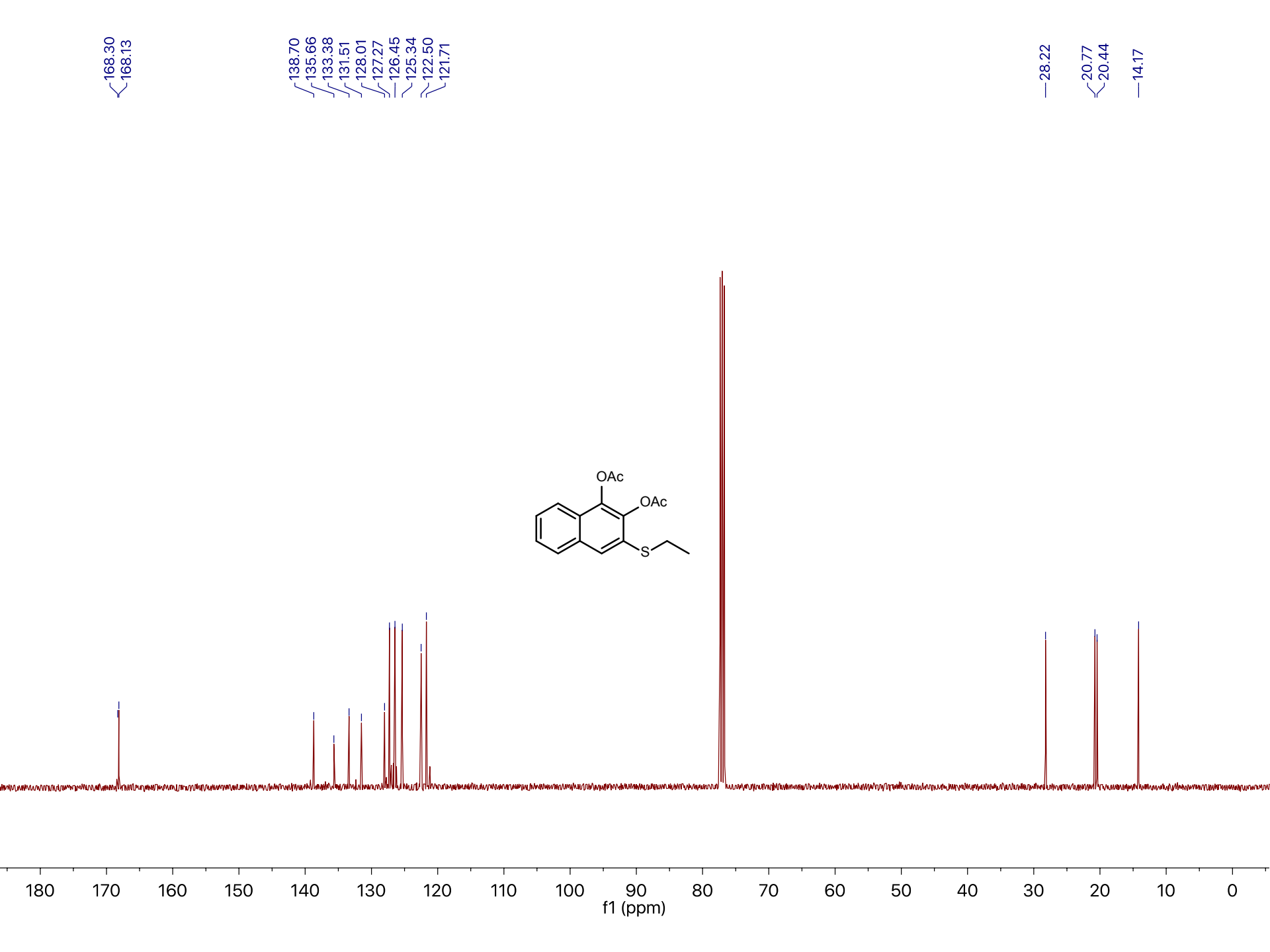
168.30
168.13
138.70
135.66
133.38
131.51
128.01
127.27
126.45
125.34
122.50
121.71
28.22
20.77
20.44
14.17
OAc
OAc
S
180
170
160
150
140
130
120
110
100
90
80
70
60
50
40
30
20
10
0
f1 (ppm)

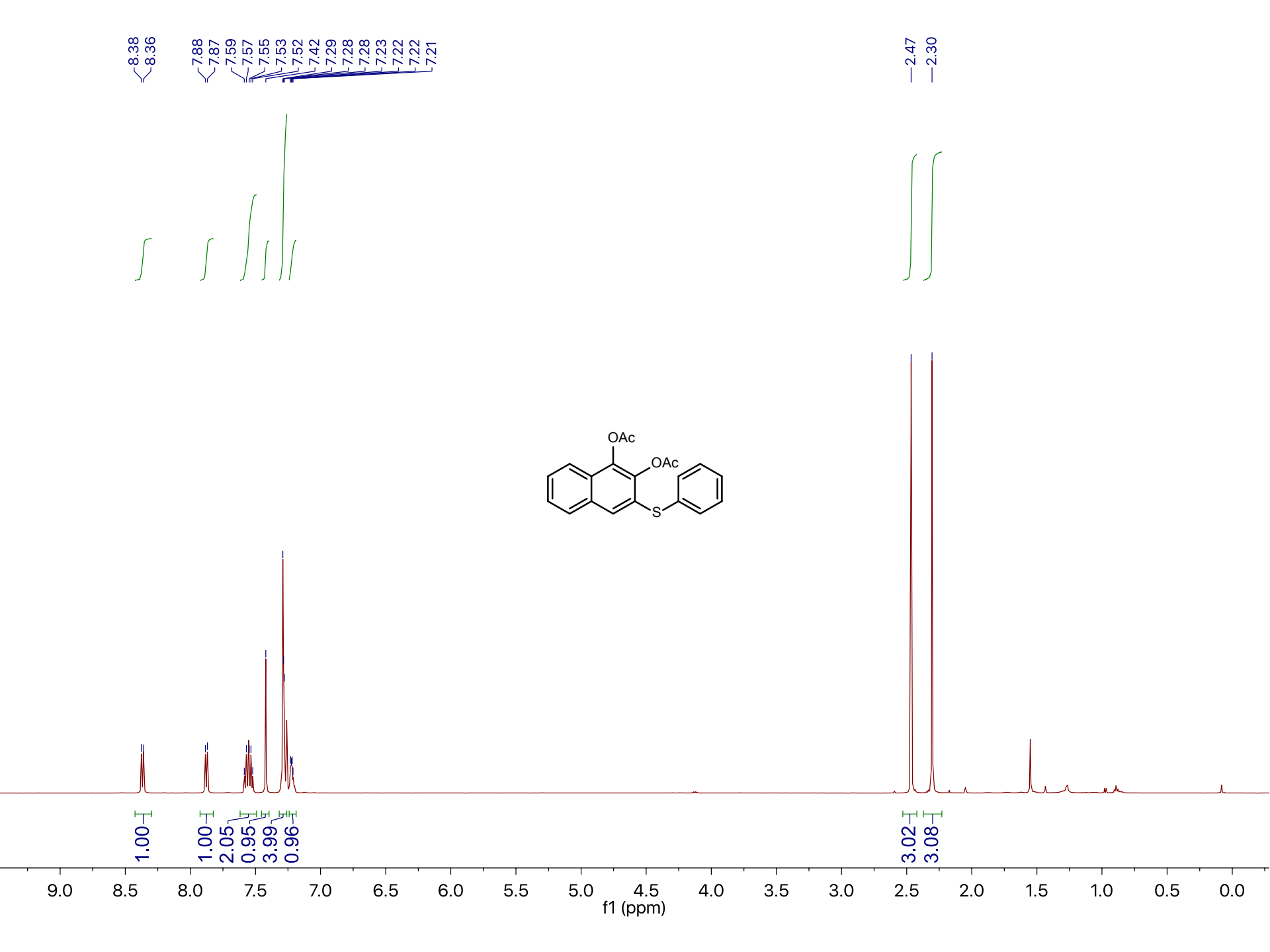
8.38
8.36
7.88
7.87
7.59
7.57
7.55
7.53
7.52
7.42
7.29
7.28
7.28
7.23
7.22
7.22
7.21
2.47
2.30
OAc
OAc
S
1.00
1.00
2.05
0.95
3.99
0.96
3.02
3.08
9.0
8.5
8.0
7.5
7.0
6.5
6.0
5.5
5.0
4.5
4.0
3.5
3.0
2.5
2.0
1.5
1.0
0.5
0.0
f1 (ppm)

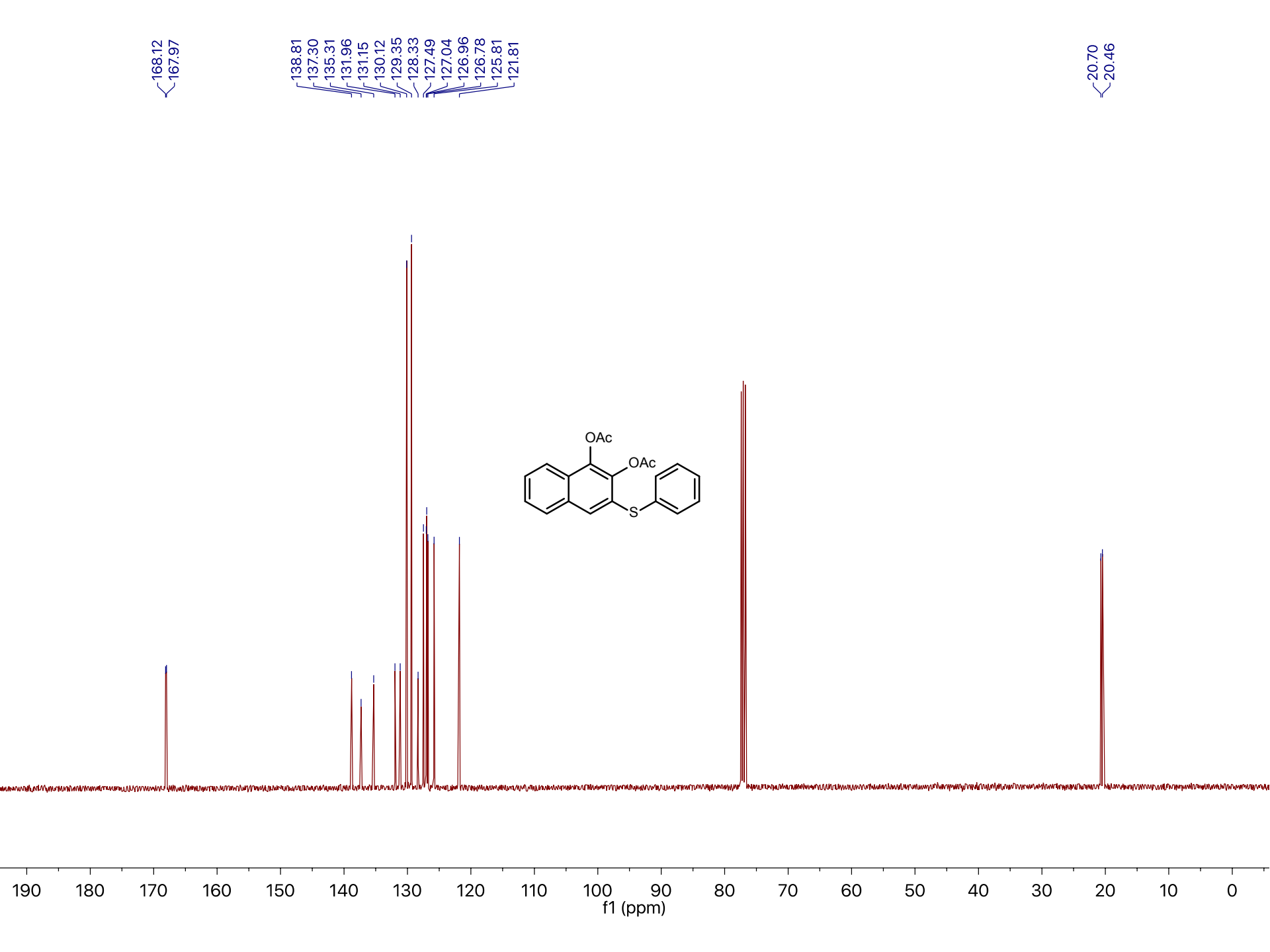
168.12
167.97
138.81
137.30
135.31
131.96
131.15
130.12
129.35
128.33
127.49
127.04
126.96
126.78
125.81
121.81
20.70
20.46
OAc
OAc
S
190
180
170
160
150
140
130
120
110
100
90
80
70
60
50
40
30
20
10
0
f1 (ppm)

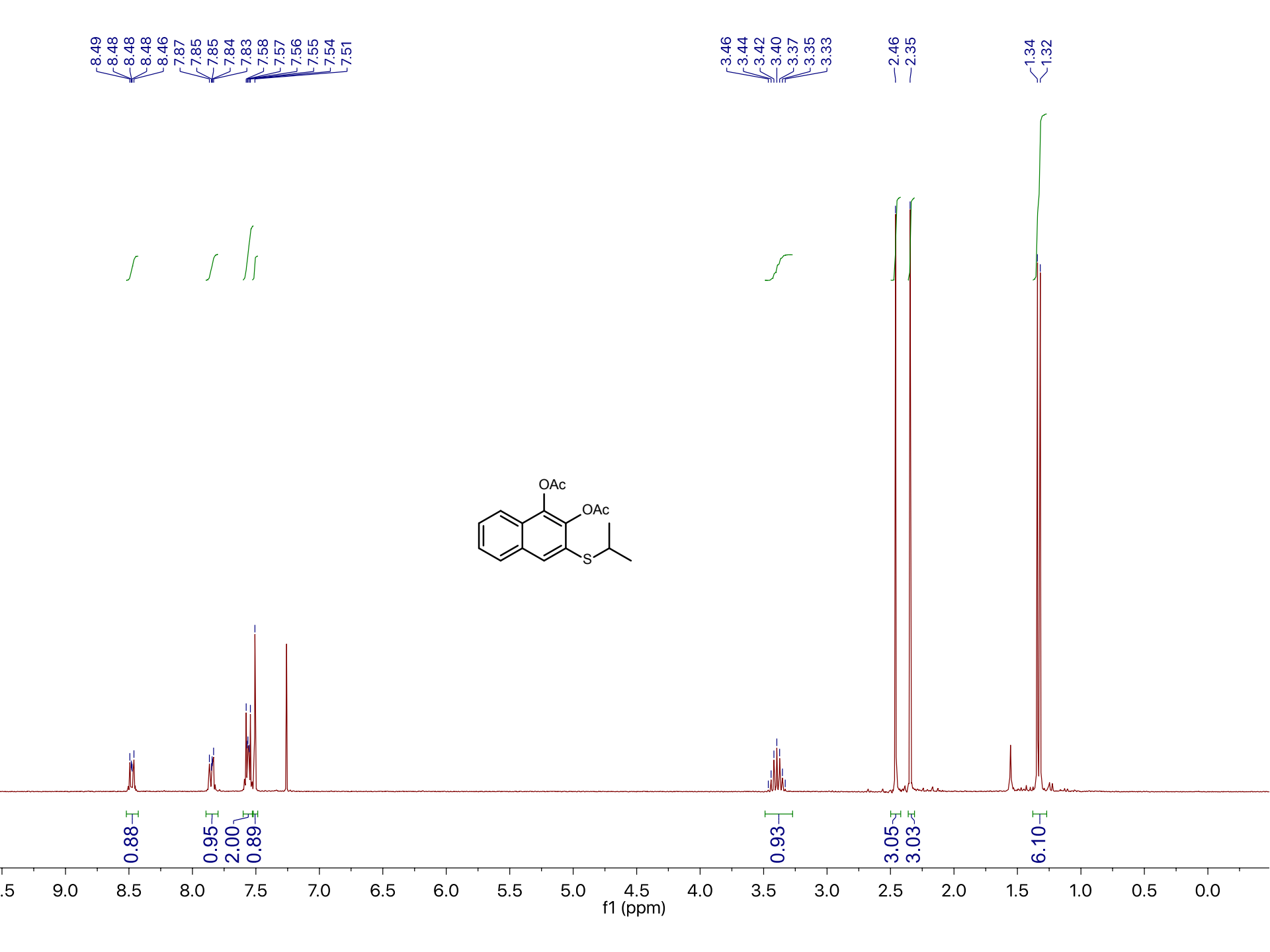
8.49
8.48
8.48
8.48
8.46
7.87
7.85
7.85
7.84
7.83
7.58
7.57
7.56
7.55
7.54
7.51
3.46
3.44
3.42
3.40
3.37
3.35
3.33
2.46
2.35
1.34
1.32
OAc
OAc
S
0.88
0.95
2.00
0.89
0.93
3.05
3.03
6.10
9.5
9.0
8.5
8.0
7.5
7.0
6.5
6.0
5.5
5.0
4.5
4.0
3.5
3.0
2.5
2.0
1.5
1.0
0.5
0.0
f1 (ppm)

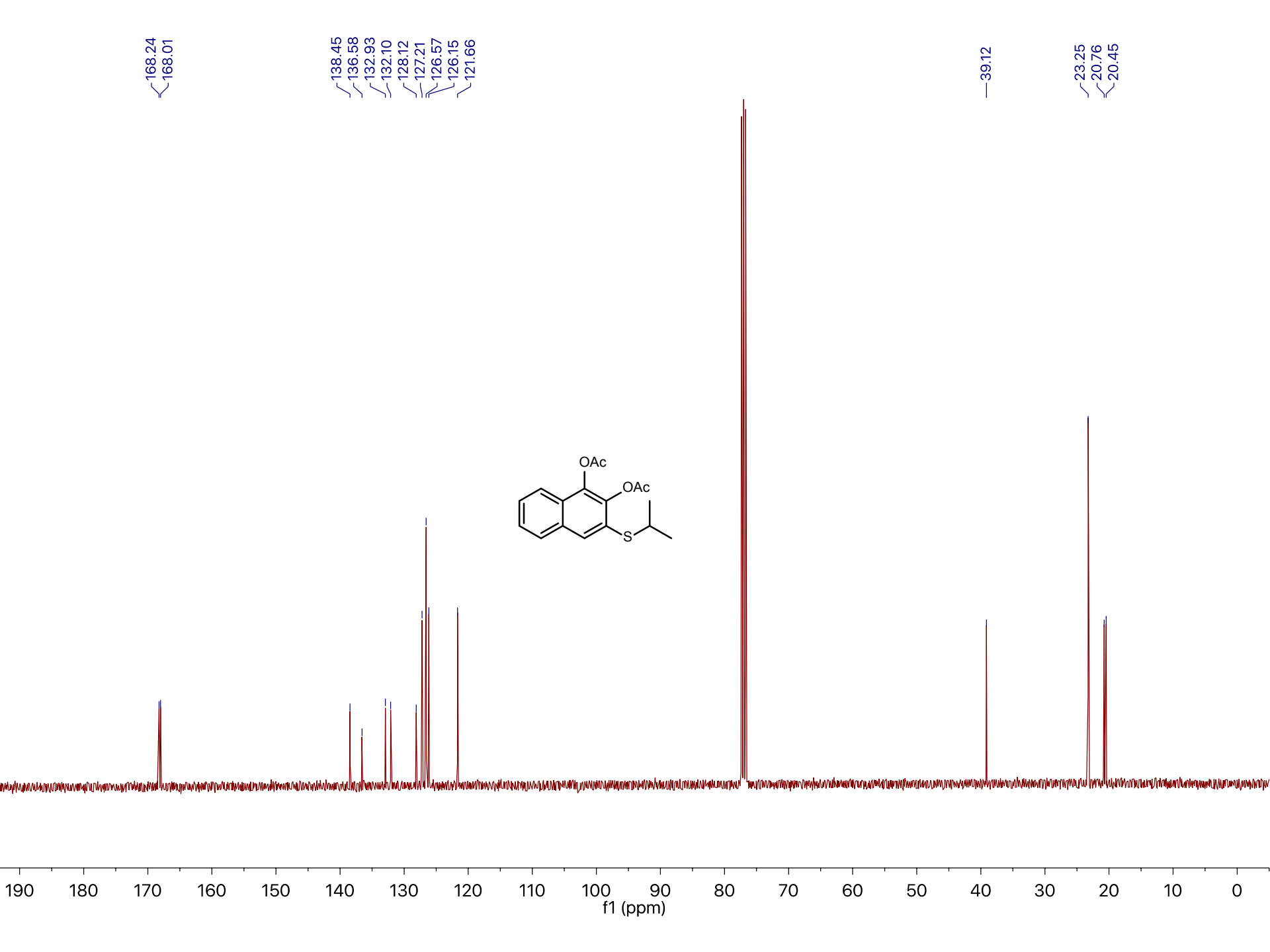
168.24
168.01
138.45
136.58
132.93
132.10
128.12
127.21
126.57
126.15
121.66
39.12
23.25
20.76
20.45
OAc
OAc
S
190
180
170
160
150
140
130
120
110
100
90
80
70
60
50
40
30
20
10
0
f1 (ppm)

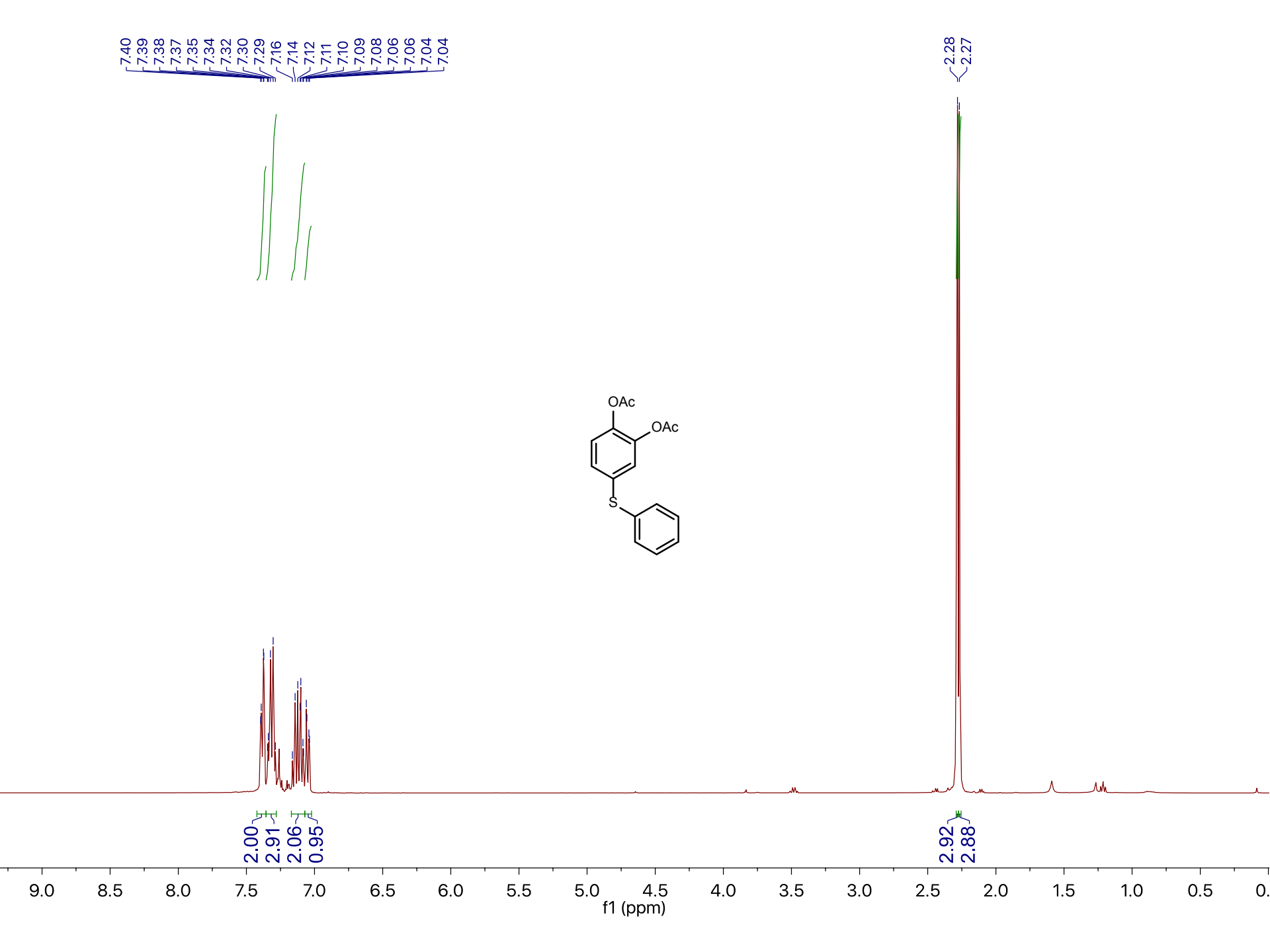
7.40
7.39
7.38
7.37
7.35
7.34
7.32
7.30
7.29
7.16
7.14
7.12
7.11
7.10
7.09
7.08
7.06
7.06
7.04
7.04
2.28
2.27
OAc
OAc
S
2.00
2.91
2.06
0.95
2.92
2.88
9.0
8.5
8.0
7.5
7.0
6.5
6.0
5.5
5.0
4.5
4.0
3.5
3.0
2.5
2.0
1.5
1.0
0.5
f1 (ppm)

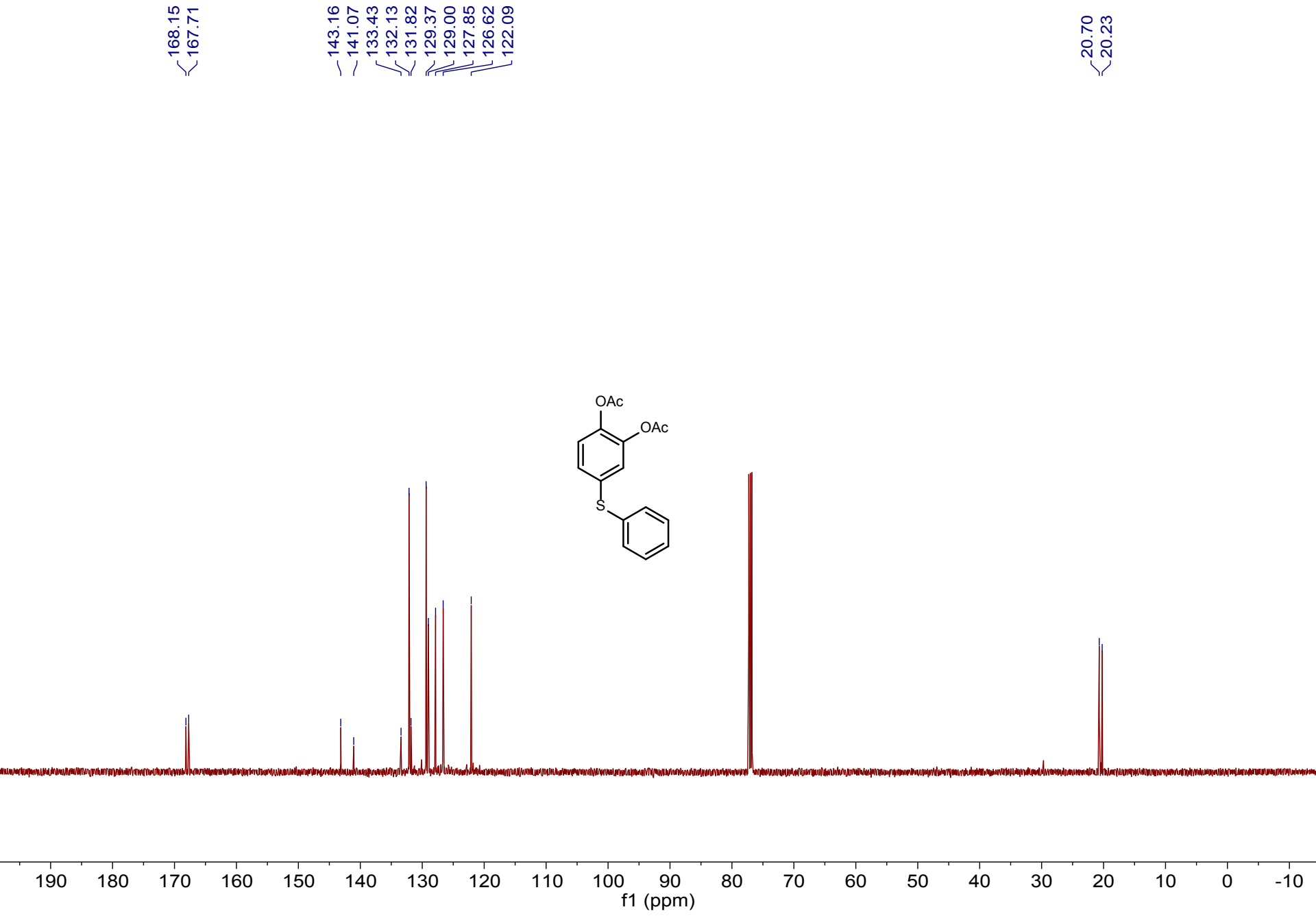
168.15
167.71
143.16
141.07
133.43
132.13
131.82
129.37
129.00
127.85
126.62
122.09
20.70
20.23
OAc
OAc
S
190
180
170
160
150
140
130
120
110
100
90
80
70
60
50
40
30
20
10
0
-10
f1 (ppm)

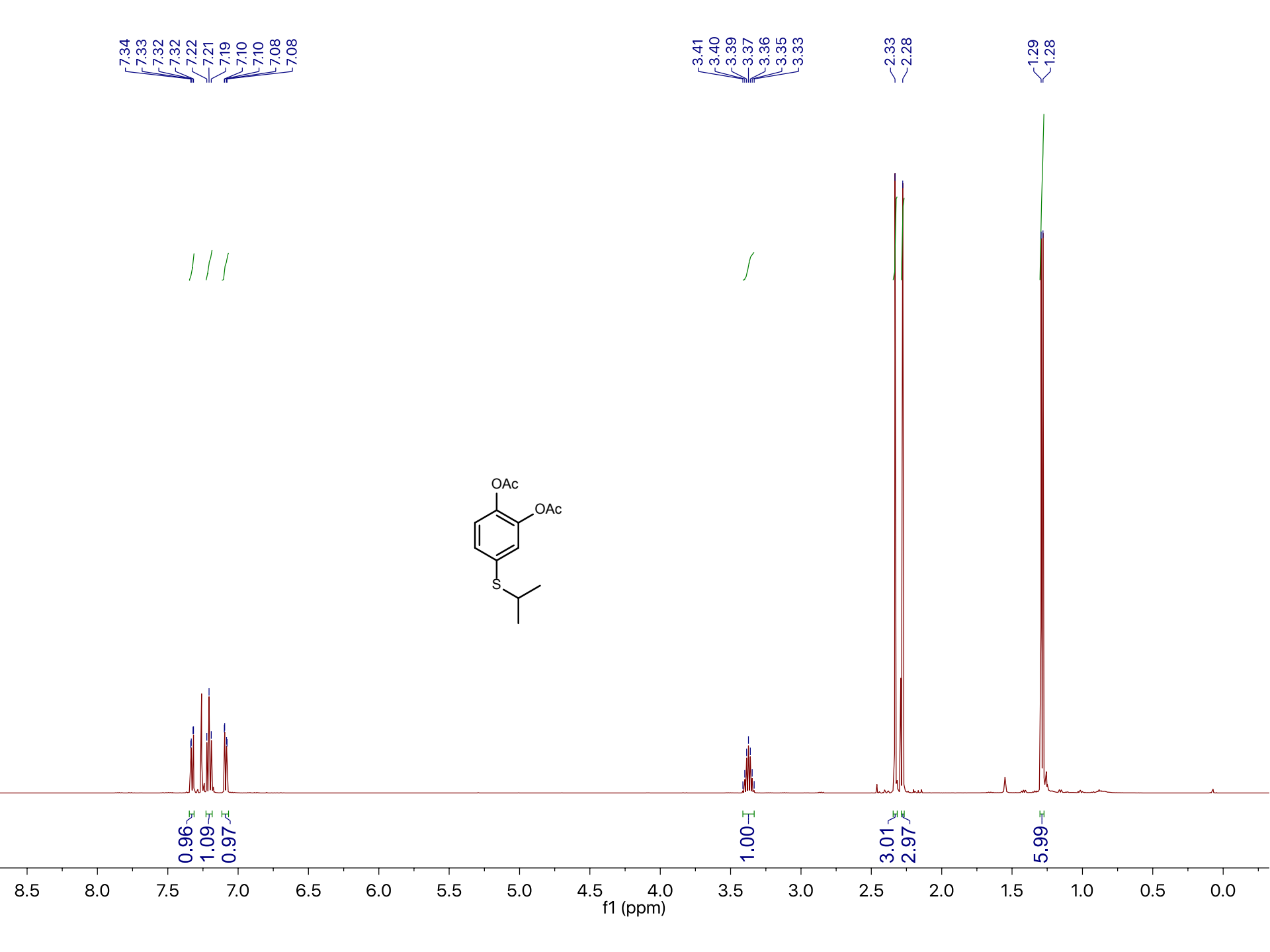
7.34
7.33
7.32
7.32
7.22
7.21
7.19
7.10
7.10
7.08
7.08
3.41
3.40
3.39
3.37
3.36
3.35
3.33
2.33
2.28
1.29
1.28
OAc
OAc
S
0.96
1.09
0.97
1.00
3.01
2.97
5.99
8.5
8.0
7.5
7.0
6.5
6.0
5.5
5.0
4.5
4.0
3.5
3.0
2.5
2.0
1.5
1.0
0.5
0.0
f1 (ppm)

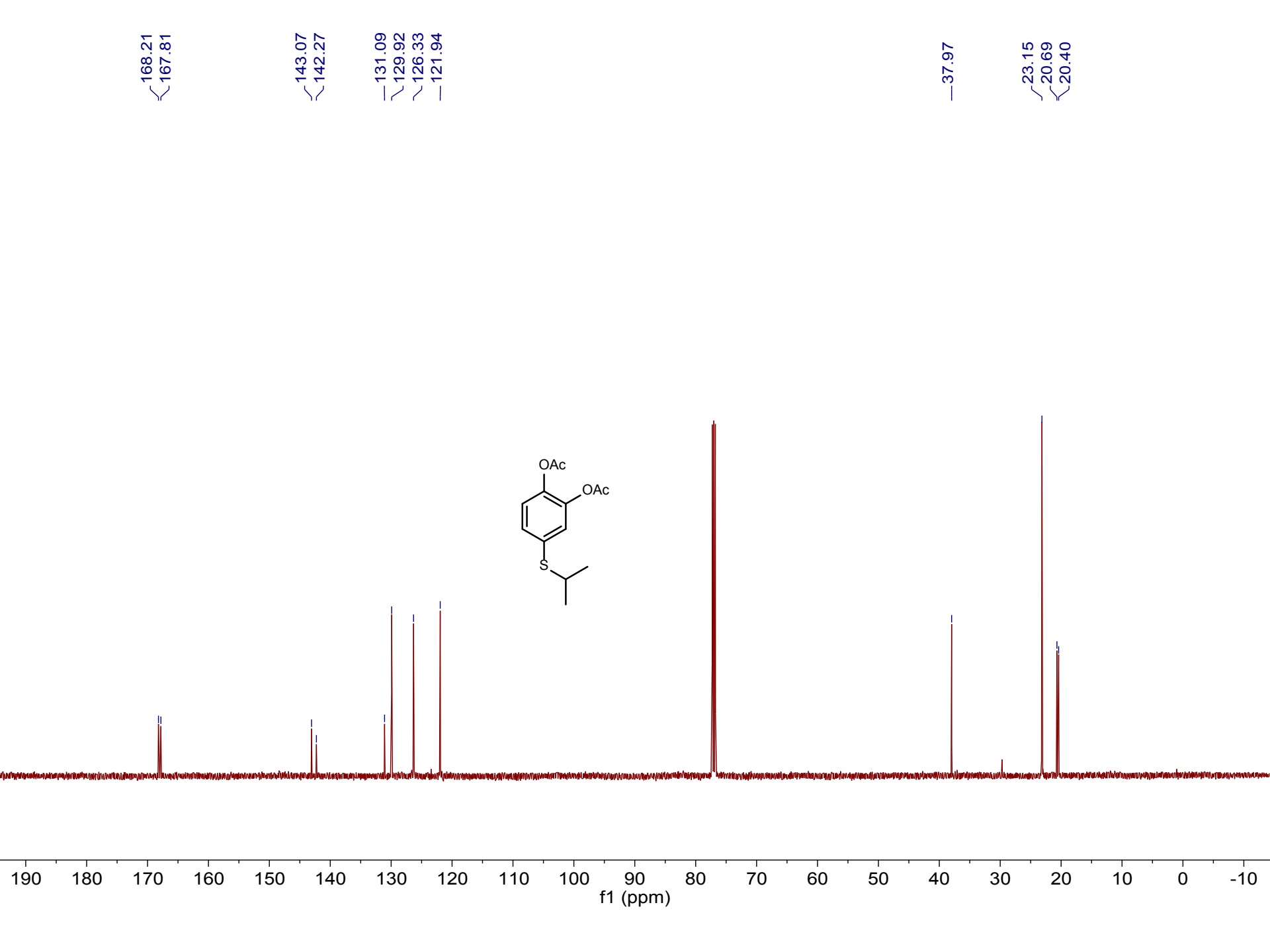
168.21
167.81
143.07
142.27
131.09
129.92
126.33
121.94
37.97
23.15
20.69
20.40
OAc
OAc
S
190
180
170
160
150
140
130
120
110
100
90
80
70
60
50
40
30
20
10
0
-10
f1 (ppm)

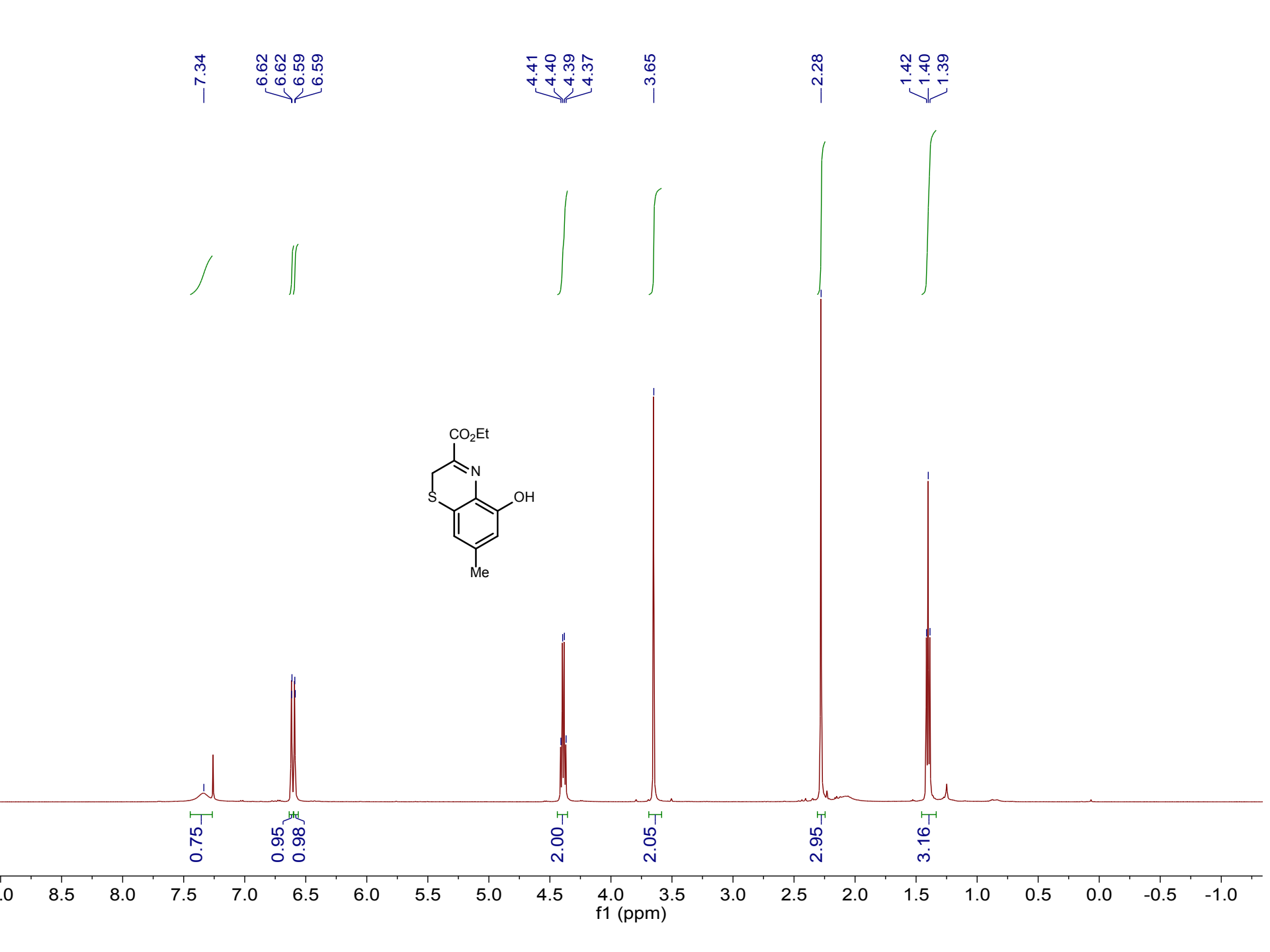
7.34
6.62
6.62
6.59
6.59
4.41
4.40
4.39
4.37
3.65
2.28
1.42
1.40
1.39
CO2Et
N
S
OH
Me
0.75
0.95
0.98
2.00
2.05
2.95
3.16
f1 (ppm)

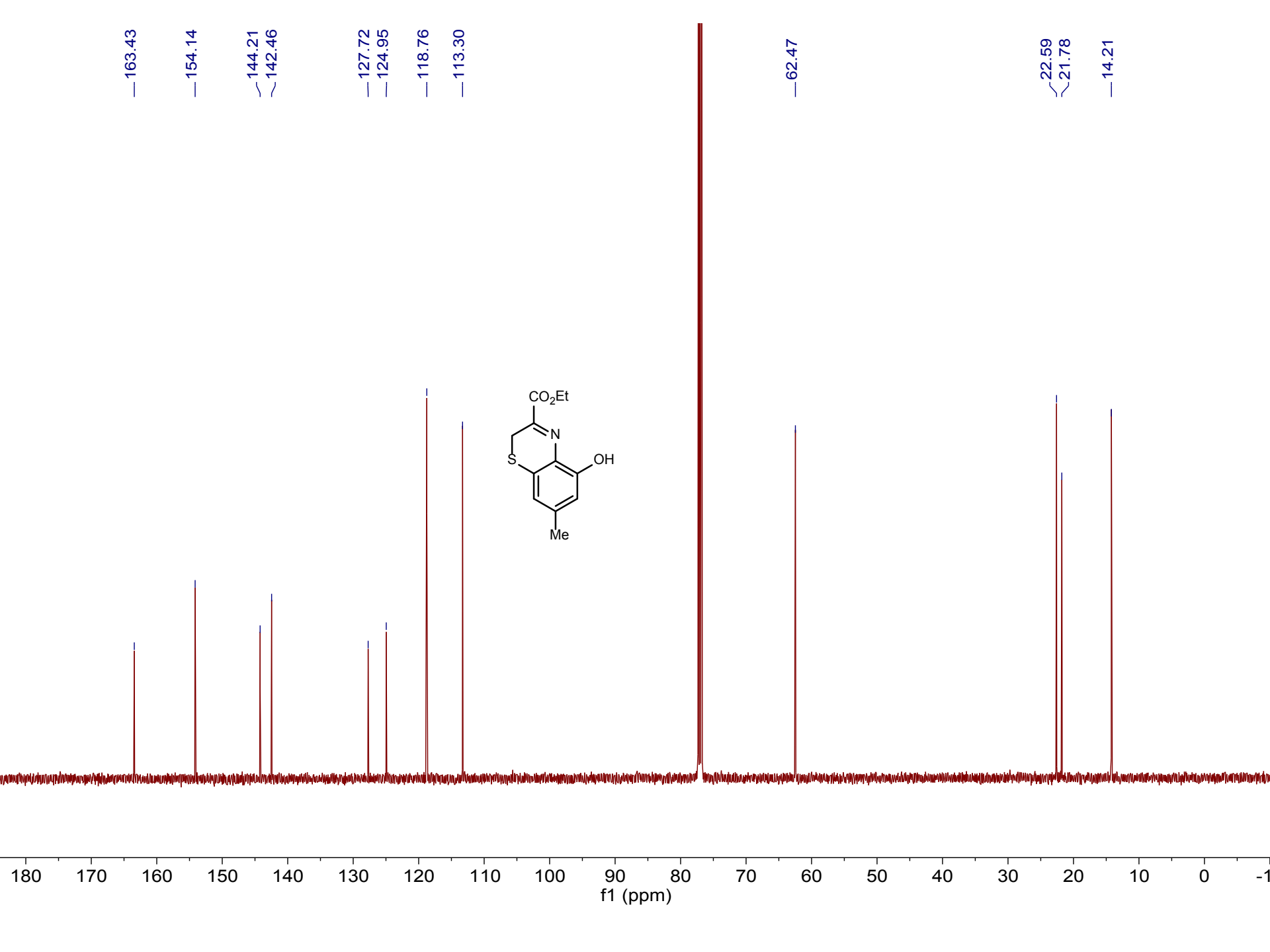
163.43
154.14
144.21
142.46
127.72
124.95
118.76
113.30
62.47
22.59
21.78
14.21
CO2Et
N
S
OH
Me
180
170
160
150
140
130
120
110
100
90
80
70
60
50
40
30
20
10
0
-1
f1 (ppm)

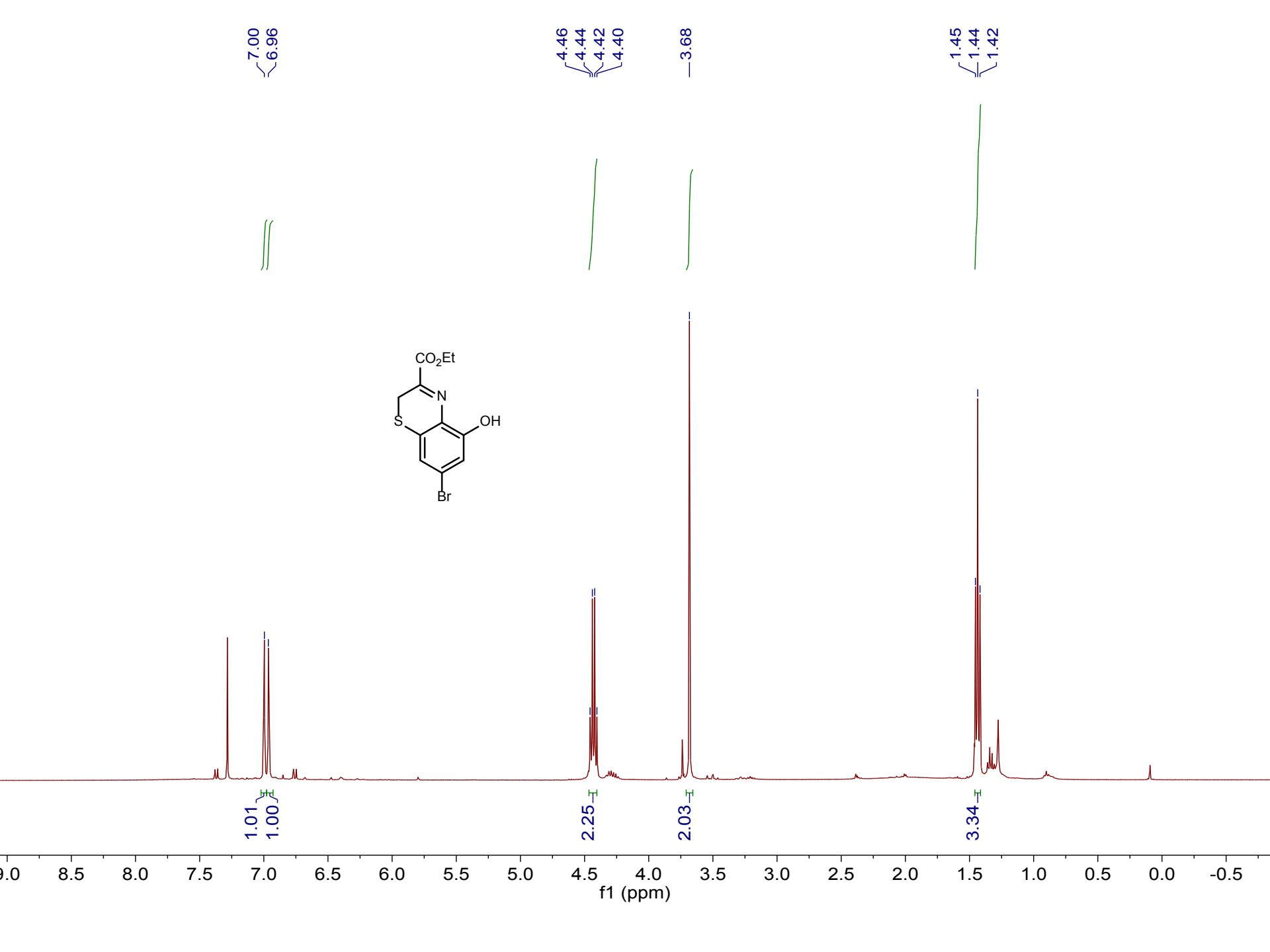
7.00
6.96
4.46
4.44
4.42
4.40
3.68
1.45
1.44
1.42
CO2Et
N
S
OH
Br
1.01
1.00
2.25
2.03
3.34
9.0
8.5
8.0
7.5
7.0
6.5
6.0
5.5
5.0
4.5
4.0
3.5
3.0
2.5
2.0
1.5
1.0
0.5
0.0
-0.5
f1 (ppm)

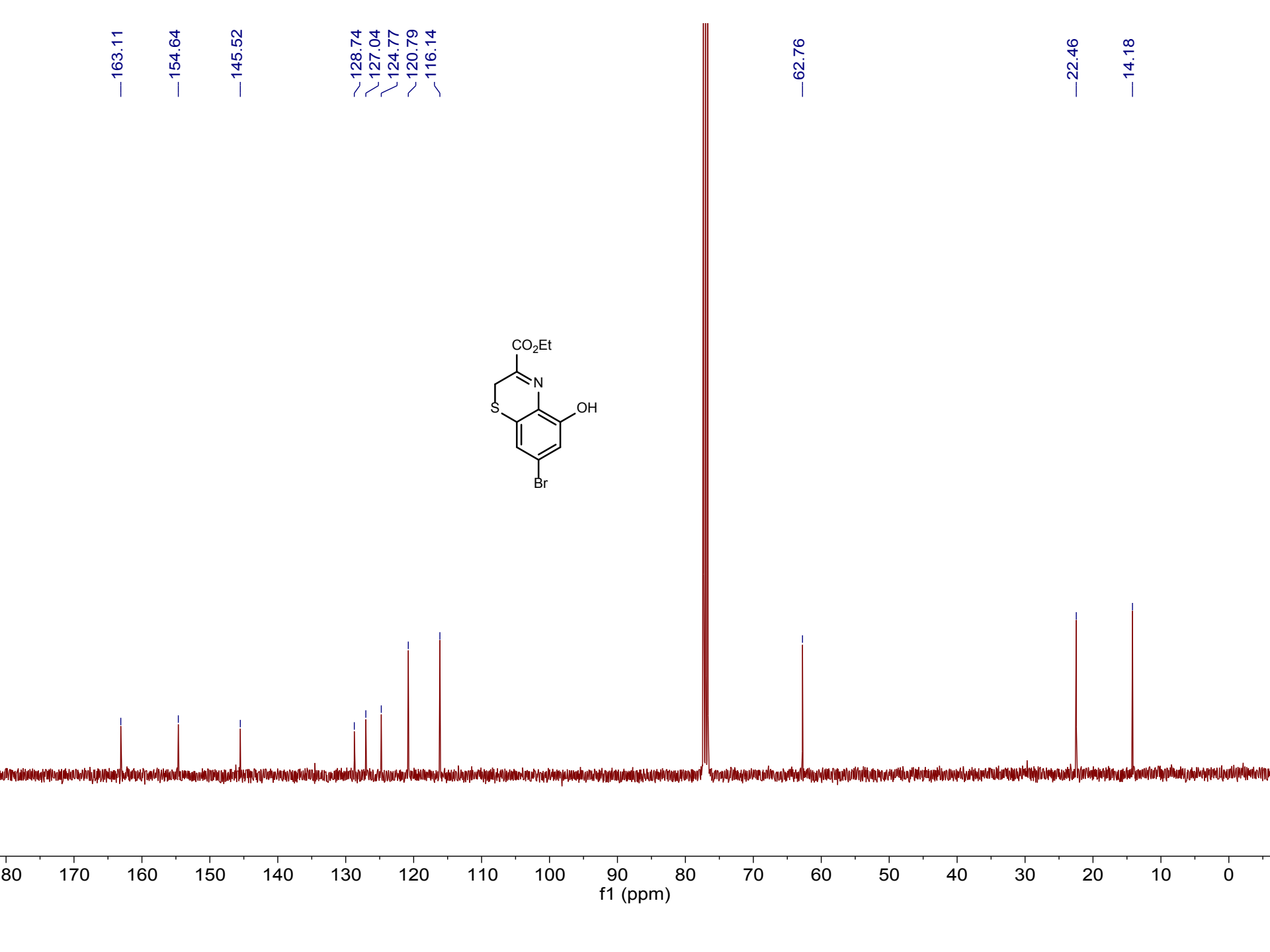
163.11
154.64
145.52
128.74
127.04
124.77
120.79
116.14
62.76
22.46
14.18
CO2Et
N
S
OH
Br
80
170
160
150
140
130
120
110
100
90
80
70
60
50
40
30
20
10
0
f1 (ppm)

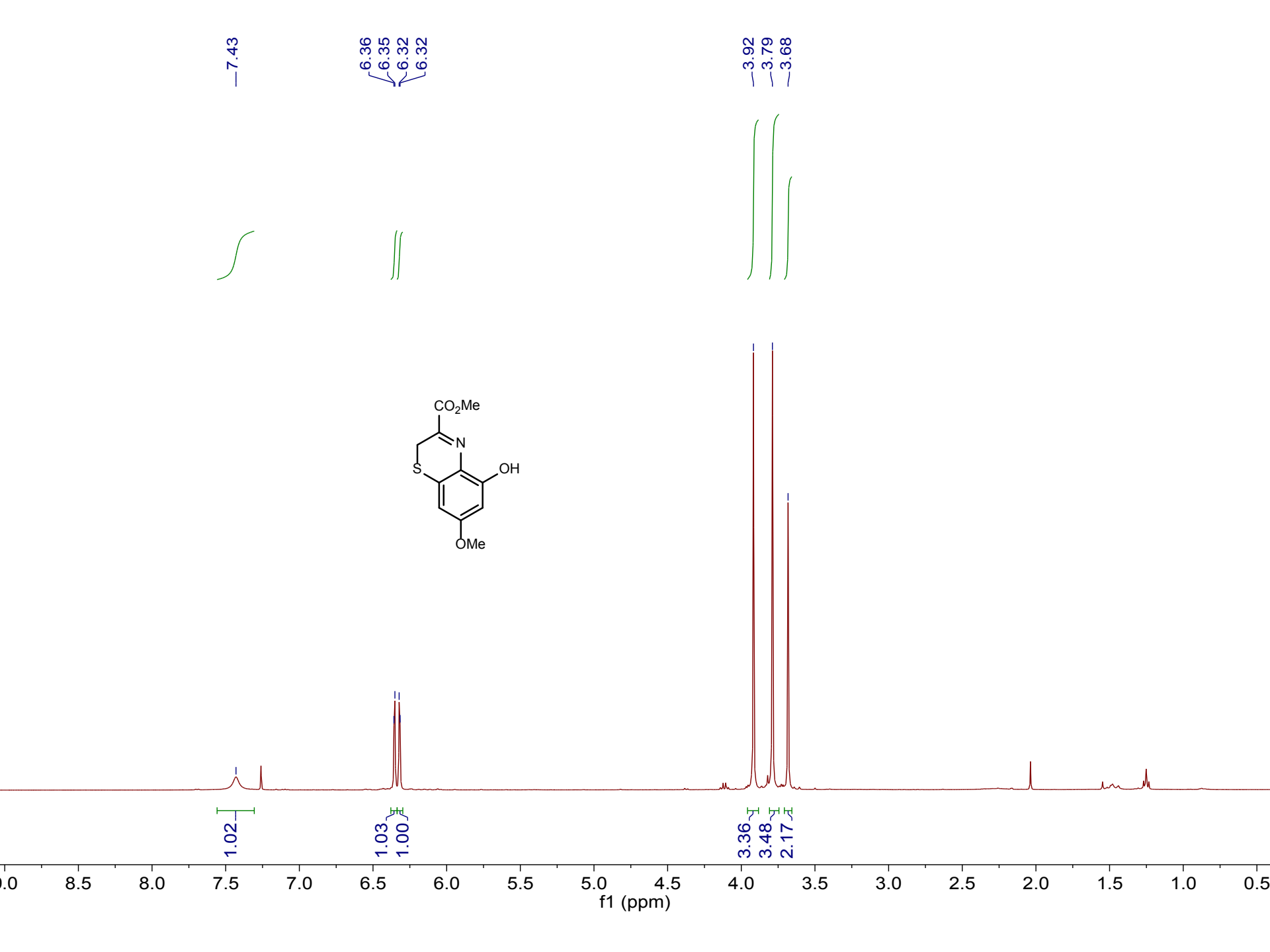
7.43
6.36
6.35
6.32
6.32
3.92
3.79
3.68
CO2Me
N
S
OH
OMe
1.02
1.03
1.00
3.36
3.48
2.17
f1 (ppm)

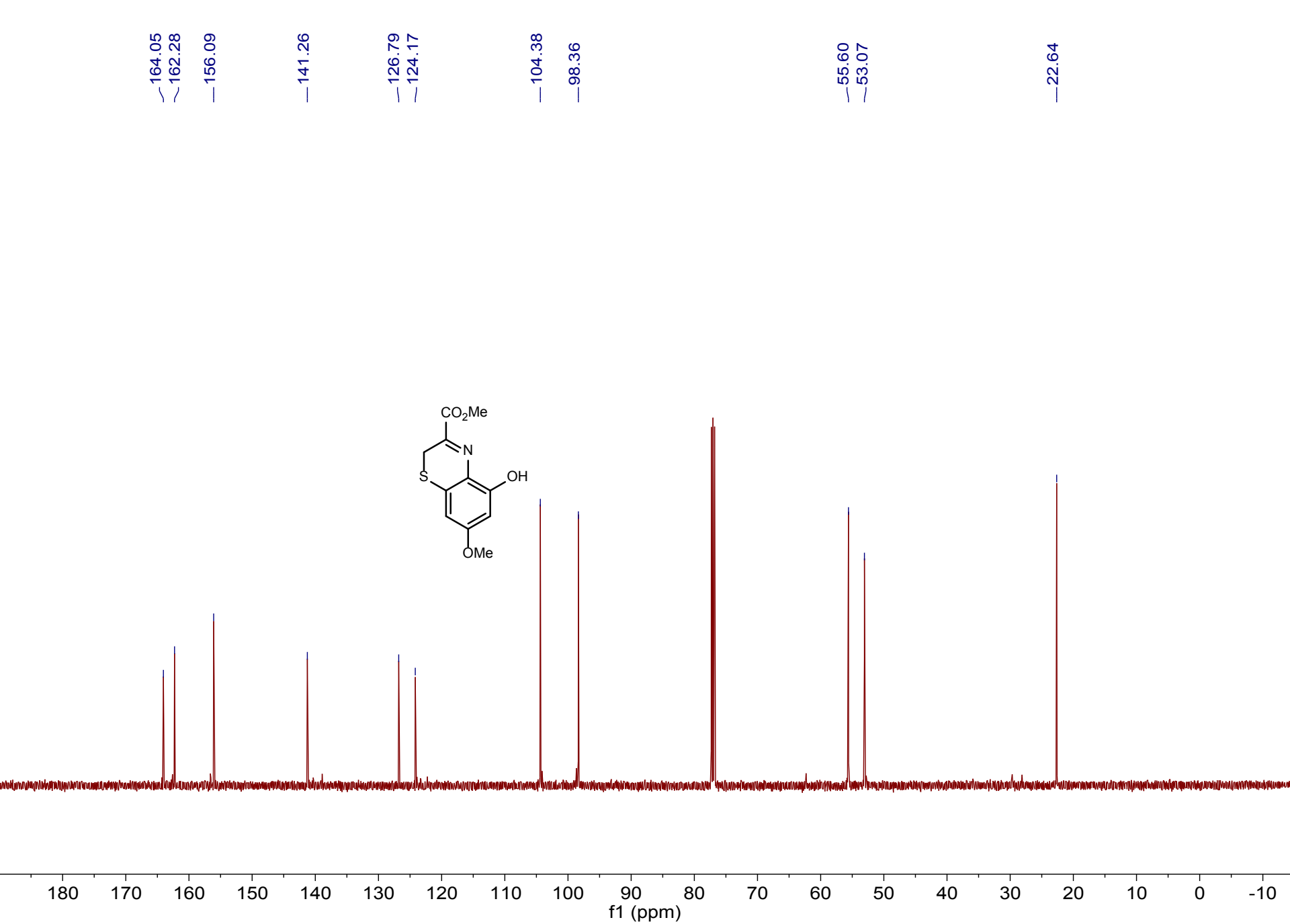
164.05
162.28
156.09
141.26
126.79
124.17
104.38
98.36
55.60
53.07
22.64
CO2Me
N
S
OH
OMe
180
170
160
150
140
130
120
110
100
90
80
70
60
50
40
30
20
10
0
-10
f1 (ppm)

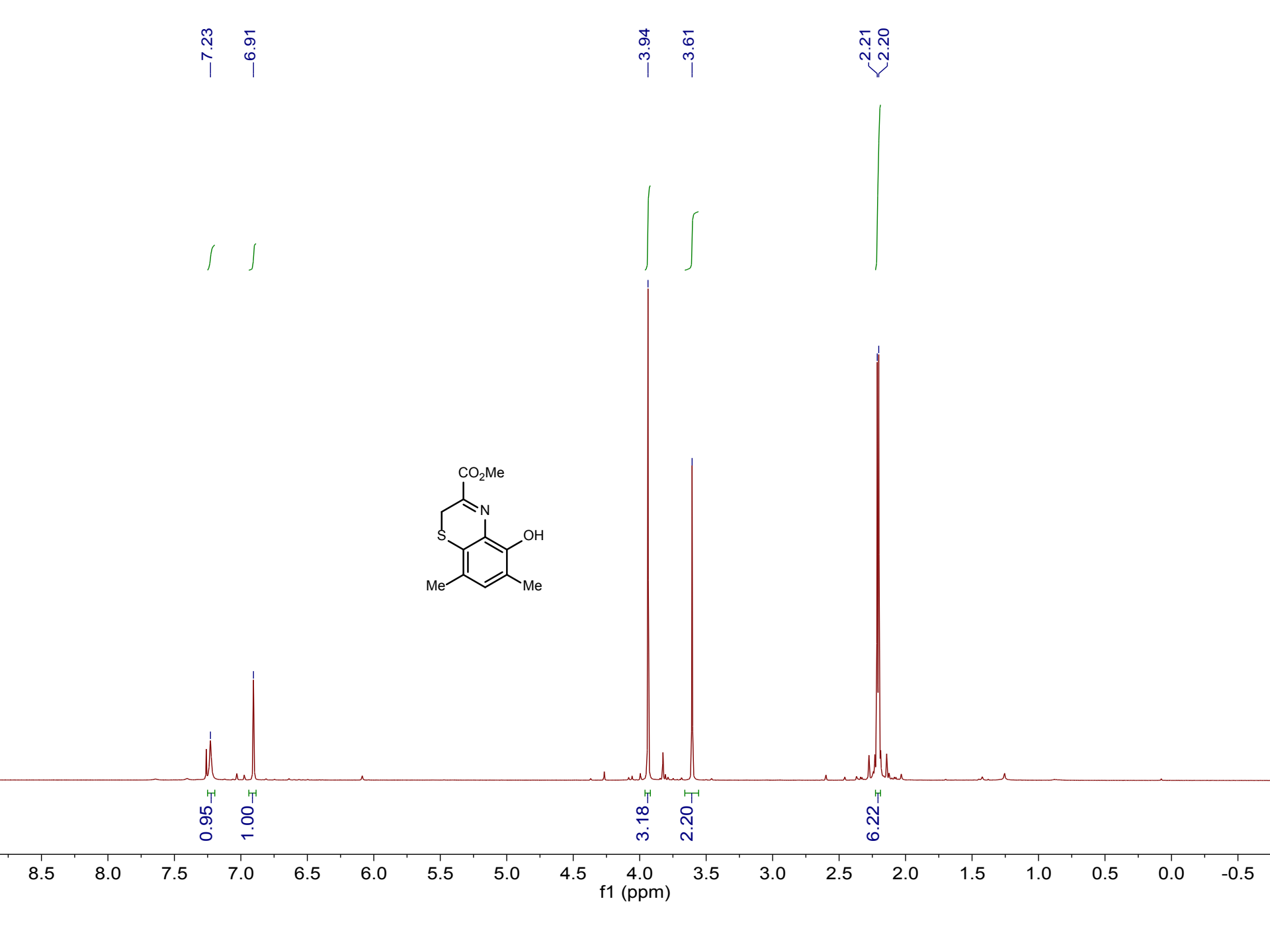
7.23
6.91
3.94
3.61
2.21
2.20
CO2Me
N
S
OH
Me
Me
0.95
1.00
3.18
2.20
6.22
8.5
8.0
7.5
7.0
6.5
6.0
5.5
5.0
4.5
4.0
3.5
3.0
2.5
2.0
1.5
1.0
0.5
0.0
-0.5
f1 (ppm)

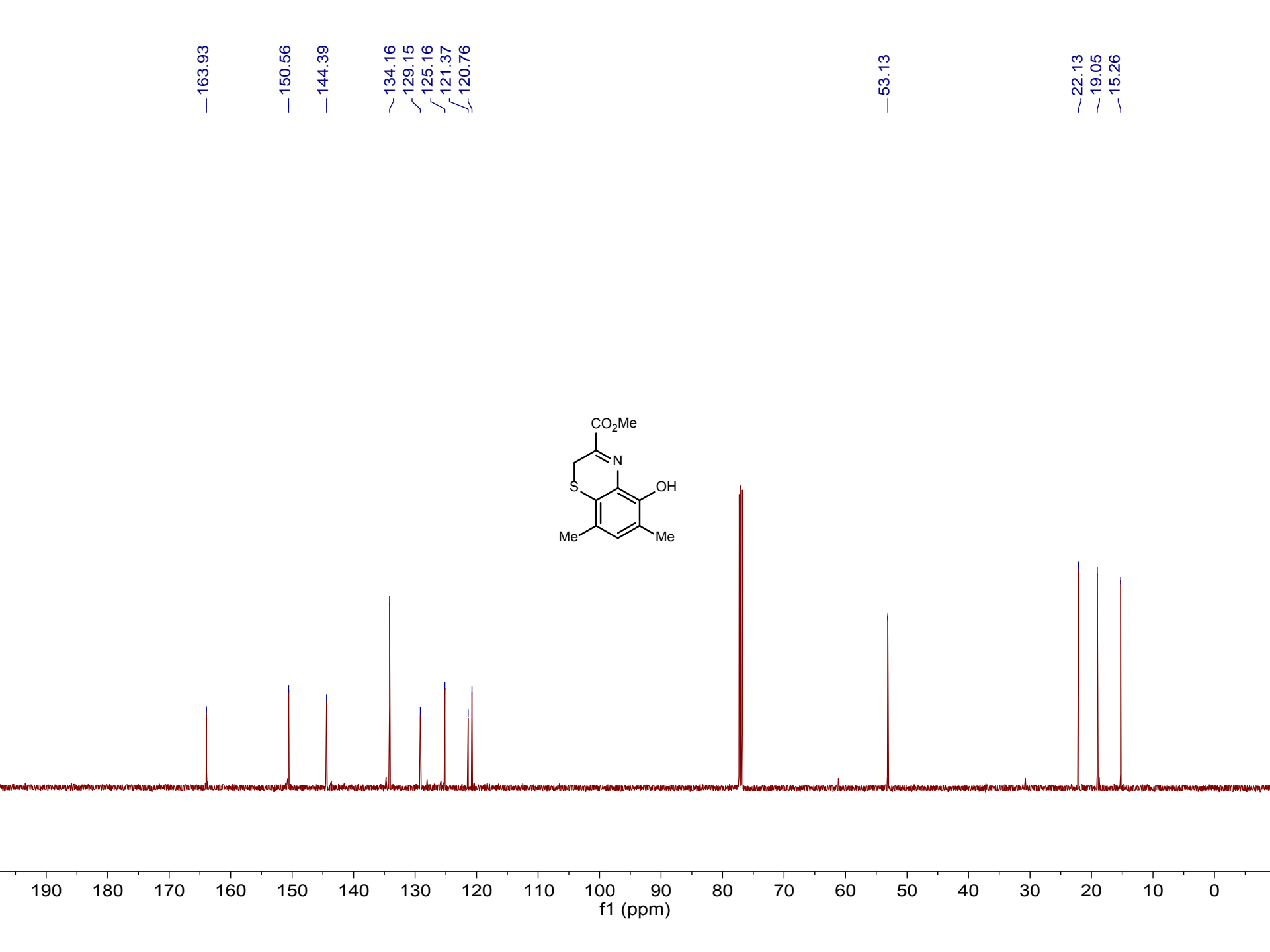
163.93
150.56
144.39
134.16
129.15
125.16
121.37
120.76
53.13
22.13
19.05
15.26
CO2Me
N
S
OH
Me
Me
190
180
170
160
150
140
130
120
110
100
90
80
70
60
50
40
30
20
10
0
f1 (ppm)

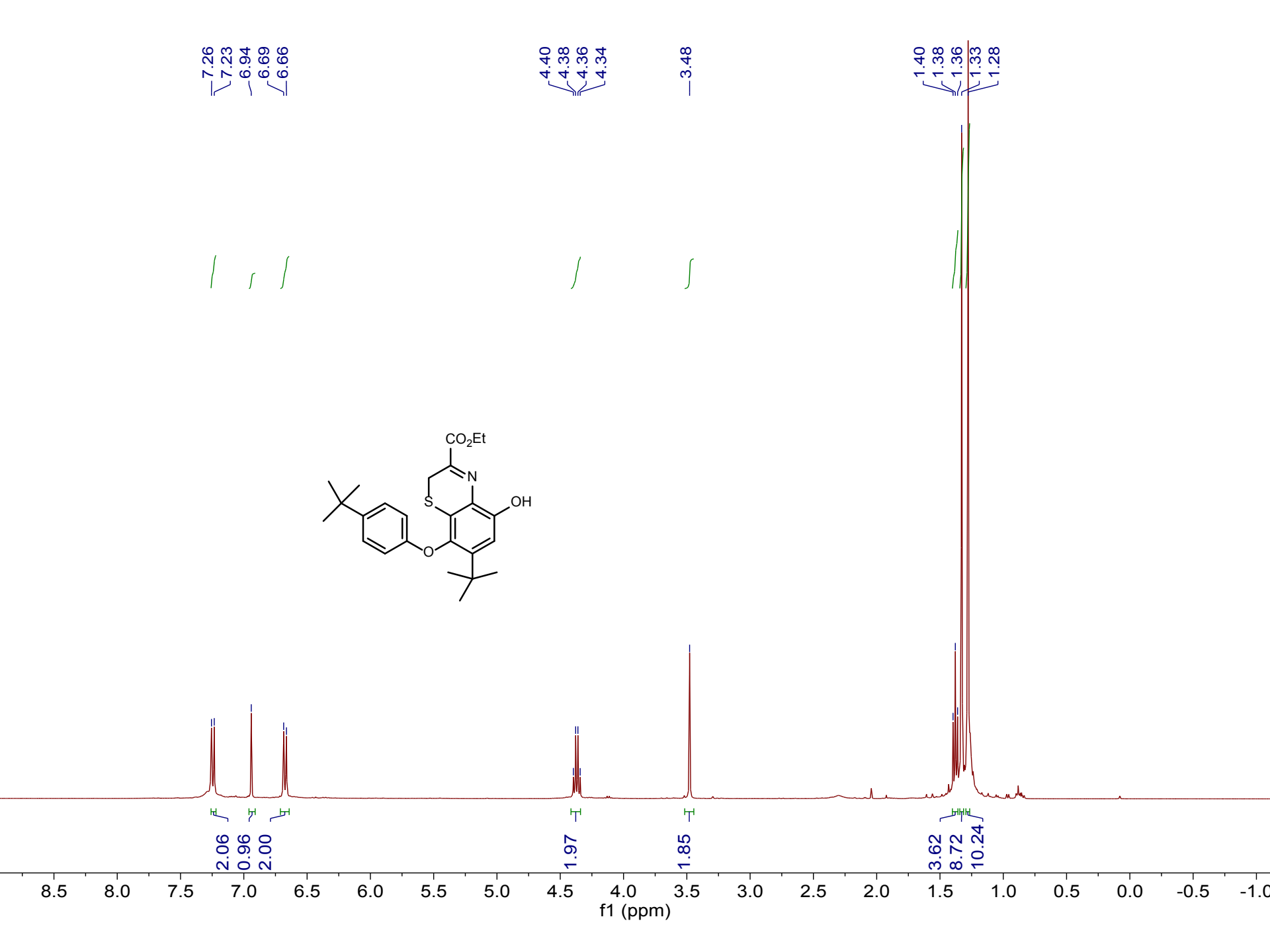
7.26
7.23
6.94
6.69
6.66
4.40
4.38
4.36
4.34
3.48
1.40
1.38
1.36
1.33
1.28
CO2Et
N
S
OH
O
2.06
0.96
2.00
1.97
1.85
3.62
8.72
10.24
8.5
8.0
7.5
7.0
6.5
6.0
5.5
5.0
4.5
4.0
3.5
3.0
2.5
2.0
1.5
1.0
0.5
0.0
-0.5
-1.0
f1 (ppm)

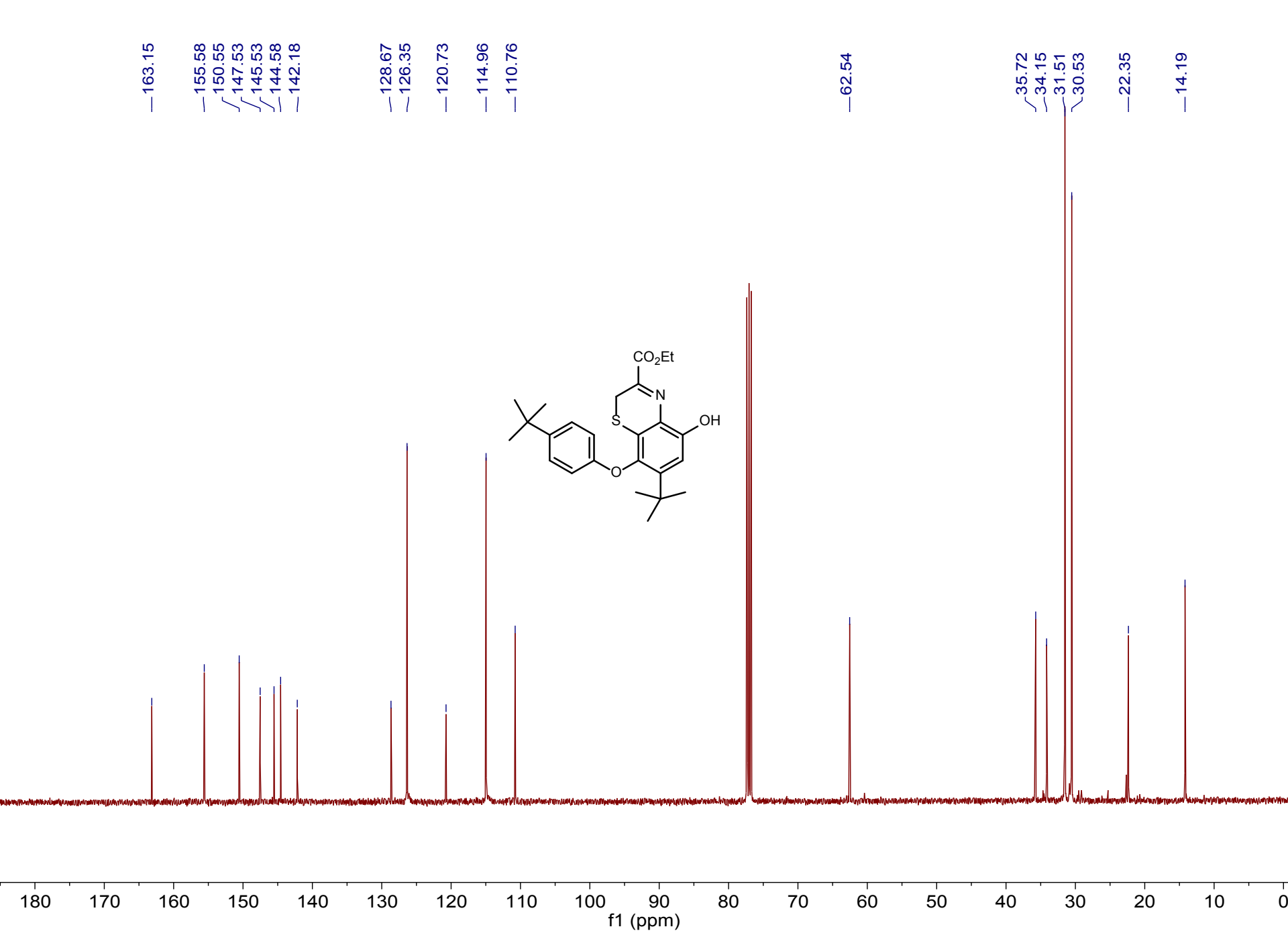
163.15
155.58
150.55
147.53
145.53
144.58
142.18
128.67
126.35
120.73
114.96
110.76
62.54
35.72
34.15
31.51
30.53
22.35
14.19
CO2Et
N
S
OH
O
180
170
160
150
140
130
120
110
100
90
80
70
60
50
40
30
20
10
0
f1 (ppm)

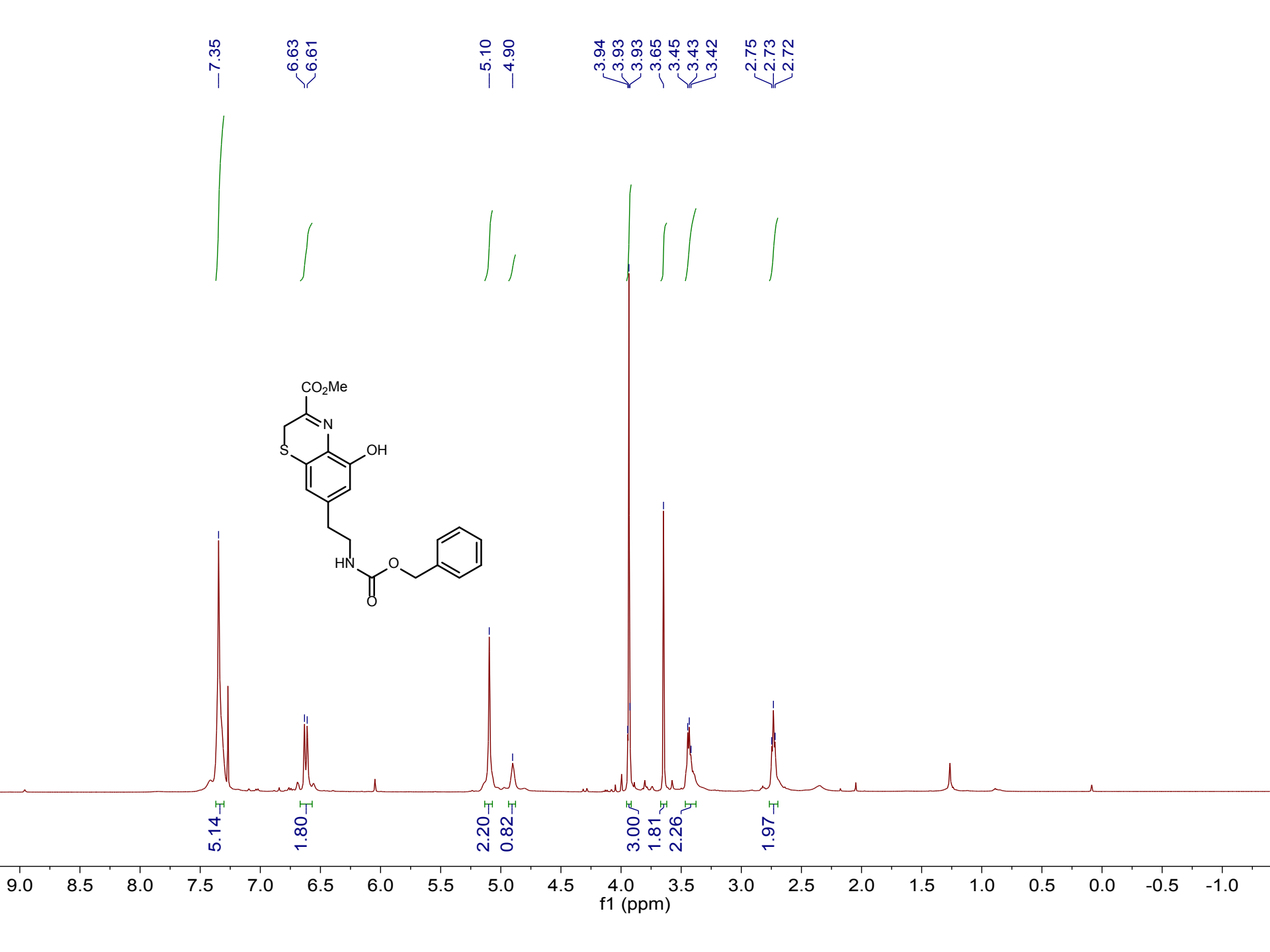
7.35
6.63
6.61
5.10
4.90
3.94
3.93
3.93
3.65
3.45
3.43
3.42
2.75
2.73
2.72
CO2Me
N
S
OH
HN
O
O
5.14
1.80
2.20
0.82
3.00
1.81
2.26
1.97
9.0
8.5
8.0
7.5
7.0
6.5
6.0
5.5
5.0
4.5
4.0
3.5
3.0
2.5
2.0
1.5
1.0
0.5
0.0
-0.5
-1.0
f1 (ppm)

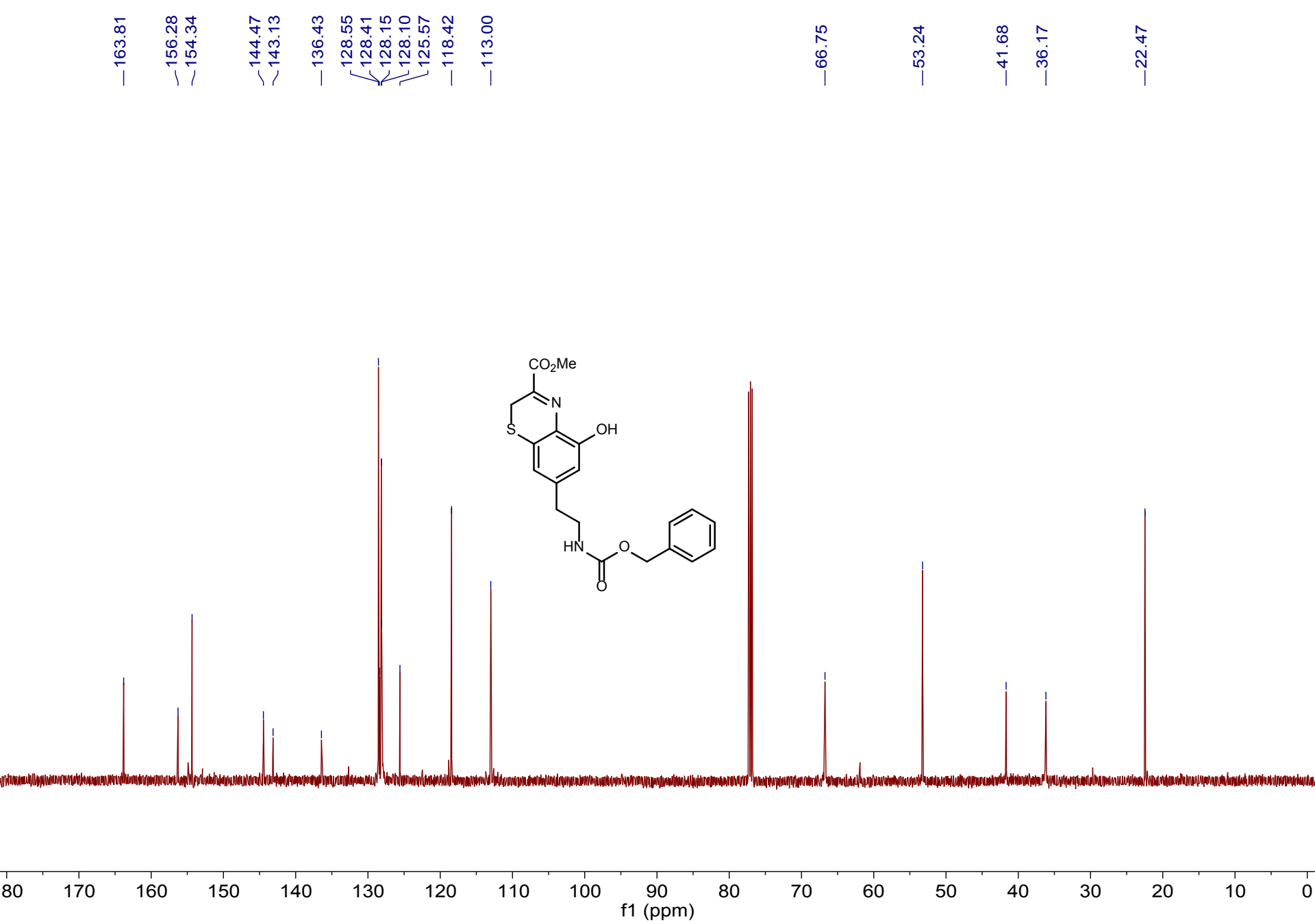
163.81
156.28
154.34
144.47
143.13
136.43
128.55
128.41
128.15
128.10
125.57
118.42
113.00
66.75
53.24
41.68
36.17
22.47
CO2Me
N
S
OH
HN
O
O
f1 (ppm)

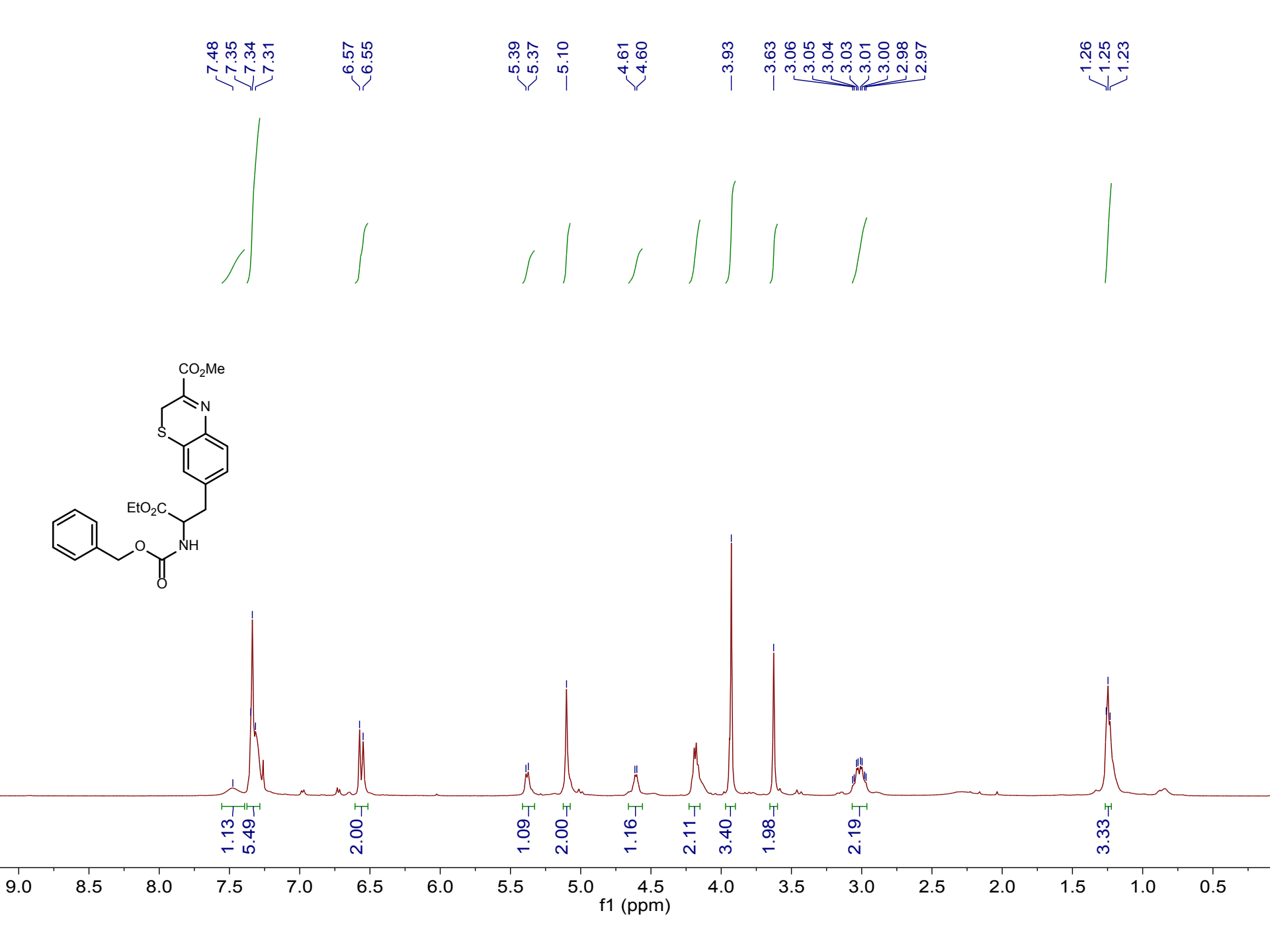
7.48
7.35
7.34
7.31
6.57
6.55
5.39
5.37
5.10
4.61
4.60
3.93
3.63
3.06
3.05
3.04
3.03
3.01
3.00
2.98
2.97
1.26
1.25
1.23
CO2Me
N
S
EtO2C
NH
O
O
1.13
5.49
2.00
1.09
2.00
1.16
2.11
3.40
1.98
2.19
3.33
9.0
8.5
8.0
7.5
7.0
6.5
6.0
5.5
5.0
4.5
4.0
3.5
3.0
2.5
2.0
1.5
1.0
0.5
f1 (ppm)

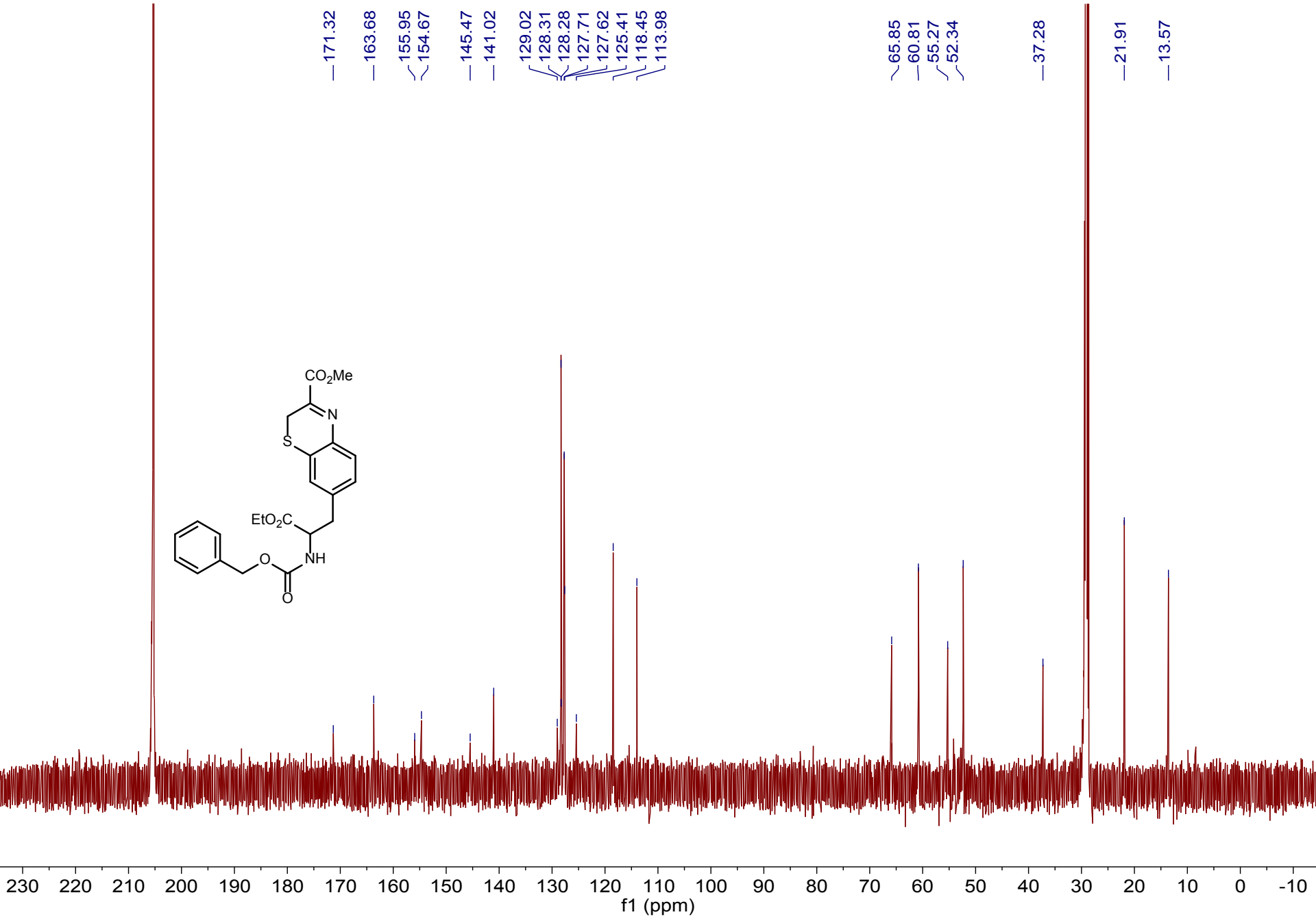
171.32
163.68
155.95
154.67
145.47
141.02
129.02
128.31
128.28
127.71
127.62
125.41
118.45
113.98
65.85
60.81
55.27
52.34
37.28
21.91
13.57
CO2Me
N
S
EtO2C
NH
O
O
230 220 210 200 190 180 170 160 150 140 130 120 110 100 90 80 70 60 50 40 30 20 10 0 -10
f1 (ppm)